

University of Nottingham
UK | CHINA | MALAYSIA

The Impact of Wind on the Building Airtightness Measurement using the Pulse Technique

YUN-SHENG HSU

MSc. BSc.

Thesis Submitted to the University of Nottingham

for the Degree of Doctor of Philosophy

October 2021

Abstract

Ventilation plays a vital role in the energy performance and indoor air quality of buildings, which can also be influenced by the uncontrolled air leakage (i.e., air infiltration) across the building envelope. As a fundamental building property, the building airtightness is a crucial factor that should be addressed in order to improve the building energy performance, indoor air quality and building durability. Minimum building airtightness requirements have been included in building regulations and voluntary standards in more and more regions.

To quantitatively understand the airtightness of the building envelope, different measurement methods for the building envelope leakages have been proposed and evolved, which typically measure the air leakage rate under a certain pressure difference. The steady pressurisation method is most commonly used, while the Pulse technique proposes an alternative solution for providing new metrics. It offers an option of high-quality fast testing, involving a low-pressure pressurisation process, typically around 4Pa. Regarding the building airtightness measurement, its uncertainty has been the key concern in many regions over the past few years. The wind impact on the airtightness measurement has been explored from different perspectives, and solutions to minimise the wind effect have been proposed, whereas the majority of work has been focused on the steady pressurisation method. Therefore, to fill the research gap, the research aims to provide in-depth insights into the wind impact on the building airtightness measurement with the Pulse technique through field testing of two case study buildings under natural wind conditions and Computational Fluid Dynamics (CFD)-based numerical simulations under steady wind conditions.

In this thesis, comparisons between the conventional steady pressurisation method and the Pulse technique were firstly presented, providing fundamental insights into how the practical measurements would be when both test methods were applied to the same house in real scenarios. Based on the experimental airtightness measurements of a five-bedroom dwelling under calm weather conditions, a good overall agreement between the two test methods was observed, with deviations of 3.93% at 7.1Pa and 4.56% at 10.6Pa for the overlapped building pressure range. In order to answer the frequently raised question associated with the dynamic nature of the Pulse test, explorations were conducted to confirm the achievement of the uniform indoor pressure distribution in a five-bedroom dwelling during the Pulse test and therefore prove the applicability and reliability of the method. To assess the wind impact on the Pulse test under natural wind conditions, a short-term experimental work consisting of 423 Pulse tests was completed over seven days in a five-bedroom detached house, and a long-term investigation with 1096 Pulse tests was performed over eight months in an outdoor chamber. The field tests demonstrated the

noticeable wind impact on the Pulse measurement, as a higher wind speed led to a significant deviation of the airtightness measurement. Based on the tests in the five-bedroom dwelling, the wind impact was not significant for the wind speed below 3.14m/s at 2.2m above ground level (i.e., approximately equivalent to the meteorological wind speed of 4.95m/s) with *RPD* <±5%, and the wind speed was below 6.10m/s at 5.0m above the ground level (i.e., approximately equivalent to the meteorological wind speed of 7.51m/s) according to the findings of the outdoor chamber. The observed threshold of wind speed that caused the Pulse measurement of the five-bedroom dwelling with unacceptable errors was 5.02m/s at 2.2m above ground level (i.e., approximately equivalent to the meteorological wind speed of 7.91m/s) with *RPD* <±10%, while the threshold was 11.65m/s at 5.0m above ground level (i.e., approximately equivalent to meteorological wind speed 14.34m/s) based on the tests in the outdoor chamber, due to the differences in the tested building configurations and airtightness levels. Besides, solutions have been explored to minimise the wind impact, such as performing multi-Pulse tests or multi-step Pulse tests and improving the algorithm to adjust the obtained Pulse measurements. Furthermore, CFD-based numerical simulations were implemented in the ANSYS Fluent based on a full-scale three-dimensional model of the building and the Pulse unit. The numerical work visually and statistically demonstrated how the pressure uniformly distributes across the internal spaces during the Pulse test. Based on the numerical simulations, the meteorological wind speed limit for the Pulse measurement with *RPD* <±10% was below 6m/s, which is in line with the wind speed limit for the fan pressurisation method stated in the ISO 9972:2015 standard (Thermal performance of buildings-Determination of air permeability of buildings-Fan pressurisation method). The numerical results also indicate that the Pulse measurement is less sensitive to the variation in the wind direction than the wind speed level, as the largest difference of the simulated average air leakage rate among the cases with different wind directions was 3.93%. Additionally, the comparison between the building model with a flat roof and a gable roof reveals the insignificant impact caused by the presence of the gable roof on the Pulse measurement, as the deviation of the air leakage rate was only 1.25%.

The research has been routinely conducted as part of the ongoing Pulse development, providing progress to the knowledge of comprehensive understandings of the wind impact on the Pulse test from practical and numerical perspectives, demonstrating how the Pulse measurement performs under different wind conditions and the reliability of the method. The findings of the wind impact in this research provide valuable supporting information for the improvement of protocols that are used to characterise building airtightness measurement and for the significance of building airtightness on the energy performance of buildings.

Published Works

Journal Paper

[1] **Yun-Sheng Hsu**, Xiaofeng Zheng, Edward Cooper, Mark Gillott, Christopher J Wood (2021). Evaluation of the indoor pressure distribution during building airtightness tests using the pulse and blower door methods. Building and Environment, 195, p.107742.

**The publication is based on the experimental work presented in Chapters 3 and 4 in this thesis.*

Conference Papers

[1] **Yun-Sheng Hsu**, Xiaofeng Zheng, Mark Gillott, Christopher J Wood (2021). A Review of Recent Developments of the Pulse Technique for Building Airtightness Measurement. 2021 The Chartered Institution of Building Services Engineers (CIBSE) Technical Symposium. London, United Kingdom.

**The publication is based on the literature review presented in Chapter 2 in this thesis.*

[2] **Yun-Sheng Hsu**, Xiaofeng Zheng, Dimitrios Kraniotis, Mark Gillott, Shin-Ku Lee, Christopher J Wood (2019). Insights into the impact of wind on the Pulse airtightness test in a UK dwelling. 40th AIVC - 8th TightVent & 6th Venticool Conference. Ghent, Belgium.

**The publication is based on the experimental work presented in Chapter 5 in this thesis.*

[3] **Yun-Sheng Hsu**, Xiaofeng Zheng, Edward Cooper, Mark Gillott, Shin-Ku Lee, Christopher J Wood (2019). Evaluation of indoor pressure distributions in a detached house using the Pulse airtightness measurement technique. 40th AIVC - 8th TightVent & 6th Venticool Conference. Ghent, Belgium.

**The publication is based on the experimental work presented in Chapter 4 in this thesis.*

[4] **Yun-Sheng Hsu**, Xiaofeng Zheng, Mark Gillott, Christopher J Wood (2019). Review of Wind Effect on Measurement of Building Airtightness. 18th International Conference on Sustainable Energy Technologies. Kuala Lumpur, Malaysia.

**The publication is based on the literature review presented in Chapter 2 in this thesis.*

[5] Christopher J Wood, Xiaofeng Zheng, Alan Vega Pasos, **Yun-Sheng Hsu**, Luke Smith (2018). An extended pressure range comparison of the blower door and novel pulse method for measuring the airtightness of two outdoor chambers with different levels of airtightness. 39th AIVC Conference. Antibes Juan-Les-Pins, France.

Acknowledgements

First of all, I would like to express my sincere gratitude to my supervisors, Dr Christopher J Wood, Prof. Mark Gillott and Dr Xiaofeng Zheng, for their consistent support, mentorship and guidance during my PhD study. I am also thankful to Dr Edward Cooper and Dr Dimitrios Kraniotis for providing thoughtful comments and recommendations on my research. I would like to extend my sincere thanks to Dr John Kaiser Calautit, Dr Tom Rogers and Dr James Pinchin for their insightful comments and suggestions during my viva examination.

I appreciate all the support I received throughout my years of study in Taiwan and the UK. My special thanks go to Dr Ko-Young Shao for his guidance and inspiration during my undergraduate study; Prof. Chin-Huai Young, Dr Shin-Ku Lee, Mr Benson Lau, Prof. Wei-Hwa Chiang and Prof. Shuo-Yan Chou for their supervision and mentorship during my postgraduate study. Their immense knowledge and plentiful experience have motivated me to pursue a doctoral degree. I would also like to show my sincere gratitude to the President and Vice President of National Taiwan University of Science and Technology, Prof. Ching-Jong Liao and Prof. Yong-Chie Heng, for their treasured support and encouragement; Prof. Jiun-Huei Proty Wu and Dr Yen-Yi Lee at the Taipei Representative Office in the UK for their help during my PhD study.

I appreciate all the support I received during my PhD study at the Department of Architecture and Built Environment. I would like to express my sincere gratitude to Prof. Saffa Riffat for offering me various part-time research opportunities, which were enormously influential in developing my research and communication skills. I am also thankful to Mr James Hazzledine, Mr Tony Gospel, Mr Daniel Cooper and Mr Carson Cheng for their technical support on all of my experimental setups. I would like to thank all the lovely colleagues in the Mark Group Research House and Sustainable Research Building for a cherished time spent together. I would also like to extend my sincere thanks to Ms Zeny Amante-Roberts for her consideration and tremendous support. My particular appreciation goes out to Dr Ziwei Chen for her endless encouragement and always being there for me.

Last but not least, I would like to express my most enormous thanks to my parents, grandparents, sister and all my family members for always believing in me and encouraging me to follow my dreams. Without their tremendous understanding, encouragement and unconditional support, it would be impossible for me to complete my study.

Thank you all for always having my back. I feel so grateful to have you all in my life.

I love all of you so much!

Table of Contents

Abstract i

Published Works iii

Acknowledgements iv

Table of Contents v

List of Figures viii

List of Tables xiii

Nomenclature xv

1. Introduction 1

1.1. Background 1

1.2. Research overview 6

1.3. Aims and objectives 7

1.4. Research methodology 8

1.5. Significance of research 10

2. Literature Review 11

2.1. Building airtightness 11

2.1.1. Concept of building airtightness 11

2.1.2. Importance of building airtightness 12

2.1.3. Building airtightness measurement 15

2.1.4. Regulation on building airtightness requirement 17

2.2. Steady pressurisation method 19

2.2.1. Blower door testing 19

2.2.2. Interpretation of measured data 21

2.2.3. Challenges of steady pressurisation method 23

2.3. Pulse technique 25

2.3.1. Fundamentals of Pulse 25

2.3.2. Development and challenges of Pulse 28

2.3.3. Other airtightness measurement methods 33

2.4. Uncertainties of building airtightness measurement 37

2.5. Wind effect on building airtightness measurement 38

2.6. Current work on addressing the wind effect on the building airtightness measurement 45

2.6.1. Wind speed and wind fluctuation during testing 45

2.6.2. Background pressure measurement 49

2.6.3. Experimental studies of addressing the wind impact on the building airtightness measurement 50

2.6.4. Numerical studies of addressing the wind impact on the building airtightness measurement 51

2.7. Summary and literature gaps 55

3. Insights into Airtightness Measurements Using the Pulse and Blower Door Testing..56

3.1. Introduction....56

3.2. Methodology....57

3.2.1. Dwelling....57

3.2.2. Equipment setup and test arrangement....59

3.3. Results analysis of the Pulse and blower door testing....63

3.4. Error analysis....68

3.5. Summary....71

4. Evaluation of Indoor Pressure Distribution and Effect of Pulse Release Location....72

4.1. Introduction and theoretical understanding....72

4.2. Test arrangement....75

4.3. Indoor pressure distribution during the Pulse test....78

4.4. Indoor pressure distribution during the blower door tests....82

4.5. Effect of the Pulse release location....84

4.6. Summary....87

5. Insights into the Wind Impact Using Pulse in a Detached Dwelling....88

5.1 Introduction....88

5.2 Investigation of wind impact on the Pulse test in a five-bedroom detached dwelling....89

5.2.1 Impact of wind speed....89

5.2.2 Impact of multiple tests....96

5.2.3 Impact of wind direction....100

5.3 Optimisation of adjustment methods for Pulse to address the wind impact....106

5.3.1 Adjustment methods for Pulse measurement results....106

5.3.2 Number of pulse release....108

5.3.3 Background pressure recording period....111

5.3.4 Sampling point for curve fitting adjustment....116

5.4 Summary....125

6. Long-term Observation of the Wind Impact on the Pulse Test....126

6.1 Introduction....126

6.2 Investigation of wind impact on the Pulse test in an outdoor chamber....126

6.2.1 Test arrangement....126

6.2.2 Impact of wind speed....131

6.2.3 Impact of wind direction....138

6.3 Seasonal effect on building leakage in eight months....143

6.4 Further work....145

6.5 Summary....145

7. CFD-Based Numerical Simulation of the Pulse Test 147
7.1 Introduction 147
7.2 Methodology 148
7.3 Simulation of indoor pressure and velocity distributions during the Pulse test 149
7.3.1 Computational domain and configurations 150
7.3.2 Results and discussions: indoor pressure and velocity distributions 160
7.3.3 Results and discussions: validation with experimental data 165
7.4 The impact of steady wind on the Pulse test 166
7.4.1 Computational domain and configurations 166
7.4.2 Results and discussions: indoor pressure distribution 172
7.4.3 Results and discussions: air leakage rate 174
7.4.4 Results and discussions: air flow rate of openings 177
7.5 The impact of wind direction on the Pulse test 185
7.5.1 Computational domain and configurations 185
7.5.2 Results and discussions: indoor pressure distribution 186
7.5.3 Results and discussions: air leakage rate 188
7.5.4 Results and discussions: air flow rate of openings 190
7.6 Simulation of the Pulse test in a building with a gable roof 198
7.6.1 Computational domain and configurations 198
7.6.2 Comparison of indoor pressure distribution 201
7.6.3 Comparison of simulated air leakage rate 202
7.6.4 Comparison of the air flow rate of openings 203
7.7 Summary 211
8. Conclusions 213
8.1 Introduction 213
8.2 Major findings 213
8.3 Recommendations for future work 218
References 220
Appendix A: Design and Preparation of a Model-Scale Pulse for Wind Tunnel Test 235
A.1 Literature review 235
A.2 Experimental set-up 239
A.3 Experiment design 241
A.4 Proposed results analysis 245
A.5 References 245

List of Figures

Figure 1-1: UK final energy consumption by sector [1] 1
Figure 1-2: Changes in energy consumption by sector and fuel from 2019 to 2020 [1] 2
Figure 1-3: Flow chart of thesis structure 9
Figure 2-1: Illustrations of (a) stack effect and neutral pressure line on a building wall and (b) infiltration and ventilation airflow [63] 11
Figure 2-2: Energy losses before and after increased airtightness [86] 15
Figure 2-3: Illustration of measuring mechanism of the blower door unit 20
Figure 2-4: (a) Installation position of the blower door [35] and (b) a photo of blower door installation 20
Figure 2-5: Examples of the air leakage log-log graph for (a) pressurisation and (b) depressurisation tests 22
Figure 2-6: Illustration of measuring mechanism of Pulse unit 25
Figure 2-7: Pressure variation with time for a typical Pulse test [142] 26
Figure 2-8: Percentage of the unsteady flow during the Pulse test [150] 27
Figure 2-9: A comparison example of pressure-leakage results for the Pulse and blower door tests [32] 28
Figure 2-10: Photos of (a) the gravity-driven piston version [28] and (b) a compressed air-driven piston version [34] 29
Figure 2-11: Photo of PULSE-50 [32] 30
Figure 2-12: Photos of (a) PULSE-40, (b) PULSE-80, (c) schemtic diagram of PULSE system composition and (d) an advanced control box [148] 31
Figure 2-13: (a) A schematic diagram [33] and (b) a photo of PULSE-60 unit 32
Figure 2-14: A photo of PULSE 2.0 system by Build Test Solutions Ltd. [152] 32
Figure 2-15: A schematic diagram of the experimental setup of the AC pressurisation method [155] 33
Figure 2-16: (a) A schematic diagram and (b) a photo of the experimental setup of Decay method and (c) pressure curve during the test using Decay method [162] 34
Figure 2-17: Monitoring arrangement for an acoustic measurement [164] 35
Figure 2-18: A photo of ATT device by ACIN instrumenten bv [166] 36
Figure 2-19: Pressure variations of (a) calm condition and (b) windy condition by ATT measurements [46] 36
Figure 2-20: Infiltration characteristics with temperature and wind effect [65] 39
Figure 2-21: (a) One-point, (b) Two-point and (c) Multi-point test methods [51] 50
Figure 3-1: Mean usable floor area by dwelling type [230] 57
Figure 3-2: Photos of the tested dwelling (a) front view, (b) back view and (c) surroundings 58
Figure 3-3: Building plans of the tested dwelling (a) ground floor and (b) first floor 58
Figure 3-4: Photos of (a) PULSE-60 unit and (b) internal pressure reference tank of PULSE-60 unit 59
Figure 3-5: Energy Conservatory Duct Blaster series B 60
Figure 3-6: Photos of ultrasonic anemometer (a) setup, (b) sensors, (c) and (d) surroundings 61
Figure 3-7: Photos of (a) installation of DBB unit and (b) PULSE-60 unit in the living room for testing 62
Figure 3-8: Building preparation for the Pulse and blower door tests 63
Figure 3-9: Air leakage rate-pressure curves for the Pulse tests 64

Figure 3-10: Air leakage rate-pressure curves for the blower door tests 65
Figure 3-11: Air leakage rate-pressure curves for the blower door and Pulse tests over the pressure range of 2-70Pa 65
Figure 3-12: Air leakage rate-pressure curves for the blower door and Pulse tests in the overlapped pressure range 66
Figure 3-13: Relative percentage difference between the Pulse and blower door tests 67
Figure 3-14: Overall errors of the Pulse and blower door tests for the overlapped pressure range 70
Figure 3-15: Overall errors for the Pulse and blower door tests at 4Pa and 50Pa 71
Figure 4-1: Diagram of the uneven pressure distribution in building under pressurisation 73
Figure 4-2: Measurement error of air mass with different percentages of V_1 and pressure difference 74
Figure 4-3: Setup locations of test equipment 75
Figure 4-4: Differential pressure transducers with five dataloggers 76
Figure 4-5: Differential pressure transducers with one datataker DT85 76
Figure 4-6: Arrangement of differential pressure transducers 77
Figure 4-7: Photos of Pulse unit and pressure tubing location in each room 78
Figure 4-8: Pressure profiles in the five rooms during the complete Pulse test 79
Figure 4-9: Pressure profiles in the five rooms during the S1 test 80
Figure 4-10: Pressure profiles in the five rooms during the S2 test 81
Figure 4-11: Pressure profiles in the five rooms during the S3 test 81
Figure 4-12: Pressure profiles in the five rooms during the DBB test at 10Pa 82
Figure 4-13: Pressure profiles in the five rooms during the DBB test at 15Pa 83
Figure 4-14: Photos of the Pulse test unit in different rooms 85
Figure 4-15: Results of 30 Pulse tests at different pulse release locations 86
Figure 5-1: Weather data of Nottingham in March 2019 [234] 89
Figure 5-2: Violin plot of 423 tests 90
Figure 5-3: Measurements of air leakage rate in the wind speed range of 0-3.5m/s 91
Figure 5-4: Relative percentage difference distribution in the wind speed range of 0-3.5m/s 91
Figure 5-5: Measurements of air leakage rate in the wind speed range of 3.5-6m/s 92
Figure 5-6: Relative percentage difference distribution in the wind speed range of 3.5-6m/s 93
Figure 5-7: Tests results in the wind speed range of 6-10m/s 94
Figure 5-8: Relative percentage difference distribution in the wind speed range of 6-10m/s 94
Figure 5-9: Violin plot of ALR results for the 423 tests, by each test, each group and first three tests 97
Figure 5-10: *RPD* results for the 423 tests, by each test, each group and first three tests 98
Figure 5-11: *RPD* distribution with the corresponding number of combinations 99
Figure 5-12: *RPD* distribution and the corresponding proportion 99
Figure 5-13: Photo of ultrasonic anemometer in the backyard of tested dwelling 100
Figure 5-14: Illustrations of (a) tested dwelling orientation and (b) anemometer orientation and wind directions with respect to tested dwelling 100
Figure 5-15: Wind rose plot of wind condition distribution of 423 tests 101

Figure 5-16: Wind rose for Nottingham [234] 102
Figure 5-17: Wind direction distribution of 423 tests 102
Figure 5-18: Illustration of different wind direction categories with tested dwelling 103
Figure 5-19: ALR measurements under different wind directions 104
Figure 5-20: Violin plot of ALR results under different wind directions 105
Figure 5-21: Flow chart of the Pulse test procedure 106
Figure 5-22: Recorded pressure differences against time and with adjustment 107
Figure 5-23: (a) Single air pulse release; (b) two air pulse releases, and (c) three air pulse releases 108
Figure 5-24: Violin plot of ALR results for Cases A, B and C 110
Figure 5-25: Relative percentage differences for Cases A, B and C 111
Figure 5-26: Illustration of Cases C, D, E, F in one air pulse release period 112
Figure 5-27: Violin plot of ALR results for Cases C, D, E and F 115
Figure 5-28: Relative percentage differences for Cases C, D, E and F 115
Figure 5-29: Illustrations of (a) Approach I, (b) II, and (c) III 118
Figure 5-30: Violin plot of ALR for Cases C, D and E with different approaches for calculating the fitted curve 123
Figure 5-31: Comparison of *RPD*s for Cases C, D and E with different approaches for calculating the fitted curve 124
Figure 6-1: Photos of (a) Pod 1 and (b) Pod 2 127
Figure 6-2: Photos of sealed (a) door and (b) window of Pod 1 127
Figure 6-3: (a) PULSE-20 unit and (b) PULSE-20 control box and datalogger 128
Figure 6-4: Photos of the connection pipe between Pod 1 and Pod 2 129
Figure 6-5: Photos of (a) nozzle outlet in Pod 1 and (b) nozzle outlet with enhanced sealing 129
Figure 6-6: Photos of (a) three sensors in Pod 1 and (b) monitoring station tripod in Pod 1 130
Figure 6-7: Photos of (a) WindSonic ultrasonic anemometer and (b) outdoor temperature sensor (PT100 RTD) 131
Figure 6-8: Site photos of Pod 1 and Pod 2 131
Figure 6-9: Annual weather data of Nottingham: (a) 2019 and (b) 2020 [234] 133
Figure 6-10: *RPD* distribution of 1096 tests according to the wind speed range 133
Figure 6-11: Measurements of air leakage rate from August 2019 to March 2020 135
Figure 6-12: Wind speed limit for Pulse testing with different *RPD* 137
Figure 6-13: (a) Illustration of the orientation of Pod 1 and (b-e) photos of four facades of Pod 1 139
Figure 6-14: Wind rose plots for tests in each month 140
Figure 6-15: Wind rose plots for all tests during the eight-month test period 141
Figure 6-16: Wind direction distribution of all tests during the eight-month testing period 141
Figure 6-17: ALR measurements at different wind direction ranges 142
Figure 6-18: ALR measurements and *RPD* in different months 144
Figure 7-1: Research structure of the investigation of the wind impact on Pulse 148
Figure 7-2: Plan views of the building layout with detailed dimensions and openings' locations 151
Figure 7-3: Sectional view of the building with detailed dimensions and openings' locations 151
Figure 7-4: Model views of the building and Pulse unit 152

Figure 7-5: Views of building model and Pulse unit in Fluent 153
Figure 7-6: Building model mesh in Fluent 155
Figure 7-7: Location of indoor monitoring points: (a) 3D perspective view and (b) plan view with dimensions ... 159
Figure 7-8: Illustration of indoor pressure variation during the entire Pulse test under no wind condition 160
Figure 7-9: Air velocity variation in each room during the Pulse test under the no wind condition 162
Figure 7-10: Plot of the indoor air velocity against the distance from the nozzle of the Pulse unit 163
Figure 7-11: Contour images of indoor pressure and air velocity at 3.2s under no wind condition 164
Figure 7-12: Views of outer domain with building model in Fluent 167
Figure 7-13: View of the outer domain mesh in Fluent 168
Figure 7-14: Illustration of the simulated steady wind condition in the outer domain in Fluent 169
Figure 7-15: Wind speed profiles for Cases II, III and IV 170
Figure 7-16: Contour images of the simulated velocity field at 0s for Cases II, III and IV 171
Figure 7-17: Location of monitoring points in the outer computational domain 172
Figure 7-18: Pressure curves of each room and overall average during the Pulse test for different wind speed Cases I, II, III and IV 173
Figure 7-19: Variations of volumetric airflow rate at ten openings during the Pulse test for Cases I, II, III and IV 177
Figure 7-20: Total volumetric airflow rate of ten openings during the Pulse test for Cases I, II, III and IV 178
Figure 7-21: Deducted volumetric flow rate at ten openings during quasi-steady period for Cases I, II, III and IV 179
Figure 7-22: Average volumetric flow rate at ten openings during quasi-steady period for Cases I, II, III and IV. 179
Figure 7-23: Plots of the average indoor pressure against the total volumetric flow rate of ten openings during the Pulse test for Cases I, II, III and IV 180
Figure 7-24: Perspective contour images of the indoor pressure at 3.2s for Cases I, II, III and IV 182
Figure 7-25: Perspective contour images of the indoor velocity at 3.2s for Cases I, II, III and IV 184
Figure 7-26: Illustration of Cases III, V, VI and VII with different wind directions 185
Figure 7-27: Contour images of the simulated wind condition at 0s for Cases III, V, VI and VII 186
Figure 7-28: Pressure curves of each room and overall average during the Pulse test for different wind condition Cases III, V, VI and VII 187
Figure 7-29: Variations of volumetric flow rate at ten openings during the Pulse test for Cases III, V, VI and VII 190
Figure 7-30: Total volumetric flow rate of ten openings during the Pulse test for Cases III, V, VI and VII 191
Figure 7-31: Deducted volumetric flow rate at ten openings during quasi-steady period for Cases III, V, VI and VII 191
Figure 7-32: Average volumetric flow rate at ten openings during quasi-steady period for Cases III, V, VI and VII 192
Figure 7-33: Plots of the average indoor pressure against the total volumetric flow rate of ten openings during the Pulse test for Cases III, V, VI and VII 193
Figure 7-34: Perspective contour images of the indoor pressure at 3.2s for Cases III, V, VI and VII 195
Figure 7-35: Perspective contour images of the indoor air velocity at 3.2s for Cases III, V, VI and VII 197
Figure 7-36: View of building model with a gable roof in Fluent 198
Figure 7-37: Front view of the location of indoor monitoring points 199

Figure 7-38: Illustration of Cases VIII and IX with different wind directions 199
Figure 7-39: Contour images of the simulated wind condition at 0s for Cases III, VIII, VI and IX 200
Figure 7-40: Pressure curves of each room and overall average during the Pulse test for Cases III, VIII, VI and IX 201
Figure 7-41: Variations of volumetric flow rate at ten openings during the Pulse test for Cases III, VIII, VI and IX 204
Figure 7-42: Total volumetric flow rate of ten openings during the Pulse test for Cases III, VIII, VI and IX 204
Figure 7-43: (a) Deducted volumetric flow rates and (b) average volumetric flow rates at ten openings during quasi-steady period for Cases III, VIII, VI and IX 206
Figure 7-44: Plots of the average indoor pressure against the total volumetric flow rate of ten openings during the Pulse test for Cases III, VI, VIII and IX 206
Figure 7-45: Perspective contour images of indoor pressure at 3.2s for Cases III, VIII, VI and IX 209
Figure 7-46: Perspective contour images of indoor velocity at 3.2s for Cases III, VIII, VI and IX 211
Figure A-1: Fan performance curve (dotted) and wind tunnel system curve (solid) by Moonen, et al. [4] 235
Figure A-2: Open-circuit wind tunnel by Vladut, et al. [8] 236
Figure A-3: Open-jet wind tunnel by Mayer, et al. [9] 236
Figure A-4: The variable roughness system by Vladut, et al. [8] 237
Figure A-5: Overview of total pressure loss calculation [3] 238
Figure A-6: Examples of Ke [3] 238
Figure A-7: Scaled building model 240
Figure A-8: Model-scale Pulse unit 241
Figure A-9: Schematic diagram of the wind tunnel [19] 241
Figure A-10: Photo of the inlet of the wind tunnel in Faculty of Engineering, University of Nottingham 242
Figure A-11: Diagrams of (a) sectional view of the wind tunnel and (b) suburban terrain in the wind tunnel [19] 242
Figure A-12: Photos of the suburban terrain inside the wind tunnel in the University of Nottingham 243
Figure A-13: Location of test building model in the wind tunnel [19] 243
Figure A-14: Photos of the round platform inside the wind tunnel 244
Figure A-15: Photos of the round platform underneath space inside the wind tunnel 244

List of Tables

Table 2-1: Summary of studies of infiltration effect on building energy performance 13
Table 2-2: Comparison of different reference pressures for building airtightness measurement 17
Table 2-3: Available minimum airtightness requirements in different countries 18
Table 2-4: Air permeability of best and normal practice for different types of buildings in the UK [132] 19
Table 2-5: EN13829, ASTM 779-10 and ISO 9972 requirements regarding the meteorological condition 40
Table 2-6: Provisions regarding wind speed limit in five tests standards 41
Table 2-7: Proceedings of 39th-40th AIVC conferences (2018-2019) 42
Table 2-8: Studies of the impact of wind fluctuations on natural ventilation 46
Table 2-9: Review on numerical studies of the wind effect on the building airtightness measurement 52
Table 3-1: Tested dwelling parameters 58
Table 3-2: List of test equipment 59
Table 3-3: Building pressure difference during the Pulse tests 63
Table 3-4: Airtightness measurement results at 4Pa and power-law equations of the Pulse tests 64
Table 3-5: Building pressure difference during the blower door tests 64
Table 3-6: Airtightness results and power-law equations of the blower door and Pulse tests 67
Table 3-7: Error analysis for the blower door test 68
Table 3-8: Error analysis for the Pulse test 68
Table 3-9: Results of overall errors of the Pulse and blower door tests for the overlapped pressure range 70
Table 4-1: Maximum pressure level in each room for the S1, S2 and S3 tests 82
Table 4-2: Maximum pressure level in each room for the DBB tests at 10 Pa and 15Pa 83
Table 4-3: Measurement results of the building permeability ($m^3/h/m^2$) for the Pulse tests at different locations 86
Table 5-1: Test result summary for the wind speed range of 0-3.5m/s 92
Table 5-2: Test result summary for the wind speed range of 3.5-6m/s 93
Table 5-3: Test result summary for the wind speed range of 6-10m/s 94
Table 5-4: Test result summary for the meteorological wind speed range of 0-16m/s 95
Table 5-5: ALR results for the 423 tests 97
Table 5-6: Case A (one air pulse release) results 109
Table 5-7: Case B (two air pulse releases) results 109
Table 5-8: Case C (three air pulse releases) results 110
Table 5-9: Four cases with different background pressure recoding periods 112
Table 5-10: Case C results 113
Table 5-11: Case D results 113
Table 5-12: Case E results 114
Table 5-13: Case F results 114
Table 5-14: Four cases with different approaches for generating the fitted curve 118
Table 5-15: Case C results with different approaches for calculating the fitted curve 119
Table 5-16: Case D results with different approaches for calculating the fitted curve 120

Table 5-17: Case D results with different approaches for calculating the fitted curve 122
Table 6-1: Parameters of Pod 1 and Pod 2 127
Table 6-2: List of test equipment 128
Table 6-3: Measured ALR for ten baseline tests 132
Table 6-4: Test result summary for tests from August 2019 to March 2020 136
Table 6-5: Test result summary for ageing effect evaluation 144
Table 7-1: Summary of the cases in the numerical study with simulation conditions 148
Table 7-2: Comparison of the building model with the tested dwelling 149
Table 7-3: Time points A and B for the Pulse test under the no wind condition 161
Table 7-4: Simulated pressure level in each room at 3.25s under the no wind condition 161
Table 7-5: Maximum air velocity in each room during Pulse test under the no wind condition 162
Table 7-6: Measured pressure level in each room at 3.25s in field testing 165
Table 7-7: Simulated ALR results under the no wind condition 166
Table 7-8: Simulated wind speed level for Cases I, II, III and IV 169
Table 7-9: Time points A and B for Cases I, II, III and IV 174
Table 7-10: Calculated ALRs and *RPDs* for Cases I, II, III and IV 175
Table 7-11: Comparison of *RPD*s between the simulation and experimental results 176
Table 7-12: Simulated wind conditions for Cases III, V, VI, VII 185
Table 7-13: Time points A and B for Cases III, V, VI and VII 188
Table 7-14: Calculated ALR and *RPDs* for Cases III, V, VI and VII 189
Table 7-15: Building configuration and wind condition for Cases III, VIII, VI and IX 200
Table 7-16: Time points A and B for Cases III, VIII, VI and IX 202
Table 7-17: Calculated ALRs and *RPDs* for Cases III, VIII, VI and IX 203
Table A-1: Scale ratios for the model-scale building 240
Table A-2: Operating parameters of the experiment 245

Nomenclature

Symbols

$a,\ b$	Coefficients
A	The effective area of the opening (m^2)
$\bar{A}$	Opening area scale ratio for the model-scale building
A_r	Area ratio
A_{ts}	The cross-section area of the test section (m^2)
$\Delta ALR_{Room_benchmark}$	The air leakage rate difference between the room and benchmark (m^3/s)
C	Air flow coefficient ($m^3/s/Pa^n$)
C_L	Air leakage coefficient ($m^3/s/Pa^n$)
C_p	Air specific heat capacity (J/kg·K)
C_t	Constant
D_{cell}	Cell hydraulic diameter (m)
D_o	Outlet diameter of contraction (m)
E_{wt}	The total energy required for operating the wind tunnel (W)
ΔE	The measurement error of isentropic expansion
f	Friction factor
f_{av}	Friction factor at the average diameter
F	The net force being applied (N)
F_s	Safety factor
H	Building height (m)
k	Conductivity (W/m·K)
K	Pressure loss coefficient
K_e	Pressure loss coefficient of a square diffuser
K_{ex}	Expansion loss coefficient
K_d	Pressure loss coefficient of a diffuser
K_f	Wall friction coefficient
l	Length (m)
l_{cell}	Honeycomb cell length (m)
l_e	The effective length of the opening (m)
L	Effective leakage area (m^2)
$\bar{L}$	Length scale ratio for the model-scale building
$\dot{m}$	Air mass flow rate (kg/s)
n	Air flow exponent
n_s	Terrain surface characteristic
n_{50}	The air change at the differential pressure of 50Pa (h^{-1})
p	The formal order of accuracy
p_d	Dynamic pressure (Pa)
P	Pressure (Pa)
$P_{livingroom}$	The living room pressure (Pa)
P_{room}	The room pressure (Pa)
$\bar{P}$	Scale ratio of pressure relative to external pressure
ΔP	The building pressure difference (Pa)

ΔP_{01}	Average zero-flow pressure difference at the start of the blower door test (Pa)
ΔP_{02}	Average zero-flow pressure difference at the end of the blower door test (Pa)
ΔP_{Room_Living}	The pressure difference between the room and the living room (Pa)
Δp_{fan}	The pressure rise caused by the fan (Pa)
Δp_{wt}	The pressure loss throughout the wind tunnel (Pa)
$P(t)$	Transient air pressure in the compressor tank (Pa)
q	Air flow rate (m^3/s)
q_{50}	Air permeability at the differential pressure of 50Pa ($m^3/h/m^2$)
$\bar{q}$	Scale ratio of volumetric airflow rate
Q	Air leakage rate (m^3/s)
Q_{in}	The net fluid flow rate of the test pace (m^3/s)
Q_{inf}	Heat losses owing to air infiltration (W)
Q_{out}	The fluid leakage rate of the test pace (m^3/s)
ΔQ	The measurement error of air leakage rate
$Q_P\{t\}$	The volumetric air flow rate in the compressor tank (m^3/s)
$q\{t\}$	Building air leakage rate (m^3/s)
r	Linear grid refinement factor
R	Gas constant (J/kg·K)
R_e	Reynolds number
R^2	The coefficient of determination
S_t	Source term
t	Time (s)
Δt	Unit of time (s)
T	Temperature (K)
u	Flow velocity (m/s)
$\bar{U}$	Scale ratio of wind speed at the building level
v	Velocity (m/s)
v_{ts}	Velocity in the test section (m/s)
V	Volume (m^3)
V'	The volume of the air receiver (m^3)
$\bar{V}$	Internal building volume scale ratio
$\overrightarrow{V}$	Velocity vector
z	Reference height (m)
z_0	Roughness length (m)

Greek letters

δm	The measurement error of air mass
δQ_e	Overall error (%)
δQ_{bias}	Bias error (%)
$\delta Q_{precision}$	Precision error (%)
$\delta Q_{modelling}$	Modelling error (%)
ρ	Air density (kg/m^3)
γ	Specific heat ratio
∂	Equivalent conical angle (°)

β	Honeycomb porosity
Δ	A grid cell (m)
Δr	Honeycomb roughness
Ω_{high}	High wind gust frequency (Hz)
Ω_{low}	Low wind gust frequency (Hz)

Abbreviations

ACH	Air Change Rate
ALR	Air Leakage Rate
CFD	Computational Fluid Dynamics
CFL	Courant–Friedrichs–Lewy
CN	Courant Number
DBB	Duct Blaster series B (blower door unit)
GCI	Grid Convergence Index
GHG	Greenhouse gas
PULSE	Pulse unit
RPD	Relative Percentage Difference
S1	The Step-one test in a three-step Pulse test
S2	The Step-two test in a three-step Pulse test
S3	The Step-three test in a three-step Pulse test
SIMPLE	Semi-Implicit Method for Pressure-Linked Equations
SST	Shear Stress Transport

Subscripts

0	Initial
4	At 4Pa
50	At 50Pa
basic	Basic grid
BD	Blower door test
benchmark	Benchmark
coarse	Coarse grid
env	Envelope
fine	Fine grid
i	Indoor
in	Inlet
m	Measured
out	Outdoor
ot	Outlet
P	Pulse test
r	Reference
s	Standard condition
x	x-axis
y	y-axis
z	z-axis

1. Introduction

1.1.Background

In recent years, energy-saving has attracted more and more attention globally. Its main purpose is to utilise the energy required for the building rationally and minimise its consumption to sustainable limits. Figure 1-1 shows the changes in each sector share of the UK's energy consumption between 1970 and 2020 according to Energy Consumption in the UK (ECUK) published in September 2021 [1]. Owing to the COVID-19 pandemic, the total energy consumption of the UK was affected; for instance, a significant decrease was noted for the transport sector. Transportation accounted for 33.5% of the final consumption in 2020 and was followed by the domestic sector (i.e., 32.5%), the industry sector (i.e.,17.4%) and the service (i.e., 16.7%).

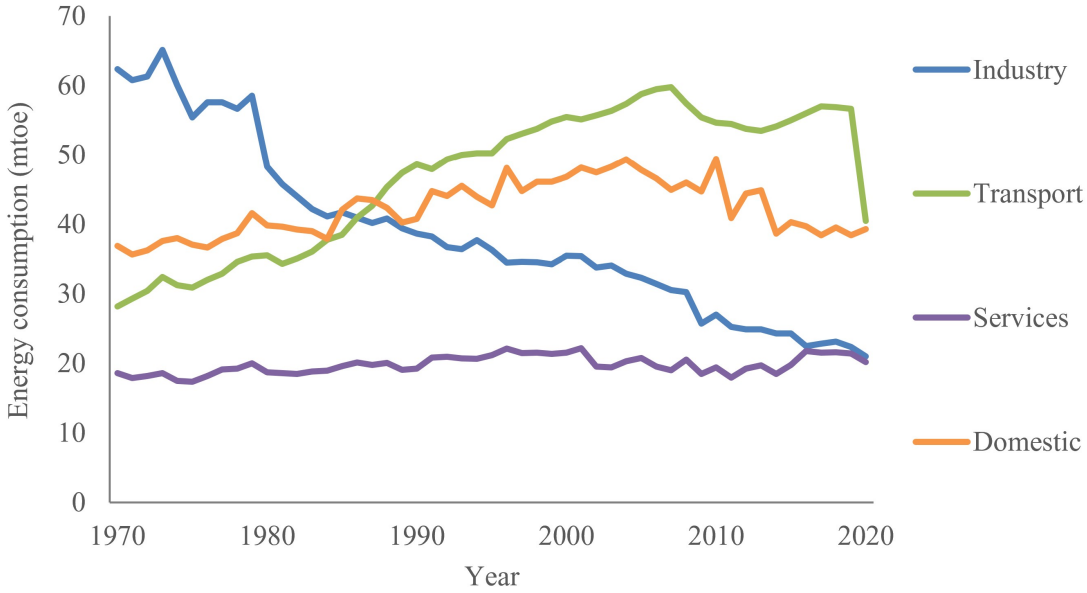


Figure 1-1: UK final energy consumption by sector [1]

The domestic energy consumption is dominated by several factors, such as household characteristics, building energy performance and electrical appliances. Between 2019 and 2020, the domestic energy consumption increased by 2.3%, while consumption of the other sectors fell (e.g., -28.6% for the transport, -6.2% for industry, and -5.6% for services), as seen in Figure 1-2. Compared to most European countries, the UK has the oldest housing stock, with approximately 38% of the housing dating back to before 1946, 40% were built between 1946-1980, and only 7% were built since 2000 [2]. Out of the total existing 29 million homes across the UK, nearly 19 million homes have Energy Performance Certificate (EPC) ratings of D or worse [3]. Owing to the poor building energy performance, additional consumptions are needed to maintain the required thermal comfort.

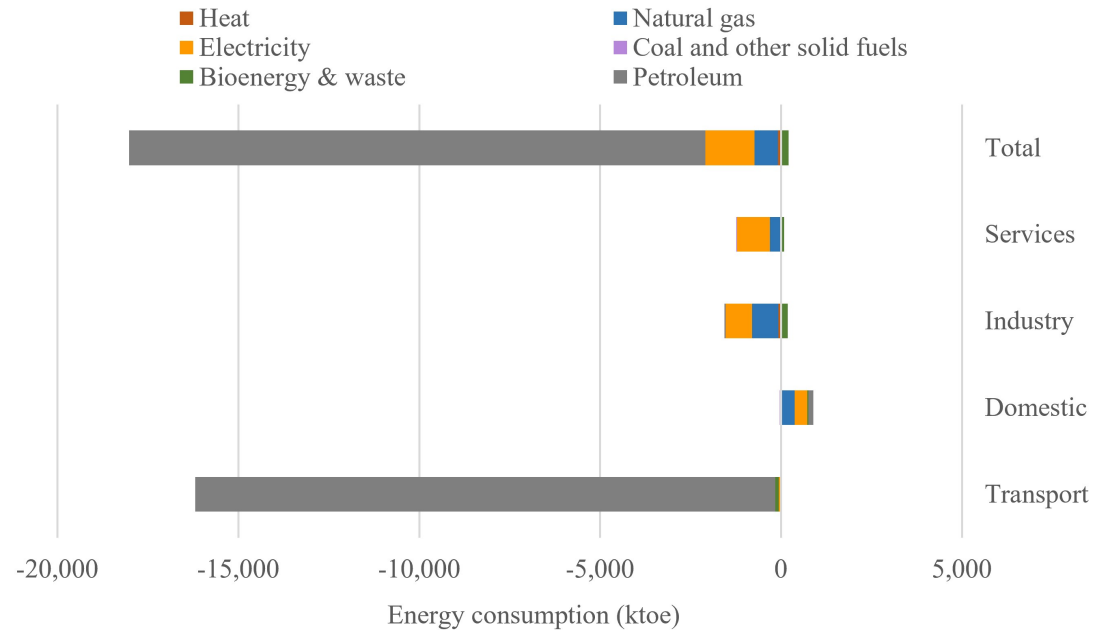


Figure 1-2: Changes in energy consumption by sector and fuel from 2019 to 2020 [1]

It is noteworthy that a great amount of energy consumption in the building sector leads to significant greenhouse gas (GHG) emissions. According to the UK Green Building Council, about 42% of the carbon emissions in the UK has resulted from the built environment. In 2007, the EU set a target of a 20% reduction in the total EU GHG emissions from the 1990 levels [4]. Additionally, the energy-saving plans include not only short-term plans but also long-term ones for the so-called "Energy Roadmap 2050" [5]. It also demonstrates that the EU countries are committed to a reduction in the GHG emissions of 80% to 95% by 2050 compared to 1990 [6, 7]. In 2019, the UK became the first major economy to announce a new target of net-zero GHG emissions by 2050. To achieve this target, huge efforts will be required from the built environment. Energy-efficient building design would be essential for improved energy performance, which could be realised through novel designs of the building construction for new houses. Moreover, it is also essential to assess and improve the construction of the existing buildings for improved energy efficiencies with fewer energy losses, as 80% of the UK buildings in 2050 have already been built [8]. It has been noted that heat losses from the building envelope are mainly attributed to heat transfer and ventilation, including infiltration [9].

Building energy performance and indoor air quality are greatly dependent upon ventilation, which is also affected by the uncontrolled air leakage (i.e. air infiltration) across the building envelope [10]. Extensive studies have explored how air infiltration affects building energy performance in different climates and regions. It has been numerically found that infiltration accounted for 10%-30% of the energy usage for space heating in a detached house in the cold climate of Finland [11]. Han, et al. [12] found that an average of 12% of the total energy consumption of an office building

in Michigan, US, was attributed to air infiltration. A considerable effect of air infiltration was noted on heat losses, which accounted for up to 40% of the total heat energy demand of industrial buildings in Germany [13]. Similar observations have been reported by Feijó-Muñoz, et al. [14], based on a field study in the Mediterranean climate areas of Spain and the Canary Islands. Guillén-Lambea, et al. [15] stated that the energy demand associated with infiltration is much lower in southern Europe (e.g., central Mediterranean cities) than in northern Europe (e.g., London, Berlin, and Pairs) with colder climates, owing to the higher infiltration rate during winter.

Airtightness is regarded as the fundamental building property that impacts infiltration and exfiltration [12]. In general, wherever the infiltration occurs, a corresponding exfiltration somewhere else in the building takes place as well [16]. Basically, the rates of air infiltration and exfiltration depend on the porosity of the building envelope, the differential pressure across the building envelope, the temperature, different natural driving forces of wind, sheltering factors and local terrain [17]. Excessive leakage may cause significant reductions in the airtightness of the building envelope. The impact of poor airtightness on the built environment has aroused wide concerns since the 1970s, for example, in regard to ventilation system performance, the hygrothermal performance of building construction materials, building energy consumption, occupancy thermal comfort, indoor air quality, noise transmission and fire resistance performance of building elements [18, 19]. The building airtightness is a crucial factor that should be concerned to enhance the building energy performance, and the minimum requirements on the building airtightness have been included in building regulations and voluntary standards in more and more countries. Locating and thus minimising air leaks on the building envelope would be of great benefit to improve the energy efficiency of existing buildings. Many studies revealed that a large amount of energy could be saved by tightening the building envelope [20-22].

Furthermore, achieving thermal comfort in the indoor environment is important, and indoor air quality is a great concern for public health. Air infiltration can facilitate pollutant transmissions into the indoor environment, which consequently affects indoor air quality and thermal comfort [23]. Therefore, an adequate airtight envelope is desired together with a suitable ventilation strategy, either through natural or mechanical ventilation, to prevent uncontrolled heat losses, transport pollutants, and provide sufficient fresh air.

To quantitatively understand the airtightness of the building envelope, different measurement methods for the building envelope leakages have been proposed and evolved [24], which typically measure the air leakage rate under a certain pressure difference. A range of pressure differences between the inside and outside the test building can be established by pressurisation or

depressurisation. The steady pressurisation method is the most commonly used method, which is implemented by a blower door test to pressurise the building to a typical range of pressure difference, 10–60Pa [25]. The blower door method has been widely accepted as a standard test in many regions and adopted as an intuitive diagnostic tool for energy-efficient houses; for instance, in energy efficiency incentive programs, Energy Star Program (EPA) in the US requires a blower door test to confirm the building airtightness [26].

The test procedure of the fan pressurisation method has been standardised in the standards, such as ISO 9972, ASTM E779, ATTMA TSL and JIS-A2201. In 2002, amendments in the Building Regulations came into force in the UK, with the introduction of mandatory air pressurisation tests for all new non-domestic buildings (e.g., with over 1000m^2 floor area) to comply with the maximum permissible leakage. Since 2006, the Building Regulations have enforced more stringent requirements in accordance with the government's commitment to improving building thermal performance and reducing GHG emissions. Mandatory airtightness testing using the conventional fan pressurisation method has been required for most newly constructed dwellings and commercial projects. Researchers and practitioners have implemented numerous field tests using the blower door method, while challenges have been noted, such as in perspectives of test practicality, flexibility, time-consuming procedure, result accuracy at low pressures and non-uniform pressure distributions in large buildings [24, 27, 28]. Therefore, these provided motivations for exploring alternative measurement approaches, for instance, AC pressurisation method, decay method, Pulse technique and acoustic method [24].

Alternatively, the leakage measurement at 4Pa could be more realistic and accurate to indicate the infiltration potential of a building envelope based on the studies [29, 30]. The new promising Pulse technique has been developed as an unsteady and dynamic approach, involving a low-pressure pressurisation process, typically around 4Pa. The technique was originally developed to address the issues of large net fluid flows and uneven pressure distributions associated with the testing of large buildings. With the Pulse technique, the building airtightness can be determined by releasing a 1.5-second air pulse from a pressurised vessel to the test building, thus establishing an instant pressure rise. The building pressure measurement is recorded continuously over a typical pressure range of 1-10Pa, which is different from the multiple-point tests over a pressure range with the steady pressurisation method. From herein, this technique is referred to under the proper noun 'Pulse', in contrast to 'pulse', which refers to the actual physical pulse of air released. In terms of practicality, the integrity of the test building could be better maintained as only a self-contained portable Pulse unit is required, and its installation does not penetrate the building fabric.

Pulse is adaptable for buildings in a variety of sizes, as multiple Pulse units could be employed for operation simultaneously. Although Pulse is a relatively newly developed transient method, its fundamental principle has been verified from many aspects [29-35].

The building airtightness measurement can be influenced by various factors, for example, building test preparation, tester's behaviour, accuracies of the measurement instrument, weather conditions, thermal draft impact and leaks with different flow exponents and linear regression [36-39]. The building airtightness under various climatic conditions is a complex process, which would be strongly influenced by the turbulent nature of the wind [40]. The error induced by wind has been regarded as a major error source in pressurisation testing [41]. Different wind speeds would lead to different infiltration rates and consequently affect the indoor pressure during the airtightness measurement [42]. Likewise, during the testing process, the outdoor wind not only results in an impact on the accuracy of airtightness measurement in the building envelope but also reduces the available days for testing.

Although Hill, et al. [43] have pointed out the building infiltration effect caused by winds in 1975, airtightness is the target topic nowadays, and many existing numerical models and studies have not widely taken into account the dynamic nature of wind. The unpredictable nature of the wind effect has been sometimes neglected, or only steady wind conditions have been considered for airtightness studies [44-55]. The majority of research conducted to explore the wind effect on the building airtightness measurement is focused on the steady pressurisation method. For example, Walker, et al. [56] applied two large measurement datasets of the blower door testing to understand the role of wind in uncertainties of measurement results. Carrié, et al. [41] established an analytical model to characterise the uncertainties caused by the steady wind in the steady pressurisation tests, and they also extended the model to simulate the impact of periodic wind on the one-point pressurisation tests [57]. Based on their findings, recommendations have been provided for practical blower door testing to minimise wind-induced errors. For instance, a multi-point test is preferred at a wind speed less than 3m/s (at 10m above ground level) when the reference pressure is 4Pa [56], while the single point test at high wind speeds above 5m/s (at building height) is not recommended [41].

Standards in different regions also have different specified wind speed limits for the pressurisation method. As Pulse has been demonstrated as a promising alternative for measuring building airtightness, there is a necessity of understanding the wind impact on Pulse and proposing adequate recommendations from practical aspects to address the wind impact on measurements in real scenarios.

1.2. Research overview

The research topic is “The Impact of Wind on the Building Airtightness Measurement using the Pulse Technique”. The importance of building airtightness has recently been widely recognised in more and more countries, with building airtightness requirements included in national regulations or energy-efficient programs to address the negative effect of poor airtightness on buildings and energy conservation [51]. Both building pressurisation and depressurisation tests have been widely accepted for compliance checks to meet energy performance requirements [58]. Regarding the measurement results of building airtightness, its uncertainty has been the key concern in many regions over the past few years. The wind could influence the measurement of building airtightness in different ways and subsequently result in inaccurate measurements. Hence, it is necessary to comprehensively examine the building permeability through the airtightness measurement in a more precise approach by taking into account the wind effect. Although the impact of wind conditions on the building airtightness measurement has been noticed, the majority of previous investigations are focused on the common steady pressurisation method by considering the steady wind impact. Limited studies are found in the literature regarding the wind impact on Pulse, especially concerning the measurement under natural wind conditions.

In 2021, the Ministry of Housing, Communities & Local Government (MHCLG) has indicated an intention to adopt an alternative airtightness testing method for new buildings based on the Pulse technique, and it is expected that this will be included in the forthcoming revisions to the Approved Documents providing guidance on Part L of the Building Regulations in England and Wales. In this thesis, the applicability and reliability of Pulse will be further evaluated from different perspectives, including comprehensive comparisons with the conventional blower door method, the uniformity of pressurisation distribution during the Pulse test, field testing of the Pulse method under natural wind conditions and computational simulation of the steady wind impact on the Pulse test. In particular, the role of wind in determining the accuracy and precision of the Pulse measurement will be examined based on a large number of field tests under natural wind conditions. Therefore, suggestions can be provided for practical applications of Pulse.

1.3. Aims and objectives

The main aim of the research is to provide in-depth insights into the wind impact on the building airtightness measurement using Pulse through both field testing and numerical simulation. In this research, field tests using Pulse will be conducted with the following objectives to comprehensively assess the reliability of Pulse and the dynamic wind impact from different perspectives, including:

- To compare with the conventional blower door method;
- To evaluate the uniformity of pressure distribution during the Pulse test;
- To assess the reliability of Pulse in a residential dwelling and an outdoor chamber under various natural wind conditions through short-term and long-term investigations of the wind impact on the Pulse test;
- To identify the threshold value of wind speed that causes results with unacceptable errors and to provide suggestions for the Pulse test with minimum wind impact;
- To improve the adjustment method for the Pulse measurements to minimise the wind impact.

In addition to performing field tests, the numerical simulations will be implemented to provide complementary insights into how other wind conditions, which are difficult to capture in experimental studies, such as steady wind conditions and wind from different directions, affect the Pulse measurements. The objectives of the numerical investigation include:

- To numerically understand how the pressure wave propagates within the indoor building spaces during the Pulse test;
- To evaluate the uniformity of pressure distribution during the Pulse test;
- To assess the steady wind impact on the Pulse measurement under different steady wind conditions (i.e., different wind speed levels and directions);
- To identify the threshold value of steady wind speed that causes results with unacceptable errors;
- To cross-validate the numerical simulations with the obtained field testing results;
- To investigate how the presence of a pitched roof influences the indoor pressure distribution during the Pulse test and how the wind might affect the Pulse measurement.

The thesis is structured accordingly and comprises eight chapters to achieve the research aim and fulfil the defined objectives:

- A comprehensive review of the existing literature to analyse, define the importance of the research and identify the research gap - Chapter 2;

- Comparison between Pulse and the steady pressurisation method - Chapter 3;
- Investigation of the uniformity of pressure distribution during the Pulse test through field testing - Chapter 4;
- Short-term field testing to examine the wind impact on the building airtightness measurement with Pulse in a large, detached UK dwelling - Chapter 5;
- Improvement on the adjustment method for the Pulse measurement to reduce wind impact - Chapter 5;
- Long-term observations of the wind impact on the building airtightness measurement with Pulse in an outdoor chamber - Chapter 6;
- Identification of the threshold value of wind speed that causes results with unacceptable errors and practical suggestions for the Pulse test to minimise the wind effect - Chapter 5 and Chapter 6;
- Numerical investigations of how different wind conditions affect the indoor and outdoor pressures of the building and the air leakage measurement during the Pulse test - Chapter 7;
- Conclusions and recommendations for future work - Chapter 8.

1.4. Research methodology

Figure 1-3 provides a flow chart illustrating the overall methodology with the detailed structure of the thesis. The research is mainly based on quantifying the collection and analysis of primary scientific data obtained from experimental field tests and Computational Fluid Dynamics (CFD) simulation. Considering the research validity and reliability, numerical and experimental approaches are adopted to evaluate the statistical data in-depth, and cross-validation is implemented between the simulation and experiment results.

In terms of field tests, the latest Pulse units are adopted. Therefore, the work also assesses the reliability and practicality of the Pulse units. Two sets of field testing are proposed under natural conditions in two different types of dwellings, respectively, to analyse the impact of various wind conditions on the Pulse testing from the practical perspectives. In addition, long-term (i.e., eight months) field testing is proposed to gain more understandings of the wind impact on the Pulse testing under various climatic conditions and assess the seasonal variation of the building airtightness under natural conditions. The detailed test arrangements and employed instrumentation for the field testing are provided in the respective chapters (i.e., Chapters 3, 4, 5, and 6). For all the tests, the tested dwelling is prepared to refer to the ISO 9972:2015 standard (Thermal performance of buildings-Determination of air permeability of buildings-Fan

pressurisation method), and the test validity is examined correspondingly. Error analysis is also performed to verify the obtained measurement results.

Due to the dynamic nature of the wind, a steady wind condition (i.e., steady wind speed level and steady wind direction) is difficult to achieve for field tests. Therefore, the CFD-based numerical simulations are conducted based on a full-scale five-bedroom building model with a flat roof to gain theoretical understandings of the steady wind impact on the Pulse measurement. The ANSYS Fluent is used to deliver the simulation of how the pressure wave propagates within the internal spaces of the test building, how the pressure distributes across different zones within the building during the Pulse test, and how the steady wind affects the Pulse measurement. In addition, considering the most common roof types in the UK, extended simulations in the building model with a pitched roof are performed to investigate the impact of the presence of a pitched roof on the indoor pressure distribution during the Pulse test and on the Pulse measurement.

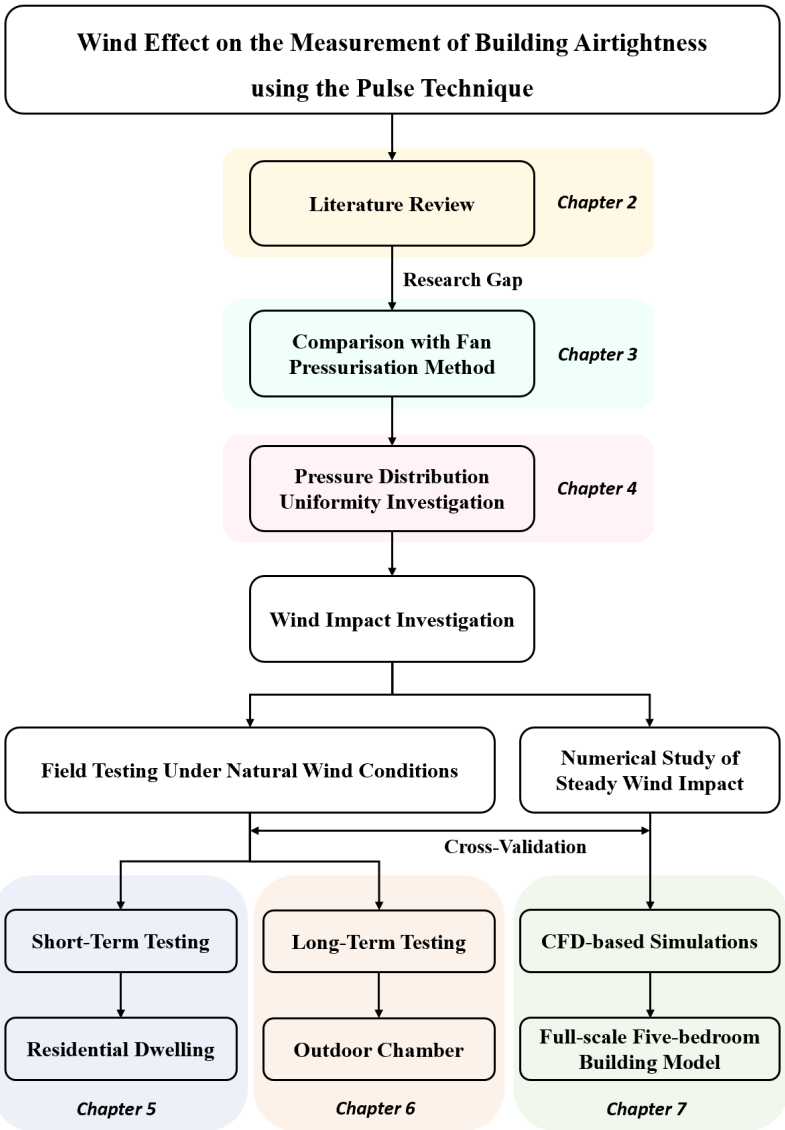


Figure 1-3: Flow chart of thesis structure

1.5. Significance of research

Only about 29% of the existing 29 million houses in the UK meet the highest energy standards [59], which indicates the importance of improving the energy performance of the existing housing stock in order to achieve the net-zero target by 2050. Therefore, there is an increasing necessity for extensively and precisely measuring the building airtightness, which is regarded as a critical factor influencing the energy efficiency and construction quality of buildings.

Different from the widely adopted fan pressurisation method, Pulse is a relatively newly developed technology in the field of building airtightness measurement. Its underlying pulse principle, feasibility and reliability have been investigated, while more in-depth explorations through both numerical studies and field-testing are needed. This research is routinely conducted as part of the ongoing Pulse development and helps to improve the understandings of the wind impact on the building airtightness measurement with Pulse under various wind conditions. In addition, the investigation presents simulation and test results as answers to the questions frequently raised by professionals in the industry and researchers in academia on the test viability owing to the dynamic nature of the Pulse test. The mandatory requirement on building airtightness for energy-efficient buildings justifies the need for a more responsive, undisruptive, non-invasive, reliable, and accurate test approach. The findings of the wind effect could help to improve protocols that are used to characterise building airtightness measurement. Therefore, this thesis contributes to new knowledge of Pulse as an improved means of measuring the building airtightness and provides valuable information for the significance of building airtightness on the energy performance of buildings.

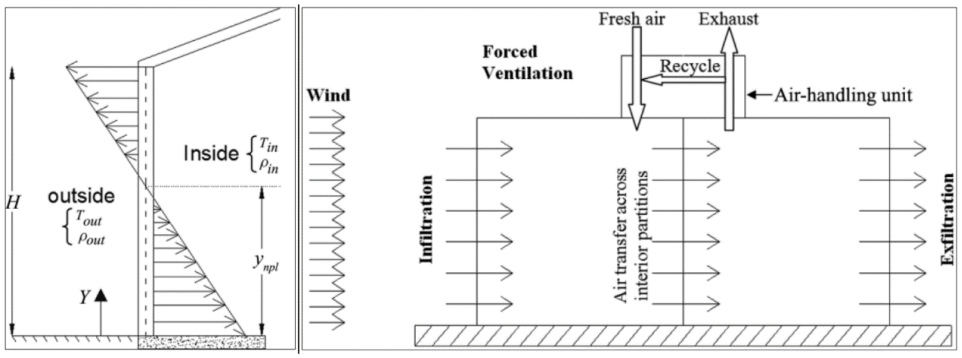
2. Literature Review

This chapter aims to provide a comprehensive introduction of the fundamental of building airtightness, existing measurement methods, how the presence of wind affects the measurement and current research on how to account for the wind impact in research and practice, to create a context for this research and identify the research gap. In detail, an overview on the state-of-the-art of building airtightness measurement methods is presented, with a focus on background research of building airtightness in Section 2.1, steady pressurisation method in Section 2.2, development and application of the Pulse technique in Section 2.3, measurement uncertainties in Section 2.4, wind effect on measurement in Section 2.5, current work on addressing wind effect in Section 2.6, and the current research gap regarding the building airtightness measurement with the Pulse technique in Section 2.7.

2.1. Building airtightness

2.1.1. Concept of building airtightness

In general, building airtightness is defined as the resistance to inward or outward air leakage through unintentional leakage cracks or gaps in the building envelope, which indicates how well the building envelope is sealed [20]. The air leakage across the building envelope is mainly driven by a pressure gradient across the building envelope, including wind-induced pressures, buoyancy pressures and additional driving pressures from mechanical ventilation systems [60]. Wind pressures are influenced by the wind characteristics, such as wind velocity, wind direction, the building envelope shape, the topography of building location and surrounding environments [61]. The buoyancy force or stack effect generally depends on the building height and the temperature difference between indoor and outdoor [62], as illustrated in Figure 2-1.



(a) (b)

Figure 2-1: Illustrations of (a) stack effect and neutral pressure line on a building wall and (b) infiltration and ventilation airflow [63]

Airtightness is the fundamental property of the building envelope that affects infiltration and exfiltration. Basically, the rates of air infiltration and exfiltration depend on the building envelope construction, the differential pressure across the building envelope, the temperature and different natural driving forces of wind [63]. Excessive leakage will result in a significant reduction in airtightness of the building envelope, and associated influences have been noted [17, 64].

2.1.2. Importance of building airtightness

As defined by Liddament [65], air infiltration is the uncontrolled flow of air through penetrations in the building fabric caused by pressure differences generated across these openings by the action of wind and temperature". Air infiltration fundamentally determined by building airtightness changes not only the amount of air entering the building but also distorts the expected airflow pattern, therefore affects the overall indoor air quality and thermal comfort, especially in cold weather [62, 66].

The heat losses owing to air infiltration can be expressed as eq. (2-1) [63].

$$Q_{inf} = \dot{m} C_p (T_i - T_{out}) \tag{2-1}$$

Where Q_{inf} represents the air infiltration energy load, $\dot{m}$ is the infiltrating air mass flow rate, T_i and T_{out} are the room and the ambient temperatures, respectively, and C_p is the air specific heat capacity. Since the 1970s, studies have reported on the energy footprint of excessive air infiltration, and a summary of some related research with their main findings is presented in Table 2-1. According to the field study by Tamura [67], the heat loss for typical residential buildings in Canada reached approximately 40% of the total building heat loss due to air permeability. Ten years later, in 1982, Persily [68] believed that one-third of the heating and cooling loads of buildings was caused by infiltration. After another ten years, in 1996, the US National Institute of Standards and Technology [69] estimated that the building air infiltration accounts for up to 15% of the total energy load of commercial offices. Emmerich, et al. [70] found that the annual energy impact of infiltration was 15% of the heating load and 4% of the cooling load for office buildings in the US. Such a trend suggests that the infiltration might have a detrimental impact on the overall building energy load as the construction quality might have improved over time, but a study [71] shows that the airtightness level of modern UK dwellings is no better than the Victorian ones. Therefore, the infiltration caused energy loss still contributes significantly to the overall building energy demand.

Table 2-1: Summary of studies of infiltration effect on building energy performance

Authors	Year	Key Findings
Harrje [72]	1979	A computer model for infiltration prediction of the whole house was developed, and simulation results demonstrate the significant impact of infiltration on energy losses.
Dickerhoff, et al. [73]	1982	Through testing of thirty-four houses in Atlanta, Georgia, Reno, Nevada, and the San Francisco Bay area, they observed that the leakages in fireplaces and ductwork were the most significant in the western houses, which caused a reduction in energy performance.
Harrje, et al. [74]	1982	Their experiments with house pressurisation revealed that walls accounted for 18-50% of the air leakages in the house, with an average of 35%, followed by ceiling details (with an average of 18%), forced-air cooling systems (with an average of 18%), windows and doors contributed to 6%–22%, with an average of 15%.
Anderlind [75]	1985	The research showed that the air leakage could take place through concentrated, larger cracks and evenly distributed smaller leakages.
Claridge, et al. [76]	1990	Calorimetric measurements were conducted on a small test cell to measure amounts of infiltration introduced under a variety of conditions. Convincing results showed that infiltration led to a notable variation in the energy load.
Liu [77]	1992	The author found the uncontrolled nature of air infiltration and the complexity of interaction between heat transfer and air flow in building components.
Energy Star [78]	2009	Abnormal infiltration resulted in inefficient HVAC systems, high utility bills, and difficulty in maintaining indoor comfort, regardless of the thermostat setting.
Wang, et al. [10]	2018	Building energy performance and indoor air quality are significantly dependent upon ventilation, which is influenced by uncontrolled air leakage (i.e., air infiltration) across the building exterior.

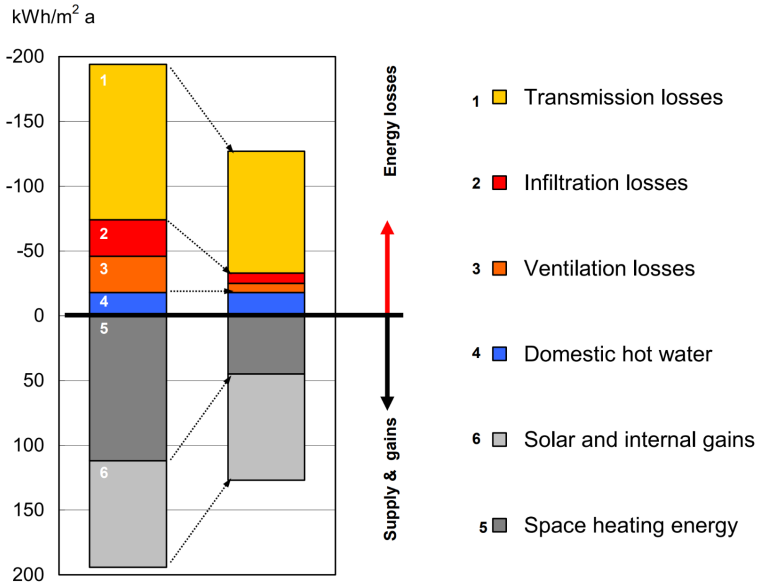
Air leakage is also crucial to ventilation system performance, because it could cause an increased air change rate and energy consumption and impact the function of the thermal resistance of insulation materials [79]. Binamu [80] stated that 53% of the ventilation heating energy in buildings is lost because of uncontrolled air leakage. Jokisalu, et al. [81] demonstrated that the building airtightness greatly influences the heat energy consumption of detached houses in cold climates. Based on their simulation results, the heat energy consumption increased from 4% to 21% when the air change rate varied from 1/h to10/h at 50Pa. Through testing a reference building located in Central Europe, Kraus, et al. [82] noted that the poor airtightness of the building resulted in more specific heat losses by ventilation. Consequently, more specific heating demand is desired for maintaining the essential indoor thermal comfort.

Poor airtightness level with excessive infiltration could also interfere with the normal operation of the mechanical ventilation system of buildings, which may result in poor indoor air quality, moisture damage to buildings, reduction in building thermal insulation, increased energy consumption with imbalanced heating and cooling systems and less efficient heat recovery devices [83-87]. As air or pollutants could be drawn in from contaminated areas owing to poor airtightness, the indoor air quality is reduced accordingly. The places that could be regarded as contaminated areas include the attic, crawlspace and outdoor. Even the building envelope could become a contamination source, which is attributed to mould or toxic materials. Evidence has been provided in the literature [88, 89], that a higher concentration of fungal spores was noted in a crawl space, which may transport to other indoor spaces. Emmerich, et al. [90] reported that the contaminants generated in the garage had been evidently transported into adjacent living spaces through air leakage. Nazaroff, et al. [91] stated that the radioactive radon gas could enter indoor through air leakage from the basement floor, which led to a higher indoor concentration. Radon is regarded as a major source of indoor air pollution and the most frequent cause of lung cancer [92]. Moreover, Pessi, et al. [93] indicated that contaminants such as small-sized actinomycete spores could enter the building interior from the wall structure, which may become airborne as respiratory allergens, causing indoor air contamination and adverse health effect for occupants. Besides, poor building airtightness could allow damp air to enter and be in contact with cool surfaces, which subsequently results in microbiological growth. For extreme cold regions, ice could be formed in and on exterior envelope components owing to poor building airtightness. The moisture convection due to the poor airtightness causes more moisture loads to form on the building structure and structural deterioration [94]. Hagentoft, et al. [95] proved that moist air was transported into the construction through air leakage. Other air leakage losses include duct leakages, such as air leaks at ventilation, heating, and air-conditioning circulation pipe joints. These losses could be quite large in normal terms, and significant energy losses occur when these ducts are passing through unconditioned spaces. Several studies have shown that the heat losses in domestic heating systems in typical North American countries could reach up to 20% due to duct leakage [96]. At the same time, pollutants may also be drawn into the building through these openings. Therefore, researches and developments have been carried out to improve pipeline sealing measures [97].

To address these impacts, requirements for building airtightness have been included in some ventilation standards using different airtightness indexes. For instance, n_{50} (in h^{-1}) represents the air changes at the differential pressure of 50Pa. The building airtightness is recommended to be around n_{50}=1h^{-1} to ensure adequate operation of ventilation devices according to the National

Building Code of Finland Part C3 [98], while in the Belgian ventilation standard NBN D50-001 [99], the criteria for airtightness are n_{50}<3h^{-1} for buildings with mechanical ventilation, and n_{50}<1h^{-1} in the case of the balanced mechanical ventilation assisted with heat recovery. On the other hand, q_{50} representing the air permeability (in m^3/h/m^2) at the differential pressure of 50Pa, is used for building regulations and energy ratings in the UK.

Therefore, to ensure proper ventilation for thermal comfort, buildings should achieve "build tight–ventilate right", meaning not be too air-tight but should be ventilated with dedicated vents [100]. The building airtightness has been considered as a crucial factor to enhance the energy performance of buildings. As seen from Figure 2-2, the increased airtightness for a typical household can contribute to a significant reduction in building energy losses [86]. Moreover, the impact of the building airtightness on the indoor security, occupants' wellbeing and health, and the design of fire compartments and critical enclosures has been noteworthy [101-103].



Left: Single family house, with assumed airtightness level n_{50} = 4.5 h^{-1}.

Right: House with increased insulation and airtightness level ($n_{50} \cong$ 1.5 h^{-1}) and mechanical ventilation with heat recovery.

Figure 2-2: Energy losses before and after increased airtightness [86]

2.1.3. Building airtightness measurement

The airtightness of the building envelope needs to be measured because visual observations are difficult to detect and quantify gaps and cracks that do exist in the building envelope. Also, leakage paths in the building envelope can be convoluted, and gaps are commonly obscured by internal architectural facings or external cladding [104]. The best way to quantitatively understand the airtightness of the building envelope is to measure leakages of the entire building envelope in a range of pressures to obtain the leakage-pressure relationship. Such a relationship can then be

mathematically described by eq. (2-2) [73], the air leakage rate through the building envelope can be characterised by the air leakage coefficient, the pressure difference and the air flow exponent.

$$Q = C_L \Delta P^n \tag{2-2}$$

Where Q is the air leakage flow rate (m^3/s), ΔP is the pressure difference and C_L ($m^3/s/Pa^n$) is the air leakage coefficient, which can be determined by correcting the air flow coefficient to the standard condition. n is the air flow exponent, which is commonly found in the vicinity of 0.65 but has the limiting values of 0.5 and 1 for simple physical considerations [105].

On the other hand, the leakage of a structure or component can also be characterised by an effective leakage area at a reference pressure difference, as given in the eq. (2-3) [106]:

$$L = \frac{Q}{\sqrt{\frac{2}{\rho}\Delta P}} \tag{2-3}$$

Where L is the effective leakage area (m^2), ρ is the air density (kg/m^3), and ΔP represents the reference pressure difference across the leakage site (Pa).

In general, the air flow rate at a specified pressure and the effective leakage area at a specified pressure demonstrate the same information but in different forms. Comparatively, flow rate formulation more directly relates to measurement equipment, while the latter provides an easy-to-relate concept of the amount of leakage in the building structure.

In practical measurement, the measured air leakage rate can be quantified as air permeability ($m^3/h/m^2$) or air change rate (h^{-1}) by normalising the air leakage rate against building envelope area or volume, respectively [107]. Considering the building envelope, the air leakage assessment involves establishing a pressure difference across the enclosure and measurement of the corresponding airflow required to achieve the pressure difference. For instance, the most commonly used reference pressure in the steady pressurisation method is 50Pa, whereas other reference pressures are also used, such as 1Pa, 4Pa, 10Pa, 25Pa and 75Pa. In such a way, the air leakage rate, as explained previously, can be denoted with the reference pressure using a subscript (e.g. Q_{50}) [108].

Table 2-2 presents a comparison of different reference pressures regarding their applications for building airtightness measurement. The Air Tightness Testing and Measurement Association (ATTMA) proposed the pressure test standard that is applied in the UK, which is based on test Method B in the ISO 9972 standard for building air permeability measurement. In terms of the technical requirement for testing, the increment in the range of applied pressure difference should be smaller than 10Pa, while the minimum pressure difference should be either 10Pa or five times

the zero-flow pressure difference, whichever is greater, and the maximum pressure difference depends on the building size: (a) small buildings: at least 50Pa, up to 100Pa and (b) large buildings: 25Pa to 50Pa considering the limitations on the fan capacity [109].

Table 2-2: Comparison of different reference pressures for building airtightness measurement

Reference Pressure	Applications
1Pa [108]	1Pa is the lowest reference pressure used in the existing literature. The measured data at the reference pressure of 1Pa is more uncertain than those of other reference pressures.
4Pa [110]	4Pa is used as the reference pressure in the ASTM (E779-99) definition of effect leakage area and ASHRAE Standards. It has also been used as a reference pressure when quoting the building air leakage rate in building regulations in Switzerland and France.
10Pa [111]	10Pa is adopted as the reference pressure in the Canadian and Dutch definition of equivalent leakage area.
25Pa [109, 112]	When measuring the duct leakage, 25Pa is preferred. In the case that the equipment could not reach the testing condition of 50Pa, 25Pa could be an alternative reference pressure value.
50Pa [113]	The most common reference pressure since the blower door testing becomes popular for building airtightness measurement. It is easy for standard blower doors to achieve 50Pa for most houses, with minimum impact of pressure noise (wind or buoyancy effects).
75Pa [114]	The pressure is too high to use in practice as some building components may change under high-pressure conditions, and it is hard to achieve 75Pa using small pressurisation equipment.

2.1.4. Regulation on building airtightness requirement

The increasing demand for more energy-efficient buildings and the need to demonstrate compliance with more stringent building regulation requirements in the future reveal the important role of airtightness in buildings [11]. Many countries have issued their minimum building airtightness requirements as listed in Table 2-3. Different countries use different ways to express the airtightness requirement, which makes it not straightforward to make a direct comparison across different countries. For example, UK, France, and Switzerland use the air permeability at the differential pressure, while Belgium, Norway, Czech Republic, Germany, and the USA usually express their requirements in air change rate at a specific reference pressure (e.g., 4 or 50Pa), Sweden and Demark use $l/s/m^2$ at a reference pressure of 50Pa, and the Netherlands uses dm^3/s at a reference pressure of 10Pa.

Table 2-3: Available minimum airtightness requirements in different countries

Country	Building Airtightness Requirement	
Belgium [99]	Dwellings with balanced mechanical ventilation: <3ach at 50Pa	
	Dwelling with heat recovery: <1ach at 50Pa	
	Passive house: 0.6ach at 50Pa	
Czech Republic [115]	Buildings with natural ventilation: 4.5ach at 50Pa	
	Buildings with mechanical ventilation	With heat recovery: 1.5ach at 50Pa
		Without heat recovery: 1ach at 50Pa
	Passive house: 0.6ach at 50Pa	
Demark [116]	1.5 l/s per m^2 floor area at 50Pa	
Finland [98]	Around 1ach at 50Pa	
France [117]	Single-family buildings: 0.6$m^3/h/m^2$ at 4Pa	
	Multi-family buildings: 1$m^3/h/m^2$ at 4Pa	
	Non-residential buildings: 1.7$m^3/h/m^2$ or 3$m^3/h/m^2$ depending on building type	
Germany [118-120]	Buildings with natural ventilation: 3ach at 50Pa	
	Buildings with mechanical ventilation: 1.5ach at 50Pa	
	Passive house: 0.6ach at 50Pa	
The Netherlands [111]	Dwellings: 200dm^3/s at 10Pa	
	Non-residential buildings: 200dm^3/s per 500m^3 at 10Pa	
Norway [121, 122]	Detached and undetected houses: 4ach at 50Pa	
	Buildings with two storeys high or less: 3ach at 50Pa	
	Building with more than two storeys: 1.5ach at 50Pa	
	Passive house: 0.6ach at 50Pa	
Sweden [123]	Dwellings: <0.8 l/m^2s at 50Pa	
	Other spaces: <1.6 l/m^2s at 50Pa	
Switzerland [124]	New buildings: <0.75$m^3/h/m^2$ at 4Pa (Recommendation at 0.5$m^3/h/m^2$)	
	Refurbished buildings: <1.5$m^3/h/m^2$ at 4Pa (Recommendation at 1$m^3/h/m^2$)	
UK [125-127]	CIBSE Technical Memoranda TM23	Buildings with natural ventilation: 10$m^3/h/m^2$ at 50Pa
		Buildings with mechanical ventilation: 5$m^3/h/m^2$ at 50Pa
	Part L Building Regulations	Basic: 10$m^3/h/m^2$ at 50Pa
		Good practice: 7$m^3/h/m^2$ at 50Pa
		Best practice: 3$m^3/h/m^2$ at 50Pa
USA [128, 129]	<0.1ach to 1.6ach at 4Pa	
	<0.53ach to 8.5ach at 50Pa	

An airtightness testing is essential to meet the requirements as stated in Compliance Testing on Part L Building Regulations (Part L1A & L2A) for new buildings in England and Wales, and Section 6 Building Standards in Scotland & Northern Ireland (Part F) [130]. Airtightness testing has been introduced as mandatory for new dwellings in the 2006 Building Regulations, by using

the first ATTMA testing standard (TS1, based on BS EN ISO9972:2015) based on the CIBSE TM23 standard [113]. As stated in the TM23 standard, the air permeability requirements for buildings with natural ventilation and mechanical ventilation are $10m^3/h/m^2$ and $5m^3/h/m^2$ at 50Pa, respectively. With regard to Part L1A, the air permeability results should be below the maximum $10m^3/h/m^2$ at 50Pa, while the standard good practice for airtightness testing is a maximum of $7m^3/h/m^2$, and the best practice is $3m^3/h/m^2$ [131]. Table 2-4 lists the air permeability of best and normal practices for different types of buildings, with reference to the standard produced by ATTMA [132].

Table 2-4: Air permeability of best and normal practice for different types of buildings in the UK [132]

	Air Permeability in ($m^3/h/m^2$) at 50Pa	
	Normal Practice	Best Practice
Building Regulations	10	---
Building Type		
Naturally Ventilated	7	3
Mixed Mode	5	2-5
Air-Conditioned	5	2
Factories and Warehouses	6	2
Superstores	5	1
Schools	9	3
Hospitals	9	5
Museums and Archival Storage	1-5	1
Cold Stores	0-3	0-2
Naturally Ventilated	9	3
Mechanically Ventilated	5	3

2.2. Steady pressurisation method

2.2.1. Blower door testing

Generally, the measurement of building airtightness can be implemented by pressurising or depressurising the building to achieve a pressure difference between inside and outside of the building and measuring the corresponding airflow rate. The steady pressurisation method is most widely adopted, by creating a range of steady pressure differences (i.e., in steps of 10-60Pa) across the building envelope with a blower fan and the corresponding airflow rate for establishing the pressure-leakage relationship of the tested dwelling through the fan is measured simultaneously. Currently, the blower door method is the well-known and widely accepted steady pressurisation method, which can also be used to measure airflows between building areas, test duct tightness

and help physically locate leaks in the building envelope with the assistance of other tools, for instance, infrared camera, smoke pen, etc. [133]. Figure 2-3 presents a schematic diagram of the blower door unit, illustrating the overall blower door measurement mechanism. Basically, a blower door unit consists of three main components, a calibrated variable speed fan, a pressure measuring instrument and a blower door mounting opening. The calibrated variable speed fan is capable of generating airflows in a specific range depending on its model capacity and configuration, which is sufficient to pressurise and depressurise a test building of various sizes to the desired pressure range.

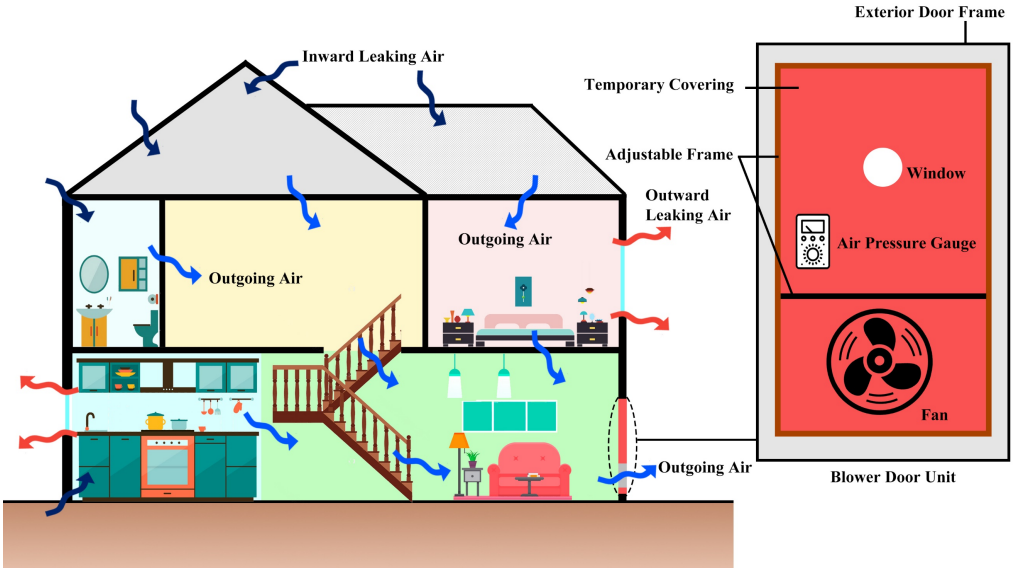
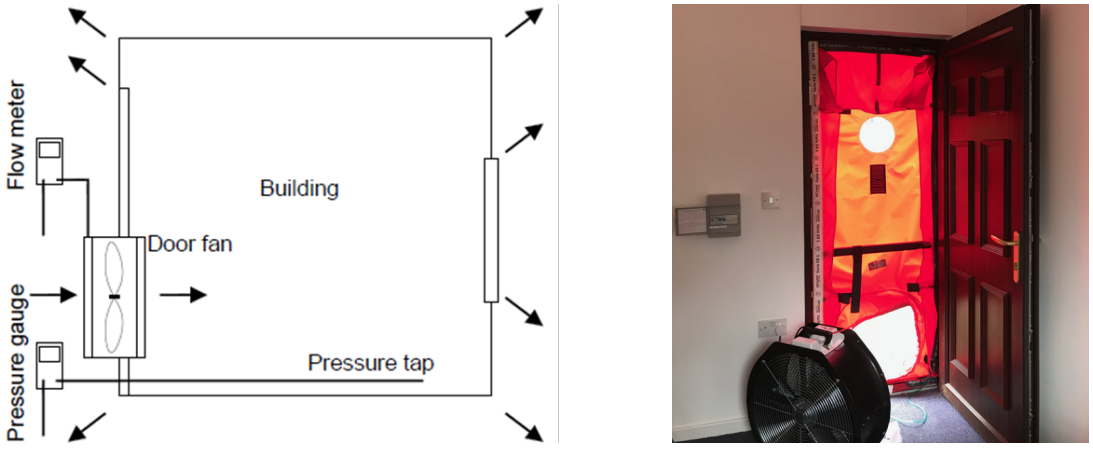


Figure 2-3: Illustration of measuring mechanism of the blower door unit

In practice, the blower door unit should be installed in an existing building fenestration such as a door or a window opening [134]. Figure 2-4(a) shows the installation position of the blower door unit inside the building, and the blower door installation for an actual test chamber is presented in Figure 2-4(b).



(a) (b)

Figure 2-4: (a) Installation position of the blower door [35] and (b) a photo of blower door installation

The blower door test provides air flow rate measurements under various building pressure differences established between indoor and outdoor, consequently building leakage characteristics and its associated energy performance can be understood [135]. For the sake of identifying the leakage location, a smoke puffer can be utilised to reveal and trace air movement while conducting the blower door testing [136]. In such a way, the building could be evaluated against standards to check if its minimum requirements are met. Furthermore, test results can be used to determine if a building requires auxiliary mechanical ventilation and to assess compliance with the building performance standards. With the measured data and indication obtained from the blower door testing, other achievements could be realised [137-139]:

- Revealing source and location of drafts, air leaks or lack of insulation, so to improve the construction quality of building envelope;
- Improvement in energy and thermal performance of buildings together with the reduction in greenhouse gas emissions;
- Reduction in carbon footprint;
- Improvement in indoor air quality;
- Less spending on utility bills;
- Improvements in efficiency and lifetime of air conditioning and heating systems.

2.2.2. Interpretation of measured data

As stated in the ISO 9972 standard, three types of test methods depend on the test purpose. For instance, Method 1 is aimed at testing in the context of clean rooms, Method 2 can be used to compare different construction techniques, and Method 3 is suitable for compliance with building airtightness specification or standard in building energy performance calculation [109]. After each blower door test, a test report is produced containing all the test data information and based on the measurement, the total amount of air flow that is required to achieve a reference pressure difference can be calculated, with reference to the standard of "Measuring Air Permeability of Building Envelopes (Dwellings)" [140].

The induced pressure difference for the blower door test is obtained by subtracting the average zero-flow pressure difference from the measured pressure difference.

$$\Delta P = \Delta P_m - \frac{\Delta P_{01} + \Delta P_{02}}{2} \tag{2-4}$$

Where ΔP and ΔP_m are the induced and measured pressure differences, respectively. In general, the pressure measuring device will be used to check the zero reading at the beginning of each test, and the fan will be temporarily covered to measure the pressure difference between the indoor

and outdoor of the building. ΔP_{01} and ΔP_{02} are the average zero-flow pressure differences obtained at the start and the end of the test.

The measured air flow rates (q_m) during testing are calculated with reference to the manufacturer's specification of the air flow rate measuring instrument (q_r).

$$q_m = f(q_r)\Delta P = \Delta P_m - \frac{\Delta P_{01} + \Delta P_{02}}{2} \tag{2-5}$$

For depressurisation testing, the air flow rate through the building envelope (q_{env}) is expressed as:

$$q_{env} = q_m \left(\frac{\rho_i}{\rho_{out}}\right) \approx q_m \left(\frac{T_{out}}{T_i}\right) \tag{2-6}$$

Where ρ_i and ρ_{out} are the air density of indoor and outdoor, respectively. T_i and T_{out} are the absolute air temperatures of indoor and outdoor.

Differently, the air flow rate through the building envelope for pressurisation testing is obtained by:

$$q_{env} = q_m \left(\frac{\rho_{out}}{\rho_i}\right) \approx q_m \left(\frac{T_i}{T_{out}}\right) \tag{2-7}$$

Therefore, the air flow coefficient (C_{env}) and air flow exponent (n) can be determined:

$$q_{env} = C_{env}(\Delta P)^n \tag{2-8}$$

A leakage graph for both pressurisation and depressurisation can be produced accordingly by plotting the air flow rate through the building envelope against the corresponding pressure differences on a log-log plot. Figure 2-5 shows log-log plot examples for the pressurisation and depressurisation tests at 50Pa. Based on the plot, the coefficient of determination (R^2) can be calculated. Referring to the ISO 9972 standard [109], valid test results require n to be in the range 0.5 to 1 and R^2 to be greater than 0.98.

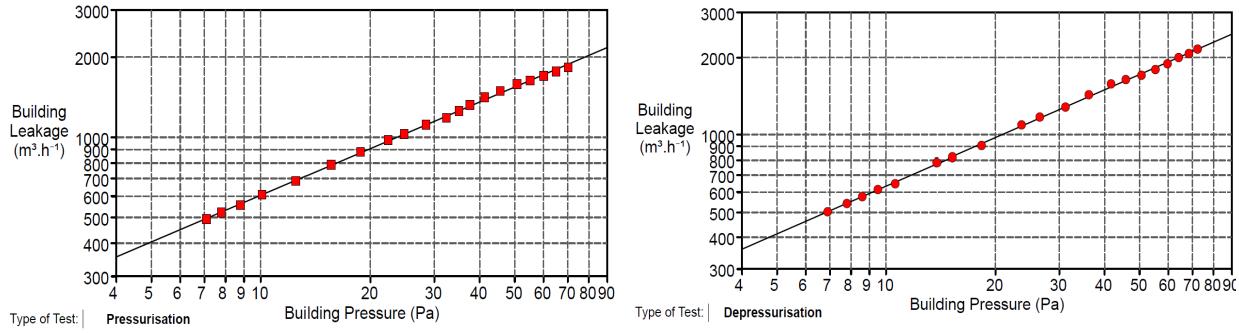


Figure 2-5: Examples of the air leakage log-log graph for (a) pressurisation and (b) depressurisation tests

The air leakage rate through the building envelope at the reference pressure difference (ΔP_r) is then calculated by:

$$Q = C_L(\Delta P_r)^n \tag{2-9}$$

Where C_L the air leakage coefficient is calculated by correcting the air flow coefficient (C_{env}) to the standard condition, which refers to 20℃ at the pressure level of 1.013×10^5Pa.

$$C_L = C_{env}\left(\frac{\rho_{out}}{\rho_s}\right)^{1-n} \approx C_{env}\left(\frac{T_s}{T_{out}}\right)^{1-n} \quad \text{for depressurisation} \tag{2-10}$$

$$C_L = C_{env}\left(\frac{\rho_i}{\rho_s}\right)^{1-n} \approx C_{env}\left(\frac{T_s}{T_i}\right)^{1-n} \quad \text{for pressurisation} \tag{2-11}$$

Where ρ_s and T_s are the air density and absolute temperature at the standard condition, respectively.

Using the air leakage rate divided by the total surface area of the building's thermal envelope, the building air permeability in the unit of $m^3/h/m^2$ at the reference pressure difference can be derived correspondingly.

In addition to measuring the building airtightness, the locations of leakage on the building envelope can be detected using the blower door testing in conjunction with another tool. For instance, (a) the subtraction method by measuring the leakage area with and without covering air barrier sheets, (b) using a thermal camera during the depressurisation test to localise air leakage pathways when there is a temperature difference between the indoor and outdoor, (c) generating smoke to visualise the airflow through the building envelope so that the locations of leakage could be detected, and (d) holding an air velocity meter against the potential leakage area to check whether a reading of air velocity is given to indicate the leakage.

2.2.3. Challenges of steady pressurisation method

As stated by Cooper, et al. [31], the 50Pa pressurisation employed in the steady pressurisation testing has been widely considered as a measure of breathability. The reason for setting the test pressure at 50Pa is that the value is much higher than the level of pressure change caused by the wind and buoyancy effects. Thus, errors resulted from the wind and buoyancy effects during testing could be ignored. Nevertheless, some challenges have been noted for the steady pressurisation method, which is explained as follows:

During testing, the pressure exerted on the building envelope is significantly higher than that under the natural condition (i.e. typically around 4Pa) [141]. Thus, the leakage under the natural condition should be extrapolated from the measurement obtained in a range of elevated high pressures, which may lead to errors. Another issue is the requirement of a large amount of airflow

for pressurisation [142]. It will be impractical to apply the steady pressurisation method, especially for large buildings, as a high-capacity fan system is needed to deliver the required amount of airflow (e.g., pressurisation testing at 50Pa for a typical large building of 100,000m^3, the required air flow rate is 1,000,000m^3/h). Although this can be limited by decreasing the pressurisation level, such as from 50Pa down to 25Pa or lower, other problems may be caused correspondingly [28]. As the pressure level approaches the pressure generated by the buoyancy and wind, the lower the pressure becomes, the less accurate the obtained measurements are due to the background noise caused by environmental conditions. Owing to the inaccuracy of the low-pressure measurement, this may cause non-negligible errors in the leakage prediction. Hence the multi-point test is preferred by typically increasing or decreasing the pressure difference, usually by 5 to 10Pa over the range of 10-60Pa [143], which demonstrates a better accuracy than the single-point test. However, more time would be consumed to proceed with a multi-point test. To minimise the effect resulted from the steady pressurisation method within an acceptable range, the standard E779-10 of ASTM 2010 [144] has been proposed to test only when the absolute value of the indoor/outdoor air temperature difference multiplied by the building height is lower than 200m°C, which also can be applied to the wind speed, preferably below 2m/s. With regard to the steady pressurisation method, other concerns have also been mentioned in the literature [24, 30-32, 35]:

- Because of the variations of pressure and ambient temperature with the weather condition, real-time leak zone measurement cannot be realised, causing unstable readings and uncertain values from the blower door testing.
- A significant amount of air discharged by the fan may cause inconvenience to the indoor environment, such as a substantial temperature change in the room, which is inconsistent with the actual heat dissipation condition.
- It is required to install the blower door to an existing window or door frame, which may affect the air leakage characteristics at the opening where the blower door is installed.
- Such a high-pressure difference may damage or alter the building structure [32].
- The difficulty of achieving an even building pressure distribution when a giant fan is employed for pressurising a large building.

2.3. Pulse technique

2.3.1. Fundamentals of Pulse

To overcome some issues of the steady pressurisation method, efforts have been made to explore and develop alternative methods [24, 145]. One of them is the Pulse technique, an unsteady approach that allows accurate testing at much lower pressures while negating the need for large air flow delivery. Basically, Pulse measures the building airtightness at low pressure by rapidly releasing a known volume of air into the test building, thereby creating an instant pressure rise that quickly reaches "quasi-steady" condition [29]. It determines the adventitious building leakage in the range of 1-10Pa and reports at 4Pa, which has been regarded as a more precise indicator of the pressure level experienced by buildings under natural conditions than the conventional steady-state measurement at 50Pa [26, 31, 33, 146, 147].

Instead of installing a fan into a doorway for blower door testing, the Pulse test unit can be placed within the building, thereby maintaining the building integrity and avoiding the need for a complex setup. Figure 2-6 presents a diagram to illustrate how the Pulse unit could be placed in the building during the measurement, with a photo of the Pulse unit (i.e., PULSE-60) and its key components annotated. A Pulse unit mainly consists of a compact compressor, an air tank, a solenoid valve, a pressure transducer, an internal pressure reference tank and a control box with an LCD screen.

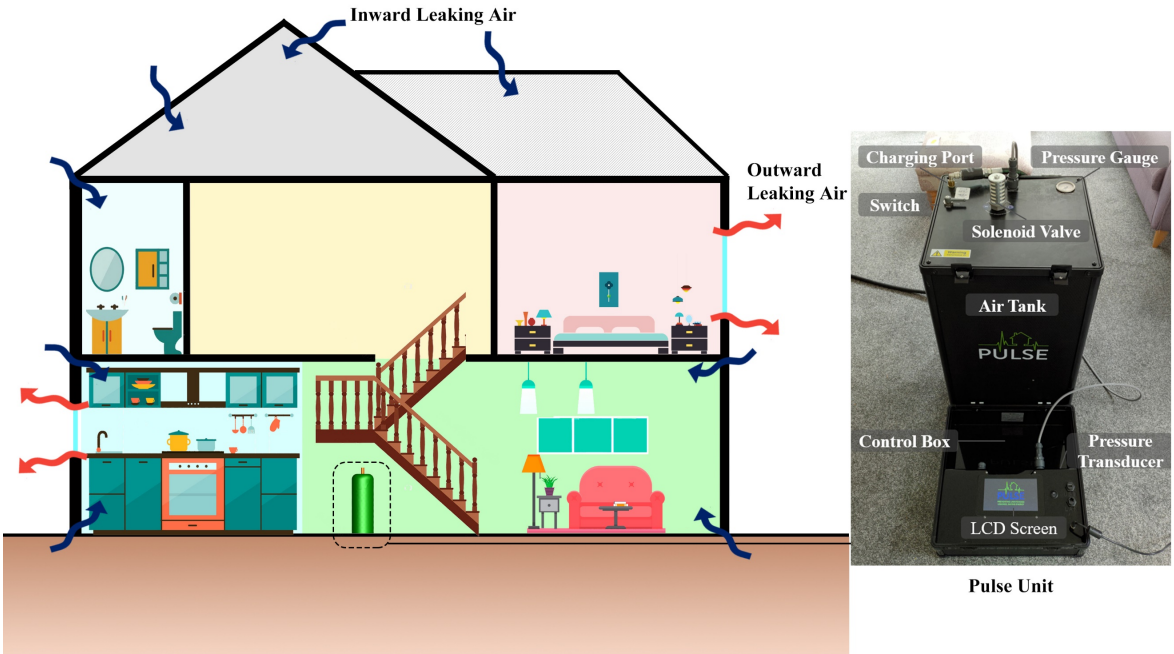


Figure 2-6: Illustration of measuring mechanism of Pulse unit

Pulse dynamically measures the airtightness of the building within a short period (e.g.,11s to 15s) [31], and the effects of wind and buoyancy force can be minimised by taking the background pressure reading at a high sampling rate in a short time window; thus high repeatability can be achieved as proved in [35]. During the Pulse test, the mass flow rate from the nozzle can be derived by measuring the transient pressure in the air receiver, while the building pressure response is measured by a differential pressure transducer with the aid of an internal pressure reference [32]. The pressure variations in the test building and tank during the Pulse test are recorded simultaneously to determine a correlation between the leakage and pressure. Typically, the building pressure readings contain three key stages: the background pressure before the air pulse release, the quasi-steady period, and the background pressure after the air pulse release [32]. In particular, the quasi-steady period is selected for examining the building airtightness. Figure 2-7 illustrates the pressure variation throughout a typical Pulse test; it can be seen that the quasi-steady period takes place in the middle part of the Pulse test.

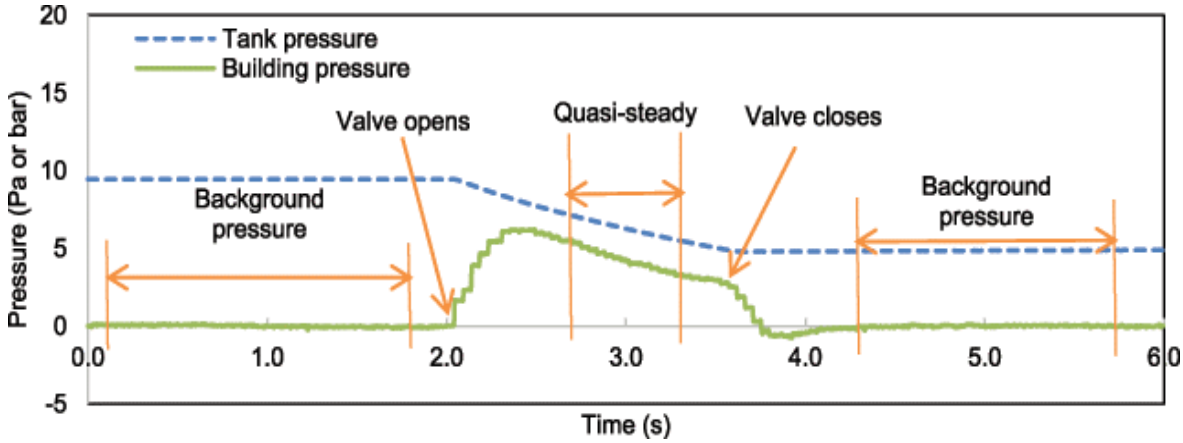


Figure 2-7: Pressure variation with time for a typical Pulse test [142]

Mathematically, the building air leakage measurement by the Pulse test can be expressed with a quasi-steady/temporal inertia model, solving a set of the continuity equation for the enclosed space and integral momentum equations for openings [148].

$$\frac{V}{\rho_i}\frac{d\rho_i}{dt} = Q_p\{t\} - q\{t\} \tag{2-12}$$

Where V is the building volume, ρ_i is the indoor air density, $Q_p\{t\}$ is the volumetric flow rate of the air released from the compressor and $q\{t\}$ is the building leakage rate. The isentropic expansion of the air is assumed as expressed in eq. (2-13):

$$\frac{P_i}{\rho_i^{\gamma}} = C_t \tag{2-13}$$

Where P_i is the indoor building pressure, γ is the specific heat ratio (1.4) and C_t is a constant. Therefore, the building leakage rate can be expressed as:

$$q\{t\} = Q_p\{t\} - \frac{V}{\gamma P_i}\frac{dP_i}{dt} \tag{2-14}$$

The volumetric flow rate of the air released from the compressor can be derived by eq. (2-15):

$$Q_p\{t\} = -\frac{V'}{\gamma R T_0}\left[\frac{P(t)}{P_0}\right]^{\frac{1-\gamma}{\gamma}}\frac{P(t)}{\rho_i} \tag{2-15}$$

Where $P(t)$ is the air transient pressure in the compressor, P_0 is the initial air pressure in the compressor and. T_0 is the initial air temperature in the compressor. R represents the gas constant (287.058 J/kg·K), and V' is the volume of the air receiver.

The main challenge for Pulse is associated with the inertia effect of air flowing through openings, which could increase the uncertainty of the measured data [149]. As addressed in [32], this type of flow is regarded as an unsteady flow. In order to determine the proportion of the unsteady flow, a momentum equation is used to quantify it, described by eq. (2-16):

$$\Delta\rho\{t\} = aq\{t\}^2 + bq\{t\} + \rho_i\frac{l_e}{A}\frac{dq}{dt} \tag{2-16}$$

Where $aq\{t\}^2 + bq\{t\}$ represents the momentum change and surface friction, $\rho_i\frac{l_e}{A}\frac{dq}{dt}$ describes the inertia effect of air flowing through an opening [32].

Whereas in the quasi-steady flow, the percentage of the unsteady flow is determined by eq. (2-17):

$$\left|\rho_i\frac{l_e}{A}\frac{dq}{dt}\right| \Big/ \left(\left|aq\{t\}^2 + bq\{t\}\right| + \left|\rho_i\frac{l_e}{A}\frac{dq}{dt}\right|\right) \times 100\% \tag{2-17}$$

An example of the percentage of the unsteady flow during the quasi-steady period in a typical Pulse test is presented in Figure 2-8. It can be noted that only about 1% of the overall flow is unsteady flow. Thus, the quasi-steady state can be regarded as being achieved.

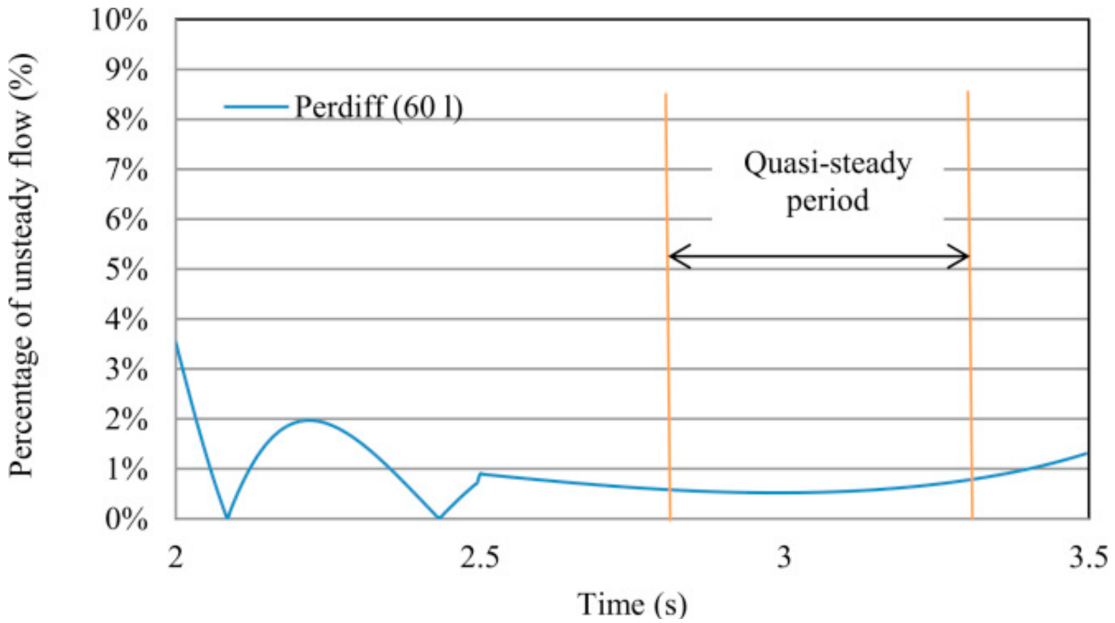


Figure 2-8: Percentage of the unsteady flow during the Pulse test [150]

A comparison of the measurement between the Pulse and blower door methods in the same test building is presented in Figure 2-9. A power-law curve in the log-log form fits well between the two test results (i.e., R^2=0.9994), which indicates a good agreement between the two test methods.

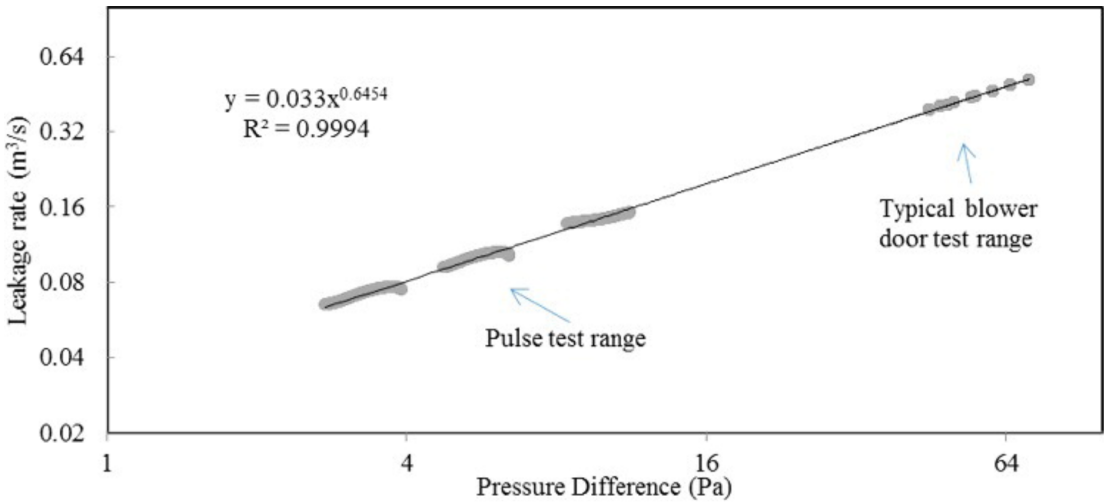


Figure 2-9: A comparison example of pressure-leakage results for the Pulse and blower door tests [32]

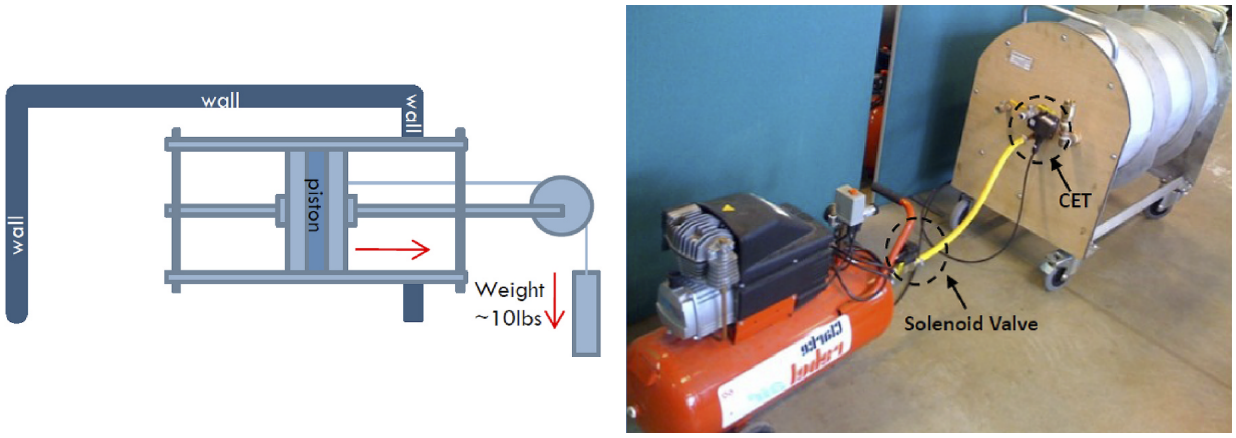
2.3.2. Development and challenges of Pulse

Pulse measures the building leaks in a dynamic manner, rather than recording every individual reading at a steady pressure level. Studies have been conducted on Pulse in regard to feasibility, reliability, repeatability, and applicability. Cooper, et al. [29], Cooper, et al. [31], Cooper, et al. [147] theoretically investigated the feasibility of Pulse via the temporal inertial model. Cooper, et al. [33] proved Pulse's accurate and reliable low-pressure measurement approach through numerical and experimental studies. Zheng, et al. [151] investigated the applicability and accuracy of the power-law and quadratic equations on predicting the air leakage at low pressures based on the experimental study under sheltered conditions.

In terms of repeatability of the Pulse test, Cooper, et al. [32] conducted the Pulse tests in a number of UK homes under different environmental conditions, and repeatability of ±8% was obtained for repeated tests in a detached house over a year time. They also observed the wind speed and direction have the greatest impact on the variation of measured air permeability. On the other hand, Zheng, et al. [150] conducted a repeatability assessment using a multi-gear portable trailer fan to provide various artificially imposed steady wind conditions. They found that a small uncertainty (i.e., within ±3%) of the Pulse test was obtained when the wind speed was below 3.5m/s at 1.5m above the ground level. However, the uncertainty increased to ±25.6% when the wind speed range was from 4.5 to 9m/s. In addition, the repeatability of the blower door and the Pulse methods was evaluated, Pulse demonstrates strong repeatability with an overall measurement uncertainty of ±5%, and the blower door testing presents a similar spread.

During the Pulse test, the pressure wave propagates at the speed of sound; therefore, the pressure within the building subjected to the rapid release of air pulse is able to equalise within a short period of time. To address the issues in testing large buildings due to the increased dimension, multiple Pulse units could be distributed evenly throughout the large building and operated simultaneously to achieve an even pressure distribution. In addition, researchers also noticed that the Pulse test location caused a minor impact on the building airtightness measurement [148, 150]. Though Pulse is newly developed, it provides reliable measured results to demonstrate building airtightness [32, 150]; thus, the testing mentioned in Section 2.2.1 using the blower door method could also be achieved through the Pulse test. After a public consultation in 2019-2020, an intention to adopt an alternative airtightness testing method for new buildings based on Pulse was indicated by the Ministry of Housing, Communities & Local Government (MHCLG). It is expected that this will be included in the forthcoming revisions to the Approved Documents providing guidance on Part L of the Building Regulations in England and Wales.

Until now, several Pulse prototypes have been developed and tested for practical applications. For instance, a concept of the gravity-driven piston version was proposed by Carey, et al. [28] in 2001 as seen in Figure 2-10(a), a compressed air-driven piston version was developed by Cooper, et al. [34] in 2004, as shown in Figure 2-10(b), and a nozzle-based version has been developed and improved since 2010 [142].



(a) (b)

Figure 2-10: Photos of (a) the gravity-driven piston version [28] and (b) a compressed air-driven piston version [34]

The nozzle-based Pulse unit avoids the need for a large separate piston unit. Figure 2-11 presents a photo of the early setup of the nozzle-based pulse unit, the PULSE-50, with a 50-litre air tank. The main components of PULSE-50 are an oil-based compressor, a compressed air tank, an internal pressure reference, a nozzle unit, and a control box.

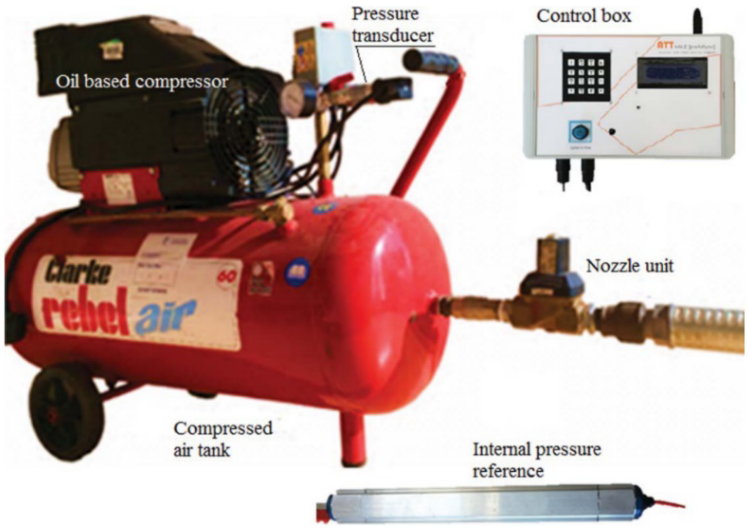
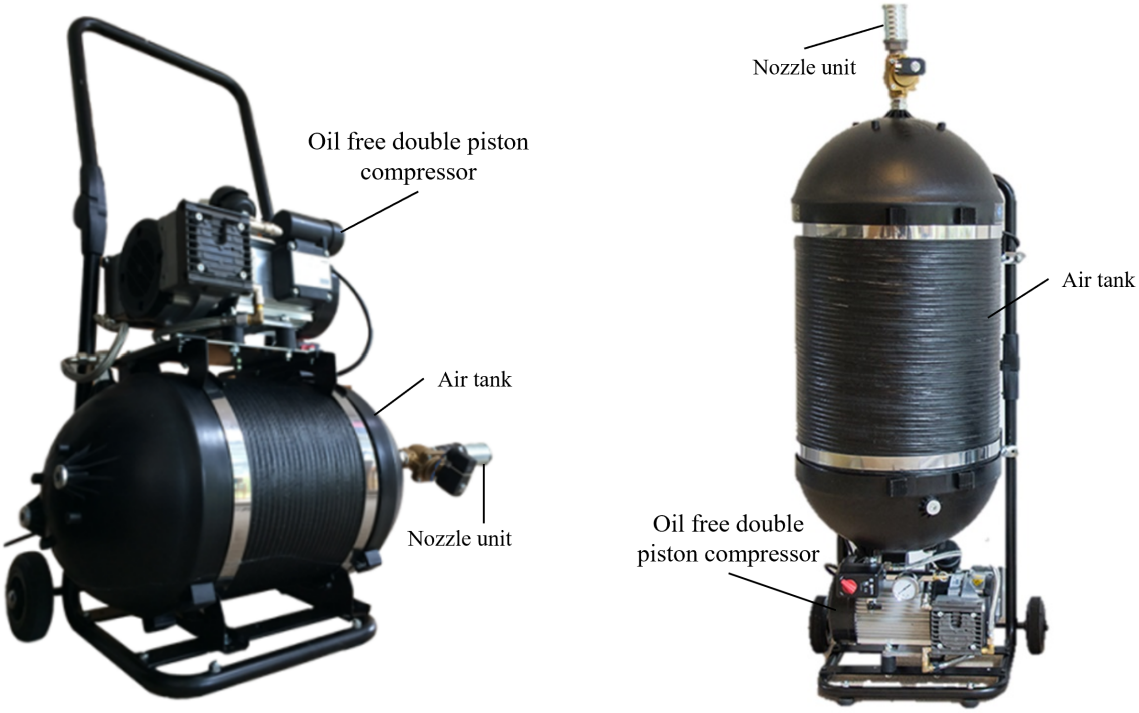
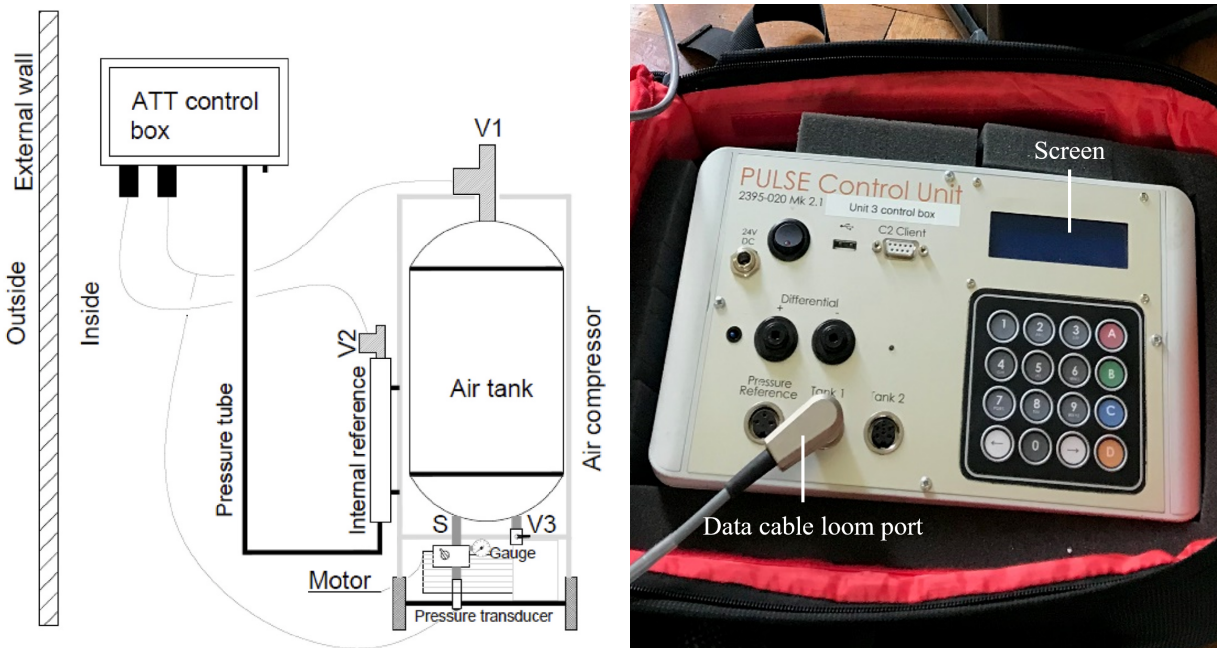


Figure 2-11: Photo of PULSE-50 [32]

To improve the portability of PULSE-50, two other versions were designed and built in 2013 by adopting lightweight, compact air tanks and oil-free double piston compressors: PULSE-40 and PULSE-80, as shown in Figure 2-12(a) and 2-12(b). A general schematic of the Pulse system composition is presented in Figure 2-12(c). Practically, a trolley structure was adopted for the sake of better mobility. Figure 2-12(d) shows a photo of the control box, which was improved for more advanced control to allow data to be directly exported to an external USB stick, with no need of using the computer to store data.



(a) (b)



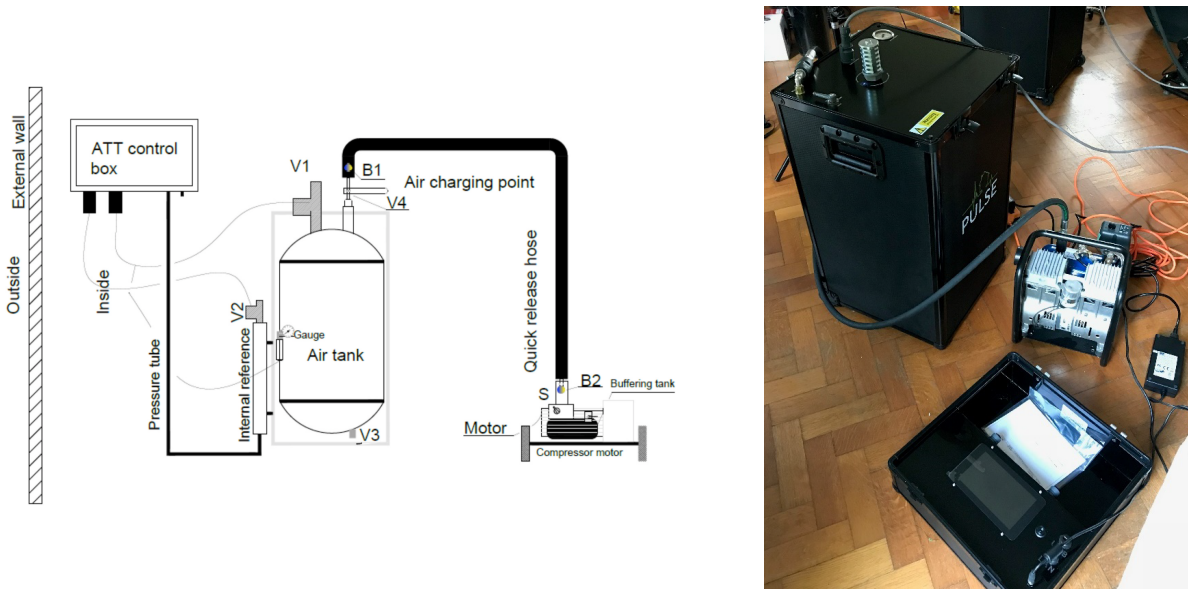
(c) (d)

Figure 2-12: Photos of (a) PULSE-40, (b) PULSE-80, (c) schemtic diagram of PULSE system composition and (d) an advanced control box [148]

Based on experimental works, researchers pointed out the importance of matching different component capacities [30]. Like the blower door method, the optimum selection of component capacity should be obtained through valid experimental data. Because different tested dwellings have different sizes (i.e., volume and envelope area) and leakage levels, the capacities of components should be adequately determined according to the application. A final prototype of the Pulse unit was developed by Build Test Solutions Ltd with improved firmware and hardware in 2016. The system schematic diagram and a photo of PULSE-60 are provided in Figure 2-13, and the key components are annotated. Several modifications and improvements were made for the PULSE-60, including:

- The overall setup of the PULSE-60 was designed with considerations of mobility, applicability, simplicity, creativity, and aesthesis. Instead of using an entire compact pulse unit design, the PULSE-60 separated the air tank, the control box, and the compressor into modular components.
- Considering an early commercial product design, a sturdy and portable container with wheels was designed for the air tank, which enabled convenient transportation and avoided any damages from a collision during transportation.
- The lid of the air tank container could be easily disassembled, and a more advanced control unit was embedded. The control unit adopted a touch screen, which allowed for easy operation.

- Real-time monitoring data can be processed while recording.
- An internal pressure reference tank was constructed inside the control box. An automated valve is installed, which normally is kept open for an equalised pressure between the inside of the tank and the ambient and is closed once the test begins to provide the reference pressure.
- PULSE-60 was designed to be adaptable for buildings in a variety of sizes, as multiple Pulse units could be employed for operation simultaneously.
- Note that this version of PULSE-60 at the time of writing has now been superseded, with a commercially available unit by the licence holders Build Test Solutions Ltd [152] (Figure 2-14).



(a) (b)

Figure 2-13: (a) A schematic diagram [33] and (b) a photo of PULSE-60 unit



Figure 2-14: A photo of PULSE 2.0 system by Build Test Solutions Ltd. [152]

Compared with the steady pressurisation method, the Pulse technique benefits from adjusting background pressure due to its short test phase and frequent sampling. The pressure difference of 4Pa has been regarded as the typical natural ventilation; however, measurement difficulties also exist for the Pulse technique because of the indeterminate nature of the external wind and buoyancy effects [149]. Different wind speeds and wind directions would cause variations in the pressure within the building, as mentioned in the literature [32, 153, 154]. The Pulse technique measures the pressure difference between the indoor of the building and the internal space of the pressure reference tank, which could be affected in accordance with the indefinite nature of the wind and buoyancy effect, thus causing errors in the measurement of the building pressure response. The Pulse technique is able to reduce the wind impact but within a limit. Therefore, there is a need to fully understand the limit to make a more informed decision on the wind conditions under which a valid Pulse test can be obtained. Furthermore, the testing weather condition requirements have been set in the standards for the fan pressurisation method, while the applicability for the Pulse technique needs to be assessed.

2.3.3. Other airtightness measurement methods

Due to the limitations in the practical application of the steady pressurisation measurement, alternative methods for the unsteady pressurisation have been proposed and tested, such as the AC pressurisation method and decay method. AC method employs a reciprocating piston to generate a repeated sinusoidal volume change to the test building, which has been reported in [155-157], and a schematic diagram of an experimental setup of the AC pressurisation method is presented in Figure 2-15.

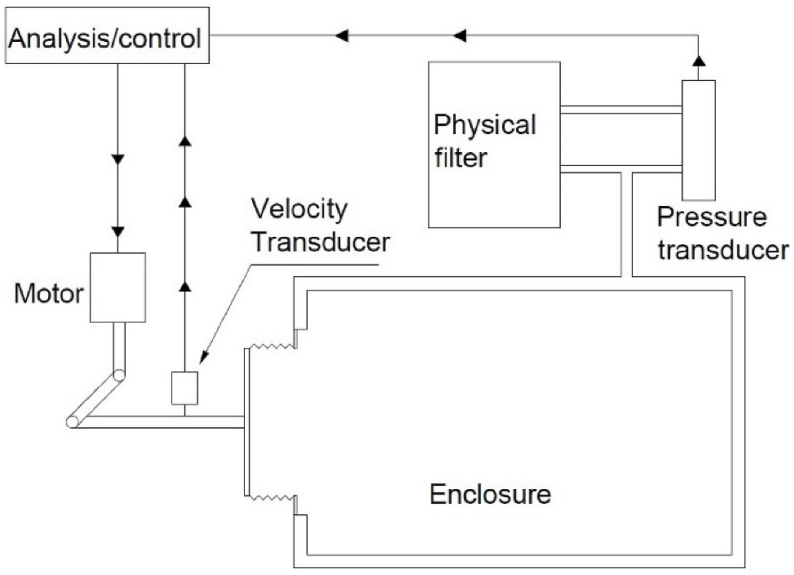
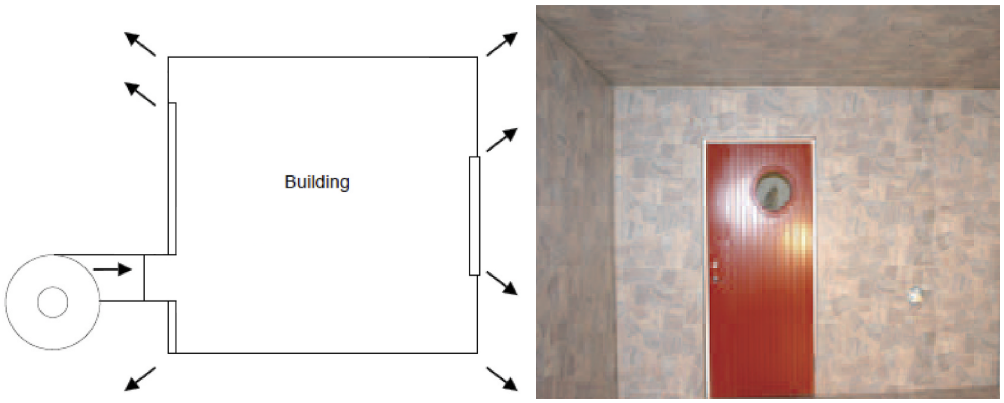
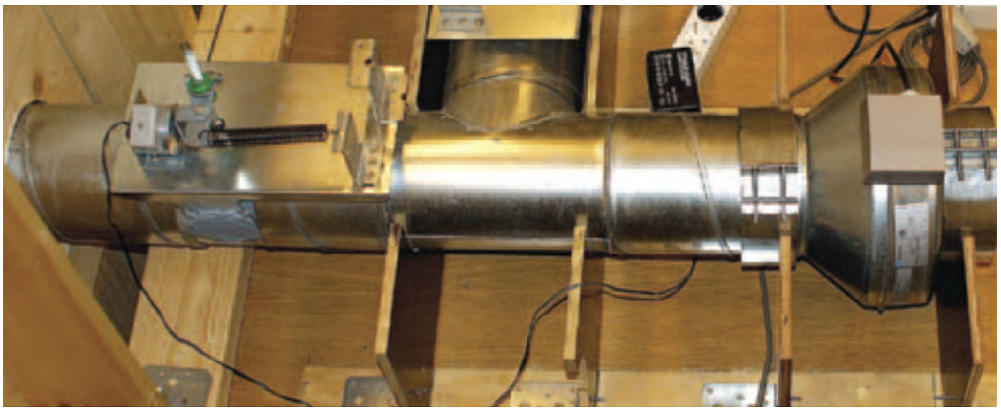


Figure 2-15: A schematic diagram of the experimental setup of the AC pressurisation method [155]

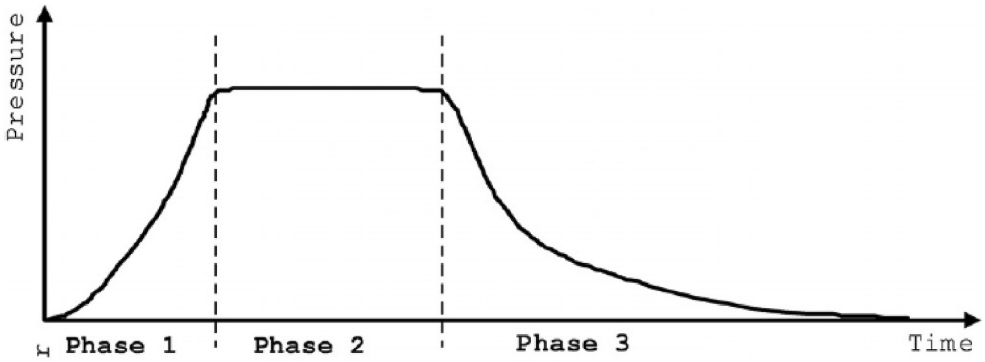
However, the AC pressurisation method has issues in frequency limitation, repeatability, accuracy, and applicability. By supplying a certain amount of air into the test space, the pressure difference between the inside and outside of the test building is created, and the Decay method monitors the decay of the pressure difference when the air supply is stopped [158]. Figure 2-16(a) and 2-16(b) show the schematic diagram and a photo of the Decay method setup, and the pressure curve during a test using the Decay method is illustrated in Figure 2-16(c). This transient pressurisation method has been explored through experimental work and numerical modelling [159-162].



(a)



(b)



(c)

Figure 2-16: (a) A schematic diagram and (b) a photo of the experimental setup of Decay method and (c) pressure curve during the test using Decay method [162]

Alternatively, an acoustic method has been proposed to measure the building airtightness through sound transmission measurements through openings. Sonoda, et al. [163] obtained a correlation between air and sound leakages through two different slits and suggested the source sound frequency of 2000Hz is favourable for the leakage measurement under a pressure difference of 50Pa. Iordache, et al. [164] carried out the acoustic measurements on both sides of each window and validated that the air permeability predicted by the acoustic protocol produced agreed well with their measured value. Varshney, et al. [165] determined the air infiltration rate using the acoustic method through different types of holes and cracks, and the obtained experimental results matched well with the measurements of the blower door test. The acoustic method has been reported to be preferable for measuring the leakage rate of a building element rather than the entire building envelope, because of the nature of sound propagation [24].

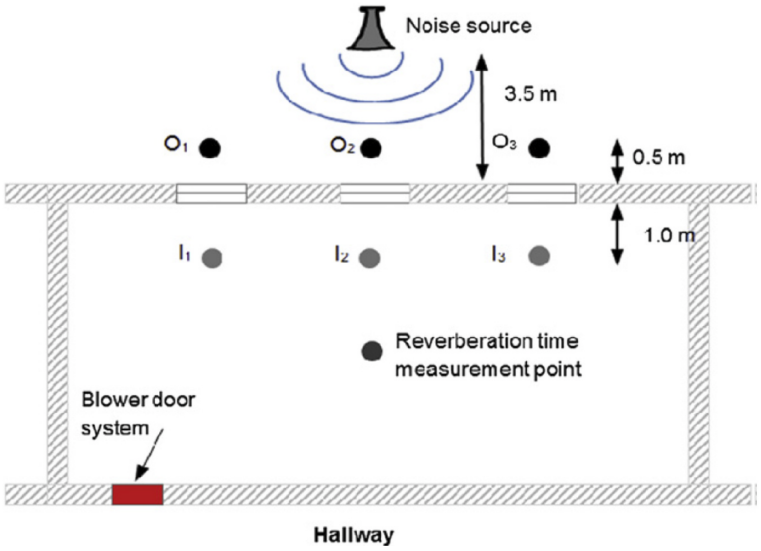


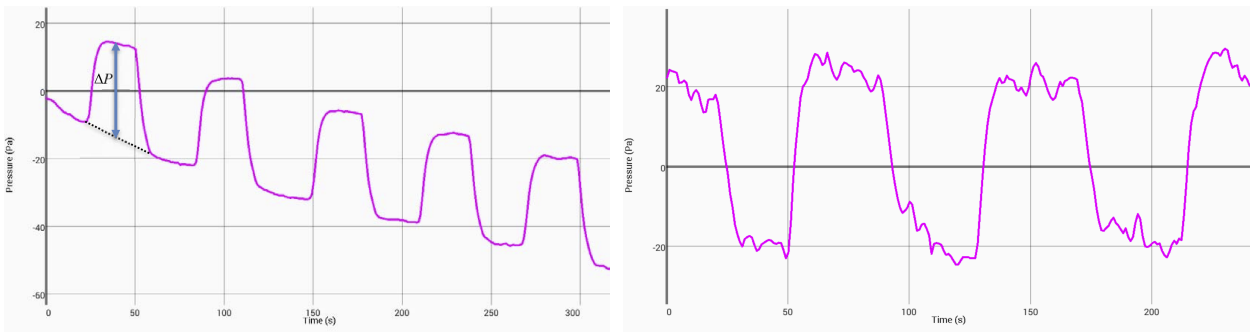
Figure 2-17: Monitoring arrangement for an acoustic measurement [164]

On the other hand, Lanooy, et al. [46] proposed a new airtightness tester device named ATT to determine the building airtightness using the existing building ventilation system to pressurise the building, and the photo of the ATT device produced by ACIN Instrumenten B.V. is presented in Figure 2-18. Instead of using an external fan in the blower door test, ATT has a compact design consisting of a pressure sensor, a reference vessel, communication hardware and an app. An airflow meter is used to measure the flow rate of the ventilation system. The fan pressurisation of the building is measured relative to the pressure in the reference vessel, which corresponds to the building pressure as the building ventilation system is switched off. The benefits of measuring the reference pressure inside the building are to avoid using a building opening for outdoor pressure measurement and minimise the wind impact on the pressure variations over the building envelope. Moreover, using the buildings ventilation system could reduce the price and time for the airtightness measurement.



Figure 2-18: A photo of ATT device by ACIN instrumenten bv [166]

Lanooy, et al. [46] performed building airtightness measurements with the ATT device on the windy condition, with their measured pressure variations presented in Figure 2-19. Their preliminary data demonstrated that the measurement is less sensitive to wind conditions as data can be obtained on a windy day where it is not achievable for the blower door testing.



(a) (b)

Figure 2-19: Pressure variations of (a) calm condition and (b) windy condition by ATT measurements [46]

To further investigate the feasibility of the new test method, airtightness measurements have been performed in 82 dwellings in the Netherlands [167]. Comprehensive comparisons between measurements of the blower door and ATT were conducted and reported in [168]. An overall good agreement of the two methods was obtained with similar airtightness results at a reference pressure of 10Pa. Compared with the blower door multi-point testing data, higher leakage measurements are obtained by ATT's single-point tests in most cases. It may be caused by the reference pressure, as ATT uses the reference as an average over the whole building while the blower door takes in one place [169]. As the building airtightness measurement is accepted and adopted widely, more practical, undisruptive, and non-invasive testing manners will be needed for both existing and new buildings.

2.4. Uncertainties of building airtightness measurement

The uncertainties of building airtightness measurement are important concerns. Common issues associated with the uncertainty of airtightness measurement has been greatly discussed; however, they are still incompletely solved in practice. There are a number of sources of uncertainty for the airtightness measurement, the most common ones are discussed below.

- Building preparation for testing and tester behaviour

Although standards have been proposed to regulate building preparation and operation procedures to eliminate the effect of tester behaviour [170], operators still have different interpretations using different test equipment on site. For instance, Delmotte, et al. [171] found the maximum variation for ten repeated tests was 4% by the same tester with the same test equipment; however, 7.9% derivation was noted for the tests conducted by different testers with different equipment.

- Uncertainties of repeatability and reproducibility

The repeatability and reproducibility of the steady pressurisation method have been widely discussed. For example, researchers found that the average air leakage rate has repeatability and reproducibility standard deviations of 1.4% and 2.4% at 50Pa, 3.5% and 5.9% at 4Pa [171]. Bracke, et al. [172] found that the maximum uncertainty of 44 repeated tests in a passive house in Belgium was 7.7%. However, field testing results proved that the repeatability and reproducibility could be improved when both the pressurisation and depressurisation tests were conducted [171, 173]. In terms of Pulse, Zheng, et al. [174] proved good repeatability in the Pulse tests with an overall measurement uncertainty of ±5%.

- Uncertainties of the measurement instrument

Different instruments are used for the steady pressurisation and Pulse tests to provide the air flow and pressure measurements, which have respective specified accuracy. Sherman, et al. [36] stated that common bias errors in the fan pressurisation testing are attributed to the measurement devices; therefore, they suggested that the inaccuracy of a flow measurement device should be within 2% and 5% for a pressure measuring device.

- Seasonal variation of building airtightness

The long-term performance of building airtightness has been explored, and a seasonal variation in building airtightness was noted. Kim, et al. [175] found that the air leakage was higher in winter and early spring than in summer months, and the seasonal variation was more noticeable for a leaky building. Similar findings were reported by Wahlgren [176], as he observed a variation of 8-10% in the building airtightness from summer to winter in three Swedish wooden houses.

Domhagen, et al. [177] also demonstrated the seasonal airtightness variation in wooden houses, which is likely caused by the varying humidity level. On the other hand, Bailly, et al. [178] found the variation is not very significant for concrete houses in France. In terms of the durability of building airtightness, Leprince, et al. [170] noted a decrease in the building airtightness during the first years after completion and then stabilised accordingly to their field studies.

- Wind and buoyancy effect

For the building airtightness measurement, there are two independent measurements, namely for pressure and airflow. It has been stated by Sherman, et al. [36] that a precision error for the fan pressurisation measurement could be attributed to wind variations because of the fluctuations during the pressure measurement. Modera, et al. [179] also indicated that wind could be a pernicious source of experimental error, leading to both precision and bias errors. When measuring the building airtightness, it is hard to measure the zero-flow pressure during the test, and the climatic conditions most generally cannot remain constant, especially because the wind could quickly change its intensity and direction [180]. In such a way, measurements are commonly recommended to be performed under low wind speed conditions or calm weather conditions. Based on the ISO 9972 standard, the overall uncertainty of the blower door test can be estimated using the error propagation calculation, which is lower than 10% under calm conditions, while it could reach up to ±20% in windy conditions [109]. More knowledge of the uncertainties due to wind for Pulse is also necessary as relevant uncertainty analysis is still limited in the literature.

2.5. Wind effect on building airtightness measurement

Outdoor natural wind could affect the internal pressure distribution and internal airflow within the building [181]. When the building openings are large, like windows, the peaks of the internal pressure may lead to risks of the structural stability of building components. Wind pressure, stack effect and mechanical ventilation are the direct forces that induce air flow within the building [182]. Kraniotis [61] demonstrated that the air exchanges across the building envelope generally resulted from wind and temperature, as depicted in Figure 2-20 produced by Liddament [65]. Besides, Shaw [183] mentioned that wind could potentially be the dominant mechanism, especially relatively small buoyancy forces for low-rise buildings. In addition, his experimental data implied that wind becomes the dominant driving force for infiltration when the temperature difference is less than 20K and wind speed is above 3.5m/s. Although infiltration measurement is different from airtightness measurement, such findings suggest that the wind can affect the pressure distribution within and around the buildings. Hence, a similar impact on the measurement of airtightness is presented.

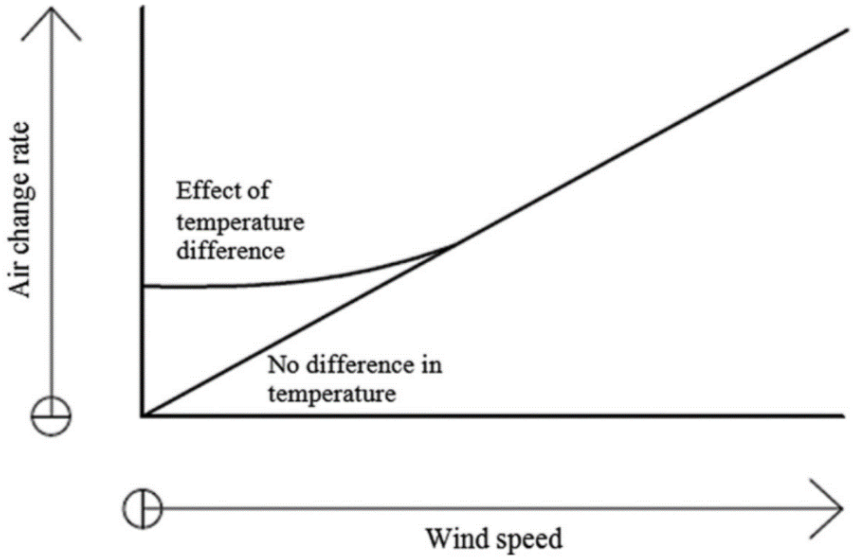


Figure 2-20: Infiltration characteristics with temperature and wind effect [65]

Owing to the variable wind speed and direction, different building penetrations would be generated, and the pressure inside the building closely relates to the outdoor wind condition as mentioned in the literature [38, 61, 184]. In addition, the effects of the wind direction and wind shielding are also critical for wind-induced penetration [185]. Researchers [175, 186, 187] observed that the uncontrolled nature of air infiltration and the complex aerodynamic phenomena which may take place around the building could indirectly affect the building pressure through the flow of small cracks. In fact, air infiltration in a building under the influence of wind pressure is a complex process, as it is strongly influenced by the turbulent characteristics of the wind [40, 188, 189]. In the numerical studies with the steady-state model, all driving forces and airflow through openings or fractures are generally averaged. For the sake of simplicity, the wind characteristics are usually represented by a typical average value at the reference height, namely the roof height or the meteorological height [190]. The fluctuations of the input parameter such as the wind speed and direction have not been widely considered for most simulation studies. In practice, even at the same wind speed, different effects will be caused due to different cracks or gaps distribution. For instance, the indoor pressure could not leak out if the direction of the leakage encountered a gust of wind. Nevertheless, the leakage speed could be accelerated if the leakage direction is in the same direction as that of a gust of wind, which causes the indoor environment with the negative pressure.

On the other hand, researchers have noted the impact of outdoor conditions on the building airtightness measurement, as air infiltration is fundamentally determined by the building airtightness. Therefore, requirements on the testing weather condition have been set in standards

for the steady pressurisation method. Examples of requirements are given in Table 2-5, including the standards of EN13829:2001, US ASTM E779-10 and the ISO 9972.

Table 2-5: EN13829, ASTM 779-10 and ISO 9972 requirements regarding the meteorological condition

	EN13829 [191]	ISO 9972 [109]	ASTM E779-10 [144]
Wind Speed	The wind speed must be Beaufort scale three or less. If measured, it should be meteorological wind speed 6m/s or less.	The strong wind shall be avoided. Recommendations: - wind speed near the ground ≤ 3m/s - meteorological wind speed ≤ 6m/s or ≤ 3 on the Beaufort scale	Low-wind pressure conditions: the wind speed is to be part of the measurement record, use a wind-measuring device or obtain readings from a nearby weather bureau. Preferred test conditions: 0-2m/s
Temperature	The product of the absolute value of the indoor/outdoor air temperature difference multiplied by the building height must be lower than 500m.K	Large indoor-outdoor temperature differences shall be avoided The product of the indoor/outdoor air temperature difference by the height of the building ≤ 250m.K	Outside temperature: 5°-35°C or 41°-95°F. The product of the indoor/outdoor air temperature difference by the height of the building shall be ≤ 200m.°C
Zero-Flow Pressure	The static pressure difference between the inside and outside of the building with the envelope closed up but with no test equipment running, must be less than 5Pa over a 30-second average.	The test is not valid if one zero low-pressure average (in absolute) ≥ 5Pa	To create a single zone for this test procedure, all interconnecting doors, except for closets which should be closed in the conditioned space, should be opened such that a uniform pressure will be maintained within the conditioned space to within ±10% of the measured inside/outside pressure difference.

For ASTM E779-10 and ISO 9972, a fan pressurisation multi-point test method is determined for characterising the air leakage of the building envelope. The EN13829 standard lists two principal test preparation methods, namely Method A and Method B. Method A measures the building when it is under normal operation (i.e., the building heating or cooling systems are running), with all air terminal devices of mechanical ventilation or air conditioning systems sealed and openings for natural ventilation closed. Method B measures the airtightness of the building envelope, with all mechanical ventilation or air conditioning systems closed and intentional ventilation openings sealed [192]. In particular, Method B adopts a multi-point test but requiring more items to be sealed for testing. It is worth noting that because of the differences in pre-testing building preparation and the required meteorological condition, the uncertainty of testing results based on the respective standard differs.

The influence of the weather condition leads to specific recommendations for wind velocity. For instance, the outdoor wind velocity for measuring building airtightness have been suggested to be no higher than 8m/s in the literature [193]. On the other hand, Kronyall [194] adopted "static wind loads and simplified load distribution models" and suggested a lower outdoor wind speed limit of 5m/s for building airtightness measurement. However, the wind speed limits mentioned in both studies did not clarify their respective wind speed reference heights. Standards specify various wind speed limits for the pressurisation method [195], such as Swedish standard SIS 021551, Norwegian standard NS 8200, American standard ASTM E779-81/ ASTM E779-10, Canadian General Standard (which is limited to depressurisation testing) and European Standard EN 13829. As listed in Table 2-6, the wind speed limits for different national standards vary, indicating the necessity of defining a more accurate value of acceptable wind speed for the Pulse test.

Table 2-6: Provisions regarding wind speed limit in five tests standards

Standard (Year)	**Wind Speed Limit**
American Standard ASTM E779-10 (2010) [144]	≤ 2.0m/s (ground wind speed)
American Standard ASTM E779-81 (1981) [196]	≤ 4.5m/s (ground wind speed)
Canadian Standard CGSB (1985) [197]	≤ 5.5m/s (meteorological wind speed)
European Standard EN 13829 (2001) [191]	≤ 6.0m/s (meteorological wind speed)
Norwegian Standard NS 8200 (1981) [198]	≤ 6.0m/s (meteorological wind speed)
Swedish Standard SIS 021551 (1980) [199]	≤ 10.0m/s (meteorological wind speed)

Although the impact of wind condition on the building airtightness measurement has been noticed, limited investigations have been implemented to clarify the wind effect on the building airtightness measurement both through the blower door and Pulse testing, and to provide a precise assessment of the building airtightness under variable wind conditions. Proceedings produced at 39th and 40th AIVC conferences (2018-2019) have been reviewed, and the relevant papers with their findings are summarised in Table 2-7. For instance, an overview of the requirements concerning wind velocity for the building airtightness measurement stated in the existing national standards is provided in the review paper by Mélois, et al. [51]. It can be found that the wind speed limit varies according to standards. Also, they emphasised the importance of considering wind fluctuations for assessing the uncertainty of building airtightness measurement. Lanooy, et al. [46] proposed a new approach to measure the building airtightness by using the existing fan pressurisation system to pressurise the building. Their testing mainly involved a reference vessel

and pressure sensor in measuring the fan pressurisation of the building relative to the pressure in the reference vessel. They stated that the advantage of measuring the reference pressure inside the building is that there is no need to use a building opening for outdoor pressure measurement and pressure variations over the building envelope because the wind effect could be averaged out. Their preliminary data demonstrated that the measurement was less sensitive to the wind conditions as data could be obtained on a windy day, which is not achievable for the blower door testing. Through a case study for a Spanish residential building, Taddeo, et al. [45] found that the air infiltration rate is a complex parameter affected by several factors, such as wind speed, wind direction and temperature gradient between the indoor and outdoor of the building. During their testing, wind speed and direction data were collected from a weather station that is 1km away from the building and corrected based on building height. They also pointed out that specific local wind distribution could be influenced by several factors, like wind gusts frequency. For the sake of simplicity, the related wind parameter was selected with the average steady speed value at the most frequent direction of each considered period. They also conducted testing to clarify the relation between air change rate, temperature difference and wind speed at low wind speed (<3m/s). They found that the change in the air change rate is less subject to the wind speed at a low wind speed condition. They also pointed out that the results could not describe the building airtightness in a complete way owing to the complexity of the combined effect, for example, variable building shapes, local wind distributions and wind gusts. It is noteworthy that many researchers mentioned the wind effect on the building airtightness measurement. However, comprehensive evaluations of the wind effect on the building airtightness measurement under different wind conditions are still needed to better understand the wind impact in real scenarios.

Table 2-7: Proceedings of 39th-40th AIVC conferences (2018-2019)

Authors	Topic	Findings Considering Wind Effect
Novák [52]	Assessment of durability of building airtightness	Outdoor wind may cause some deformations of the building structure, which affects the building airtightness. An estimation of the wind effect was considered for assessing the uncertainty of test results (for air change rate at 50Pa).
Remion, et al. [47]	Assessment of the performance of hybrid and natural ventilation systems	For models used on standards to compute air flow within buildings, data of the wind speed and direction are required. However, the unstable behaviour of the wind is difficult to predict accurately for simulation. The average of the wind introduced in empirical models resulted in huge uncertainties. Comparatively, CFD modelling can better account for the wind effect.

Authors	Topic	Findings Considering Wind Effect
Yamasawa, et al. [48]	Ventilation performance of natural ventilation building	The unstable wind condition would affect the natural ventilation of the interior spaces, thus making it difficult to predict the natural ventilation performance.
Sajima, et al. [49]	Ventilation performance of office building	
Breesch, et al. [55]	Ventilation cooling in a school building	
Marrero, et al. [53]	Effects of meteorological factors on CO_2 concentrations	Outdoor CO_2 concentration can be influenced by the level and the direction of the wind.
Mélois, et al. [51]	Review on wind speed in building airtightness test protocols	Based on the literature review, requirements regarding the wind condition for building airtightness measurement were compared among available national standards. Most of the existing studies considered steady wind (e.g., in numerical studies) and low wind speeds (e.g., experimental work), while in fact, tests are normally performed under unsteady and not a low wind speed level. The wind fluctuation may induce significant uncertainties on the measurement results as time variations in the measured pressures and flows can be induced.
Prignon, et al. [50]	Assessment of uncertainties in airtightness measurements using different regression methods	The comparison between the calculated uncertainty and the standard deviation using different regression methods showed that variable sources influenced the building airtightness measurement's uncertainty. The wind is one of the uncertainty sources when measuring the building airtightness. The mean wind speed with 10-minutes averages was adopted for assessment.
Qabbal, et al. [54]	Factors influencing the pressure homogeneity during airtightness testing	Parameters that are likely to influence the pressure distribution during the building airtightness testing in a large building were investigated through the numerical study. The results revealed that the pressure homogeneity was influenced when the air leakage was located in an incorrectly connected location and/or the leak was located in one place. However, the effect of the outdoor wind speed and temperature has been neglected as very low and steady wind speed was assumed in the numerical study.
Lanooy, et al. [46]	New method to measure building airtightness	A new methodology was proposed to determine the building airtightness by pressurisation with the existing building fan system. The newly developed method for measuring the building airtightness was found to be less subject to the outdoor wind condition as the wind fluctuations are averaged out over the whole building envelope.

Authors	Topic	Findings Considering Wind Effect
Taddeo, et al. [45]	Comparison of experimental methodologies to estimate air infiltration rate	The obtained experimental results of the air infiltration rate indicated that the wind speed, the wind direction and the outdoor temperature were critical parameters. Although these factors clearly influenced the external air infiltration rate, it was hard to completely describe the building airtightness due to the complexity of the phenomenon, such as the building shape, local wind distribution and wind gusts.
Pasos, et al. [44]	Measurement of building infiltration and air leakage rates	Different weather conditions were monitored during testing, including the wind and temperature conditions in the constant concentration tracer gas test. The results showed that the high wind speed had a relatively greater impact on the Pulse test at lower pressures. Under the high wind speed condition, the lower range measurements should be discarded for the Pulse test data analysis to minimise the wind impact on the Pulse test.
Novák [200]	Influence of the external pressure tap position on the airtightness test result	The position of the external pressure tap may influence an airtightness test result. The influence of the external pressure tap position on the airtightness measurement would be amplified with the increasing wind speed. The averaging of multiple readings as placing the external pressure taps at different locations led to high R^2 value as required by the ISO 9972 standard and, hence, reduced wind impact on the measurement results.
Delmotte [201]	Airtightness of buildings – Considerations regarding place and nature of pressure taps	The static pressure taps were used and placed away from the building and possible obstacles to minimise the measurement uncertainty with the fan pressurisation method.
Rolfsmeier [202]	New findings on measurements of very airtight buildings and apartments	Measuring equipment was recommended to be installed on the downwind side (lee side) of the tested building and to measure the outside building pressure there under windy conditions. More points above 50Pa should be measured at windy conditions. Different pressure stages should be controlled more slowly and possibly for greater tolerance. Longer measuring time is recommended for accuracy.
Mélois, et al. [203]	Designing a model-scale experiment to evaluate the impact of steady wind on building air leakage measurements	A model-scale experiment was designed in the controlled laboratory condition using a wind tunnel. The design of the wind tunnel was optimised to provide steady wind with wind speed ranging from 0-12m/s. Only test design and arrangement were presented, and the corresponding results were not provided in the paper.
Kraniotis, et al. [204]	CFD modelling of fan pressurisation method in buildings – The impact of dynamic-wind on airtightness tests	A CFD-based numerical study was presented for investigating the impact of the unsteady wind on the airtightness measurement using the fan pressurisation method. Two houses were modelled in cross-laminated-timber (CLT) under different scenarios (e.g., various leakage locations, fan placement, and wind profiles). Even when the fan placed leeward, the wind speed above 6m/s resulted in a great uncertainty (e.g., 40-60%) in the depressurisation test.

2.6. Current work on addressing the wind effect on the building airtightness measurement

A number of studies have been conducted to address the uncertainties of the building airtightness measurement associated with the wind effect. Based on the literature review, both numerical investigations (e.g., numerical modelling and CFD transient modelling) and experimental testing have been conducted to investigate the wind impact on the building airtightness measurement, including the background pressure measurement, wind speed and wind fluctuations during the test. At the end of this section, Table 2-9 presents a summary of detailed reviews on representative studies that have been conducted in recent years to investigate the impact of wind on the measurement of building airtightness. Their respective key findings with limitations are summarised and discussed respectively, and the research gap is identified, which this research will aim to fill.

2.6.1. Wind speed and wind fluctuation during testing

It has been noted that a proper definition of wind speed is hard to find in the existing literature. Typically, there are two different definitions of wind speed: (a) the meteorological wind speed, which represents wind speed at 10 meters from the ground and (b) the local wind speed representing the wind speed at the height of the building. Additionally, the ISO 9972 standard provides another wind speed reference, which is the wind speed near the ground. Due to different wind speed references, confusion might occur, and significant differences can be noticed for measuring or calculating wind speed [27, 205, 206]. It is found that researchers employed different definitions of wind speed for investigating the wind effect on building airtightness measurement, and sometimes the wind speed was not clearly indicated. For instance, Walker, et al. [56] directly employed wind speed and direction taken from meteorological towers at the test site, while Bailly, et al. [173] adopted the wind speed at the height of the wall of 10m. Another issue is that the wind speed is usually measured only before and after the test, while the variation in wind speed during testing is ignored. The fact that the wind enters the room directly from the blower door during the test could also introduce the error into the measurement. Mean wind velocity is commonly used for investigating the effect of wind conditions on building airtightness measurement. For example, Kraniotis, et al. [184] used an ultrasonic anemometer to monitor the outdoor wind characteristics, such as the direction angle and the instantaneous velocity. They carried out seven measurements with mean wind speed ranging from 2.9m/s to 5.3m/s. Carrié, et al. [41] studied the uncertainties in building pressurisation tests by focusing on only steady wind model error stemming from the

heterogeneous pressure distribution around the building. They used mean wind speed at the building level ranging from 0 to 10m/s for simulation with both one-point and two-point methods. The results demonstrated that the uncertainty caused by the wind effect on the estimated air flow rate was relatively small at the high-pressure point but significant at a low-pressure point. It might be essential to propose a standard to regulate the measurement of wind speed at an agreed reference height so that such misunderstandings could be avoided.

On the other hand, the unsteady wind is identified as a factor of uncertainty towards an accurate estimation of air exchanges in natural ventilation studies [207]. The associated impact of wind fluctuation on natural ventilation has been well discussed in the literature. Table 2-8 presents a list of some research work with their main findings.

Table 2-8: Studies of the impact of wind fluctuations on natural ventilation

Authors	Year	Key Findings
Cockroft, et al. [208]	1976	A theoretical pulsation flow model studied the ventilation of an enclosure with a single opening subjected to a turbulent impinging airstream. The simulation indicated the magnitudes of ventilating airflows that may be generated by turbulent wind. They mentioned that the turbulent nature of wind caused air diffusion through openings and cracks in the building envelope.
Phaff, et al. [209]	1980	An empirical correlation to predict the ventilation rate across an opening or a crack was provided by considering both buoyancy forces and wind phenomena. Their results implied that the fluctuating wind was only represented by an additional pressure drop as a function of the flow exponent *n*.
Ethridge, et al. [210]	1980	An air infiltration predictive model for multi-cell buildings was developed to evaluate the impact of wind fluctuation. Based on obtained data, they thought that additional ventilation resulting from turbulence only occurs when the fluctuations are large enough to cause flow reversal. They also proposed an additional term to quantify the occurrences of large mean pressures.
Sasaki, et al. [211]	1987	Their results indicated that the air flow fluctuation through the cracks could be influenced not only by the static resistance of the crack but also by the crack depth, the air volume behind the crack, and the wind fluctuations. However, the computation requirements for solving linear differential equations might restrict the practical application of the model.
Crommelin, et al. [212]	1988	Work was conducted using a scale model in a wind tunnel to predict the ventilation rate through a single opening using N_2O as a tracer gas. Empirical coefficients to calculate the isothermal ventilation caused by the wind and the turbulence in the tunnel were derived.
Haghighat, et al. [213-215]	1991	A power spectrum analysis linearization technique was adopted to model pulsating airflow due to turbulent wind-induced pressures. The concept of aerodynamic admittance functions was employed to modify the wind pressure spectra for deriving the average fluctuating wind pressure over an opening.
Dascalaki, et al. [216]	1995	A correction factor for enhancing the existing ventilation work was proposed based on the Grashof and Reynolds numbers by taking into account the dynamic characteristics of wind.

Authors	Year	Key Findings
Etheridge [217, 218]	2000	They presented numerical results of unsteady wind pressures on the instantaneous flow rates in certain types of purpose-designed naturally ventilated buildings. The data show that inertia reduces the occurrence of flow reversal and may impede the reestablishment of the correct flow when the reversal is formed by some hysteresis effect.
Miguel, et al. [219, 220]	2001	Details were described for air infiltration in enclosed space. The momentum equation was established for a mathematical model to characterise air infiltration induced by fluctuating pressures. It is proved that their method can be used for simulating enclosures with a porous material (ventilation filters or screens) and apertures. Their experimental data validated the developed method.
Wang, et al. [221]	2012	An empirical model was developed for estimating the mean and the fluctuating ventilation rate of wind-driven natural ventilation. The simulation data showed the ventilation rate and wind velocity were linearly correlated.
Ai, et al. [222]	2014	A large eddy simulation (LES) model combined with the tracer gas concentration decay method was used to assess the fluctuating ventilation characteristics through a single opening under different wind directions. Based on their results, they pointed out that for windward ventilation, the velocity and pressure fields around the opening were relatively stable in terms of windward ventilation, which limited turbulence diffusion across the opening, while for lateral ventilation, the velocity and pressure fields were very unsteady. It indicated that wind direction greatly affected the airflow exchange at a single opening.
Mahrt, et al. [223]	2015	The dependence of turbulence quantities on wind speed and stability was examined with nocturnal data. A good agreement with previous studies was found. The turbulent velocities increased slowly with wind speed until the wind speed increased to a transition and then increased more rapidly with further wind speed. The data also showed that the impact of stratification was relatively small for the weakest winds. Owing to the influence of stratification and site-dependent non-stationarity in the weak-wind regime, the relationship between the turbulence and the wind speed could not be regarded as universal.
Antoniou, et al. [224]	2017	New ventilation indicated, namely air delay, was introduced to describe the outdoor urban ventilation. CFD simulations using Reynolds-Averaged Navier-Stokes (RANS) and Large Eddy Simulation (LES) approaches were conducted for ventilation simulation in a dense district, and comparison was given between the two approaches. Simulation results demonstrated that the LES was more capable of accurately predicting the mean wind speed and turbulence intensity in a complex urban area.

For most of the existing literature in the field of building airtightness, a steady wind condition has been commonly considered or assumed in numerical studies, and the low wind speed condition is preferred for experimental work. For instance, Walker, et al. [56] only selected measurements under low wind speed conditions (i.e., meteorological wind speed less than 3m/s) for analysis. Another limitation of their studies is the lack of assessment with consideration of wind fluctuations like gust frequency. In practice, building airtightness measurements could be conducted under unsteady wind conditions rather than only at very low wind speeds and the same direction. It has been found that the wind fluctuation could result in noticeable uncertainties

because the measured pressure and air flow vary during the testing period. A number of researchers have discussed the impacts of wind fluctuation on building infiltration. In the thesis of Kraniotis [61], a multivariate model considering the wind speed, direction, gustiness and gust strength was developed to estimate the infiltration rates of a building and to provide a better understanding of the wind effect. The results demonstrate that the steady-state wind characteristics are not precise enough to describe neither the dynamic behaviour of air infiltration nor the dynamics of indoor airflow. He found that wind gustiness has a key role in calculating air infiltration rate. Along with other wind characteristics, like the wind speed and direction, gusts have the potential of governing the resultant air exchanges that take place across the leakage paths of the building envelope. The research is limited to low-rise buildings.

The leakage distribution and rate that correlates with unsteady wind phenomena have not been identified, and more measurements of leakage rates in buildings could be conducted to provide a better understanding of air infiltration under natural conditions. In another study, Kraniotis, et al. [225] studied the impact of wind direction and wind gust frequency in a cross-infiltrated single-compartment building numerically. A parametrical study of the external leakage distribution was carried out and finally linked to wind gustiness based on CFD transient analysis. It has been seen that the wind gust frequency increases the estimation uncertainty of the building infiltration rate. In addition, when the gust frequency is high, even the oblique angles could result in relatively high leakage rates. They also pointed out that the location of leakage paths and the distribution on the building envelope is another factor causing the air exchange rate variation, especially under more severe wind gust conditions. However, the study only accounts for two scenarios of wind gust frequency (i.e., Ω_{high}=0.5Hz and Ω_{low}=0.1Hz) and five angles of wind direction, it may not be precise enough to reflect the exact climatic condition. In another study conducted by Kraniotis, et al. [184], tracer gas techniques were employed to measure the infiltration rates of a room, and the dynamic wind characteristics were analysed in the frequency domain (i.e. spectral analysis and Fast Fourier Transform). A good agreement was observed with the numerical simulation in [225], that the high wind fluctuation frequency led to the potential of a higher air change rate. As airtightness fundamentally determines the air infiltration, wind fluctuation could also affect the measurement of airtightness. However, based on the review, it can be noted that explorations of the effect of wind fluctuation on the building airtightness measurement are still needed, in particular comprehensive investigations on various wind conditions using both the blower door and Pulse methods.

2.6.2. Background pressure measurement

Due to the fact that the wind pressure induced on the upwind façade and the other building façades are not identical, the position of the installed pressure probe also affects the testing results [226]. It has been proved that the pressure uncertainty caused by the wind and by instrumentation inaccuracies is one of the major sources of uncertainty for the fan pressurisation measurement. Modera, et al. [179] proposed a methodology to reduce the effect of wind on the fan pressurisation test by using multiple fan pressurisation measurements at a single site and employing four-surface pressure averaging and time averaging of pressure and flow data. The data evidently showed that the combined surface-averaging and time averaging technique significantly reduce the uncertainty under the calm conditions, and the uncertainty remains below 11% when the wind speed increases up to 5m/s. Therefore, they recommended using the surface-pressure averaging for a more accurate building airtightness measurement. Based on the simulation using single-zone building under isothermal conditions, Leprince, et al. [39] suggested that it is necessary either to have a constraint on the wind speed with a maximum of 6m/s or to have a constraint on zero-flow pressure at a maximum pressure of 5Pa to address the uncertainty caused by the steady wind on building airtightness measurement.

On the other hand, Novák [200] conducted an experiment to quantify the variability of the airtightness measurement results under repeatable conditions with different external pressure tap positions in the function of the wind speed. Novák found that the impact of external pressure tap position was not noticeable on the repeatability under the testing wind conditions (according to ISO 5725-6 standard), that may be because of the low wind speed and some technical measures, such as T-pieces, longer recording period and distance of the pressure taps from facades. Based on the experimental investigation, he thought multiple tests by placing external pressure taps at different places could contribute to a more accurate reading with reduced uncertainty owing to wind impact. For future work, he recommended a more extensive experiment under more variable wind conditions.

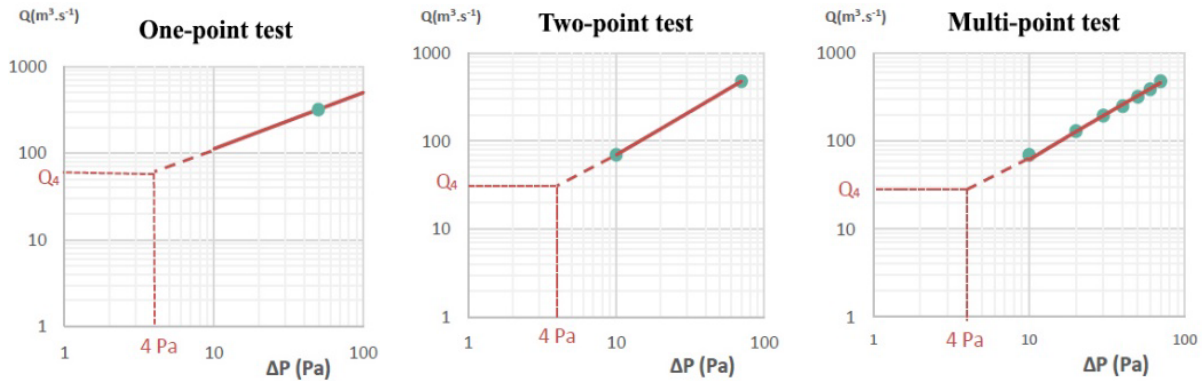
Similarly, Delmotte [201] discussed the effect of the nature of the pressure tap and the place of the external pressure tap on building airtightness measurements. The effects were attributed to the wind impact on the building and the dynamic pressure that the wind-generated. Based on his findings, he stated that it is important to use static pressure taps and place them away from the building and possible obstacles.

For airtightness measurements using the fan pressurisation method, the zero-flow pressure approximation has not been widely taken into account for calculating uncertainties. To address

this issue, Prignon, et al. [227] demonstrated a method to quantify this source of uncertainty in airtightness measurement. They adopted the method for 31 zero-flow pressure tests on a newly constructed apartment within 15 days in Brussels, Belgium. They recommended multi-level modelling to estimate the uncertainties due to the zero-flow pressure approximation. Their findings indicated the noticeable impact of zero-flow approximation on the regression technique, as uncertainties in zero-flow pressure account for more than 75% of the envelope pressure uncertainties regardless of the wind conditions. Based on measurement results, they noticed the zero-flow pressure approximation uncertainty was ±0.45Pa, ±0.91Pa and ±1.52Pa, respectively, under low, medium, and high wind conditions. However, a reduction in the uncertainty could be obtained when a longer zero-flow pressure measurement period was enabled. The approximation period should be increased to 60s on medium-wind days as the uncertainty could be reduced by 11%, and 90s on high-wind days with an uncertainty reduction of 9%.

2.6.3. Experimental studies of addressing the wind impact on the building airtightness measurement

Mélois, et al. [51] summarised three different test methods for building pressurisation testing, namely one-point, two-point and multi-point test methods, illustrated respectively in Figure 2-21.



(a) (b) (c)

Figure 2-21: (a) One-point, (b) Two-point and (c) Multi-point test methods [51]

Walker, et al. [56] assessed the one-point and multi-point testing to determine building leakage at 4Pa. The uncertainty of the testing results has been assessed, and comparisons have been conducted based on two large datasets containing thousands of fan pressurisation tests. Multi-point testing was recommended based on their results, as 90% of the multi-point tests provided lower errors in estimating the building envelope leakage at 4Pa. For instance, at the meteorological wind speed below 6m/s, the total error of a multi-point test reduced by 10% compared with that of the one-point test. For standards like ASTM 779-03 and ISO 9972, the multi-point test method is also preferred.

To minimise the wind impact, Rolfsmeier [202] suggested the installation of measurement equipment could be on the down/leeward building side, and multiple tests above 50Pa (EN 13289 and ISO 9972 standards) are needed to measure the building airtightness. Also, they recommend the slow control of different pressure stages for greater tolerance and longer measuring time for increased accuracy. According to their findings, they stated that the measuring time for one measuring point, which normally takes 10-15s, could be extended to 60-120s under gusty wind conditions. Most of the investigations addressing the wind impact on the building airtightness measurement have been conducted for the fan pressurisation method, while limited studies related to the test performance of the Pulse test under different wind conditions have been found in the literature. Cooper, et al. [32] conducted the Pulse tests in a range of UK homes under various environmental conditions, and repeatability of ±8% was obtained for repeated tests in a detached house over a year. They also observed the wind speed and direction have the greatest impact on the variation of measured air permeability.

On the other hand, Zheng, et al. [150] conducted a repeatability assessment to the Pulse test by using a multi-gear portable trailer fan to provide various artificially imposed steady wind conditions. They found that a small uncertainty (i.e., within ±3%) was obtained when the wind speed was below 3.5m/s at 1.5m above the ground level. However, the uncertainty increased up to ±25.6% when the wind speed was increased to 9m/s.

2.6.4. Numerical studies of addressing the wind impact on the building airtightness measurement

Regarding the investigation of wind effect on the building airtightness measurement, the majority of current works are based on numerical modelling and simulations for pressurisation testing. Table 2-9 summarises the findings and limitations of the numerical studies investigating the wind effect on the building airtightness measurement. Kraniotis, et al. [225] conducted a CFD-based numerical study for investigating the impact of unsteady wind on airtightness measurement using the fan pressurisation method. They modelled two test houses in cross-laminated-timber (CLT) and simulated various leakage locations, fan placement and wind profiles. In terms of the steady-state, the impact of various wind speeds on airtightness tests was analysed, while for the transient analysis, the turbulent wind was considered. Historical data about surface roughness and wind speed at the height of 10m have been collected and used as the input of the wind profile. Based on their simulation results, they noticed that even when the fan was placed leeward, the wind speed above 6m/s resulted in great uncertainty (e.g., 40-60%) in the depressurisation test. A numerical evaluation of the wind effect on testing uncertainties has been conducted by Carrié, et

al. [41] using both one-point and two-point methods. Their simulation results implied that the maximum combined uncertainty at a reference pressure of 4Pa was worse for the two-point method than in one-point with a full range of leakage distribution. It could be pointed out that the selection of the test method for measuring building airtightness depended on the wind condition, so it is critical to choose a proper method in order to minimise uncertainties owing to the wind effect. Bailly, et al. [173] suggested that the measurement of building airtightness could be valid when wind speed was lower than 8m/s, which has not been well stated in the ISO9972 standard. Also, two sets of measurements in the pressurisation and depressurisation tests were needed to minimise the wind impact on the building airtightness measurement. On the other hand, Carrié, et al. [57] proposed an approach to quantify uncertainties of one-point pressurisation tests under periodic wind conditions. The impact of wind fluctuations should be considered for practical measurement, as their simulation results demonstrated that the wind fluctuation could yield much larger uncertainties than the average wind alone during the pressurisation test. Nevertheless, very few numerical studies have been noted in the literature for addressing the wind impact on the building airtightness measurement using Pulse.

Table 2-9: Review on numerical studies of the wind effect on the building airtightness measurement

Authors	Year	Key Findings and Limitations
Bailly, et al. [173]	2012	**Key Findings:** Simulations of the measurement protocol with software CONTAM were conducted under variable wind conditions and airtightness levels. Three main impacts on the uncertainty were mentioned: wind speed, leak distribution and pressure correction with zero-flow pressure difference. Referred to ISO 9972 standard, they further suggested that valid tests could be conducted when wind speed was lower than 8m/s. They also found that the wind impact greatly depended on the leakage distribution on the envelope instead of airtightness level. To minimise the wind impact on building airtightness measurement, they recommended that both pressurisation and depressurisation measurements are needed.
		Limitations: The numerical study adopted a single-zone model building for an investigation. The stack effect has not been included, and simulations were conducted under isothermal conditions. The wind speed was defined on the basis of 10m height with a range of 0-9m/s, and it was treated as constant during testing, which could not exactly reflect the real scenario as the wind fluctuation was neglected.

Authors	Year	Key Findings and Limitations
Kraniotis, et al. [225]	2013	**Key Findings:** Through CFD simulation, the impact of wind direction and wind gust frequency was investigated for a cross-infiltrated building. The results demonstrated that high wind gust frequency increased the uncertainty of estimating the building infiltration rate. In addition, when the gust frequency was high, even the oblique angles could result in relatively high leakage rates. They also pointed out that the location of leakage paths and distribution on the building envelope was another two factors causing air exchange rate variations, especially under more severe wind gust conditions.
		Limitations: In this transient analysis, only two scenarios of the wind gust frequency (i.e., Ω_{high}=0.5Hz and Ω_{low}=0.1Hz) and five angles of the wind direction were defined for simulation. It is hard to predict and describe the wind fluctuation based on the limited observations. In order to validate the developed numerical model, reliable experimental data under the real testing condition is needed.
Walker, et al. [56]	2013	**Key Findings:** Through two large datasets of blower door measurements, the associated uncertainty was assessed for both one-point and multi-point tests. The data implied that multipoint testing was comparatively better at estimating equivalent leakage area at 4Pa than one-point testing. Compared with the total error of the one-point test, the total error of the multi-point test was reduced by 10% under meteorological wind speed below 6m/s and 25-30% under meteorological wind speed above 6m/s.
		Limitations: The wind speed and direction were directly taken from the meteorological tower at the test site. However, wind fluctuation like gust frequency has not been considered. Some tests were eliminated due to the above limits on pressure exponent or lack of a low wind speed test.
Kraniotis, et al. [184]	2014	**Key Findings:** By adopting the tracer gas technique, the infiltration rates of a room were estimated through the CO_2 decay method, and the dynamic wind characteristics were analysed in the frequency domain. An ultrasonic anemometer was used for monitoring outdoor wind characteristics, like the direction angle and the instantaneous velocity. Moreover, the turbulence intensity was calculated, and spectral analysis was performed to identify the dynamic characteristics of the unsteady wind. The results indicated that high wind fluctuations frequency led to the potential to cause a higher air change rate.
		Limitations: Seven measurement periods were presented in the study, and the mean wind speed ranges only from 2.9 to 5.3m/s. More data could be produced for a more detailed view of the wind-driven infiltration, especially in cases where the wind effect was more significant than the buoyancy forces. Also, results were needed to clarify the role of the wind fluctuation frequency with investigations of the local building dynamic phenomena to find the leakage magnitude and distribution.

Authors	Year	Key Findings and Limitations
Carrié, et al. [41]	2016	**Key Findings:** The wind effect on uncertainties in building pressurisation tests were quantified and assessed using a simplified isothermal model. Both one-point and two-point methods were adopted for simulation. They looked more specifically at the governing equations to provide the airflow rate through the blower door as a function of wind speed. It was noted that the model error due to the wind on the estimated airflow rate was relatively small at the high-pressure point, while it became significant at a low-pressure point.
		Limitations: The isothermal model only quantifies the uncertainties in the building pressurisation tests; however, its effect on the depressurisation test for the blower door method has not been considered. In the simplified model, the stack effect was not considered, and the building was assumed as one single pressure zone. In addition, the presented simulation focused on only the steady wind model error stemming from the heterogeneous pressure distribution around the building. The steady wind velocity ranged from 0-10m/s. The effect of the wind fluctuation has been excluded.
Leprince, et al. [39]	2018	**Key Findings:** The study is an updated work of [41]. The data indicated that the error lay within 12% for wind speeds up to 10m/s at 50Pa; however, it could reach up to 60% at the low-pressure point (i.e., 10Pa). In addition, the uncertainty owing to wind became dominant at 5m/s for 10Pa and 4m/s for the two-point test extrapolated at 4Pa. They suggested that 6m/s is a relevant limit value for the high-pressure station (50Pa) but is too high for low-pressure measurements.
		Limitations: The building was simply represented by a single zone, and tests were performed under isothermal conditions. For their measurements and analysis, several sources of uncertainty have not been considered, such as the wind fluctuation, the leakage with variable flow exponents, the linear regression, the thermal draft, the tester behaviour, and the building preparation.
Carrié, et al. [57]	2020	**Key Findings:** The study is an extended work of [41]. Studied a new numerical approach to simulate the impact of periodic wind on the one-point pressurisation test by assuming leaks as perfect sharp-edged orifices. Simulation results proved the noticeable impact of wind fluctuations and wind frequency on measurements with larger uncertainties. Also, they pointed out the importance of considering zero-flow pressure uncertainty for accurate measurement.
		Limitations: The building for simulation was idealised, with all leaks on the windward side were represented as a single sharp-edged opening. The simulation was limited to the one-point pressurisation test at a given pressure station based on the few test cases that were previously conducted. The simulation of the periodic wind condition was based on a simple relationship of the wind pressure by ignoring the time lag issue between the upstream and downstream wind signals.

2.7. Summary and literature gaps

The building airtightness has been seen as a critical indicator of building quality and building energy efficiency. The steady pressurisation method has been applied widely as a standard method for measuring the building airtightness, while Pulse offers an alternative solution for providing new metrics. It is expected that the adoption of Pulse as an alternative airtightness test method for new buildings will be included in the forthcoming revisions to the Approved Documents providing guidance on Part L of the Building Regulations in England and Wales, there is a need to conduct more in-depth explorations of the Pulse test.

Based on the review of the literature, extensive studies on the building airtightness measurement have been carried out either through experimental or numerical work, from different perspectives, such as improvements in the measurement technique with associated accuracies and addressing the uncertainties resulting from various sources. A number of studies have been identified in the literature exploring the wind effect on measuring building airtightness and proposing solutions to minimise the wind effect, mostly focused on the steady pressurisation method, i.e., the blower door. These investigations have taken the direction of different perspectives, such as understanding the uncertainties caused by the zero-flow pressure measurement and the steady wind and wind fluctuations through numerical and experimental approaches. However, some studies focused on only the steady-state wind characteristics, which is not adequate to entirely describe the dynamic behaviour of air infiltration and indoor airflow pattern. In such a way, an incomplete image of the real energy consumption of a building may be provided due to neglecting the dynamic characteristics of wind and infiltration. The current work addressing the unsteady wind effect only contains limited simulations or field tests, which is not comprehensive enough to reflect the real climatic condition as the wind fluctuations are unpredictable and changeable.

Therefore, the research gap has been highlighted as limited studies have been conducted to explore the impact of the wind condition on the Pulse measurement through field testing and numerical simulation. This could contribute to a more comprehensive evaluation of the uncertainty of measuring building airtightness with the Pulse testing. Improvements in protocols that are used to characterise building airtightness measurement could also be realised with the inclusion of consideration of wind effect.

3. Insights into Airtightness Measurements Using the Pulse and Blower Door Testing

3.1. Introduction

The well-known blower door is a steady fan pressurisation method that is implemented typically in a range of high pressures (i.e., 10-60Pa), while the newly developed Pulse adopts an unsteady approach in a range of low pressures (i.e., 1-10Pa). Along with the development and validation of Pulse, a number of research have been conducted to compare both test methods from different perspectives. Some comparisons were made based on a single-point assessment by mainly focusing on the common pressure levels (i.e., 4Pa and 50Pa). Therefore, one of the tests should be extrapolated for a direct comparison, which results in noticeable extrapolation errors (e.g., up to ±50%) between low pressure and high pressure [32, 148]. Due to the lack of measurement in higher pressures (e.g.,>10Pa), a more significant error occurs in the exploitation of the Pulse testing to 50Pa. To achieve direct comparisons over a wide range of pressure levels, comparative studies were conducted in small-volume chambers (13-21m^3), such as 15-50Pa and 5-23Pa as reported in studies [174, 228]. A good agreement of airtightness measurement in the sheltered condition was obtained between the two test methods, with a maximum discrepancy of 7.4%.

This chapter aims to provide complementary insights into both test methods from different perspectives and also establish a baseline for further investigation. Experimental work was performed in a five-bedroom dwelling in the UK under natural environment conditions using both Pulse and blower door methods. Due to the dwelling volume and equipment limitation, the testing pressure level range in this comparison study is 6.9-72.3Pa for blower door testing and 3-10.6Pa for the Pulse testing, respectively. All measurement data are extrapolated based on the Power law in order to compare the test methods over a wide pressure range from 2Pa to 70Pa. Also, single-point assessment is conducted by extrapolating airtightness measurement results based on the Power law to compare the measurements at the same pressure level of 4Pa and 50Pa. A direct comparison between the two methods is provided over the overlapped pressure level range regarding the measured air leakage rate and overall error associated with measurements.

3.2. Methodology

3.2.1. Dwelling

According to the English Housing Survey, the average (mean) usable floor area of English dwellings in 2018 was 94m^2 [229], and if multiplied by a typical floor to ceiling height of 2.5m, the average property volume is about 235m^3. According to the English Housing Survey [230], the mean usable floor area by dwelling type is presented in Figure 3-1. It can be seen that the majority of dwelling types have a mean volume below 300m^3, while the detached house has a mean volume of 381m^3.

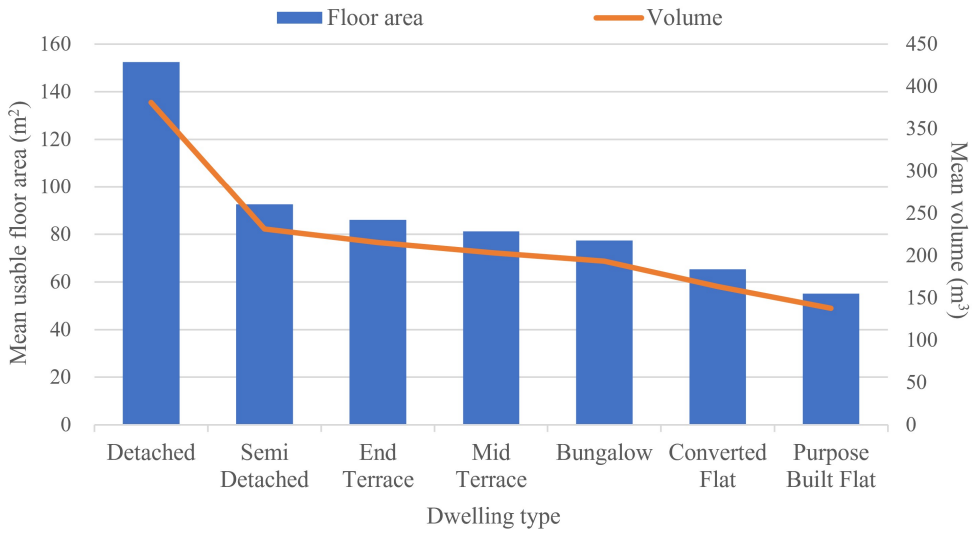


Figure 3-1: Mean usable floor area by dwelling type [230]

A five-bedroom detached house located on the University of Nottingham's University Park campus was chosen as the test building. Figure 3-2 shows the front and back views of the dwelling and the surroundings, and Figure 3-3 presents the floor plans with dimensions. The house has one bedroom, one living room, one kitchen on the ground floor and four bedrooms on the first floor.



(a)

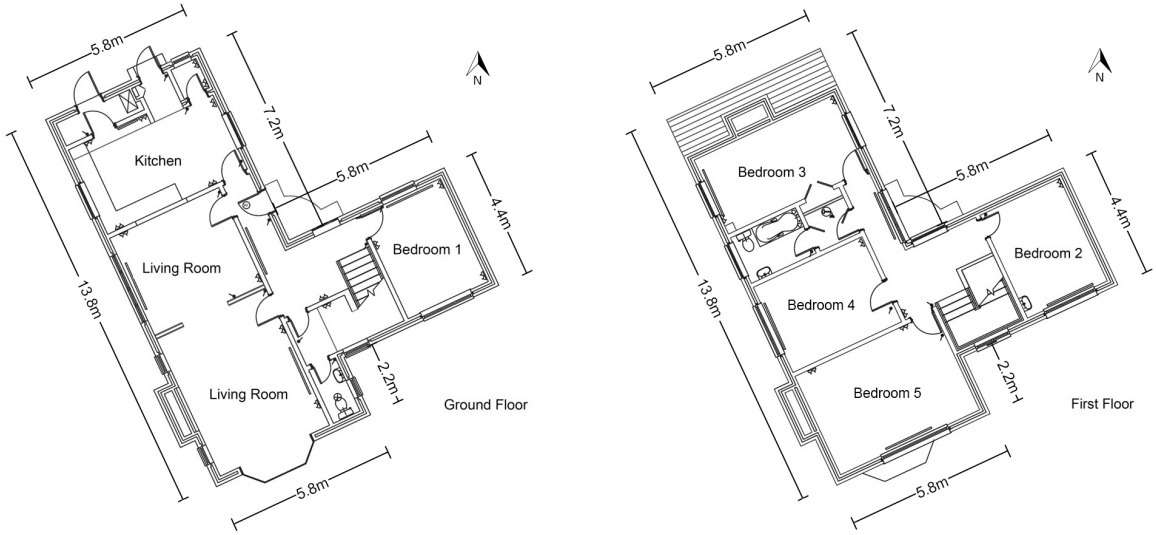


(b)



(c)

Figure 3-2: Photos of the tested dwelling (a) front view, (b) back view and (c) surroundings



(a) (b)

Figure 3-3: Building plans of the tested dwelling (a) ground floor and (b) first floor

The tested dwelling is a typical UK residential house, and the building parameters are listed in Table 3-1. This house has a volume of 447m^3, which is above the average volume of detached houses, as seen in Figure 3-1. Therefore, the size of this house is large enough to represent the worst-case scenario, providing a good case for comparing the two test methods in a building of large volume with challenges of pressurisation and achieving the uniform pressure distribution.

Table 3-1: Tested dwelling parameters

Dwelling	Wortley 5 - University of Nottingham, University Park, Nottingham
Type	Five-bedroom detached house
Year	Built in 1950 and retrofitted in 2018
Volume (m^3)	447
Envelope Area (m^2)	416

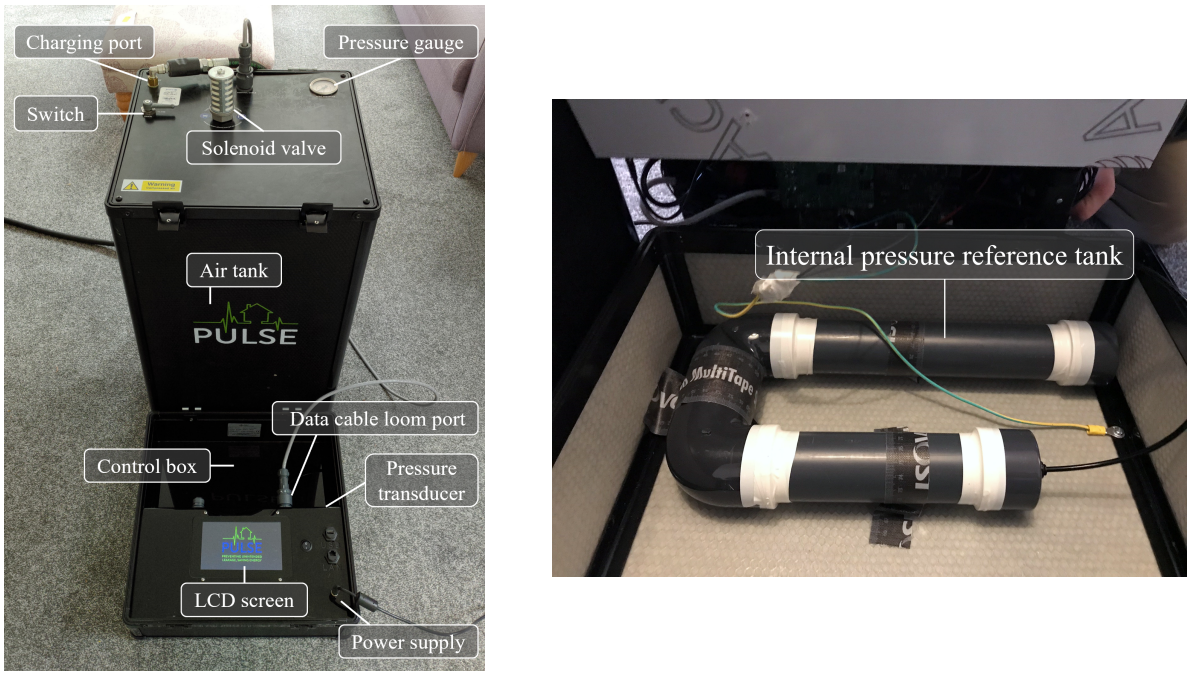
3.2.2. Equipment setup and test arrangement

A number of devices were used for this experimental work, as listed in Table 3-2.

Table 3-2: List of test equipment

Airtightness	Others
PULSE-60	Ultrasonic anemometer (WindSonic™)
	Differential pressure transducers (FCO44)
Duct Blaster series B (DBB)	Temperature sensors (PT100 RTD)
	Data loggers (Datataker DT85)

A PULSE-60 unit was used, as shown in Figure 3-4(a), which consists of a 58.5-litre lightweight aluminium air tank and oil-free compact air compressor. A ¾ inch (BSP) solenoid valve was installed at the outlet, allowing the release of the compressed air from the air tank into the indoor spaces. In addition, the Pulse test data, such as the chamber and tank pressures, were recorded and analysed by the on-board PULSE-60 control box, with results displayed on the LCD screen, as seen in Figure 3-4(a). Uniquely, an internal pressure reference tank is constructed inside the control box of the PULSE-60, as shown in Figure 3-4(b). An automated valve is installed on the internal pressure reference tank, which normally is kept open for an equalised pressure inside the tank with the ambient environment and closed once the test starts to provide a reference pressure. In this study, a complete three-step Pulse test consists of three consecutive pulses, namely S1, S2 and S3 (i.e., three separate pulses are achieved from one compressed air tank without recharging).



(a) (b)

Figure 3-4: Photos of (a) PULSE-60 unit and (b) internal pressure reference tank of PULSE-60 unit

For the blower door test, Duct Blaster series B (DBB), which is manufactured by The Energy Conservatory (US), was employed. A photo of the DBB unit is presented in Figure 3-5. The unit is mainly composed of an adjustable doorframe, a flexible canvas panel, a variable-speed fan, a DG-1000 digital pressure and a flow gauge. An exterior pressure tap was placed outside at some distance away from the building (i.e., 3m) but not close to any obstacles to measuring the outside pressure as the reference pressure value.

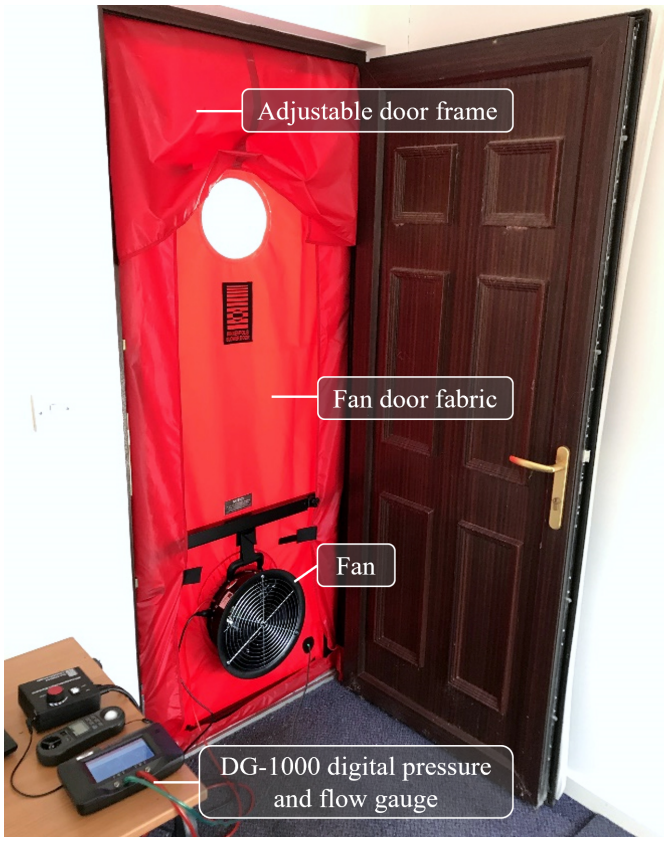


Figure 3-5: Energy Conservatory Duct Blaster series B

In order to obtain the weather condition during testing, an ultrasonic anemometer was applied to monitor the outdoor wind condition with an accuracy of ±3%, as seen in Figure 3-6(a) and Figure 3-6(b), and thermocouples were used to measure ambient temperature. The anemometer was installed at the height of 2.2m above the ground in the backyard and a distance of 12m away from the perimeter of the test building. Figure 3-6(c) and Figure 3-6(d) provide photos of the surrounding environment of the ultrasonic anemometer; there were no significant obstructions within a radius of 12m of the anemometer in the open backyard, except for sparse tree branches and grass on the ground. A Datataker DT85 data logger was used for the acquisition of the weather data, with an accuracy of ±0.1%. All employed instruments with their respective accuracies can be found in Table 3-7 and Table 3-8.



Figure 3-6: Photos of ultrasonic anemometer (a) setup, (b) sensors, (c) and (d) surroundings

In this comparative study, the DBB was installed at the main entrance door of the dwelling, as shown in Figure 3-7(a). The pressurisation and depressurisation tests were performed sequentially. The PULSE-60 unit was placed in the living room on the ground floor, as seen in Figure 3-7(b). For both tests, the dwelling was prepared according to the ISO 9972 standard; for instance, all the ventilation openings were sealed with TechnoSol sealing tape (Figure 3-8), and the interconnecting doors were kept open for establishing a homogeneous pressure within the house. All experimental tests were conducted in July 2018 under natural outdoor conditions, and the

weather was sunny and calm without rain. The recorded average outdoor temperature was around 20℃. During the testing, the outdoor wind speed was monitored continuously by the ultrasonic anemometer. In this study, all experimental tests were conducted separately but all under a wind speed less than 0.45m/s at 2.2m above ground level, which can be regarded as the calm condition based on the Beaufort scale [109]. The purpose of this arrangement was to minimise the wind impact on the Pulse and blower door measurements. Furthermore, the corresponding test validity was examined with checks of the background pressure and zero-flow pressure difference.



(a)



(b)

Figure 3-7: Photos of (a) installation of DBB unit and (b) PULSE-60 unit in the living room for testing

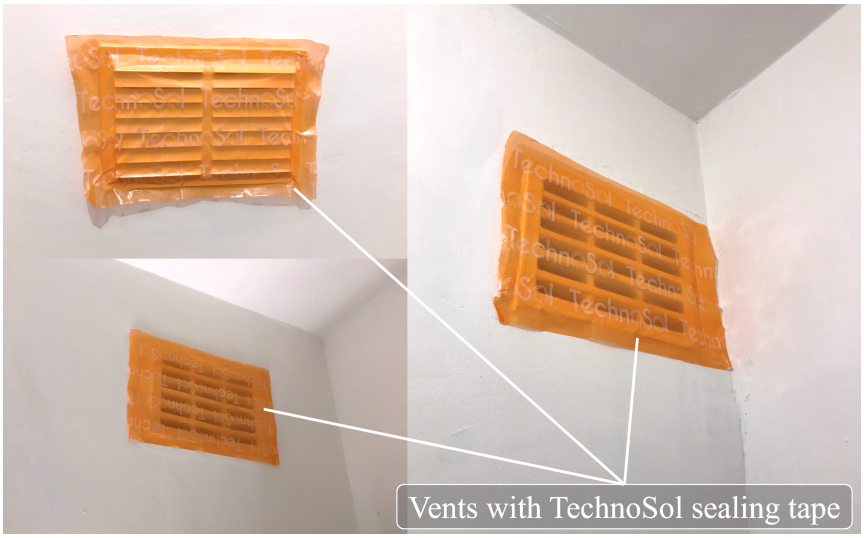


Figure 3-8: Building preparation for the Pulse and blower door tests

3.3. Results analysis of the Pulse and blower door testing

A three-step Pulse test was conducted to achieve leakage measurements in a wide range of building pressure. Table 3-3 lists the respective ranges of the pressure difference during the three-step Pulse testing. The tested dwelling has a volume of 447m^3, and the PULSE-60 unit can pressurise the air tank (with a capacity of 58.50 Litre) up to 10bar. In this study, the largest achievable pressure rise is about 10.6Pa (i.e., S1 test) within the dwelling with the initial tank pressure of 8.5bar. For the following S2 and S3 tests, the initial tank pressure was 6.8bar and 5.0bar, respectively.

Table 3-3: Building pressure difference during the Pulse tests

Three-Step Pulse	ΔP Range (Pa)
S1	7.6 ~ 10.6
S2	5.0 ~ 7.2
S3	3.0 ~ 4.6
Overall Range	3.0 ~ 10.6

Figure 3-9 presents the building air leakage rate based on the Pulse test in a pressure range of 3-10.6Pa. The power-law equation was fitted to the leakage-pressure curves, and details are listed in Table 3-4 with the measured air leakage rate at 4Pa, derived equation coefficients and the corresponding coefficient of determination. In Table 3-4, the pressure difference between the indoor and outdoor during the Pulse test is represented as ΔP; C and n are the flow coefficient (m^3/s/Pa^n) and the air flow exponent, as described in the power-law equation $Q=C\Delta P^n$. Q is the air leakage rate, and R^2 is the coefficient of determination, representing the quality of the curve-fit. The test validity was assessed by referring to the standard, for instance, n in the range 0.5 to 1 and R^2 >0.98.

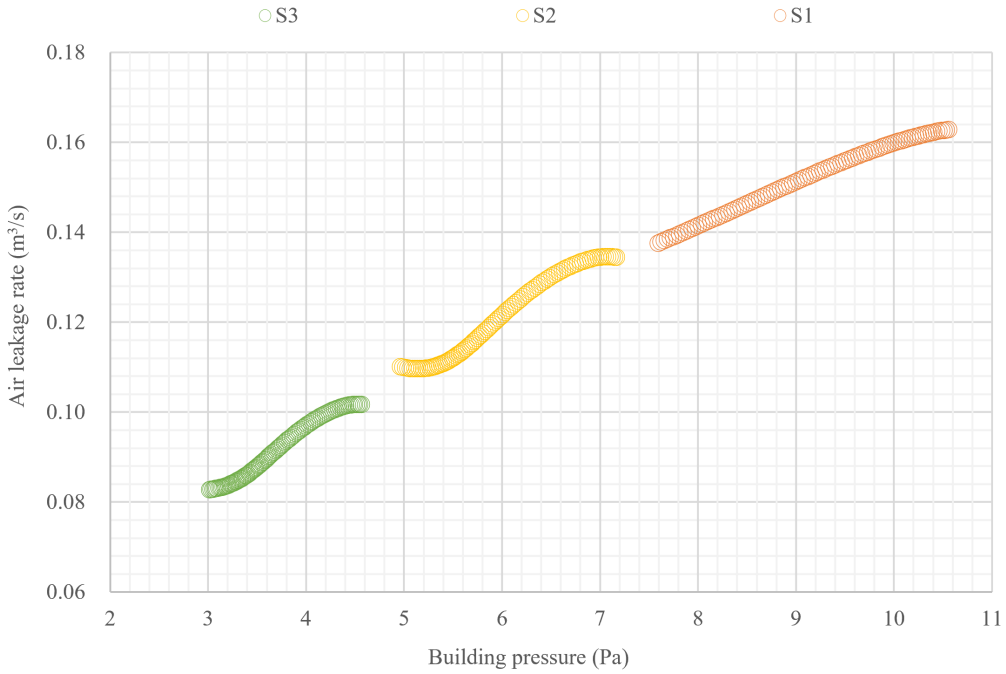


Figure 3-9: Air leakage rate-pressure curves for the Pulse tests

Table 3-4: Airtightness measurement results at 4Pa and power-law equations of the Pulse tests

	S1	S2	S3	Overall Results
ALR (m^3/s)	0.098	0.091	0.096	0.096
Permeability ($m^3/m^2/h$)	0.846	0.785	0.829	0.828
ACH (h^{-1})	0.787	0.730	0.772	0.770
ELA (m^2)	0.038	0.035	0.037	0.038
C	0.047	0.034	0.042	0.044
n	0.535	0.714	0.602	0.567
R^2	0.997	0.971	0.985	0.996

In terms of the blower door measurements, the building pressure difference ranged from 6.9-72.3Pa during the pressurisation testing and from 7.1-70.2Pa during depressurisation testing, as listed in Table 3-5.

Table 3-5: Building pressure difference during the blower door tests

Blower Door	**ΔP Range (Pa)**
Pressurisation	6.9 ~ 72.3
Depressurisation	7.1 ~ 70.2

Figure 3-10 presents the measured building air leakage rate-pressure curves for the blower door tests, and the detailed results at 50Pa fitted with a power-law equation are provided in Table 3-6.

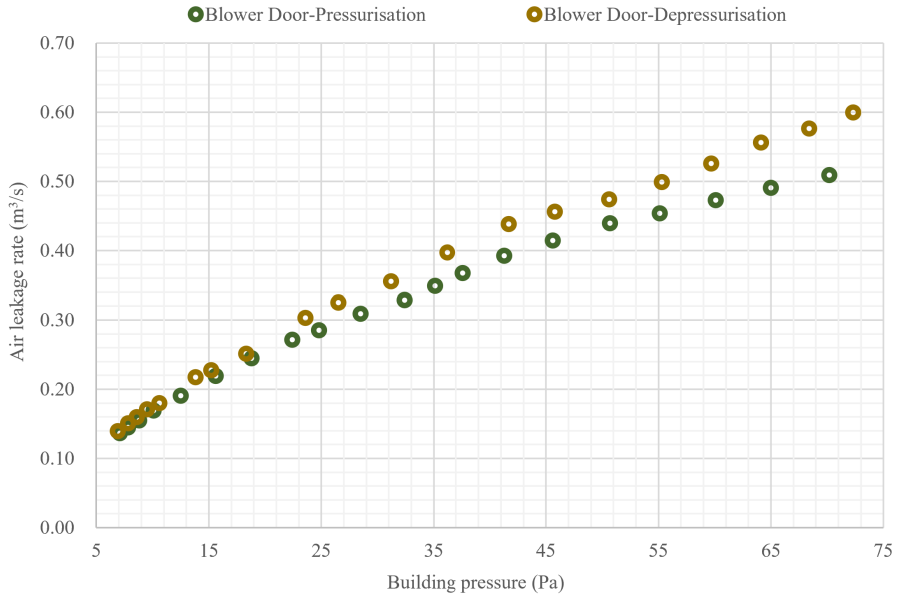


Figure 3-10: Air leakage rate-pressure curves for the blower door tests

In comparison, the air leakage rate-pressure curves for the blower door (i.e., pressurisation and depressurisation) and the Pulse testing are shown in Figure 3-11. As seen, the power-law equation was fitted to the leakage-pressure curves, and all data were extrapolated based on the Power law in order to compare the testing over the whole pressure range of 2Pa to 70Pa. It can be noticed that the obtained air leakage rate of the Pulse test is lower than that of the blower door pressurisation test. One of the reasons for this discrepancy may be because both pressurisation and depressurisation tests were conducted without sealing the door frame, i.e., leakage difference caused by the installation of the blower door unit. In addition, some drainage grooves in the door frame itself were observed and may contribute to the discrepancy, together with the valving effects of some building elements [228].

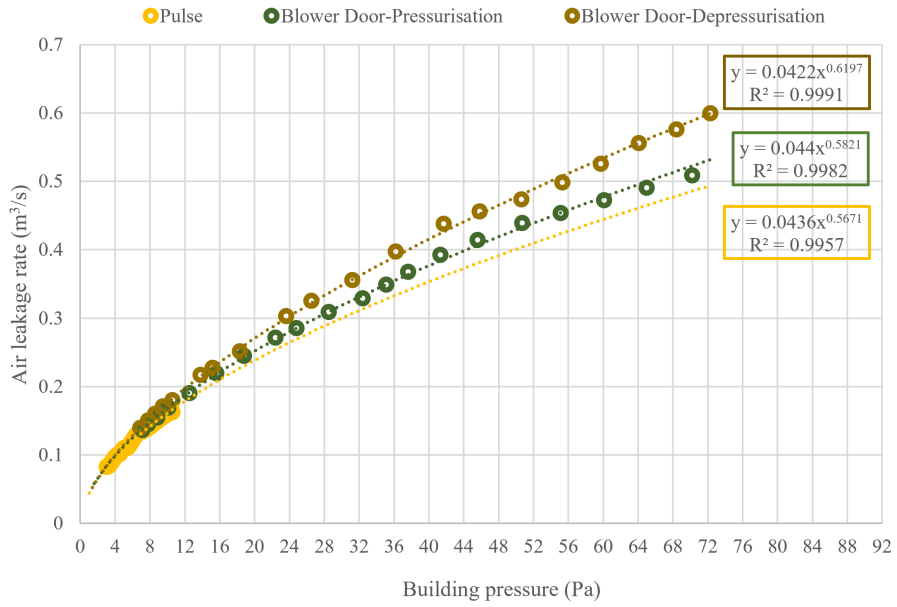


Figure 3-11: Air leakage rate-pressure curves for the blower door and Pulse tests over the pressure range of 2-70Pa

For comparison, Figure 3-12 presents the air leakage rate-pressure curves for both the blower door (pressurisation and depressurisation) and Pulse tests, covering the overlapped pressure range. Due to the different test approaches and the limitation in practical testing, the building pressure difference between the indoor and outdoor, where the tests overlap, is from 7.1Pa to 10.6Pa.

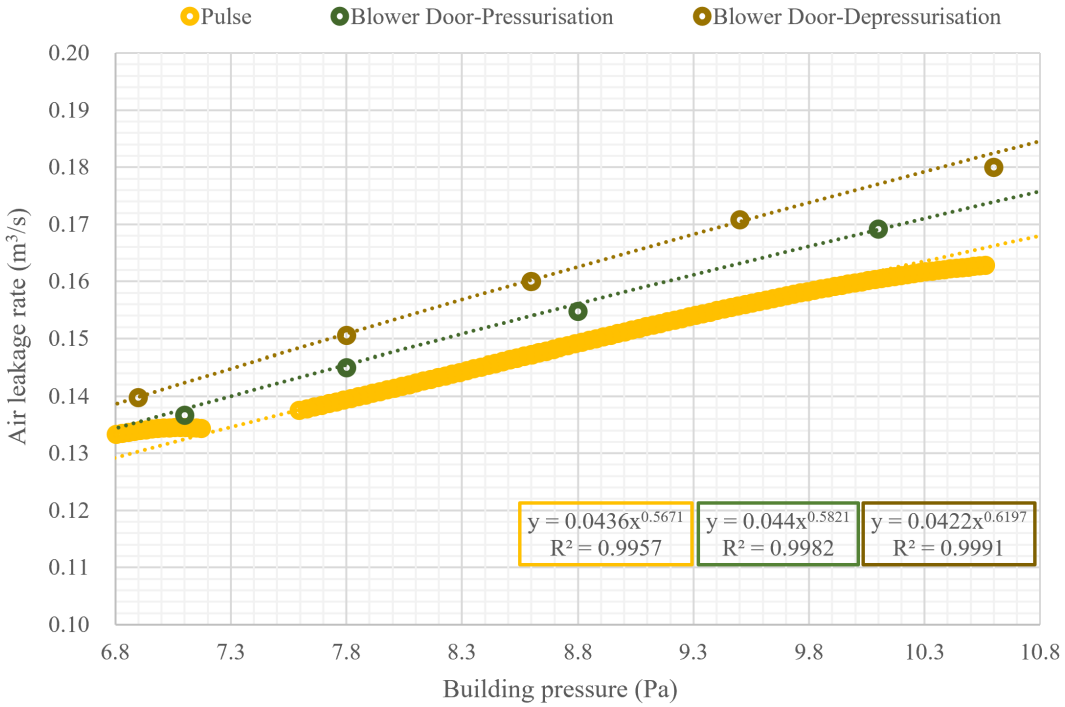


Figure 3-12: Air leakage rate-pressure curves for the blower door and Pulse tests in the overlapped pressure range

For direct comparison between the two testing methods over the overlapped pressure range, the relative percentage difference (*RPD*) defined by eq.(3-1), is used to describe the difference of measured air leakage rate between the blower door test (Q_{BD}) against the Pulse test (Q_P).

$$RPD = (Q_{BD-}Q_P)/Q_P \tag{3-1}$$

As shown in Figure 3-13, regarding the pressurisation test results of the two test methods, the blower door pressurisation result deviates from the Pulse result by 3.93% at 7.1Pa and 4.56% at 10.6Pa. Hence, a reasonably good agreement between the blower door and Pulse tests are obtained. As recommended by the ISO 9972 standard, both pressurisation and depressurisation measurements have been implemented, and the average of the pressurisation and depressurisation test results was derived (as seen in Figure 3-13). Based on the measured air leakage rate, the difference between the pressurisation and depressurisation tests is also noted, i.e., 3.24% at 7.1Pa and 4.81% at 10.6Pa. The difference, albeit small, could be caused by the combination of valving effects in leaks under different flow directions and biases in the two measurement procedures [56, 231]. Therefore, it is understandable that the pressurisation test result agreed with the Pulse test result slightly better than the depressurisation test result.

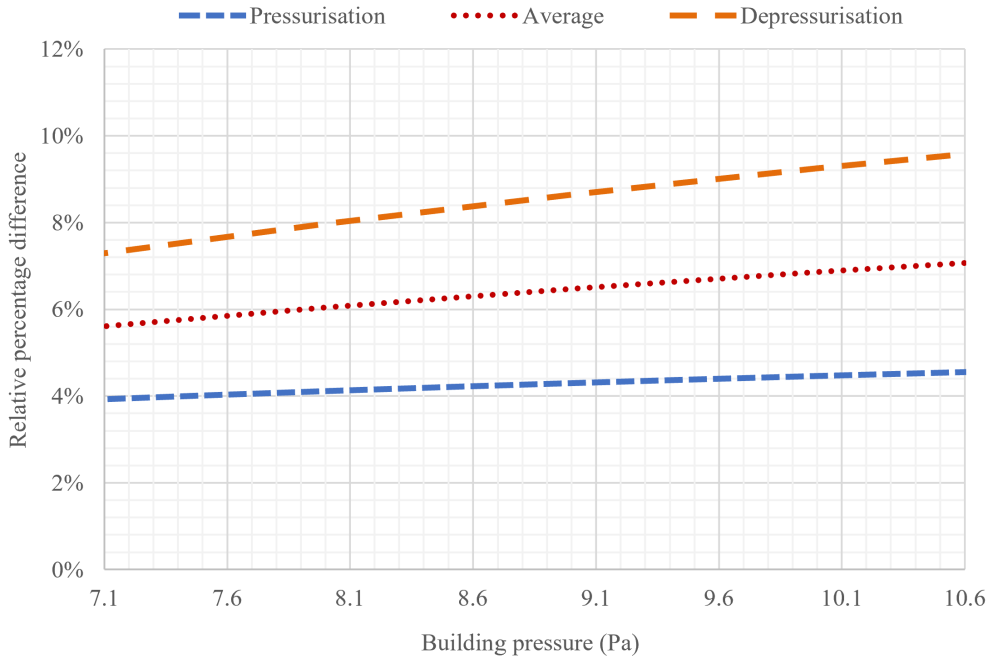


Figure 3-13: Relative percentage difference between the Pulse and blower door tests

Airtightness measurement results were extrapolated based on the Power law for comparing the testing at the same pressure level of 4Pa and 50Pa, as presented in Table 3-6. In terms of the measured air leakage rate, the *RPD* is 3.13% for the pressurisation test presented at 4Pa and 4.17% for the depressurisation test. In terms of the tests at 50Pa, the extrapolated air leakage rate for the Pulse test deviates from the direct measurement of pressurisation testing by 6.98%. Compared with the *RPD* of the overlapped pressure range, the larger *RPD* at 4Pa/50Pa is mainly attributed to the uncertainties in extrapolation. It is impractical to achieve a direct comparison in a wide pressure range using both test methods in a typical dwelling, as the very high mass flow rate of air pulse will be required to pressurise the building.

Table 3-6: Airtightness results and power-law equations of the blower door and Pulse tests

		Pulse	Blower Door-Pressurisation	Blower Door-Depressurisation
@4Pa	ALR (m^3/s)	0.096	0.099	0.100
	Permeability ($m^3/h/m^2$)	0.828	0.857	0.865
	ACH (h^{-1})	0.770	0.797	0.805
	ELA (m^2)	0.038	0.038	0.039
@50Pa	ALR (m^3/s)	0.401	0.429	0.477
	Permeability ($m^3/h/m^2$)	3.470	3.713	4.128
	ACH (h^{-1})	3.230	3.455	3.842
	ELA (m^2)	0.156	0.167	0.185

3.4. Error analysis

The overall error (δQ_e) associated with airtightness measurements for Pulse and blower door tests is determined by taking three sources into consideration, including instrumentation accuracy for bias error (δQ_{bias}), environmental conditions for precision error ($\delta Q_{precison}$) and model specification for modelling error ($\delta Q_{modelling}$) [36, 41, 148].

$$\delta Q_e = \sqrt{\delta^2 Q_{bias} + \delta^2 Q_{precison} + \delta^2 Q_{modelling})} \quad (3\text{-}2)$$

It is known that the impact of the wind may be the most pernicious error source as both precision and bias errors can be caused. The ISO 9972 standard recommends the ground wind speed for valid testing should be less than 3m/s or smaller than three on the Beaufort scale. To minimise the wind effect on measurements, measures have been taken in this study. For instance, all the tests were conducted under steady wind conditions (i.e., <0.45m/s, 2.2m above ground, 0 on Beaufort scale) with multipoint testing for the blower door method and multiple air pulse releases in the Pulse testing. In addition, based on the numerical study by Carrié, et al. [41], the steady wind-induced errors for pressurisation testing at reference pressures of 4Pa and 50Pa are minor and negligible in the wind speed range of 0-1m/s. Table 3-7 and 3-8 below list the error sources for both the Pulse and blower door tests and the measuring instruments with their respective accuracies. For the uncertainty of building volume measurement, the reference value generally varies from 3% to 10%, as stated in the ISO 9972 standard [109], and the highest value of 10% is considered herein.

Table 3-7: Error analysis for the blower door test

Error Sources	Measurement Instrument	Unit	Precision
Building parameter	---	m^3	±10%
Building pressure	DBB built-in pressure transducer	Pa	±0.9%
	Differential pressure transducer (FCO44)	Pa	±0.25%
Atmospheric pressure	Pressure transducer	hPa	±3%
Indoor air temperature	Indoor thermocouples (PT100 RTD)	℃	±0.2
Outdoor air temperature	Outdoor Thermocouple (PT100 RTD)	℃	±0.2
Fan flow rate	---	m^3/h	±3.0%

Table 3-8: Error analysis for the Pulse test

Error Sources	Measurement Instrument	Unit	Precision
Building parameter	---	m^3	±10%
Building pressure	PULSE-60 built-in pressure transducer	Pa	±0.40%
	Differential pressure transducer (FCO44)	Pa	±0.25%
Indoor air temperature	PULSE-60 built-in thermocouple	℃	±0.08
Tank air pressure	PULSE-60 built-in pressure transducer	Pa	±0.2%
Tank volume	---	Litre	±0.4
Tank air temperature	PULSE-60 built-in thermocouple	℃	±0.08

The bias error analysis for the blower door test is conducted, with reference to the studies by Sherman, et al. [36], Carrié, et al. [41], Carrié, et al. [57] and the ISO 9972 standard Annex C [109], and a similar approach has also been discussed in the research by Zheng, et al. [148]. The two independent errors are mainly from pressure and air flow measurements. The detailed calculations of the induced pressure difference during the blower door tests and the air leakage rate through the building envelope at the reference pressure difference are presented in Section 2.2.2 (i.e., eq. 2-4 to 2-11). The calculations of the measured building air leakage rate by the Pulse test are described in Section 2.3.1 (i.e., eq. 2-12 to 2-15).

The overall bias error of the measured building leakage rate can be expressed as:

$$\delta Q_{bias} = \sqrt{\Delta Q^2 + \Delta E^2} \tag{3-3}$$

Where ΔQ^2 relates to the measurement of air flow rate in the tank and ΔE^2 occurs in the measurement of isentropic expansion.

The precision error is calculated according to procedures described in Annex C in ISO 9972 standard [109]. Environmental variations during the tests are treated as the key source for the precision error. Model specification (or modelling) errors for the blower door and Pulse tests is calculated with reference to studies [36, 41, 148]. The key model specification error is related to the assumption that the flow can be extrapolated using a power-law formulation; thus, the error can be caused by extrapolating data beyond the measurement limits [151].

Based on the obtained data for the blower door and Pulse tests, Figure 3-14 shows the overall error for their overlapped building pressure testing range and detailed results for the tests are provided in Table 3-9. Due to the different test approaches, the building pressure during the Pulse, the fan pressurisation and depressurisation tests could not achieve the exact same pressure level. As it can be seen, the overall measurement errors for the Pulse test, the fan pressurisation and the depressurisation tests are lower than 10% under the calm weather condition, which is in line with the expectation stated in the ISO 9972 standard. Hence it demonstrates the validity of the obtained measurement results in this study. Over the tested building pressure range, the average overall error is 1.60% for the Pulse test and 2.94% for the fan pressurisation test, with a small difference in the overall error (i.e., 1.34%). This also verifies the good overall agreement between the two pressurisation tests. In terms of the depressurisation test, the average overall error is about 7.46%. The larger overall error is attributed to the combination of the blower door frame leakage, valving effect of leaks and different component behaviours during the depressurisation testing.

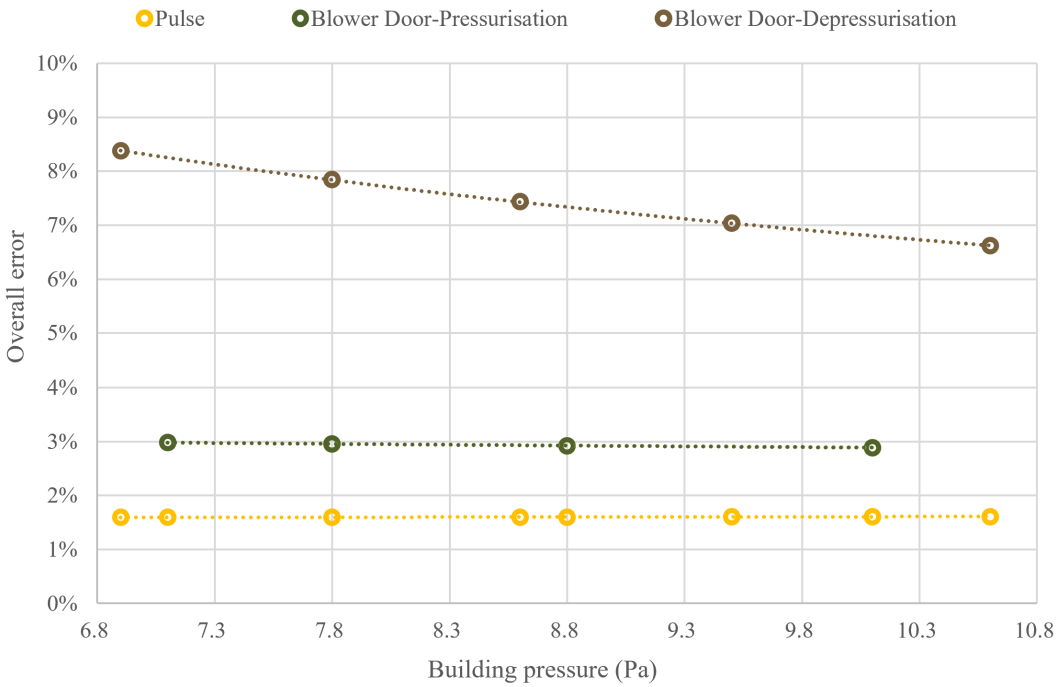


Figure 3-14: Overall errors of the Pulse and blower door tests for the overlapped pressure range

Table 3-9: Results of overall errors of the Pulse and blower door tests for the overlapped pressure range

Building Pressure (Pa)	Overall Error		
	Pulse	Blower Door-Pressurisation	Blower Door-Depressurisation
6.9	1.59%	---	8.83%
7.1	1.59%	2.98%	---
7.8	1.60%	2.96%	7.84%
8.6	1.60%	---	7.44%
8.8	1.60%	2.92%	---
9.5	1.60%	---	7.04%
10.1	1.61%	2.89%	---
10.6	1.61%	---	6.62%
Average	1.60%	2.94%	7.46%
Difference (Between Pulse and Blower Door)	---	1.34%	5.86%

Comparisons of the overall error for the blower door and Pulse tests at 4Pa and 50Pa are presented in Figure 3-15. The overall error for Pulse testing is approximately 0.80% at 4Pa and 1.83% at 50Pa, while the pressurisation test has an overall error of 3.19% at 4Pa and 1.46% at 50Pa, and depressurisation of 10.96% at 4Pa and 5.47% at 50Pa. As suggested by Sherman, et al. [36], to minimise the uncertainty within blower door testing, the low-pressure point should range from 10 to 20Pa, while the high-pressure point is in a range of 40-60Pa. The blower door tests in this study were conducted by following these rules, covering a pressure range of around 7Pa to 70Pa. Therefore, the average error of the blower door testing is less than 4% at 50Pa.

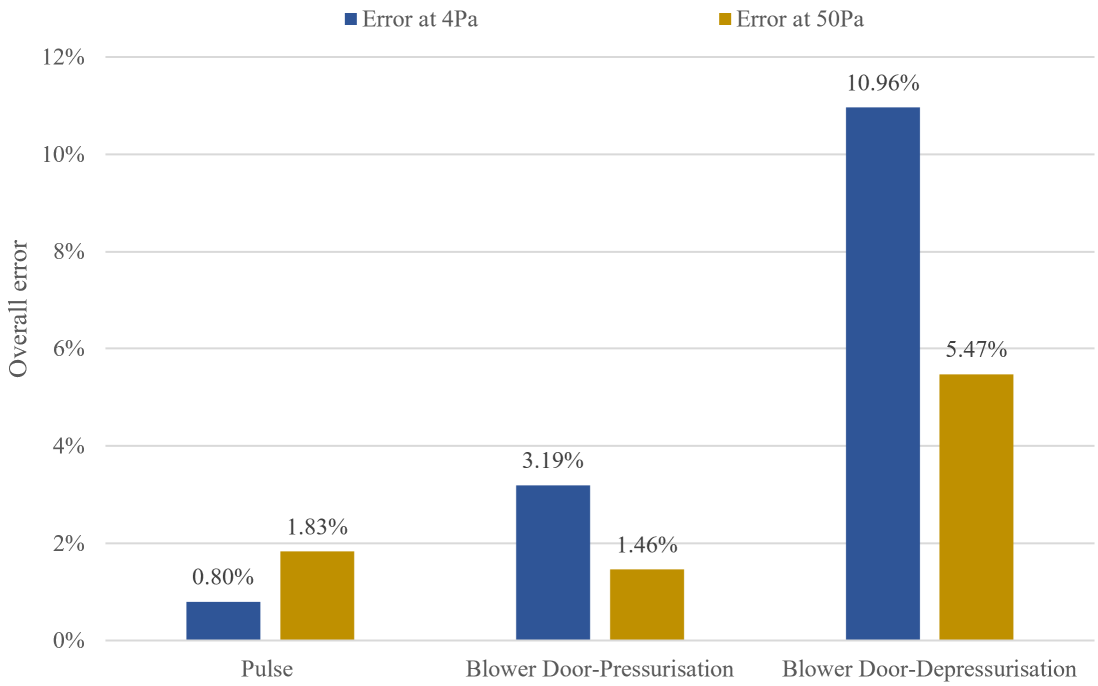


Figure 3-15: Overall errors for the Pulse and blower door tests at 4Pa and 50Pa

3.5. Summary

In this chapter, a comprehensive comparison between the blower door and Pulse testing was conducted based on the experimental work of a five-bedroom dwelling under calm weather conditions where the wind speed was less than 0.45m/s. The results demonstrate a good overall agreement of building air leakage rate, with deviations of 3.93% at 7.1Pa to 4.56% at 10.6Pa for the overlapped building pressure range. Comparison of airtightness measurements presented at 4Pa and 50Pa between the two methods were conducted based on data extrapolation. Due to the uncertainties of extrapolation, large differences between the two methods are noted compared with the direct comparison over the overlapped pressure range. However, due to the limitation of equipment, it is not practical to pressurise the testing dwelling to high pressure (e.g., 50Pa) by Pulse to directly compare with the fan pressurisation test method. The average overall error over the tested building pressure range is 1.60% for the Pulse testing, 2.94% for pressurisation testing and 7.46% for depressurisation testing.

The comparison provides some complementary insights into the range of measurements that could be expected, with an associated error when both test methods are applied to the same house in real scenarios. The error analysis also proves that the overall measurement errors of both testing methods align with the uncertainties reported in the literature, and thus the study provides a valid assessment.

4. Evaluation of Indoor Pressure Distribution and Effect of Pulse Release Location

4.1. Introduction and theoretical understanding

The increasing demand for more energy-efficient buildings and the need to demonstrate compliance with more stringent building regulation requirements in the future reveal the important role of airtightness in buildings [232, 233]. As mentioned in Chapter 2, the blower door method is a well-known and widely accepted steady-state pressurisation method. For the blower door test, a range of steady pressure differences across the building exterior is created with a blower door fan, and the corresponding air flow rate through the fan is measured simultaneously for establishing the pressure-leakage relationship of the tested dwelling. However, some issues have been noted for building airtightness testing using the steady pressurisation method, such as the impracticability in large buildings owing to the requirement of a large amount of airflow for pressurisation. The need of addressing these issues was the original impetus for developing Pulse. Pulse is designed to measure the building air leakage at low pressures in a dynamic manner, with a flexible installation [28], thereby mitigating the need for a large amount of airflow and enabling even distribution of the testing unit. The first development of Pulse was focused on the domestic application due to various reasons, such as the ease of proof of concept and more realistic approach.

During the Pulse test, a pulse in the internal air pressure is created by the release of a short burst of air from a pressurised air tank into the indoor space, and a period of quasi-steady flow is achieved accordingly. For context, a typical air tank would be of volume 40-Litre at 10bar pressure for a 3 to 4-bedroom modern residential dwelling in the UK. Based on the previous investigations to deliver a quasi-steady flow, the unsteady flow should only account for a small percentage of the overall flow; a 1% threshold was chosen in the studies [29, 30] to provide an optimal accuracy. Another concern for using the steady pressurisation method for buildings of large volume is the difficulty of achieving an even building pressure distribution [28]. Different sources during the steady pressurisation testing may contribute to an uneven pressure distribution within the building when it is pressurised, such as the installation of the equipment being limited to the availability and accessibility of fenestration and a large amount of airflow occurring at the concentrated space.

Pressure variations in the building and tank are measured during the Pulse test in order to establish the pressure-leakage relationship. Considering the background pressure variation, the adjustment method for the Pulse testing deducts the background pressure from raw data [142]. However, peer

researchers and practitioners have questioned the reliability and accuracy of Pulse, mainly due to the likelihood of uneven pressure distribution over a short test period. During the Pulse test, the pressure wave propagates at the speed of sound; therefore, the pressure within the building subjected to the rapid release of air is able to equalise within a short period of time. To address the issues in testing large buildings due to the increased dimension, it is considered that multiple Pulse units could be distributed evenly throughout the large building and operated simultaneously to achieve an even pressure distribution. Therefore, there is a necessity to provide insight into exploring the indoor pressure distribution during the Pulse pressurisation process.

Uneven pressure distributions could result in an error in the calculation of leakage area at a reference pressure, inaccurate quantification of required air flow rate, and thus inaccurate building airtightness measurements. Therefore, being conscious that the actual pressure distribution is more complex, Figure 4-1 provides a simplified diagram to describe the mathematical problem regarding the uneven pressure distribution in a test space with two different pressure levels established by a net fluid flow rate Q_{in}. Q_{out} is the rate of the airflow leaking out of the test space. The sensor is placed in the central zone giving a pressure reading of P_2 to represent the pressure in the whole zone, and the actual pressure in the outer zone is represented by P_1. Therefore, based on the assumption of a uniform indoor temperature, the measurement error of air mass (δm) within the test building can be described by eq. (4-1) using the continuity equation and ideal gas law:

$$\delta m = \frac{P_2 - \left(\frac{P_1V_1 + P_2V_2}{V_1 + V_2}\right)}{\frac{P_1V_1 + P_2V_2}{V_1 + V_2}} = \frac{|P_2 - P_1|V_1}{P_1V_1 + P_2V_2} \tag{4-1}$$

Where V_1 and V_2 are volumes of the outer zone and the centre zone, respectively.

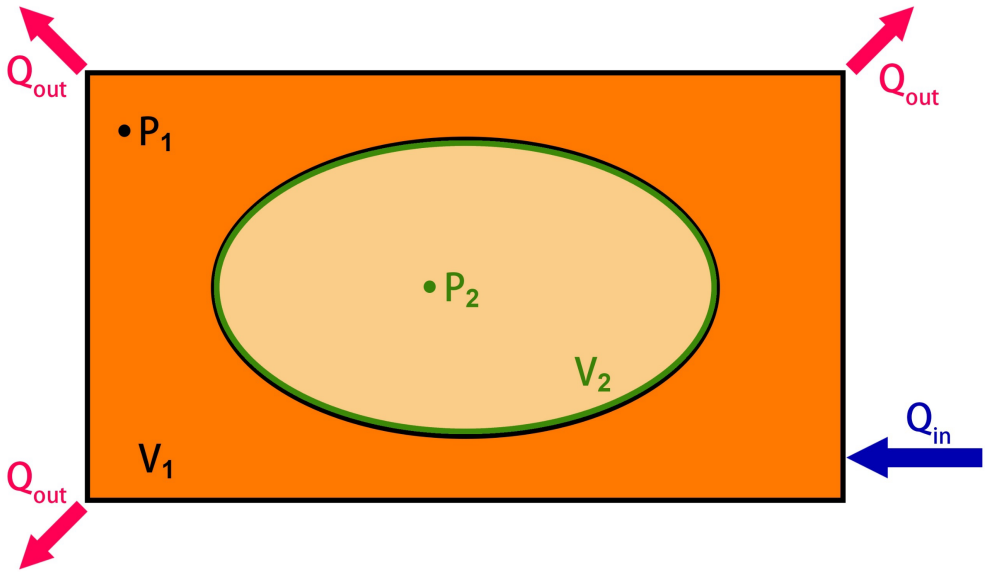


Figure 4-1: Diagram of the uneven pressure distribution in building under pressurisation

As seen, the error is determined by the pressure difference between P_1 and P_2, and the volume V_1. It thus indicates that a uniform pressure distribution within the test space could contribute to minimising δm. Figure 4-2 presents examples of how the uneven pressure distribution (represented by $\frac{P_1}{P_2}$) and the different size of V_1 (represented by $\frac{V_1}{V_2}$) influences the measurement of the air mass. It can be noted that the measurement error increases remarkably as the size of V_1 increases, and the impact is greater at a larger pressure difference. Hence, evaluation needs to be given to the level of the error produced by various levels of pressure uniformity, which can be obtained according to the achieved uniformity in both the Pulse and blower door tests. The corresponding error in the calculated building air leakage can then be provided. This evaluation can be done according to two different scenarios, different sizes of V_1 and the different percentage differences between P_1 and P_2.

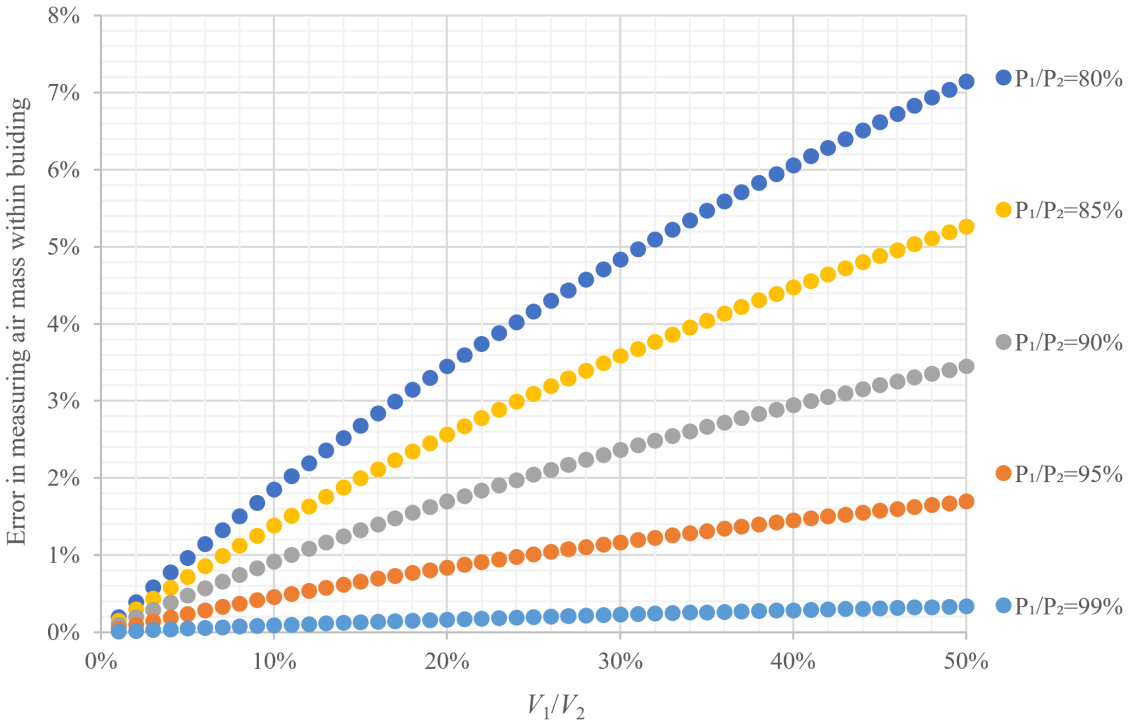


Figure 4-2: Measurement error of air mass with different percentages of V_1 and pressure difference

In this chapter, experimental work is focused on the domestic application of Pulse by performing the Pulse tests in a five-bedroom detached house to verify whether a uniform indoor pressure distribution can be achieved during the pulse pressurisation process. This distribution is also compared with that of a steady pressurisation test. In addition, the effect of the pulse release location on the building airtightness measurement is also investigated. The tests are routinely done as part of the ongoing development of the Pulse technique, and the investigation presents results of testing using the latest Pulse equipment as an answer to the aforementioned questions.

4.2. Test arrangement

The five-bedroom detached house mentioned in Chapter 3 was chosen as the test building, as per the photos provided in Figure 3-2. The same experimental setup for Pulse (i.e., PULSE-60 unit) and blower door (i.e., Duct blaster series B) testing was used. For both Pulse and blower door tests, the dwelling was prepared according to the ISO 9972 standard; therefore, the interconnecting doors were kept open for establishing a homogeneous pressure within the house. Figure 4-3 shows the locations of the Pulse unit and the pressure transducers within the tested dwelling. During the testing, the weather was sunny and calm without rain, with an average outdoor temperature of around 19℃. The outdoor wind speed was monitored continuously by the ultrasonic anemometer at the height of 2.2m above ground level in the backyard and a distance of 12m away from the perimeter of the test building, with no significant obstructions in its vicinity. In this study, all experimental tests were conducted separately, but all under wind speeds less than 0.45m/s at 2.2m above ground level, which can be regarded as the calm condition based on the Beaufort scale [109]. The purpose of this arrangement was to minimise the wind impact on the indoor pressure distribution, so insights on the pressure distribution during the Pulse and blower door tests could be gained. Furthermore, the corresponding test validity was examined with checks of the background pressure and zero-flow pressure difference.

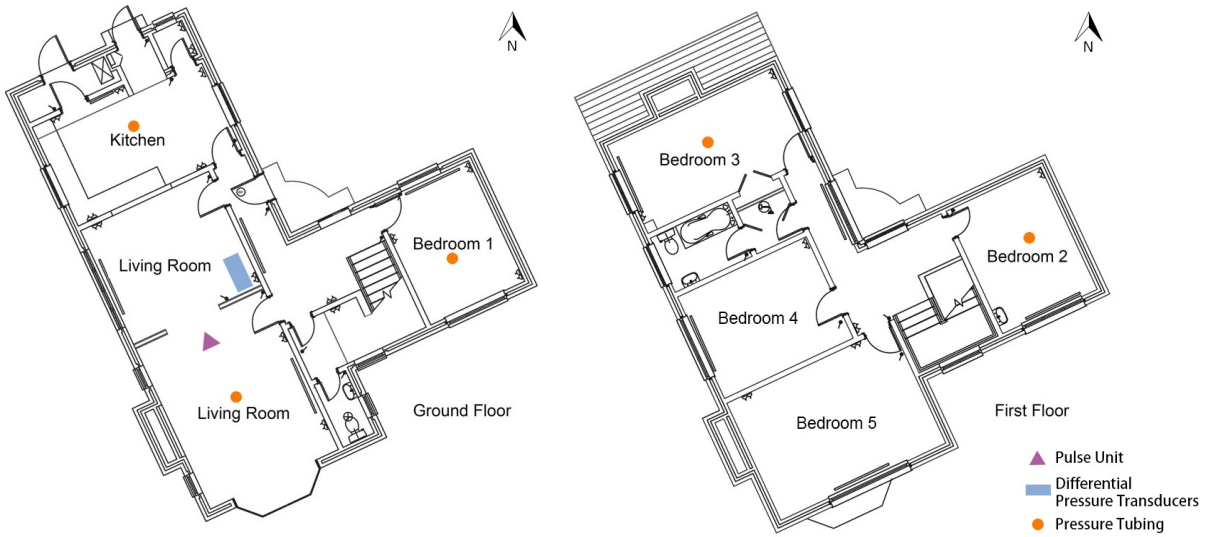


Figure 4-3: Setup locations of test equipment

Five differential pressure transducers were utilised to measure the indoor pressure distribution. Preliminary work was conducted by connecting each differential pressure transducer to a separate datalogger, as seen in Figure 4-4. However, the difference in the recording time step of the five independent dataloggers was noticeable and inevitable, which led to uncertainties in analysing the

rapid pressure variation during the air pulse release. To overcome this, the pressure transducers were required to be connected to the same datalogger, as shown in Figure 4-5. However, an increased number of transducers on one datalogger came at the expense of sampling rate and therefore, a balance between the sample rate and the number of pressure transducers was made. This limited the number of rooms that could be monitored within the dwelling. The readings of all differential pressure transducers were recorded at a sampling rate of 4Hz. The accuracy of the differential pressure transducer is ±0.25%, and all the five pressure transducers were calibrated by connecting to the same tapping point.



Figure 4-4: Differential pressure transducers with five dataloggers

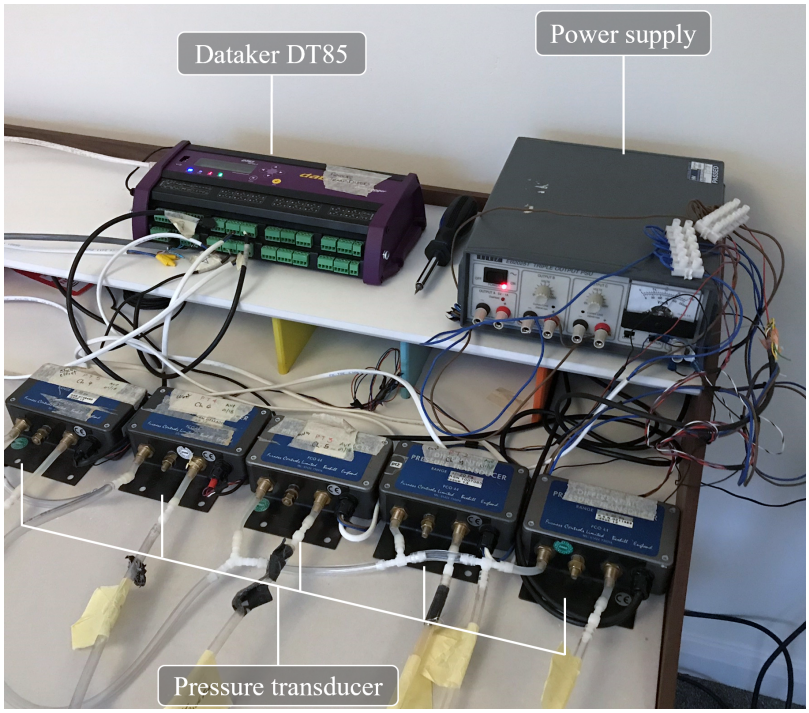


Figure 4-5: Differential pressure transducers with one datataker DT85

Differential pressure transducers have two inlet ports, one for the reference pressure and the other connected to each room whose pressure is to be monitored. Figure 4-6 presents a flow chart for the arrangement of differential pressure transducers used in this study. The reference pressure was obtained by placing the pressure tubing in the attic space of the tested dwelling, giving the same pressure as that of the outdoor environment but greatly minimising the impact of the varying outdoor weather conditions (e.g., rain, gust wind). The five pressure transducers connecting to the data logger are placed in the living room, and the pressure tubes connected to each room had the same specification in terms of material and dimensions (e.g., length and diameter). Figure 4-7 shows the photos of the pressure tubes in each room.

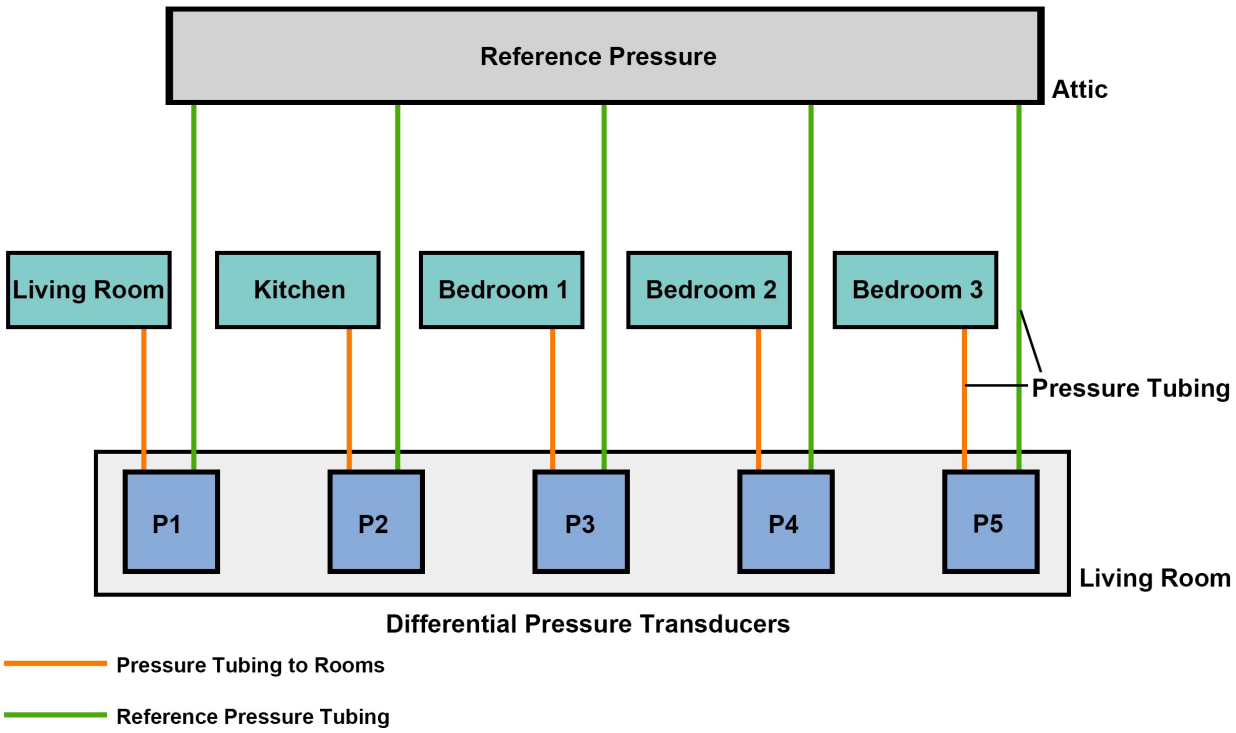


Figure 4-6: Arrangement of differential pressure transducers



(a) PULSE-60 unit in living room (b) Living room (c) Kitchen

(d) Bedroom (e) Bedroom 2 (f) Bedroom 3

Figure 4-7: Photos of Pulse unit and pressure tubing location in each room

4.3. Indoor pressure distribution during the Pulse test

It is worth noting that the sampling rate of 4Hz is perhaps insufficient in capturing the complete profile of how the indoor pressures across the internal spaces might vary during the rapid and dynamic air pulse releasing process. However, it still allows us to gain an improved understanding of how the pressures across the building's internal spaces respond simultaneously to the release of an air pulse in the Pulse test. The long pressure tubes, which were used to minimise the error caused by the equipment setup, also served as pneumatic low-pass filters for pressure readings, and therefore an increased sampling rate would not achieve a significant improvement in the pressure readings. It is a limitation in this experimental study. Nevertheless, the experimental investigations on the impact of the pulse release location on the Pulse measurement and its

comparison with the blower door measurement provide complementary validations for the uniformity of the pressure distribution from the testing perspective.

A series of Pulse tests have been conducted in the house to verify whether a uniform pressure distribution across the internal spaces of the test building can be achieved during the air pulse release so that the viability of the Pulse test for accomplishing building airtightness measurement at 4Pa in a very short period can also be evaluated. The Pulse unit was located in the centre of the living room on the ground floor, and the indoor pressure distributions for five rooms on both floor levels (i.e., the living room, the kitchen and the three bedrooms) were measured respectively during the pulse pressurisation process. Figure 4-8 illustrates the pressure variation in each room during the complete three-step of the Pulse test (i.e., S1, S2 and S3). A three-step Pulse test consists of three consecutive pulses, and therefore the 1.5-second pressure rise in the third pulse (S3) is much lower than that of the first one (S1) due to the declining tank air pressure. It can be noted that the curves representing the pressure responses in the five rooms are nearly identical, which indicates a good uniformity of the pressure distribution across the five rooms during the pulse release has been achieved. More discussions for each step of the Pulse tests are given in the following sections.

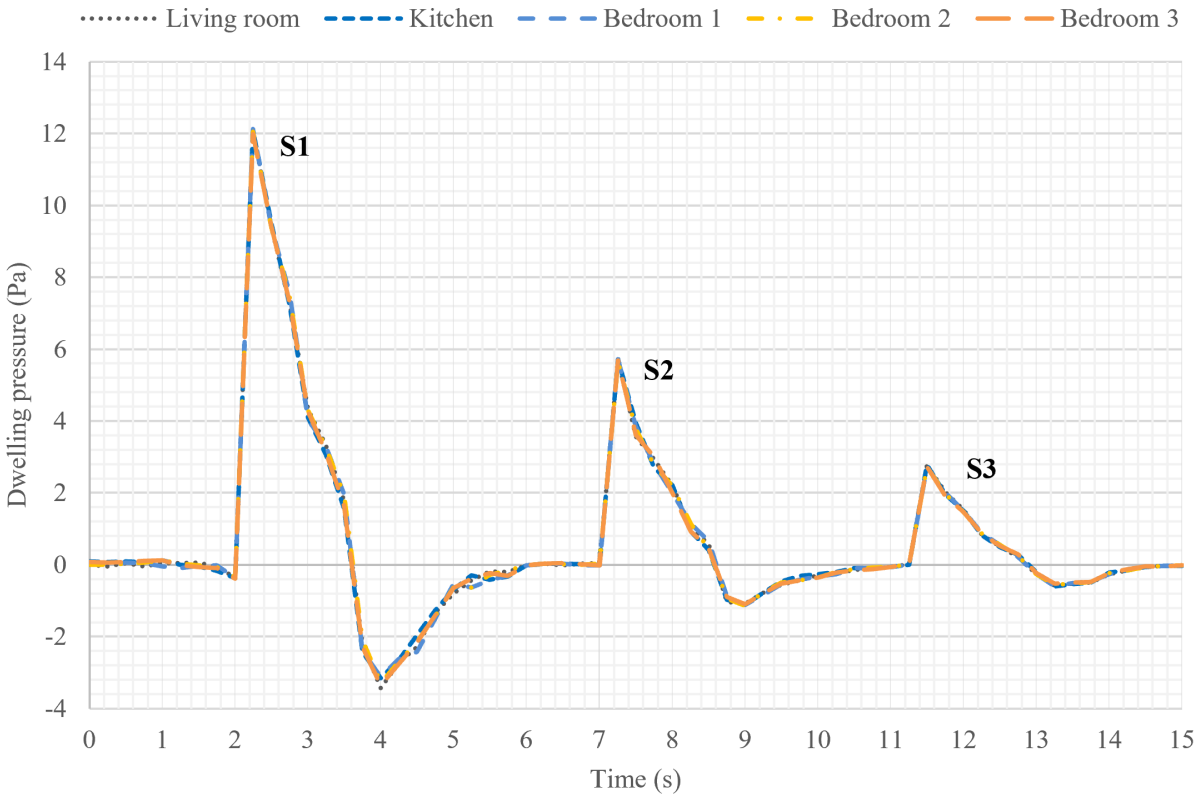


Figure 4-8: Pressure profiles in the five rooms during the complete Pulse test

Figure 4-9 shows the measured pressure variation of each room during S1. Similar trends were observed in the five rooms, and the indoor pressure of every room reached around 12Pa at 2.25s,

i.e., 0.25 seconds after the valve opened and released the compressed air from the tank into indoor spaces. Only slight differences were noted at the peak level.

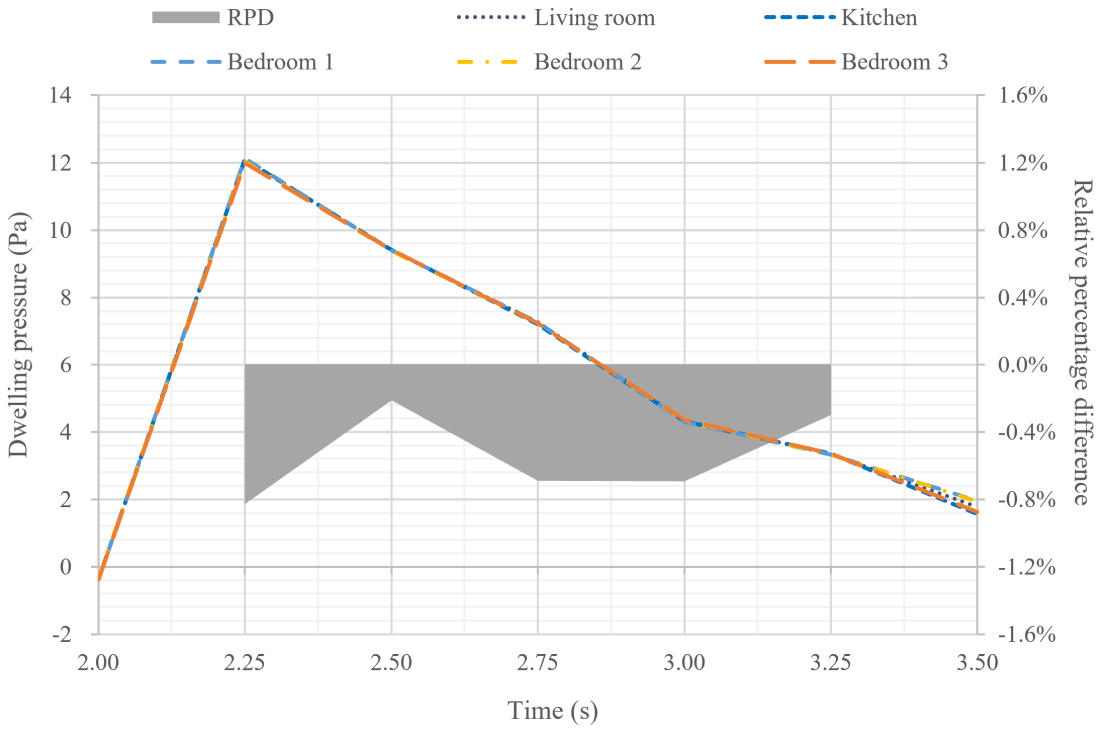


Figure 4-9: Pressure profiles in the five rooms during the S1 test

For the evaluation purpose, the Pulse unit was placed in the living room, and its pressure is regarded as the baseline against which the pressures of the other four rooms are compared. Therefore, the relative percentage difference (*RPD*) between the pressures in other rooms and the living room can be calculated using eq. (4-2).

$$RPD = (\Delta P_{Room_Living})/P_{livingroom} \tag{4-2}$$

Where $\Delta P_{Room_Living} = P_{room} - P_{livingroom}$, ΔP_{Room_Living} represents the pressure difference between the room pressure (P_{room}) and the living room pressure ($P_{livingroom}$).

As seen in Figure 4-9, *RPD* is only calculated for the pulse period during the air pulse release, but the pressures at the start and the end of the pulse release are not considered due to being unstable as the valve opens or closes. For S1, the highest *RPD* is approximately 0.83%, which was observed in Bedroom 3 with a pressure level of 11.99Pa in comparison to 12.09Pa in the living room.

The results of pressure variation in the five rooms for S2 are presented in Figure 4-10. At 7.25s, i.e., 0.25 seconds after the pulse of air was released into the interior rooms, the maximum pressure level was obtained for each room, ranging from 5.65Pa to 5.73Pa. Compared with the curves of the S1 test in Figure 4-9, some differences were seen among the five pressure curves of S2. The maximum *RDP* for S2 is around 1.40%, between Bedroom 2 with a room pressure of 5.65Pa and the living room of 5.73Pa, which is higher than that of S1.

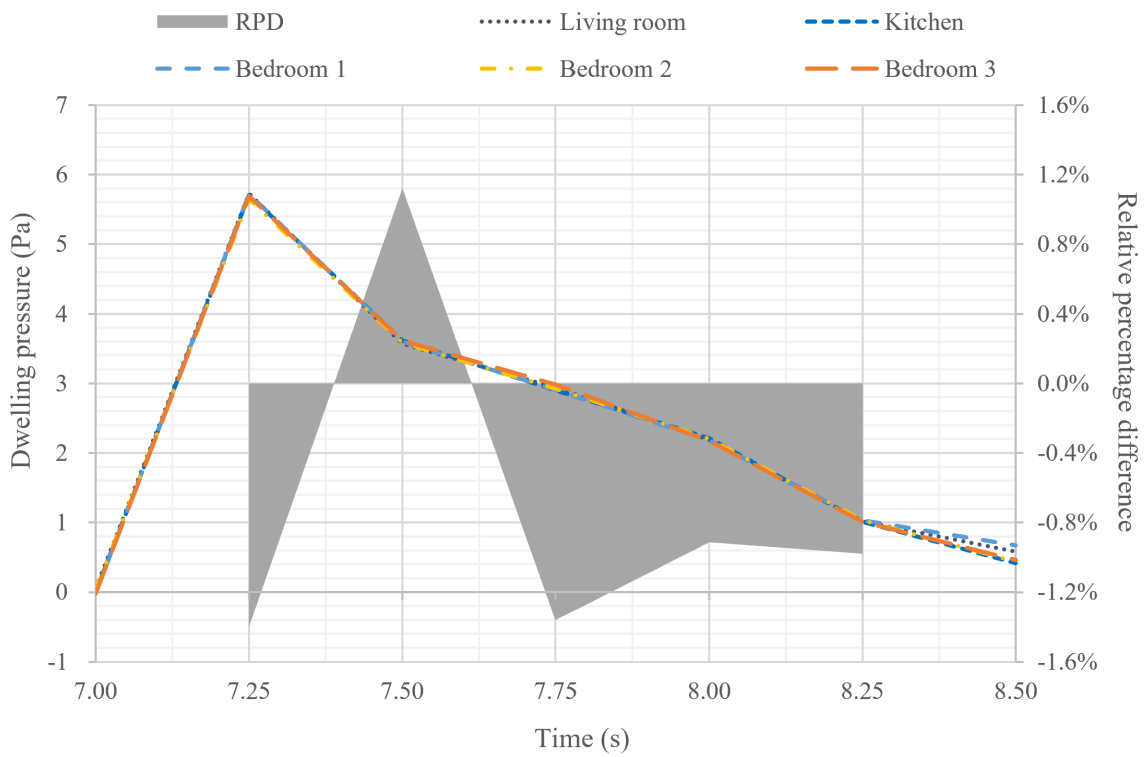


Figure 4-10: Pressure profiles in the five rooms during the S2 test

Figure 4-11 demonstrates the pressure variations in the five rooms during S3. The pressure in each room peaked around 2.7Pa at 11.25s, i.e., 0.25 seconds after the release of air pulse. The highest *RPD,* 1.45%, was observed between Bedroom 1 (2.72Pa) and the living room (2.76Pa), which is slightly higher than that of S2.

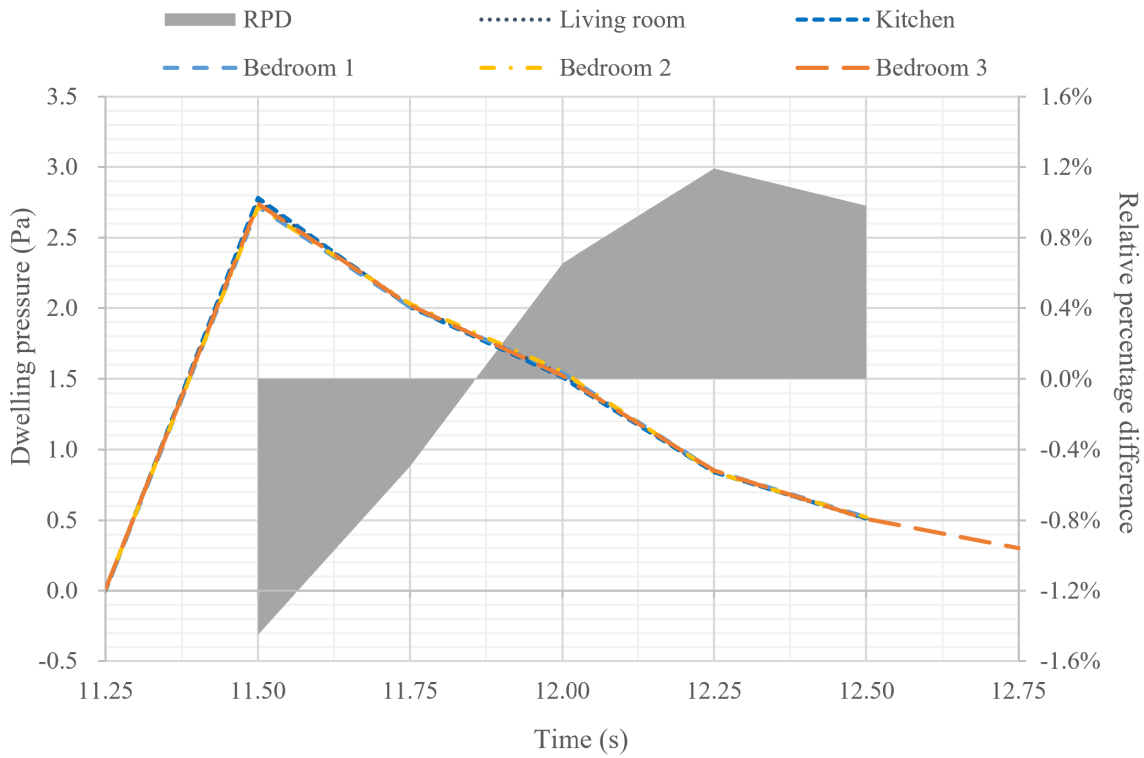


Figure 4-11: Pressure profiles in the five rooms during the S3 test

Table 4-1 list the detailed data for the measured pressure level in each room during the S1, S2 and S3 tests. It can be seen that the *RPD* is within ±1.5% for the three Pulse tests, which thus confirms the uniformity of pressure distribution during the Pulse test.

Table 4-1: Maximum pressure level in each room for the S1, S2 and S3 tests

	Living Room	Kitchen	Bedroom 1	Bedroom 2	Bedroom 3	*RPD**
S1	12.09 Pa	12.09 Pa	12.13 Pa	12.04 Pa	11.99 Pa	-0.83%
S2	5.73 Pa	5.71 Pa	5.72 Pa	5.65 Pa	5.69 Pa	-1.40%
S3	2.76 Pa	2.78 Pa	2.72 Pa	2.72 Pa	2.74 Pa	-1.45%

*The maximum relative percentage difference between the living room and the other rooms

4.4. Indoor pressure distribution during the blower door tests

In order to provide a benchmark comparison, experimental work was also undertaken to investigate the uniformity of the pressure distribution within the house during the blower door testing. Due to the limited measurement range (±20Pa) of the differential pressure transducers used in the Pulse unit, the uniformity of the pressure distribution was only investigated at 10Pa and 15Pa. Figure 4-12 and Figure 4-13 present the respective results. The overall measurement lasted about 15 seconds after the building pressure became steady. For the evaluation purpose, the relative percentage difference (*RPD*) is also calculated based on eq. (4-2).

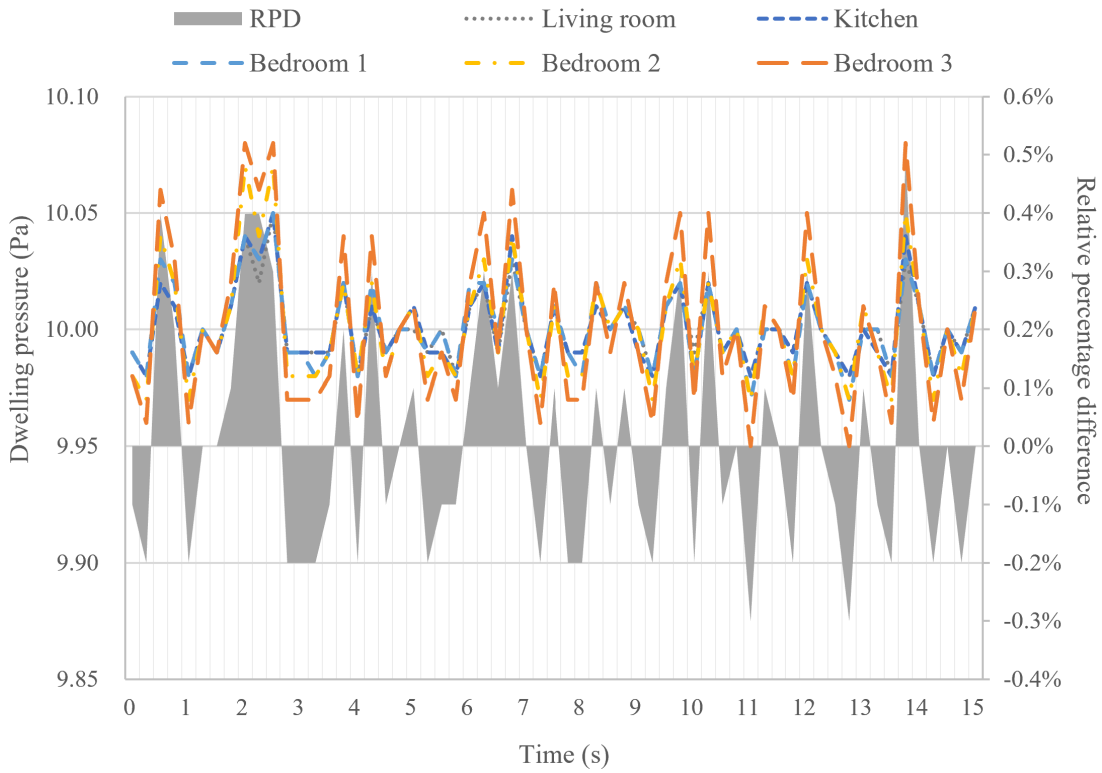


Figure 4-12: Pressure profiles in the five rooms during the DBB test at 10Pa

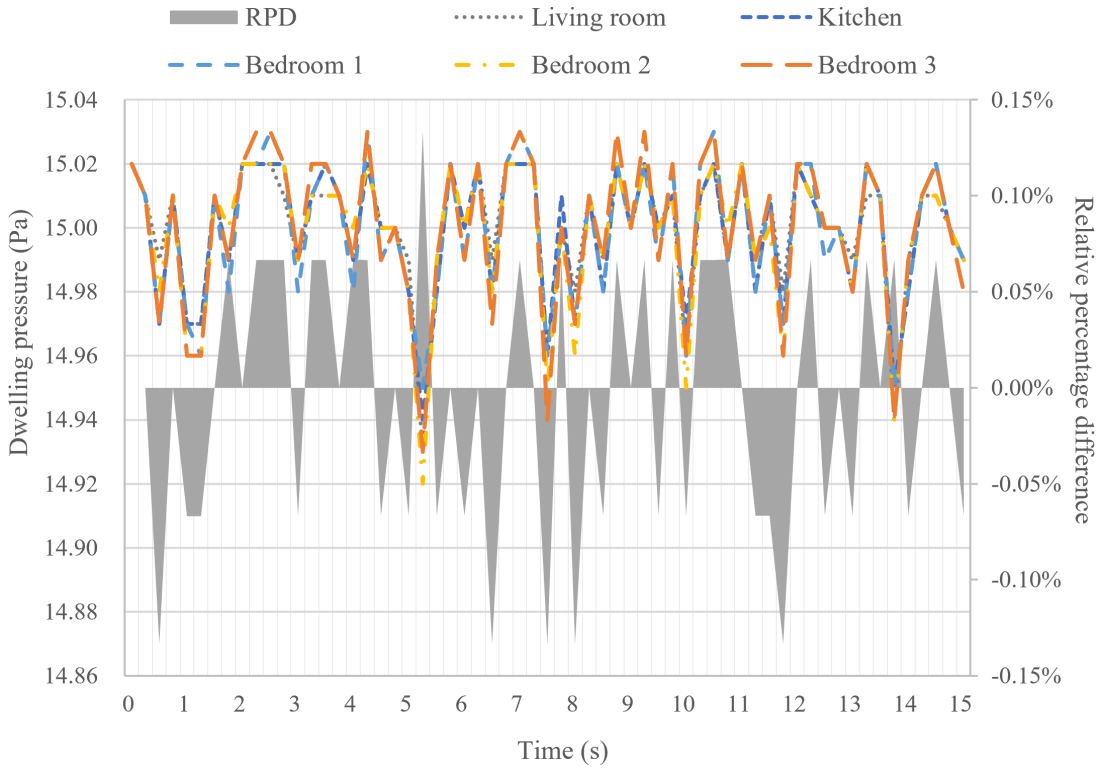


Figure 4-13: Pressure profiles in the five rooms during the DBB test at 15Pa

As seen from both figures, the overall trend of the pressure variation in each room is similar. For a test at 10Pa, the pressure difference between the living room and other rooms is about 0.05Pa, with a relative percentage difference of 0.50%, while only 0.03Pa of the pressure difference is observed for testing at 15Pa with an *RPD* of 0.13%. Considering the accuracy of the pressure transducers (i.e., 0.25%), a uniform pressure distribution across the internal spaces has been demonstrated for the fan pressurisation test. Table 4-2 below lists the detailed data for the measured pressure level in each room during the blower door tests.

Table 4-2: Maximum pressure level in each room for the DBB tests at 10 Pa and 15Pa

	Living Room	Kitchen	Bedroom 1	Bedroom 2	Bedroom 3	*RPD**
DDB 10 Pa	10.03 Pa	10.04 Pa	10.03 Pa	10.05 Pa	10.08 Pa	0.50 %
DDB 15 Pa	14.93 Pa	14.94 Pa	14.95 Pa	14.92 Pa	14.93 Pa	0.13 %

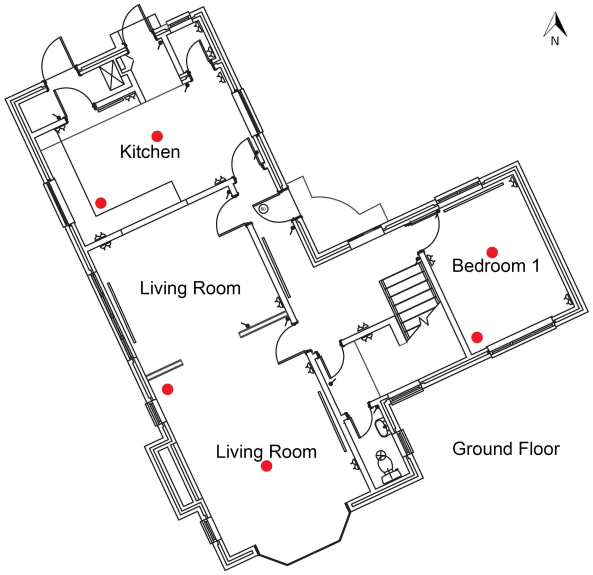
*Relative percentage difference between maximum and minimum

Based on the error analysis mentioned in Section 3.4, the uncertainties for the pressure distribution measurement during the blower door and Pulse tests are also calculated, accounting for the error sources in the blower door and Pulse tests, the pressure measurement and the data logging error. The overall error for pressure distribution measurement is approximately 1.62% for the Pulse test and 2.95% for the blower door pressurisation testing at 10Pa and 15Pa. Therefore, the obtained

data can reinforce the finding that a uniform indoor pressure distribution can be achieved during the pulse pressurisation process.

4.5. Effect of the Pulse release location

Investigations were made to understand any potential effect of the specific pulse release location on the building airtightness measurement by performing tests at various locations within the building. The evaluation could also provide a secondary validation to the fact that the even pressure distribution given by the Pulse test is able to provide a consistent measurement even when the location of placing the Pulse unit is changed. Figure 4-14 illustrates the floor plan of the dwelling with marked test points. In total, six locations on the ground floor were selected, including the living room, the living room corner, Bedroom 1, the Bedroom 1 corner, the kitchen, and the kitchen corner.



(a) Pulse test location diagram



(B) Kitchen



(c) Bedroom 1 (d) Living room corner

Figure 4-14: Photos of the Pulse test unit in different rooms

At each test location, five repeated tests were implemented under calm weather conditions (i.e., wind speed <0.45m/s). Figure 4-15 presents the building airtightness measurement results for the 30 tests at the different pulse release locations, with the results listed in Table 4-3. The average building permeability value is calculated based on the five tests for each location. The average permeability for the pulse release in the living room, the living room corner, Bedroom 1, the Bedroom 1 corner, the kitchen and the kitchen corner are 0.725, 0.721, 0.721, 0.728, 0.731 and 0.716 $m^3/h/m^2$, respectively. A subtle difference in the average building permeability is noted with a variability of 1.05%, which can be considered acceptable due to intrinsic measurement uncertainty. Therefore, the obtained results reveal that the Pulse test location in this study has little effect on the building airtightness measurement. This is in line with similar observations, which have been reported in previous experimental investigations in studies [148, 150].

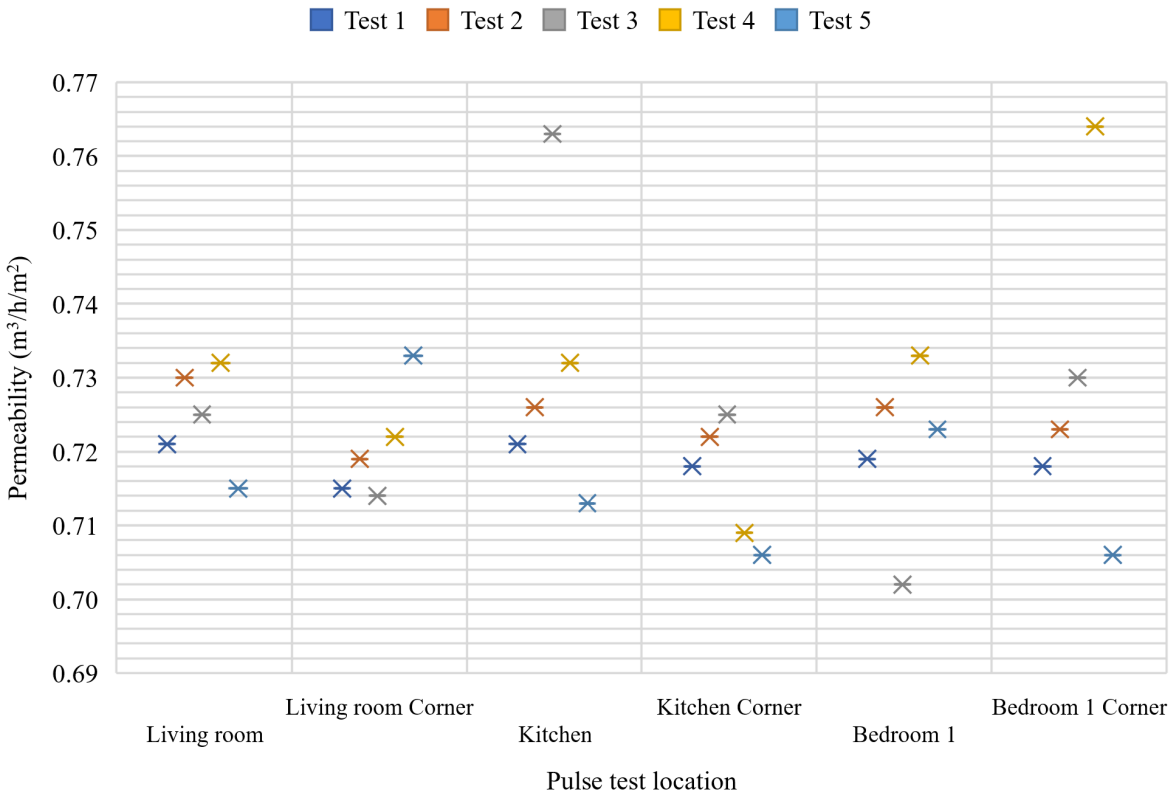


Figure 4-15: Results of 30 Pulse tests at different pulse release locations

Table 4-3: Measurement results of the building permeability (m³/h/m²) for the Pulse tests at different locations

	Living Room	Living Room Corner	Kitchen	Kitchen Corner	Bedroom 1	Bedroom 1 Corner
Test 1	0.721	0.715	0.721	0.718	0.719	0.718
Test 2	0.730	0.719	0.726	0.722	0.726	0.723
Test 3	0.725	0.714	0.763	0.725	0.702	0.730
Test 4	0.732	0.722	0.732	0.709	0.733	0.764
Test 5	0.715	0.733	0.713	0.706	0.723	0.706
Average	0.725 (±1.38%) *	0.721 (±1.66%)	0.731 (±4.38%)	0.716 (±1.40%)	0.721 (±2.64%)	0.728 (±4.95%)
Overall Average				0.724		
%**	0.15%	0.40%	1.03%	1.05%	0.40%	0.65%

* Highest relative percentage difference between each test and average
** Relative percentage difference between location average and an overall average

4.6. Summary

Pulse adopts an unsteady approach to measure building airtightness at low pressures. Due to the rapid dynamic nature of Pulse, the uniformity of the pressure distribution across the internal space of the test building during the pulse period has been frequently questioned. In this chapter, experimental investigations were made in a five-bedroom detached house using the PULSE-60 unit and the fan pressurisation to measure building airtightness under calm weather conditions (i.e., wind speeds less than 0.45m/s). The pressure distributions among five different rooms within the building were monitored together with the building permeability. A minor pressure difference within the building during the Pulse test was observed, but the deviation is not significant, with the highest relative percentage difference of 1.40% in S2 and 1.45% in S3 test when comparing the pressure in each room with the living room pressure. In terms of the blower door tests, the relative percentage difference of the maximum pressure level in each room is 0.50% at 10Pa and 0.13% at 15Pa, which is lower than that of the Pulse tests. The error analysis also proved the validity of the assessment study. Furthermore, a minor impact of the Pulse test location on the building airtightness measurement was observed with a subtle variation (i.e., 1.05%) in the building air permeability when the Pulse tests were conducted at different locations inside the building. The work extends the explorations of Pulse in practical aspects, providing a full image of the uniform pressure distribution within the building during the test and proving the applicability and reliability of the technique. The study is based on tests performed with a single Pulse unit in a five-bedroom dwelling of a relatively large volume when compared to the vast majority of residential UK dwellings, thus representing a potential worst-case scenario. Hence, the findings are also applicable to smaller buildings.

5. Insights into the Wind Impact Using Pulse in a Detached Dwelling

5.1 Introduction

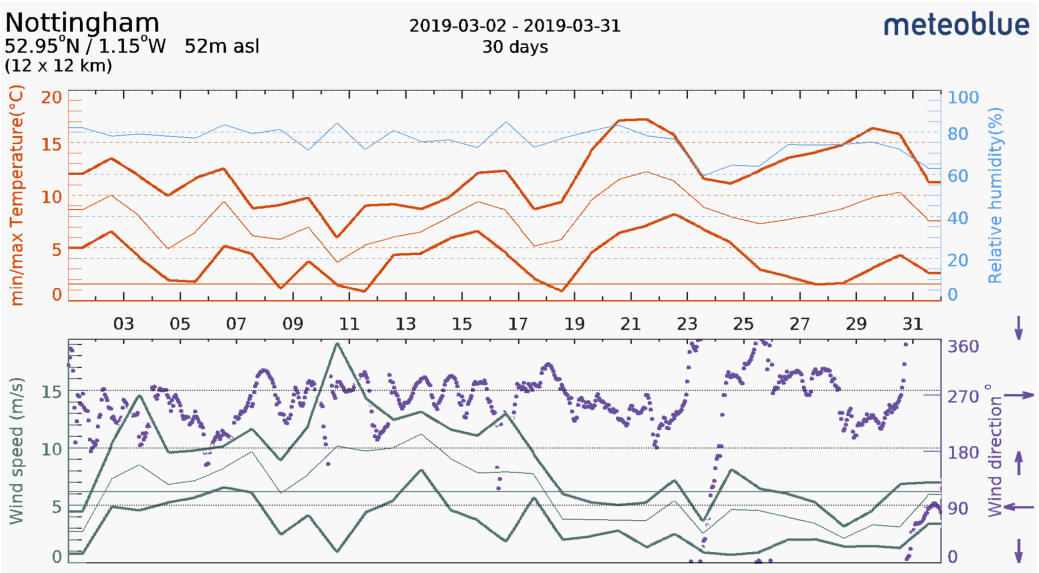
As discussed in Chapter 2, the wind effect is one of the main sources of uncertainty for airtightness testing. Owing to the indefinite nature of the wind and buoyancy effects, the building pressure difference between the indoor and the outdoor environment could be influenced, thus leading to an imprecise measurement of the building airtightness. Many studies noted that the outdoor weather condition, particularly the wind, can significantly influence building airtightness measurement. For example, the ISO 9972 standard suggests a meteorological wind speed limit of 6m/s or 3m/s near ground level for the fan pressurisation test. However, there are few studies that consider the validity of Pulse under windy conditions. Cooper, et al. [32] conducted a series of Pulse tests over a year period to investigate the impact of environmental conditions, including the air temperature, wind speed and direction. They observed a greater effect of the wind condition on the airtightness measurement. Zheng, et al. [150] performed Pulse tests in an outdoor chamber under different steady wind speed levels, and the artificial wind was created by a multi-gear portable trailer fan. Their findings indicate that high wind speeds (i.e., 4-9m/s) result in less repeatability of the Pulse measurement, with large uncertainties. They suggested a model-scale experiment in a wind tunnel to further investigate the steady wind impact on the Pulse test.

On the other hand, most of the investigations addressing the wind impact on building airtightness measurement have been conducted for the fan pressurisation method, while limited studies related to the test performance of Pulse under different wind speeds and directions have been found in the literature. In this chapter, a number of Pulse tests are implemented for measuring the building airtightness of a five-bedroom detached house under a range of natural wind conditions. The Pulse tests are performed in the same building as the one introduced in Chapters 3 and 4. The experimental work entailing 423 tests were conducted over seven days in March 2019. All the tests were accomplished in a short period in order to minimise the impact of variable ambient conditions. The viability of Pulse for delivering airtightness measurements under different wind conditions is evaluated. The impacts of the wind speed and the wind direction on the Pulse test are analysed respectively based on the experimental data. Additionally, different aspects are discussed to minimise the wind impact on the Pulse measurement in practical testing scenarios, including the necessity of implementing the multiple Pulse tests and the optimisation of the adjustment method for the obtained Pulse measured results.

5.2 Investigation of wind impact on the Pulse test in a five-bedroom detached dwelling

5.2.1 Impact of wind speed

In total, 423 tests were implemented under various natural wind conditions, and every test was a three-step pulse test, i.e., contained three successive pulse releases. Figure 5-1 provides the weather data of Nottingham from meteoblue.com [234] during March 2019; the average temperature during the testing period (i.e., 9th March to 15th March 2019) was around 6.34℃, the average meteorological wind speed was approximately 9.26m/s, and the highest meteorological wind speed was 19.12m/s.



**Red lines: the daily temperature; Light blue line: the daily relative humidity; Grey lines: the meteorological wind speed, and Purple dots: the wind direction.*

Figure 5-1: Weather data of Nottingham in March 2019 [234]

During the testing, the outdoor wind condition was measured by an ultrasonic anemometer. The anemometer was installed at the height of 2.2m above the ground in the backyard and a distance of 12m away from the perimeter of the test building, with no significant obstructions within a radius of 12m of the anemometer, except for sparse tree branches and grass on the ground. From herein, the mentioned wind speed in this section refers to the wind speed measured at 2.2m above ground level. Overall, the monitored natural wind condition of 423 tests is in the wind speed range of 0-10m/s, and the wind direction degree of 60° to 300°. In this section, the analysis is focused on the wind speed impact, while the wind direction impact is investigated later in Section 5.2.3.

Due to a large number of test results, analysis is conducted by grouping these tests on the basis of the wind speed range (i.e., 0-3.5m/s; 3.5-6m/s and 6-10m/s). During the entire period of each test,

the outdoor wind speed was continuously recorded, and the highest wind speed during a test was selected as the corresponding wind speed of the test. The reasons for selecting the highest wind speed of each test for analysis are: (a) representing the threshold value of the wind speed during the entire test and (b) taking into account the occurrence of gusty winds during the test period. Therefore, 133 tests have their highest wind speeds in the range of 0-3.5m/s, 3.5-6m/s with 173 tests and 6-10m/s with 117 tests. The average wind speed of all the 423 tests is 4.76m/s.

A violin plot is presented in Figure 5-2, depicting the full distribution shape of the measured air leakage rate (ALR) of all 423 tests across different wind speed ranges. A marker for the median of the data (in blue colour) and a marker for the interquartile range (in green colour) are included. The shape of the distribution of the 423 tests demonstrates that the ALRs are centralised around the interquartile range. It can be clearly seen that the distribution shape varies significantly across the wind speed range with different median ALRs, which indicates that the wind speed affects the measurement of building airtightness. Detailed analysis of each wind speed range is presented in the following sections.

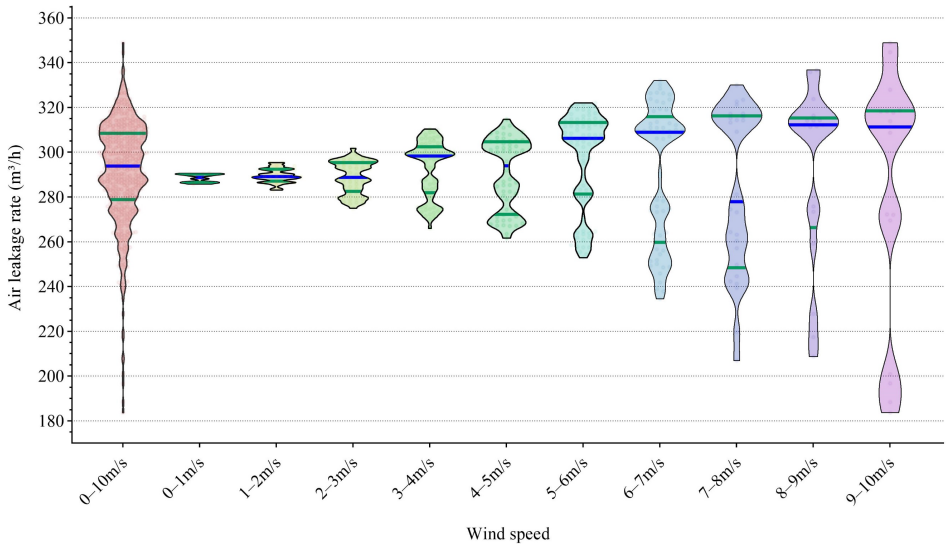


Figure 5-2: Violin plot of 423 tests

0-3.5m/s

Figure 5-3 shows the test results of ALR in the wind speed range of 0-3.5m/s, which includes a total of 133 tests. Among these tests, three tests were performed at low wind speed conditions (i.e., <0.5m/s). The average ALR of the three tests is 288.02m³/h, which is used as the baseline ALR value in this assessment. Hence, the relative percentage difference (*RPD*) is used to indicate the wind impact on building airtightness measurement, which is given by the relative difference between the ALR of each single test and the baseline ALR. The respective *RPD*s of the 133 tests are also provided in Figure 5-3. It can be clearly noted that the *RPD* becomes larger as the wind speed increases.

For a more detailed evaluation, Figure 5-4 provides an overview of how the *RPD*s of the 133 tests are distributed within the speed range of 0-3.5m/s, and the maximum *RPD*s under different wind speed ranges could be easily noted. For instance, in the wind speed range of 1.69-2.0m/s, the maximum *RPD* is about 2.54%, while in the wind speed range of 3.25-3.37m/s, the maximum *RPD* is 6.54%. Compared to the baseline ALR, similar ALR results were obtained when the wind speed was below 2.08m/s, with the maximum *RPD* within ±3%. Also, it can be noted that the *RPD* fell outside ±5% when the outdoor wind speed was higher than 3.14m/s, which indicates that a more accurate building airtightness measurement could be achieved for the Pulse test when the wind speed is around 3m/s. The highest *RPD* of 7.7% was observed among all the 133 tests in the assessed wind range, i.e., 0-3.5m/s. Table 5-1 summarises the corresponding wind speed limit with the *RPD* based on the obtained results.

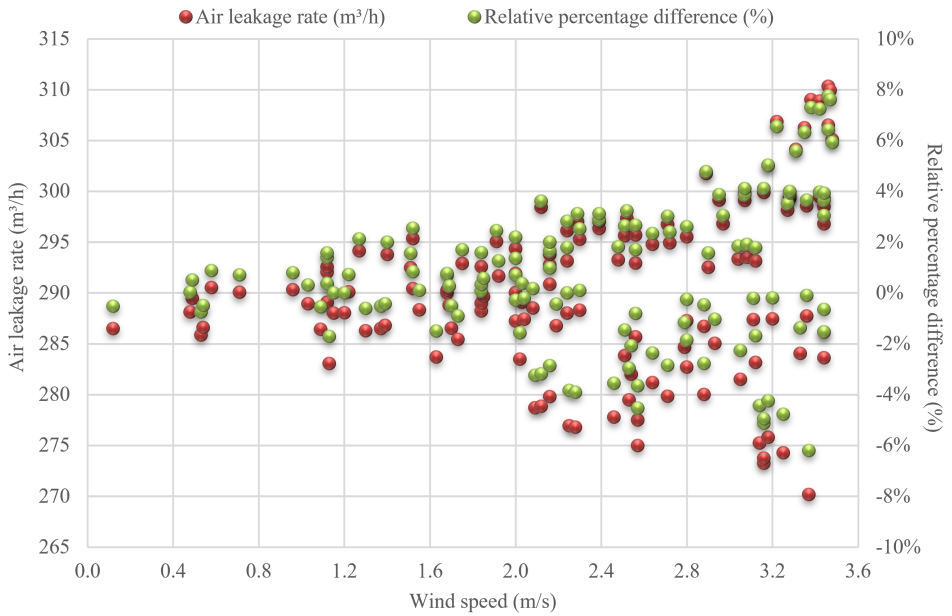


Figure 5-3: Measurements of air leakage rate in the wind speed range of 0-3.5m/s

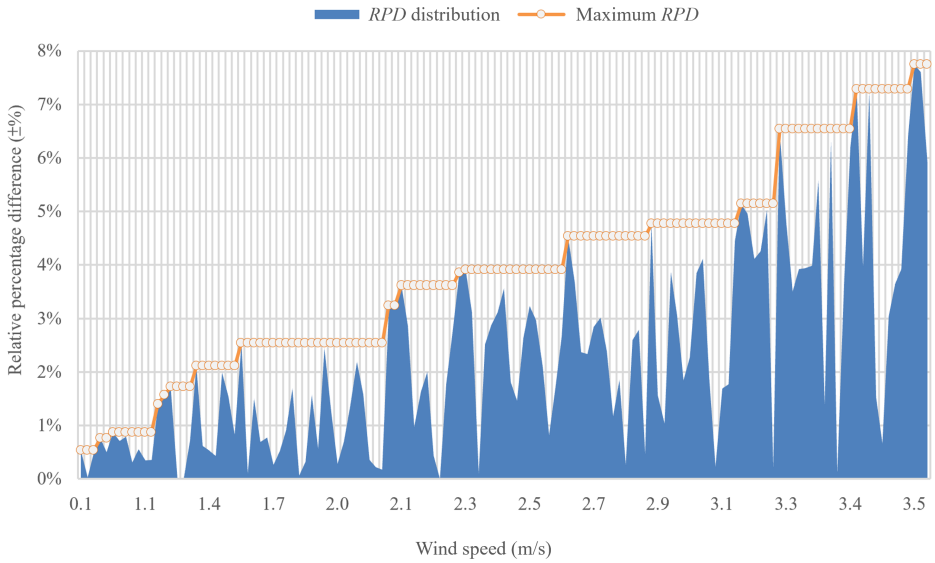


Figure 5-4: Relative percentage difference distribution in the wind speed range of 0-3.5m/s

Table 5-1: Test result summary for the wind speed range of 0-3.5m/s

Wind Speed (Ground Level)			**Number of Tests**			
0 - 3.5 m/s			133 tests			
Wind Speed Limit (m/s) with Maximum Relative Percentage Difference (%)						
<±1%	<±2%	<±3%	<±4%	<±5%	<±6%	<±7%
1.09m/s	1.22m/s	2.08m/s	2.56m/s	3.14m/s	3.20m/s	3.37m/s

3.5-6m/s

There are, in total, 173 tests that have been performed in the wind speed range of 3.5-6m/s. The measured ALR results and the *RPD* of each test are presented in Figure 5-5. Similar trends are seen; as the wind speed increases, the deviation of the measured ALR from the baseline ALR becomes higher. The *RPD*s are higher than those in the lower wind speed range of 0-3.5m/s, and the highest *RPD* is approximately ±12.19% in the wind speed range of 3.5-6m/s.

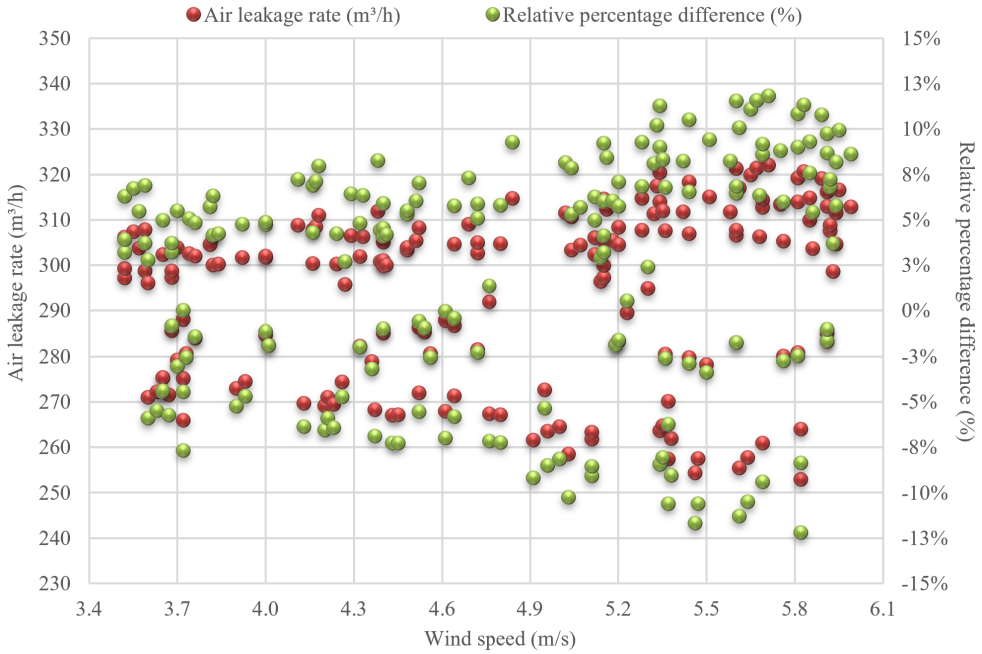


Figure 5-5: Measurements of air leakage rate in the wind speed range of 3.5-6m/s

Figure 5-6 illustrates the *RPD* distribution of the 173 tests in the wind speed range of 3.5-6m/s, and Table 5-2 lists the *RPD* levels with the corresponding wind speed limits. According to the results, when the wind speed exceeded 5.02m/s, the corresponding *RPD* was higher than ±10%. Compared to the wind speed limit stated in the available standards for the fan pressurisation testing, for example, ASTM E779-03, the suggested ground wind speed limit is 2m/s, and a wind speed limit of 3m/s at near ground level or meteorological wind speed of <6m/s is also regulated in the ISO 9972 standard. Based on the obtained results in this study, the building airtightness measurement using Pulse is not suggested at a wind speed higher than around 5.02m/s (i.e., at the

ground level of 2.2m) as a more significant deviation (i.e., >±10%) could occur. This investigation also implies the validity of Pulse under windy conditions.

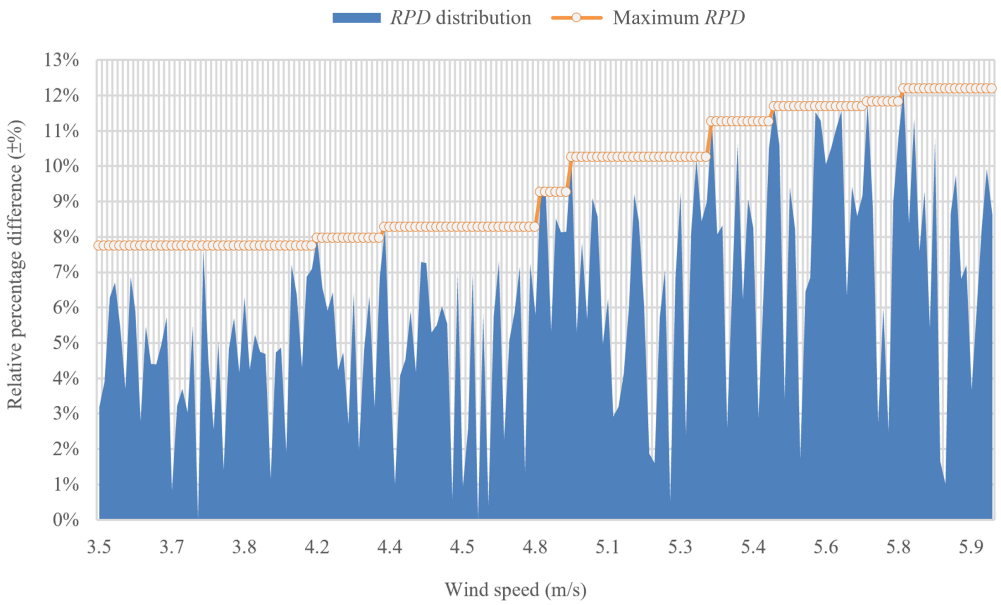


Figure 5-6: Relative percentage difference distribution in the wind speed range of 3.5-6m/s

Table 5-2: Test result summary for the wind speed range of 3.5-6m/s

Wind Speed (Ground Level)			**Number of Tests**		
3.5 - 6.0 m/s			173 tests		
Wind Speed Limit (m/s) with Maximum Relative Percentage Difference (%)					
<±8%	<±9%	<±10%	<±11%	<±12%	<±13%
4.38m/s	4.80m/s	5.02m/s	5.33m/s	5.81m/s	5.99m/s

6-10m/s

For the wind speed range of 6-10m/s, 117 tests have been carried out. Figure 5-7 shows the corresponding ALR measurements and the *RPD* of tests. A larger difference against the baseline ALR (288.02m³/h) was observed under the wind condition of 6 to 10m/s. For example, at the wind speed of 9.35m/s, the ALR reached 348.95m³/h, while 183.67m³/h was obtained at a wind speed of 9.66m/s, with a significant deviation of -36.23%. The *RPD* distribution in the wind speed ranging from 6-10m/s is presented in Figure 5-8, and the detailed data is listed in Table 5-3. As shown in the figure, even in the lower wind speed range of 6.03-6.37m/s, the maximum *RPD* is around 13.39%, which is higher than the data in the wind speed range of 0-6m/s. Furthermore, the *RPD* rose beyond ±20% when the outdoor wind speed was higher than 7.37m/s. Therefore, the results imply that for the Pulse testing, the wind impact should be taken into account under the high wind speed condition as the measured building airtightness could vary considerably, leading to inaccurate results.

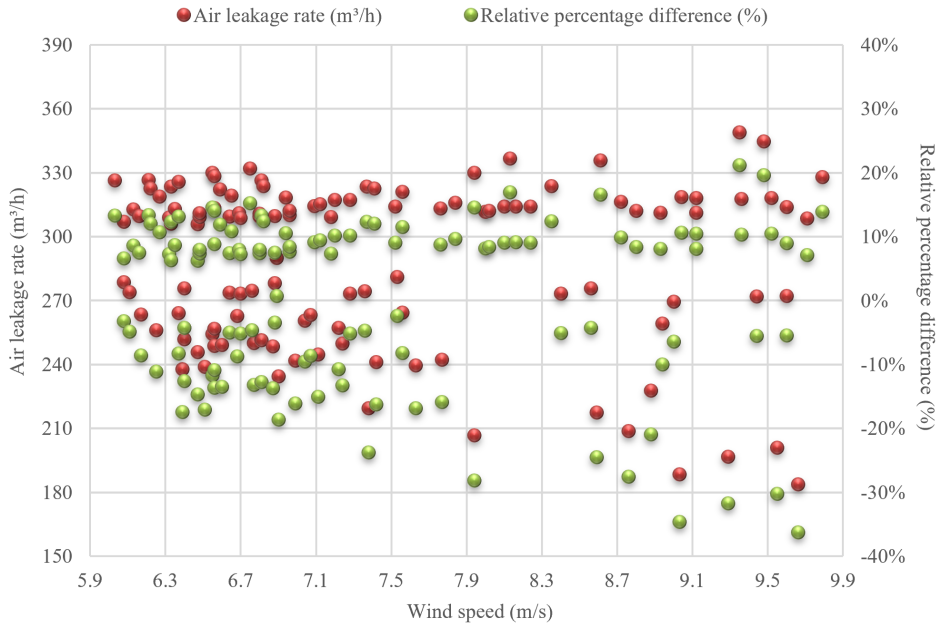


Figure 5-7: Tests results in the wind speed range of 6-10m/s

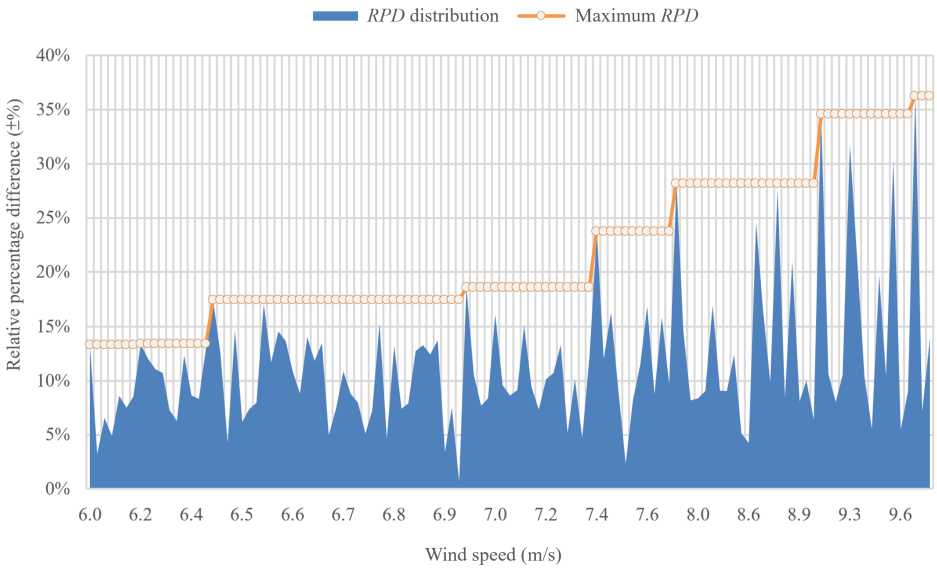


Figure 5-8: Relative percentage difference distribution in the wind speed range of 6-10m/s

Table 5-3: Test result summary for the wind speed range of 6-10m/s

Wind Speed (Ground Level)				**Number of Tests**		
6.0 - 10.0 m/s				117 tests		
Wind Speed Limit (m/s) with Maximum Relative Percentage Difference (%)						
<±14%	<±18%	<±19%	<±24%	<±29%	<±35%	<±37%
6.37m/s	6.89m/s	7.37m/s	7.84m/s	9.00m/s	9.60m/s	9.79m/s

Overall

To better understand the indication of the findings in this study, the wind speed limits obtained in Tables 5-1, 5-2 and 5-3 are then calculated to the corresponding meteorological wind speed based on the test location. It is known that the wind speed rises with the increasing height above the

ground level. To estimate the vertical wind speed profile, two approaches are commonly used, including the log law (eq. 5-1) [235] and the power law (eq. 5-2) [236].

$$v_2 = v_1 \cdot \frac{\ln \frac{z_2}{z_0}}{\ln \frac{z_1}{z_0}} \tag{5-1}$$

Where, z is the reference height and z_0 is the surface roughness length.

$$v_2 = v_1 \cdot (\frac{z_2}{z_1})^{n_s} \tag{5-2}$$

Where, n_s is the terrain surface characteristic based on the typology.

Manwell, et al. [235] listed the values of surface roughness length for various types of terrain, and Dalila, et al. [237] reported various terrain surface characteristics. In accordance with the urban environment in the field tests, z_0 is chosen as 0.1m (i.e., few trees) for log law extrapolation, and n_s is chosen as 0.3 (i.e., a small town with some trees) for power law extrapolation. In the field tests, measurements of the wind speed were also taken at 0.5m, 1m, 1.2m, 1.5m and 2m. By comparing the measured data with the extrapolated values using the two approaches, the power law profiles matched well with the measured data.

Based on the calculation, Table 5-4 summarises the corresponding meteorological wind speed limit with the *RPD* ranges. It can be seen that the threshold value of the meteorological wind speed is approximately 7.91m/s for the *RPD* within ±10%.

Table 5-4: Test result summary for the meteorological wind speed range of 0-16m/s

Meteorological Wind Speed	Number of Tests	Wind Speed Limit (m/s) with Maximum *RPD* (%)						
0 - 6m/s	133 tests	<±1%	<±2%	<±3%	<±4%	<±5%	<±6%	<±7%
		1.72m/s	1.92m/s	3.28m/s	4.03m/s	4.95 m/s	5.04 m/s	5.31 m/s
6 - 10m/s	173 tests	<±8%	<±9%	<±10%	<±11%	<±12%	<±13%	
		6.90m/s	7.56m/s	7.91m/s	8.39m/s	9.15m/s	9.43m/s	
10 - 16m/s	117 tests	<±14%	<±18%	<±19%	<±24%	<±29%	<±35%	<±37%
		10.03m/s	10.85m/s	11.61m/s	12.35m/s	14.17m/s	15.12m/s	15.42m/s

Different wind speed limits for the fan pressurisation method are available in different standards, such as <2m/s ground wind speed in the American standard ASTM E779 [144], <5.5m/s metrological wind speed for Canadian Standard [197] and <6m/s metrological wind speed for the European Standard EN 13829 [191]. The experiment work of the 423 tests provides insights into whether these wind speed limits also apply to the Pulse testing. According to the observations, it is preferred to perform the Pulse test under the wind speed <2.08m/s (i.e., meteorological wind speed of 3.28m/s) with the *RPD* <±3%, and the test is advised to be performed at <5.02m/s (i.e.,

meteorological wind speed of 7.91m/s) for the *RPD* within ±10%. Different from Zheng, et al. [238] using a multi-gear portable trailer fan to provide various artificially imposed steady wind conditions, this study was conducted under natural wind conditions with unpredictable wind characteristics. Both studies investigated the wind speed limit that allowed Pulse to produce repeatable and accurate measurements. For the *RPD* within ±3%, Zheng, et al. [238] found the test conditions were under the steady wind speeds below 3.5m/s at 1.5m above ground level with a fixed wind direction, while the wind speed below 2.08m/s at 2.2m above ground level under natural wind conditions was noted in this study.

A different pattern in the airtightness variation is shown between the two studies when the wind level was beyond the limit. This might be attributed to: (a) the different building configurations, i.e., the small-size outdoor chamber and the five-bedroom dwelling; (b) different wind conditions experienced in the studies, i.e., the artificially imposed steady wind in a fixed direction in contrast to the natural wind conditions with unprecedented wind directions and fluctuations; (c) the analysis presented in this section does not consider the wind direction impact; and (d) the occurrence of wind gust during the test period, which may influence the building airtightness measurement, but was not able to be monitored by the anemometer due to the distance between the anemometer and the test building, and the duration of the gusty the wind gust lasted.

5.2.2 Impact of multiple tests

Conducting multiple tests would be a solution to minimising the wind impact on building airtightness measurement; hence multi-point method is preferred for the fan pressurisation testing, as discussed in Section 2.6.3. In this section, an assessment is conducted to evaluate how multiple Pulse tests could contribute to minimising the wind impact on the airtightness measurement.

With a wind speed interval of 0.5m/s, the total 423 tests can be divided into 20 groups for more in-depth discussions (i.e., from Group A: 0-0.5m/s to Group T: 9.5-10m/s). Assessments are performed based on three cases to include all the practical testing scenarios, which are: (1) each test, (2) multiple tests in each group and (3) the first three tests in each group. Table 5-5 lists the detailed results for Group A to Group T, with regard to the ALRs for each case and the corresponding *RPD*s by comparing with the baseline ALR.

The violin plot in Figure 5-9 shows the shapes of ALR distribution for the three cases, which clearly visualises the difference between the three cases. By conducting the multiple Pulse tests, the difference of ALR between different wind speed ranges is much less significant compared with the ALR that is obtained from a single Pulse test under various wind conditions. Although

the median ALRs for the three cases are close, the interquartile range describing the range in values of the central 50% of ALRs differs widely in the three cases, suggesting the necessity of the multiple Pulse tests to minimise the wind impact on the airtightness measurement.

Table 5-5: ALR results for the 423 tests

Test Group	Wind Speed (Ground Level)[1]	Number of Tests	Group Average ALR	First Three Tests Average ALR	Relative Percentage Difference		
					Each Test[2]	Each Group[3]	First Three Tests[4]
A	0 – 0.5 m/s	3	288.02	288.02	-0.53%	0.00%	0.00%
B	0.5 – 1.0 m/s	5	288.66	287.64	-0.76%	0.22%	-0.13%
C	1.0 – 1.5 m/s	15	288.97	288.12	-1.72%	0.33%	0.03%
D	1.5 – 2.0 m/s	17	290.01	292.74	2.54%	0.69%	1.64%
E	2.0 – 2.5 m/s	28	288.84	289.72	-3.91%	0.28%	0.59%
F	2.5 – 3.0 m/s	26	288.63	292.25	-4.53%	0.21%	1.47%
G	3.0 – 3.5 m/s	39	293.85	291.30	7.74%	2.02%	1.14%
H	3.5 – 4.0 m/s	33	291.13	300.87	-7.68%	1.08%	4.46%
I	4.0 – 4.5 m/s	33	292.31	296.14	-7.28%	1.49%	2.82%
J	4.5 – 5.0 m/s	23	286.88	287.92	-9.18%	-0.40%	-0.03%
K	5.0 – 5.5 m/s	43	293.33	278.19	-11.69%	1.84%	-3.42%
L	5.5 – 6.0 m/s	41	301.65	301.69	-12.19%	4.73%	4.74%
M	6.0 – 6.5 m/s	24	294.78	304.01	-17.47%	2.35%	5.55%
N	6.5 – 7.0 m/s	33	288.54	274.40	-18.60%	0.18%	-4.73%
O	7.0 – 7.5 m/s	16	281.42	279.31	-23.77%	-2.29%	-3.03%
P	7.5 – 8.0 m/s	10	282.87	286.57	-28.18%	-1.79%	-0.50%
Q	8.0 – 8.5 m/s	8	312.50	312.63	16.93%	8.50%	8.54%
R	8.5 – 9.0 m/s	9	273.82	276.31	-27.56%	-4.93%	-4.07%
S	9.0 – 9.5 m/s	10	288.59	258.85	-34.59%	0.20%	-10.13%
T	9.5 – 10 m/s	7	275.05	263.75	-36.23%	-4.50%	-8.43%
Based on Low Wind Speed Conditions 0 – 0.5 m/s (3 Tests)			Baseline: Average ALR (m³/h)				
			288.02				

1. Wind speed measured at the height of 2.2m above ground.
2. The maximum relative percentage difference of ALR of each single test to the baseline ALR.
3. The relative percentage difference of average ALR of each group to the baseline ALR.
4. The relative percentage difference of average ALR of the first three tests to the baseline ALR.

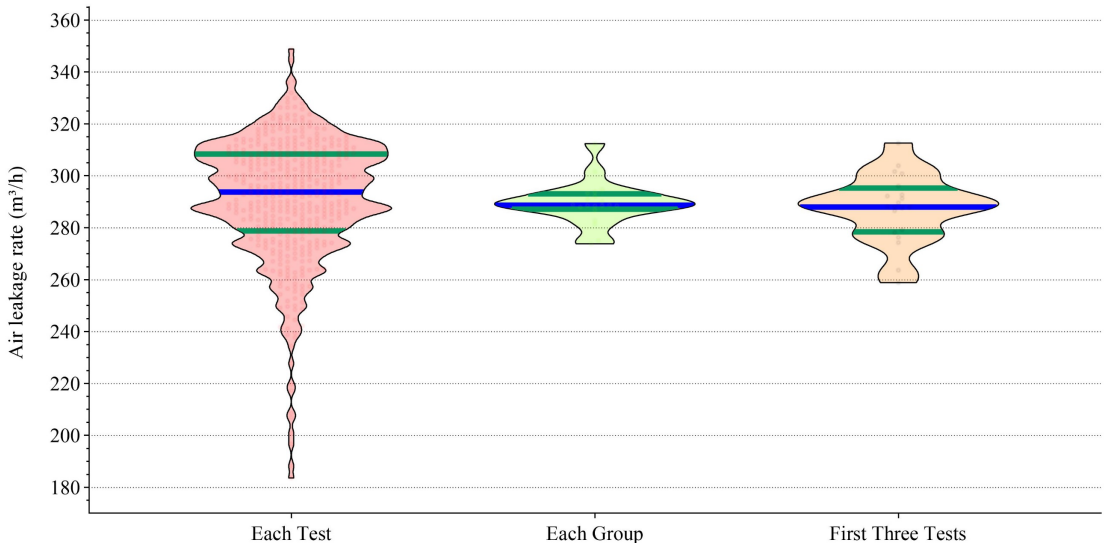


Figure 5-9: Violin plot of ALR results for the 423 tests, by each test, each group and first three tests

The corresponding *RPD* distributions are presented in Figure 5-10. It can be clearly seen that an increased number of the Pulse tests contributes to minimising the wind impact on the building

airtightness measurement. For instance, for the single Pulse test conducted in the wind speed range of 5.0-5.5m/s (i.e., Group K), the maximum *RPD* was approximately -11.69%. By considering the first three tests in Group K, the *RPD* reduced to -3.42%, and the *RPD* was only around 1.84% when taking all the 43 tests in Group K into consideration. Although it would be impractical to conduct a number of the Pulse tests in practice, the three Pulse tests could also make a difference. The difference became more significant under more windy conditions; for example, the *RPD* decreased by 6.6% in Group G (i.e., 3-3.5m/s), while the reduction in *RPD* was 17.8% in Group T (i.e., 9.5-10m/s).

On the other hand, the *RPD* of each group fell within ±5% when the wind speed was below 8m/s, and the *RPD* of the first three tests fell within ±5% when the wind speed was below 6m/s. However, the recommended wind speed limit for a single Pulse test is about 3.14m/s for an *RPD* within ±5%, as discussed in Section 5.2.1. Therefore, in practical circumstances, the multiple Pulse tests could be a solution to obtaining the building airtightness measurement with a reduced wind impact under inevitable windy conditions.



Figure 5-10: *RPD* results for the 423 tests, by each test, each group and first three tests

Besides evaluating the first three tests in each group, further investigations are conducted to provide insights into how the *RPD* reduces when comparing a single Pulse test with three multiple tests that are randomly selected from all 423 tests. Theoretically, the total number of combinations for three multiple tests is 12,525,171. The *RPD* distribution is provided with the corresponding

number of combinations in Figure 5-11. The *RPD* of 3% has the highest probability with the most combinations (i.e., 1,142,399 combinations, accounting for 9%).

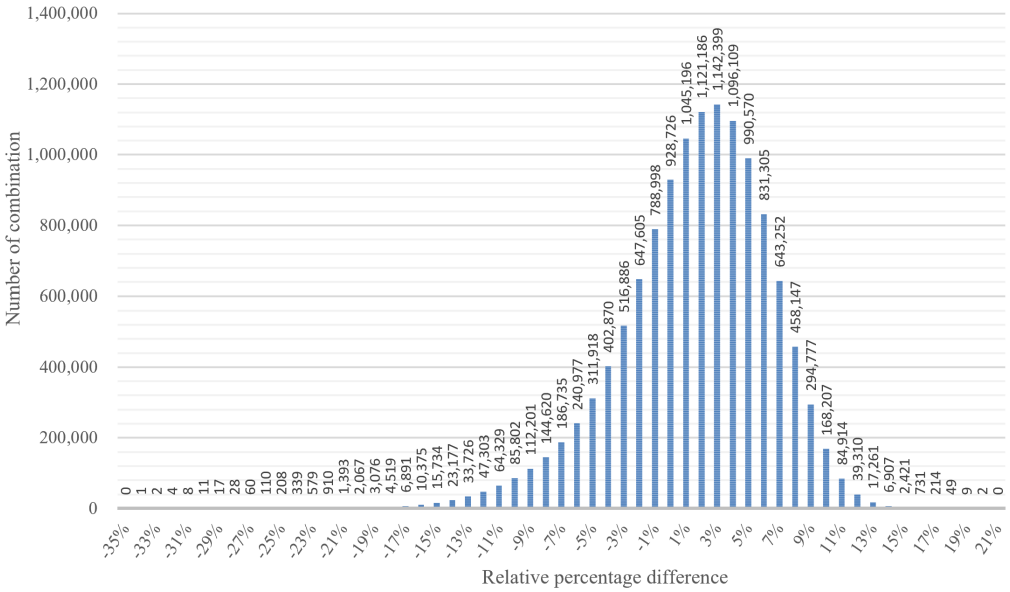


Figure 5-11: *RPD* distribution with the corresponding number of combinations

The pie chart in Figure 5-12 shows the proportion of each *RPD* among all combinations in the wind speed range of 0-10m/s. The results show that the majority of the three multiple Pulse tests (i.e., 97.07%) could achieve an *RPD* within ±10%, while the *RPD* <±3% accounts for 49.43%, and 71.80% of the combinations have an *RPD* <±5%. Only a very small proportion (i.e., 2.93%) has an *RPD* beyond ±11%. Therefore, the assessment shows by performing multiple Pulse tests, the impact of adverse wind conditions on the Pulse measurement can be significantly reduced.

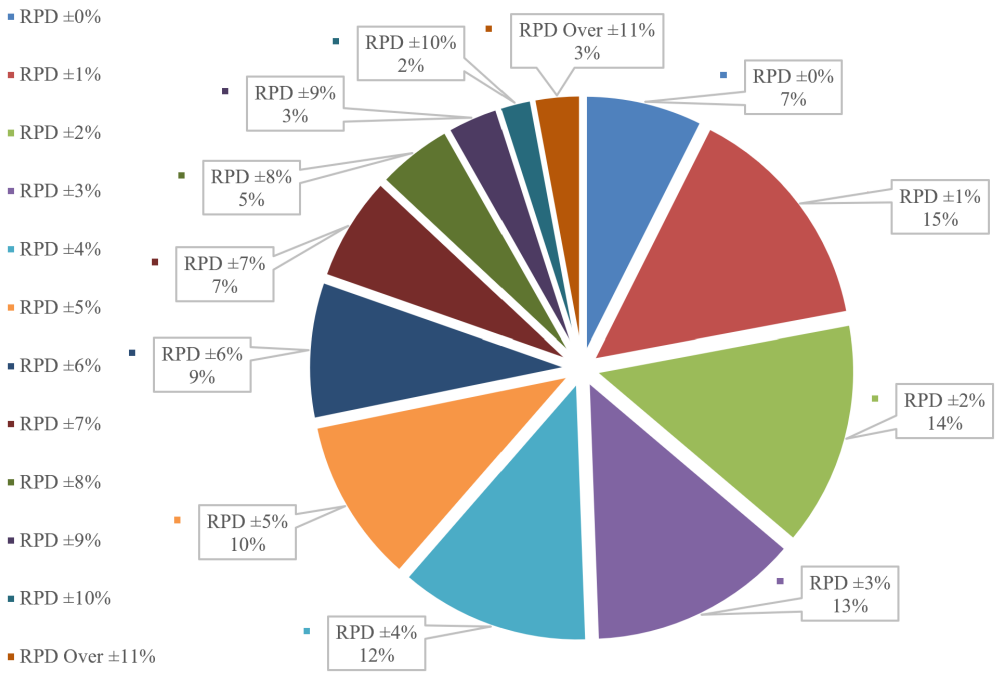


Figure 5-12: *RPD* distribution and the corresponding proportion

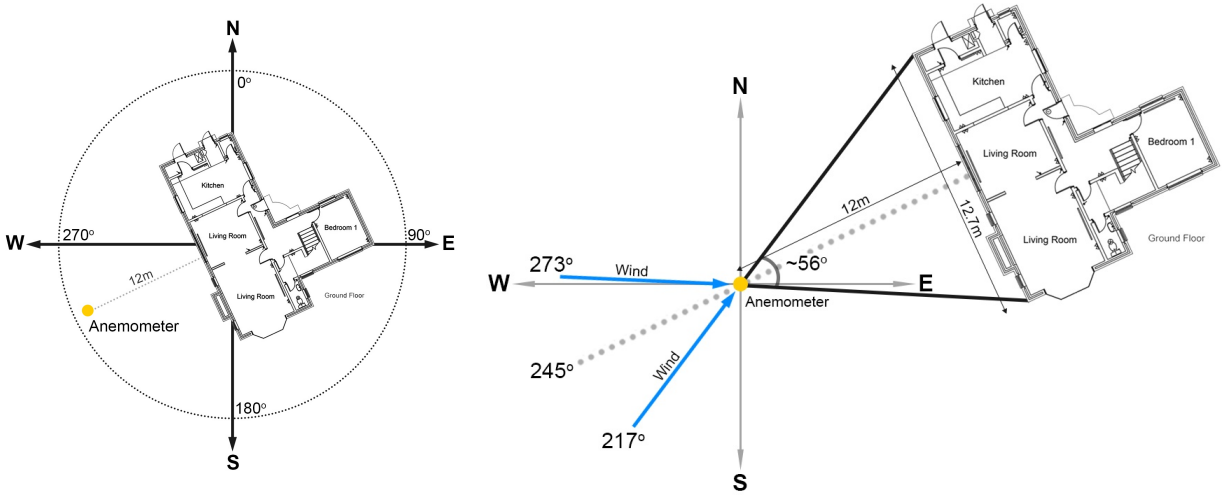
5.2.3 Impact of wind direction

As introduced in Section 5.2.1, an ultrasonic anemometer was installed in the backyard of the tested dwelling at the height of 2.2m above ground to record the outdoor wind conditions during the Pulse testing, including the wind speed as well as the wind direction. Figure 5-13 presents the photo of the employed anemometer in the backyard, at a distance of 12m away from the nearest perimeter of the test building.



Figure 5-13: Photo of ultrasonic anemometer in the backyard of tested dwelling

In terms of site analysis, the tested dwelling orientation is shown in Figure 5-14(a). Considering the anemometer orientation and building geometry, for the wind blowing to edges of the façade facing the backyard, the corresponding wind direction degree measured by the anemometer ranges from 217° to 273° as illustrated in Figure 5-14(b).



(a) (b)

Figure 5-14: Illustrations of (a) tested dwelling orientation and (b) anemometer orientation and wind directions with respect to tested dwelling

In total, 423 Pulse tests have been conducted under different wind conditions. A wind rose plot is produced in Figure 5-15, to provide an overview of the wind condition distribution of the 423 tests, and the vertical axis represents the number of the Pulse tests. It can be seen that most of the tests were conducted with the wind direction degree from 220 to 270°, which is mainly attributed to the prevailing west to south-westerly winds in the UK. The wind rose for Nottingham, produced by meteoblue.com [234] is presented in Figure 5-16, based on the historical annual weather data of Nottingham. It can be noted that the predominant wind is between the south-southwest (SSW) and west (W) direction. In addition, the dominant directions of the wind were in the range of 180-300° during the testing period, as shown in the weather data chart in Figure 5-1. Owing to the anemometer location and building orientation (Figure 5-14), the wind coming from the north-northwest (NNW) to the southeast (SE) could not be easily monitored during the tests.

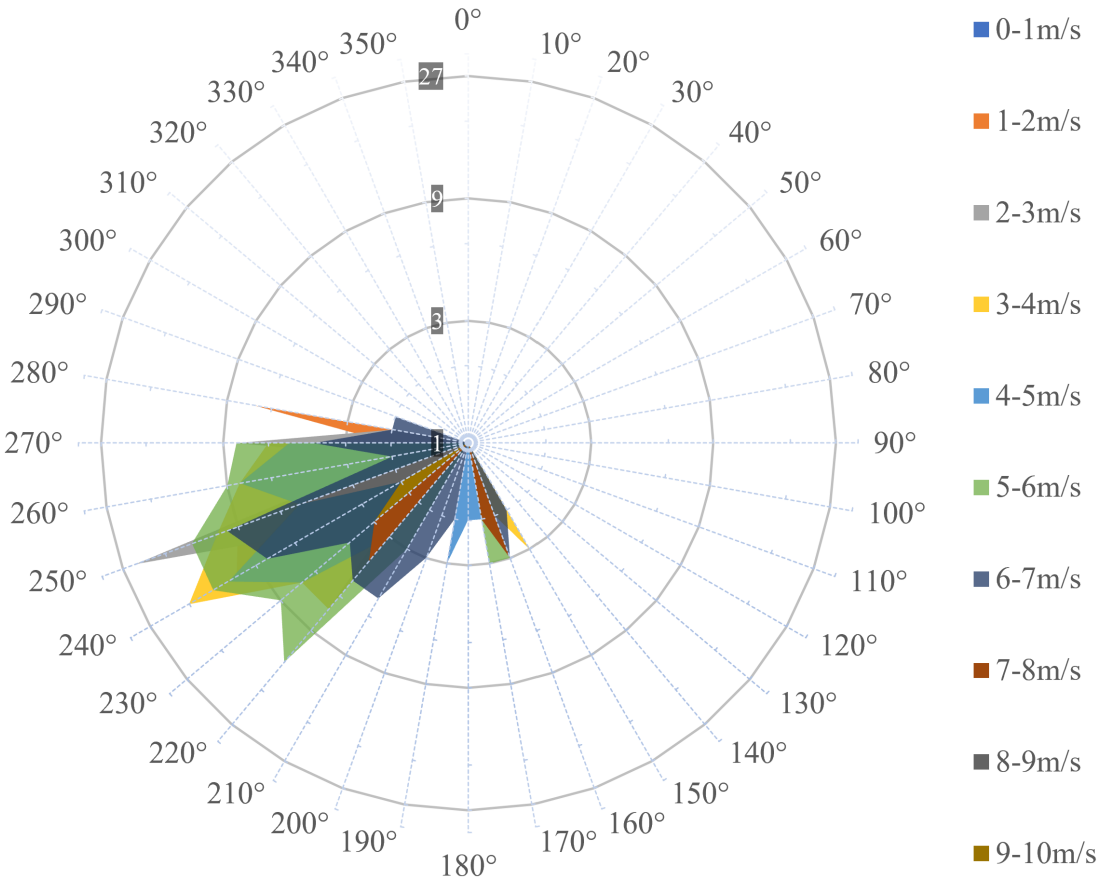


Figure 5-15: Wind rose plot of wind condition distribution of 423 tests

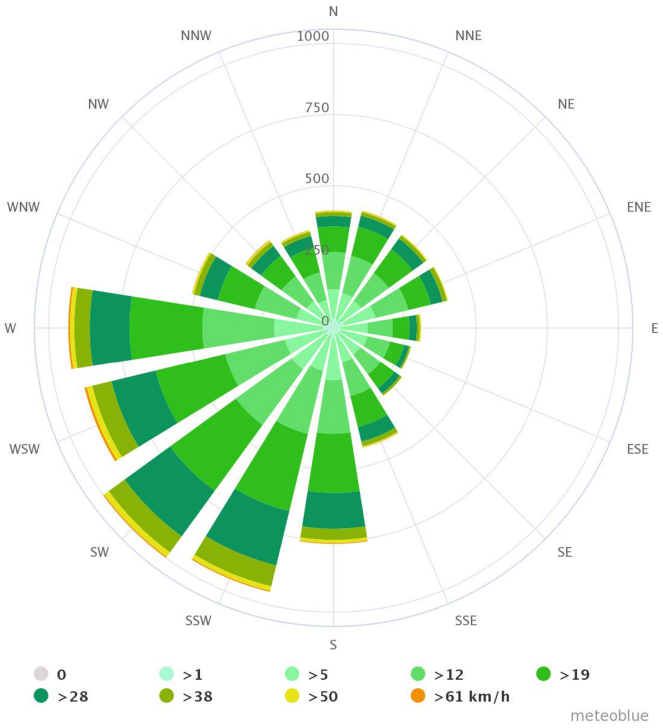


Figure 5-16: Wind rose for Nottingham [234]

More specifically, the wind direction distribution and the associated number of tests is shown in Figure 5-17. The wind direction range for all the 423 tests is from direction degree of 60° to 300°, while no tests have been conducted with the wind direction from 300° to 60° due to climatic characteristics in Nottingham during the test period. Comparatively, the wind direction degree of 250° has the greatest number of the Pulse tests, in total about 85 tests, accounting for 20.1% of the total 423 tests, followed by the wind direction degree of 240° with 78 tests.

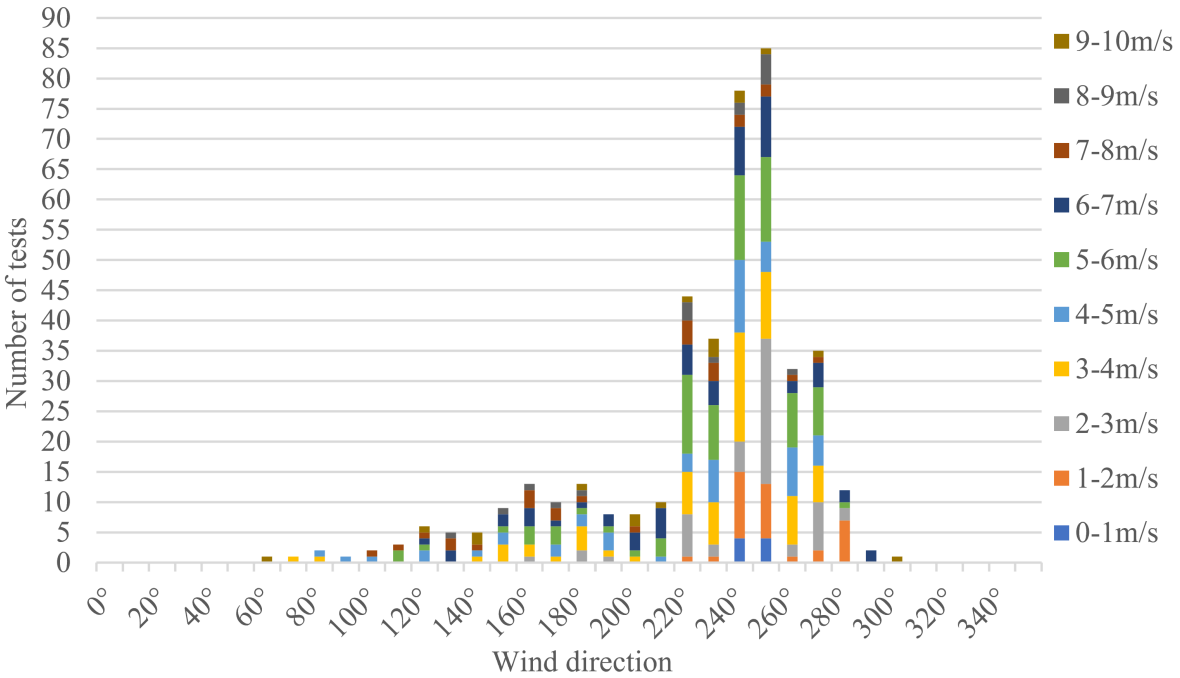
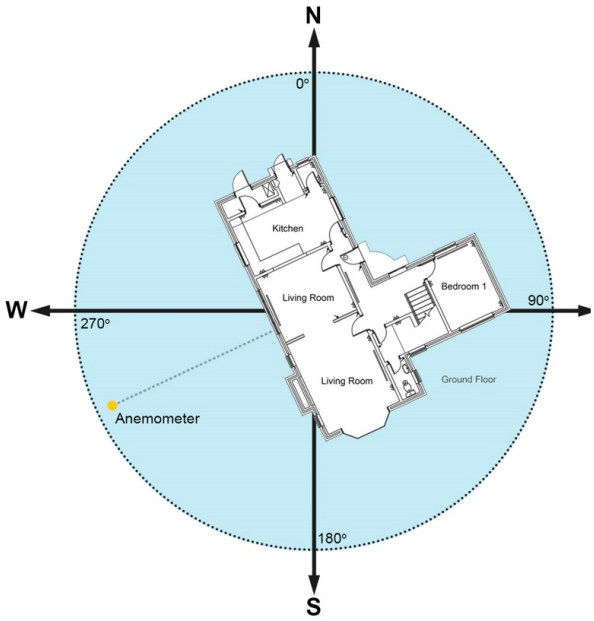
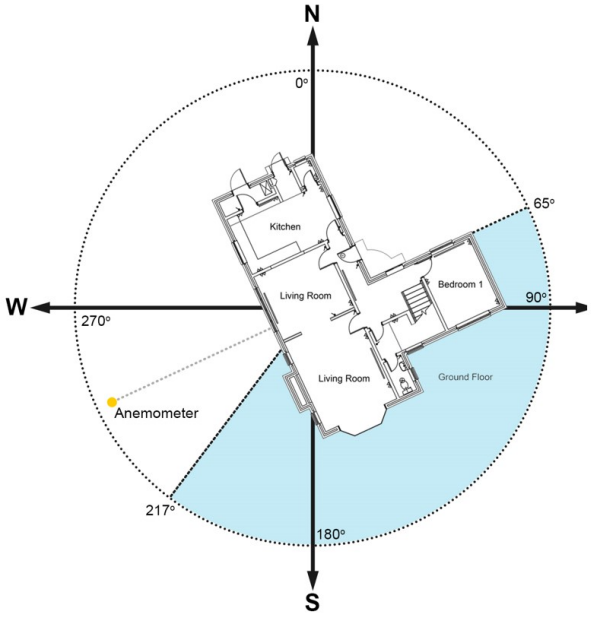


Figure 5-17: Wind direction distribution of 423 tests

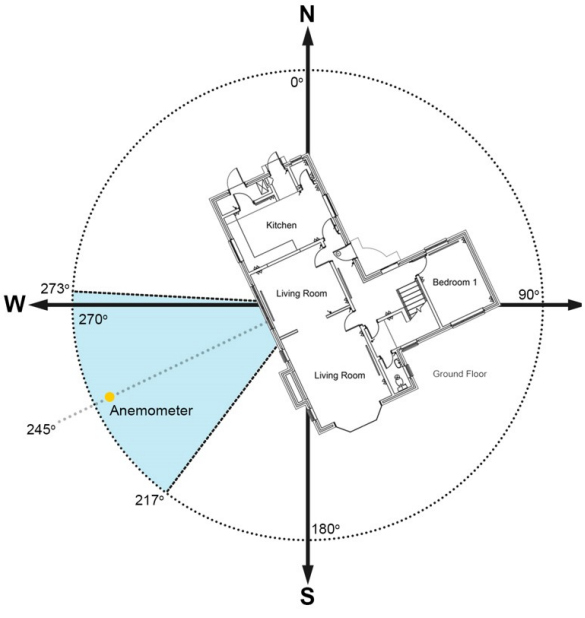
For analysis, the 423 tests are categorised into three groups according to the wind direction degree in respect to tested dwelling, such as Group 1: 65°-217°; Group 2: 217°-273° and Group 3: 273°-65°. There are 101 tests in Group A, 301 tests in Group B, and 21 tests in Group C. Figure 5-18 depicts the respective wind direction categories experienced by tested dwelling during testing, showing the windward/leeward façades of the house in different wind directions categories.



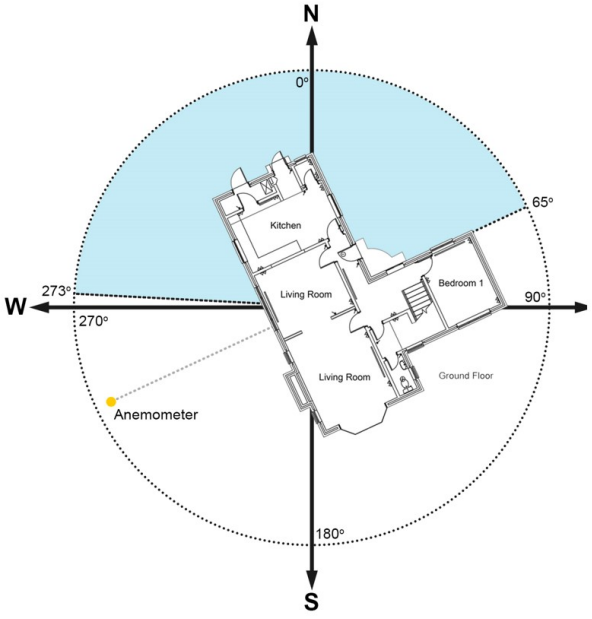
Wind Direction 0° - 360°



Group A: Wind Direction 65° - 217°



Group B: Wind Direction 217° - 273°



Group C: Wind Direction 273° - 65°

Figure 5-18: Illustration of different wind direction categories with tested dwelling

The measured ALRs under different wind directions are plotted in Figure 5-19. Group B has the largest number of tests in the wind speed range of 0.1-9.8m/s, while the wind speed range of Group A is 2.0-9.7m/s, and fewer tests were implemented in Group C with the wind speeds mainly

fell in the range of 1.1-2.7m/s and 5.7-6.8m/s. In the overlapped wind speed range of 2-3m/s, the tests in Group B provided ALR measurement results higher than those of Group A and C, with the average ALR of 294.64m³/h, 276.04m³/h for Group A and 281.36m³/h for Group C. In the wind speed range of 6-7m/s, larger differences among the three groups were noted; Group C has larger average ALR results (i.e., 328.13m³/h), which is approximately 5.74% higher than that of Group B (i.e., 309.31m³/h) and 21.84% higher than Group A (i.e., 256.47m³/h). It can also be seen from the figure, the tests in Group B provided measurement results that were less susceptible to the variation in wind direction, with the maximum difference of 22.15% in the ALR measurements over the tested wind speed range, while the maximum difference reached 55.53% for Group A.

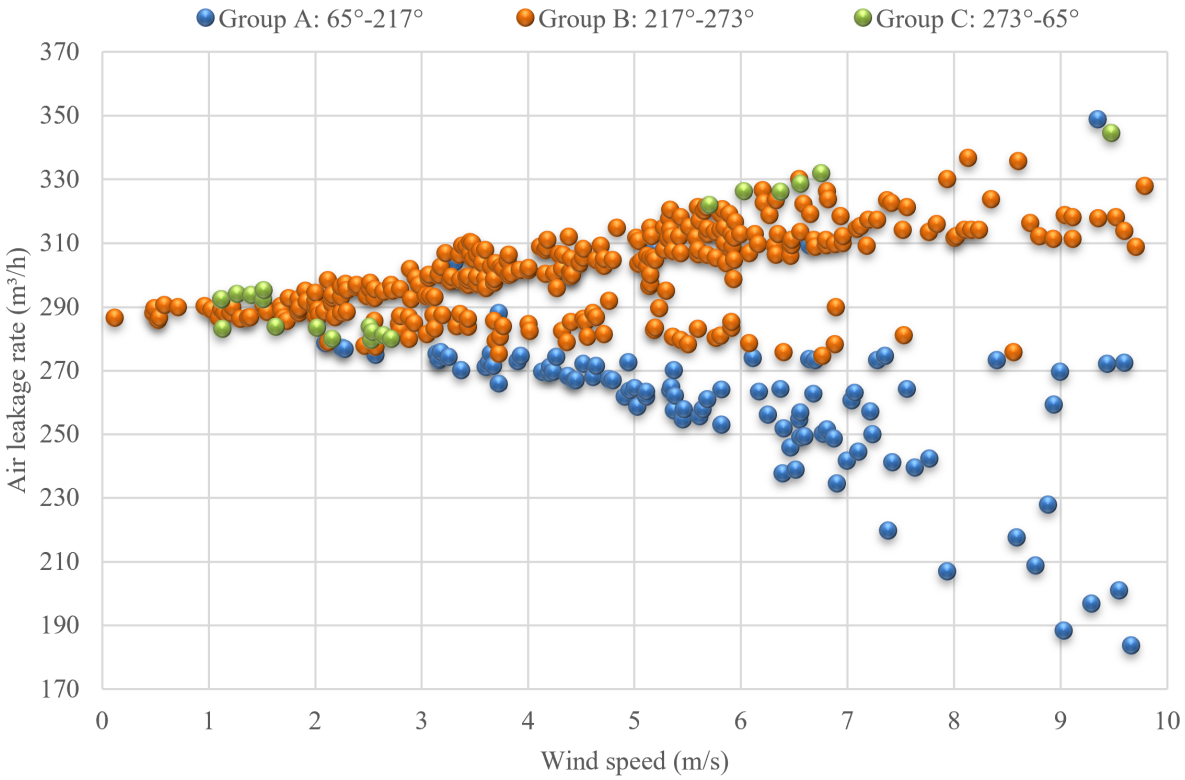


Figure 5-19: ALR measurements under different wind directions

This could also be observed in the violin plot in Figure 5-20, as the three groups have distinct distribution shapes. In addition, each group has different median ALRs and interquartile ranges. Comparatively, Group A and Group C have relatively larger dispersions of the ALR data, while the ALRs of Group B are more centralised in the interquartile range. In this study, Group B has the greatest number of tests (i.e., 71% of the total tests), owing to the UK's prevailing west to south-westerly winds, while 24% of the tests were in Group A, and 5% in Group C. Hence, based on the obtained data, the Pulse test is preferably performed in the tested dwelling, with the wind direction in the range of 217°-273°, for a reduced impact of the wind direction on the airtightness measurement. This finding may not be appliable to the Pulse testing in other buildings, as the

building configuration and local wind characteristics vary; nevertheless, it provides insights into the wind direction effect on the Pulse test under natural conditions.

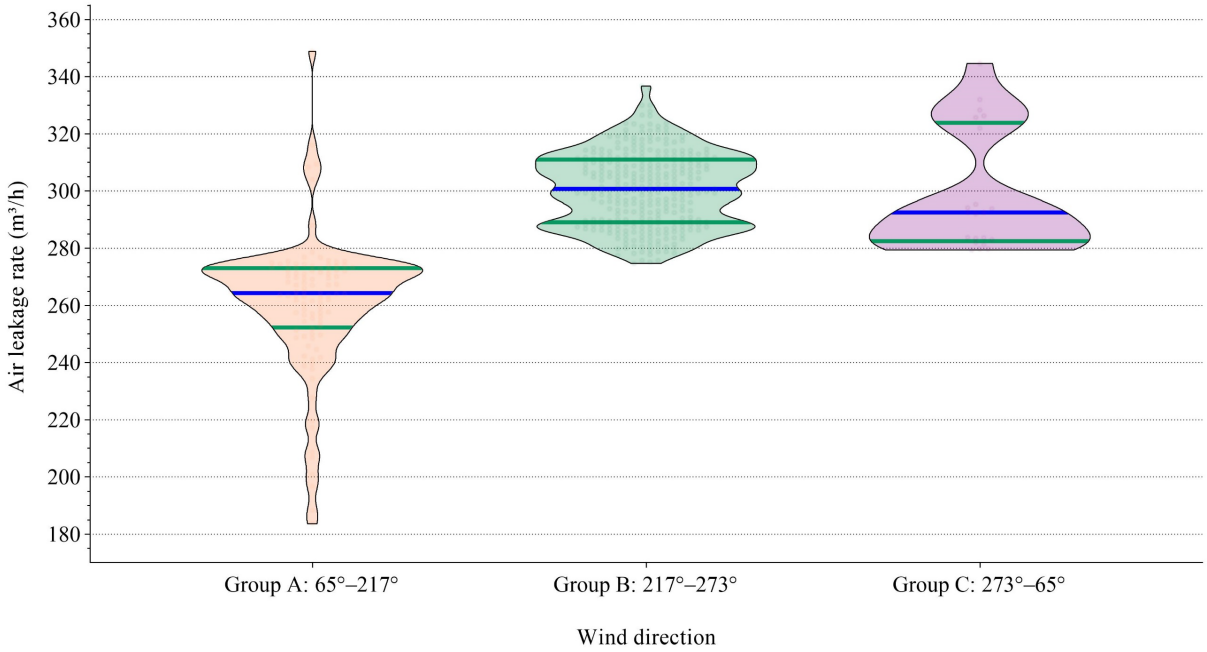


Figure 5-20: Violin plot of ALR results under different wind directions

Furthermore, the impact of the wind direction is less significant when the corresponding wind speed is at a low level. It can be noted from Figure 5-19, the average ALR measurement for tests in Group B is around 289.13m³/h in the wind speed range of 0-2m/s with a difference of 3% between the highest and the lowest measurements, while the discrepancy becomes more noticeable for the wind speed above 3m/s, with the maximum difference of 61.07m³/h in the wind speed range of 8-9m/s. Similar results are found when comparing different groups. For instance, at a wind speed of 1.5m/s, the ALR of 292.48m³/h was measured in Group C, while the measurement of 290.40m³/h was obtained in Group B, with a difference of 2.07m³/h. However, the difference becomes much larger when the measurement of Group B is compared with that of Group C at the wind speed of 6.8m/s, which is 57.27m³/h, and the difference between Group C and Group A at the wind speed of 9.5m/s reached up to 117.25m³/h. This is also because of the limited available tests in Group C. Therefore, a similar recommendation could be made, as discussed in Section 3.1, that the Pulse test is recommended at the calm wind condition (e.g., at lower wind speed level) for accurate building airtightness measurement with minimal wind impact.

5.3 Optimisation of adjustment methods for Pulse to address the wind impact

5.3.1 Adjustment methods for Pulse measurement results

Figure 5-21 illustrates the flow chart of the Pulse test procedure in this study, beginning with the building preparation and Pulse unit set-up, followed by the determination of the number of the air pulse releases, the implementation of the Pulse test, the data process and the data output based on the test quality check criteria. Referring to criteria for test validity of the fan pressurisation method in the ISO 9972 standard, the test result validity for each Pulse test at 4Pa is examined in this study based on the three main criteria: (1) The maximum recorded quasi-steady-state pressure >4Pa and the recorded minimum quasi-steady-state pressure <4Pa; (2) the air flow exponent (n) in the range 0.5 to 1, and (3) the coefficient of determination (R^2) in the log-log plot >0.98.

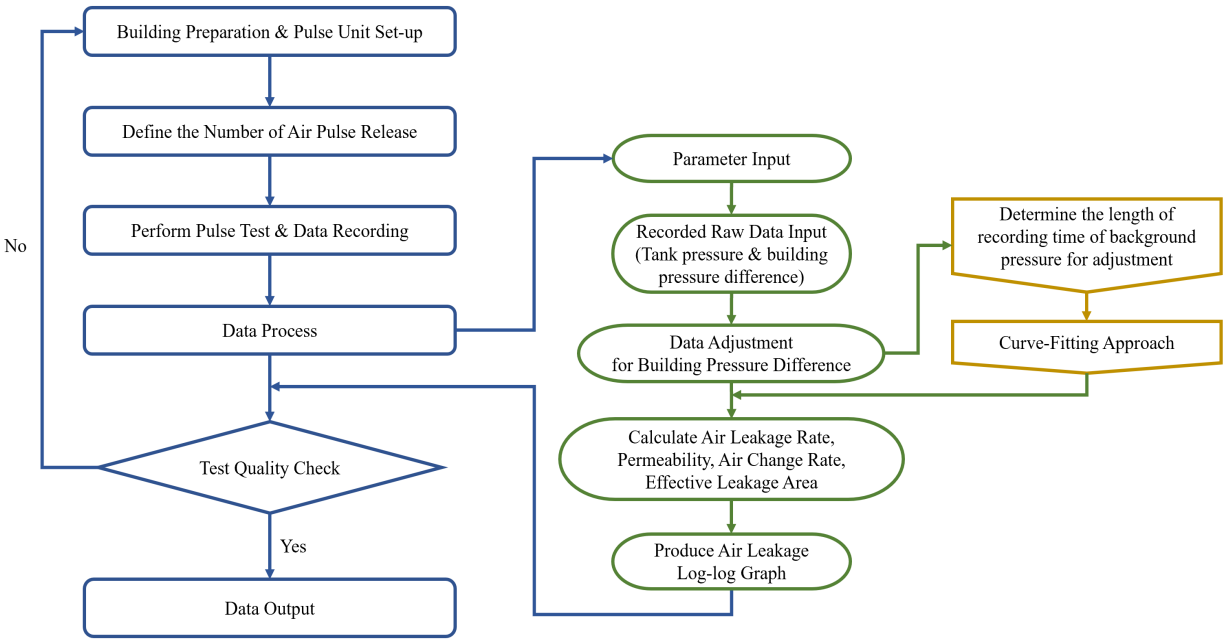


Figure 5-21: Flow chart of the Pulse test procedure

During the Pulse test, the raw data consisting of continuous records of both the tank and building pressures during the entire Pulse testing period were recorded in the control box at three key stages: (1) background pressure before the pulse release; (2) quasi-steady period during the pulse release; (3) background pressure after the pulse release until indoor pressure becomes steady for recording. After the process of the data, a leakage graph is produced by plotting the building leakage rate against the corresponding pressure differences on a log-log plot. An example plot of recorded building pressure difference against time (i.e., red line) is provided in Figure 5-22.

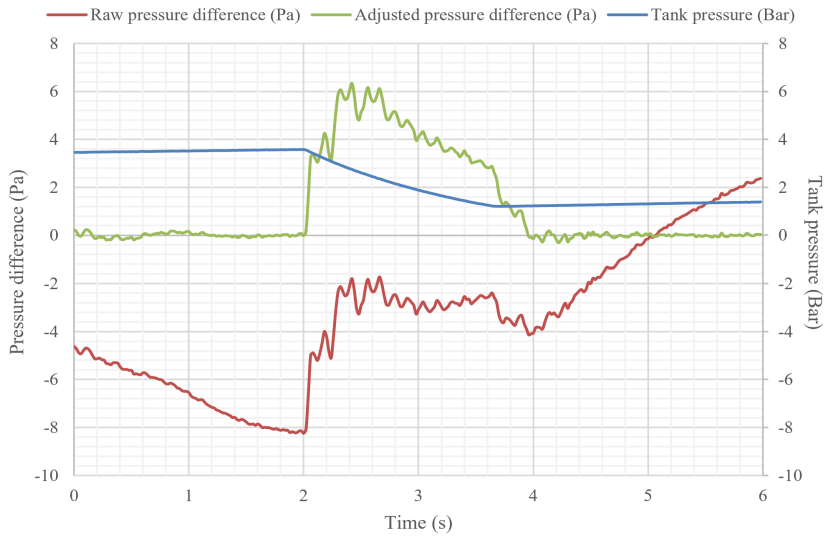


Figure 5-22: Recorded pressure differences against time and with adjustment

The variation of the pressure difference before and after the imposed pulse is noticeable (e.g., around -4Pa to +2Pa), which is mainly attributed to the wind and buoyancy impact. Based on the theoretical research by Cooper, et al. [29], the still-air pulse can be obtained by subtracting the building pressure difference variation owing to wind and buoyancy effects from the recorded pressure data. To justify the variation of the pressure difference due to wind and buoyancy effects during the pulse release, interpolation from the recorded pressure difference between the start and endpoint of the pulse release should be considered. Therefore, an adjustment to the recorded measurement was proposed by Cooper, et al. [30], by fitting a curve to the data before and after the pulse and then subtracting the curve from the raw data. As presented in the flow chart in Figure 5-21, the calculation of the building airtightness is conducted based on the adjusted building pressure values. An example of the adjusted pressure difference is represented in the green line in Figure 5-22. Furthermore, the uncertainty related to the curve-fitting is usually small, as demonstrated by the repeatability testing in [30].

In this section, improvements on the adjustment method are investigated to minimise the wind and buoyancy impact to the measurement of the building pressure induced by the air pulse released during the Pulse testing. In general, three perspectives will be discussed based on the experimental work, including: (1) the appropriate number of pulse releases in a one complete Pulse test; (2) the optimum time duration for recording the background building pressure and (3) the optimum sampling point for curve fitting adjustment. As presented in Section 5.2, the total 423 tests conducted in the detached dwelling under various wind conditions are used in the following sections. The validity of each test is assessed accordingly as the adjustment method is optimised from the above-mentioned three perspectives, ensuring the evaluation of the adjustment methods meets the valid test requirement.

5.3.2 Number of pulse release

A complete Pulse test could contain a single air pulse release, two air pulse releases or three air pulse releases, as shown in Figure 5-23. The PULSE-60 unit employed for this experimental work allows up to three pulse releases in one complete Pulse test. It is also noteworthy that the reduction in the building pressure is attributed to the decreasing tank pressure as there is no charging of the tank between successive pulses.

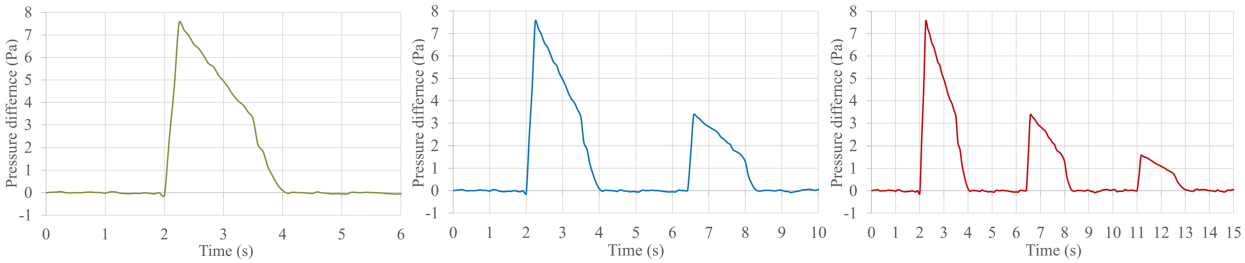


Figure 5-23: (a) Single air pulse release; (b) two air pulse releases, and (c) three air pulse releases

All the tests were conducted with three air pulse releases in this experimental study; nevertheless, the measured ALRs are assessed based on three different cases: (1) Case A: measurement of the first air pulse release; (2) Case B: measurement of the first two air pulse releases and (3) Case C: measurement of all three air pulse releases. Based on the test validity assessment for all 423 tests, 393 tests are valid for the evaluation of the three cases. A similar method was used to process the data, as mentioned in Section 5.2. Based on the tests at low wind speed conditions (i.e., 0-1m/s), the average ALR can be obtained correspondingly as the baseline ALR of each case. The *RPD* is used to indicate the wind impact on building airtightness measurement, which is calculated by comparing the ALR of each Pulse test with the baseline ALR. For Case A with one air pulse release, there were 54 tests under the wind speed lower than 1m/s; thus, the corresponding average ALR is 313.21m³/h. For Case B consisting of two pulse releases, 42 tests were found under the wind speed lower than 1m/s, with an average ALR of 291.80m³/h. Only five tests in Case C were under the wind speed below 1m/s, with an ALR of 287.73m³/h. The reason for the different number of tests in the three cases is because of the dynamic nature of wind and different test durations. A test with a single air pulse release lasts about 6 seconds, while 15 seconds is needed for a test with three pulses release; thus, the wind speed highly likely varies over the test duration. The calculated *RPD* results for the three cases are shown in Table 5-6, Table 5-7, Table 5-8, respectively. For a better presentation of measured data, assessment for each case was conducted by dividing the 393 tests into 20 groups according to the wind speed level during the testing. The *RPD* of each group is also calculated by comparing the group average ALR with the case baseline ALR.

Table 5-6: Case A (one air pulse release) results

Test Group	Wind Speed (Ground Level)[1]	Number of Tests	Group Average ALR	Relative Percentage Difference	
				Each[2]	Group[3]
A	0 – 0.5 m/s	15	310.31	14.13%	0.93%
B	0.5 – 1.0 m/s	39	314.33	17.68%	0.36%
C	1.0 – 1.5 m/s	38	321.43	30.63%	2.62%
D	1.5 – 2.0 m/s	48	329.84	35.95%	5.31%
E	2.0 – 2.5 m/s	51	313.10	35.06%	0.04%
F	2.5 – 3.0 m/s	36	313.22	15.47%	0.00%
G	3.0 – 3.5 m/s	30	327.92	43.53%	4.69%
H	3.5 – 4.0 m/s	29	313.86	45.70%	0.21%
I	4.0 – 4.5 m/s	21	347.08	27.55%	10.81%
J	4.5 – 5.0 m/s	21	334.64	32.92%	6.84%
K	5.0 – 5.5 m/s	21	334.11	26.78%	6.67%
L	5.5 – 6.0 m/s	7	357.66	35.66%	14.19%
M	6.0 – 6.5 m/s	9	346.72	25.98%	10.70%
N	6.5 – 7.0 m/s	7	335.14	36.85%	7.00%
O	7.0 – 7.5 m/s	8	311.32	44.40%	0.60%
P	7.5 – 8.0 m/s	5	325.91	10.96%	4.05%
Q	8.0 – 8.5 m/s	2	354.06	29.65%	13.04%
R	8.5 – 9.0 m/s	2	321.87	8.33%	2.76%
S	9.0 – 9.5 m/s	3	348.93	21.90%	11.40%
T	9.5 – 10 m/s	1	354.91	13.31%	13.31%
Based on Low Wind Speed Conditions		Baseline ALR (m³/h)		Each Avg. *RPD*	Group Avg. *RPD*
0 – 1m/s (54 Tests)		313.21		27.62%	5.78%

1. Wind speed measured at the height of 2.2m above ground
2. The maximum relative percentage difference of ALR of each single test to the baseline average ALR
3. The relative percentage difference of average ALR of each group to the baseline average ALR

Table 5-7: Case B (two air pulse releases) results

Test Group	Wind Speed (Ground Level)[1]	Number of Tests	Group Average ALR	Relative Percentage Difference	
				Each[2]	Group[3]
A	0 – 0.5 m/s	8	290.92	4.59%	0.30%
B	0.5 – 1.0 m/s	34	292.00	11.29%	0.07%
C	1.0 – 1.5 m/s	39	290.60	11.92%	0.41%
D	1.5 – 2.0 m/s	41	291.03	10.71%	0.26%
E	2.0 – 2.5 m/s	48	288.04	15.93%	1.29%
F	2.5 – 3.0 m/s	28	294.64	11.09%	0.97%
G	3.0 – 3.5 m/s	39	300.27	35.09%	2.90%
H	3.5 – 4.0 m/s	33	286.75	21.09%	1.73%
I	4.0 – 4.5 m/s	25	297.57	24.69%	1.98%
J	4.5 – 5.0 m/s	17	297.95	11.65%	2.11%
K	5.0 – 5.5 m/s	28	294.39	18.48%	0.89%
L	5.5 – 6.0 m/s	9	301.45	12.88%	3.31%
M	6.0 – 6.5 m/s	11	299.14	11.09%	2.51%
N	6.5 – 7.0 m/s	9	297.90	8.45%	2.09%
O	7.0 – 7.5 m/s	6	276.37	34.71%	5.29%
P	7.5 – 8.0 m/s	5	278.68	41.42%	4.49%
Q	8.0 – 8.5 m/s	4	300.91	12.64%	3.12%
R	8.5 – 9.0 m/s	2	295.31	2.77%	1.20%
S	9.0 – 9.5 m/s	4	307.72	8.16%	5.46%
T	9.5 – 10 m/s	3	305.32	11.25%	4.63%
Based on Low Wind Speed Conditions		Baseline ALR (m³/h)		Each Avg. *RPD*	Group Avg. *RPD*
0 – 1m/s (42 Tests)		291.80		16.00%	2.25%

1. Wind speed measured at the height of 2.2m above ground
2. The maximum relative percentage difference of ALR of each single test to the baseline average ALR
3. The relative percentage difference of average ALR of each group the baseline average ALR

Table 5-8: Case C (three air pulse releases) results

Test Group	Wind Speed (Ground Level)[1]	Number of Tests	Group Average ALR	Relative Percentage Difference	
				Each[2]	Group[3]
A	0 – 0.5 m/s	1	281.39	2.20%	2.20%
B	0.5 – 1.0 m/s	4	289.31	6.13%	0.55%
C	1.0 – 1.5 m/s	15	286.31	10.98%	0.49%
D	1.5 – 2.0 m/s	14	288.70	9.75%	0.34%
E	2.0 – 2.5 m/s	26	286.05	7.37%	0.58%
F	2.5 – 3.0 m/s	23	289.86	7.33%	0.74%
G	3.0 – 3.5 m/s	35	292.05	10.38%	1.50%
H	3.5 – 4.0 m/s	32	288.42	15.94%	0.24%
I	4.0 – 4.5 m/s	31	291.41	13.90%	1.28%
J	4.5 – 5.0 m/s	22	288.40	14.36%	0.23%
K	5.0 – 5.5 m/s	42	290.99	17.45%	1.13%
L	5.5 – 6.0 m/s	39	294.55	17.52%	2.37%
M	6.0 – 6.5 m/s	24	298.38	18.89%	3.70%
N	6.5 – 7.0 m/s	31	294.03	18.33%	2.19%
O	7.0 – 7.5 m/s	15	287.74	14.86%	0.00%
P	7.5 – 8.0 m/s	8	292.56	18.15%	1.68%
Q	8.0 – 8.5 m/s	8	308.99	11.07%	7.39%
R	8.5 – 9.0 m/s	8	279.89	17.63%	2.72%
S	9.0 – 9.5 m/s	9	300.19	15.59%	4.33%
T	9.5 – 10 m/s	6	284.86	16.49%	1.00%
Based on Low Wind Speed Conditions 0 – 1m/s (5 Tests)			Baseline ALR (m³/h) 287.73	Each Avg. *RPD* 13.22%	Group Avg. *RPD* 1.73%

1. Wind speed measured at the height of 2.2m above ground
2. The maximum relative percentage difference of ALR of each single test to the baseline average ALR
3. The relative percentage difference of average ALR of each group to the baseline average ALR

All ALR data of Case A, B and C are plotted in the violin plot in Figure 5-24. When comparing the distribution shape of ALR in each Pulse test for the three cases, the ALRs in Case A disperse in a wider range. Case B and Case C had similar median ALR, while Case C had more ALR results concentrated in the interquartile range. Similar findings can be observed for the group ALR for the three cases. The plot reflects that the number of the air pulse release in a complete Pulse test leads to different ALR measurements, as different distribution shapes are noted for the three cases.

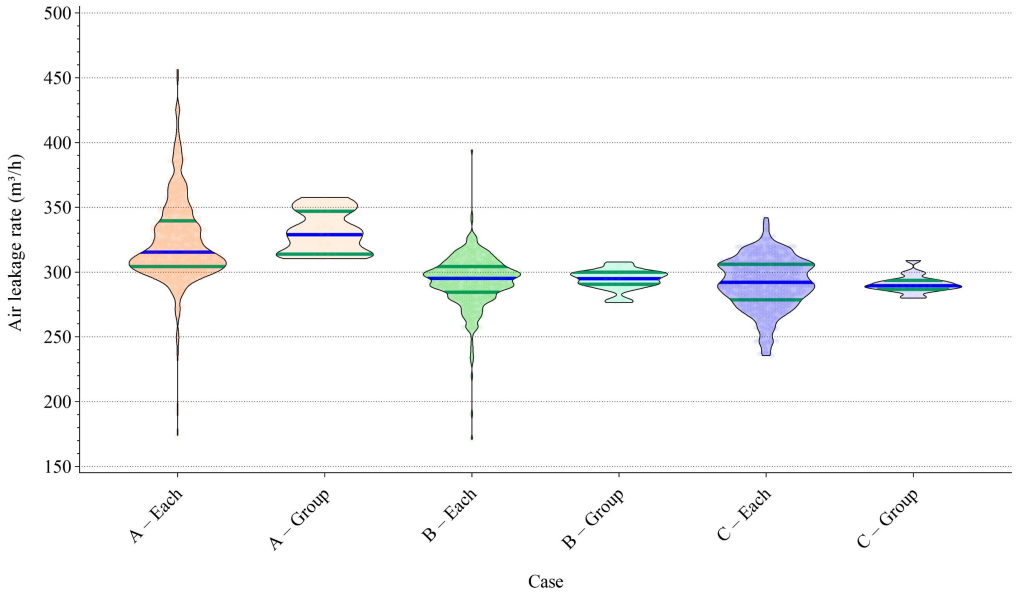


Figure 5-24: Violin plot of ALR results for Cases A, B and C

Figure 5-25 presents the comparison of the three cases in regard to the average *RPD* of each test and group. The results show that Case C has a much lower average *RPD*s than the other two cases, revealing that the three-step Pulse test could be less affected by wind. This is because, with three air pulse releases, more data can be recorded over the established pressure range during the Pulse test, thus contributing to a more comprehensive image of the building pressure variation and leakage curve with minimised reliance on data extrapolation. In practical testing, the recorded pressure data in the quasi-steady period may not cover 4Pa for a one-step Pulse test; therefore, the air leakage rate at 4Pa is derived by extrapolation based on the Power law. This induces extrapolation uncertainties due to the limited data. However, a Pulse with three pulse releases includes recorded pressure data for three respective quasi-steady periods; thus, three leakage curves can be produced and used to obtain the air leakage rate at 4Pa with minimised extrapolation uncertainties. Though a complete three-step Pulse test lasts longer, with a risk of occurrence of varying wind conditions, the evaluation in this section suggests that accurate measurements could be obtained with reduced wind impact. Furthermore, a similar finding can be observed as discussed in Section 5.2.2, and the group average *RPD* is much lower than the *RPD* of a single test in each case, which implies that the multiple Pulse and multi-step Pulse tests contribute to minimising the wind impact on building airtightness measurement.

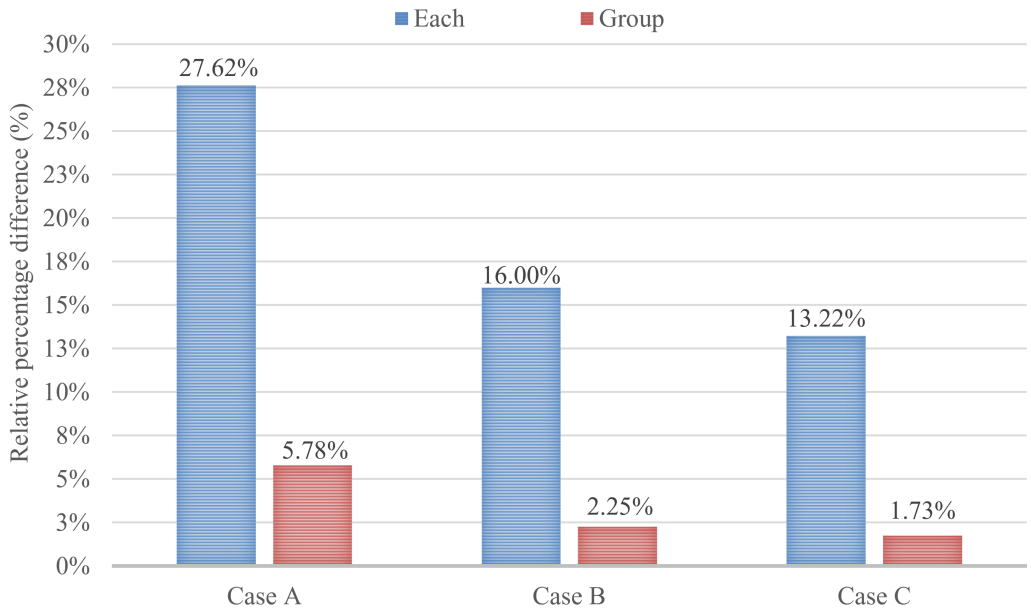


Figure 5-25: Relative percentage differences for Cases A, B and C

5.3.3 Background pressure recording period

As the raw data pressure curve illustrated in Figure 5-22, the wind and buoyancy effects can be apparently noticed before and after the air pulse release. During the entire Pulse test of 6 seconds, the background pressure is commonly recorded from the beginning (0s) until the pulse releases at

2s, and the pulse release lasts 1.5s (i.e., from 2s to 3.5s), then the background pressure is measured again from 4.5s to the end at 6s, as the indoor pressure is not steady enough for recording during 3.5s to 4.5s. Therefore, the common curve-fit adjustment covers the two recording periods of the background pressure: (1) the first 2s before the start of pulse release; and (2) 1.5s after the end of pulse release, where the indoor pressure becomes valid for recording (i.e., from the point at 4.5s to 6s). It is necessary to investigate the optimal time period for recording the background pressure before and after the imposed pulse, which can contribute to reflecting a full image of the changes in the background pressure during the Pulse test. In addition, the optimal background pressure recording period allows the determination of the optimal testing duration for a complete Pulse test, which can provide complementary information for the operator. In this study, four different cases are proposed and compared with different recording periods of the background pressure, and their respective details are listed in Table 5-9. Figure 5-26 illustrates the background pressure recording period in one pulse release period for each case.

Table 5-9: Four cases with different background pressure recoding periods

Case	Number of Pulse Release	Period for Recording Background Pressure	
		Before the Pulse Release	After the Pulse Release*
C	3	2s	1.5s
D	3	1.5s	1.5s
E	3	1.0s	1.0s
F	3	0.5s	0.5s

*When the indoor pressure becomes valid for recording after the pulse release ends

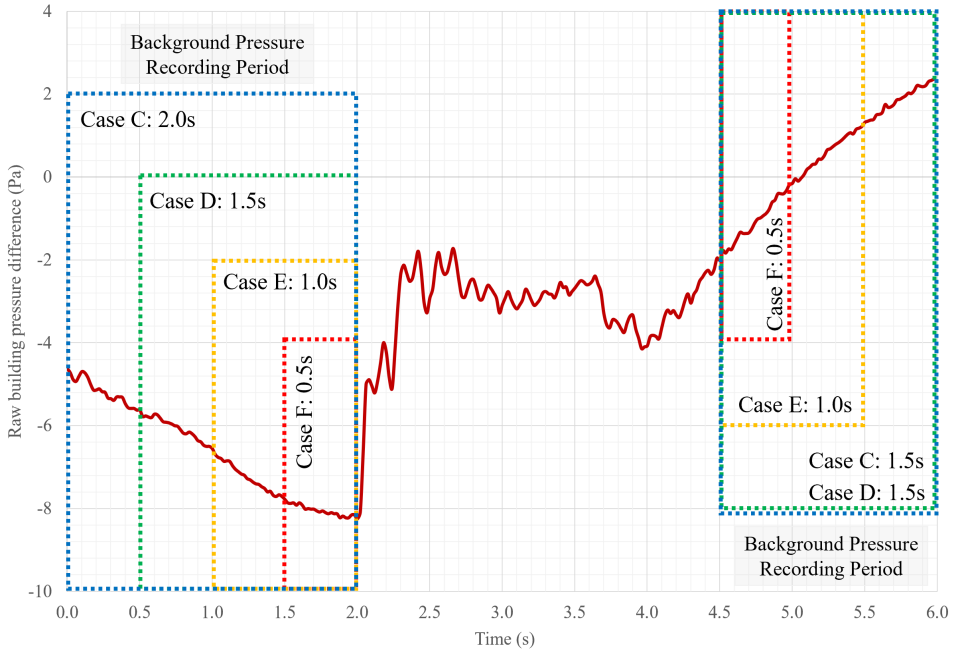


Figure 5-26: Illustration of Cases C, D, E, F in one air pulse release period

All the four cases consist of tests with three pulse releases, and 393 tests are valid for evaluation based on the validity assessment. The average ALR and *RPD* based on different recording times

of background pressure are calculated, and the respective results of the four cases are listed in Table 5-10, Table 5-11, Table 5-12 and Table 5-13. By applying the adjustment to the obtained measured data based on different recording periods of background pressure, different building airtightness results are noticed in the four cases.

Table 5-10: Case C results

Test Group	Wind Speed (Ground Level)[1]	Number of Tests	Group Average ALR	Relative Percentage Difference	
				Each[2]	Group[3]
A	0 – 0.5 m/s	1	281.39	2.20%	2.20%
B	0.5 – 1.0 m/s	4	289.31	6.13%	0.55%
C	1.0 – 1.5 m/s	15	286.31	7.98%	0.49%
D	1.5 – 2.0 m/s	14	288.70	9.75%	0.34%
E	2.0 – 2.5 m/s	26	286.05	7.37%	0.58%
F	2.5 – 3.0 m/s	23	289.86	7.33%	0.74%
G	3.0 – 3.5 m/s	35	292.05	10.38%	1.50%
H	3.5 – 4.0 m/s	32	288.42	15.94%	0.24%
I	4.0 – 4.5 m/s	31	291.41	13.90%	1.28%
J	4.5 – 5.0 m/s	22	288.40	14.36%	0.23%
K	5.0 – 5.5 m/s	42	290.99	17.45%	1.13%
L	5.5 – 6.0 m/s	39	294.55	17.52%	2.37%
M	6.0 – 6.5 m/s	24	298.38	18.89%	3.70%
N	6.5 – 7.0 m/s	31	294.03	18.33%	2.19%
O	7.0 – 7.5 m/s	15	287.74	14.86%	0.00%
P	7.5 – 8.0 m/s	8	292.56	18.15%	1.68%
Q	8.0 – 8.5 m/s	8	308.99	11.07%	7.39%
R	8.5 – 9.0 m/s	8	279.89	17.63%	2.72%
S	9.0 – 9.5 m/s	9	300.19	15.59%	4.33%
T	9.5 – 10 m/s	6	284.86	16.49%	1.00%
Based on Low Wind Speed Conditions 0 – 1m/s (5 Tests)		Baseline ALR (m³/h)		Each Avg. *RPD*	Group Avg. *RPD*
		287.73		13.22%	1.73%

1. Wind speed measured at the height of 2.2m above ground.
2. The maximum relative percentage difference of ALR of each single test to the baseline average ALR
3. The relative percentage difference of average ALR of each group to the baseline average ALR

Table 5-11: Case D results

Test Group	Wind Speed (Ground Level)[1]	Number of Tests	Group Average ALR	Relative Percentage Difference	
				Each[2]	Group[3]
A	0 – 0.5 m/s	1	282.80	2.46%	2.46%
B	0.5 – 1.0 m/s	4	291.73	6.37%	0.62%
C	1.0 – 1.5 m/s	15	287.94	13.21%	0.69%
D	1.5 – 2.0 m/s	14	289.57	10.21%	0.13%
E	2.0 – 2.5 m/s	26	287.20	8.56%	0.94%
F	2.5 – 3.0 m/s	23	290.24	5.87%	0.10%
G	3.0 – 3.5 m/s	35	293.28	11.50%	1.15%
H	3.5 – 4.0 m/s	32	288.94	13.64%	0.34%
I	4.0 – 4.5 m/s	31	292.10	13.04%	0.74%
J	4.5 – 5.0 m/s	22	289.60	13.35%	0.12%
K	5.0 – 5.5 m/s	42	292.63	19.68%	0.93%
L	5.5 – 6.0 m/s	39	295.12	18.13%	1.79%
M	6.0 – 6.5 m/s	24	301.23	18.30%	3.90%
N	6.5 – 7.0 m/s	31	296.73	17.46%	2.34%
O	7.0 – 7.5 m/s	15	290.40	13.14%	0.16%
P	7.5 – 8.0 m/s	8	295.03	16.42%	1.75%
Q	8.0 – 8.5 m/s	8	310.85	11.75%	7.21%
R	8.5 – 9.0 m/s	8	282.37	17.93%	2.61%
S	9.0 – 9.5 m/s	9	304.96	15.20%	5.18%
T	9.5 – 10 m/s	6	290.32	15.50%	0.13%
Based on Low Wind Speed Conditions 0 – 1m/s (5 Tests)		Baseline ALR (m³/h)		Each Avg. *RPD*	Group Avg. *RPD*
		289.94		13.09%	1.66%

1. Wind speed measured at the height of 2.2m above ground.
2. The maximum relative percentage difference of ALR of each single test to the baseline average ALR
3. The relative percentage difference of average ALR of each group to the baseline average ALR

Table 5-12: Case E results

Test Group	Wind Speed (Ground Level)[1]	Number of Tests	Group Average ALR	Relative Percentage Difference	
				Each[2]	Group[3]
A	0 – 0.5 m/s	1	282.47	2.91%	2.91%
B	0.5 – 1.0 m/s	4	293.07	8.15%	0.73%
C	1.0 – 1.5 m/s	15	286.37	17.95%	1.57%
D	1.5 – 2.0 m/s	14	288.87	12.98%	0.72%
E	2.0 – 2.5 m/s	26	284.32	13.76%	2.28%
F	2.5 – 3.0 m/s	23	287.50	8.71%	1.19%
G	3.0 – 3.5 m/s	35	291.95	14.36%	0.34%
H	3.5 – 4.0 m/s	32	287.11	22.34%	1.32%
I	4.0 – 4.5 m/s	31	290.61	14.56%	0.12%
J	4.5 – 5.0 m/s	22	289.32	9.64%	0.56%
K	5.0 – 5.5 m/s	42	291.66	17.72%	0.24%
L	5.5 – 6.0 m/s	39	292.99	18.42%	0.70%
M	6.0 – 6.5 m/s	24	298.34	15.92%	2.54%
N	6.5 – 7.0 m/s	31	296.23	15.96%	1.81%
O	7.0 – 7.5 m/s	15	292.74	13.34%	0.61%
P	7.5 – 8.0 m/s	8	298.47	17.92%	2.58%
Q	8.0 – 8.5 m/s	8	313.10	14.99%	7.61%
R	8.5 – 9.0 m/s	8	283.03	20.18%	2.72%
S	9.0 – 9.5 m/s	9	306.93	17.60%	5.49%
T	9.5 – 10 m/s	6	291.83	14.85%	0.30%
Based on Low Wind Speed Conditions 0 – 1m/s (5 Tests)		Baseline ALR (m³/h)		Each Avg. *RPD*	Group Avg. *RPD*
		290.95		14.61%	1.82%

1. Wind speed measured at the height of 2.2m above ground.
2. The maximum relative percentage difference of ALR of each single test to the baseline average ALR
3. The relative percentage difference of average ALR of each group to the baseline average ALR

Table 5-13: Case F results

Test Group	Wind Speed (Ground Level)[1]	Number of Tests	Group Average ALR	Relative Percentage Difference	
				Each[2]	Group[3]
A	0 – 0.5 m/s	1	262.64	5.55%	5.55%
B	0.5 – 1.0 m/s	4	281.94	10.45%	1.39%
C	1.0 – 1.5 m/s	15	282.61	41.05%	1.63%
D	1.5 – 2.0 m/s	14	290.81	57.07%	4.58%
E	2.0 – 2.5 m/s	26	274.65	23.55%	1.24%
F	2.5 – 3.0 m/s	23	283.73	15.04%	2.03%
G	3.0 – 3.5 m/s	35	288.01	23.66%	3.57%
H	3.5 – 4.0 m/s	32	283.09	40.98%	1.80%
I	4.0 – 4.5 m/s	31	295.79	14.83%	6.37%
J	4.5 – 5.0 m/s	22	311.00	9.84%	11.84%
K	5.0 – 5.5 m/s	42	287.89	41.70%	3.53%
L	5.5 – 6.0 m/s	39	280.79	27.97%	0.97%
M	6.0 – 6.5 m/s	24	296.98	26.13%	6.80%
N	6.5 – 7.0 m/s	31	290.70	32.95%	4.54%
O	7.0 – 7.5 m/s	15	296.76	23.17%	6.72%
P	7.5 – 8.0 m/s	8	274.71	32.90%	1.21%
Q	8.0 – 8.5 m/s	8	309.77	25.63%	11.39%
R	8.5 – 9.0 m/s	8	286.58	44.56%	3.06%
S	9.0 – 9.5 m/s	9	317.88	45.21%	14.31%
T	9.5 – 10 m/s	6	289.65	27.54%	4.16%
Based on Low Wind Speed Conditions 0 – 1m/s (5 Tests)		Baseline ALR (m³/h)		Each Avg. *RPD*	Group Avg. *RPD*
		278.08		28.49%	4.83%

1. Wind speed measured at the height of 2.2m above ground.
2. The maximum relative percentage difference of ALR of each single test to the baseline average ALR
3. The relative percentage difference of average ALR of each group to the baseline average ALR

All the ALR results of Case C, Case D, Case E and Case F are shown in the violin plot in Figure 5-27. In a comparison of the distribution shape of ALR for all cases, Case F has more dispersed ALR results, while Case C, Case D, Case E have similar median ALRs, with centralised results in the interquartile ranges. Figure 5-28 presents the comparison of the four cases regarding the average *RPD*s of each Pulse test and group.

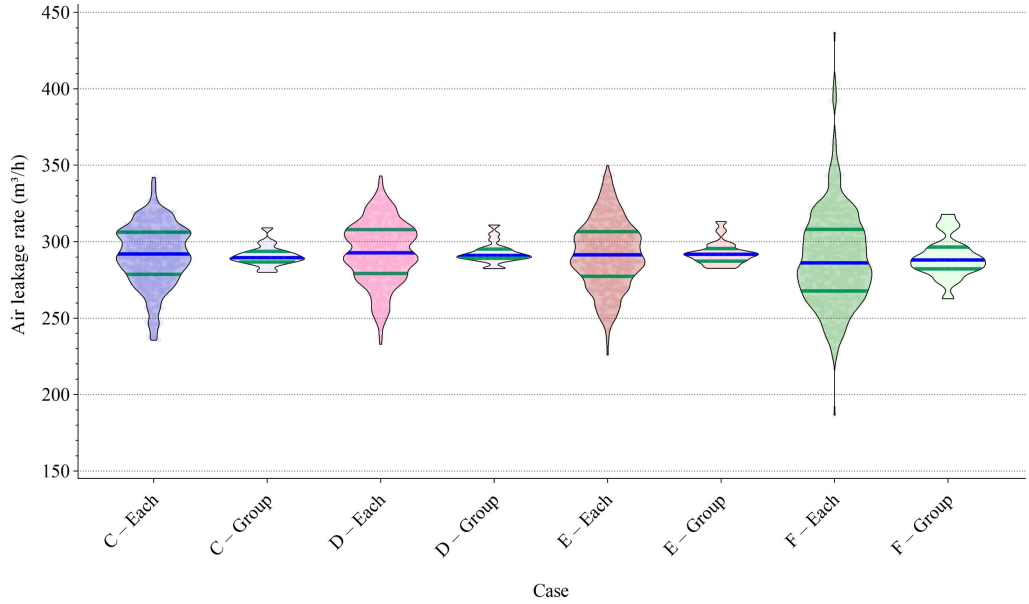


Figure 5-27: Violin plot of ALR results for Cases C, D, E and F

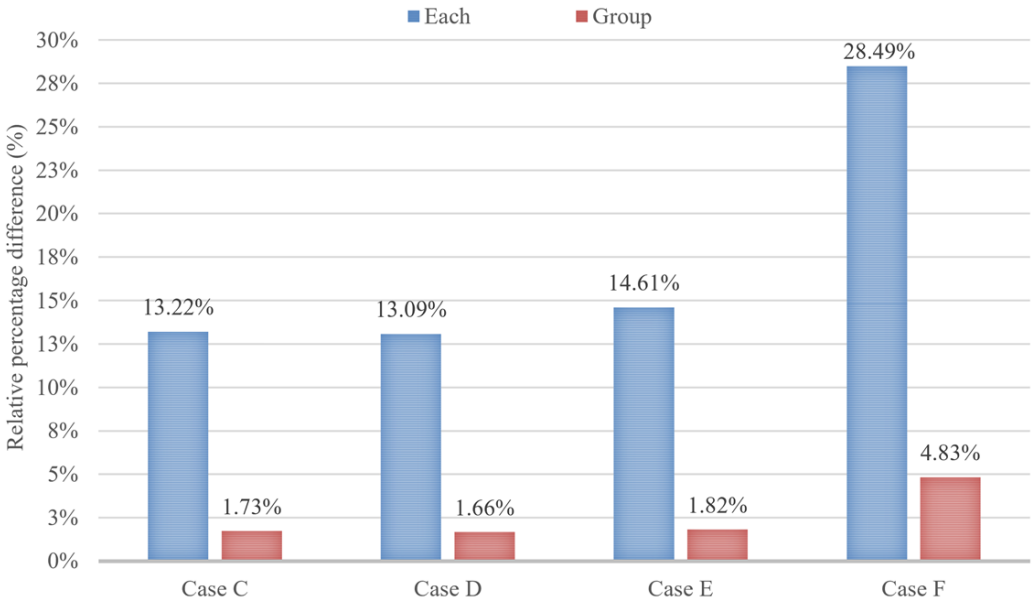


Figure 5-28: Relative percentage differences for Cases C, D, E and F

Among the four cases, a lower *RPD* is obtained when the curve-fitting procedure is processed for Case D. Small differences in terms of the average *RPD*s of each Pulse test and group are noticed for Case C, Case D, Case E, while the average *RPD* of each test increases to 28.49% and group average *RPD* is 4.83% for Case F with the shortest time for recording the background pressure (i.e., 0.5s). Based on the results of the tested dwelling, Case D provides an optimum adjustment

to the airtightness measurement with minimised wind and buoyancy effects. Case C is mostly adopted for adjusting the obtained Pulse measurements. Nevertheless, only slight differences of the average *RPD*s of each Pulse test and the group from Case D (i.e., deviation of 0.07% for group *RPD* and 0.13% for each test *RPD*) is observed in this study. This difference may vary depending on the test conditions and tested dwelling. The finding can also be used for optimising Pulse to provide an accurate and full image of the changes in the background pressure during the Pulse testing.

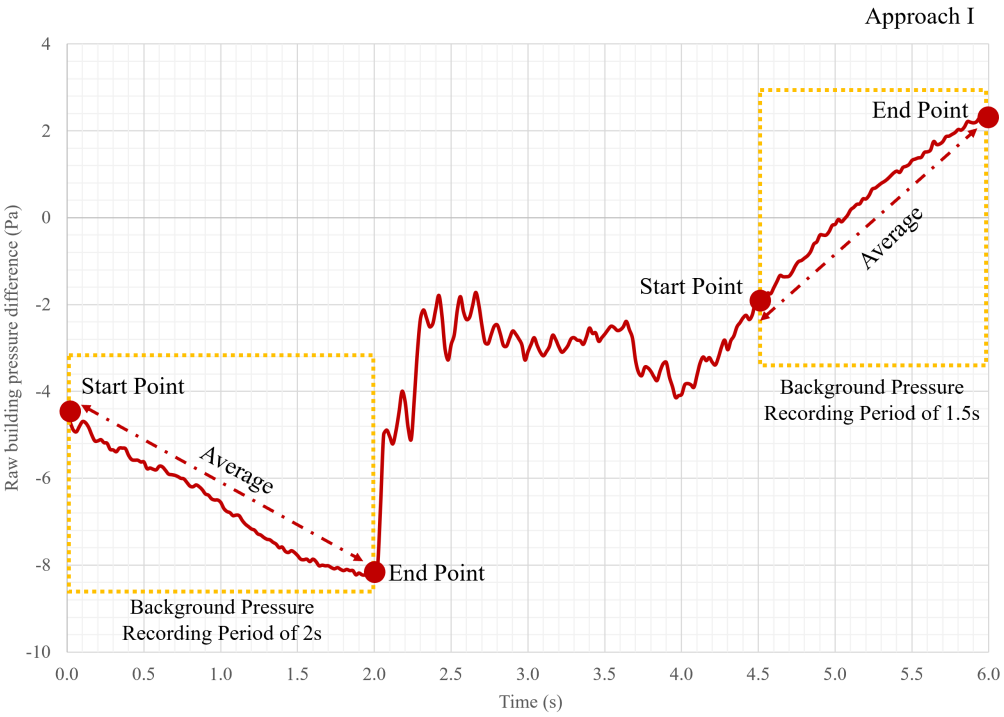
5.3.4 Sampling point for curve fitting adjustment

For the fan pressurisation method, the zero-flow pressure differences are recorded at least over 30 seconds at the starting and the end of the testing, and a minimum of ten values are required. The average of the obtained zero-flow pressure differences is determined for the positive values, negative values as well as all values, respectively. The three average values are used for the test validity check, i.e., the absolute value of each average value should be below 5Pa. The induced pressure difference during the blower door test is derived by subtracting the average zero-flow pressure difference of all values from each of the measured pressure differences.

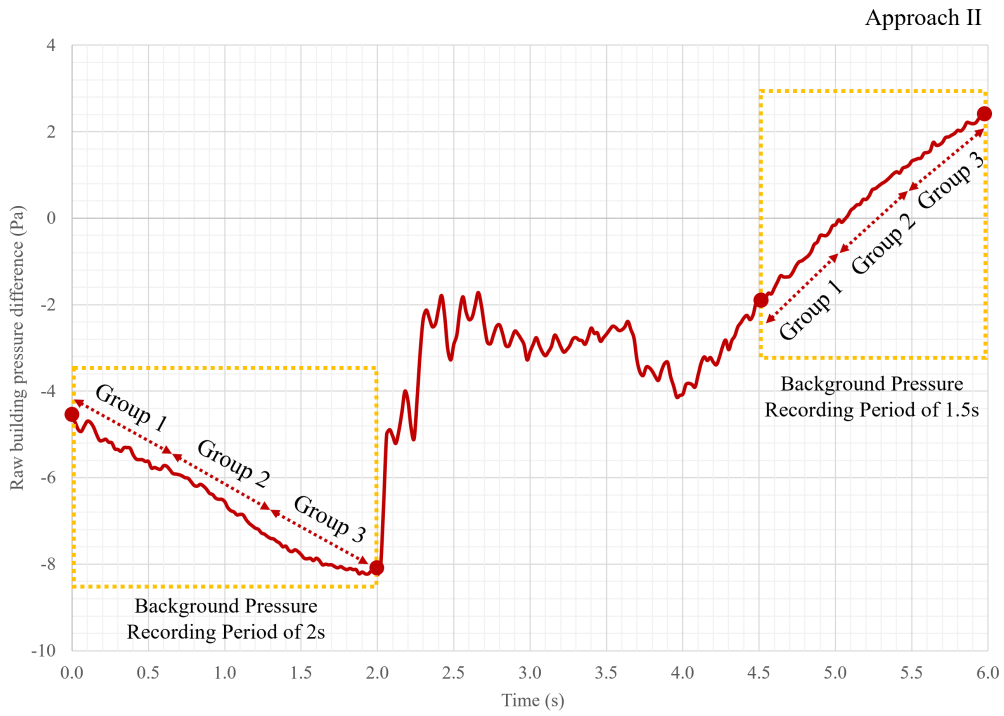
Different from the fan pressurisation method, Pulse requires less recording time for the background pressure. During the Pulse testing, the background pressure was continuously recorded by an embedded pressure transducer in the PULSE-60 unit with a measurement frequency of 50Hz. For instance, in total, 100 measured points of the background pressure can be produced for a recording period of 2s. The curve-fit approach for adjusting the obtained background pressure differences during the recording period at the starting and the end of the air pulse release is based on: the first measured value of the background pressure difference at the start point, the average of all values during the recording period (i.e., the average value of all the 100 measured points in the 2-second recording period) and the last measured value of the background pressure different at the endpoint (i.e., the 100^{th} measured point in the 2-second recording period).

As the curve-fit procedure for adjusting the measured data relies on the recorded background pressure, it would be interesting to investigate an optimal method to process the recorded background pressure data for a better curve-fit procedure in adjusting for the measured data in the tested dwelling. As discussed in Section 5.3.3, Case C, Case D and Case E provide relatively better adjustments to the airtightness measurement with minimised wind and buoyancy effects. Therefore, in this section, more analyses are conducted for Case C, Case D and Case E by

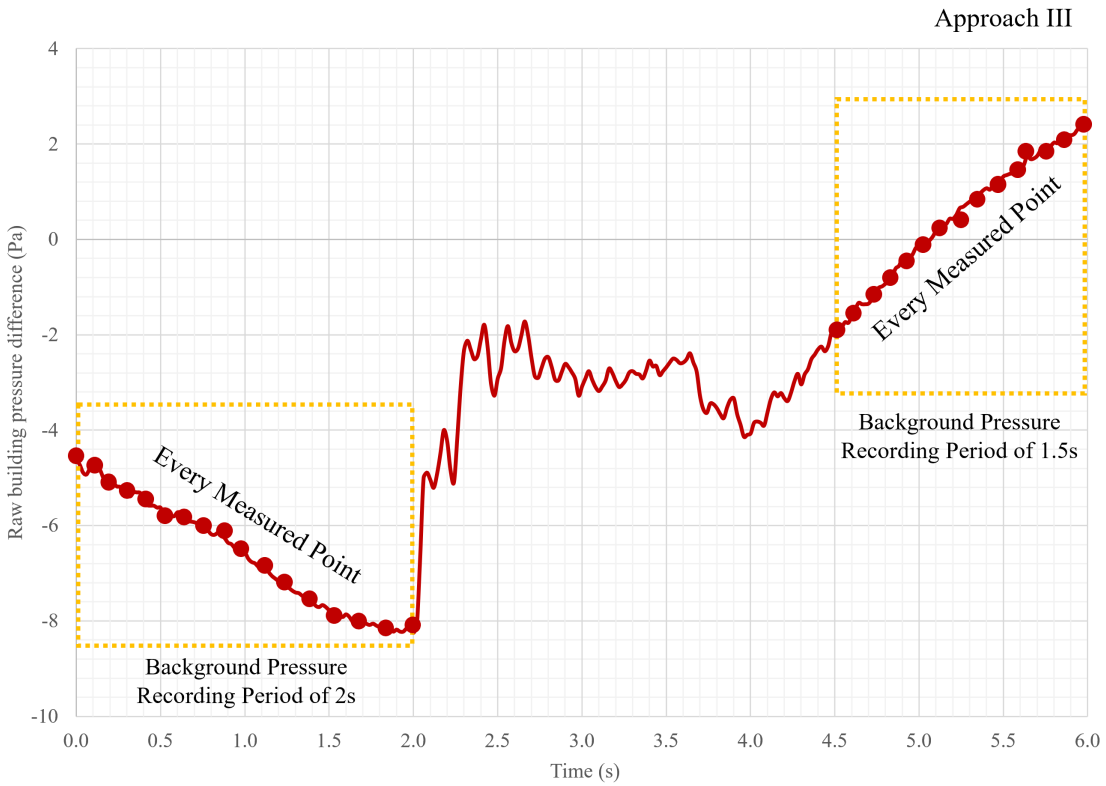
considering different approaches of accounting for the background pressure as depicted in Figure 5-29: (I) based on the first and the last measured points during the recording period, and the average value during the recording period; (II) based on the average value for each group by dividing all the obtained measured points into three groups; and (III) based on every measured value of the background pressure. Therefore, in total, 9 cases are proposed for analysis in this section, and Table 5-14 lists the details for each case.



(a) Approach I



(b) Approach II



(c) Approach III

Figure 5-29: Illustrations of (a) Approach I, (b) II, and (c) III

Table 5-14: Four cases with different approaches for generating the fitted curve

Case	Number of Pulse Release	Recording Period of Background Pressure		Calculation Approaches for Curve Fitting
		Before the Pulse Release	After the Pulse Release*	
C-I	3	2s	1.5s	Three points
C-II	3	2s	1.5s	Three groups
C-III	3	2s	1.5s	Every measured background pressure point
D-I	3	1.5s	1.5s	Three points
D-II	3	1.5s	1.5s	Three groups
D-III	3	1.5s	1.5s	Every measured background pressure point
E-I	3	1.0s	1.0s	Three points
E-II	3	1.0s	1.0s	Three groups
E-III	3	1.0s	1.0s	Every measured background pressure point

*When the indoor pressure becomes valid for recording after the pulse release ends

Based on the validity assessment for all the 423 tests, 382 tests can be used for evaluating the three different approaches. Tables 5-15, 5-16 and 5-17 present the detailed results of *RPD* for each single test and group.

Table 5-15: Case C results with different approaches for calculating the fitted curve

Case C – Approach I

Test Group	Wind Speed (Ground Level)[1]	Number of Tests	Group Average ALR	Relative Percentage Difference	
				Each[2]	Group[3]
A	0 – 0.5 m/s	1	281.39	2.20%	2.20%
B	0.5 – 1.0 m/s	4	289.31	6.13%	0.55%
C	1.0 – 1.5 m/s	14	287.58	10.98%	0.05%
D	1.5 – 2.0 m/s	14	288.70	9.75%	0.34%
E	2.0 – 2.5 m/s	26	286.05	7.37%	0.58%
F	2.5 – 3.0 m/s	22	290.53	7.33%	0.97%
G	3.0 – 3.5 m/s	33	291.68	10.38%	1.37%
H	3.5 – 4.0 m/s	32	288.42	15.94%	0.24%
I	4.0 – 4.5 m/s	31	291.41	13.90%	1.28%
J	4.5 – 5.0 m/s	21	288.97	14.36%	0.43%
K	5.0 – 5.5 m/s	42	290.99	17.45%	1.13%
L	5.5 – 6.0 m/s	39	294.55	17.52%	2.37%
M	6.0 – 6.5 m/s	22	298.68	18.89%	3.81%
N	6.5 – 7.0 m/s	28	295.72	18.33%	2.78%
O	7.0 – 7.5 m/s	15	287.74	14.86%	0.00%
P	7.5 – 8.0 m/s	8	292.56	18.15%	1.68%
Q	8.0 – 8.5 m/s	8	308.99	11.07%	7.39%
R	8.5 – 9.0 m/s	8	279.89	17.63%	2.72%
S	9.0 – 9.5 m/s	9	300.19	15.59%	4.33%
T	9.5 – 10 m/s	5	283.96	16.49%	1.31%
Based on Low Wind Speed Conditions 0 – 1 m/s (5 Tests)		Baseline ALR (m³/h)		Each Avg. *RPD*	Group Avg. *RPD*
		287.73		13.22%	1.78%

1. Wind speed measured at the height of 2.2m above ground.
2. The maximum relative percentage difference of ALR of each single test to the baseline average ALR
3. The relative percentage difference of average ALR of each group to the baseline average ALR

Case C – Approach II

Test Group	Wind Speed (Ground Level)[1]	Number of Tests	Group Average ALR	Relative Percentage Difference	
				Each[2]	Group[3]
A	0 – 0.5 m/s	1	292.80	0.10%	0.10%
B	0.5 – 1.0 m/s	4	293.16	8.06%	0.02%
C	1.0 – 1.5 m/s	14	290.17	6.79%	0.99%
D	1.5 – 2.0 m/s	14	291.59	11.64%	0.51%
E	2.0 – 2.5 m/s	26	290.04	12.36%	1.04%
F	2.5 – 3.0 m/s	22	294.76	10.55%	0.57%
G	3.0 – 3.5 m/s	33	295.52	12.69%	0.83%
H	3.5 – 4.0 m/s	32	290.49	29.93%	0.89%
I	4.0 – 4.5 m/s	31	291.74	16.47%	0.46%
J	4.5 – 5.0 m/s	21	286.67	17.86%	2.19%
K	5.0 – 5.5 m/s	42	291.49	33.92%	0.55%
L	5.5 – 6.0 m/s	39	301.72	27.62%	2.94%
M	6.0 – 6.5 m/s	22	296.59	22.97%	1.19%
N	6.5 – 7.0 m/s	28	303.45	44.43%	3.54%
O	7.0 – 7.5 m/s	15	283.72	24.77%	3.20%
P	7.5 – 8.0 m/s	8	286.45	30.73%	2.27%
Q	8.0 – 8.5 m/s	8	308.74	11.22%	5.34%
R	8.5 – 9.0 m/s	8	274.55	20.49%	6.33%
S	9.0 – 9.5 m/s	9	291.13	22.59%	0.67%
T	9.5 – 10 m/s	5	283.79	23.92%	3.17%
Based on Low Wind Speed Conditions 0 – 1 m/s (5 Tests)		Baseline ALR (m³/h)		Each Avg. *RPD*	Group Avg. *RPD*
		293.09		19.45%	1.84%

1. Wind speed measured at the height of 2.2m above ground.
2. The maximum relative percentage difference of ALR of each single test to the baseline average ALR
3. The relative percentage difference of average ALR of each group to the baseline average ALR

Case C – Approach III

Test Group	Wind Speed (Ground Level)[1]	Number of Tests	Group Average ALR	Relative Percentage Difference	
				Each[2]	Group[3]
A	0 – 0.5 m/s	1	292.09	0.04%	0.04%
B	0.5 – 1.0 m/s	4	291.96	6.24%	0.01%
C	1.0 – 1.5 m/s	14	290.10	6.62%	0.64%
D	1.5 – 2.0 m/s	14	290.86	10.28%	0.38%
E	2.0 – 2.5 m/s	26	288.41	10.72%	1.23%
F	2.5 – 3.0 m/s	22	293.73	8.54%	0.60%
G	3.0 – 3.5 m/s	33	294.90	11.63%	1.00%
H	3.5 – 4.0 m/s	32	290.16	28.24%	0.62%
I	4.0 – 4.5 m/s	31	291.66	15.26%	0.11%
J	4.5 – 5.0 m/s	21	286.60	17.85%	1.84%
K	5.0 – 5.5 m/s	42	291.82	29.79%	0.06%
L	5.5 – 6.0 m/s	39	300.86	24.52%	3.04%
M	6.0 – 6.5 m/s	22	296.88	20.66%	1.68%
N	6.5 – 7.0 m/s	28	299.25	21.76%	2.49%
O	7.0 – 7.5 m/s	15	283.44	22.25%	2.92%
P	7.5 – 8.0 m/s	8	286.69	27.18%	1.81%
Q	8.0 – 8.5 m/s	8	308.97	9.71%	5.82%
R	8.5 – 9.0 m/s	8	274.70	20.82%	5.92%
S	9.0 – 9.5 m/s	9	285.76	25.98%	2.13%
T	9.5 – 10 m/s	5	281.71	22.02%	3.52%
Based on Low Wind Speed Conditions 0 – 1 m/s (5 Tests)		Baseline ALR (m³/h)		Each Avg. *RPD*	Group Avg. *RPD*
		291.98		17.01%	1.79%

1. Wind speed measured at the height of 2.2m above ground.
2. The maximum relative percentage difference of ALR of each single test to the baseline average ALR
3. The relative percentage difference of average ALR of each group to the baseline average ALR

Table 5-16: Case D results with different approaches for calculating the fitted curve

Case D – Approach I

Test Group	Wind Speed (Ground Level)[1]	Number of Tests	Group Average ALR	Relative Percentage Difference	
				Each[2]	Group[3]
A	0 – 0.5 m/s	1	282.80	2.46%	2.46%
B	0.5 – 1.0 m/s	4	291.73	6.37%	0.62%
C	1.0 – 1.5 m/s	14	289.11	13.21%	0.29%
D	1.5 – 2.0 m/s	14	289.57	10.21%	0.13%
E	2.0 – 2.5 m/s	26	287.20	8.56%	0.94%
F	2.5 – 3.0 m/s	22	290.86	5.87%	0.32%
G	3.0 – 3.5 m/s	33	292.79	11.50%	0.98%
H	3.5 – 4.0 m/s	32	288.94	13.64%	0.34%
I	4.0 – 4.5 m/s	31	292.10	13.04%	0.74%
J	4.5 – 5.0 m/s	21	290.14	13.35%	0.07%
K	5.0 – 5.5 m/s	42	292.63	19.68%	0.93%
L	5.5 – 6.0 m/s	39	295.12	18.13%	1.79%
M	6.0 – 6.5 m/s	22	301.77	18.30%	4.08%
N	6.5 – 7.0 m/s	28	298.38	17.46%	2.91%
O	7.0 – 7.5 m/s	15	290.40	13.14%	0.16%
P	7.5 – 8.0 m/s	8	295.03	16.42%	1.75%
Q	8.0 – 8.5 m/s	8	310.85	11.75%	7.21%
R	8.5 – 9.0 m/s	8	282.37	17.93%	2.61%
S	9.0 – 9.5 m/s	9	304.96	15.20%	5.18%
T	9.5 – 10 m/s	5	289.87	15.50%	0.03%
Based on Low Wind Speed Conditions 0 – 1 m/s (5 Tests)		Baseline ALR (m³/h)		Each Avg. *RPD*	Group Avg. *RPD*
		289.94		13.09%	1.68%

1. Wind speed measured at the height of 2.2m above ground.
2. The maximum relative percentage difference of ALR of each single test to the baseline average ALR
3. The relative percentage difference of average ALR of each group to the baseline average ALR

Case D – Approach II

Test Group	Wind Speed (Ground Level)[1]	Number of Tests	Group Average ALR	Relative Percentage Difference	
				Each[2]	Group[3]
A	0 – 0.5 m/s	1	293.99	1.17%	1.17%
B	0.5 – 1.0 m/s	4	298.35	7.32%	0.29%
C	1.0 – 1.5 m/s	14	289.73	7.18%	2.61%
D	1.5 – 2.0 m/s	14	292.85	10.98%	1.56%
E	2.0 – 2.5 m/s	26	290.07	8.62%	2.49%
F	2.5 – 3.0 m/s	22	294.42	5.34%	1.03%
G	3.0 – 3.5 m/s	33	295.39	13.41%	0.70%
H	3.5 – 4.0 m/s	32	289.93	30.69%	2.54%
I	4.0 – 4.5 m/s	31	291.83	22.23%	1.90%
J	4.5 – 5.0 m/s	21	288.04	21.30%	3.17%
K	5.0 – 5.5 m/s	42	293.47	31.18%	1.35%
L	5.5 – 6.0 m/s	39	302.04	20.81%	1.53%
M	6.0 – 6.5 m/s	22	298.15	17.43%	0.23%
N	6.5 – 7.0 m/s	28	303.09	23.13%	1.89%
O	7.0 – 7.5 m/s	15	284.21	23.92%	4.46%
P	7.5 – 8.0 m/s	8	287.77	29.55%	3.26%
Q	8.0 – 8.5 m/s	8	310.25	12.76%	4.29%
R	8.5 – 9.0 m/s	8	274.61	30.60%	7.69%
S	9.0 – 9.5 m/s	9	296.35	9.87%	0.38%
T	9.5 – 10 m/s	5	284.70	26.65%	4.30%
Based on Low Wind Speed Conditions 0 – 1 m/s (5 Tests)		Baseline ALR (m^3/h)		Each Avg. *RPD*	Group Avg. *RPD*
		297.48		17.71%	2.34%

1. Wind speed measured at the height of 2.2m above ground.
2. The maximum relative percentage difference of ALR of each single test to the baseline average ALR
3. The relative percentage difference of average ALR of each group to the baseline average ALR

Case D – Approach III

Test Group	Wind Speed (Ground Level)[1]	Number of Tests	Group Average ALR	Relative Percentage Difference	
				Each[2]	Group[3]
A	0 – 0.5 m/s	1	293.50	0.32%	0.33%
B	0.5 – 1.0 m/s	4	294.73	6.19%	0.08%
C	1.0 – 1.5 m/s	14	290.18	6.53%	1.46%
D	1.5 – 2.0 m/s	14	291.56	10.34%	0.99%
E	2.0 – 2.5 m/s	26	289.44	7.94%	1.71%
F	2.5 – 3.0 m/s	22	293.70	6.19%	0.27%
G	3.0 – 3.5 m/s	33	295.20	10.73%	0.24%
H	3.5 – 4.0 m/s	32	289.91	32.44%	1.55%
I	4.0 – 4.5 m/s	31	292.28	18.12%	0.75%
J	4.5 – 5.0 m/s	21	287.74	19.62%	2.29%
K	5.0 – 5.5 m/s	42	293.27	31.45%	0.41%
L	5.5 – 6.0 m/s	39	301.53	21.36%	2.39%
M	6.0 – 6.5 m/s	22	298.31	19.12%	1.30%
N	6.5 – 7.0 m/s	28	303.93	23.21%	3.21%
O	7.0 – 7.5 m/s	15	284.10	22.09%	3.52%
P	7.5 – 8.0 m/s	8	287.28	27.75%	2.45%
Q	8.0 – 8.5 m/s	8	310.14	11.01%	5.32%
R	8.5 – 9.0 m/s	8	274.37	24.58%	6.83%
S	9.0 – 9.5 m/s	9	289.65	15.75%	1.64%
T	9.5 – 10 m/s	5	285.68	21.55%	2.99%
Based on Low Wind Speed Conditions 0 – 1 m/s (5 Tests)		Baseline ALR (m^3/h)		Each Avg. *RPD*	Group Avg. *RPD*
		294.48		16.81%	1.99%

1. Wind speed measured at the height of 2.2m above ground.
2. The maximum relative percentage difference of ALR of each single test to the baseline average ALR
3. The relative percentage difference of average ALR of each group to the baseline average ALR

Table 5-17: Case D results with different approaches for calculating the fitted curve

Case E – Approach I

Test Group	Wind Speed (Ground Level)[1]	Number of Tests	Group Average ALR	Relative Percentage Difference	
				Each[2]	Group[3]
A	0 – 0.5 m/s	1	282.47	2.91%	2.91%
B	0.5 – 1.0 m/s	4	293.07	8.15%	0.73%
C	1.0 – 1.5 m/s	14	287.42	17.95%	1.21%
D	1.5 – 2.0 m/s	14	288.87	12.98%	0.72%
E	2.0 – 2.5 m/s	26	284.32	13.76%	2.28%
F	2.5 – 3.0 m/s	22	288.50	7.73%	0.84%
G	3.0 – 3.5 m/s	33	292.11	14.36%	0.40%
H	3.5 – 4.0 m/s	32	287.11	22.34%	1.32%
I	4.0 – 4.5 m/s	31	290.61	14.56%	0.12%
J	4.5 – 5.0 m/s	21	290.01	14.42%	0.32%
K	5.0 – 5.5 m/s	42	291.66	17.72%	0.24%
L	5.5 – 6.0 m/s	39	292.99	18.42%	0.70%
M	6.0 – 6.5 m/s	22	298.70	15.92%	2.66%
N	6.5 – 7.0 m/s	28	296.67	15.96%	1.97%
O	7.0 – 7.5 m/s	15	292.74	13.34%	0.61%
P	7.5 – 8.0 m/s	8	298.47	17.92%	2.58%
Q	8.0 – 8.5 m/s	8	313.10	14.99%	7.61%
R	8.5 – 9.0 m/s	8	283.03	20.18%	2.72%
S	9.0 – 9.5 m/s	9	306.93	17.60%	5.49%
T	9.5 – 10 m/s	5	294.01	14.85%	1.05%
Based on Low Wind Speed Conditions 0 – 1 m/s (5 Tests)		Baseline ALR (m³/h)		Each Avg. *RPD*	Group Avg. *RPD*
		290.95		14.80%	1.82%

1. Wind speed measured at the height of 2.2m above ground.
2. The maximum relative percentage difference of ALR of each single test to the baseline average ALR
3. The relative percentage difference of average ALR of each group to the baseline average ALR

Case E – Approach II

Test Group	Wind Speed (Ground Level)[1]	Number of Tests	Group Average ALR	Relative Percentage Difference	
				Each[2]	Group[3]
A	0 – 0.5 m/s	1	300.03	0.45%	0.45%
B	0.5 – 1.0 m/s	4	301.72	6.25%	0.11%
C	1.0 – 1.5 m/s	14	289.05	9.31%	4.09%
D	1.5 – 2.0 m/s	14	292.19	14.00%	3.05%
E	2.0 – 2.5 m/s	26	291.19	9.36%	3.38%
F	2.5 – 3.0 m/s	22	289.49	11.05%	3.95%
G	3.0 – 3.5 m/s	33	291.53	16.99%	3.27%
H	3.5 – 4.0 m/s	32	291.96	20.70%	3.12%
I	4.0 – 4.5 m/s	31	292.08	21.08%	3.09%
J	4.5 – 5.0 m/s	21	287.78	19.97%	4.51%
K	5.0 – 5.5 m/s	42	295.72	21.42%	1.88%
L	5.5 – 6.0 m/s	39	303.67	47.88%	0.76%
M	6.0 – 6.5 m/s	22	293.63	19.62%	2.57%
N	6.5 – 7.0 m/s	28	293.40	24.13%	2.65%
O	7.0 – 7.5 m/s	15	282.64	25.33%	6.22%
P	7.5 – 8.0 m/s	8	287.69	32.07%	4.54%
Q	8.0 – 8.5 m/s	8	314.54	13.77%	4.37%
R	8.5 – 9.0 m/s	8	281.15	45.35%	6.71%
S	9.0 – 9.5 m/s	9	264.05	77.48%	12.39%
T	9.5 – 10 m/s	5	293.48	11.46%	2.62%
Based on Low Wind Speed Conditions 0 – 1 m/s (5 Tests)		Baseline ALR (m³/h)		Each Avg. *RPD*	Group Avg. *RPD*
		301.38		22.38%	3.69%

1. Wind speed measured at the height of 2.2m above ground.
2. The maximum relative percentage difference of ALR of each single test to the baseline average ALR
3. The relative percentage difference of average ALR of each group to the baseline average ALR

Case E – Approach III

Test Group	Wind Speed (Ground Level)[1]	Number of Tests	Group Average ALR	Relative Percentage Difference	
				Each[2]	Group[3]
A	0 – 0.5 m/s	1	296.86	1.34%	1.34%
B	0.5 – 1.0 m/s	4	301.91	6.78%	0.34%
C	1.0 – 1.5 m/s	14	288.02	10.17%	4.28%
D	1.5 – 2.0 m/s	14	292.52	11.01%	2.78%
E	2.0 – 2.5 m/s	26	291.38	8.88%	3.16%
F	2.5 – 3.0 m/s	22	289.28	10.80%	3.86%
G	3.0 – 3.5 m/s	33	292.98	16.56%	2.63%
H	3.5 – 4.0 m/s	32	291.14	19.70%	3.24%
I	4.0 – 4.5 m/s	31	291.18	21.73%	3.23%
J	4.5 – 5.0 m/s	21	287.33	20.93%	4.51%
K	5.0 – 5.5 m/s	42	295.11	16.47%	1.92%
L	5.5 – 6.0 m/s	39	301.22	23.52%	0.11%
M	6.0 – 6.5 m/s	22	294.62	18.70%	2.09%
N	6.5 – 7.0 m/s	28	296.13	21.08%	1.59%
O	7.0 – 7.5 m/s	15	282.71	24.45%	6.04%
P	7.5 – 8.0 m/s	8	288.16	30.80%	4.23%
Q	8.0 – 8.5 m/s	8	313.30	14.76%	4.12%
R	8.5 – 9.0 m/s	8	277.75	43.89%	7.69%
S	9.0 – 9.5 m/s	9	263.03	74.11%	12.58%
T	9.5 – 10 m/s	5	292.13	13.80%	2.91%

Based on Low Wind Speed Conditions 0 – 1 m/s (5 Tests)	Baseline ALR (m³/h)	Each Avg. *RPD*	Group Avg. *RPD*
	300.90	20.47%	3.63%

1. Wind speed measured at the height of 2.2m above ground.
2. The maximum relative percentage difference of ALR of each single test to the baseline average ALR
3. The relative percentage difference of average ALR of each group to the baseline average ALR

The violin plot in Figure 5-30 includes all the ALR data for all the cases. The distinct differences among these cases can be visually observed from their respective shapes of distribution. Approach II and Approach III result in a wider dispersion of ALR results for all cases, especially Case E-II and Case E-II have much wider scattered results.

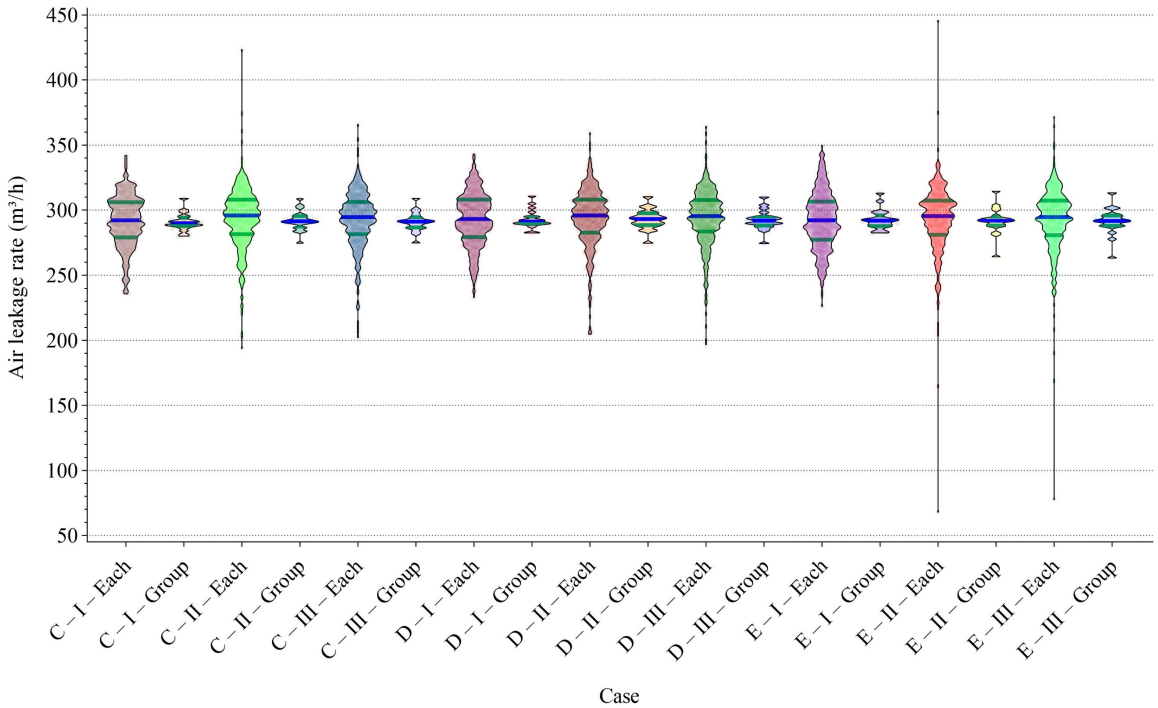


Figure 5-30: Violin plot of ALR for Cases C, D and E with different approaches for calculating the fitted curve

The results of different approaches for Cases C, D and E, are summarised in Figure 5-31. Approach II has the highest *RPD* for the three cases, followed by Approach III and the lowest *RPD* of 13.1% occurs in Case D with Approach I. As seen from the comparison, different approaches have different effects on the three cases with different recoding periods of background pressure. For instance, Approach II has the highest *RPD* of 22.4% in Case E, while the *RPD* of 17.7% was found in Case D. This indicates it is important to optimise the recording of background pressure for curve fitting.

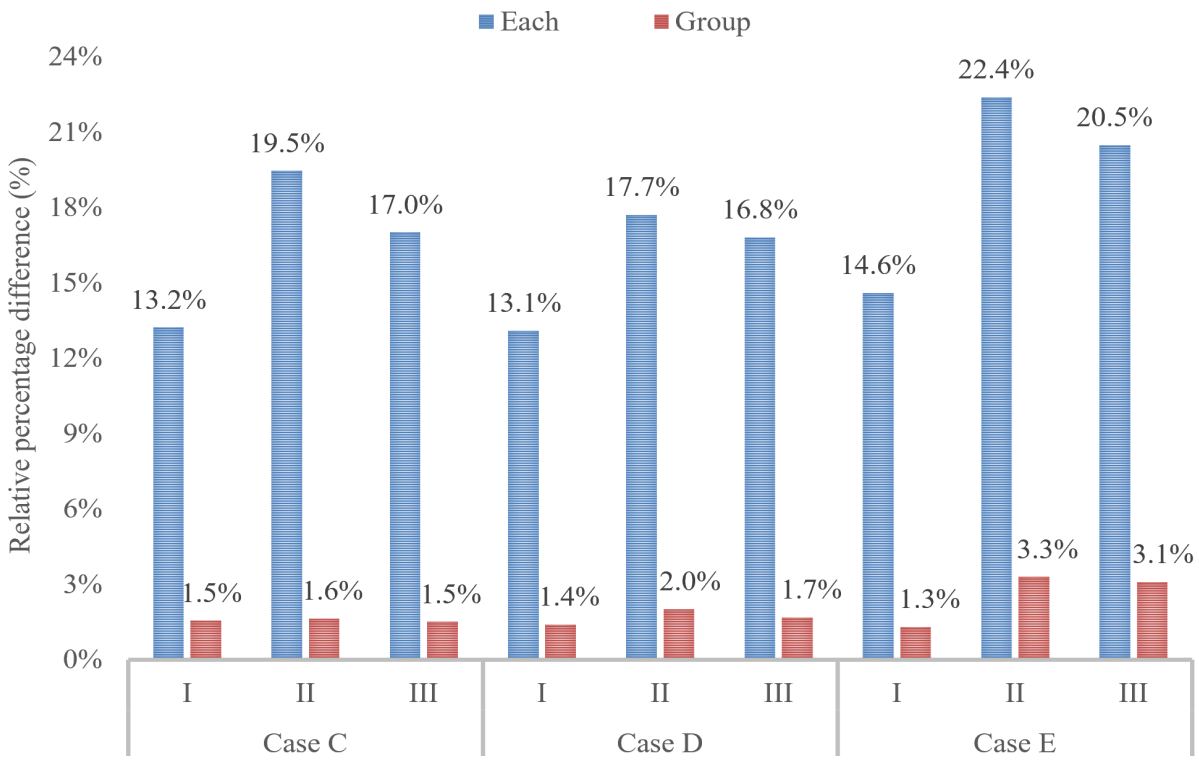


Figure 5-31: Comparison of *RPD*s for Cases C, D and E with different approaches for calculating the fitted curve

Overall, based on the data obtained under the reported test conditions, the optimal curve-fit approach for the Pulse measurement of the tested dwelling with minimum wind and buoyancy effects are considered: (1) with three separate air pulse releases in a complete Pulse test, (2) the background pressure recording period of 1.5s before the release of the air pulse and 1.5s after the completion of the pulse release, and (3) adjustment based on the first and the last measured values of the background pressure during the recording period, and the average value of all the measured background pressures during the recording period.

5.4 Summary

In this chapter, the wind impact on the Pulse testing was evaluated from different perspectives accounting for the wind speed, the wind direction, and the achieved pressure range. Based on the experimental data in the tested dwelling, the preferred test wind condition for the Pulse measurement with the *RPD* within ±10% is under wind speed lower than 5.02m/s at 2.2m above ground level (i.e., approximately equivalent to meteorological wind speed 7.91m/s based on test the location). When the wind speed is above 7.37m/s at 2.2m above ground level (i.e., approximately equivalent to meteorological wind speed 11.61m/s), the *RPD* of a single Pulse test in the tested dwelling could exceed ±20%, which indicates that the measurement faces a large uncertainty owing to the wind impact. The findings of the suggested wind speed limit in this study could also be used as supporting information for considering the wind impact when conducting the Pulse testing in practical conditions. In addition, the experimental results also imply the necessity of the multiple Pulse tests in practical testing, which contributes to minimising the wind impact on the building airtightness measurement. On the other hand, the impact of the wind direction on the Pulse testing was also noted, and more tests were implemented in the tested dwelling with the wind direction in the range of 217°-273°, with smaller *RPD*s than those of other wind directions, due to the prevailing west to south-westerly winds. It is noteworthy that the lower the corresponding wind speed is, the less significant the wind direction impact becomes.

Furthermore, potential improvements on the algorithm for adjusting the obtained Pulse measurements in the tested dwelling to minimise the wind and buoyancy effects were investigated from three different aspects. Results demonstrate that for a Pulse measurement with the minimised wind and buoyancy effects, a multiple-step Pulse test (e.g., three separate air pluses in a complete Pulse test) is suggested, and the recording duration of the background pressure measurement needs to be high enough in order to capture the representative background pressure trend. The optimal curve-fitting adjustment for the measurements of the tested dwelling considers: (a) impose three separate pulses in a Pulse test; (b) record of the background pressure for 1.5s before the air pulse release and 1.5s after the completion of the pulse release; and (c) determining the fitted curve based on the measured background pressure at the start point, the average pressure during recording period and at the endpoint. The work could provide practical information for deploying Pulse to measure building airtightness more accurately with minimised wind impact, which will be also beneficial for the wider applicability of Pulse.

6. Long-term Observation of the Wind Impact on the Pulse Test

6.1 Introduction

The 7-days experimental work presented in Chapter 5 provides evidence of the wind impact on the building airtightness measurement with Pulse. This chapter aims to extend the investigation of the wind impact through long-term observations on the leakage variation of an outdoor chamber under various wind conditions, which provides complementary insights into the understanding of the wind impact on the Pulse test in real scenarios. The experimental work lasted for, in total, eight months, from August 2019 to March 2020. Considering the period of the experimental work, the seasonal impact on the building airtightness is also discussed, focusing on the ageing effect of the outdoor chamber during the eight-month testing period.

Furthermore, the model-scale experiment was proposed to perform the Pulse testing under controlled wind conditions in a wind tunnel. The work was initially planned to use the available wind tunnel and experimental facilities in the Faculty of Engineering, University of Nottingham, to further investigate the steady wind impact on the Pulse test. However, the proposed work was forced to terminate due to non-access to the facility during the Pandemic. As limited model-scale experiments have been found in the literature exploring the steady wind impact on the Pulse test in a wind tunnel, the entire experimental design for the wind tunnel testing provides useful information on the possible experimental facilities for future wind impact explorations, which has been added to Appendix A.

6.2 Investigation of wind impact on the Pulse test in an outdoor chamber

6.2.1 Test arrangement

Two test pods located in the department of Architecture and Built Environment, University of Nottingham, are used to conduct the experimental work. Their photos are presented in Figure 6-1, and their respective parameters are listed in Table 6-1. Though the two pods have much smaller volumes than typical houses, they are designed and constructed based on 2010 UK building regulations (Pod 1) and the Passivhaus standard (Pod 2), respectively. According to the Passivhaus standard, Pod 2 is more airtight than Pod 1. Due to the ageing process, both pods have become leakier over the years but still maintain very different leakage characteristics from each other. There are various sources of leaks within a typical dwelling, such as pipework, ducts, fixtures, doors, windows and building envelope. Both pods are built primarily for experimental purposes,

with modular construction and a reduced number of building elements, such as pipework, vents, and ducting. Hence, the impact of other influencing factors on the experimental investigation in this study can be minimised, such as the building shape and leaks in building elements.

Table 6-1: Parameters of Pod 1 and Pod 2

	Pod 1	Pod 2
Volume (m^3)	21	22
Envelope Area (m^2)	47	48
Dimension	3m(W)*4m(L)*3m(H)	3.3m(W)*4.3m(L)*3.3m(H)
Building Standard	UK Building Standard	Passivhaus Standard

In this experimental study, Pod 1 was chosen as the test chamber because it has a leakage level that is more representative of a typical UK dwelling. On the other hand, Pod 2 was used as the control room, where the tester was based, in order to eliminate the influences of personnel on testing in Pod 1.



(a) (b)

Figure 6-1: Photos of (a) Pod 1 and (b) Pod 2

As shown in Figure 6-2, both the door and window of Pod 1 were locked and sealed with sealing tape to maintain a consistent test condition throughout the long-term test period and avoid accidental opening.



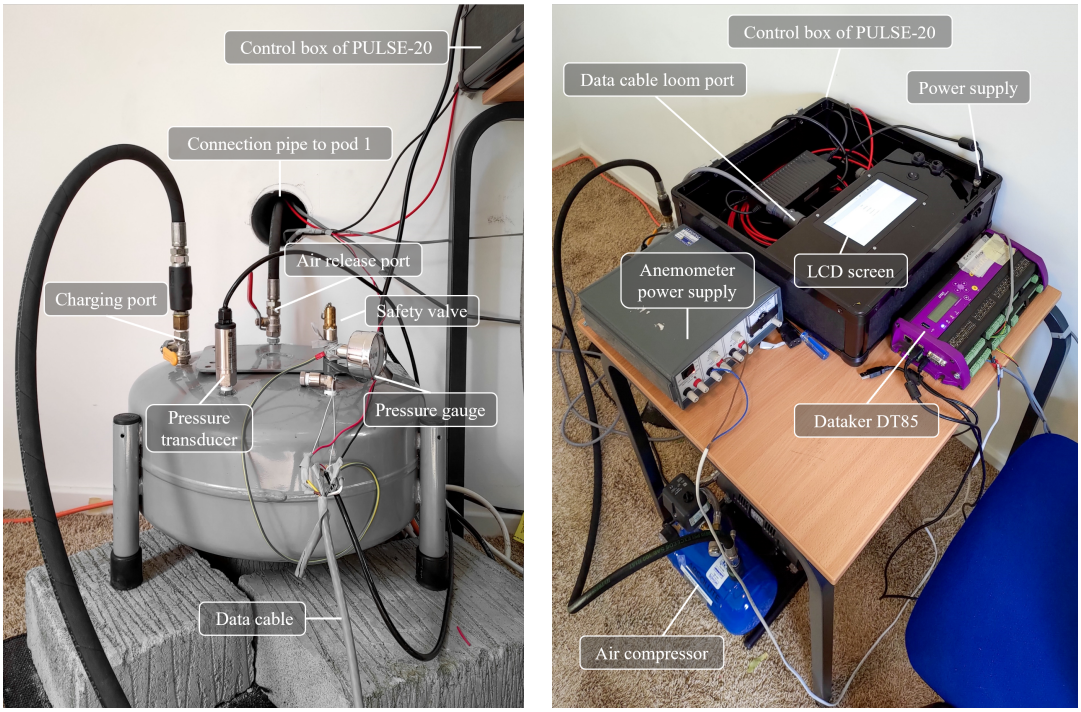
(a) (b)

Figure 6-2: Photos of sealed (a) door and (b) window of Pod 1

Table 6-2 summarises the experimental instrumentation in this study, with their respective accuracies. Due to the small volume of Pod 1, the Pulse unit employed in this study is the PULSE-20 unit, which incorporates a 20-litre stainless steel tank and oil-free double piston compressor, as shown in Figure 6-3(a). As seen in Figure 6-3(b), the PULSE-20 unit with its control box and data logger were all placed in Pod 2 so that the tester was able to control the unit and monitor the testing process remotely without affecting the measurement process in Pod 1. During the Pulse test, the pressure transducer and temperature sensors inside the control box of the PULSE-20 unit measured the building pressure and ambient temperature, and the measured data were recorded and analysed by the control box of the PULSE-20 unit, where results were simultaneously displayed on the LCD screen.

Table 6-1: List of test equipment

Airtightness	Others	Accuracy
PULSE-20	Pressure transducers (PULSE-20 built-in)	±0.40%
	Temperature sensors (PULSE-20 built-in)	±0.08℃
	Ultrasonic anemometer (WindSonic^{TM})	±3.00%
	Temperature sensors (PT100 RTD)	±0.2℃
	Data logger (Datataker DT85)	±0.10%

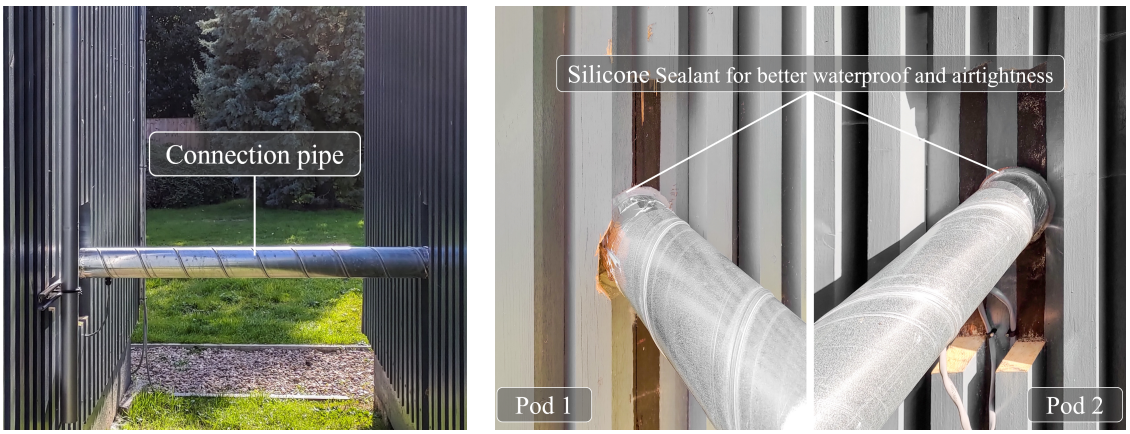


(a) (b)

Figure 6-3: (a) PULSE-20 unit and (b) PULSE-20 control box and datalogger

The PULSE-20 outlet utilises a ¼inch (BSP) solenoid valve to release the compressed air from the air tank into the test space, which delivers the 1.5-second pressure rise. To enable the air pulse release from the air tank in Pod 2 to be delivered to the testing space of Pod 1, modifications on the experimental facilities have been conducted. A connection pipe (i.e., length of 1.2m) was

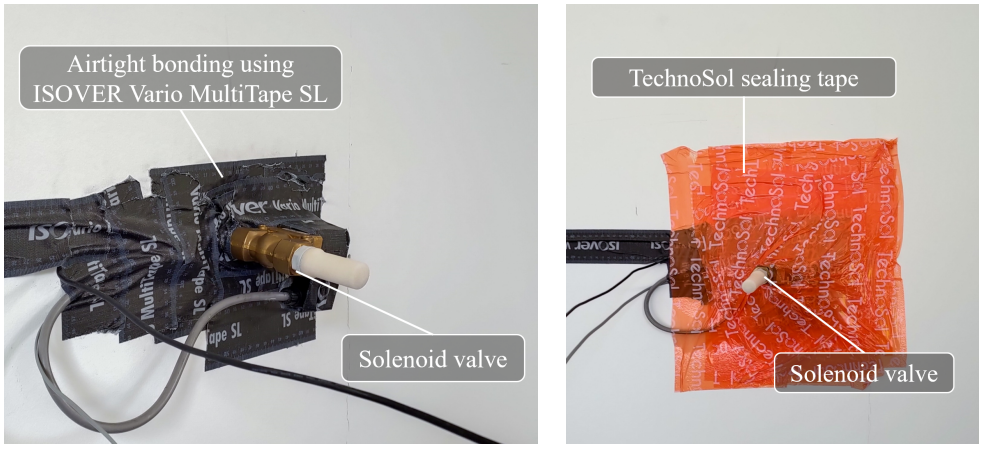
designed between the two pods with waterproof coating and proper sealings on both ends to allow the transfer of air pulse into Pod 1 but prevent any ambient airflows or rainwater from entering. Photos of the connection pipe are presented in Figure 6-4. As noted in Figure 6-3(a), an extended hydraulic hose assembly was coupled to the valve outlet and then connected to the connection pipe through a drilled hole in the wall of Pod 2. The selected hydraulic hose assembly is highly durable with high tensile steel wire reinforcing and maximum operating pressure of 400bar, which ensure its durability during the pulse release. The holes in the walls were drilled precisely with designated dimensions and care without causing any other leaks in the two pods. Considering the volume of the coupled hydraulic hose assembly to the air tank, the total volume of the entire unit is 20.05 Litres.



(a) (b)

Figure 6-4: Photos of the connection pipe between Pod 1 and Pod 2

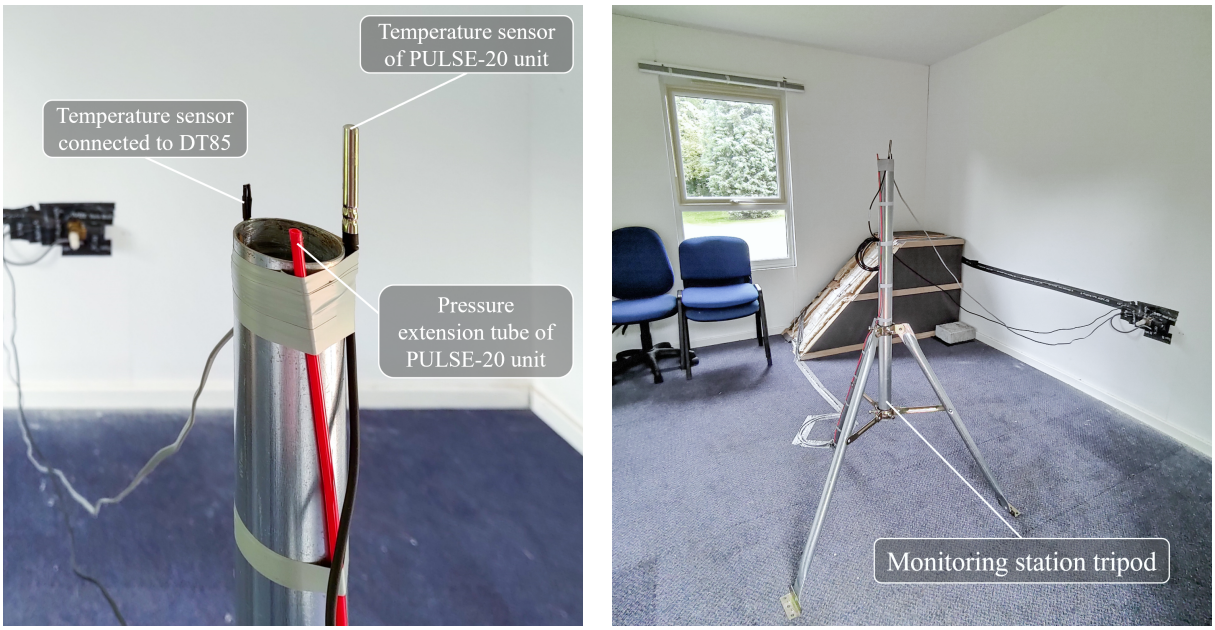
Figure 6-5(a) shows the solenoid valve on the wall of Pod 1. The nozzle releases the air pulse into the indoor space of Pod 1, which is transported from the PULSE-20 unit in Pod 2 via the connection pipe. Sealant and ISOVER Vario MultiTape was firstly applied around the nozzle for airtight bonding, and TechnoSol sealing tape was used to enhance the sealing further and eliminate leaks around the solenoid valve, as shown in Figure 6-5(b).



(a) (b)

Figure 6-5: Photos of (a) nozzle outlet in Pod 1 and (b) nozzle outlet with enhanced sealing

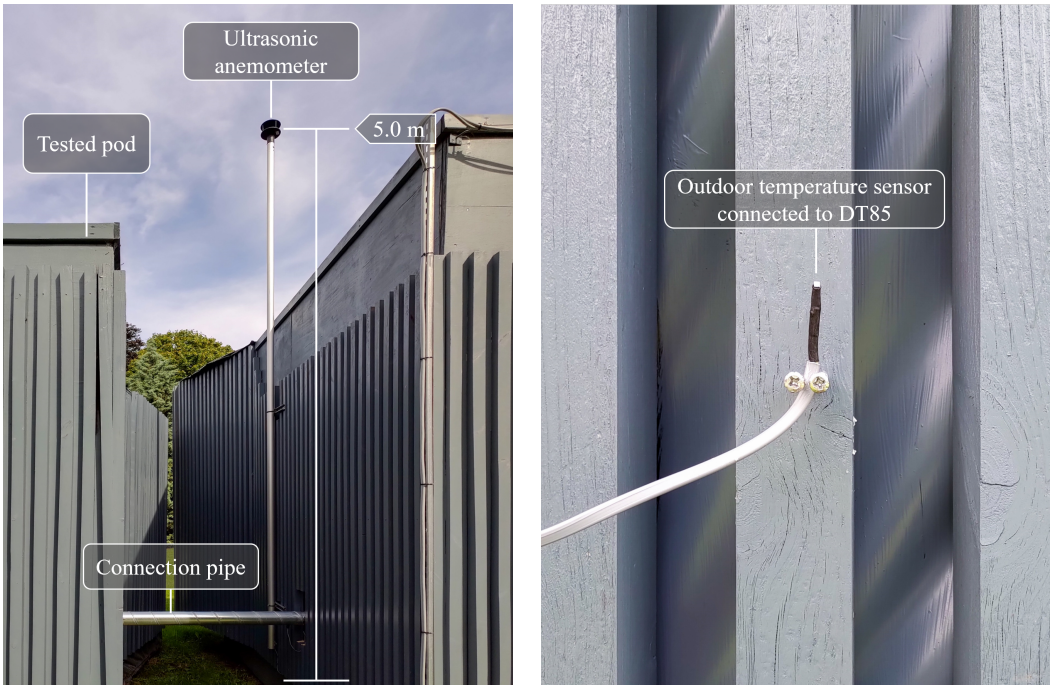
In Pod 1, three sensors were installed within the interior space to measure various parameters, as shown in Figure 6-6(a), including a thermocouple to measure the room temperature, a pressure transducer to measure the indoor pressure and a backup temperature sensor for cross-checking. The three sensors were fixed onto a tripod stand, as seen in Figure 6-6(b), at the height of 1.5-meter above the ground floor. Both the pressure transducer and the thermocouple were connected to the control box of the PULSE-20 unit; thus, the indoor pressure and temperature data were recorded by the control box at a sample rate of 50Hz. The temperature data obtained by the backup temperature sensor was recorded by a Datataker DT85 data logger, with a sampling rate of 4Hz.



(a) (b)

Figure 6-6: Photos of (a) three sensors in Pod 1 and (b) monitoring station tripod in Pod 1

Figure 6-7 presents the photos of the outdoor monitoring devices in this study. For the wind condition monitoring, an ultrasonic anemometer was installed at the height of 5m above ground level (i.e., 2m above the rooftop of Pod 1). From herein, the mentioned wind speed in this section refers to the wind speed measured at 5m above ground level. Additionally, a shielded temperature sensor was used to measure the outdoor temperature during the testing. All tests were conducted under similar conditions with a temperature difference of 5℃ between the indoor and outdoor of Pod 1, which minimised the impact of outdoor temperature on the air leakage. All the outdoor weather data were acquired by the Datataker DT85 at a sampling rate of 4Hz. The site overview of Pod 1 and Pod 2 with the experimental setup can be seen from the photos in Figure 6-8.



(a) (b)

Figure 6-7: Photos of (a) WindSonic ultrasonic anemometer and (b) outdoor temperature sensor (PT100 RTD)



(a) (b)

Figure 6-8: Site photos of Pod 1 and Pod 2

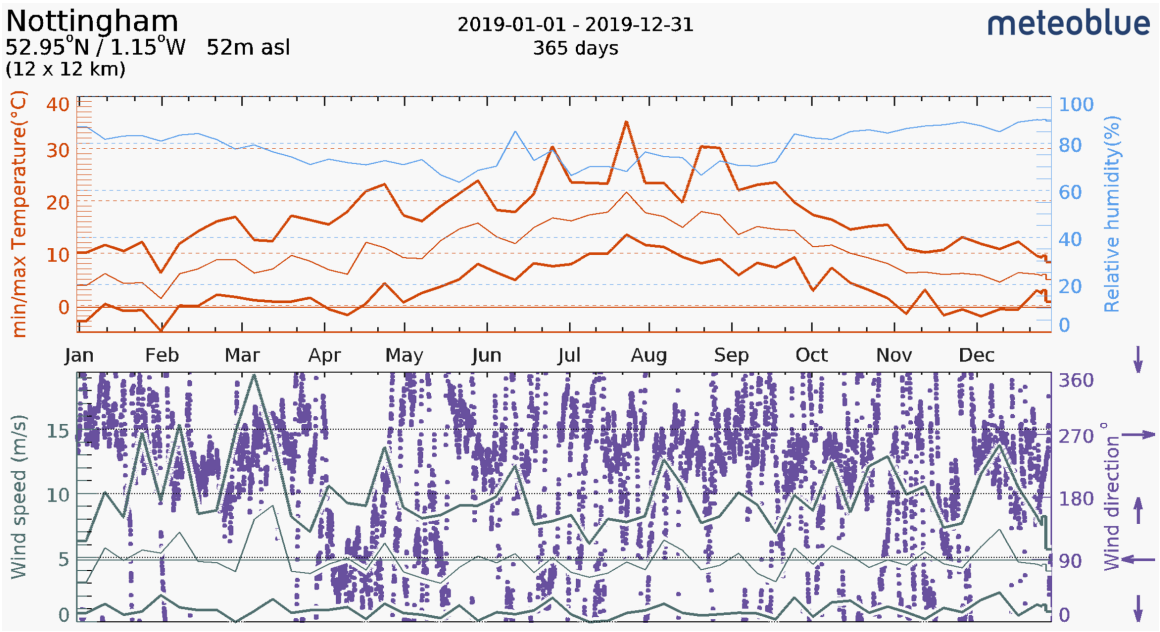
6.2.2 Impact of wind speed

In this study, in order to evaluate the wind impact on the Pulse testing over a long period, a baseline air leakage rate (ALR) at 4Pa is needed. Therefore, ten pre-tests have been initially performed at the wind speed below 0.7m/s to establish the baseline reference, and every test was a three-step pulse test, i.e., contained three successive pulse releases. The measured ALR for baseline tests and the test wind conditions are listed in Table 6-3. The corresponding measured ALR of the ten baseline tests were averaged to determine the baseline ALR for assessment, which is 25.17m³/h.

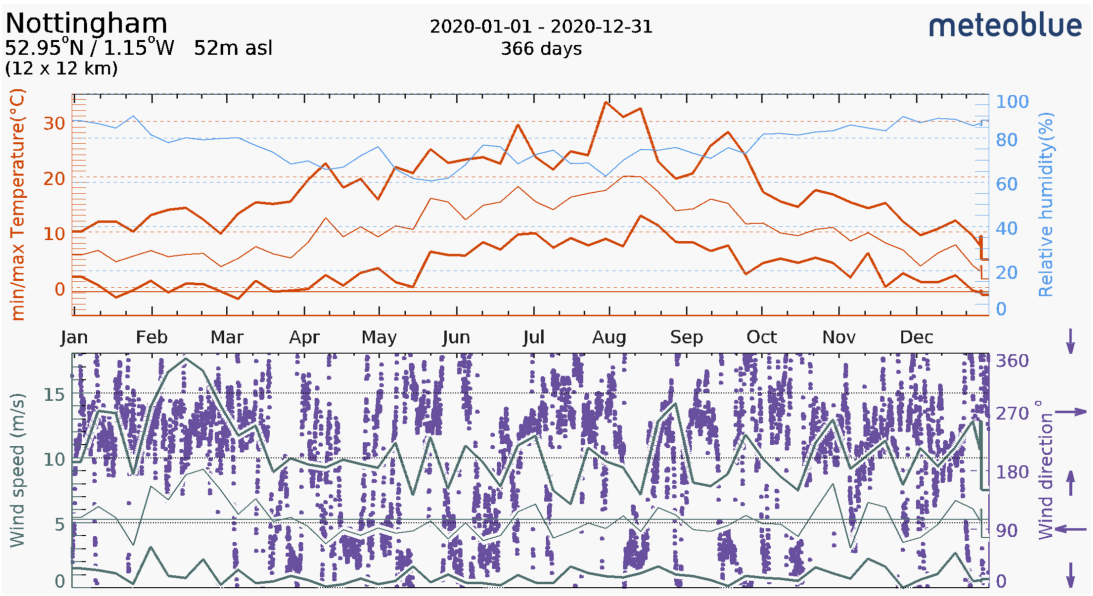
Table 6-3: Measured ALR for ten baseline tests

No.	ALR (m³/h)	Wind Speed (m/s)	Wind Direction (deg˚)
Baseline Test 1	25.24	0.07	232
Baseline Test 2	25.15	0.08	207
Baseline Test 3	25.11	0.09	243
Baseline Test 4	25.18	0.12	243
Baseline Test 5	25.24	0.13	202
Baseline Test 6	25.20	0.20	14
Baseline Test 7	25.19	0.23	228
Baseline Test 8	25.23	0.39	231
Baseline Test 9	25.12	0.48	327
Baseline Test 10	25.03	0.68	220

The test period of the long-term monitoring lasted eight months (i.e., from August 2019 to March 2020), and in total, 1096 tests were accomplished at various natural wind conditions (i.e., wind speed ranging from 0 to 12m/s, and wind direction ranging from 150° to 40°). Each test was a three-step pulse test. The majority of the Pulse tests were conducted at the wind speed ranging from 1-10m/s (i.e., approximately equivalent to meteorological 1.23-12.31m/s based on the test location). According to the weather data of Nottingham published on meteoblue.com [234] in Figure 6-9, the average temperature during the testing period (i.e., August 2019 to March 2020) is 9.25℃, the average meteorological wind speed is approximately 5.81m/s, with the highest meteorological wind speed of 17.43m/s. Hence, the obtained wind data by the anemometer during the eight-month test period are in line with the weather station data.



(a)



(b)

**Red lines: the daily temperature; Light blue line: the daily relative humidity; Grey lines: the meteorological wind speed, and Purple dots: the wind direction.*

Figure 6-9: Annual weather data of Nottingham: (a) 2019 and (b) 2020 [234]

Similar to the evaluation in Chapter 5, the relative percentage difference (*RPD*) is used to indicate the wind impact on the Pulse measurement, which is calculated by comparing the ALR of every single test with the baseline ALR. Figure 6-10 summarises the distribution of *RPD* for all 1096 tests based on the wind speed range. The results demonstrate that the higher wind speed during the Pulse testing contributes to a higher *RPD*, which consequently causes uncertainties in the measurement.

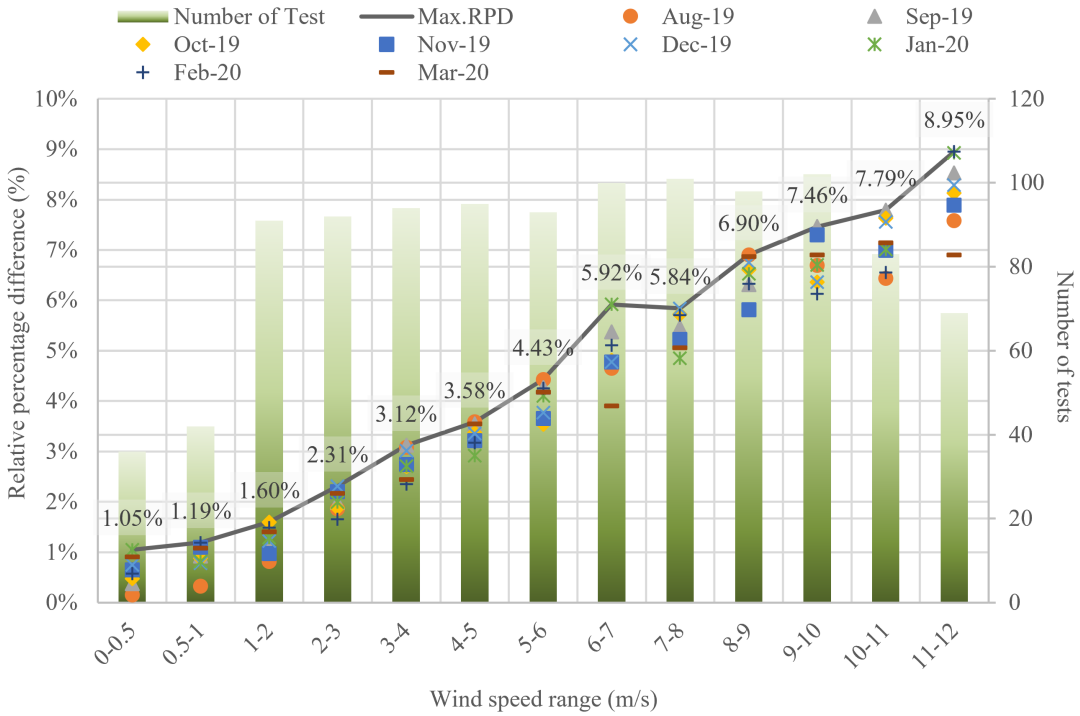


Figure 6-10: *RPD* distribution of 1096 tests according to the wind speed range

Table 6-4 summarises the number of tests conducted in each month, and the maximum *RPD*s in different wind speed ranges are also listed based on each month's testing results. The measured ALR and the corresponding *RPD* of each test in each month are plotted in Figure 6-11. The total number of tests implemented in each month is 113 tests in August 2019, 154 tests in September 2019, 151 tests in October 2019, 150 tests in November 2019, 146 tests in December 2019, 136 tests in January 2020, 128 tests in February 2020, and 118 tests in March 2020. Generally, the maximum *RPD* of each month takes place at a high wind speed level. All the 1096 tests have *RPD* below ±9%, with the highest *RPD* of -8.95% obtained in a test in February 2020 under a wind speed of 11.43m/s. Similar measurements were obtained for the eight-month tests, whereas the difference of the maximum *RPD* among all eight months varies in different wind speed ranges. For example, in the wind speed range of 0-0.5m/s, the difference is approximately 0.9% between the maximum RPDs of the eight months, while the difference increases to 2.05% in the wind speed range of 11-12m/s. The difference of the maximum *RPD* among all eight months may be attributed to the limited number of tests conducted in the certain wind speed range and the occurrence of wind gusts with unpredicted changes in the wind direction. Moreover, it can be clearly seen that the *RPD* increases with the higher wind speed. For instance, under the wind speed of 0-0.5m/s, the average of the eight-month maximum *RPD* is about 0.62%, while it reaches up to 8.15% in the wind speed range of 11-12m/s. It is also interesting to notice in Figure 6-10 that under windy conditions, a few tests still provided very close measurement results to the baseline ALR. This is maybe because: (a) the wind gust during the test was monitored by the anemometer, reflecting a wind speed variation, while the wind gust only caused a minor effect on the measurement, as it blew from a different direction, not against Pod 1; and (b) the wind gust may take place in the time gap of the successive pulses or during the background pressure recording period, which may only result in a minor influence on the Pulse measurement.

The results reflect the noticeable impact of wind speed on the Pulse test and the importance of considering the wind condition for the Pulse testing in real scenarios. Regarding the wind speed limit for *RPD* within ±5%, different findings were noticed for the eight-month tests. For instance, the suggested wind speed with *RPD* within ±5% is below 6.95m/s based on the test results in August 2019, below 7.25m/s based on the test results in October 2019, below 6.10m/s based on the January 2020's testing results, and below 7.43m/s based on the March 2020's results.

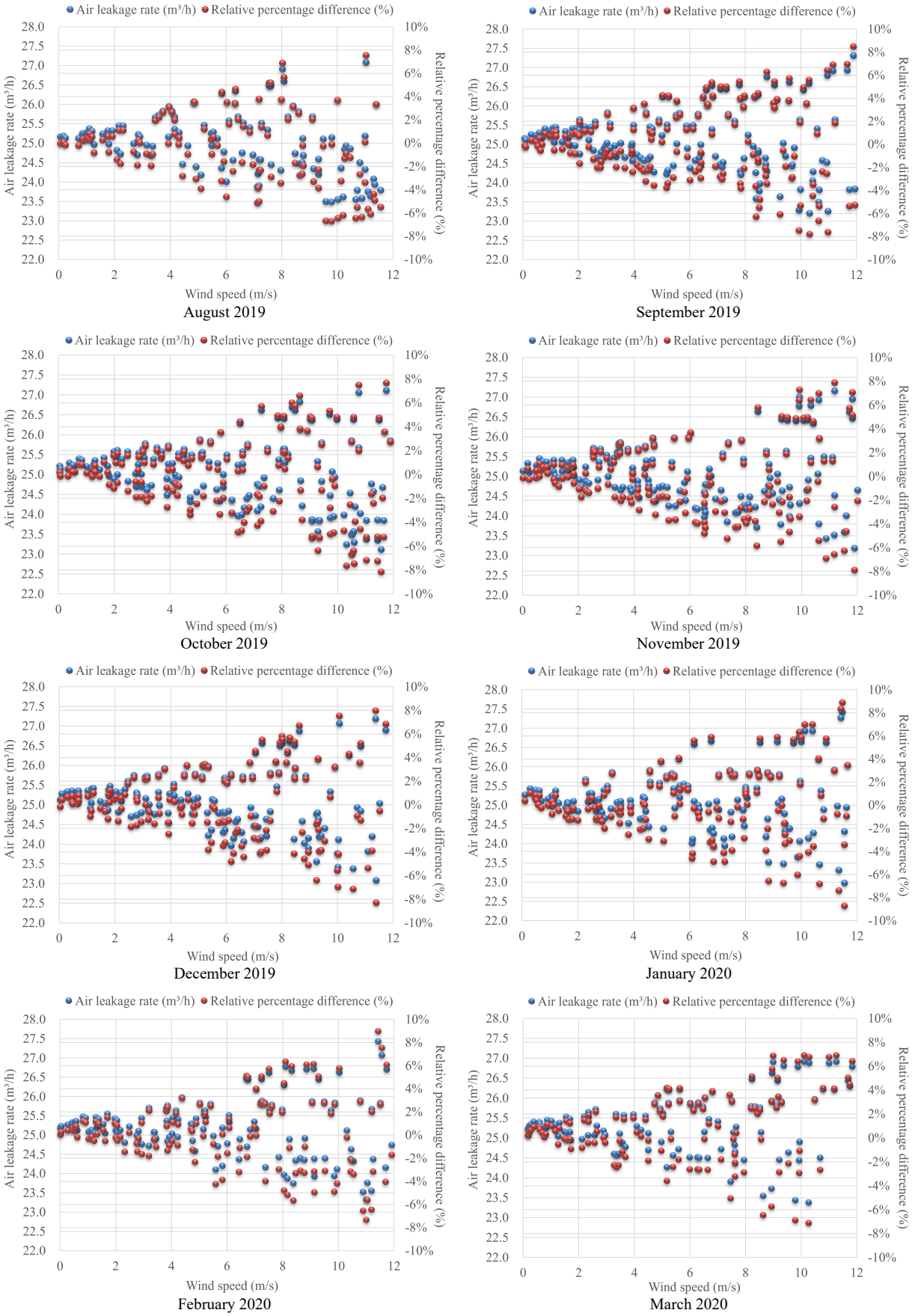


Figure 6-11: Measurements of air leakage rate from August 2019 to March 2020

Table 6-4: Test result summary for tests from August 2019 to March 2020

Wind Speed	Number of Tests								Maximum *RPD*											
	08/19	09/19	10/19	11/19	12/19	01/20	02/20	03/20	08/19	09/19	10/19	11/19	12/19	01/20	02/20	03/20	Max.*	Min.*	Diff.*	Aver.*
0 - 0.5m/s	3	4	4	5	6	4	5	5	0.15%	0.37%	0.48%	0.65%	0.74%	1.05%	0.58%	0.90%	1.05%	0.15%	0.90%	0.62%
0.5 - 1m/s	4	6	4	6	5	5	6	6	0.33%	0.92%	0.88%	1.10%	0.78%	0.82%	1.19%	1.08%	1.19%	0.33%	0.86%	0.89%
1 - 2m/s	9	13	12	12	12	12	11	10	0.82%	1.07%	1.60%	0.98%	1.22%	1.29%	1.49%	1.40%	1.60%	0.82%	0.78%	1.23%
2 - 3m/s	8	14	12	12	12	13	11	10	1.86%	1.99%	1.88%	2.20%	2.31%	2.00%	1.65%	2.16%	2.31%	1.65%	0.66%	2.01%
3 - 4m/s	8	13	14	16	13	10	10	10	3.08%	3.12%	2.70%	2.74%	3.02%	2.71%	2.35%	2.44%	3.12%	2.35%	0.77%	2.77%
4 - 5m/s	10	13	13	15	13	10	11	10	3.58%	3.55%	3.37%	3.21%	3.35%	2.92%	3.18%	3.55%	3.58%	2.92%	0.66%	3.34%
5 - 6m/s	9	13	12	11	15	11	11	11	4.43%	4.27%	3.54%	3.66%	3.77%	4.10%	4.25%	4.18%	4.43%	3.54%	0.89%	4.03%
6 - 7m/s	11	16	13	12	14	13	10	11	4.65%	5.38%	4.81%	4.77%	4.77%	5.92%	5.11%	3.90%	5.92%	3.90%	2.02%	4.91%
7 - 8m/s	13	14	12	11	15	13	12	11	5.20%	5.47%	5.72%	5.23%	5.84%	4.85%	5.71%	5.06%	5.84%	4.85%	0.99%	5.39%
8 - 9m/s	10	14	12	12	15	12	12	11	6.90%	6.31%	6.61%	5.81%	6.75%	6.53%	6.33%	6.87%	6.90%	5.81%	1.09%	6.51%
9 - 10m/s	8	15	17	14	11	15	11	11	6.69%	7.46%	6.36%	7.30%	6.36%	6.70%	6.13%	6.90%	7.46%	6.13%	1.33%	6.74%
10 - 11m/s	13	13	13	13	9	9	7	6	6.43%	7.79%	7.63%	6.99%	7.56%	7.01%	6.55%	7.14%	7.79%	6.43%	1.36%	7.14%
11 - 12m/s	7	6	13	11	6	9	11	6	7.58%	8.53%	8.13%	7.89%	8.29%	8.93%	8.95%	6.90%	8.95%	6.90%	2.05%	8.15%
Total	113	154	151	150	146	136	128	118												

*Max.: The highest maximum *RPD* among the eight-month's results.

*Min.: The lowest maximum *RPD* among the eight-month's results.

*Diff.: The difference between the highest and lowest maximum *RPD*.

*Aver.: The average maximum *RPD* among the eight-month's results

Overall Comparison

Figure 6-12 presents the wind speed limit with different *RPD* levels based on the measurements of all the 1096 tests. The obtained measurement results imply that the wind speed during the Pulse test on Pod 1 should not exceed 6.10m/s (i.e., equivalent to the meteorological wind speed of 7.51m/s based on the test location) to ensure the corresponding *RPD* within ±5%.

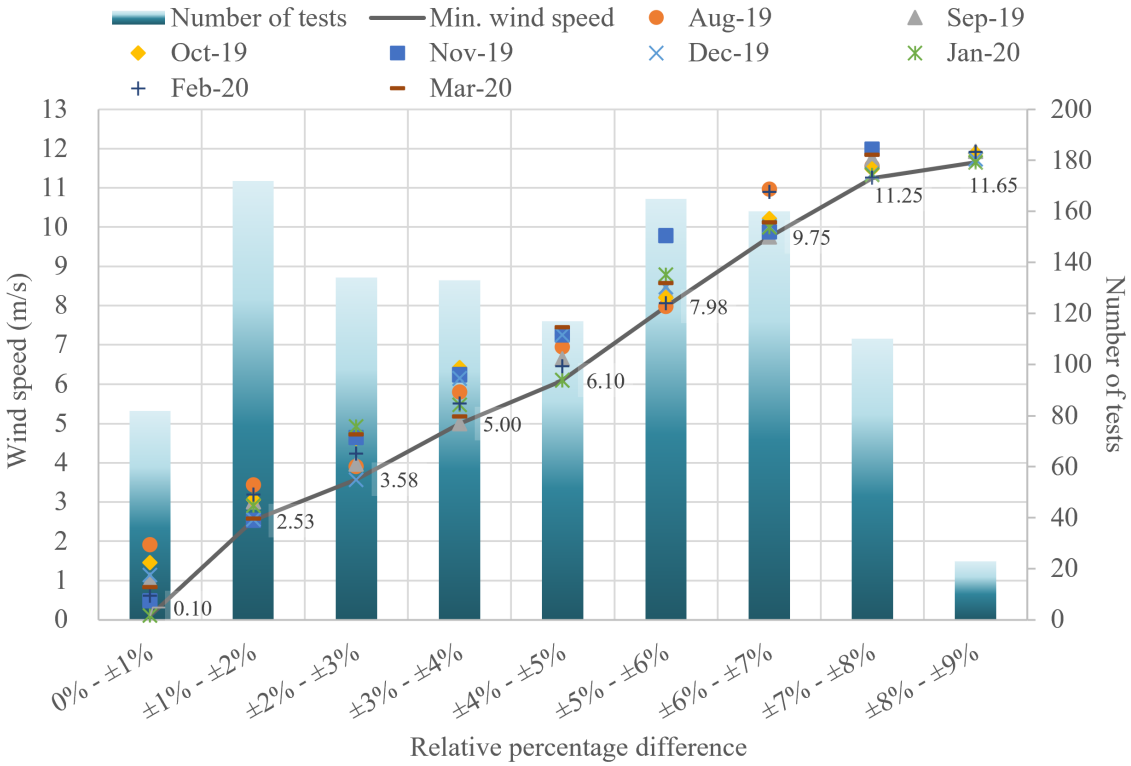


Figure 6-12: Wind speed limit for Pulse testing with different *RPD*

Compared to the findings in Chapter 5, the impact of wind speed is less significant on the Pulse testing in Pod 1, especially under the high wind speed conditions. For instance, the difference of the maximum *RPD*s for the Pulse tests in the five-bedroom dwelling at the wind speed of 0-0.5m/s and 9.5-10m/s is approximately 35.7%, while the difference is approximately 6.4% based on this long-term observational study in Pod 1. This may be caused by the following reasons:

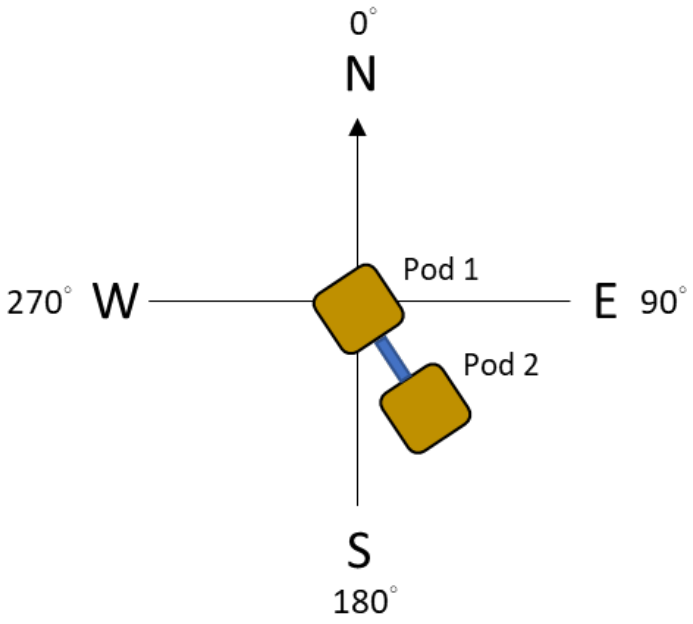
Firstly, the position of the ultrasonic anemometer. In this long-term testing, the anemometer was placed to measure the wind characteristics at 5m above ground level, higher than that of the experimental work presented in Chapter 5 (i.e., 2.2m above ground level). It is known that the wind speed increases with height; thus, the corresponding wind speed mentioned herein is higher than that of Chapter 5. According to the ISO 9972 standard, the fan pressurisation method is suggested at the wind speed near the ground level below 3m/s or the meteorological wind speed below 6m/s. For *RPD* within ±5%, the Pulse test is not suggested at a wind speed higher than around 3.14m/s at 2.2m above the ground level based on the observations presented in Chapter 5

(i.e., approximately equivalent to the meteorological wind speed of 4.95m/s based on the test location), and the wind speed limit is 6.10m/s at 5m above the ground level based on the explorations in this chapter (i.e., approximately equivalent to the meteorological wind speed of 7.51m/s). This also indicates the importance of clarifying the specific wind speed reference point for the building airtightness measurement conducted in the field test.

Secondly, the presence of the small in-between area of Pod 1 and Pod 2 may influence the wind-flow pattern around Pod 1 during the Pulse testing. Another reason is the surrounding environment. The anemometer was installed in the open backyard of the five-bedroom detached dwelling, which was free of significant obstructions within a radius of 12m of the anemometer, except tree branches and grass on the ground. However, due to the site location, as seen in Figure 6-8, there is a taller building at a distance of 5m from Pod 2. This may lead to some influences on the wind flows around Pod 1 because of the sheltering and channelling effects. Moreover, Pod 1 has a much smaller volume than the five-bedroom dwelling, as shown in Figure 6-8. Owing to the simplified building construction, Pod 1 is more airtight with fewer building elements that could contribute to building leaks. Therefore, the significance of the wind speed impact in the building airtightness measurement is not as noticeable as that in large volume buildings.

6.2.3 Impact of wind direction

In terms of site analysis, the orientation of Pod 1 is illustrated in Figure 6-13(a), Figure 6-13(b), (c), (d), and (e) show respective photos of the four façades of Pod 1.



(a)



(b) Front (Southwest)



(c) Side (Northwest)



(d) Back (Northeast)



(e) Side (Southeast)

Figure 6-13: (a) Illustration of the orientation of Pod 1 and (b-e) photos of four facades of Pod 1

The wind condition distribution (i.e., wind speed and wind direction) of the Pulse tests in each month is presented in the wind rose plot in Figure 6-14, and a wind rose plot of the 1096 tests over the eight-month testing period is shown in Figure 6-15, The vertical axis represents the number of the Pulse tests. As can be seen, most of the months have the wind direction between 200° and 240°. According to the weather data provided by Windfinder.com [239], the two dominant wind directions during the eight testing months are southwest and west-southwest (i.e., 214°-258°). Hence, the wind data gathered by the anemometer in this study match with the recorded data from the weather station.

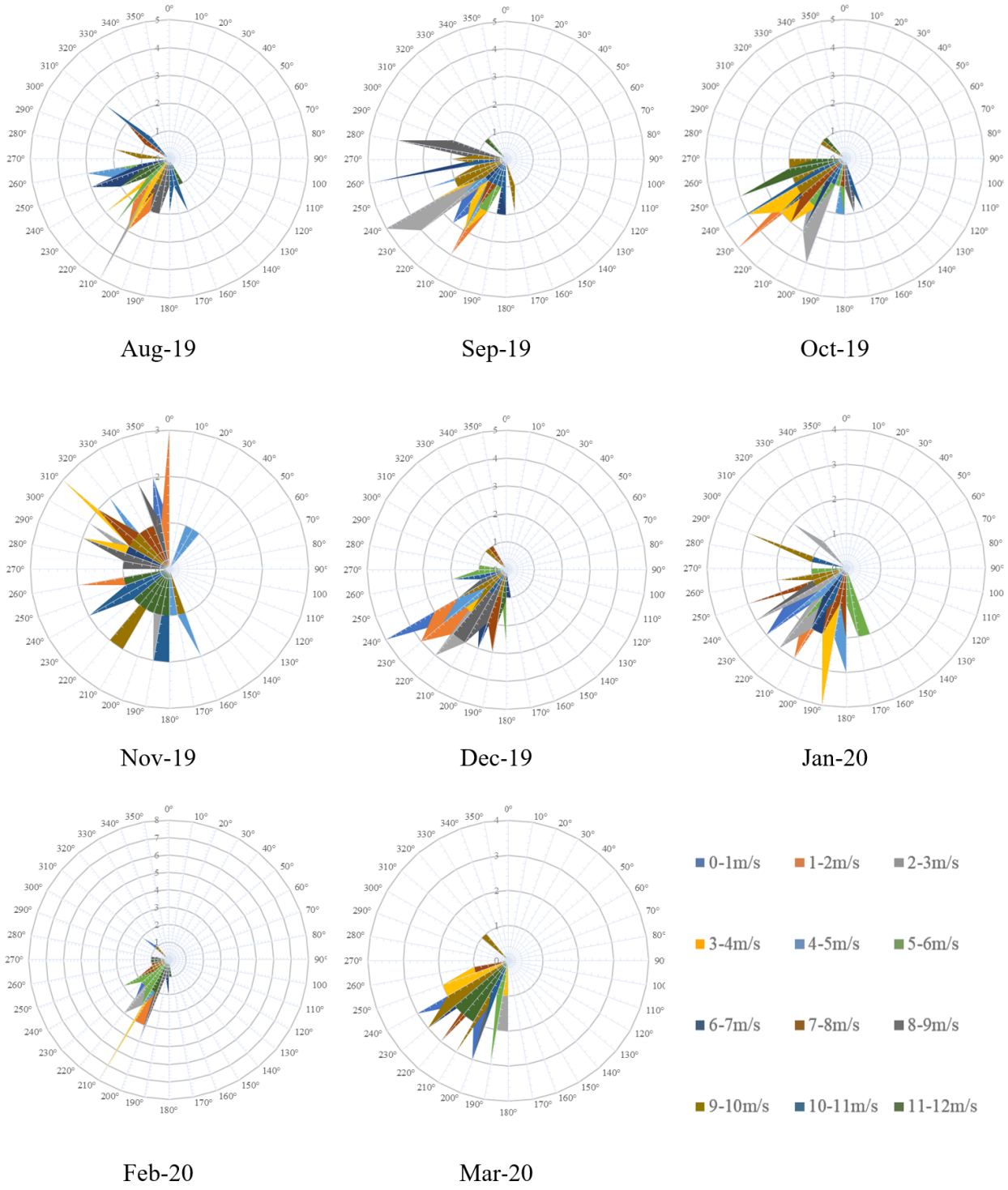


Figure 6-14: Wind rose plots for tests in each month

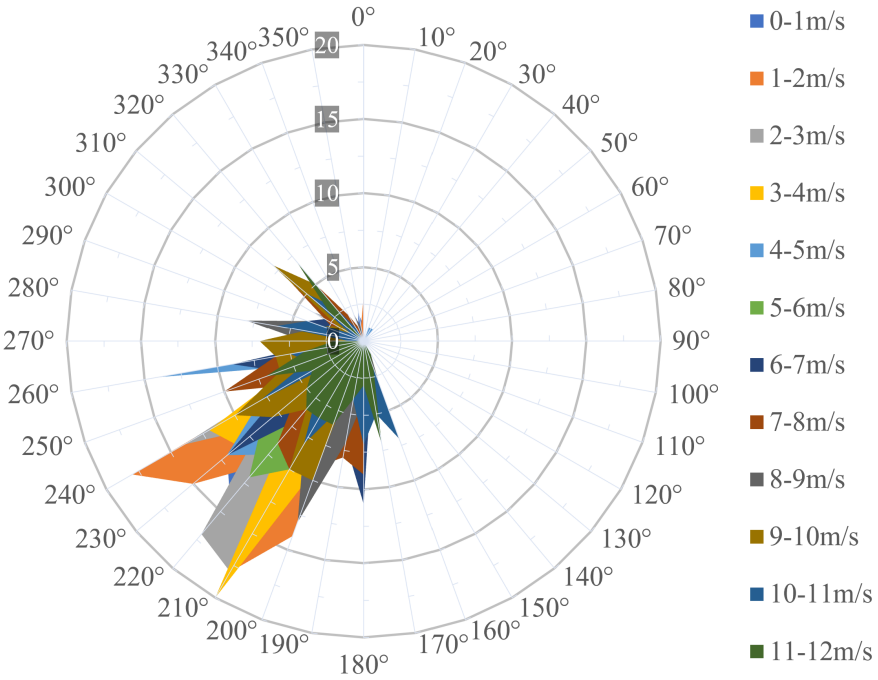


Figure 6-15: Wind rose plots for all tests during the eight-month test period

More specifically, the wind direction distribution and the associated number of the Pulse test is produced in Figure 6-16. The common wind direction range during the eight-month test period was from 160° to 340°, while very few tests were implemented with the wind direction from 0° to 160° due to the climatic characteristic in Nottingham. Comparatively, the wind direction degree of 210° has the greatest number of the Pulse tests, in total about 139 tests, accounting for around 12.68% of the total 1096 Pulse tests, followed by the wind direction degree of 240° with 117 tests and the wind direction degree of 200° with 130 tests.

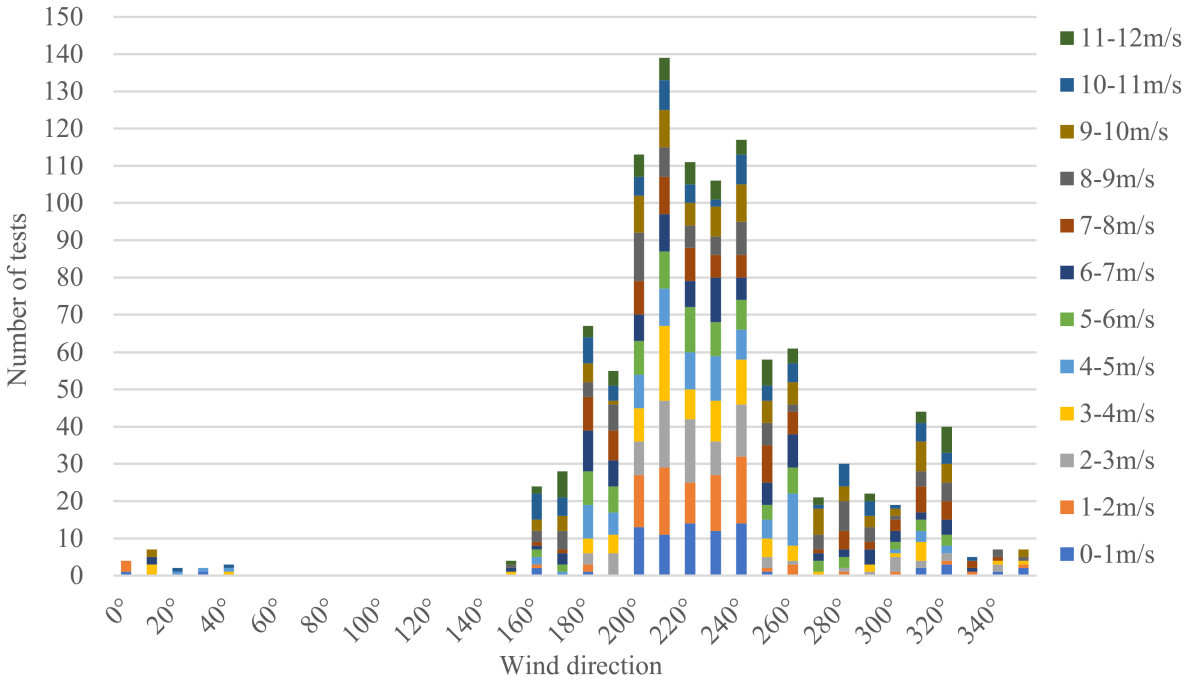


Figure 6-16: Wind direction distribution of all tests during the eight-month testing period

For analysis, the 1096 tests are categorised into four groups according to the associated wind direction degree, such as Group 1: 0°-90°; Group 2: 90°-180°; Group 3: 180°-270° and Group 4: 270°-360°. Figure 6-17 summarises the measured average ALR in each group and the corresponding number of tests in each group. There are 18 tests in Group 1, 56 tests in Group 2, 827 tests in Group 3 and 195 tests in Group 4. The obtained results indicate that the wind direction influences the building airtightness measurement, but the impact is not as considerable as that of wind speed. There is only a minor difference in the group average ALR for Group 1, 2, 3, with a difference of 1%, whereas Group 4 has the lowest average ALR, which is because that the windward façade of Pod 1 for the wind direction of Group 4 has no doors and windows (as seen in Figure 6-20c). Among all groups, the largest difference is found between Group 3 (average ALR of 25.31m³/h) and Group 4 (average ALR of 24.60m³/h), approximately 0.71m³/h (i.e., 2.8%). The reason for the minor effect of the wind direction on the airtightness measurement may include: the small volume of Pod 1 with an airtight envelope, the site location of Pod 1 with a taller building nearby influencing the wind flow pattern, and also uncertainties owing to the less available tests in Group 4 compared to Group 3.

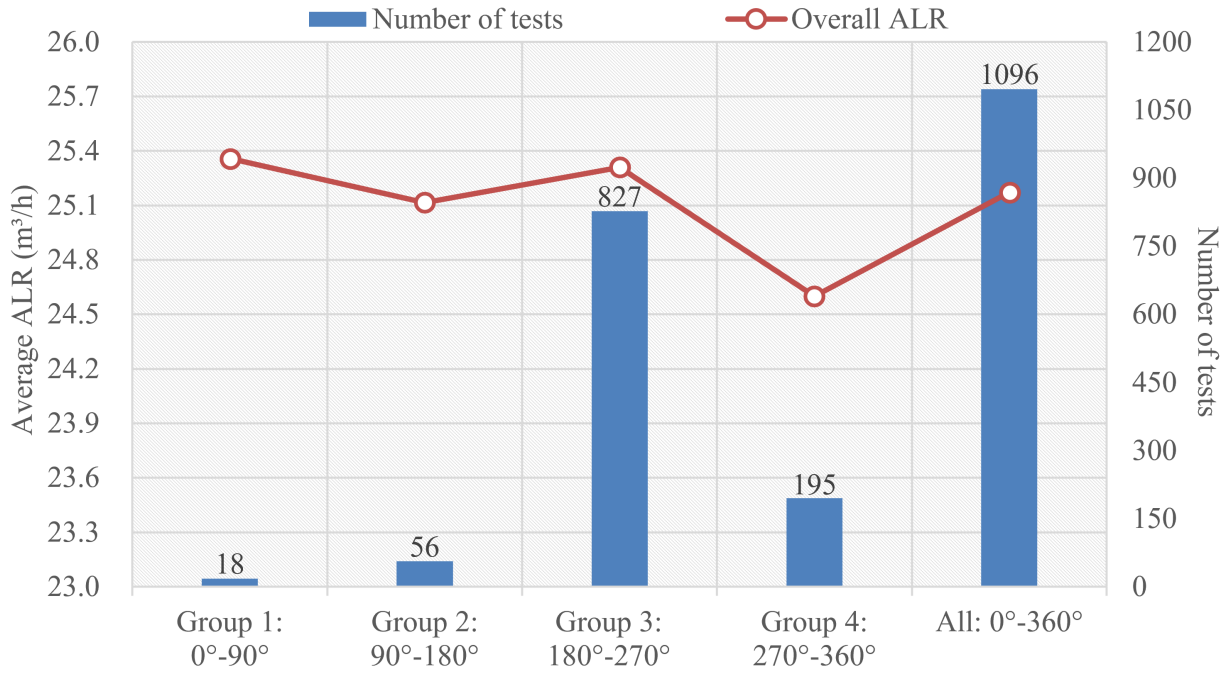


Figure 6-17: ALR measurements at different wind direction ranges

The wind direction impact is less significant when the corresponding wind speed is at a low level. For instance, the average ALR measurement for Group 1 is around 25.19m³/h in the wind speed range of 0-2m/s with 0.31m³/h (1.2%) difference between the highest and the lowest values, while the discrepancy becomes more noticeable for the wind speed above 3m/s, with the maximum difference of 3.20m³/h in the wind speed range of 9-11m/s. Similar results are found when

comparing different groups. For instance, at the wind speed ranging in 1-1.5m/s, the average ALR of 25.11m³/h was measured in Group 1, while the average measurement of 25.23m³/h was obtained in Group 3 and 24.94m³/h in Group 4, with a difference of 0.12m³/h and 0.17m³/h, respectively. However, the difference becomes more noticeable at the wind speed of 9.5-10m/s, which is 27.01m³/h for Group 1, 24.98m³/h for Group 2, 25.26m³/h for Group 3 and 24.24m³/h for Group 4. Hence, as discussed previously in Chapter 5, the Pulse test is recommended at lower wind speed for an accurate building airtightness measurement, simultaneously taking into account of the impact of wind direction.

6.3 Seasonal effect on building leakage in eight months

The experiment work has been conducted for eight months from 2019 to 2020, covering meteorological seasons of summer (August 2019), autumn (September 2019, October 2019, November 2019), winter (December 2019, January 2020, February 2020) and spring (March 2020), and temperatures varied from 3.8℃ to 21.9℃. Therefore, the seasonal variation of building airtightness of Pod 1 can be analysed based on the obtained data. The long-term performance of the airtightness of Pod 1 is listed in Table 6-5 and shown in Figure 6-18. The evaluation of the ageing effect is based on the Pulse tests each month at the wind speed below 1m/s and the wind direction between 180-270°, which minimises the wind impact on the building airtightness measurement. The baseline ALR is determined as the average ALR of the pre-tests, which is 25.18m^3/h. The *RPD* is calculated by comparing the average ALR of each month with the baseline ALR. The higher *RPD* obtained in November 2019 may be caused by the limited valid tests in that month (i.e., only three tests) and also more diverse wind characteristics as seen in Figure 6-9 (i.e., with a wide range of wind direction). Overall, the seasonal variation on the building airtightness is not noticeable, with the highest *RPD* of 0.58%. It may be due to: (a) the measurement uncertainty caused by the equipment, and (b) the sealing tapes around the windows and door dried out, causing the variation of ALR.

On the other hand, the average ALR is slightly higher in winter than in summer, for instance, 25.29m^3/h in winter and 25.18m^3/h in summer. This is in line with the findings discussed in [175]. Based on the one-year investigation of the impact of environmental conditions on the building airtightness by Cooper, et al. [32], their obtained ALR in November is slightly higher than that of August under similar wind conditions. The insignificant seasonal variation of airtightness maybe because that Pod 1 is a relatively smaller volume and more airtight than typical dwellings. Also, the physical form has been maintained throughout the test period, for example, the door and

window of Pod 1 are sealed and no changes in building preparation between each test. In addition, the test lasts about eight months, and the seasonal variation may become more noticeable based on years' observations.

Table 6-5: Test result summary for ageing effect evaluation

	Number of Tests	Average ALR (m³/h)	*RPD*
Baseline Test	8	25.18	0.00%
Aug-19	7	25.19	0.08%
Sep-19	10	25.22	0.17%
Oct-19	8	25.26	0.32%
Nov-19	3	25.32	0.58%
Dec-19	11	25.27	0.37%
Jan-20	9	25.29	0.44%
Feb-20	8	25.30	0.51%
Mar-20	10	25.32	0.56%

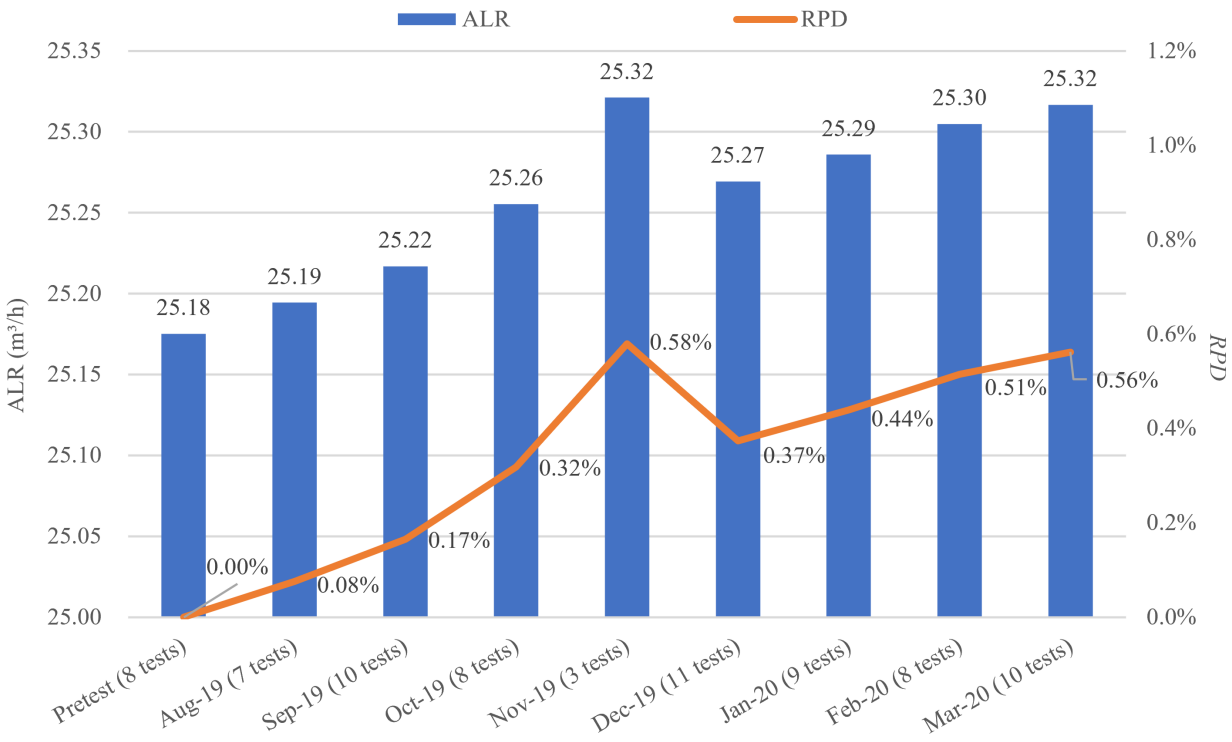


Figure 6-18: ALR measurements and *RPD* in different months

6.4 Further work

Considering the difficulty of establishing controllable wind conditions to characterise the wind impact on the Pulse tests in real scenarios, extended work could be conducted with a model-scale experiment in a wind tunnel to investigate how the steady wind affects the Pulse test and thus obtain an improved understanding of how the Pulse test is affected by various wind conditions. Moreover, the uncertainty induced by the wind impact on the Pulse test could be assessed based on the model-scale experiments in controlled laboratory conditions. The design of the model-scale experiment in a wind tunnel was prepared in September 2019. However, due to the global pandemic, all the planned works have been disrupted and suspended since March 2020. Because of the prolonged lockdown in the UK, the model-scale experiment with the wind tunnel facilities eventually was not able to be performed in the laboratory at the University of Nottingham. Nevertheless, the preliminary work can be found in the supplementary material in Appendix-A, including the literature review, the test arrangement, the test methodology and the design of experimental facilities for the proposed model-scale experiment using a wind tunnel. The constructed experimental facility and the presented methodology would be useful for future evaluation of the steady wind impact on the Pulse measurement in controlled conditions.

6.5 Summary

In this chapter, complementary insights into the wind impact on the Pulse testing were provided based on the eight-month observations in an outdoor test pod. The explorations over the eight months also demonstrate how the Pulse measurement performs under different wind conditions in real scenarios and the reliability of Pulse. Over the eight-month of the Pulse testing in the outdoor test pod, the wind conditions varied significantly, and the noticeable impact of the wind speed was also apparent in line with the observations discussed in relation to the five-bedroom dwelling of Chapter 5. A higher wind speed could contribute to a large deviation of the airtightness measurement. In terms of the threshold of wind speed that causes results with unacceptable errors, the Pulse test in the outdoor chamber with the *RPD* within ±10%, the wind speed should be less than 11.65m/s at 5.0m above ground level (i.e., approximately equivalent to meteorological wind speed 14.34m/s). This finding is different from the suggestion for the fan pressurisation method stated in the ISO 9972 standard (i.e., below the meteorological wind speed of 6m/s), and from the findings discussed in Chapter 5 (i.e., below meteorological wind speed 7.91m/s), due to the test building configuration, the position of the ultrasonic anemometer and the surrounding environment in the test location. The threshold value of the meteorological wind speed of

11.61m/s with the *RPD* <±20% discussed in Chapter 5 was not applicable to the Pulse test in the outdoor chamber, as the corresponding *RPD* is in the range of 6-7%. This is owing to the fact that the two tested buildings have different building configurations and airtightness levels, causing the wind impact on the Pulse measurement of the outdoor chamber to be not as significant as that of the five-bedroom dwelling presented in Chapter 5. The results also indicate the importance of clarifying the specific wind speed reference point for the building airtightness measurement conducted in the field test.

Moreover, the airtightness measurement could be less affected by the wind direction under the lower wind speed conditions. Additionally, a minor seasonal variation (i.e., 0.58%) of the Pod's airtightness was observed over the eight months, which may be due to a seasonal effect or potentially a degradation of the sealing tape around the window, door and ductwork. Nevertheless, the average ALR is slightly higher in winter than that of summer, by approximately 0.11m^3/h. Furthermore, the supplementary materials were given in Appendix A for the proposed model-scale experiment work with a wind tunnel, which could provide useful information for future model scale experimental investigations of the steady wind impact on the Pulse test.

7. CFD-Based Numerical Simulation of the Pulse Test

7.1 Introduction

In this chapter, CFD-based simulations using the ANSYS Fluent are conducted to numerically investigate how the pressure wave propagates within the internal spaces of a building and how various wind conditions affect the pressure distribution and, subsequently, the Pulse measurement. The CFD-based numerical simulations aim to extend the exploration of the wind impact on the Pulse test. The numerical simulations will be cross-validated to the experimental results obtained from the tests performed inside the five-bedroom detached dwelling presented in Chapters 3, 4, and 5, thus providing complementary insights into Pulse under different steady wind conditions. The building and the Pulse unit models are established based on the dimensions and specifications of the experimentally tested dwelling and the PULSE-60 unit used for the tests. The simulations are implemented to understand how the pressure wave propagates within the building during the pulse test and the steady wind impact on the Pulse measurements under various scenarios, such as under various wind speed levels, various wind directions and the presence of a gable roof.

As Pulse is a relatively newly developed technique for measuring the building airtightness, very limited simulation studies have been reported in the literature. Cooper, et al. [33] performed CFD simulations to prove the uniformity of air pressure distribution in the tank and the uniformity of density during the pulse period, which were based on a simplified two-dimensional axisymmetric domain and the distribution of the leakage pathways in the building envelope was represented by a circular opening. The assumption on which the theoretical model was based has been validated by the numerical investigation. Differently, the simulations in this study focus on the three-dimensional computational fluid dynamics modelling of a full-scale dwelling and the Pulse unit. To provide a full picture of the research, Figure 7-1 presents the overview of how the investigations of the wind impact are structured and conducted from different perspectives in this research. Table 7-1 list the simulated cases in this study with their respective simulation conditions. The main objectives of the numerical investigations are to provide a different perspective into how the steady wind condition influences the Pulse measurement, such as gaining an understanding of how different steady wind speeds and wind directions (which are difficult to achieve in the experiment studies) affect the Pulse test. Also, the simulation results could provide evidence in terms of the reliability and practicality of the Pulse test under various steady wind conditions and complementary understandings of the wind impact on the Pulse test.

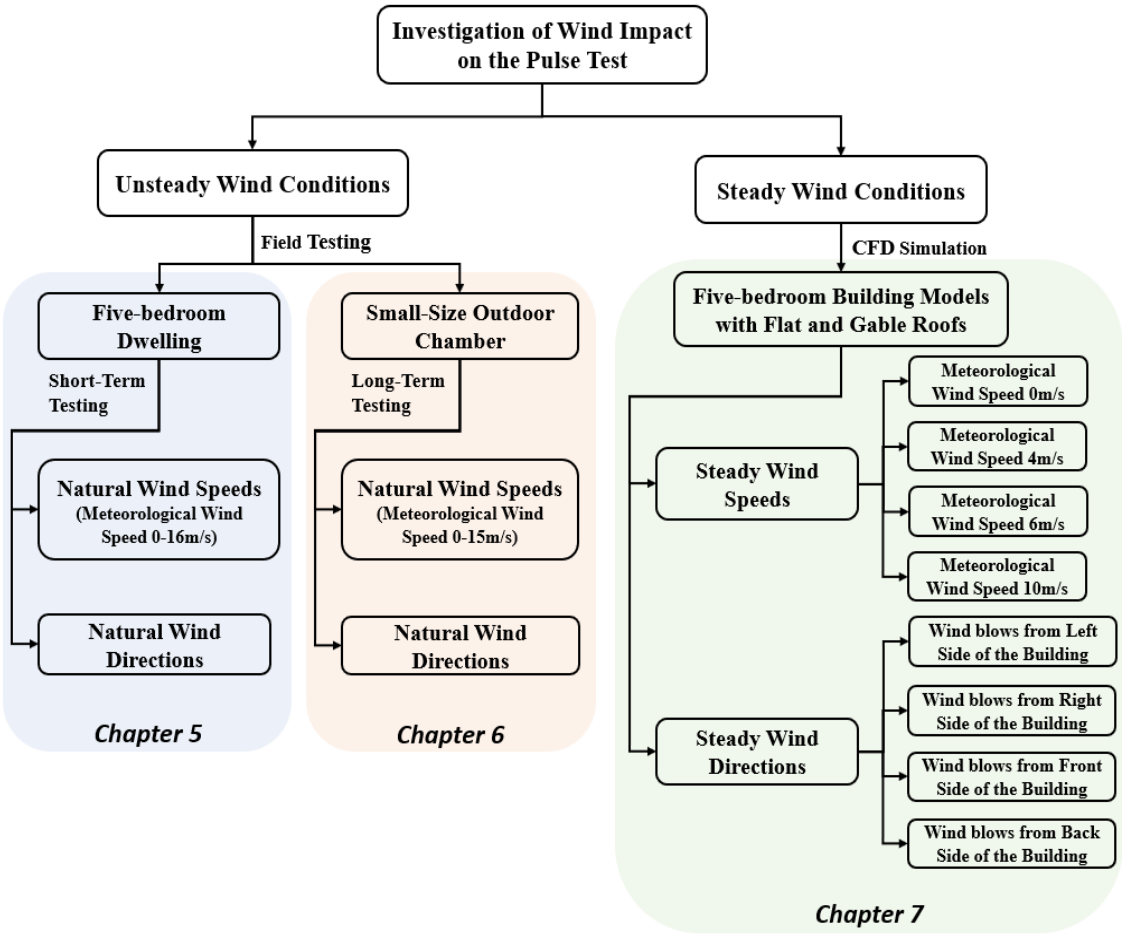


Figure 7-1: Research structure of the investigation of the wind impact on Pulse

Table 7-1: Summary of the cases in the numerical study with simulation conditions

Case	Roof Type	Wind Speed at 10m above Ground	Wind Direction
I	Flat	0m/s	along positive x-axis
II	Flat	4m/s	along positive x-axis
III	Flat	6m/s	along positive x-axis
IV	Flat	10m/s	along positive x-axis
V	Flat	6m/s	along negative x-axis
VI	Flat	6m/s	along negative z-axis
VII	Flat	6m/s	along positive z-axis
VIII	Pitched	6m/s	along positive x-axis
IX	Pitched	6m/s	along negative z-axis

7.2 Methodology

Referred to the size and configuration of the tested five-bedroom dwelling in the experimental studies reported in Chapter 3, a three-dimensional full-scale model of the five-bedroom house is established in SolidWorks. Different from the tested dwelling, a rectangular building plan is adopted for modelling, while the room layout is kept the same as the tested dwelling, with

considerations of: (1) in the numerical simulation, wind direction is set to be normal to the building façade. Therefore, numerical investigations with the rectangular building geometry could provide a straightforward understanding of how different steady wind conditions influences the Pulse measurement. Whereas an L-shape building causes complexity in the wind flow pattern around the building and the occurrence of stagnation phenomenon in the corners under different wind conditions, and (2) simplicity of the rectangular building shape for simulation and required simulation time. Table 7-2 presents the differences between the established building model and the tested dwelling in terms of the building layout, internal volume, and envelope area. Only slight differences are noted with regard to building volume and envelope area. Further modelling details are presented in Section 7.3.1. The computational simulations are implemented in the ANSYS Fluent 2020R2 platform, and configurations are described in detail in the following sections.

Table 7-2: Comparison of the building model with the tested dwelling

	Total Number of Rooms	Building Internal Volume	Envelope Area
Tested Dwelling	7	447m^3	416m^2
Building Model	7	450m^3	410m^2
Discrepancy	-	0.67%	1.44%

As with the evaluation method used for the field testing presented in Chapter 5, a number of monitoring points are defined in the numerical simulation to record the transient data, including air pressure, air density and air velocity in each room within the building, volumetric airflow rate of designated building openings and wind condition. Therefore, the analysis is carried out based on the obtained numerical results covering various aspects, such as assessing the uniformity of the indoor pressure distribution, the indoor air velocity distribution, the airflow profile through openings, and the overall air leakage rate under various wind conditions.

7.3 Simulation of indoor pressure and velocity distributions during the Pulse test

Firstly, the simulation is conducted in order to visualise the dynamic process of the Pulse test to understand both the pressure wave propagation and the uniformity of the pressure distribution within the building during the air pulse test. As the experimental work in Chapter 4 was performed under calm wind conditions, the numerical simulation reported in this section is based on the condition with no outdoor wind to facilitate the cross-validation between the numerical investigation and the experimental results. Moreover, the simulations visualise the velocity distribution of the indoor spaces during the Pulse test, which could be challenging to achieve through field testing.

7.3.1 Computational domain and configurations

Modelling of the building with the Pulse unit

Figure 7-2 presents the layout of the building model with detailed dimensions in the plan view, and the sectional view of the building model is shown in Figure 7-3. The exterior dimension of the building model is 5.2m (W)*18.2m (L)*5.3m (H), with a wall thickness of 0.1m. However, the entire internal space of the building model is determined as the fluid domain in the numerical simulation, with the dimension of 5m (W)*18m (L)*5m (H), an envelope area of 410m^2 and a volume of 450m^3. The distribution of the leakage pathways on the building envelope is represented by circular openings, where the released air from the air tank of the Pulse unit during the Pulse test is discharged through during testing. The circular openings are regarded as circular orifices, and the discharge of the fluid depends on the depth of the orifice as per the study by Huebsch, et al. [240]. In this numerical study, they are assumed as thin plate circular orifices, as they are located on the inner building envelope, of which the fluid domain has negligible thickness. Kurita [241] and Blair, et al. [242] reported the discharge coefficient of various duct end geometries, and the typical value of the circular sharp-edged orifice plate is stated as 0.61, which is used for the proposed openings in this study.

In this numerical study, simulations are performed on the basis of a single air pulse release. Therefore, referring to the Pulse measurements with a single air pulse release presented in Section 5.3.2 (i.e., Table 5-5 Case A), the measured permeability of the tested dwelling is 0.777m^3/h/m^2 at 4Pa under a wind speed of 0.06m/s (i.e., air leakage rate of 0.08979m^3/s). Taking the measured permeability and the discharge coefficient into account, in total, ten circular openings across the building envelope are proposed at different locations, with a total area of 0.058m^2. In such a way, each opening has an area of 0.0058m^2 (i.e., a radius of 0.043m) and the specific location for each opening is shown in Figure 7-2.

The Pulse unit model was built in SolidWorks, with reference to the configuration of the PULSE-60 unit that was employed in the experimental studies, which contains an air tank with an effective volume of 58.5L. In the experimental study, a ¾ inch (BSP) solenoid valve was installed at the air tank outlet with an effective area of 0.0016m^2, working together with a silencer to release the compressed air from the air tank into the indoor spaces. Therefore, a cylindrical nozzle is created for the Pulse unit model with the same effective area as the silencer used in the PULSE-60 unit, which diffuses the compressed air through its surface into the indoor spaces. Same as the experimental setup, the Pulse unit model is also located in the living room on the ground floor, as illustrated in Figure 7-2(b).

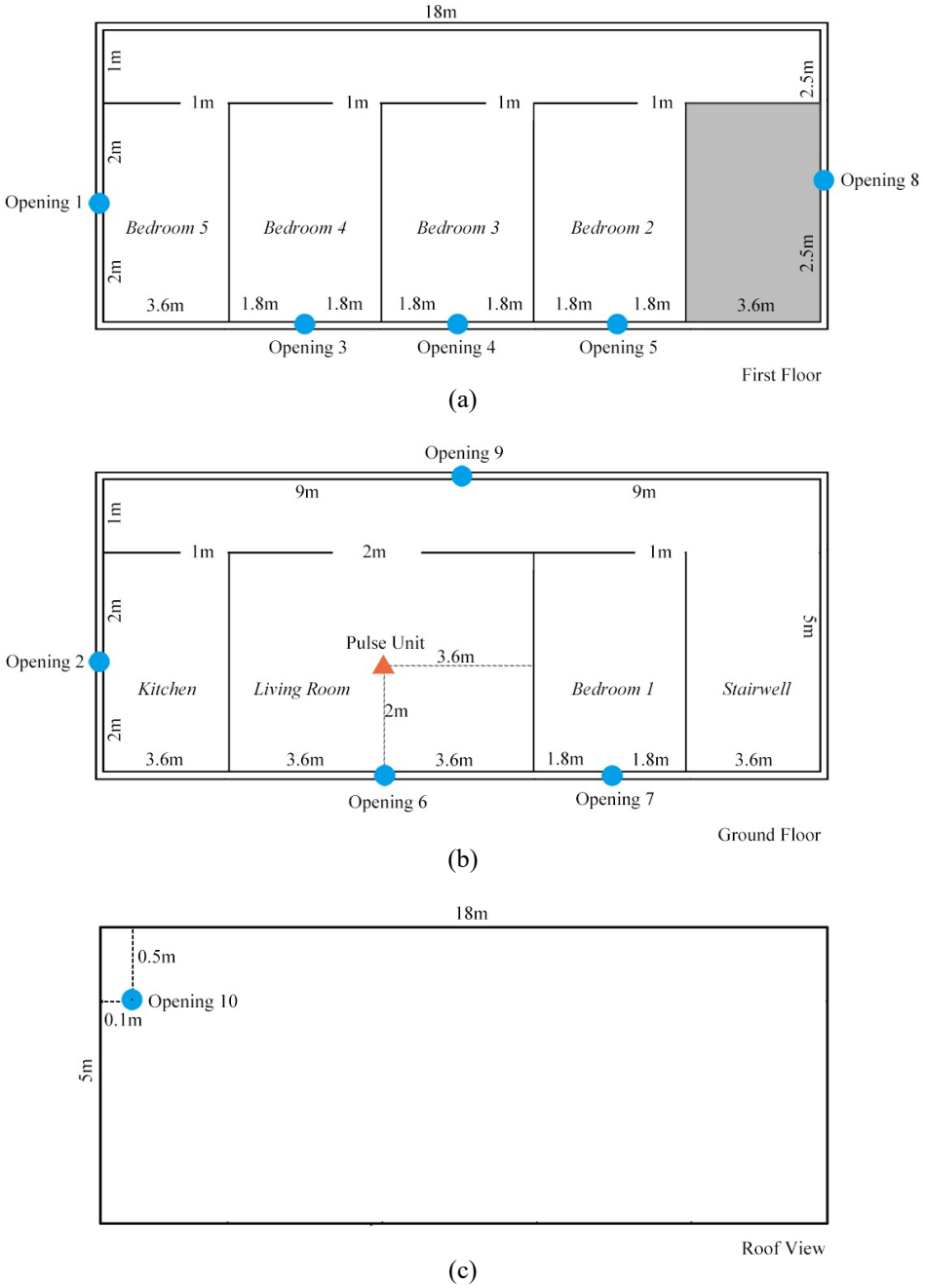


Figure 7-2: Plan views of the building layout with detailed dimensions and openings' locations

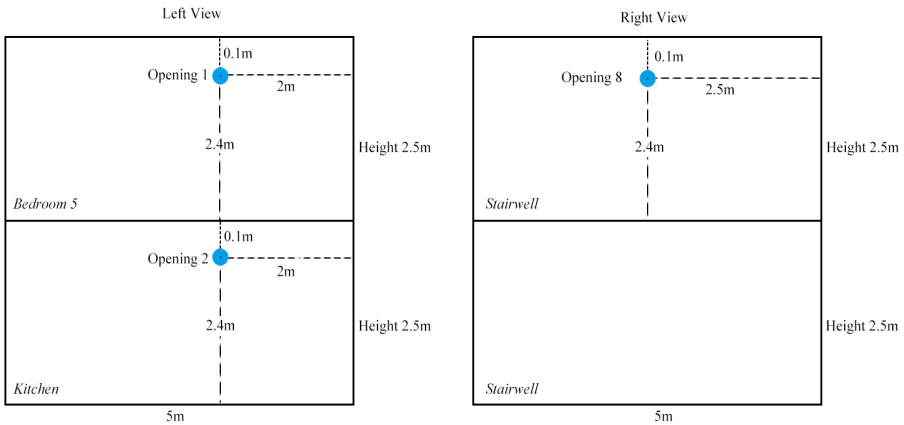
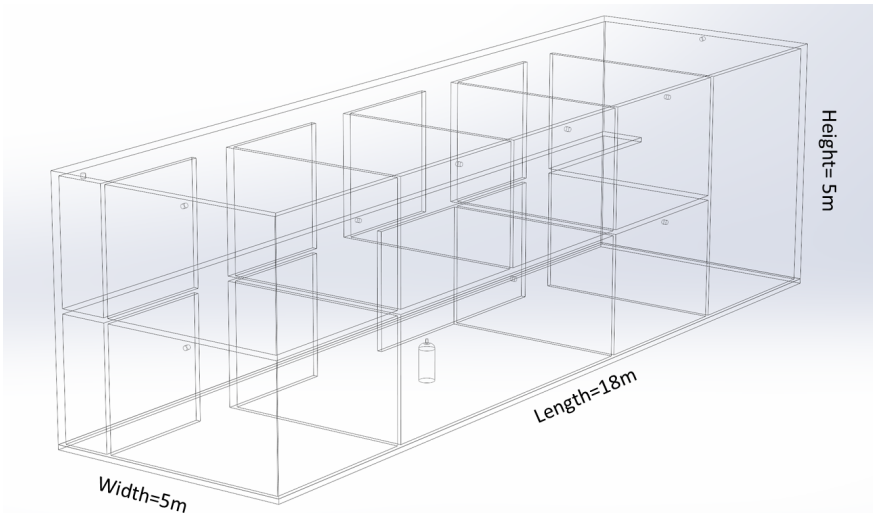
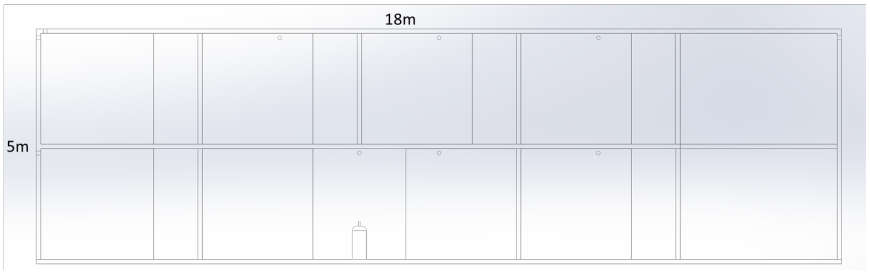


Figure 7-3: Sectional view of the building with detailed dimensions and openings' locations

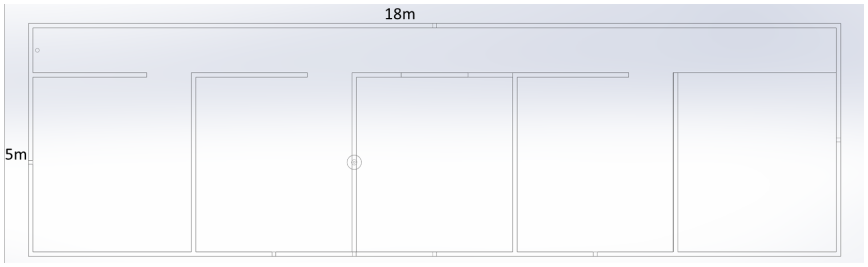
Figure 7-4 presents different views of the building wireframe model with ten circular openings on the envelope and the Pulse unit.



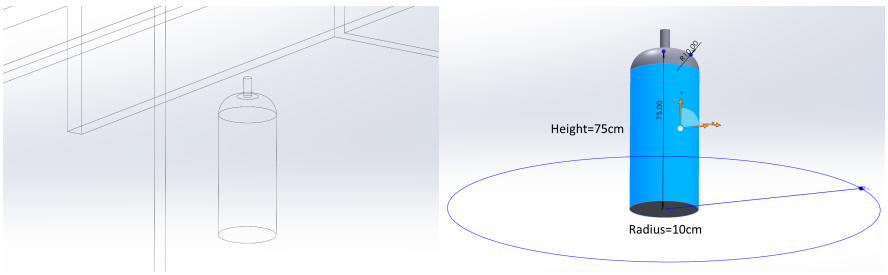
(a) 3D model perspective view



(b) Building model front view



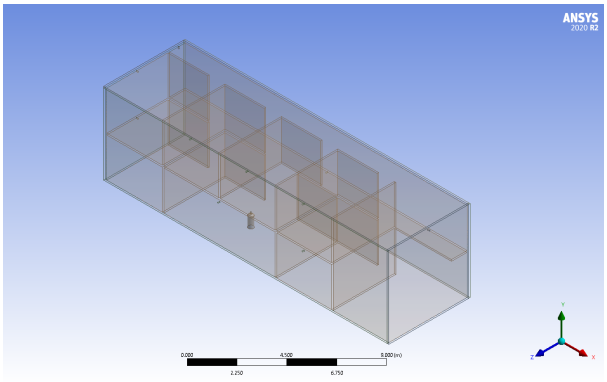
(c) Building model top view



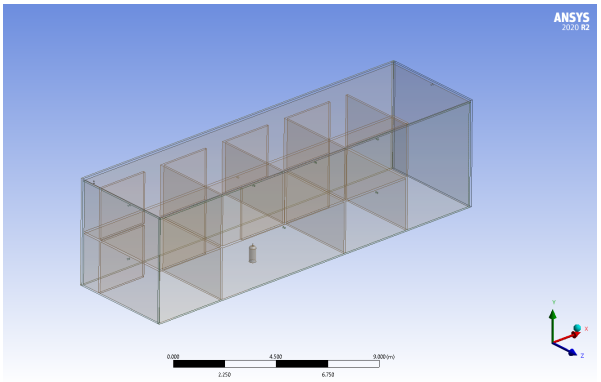
(d) Pulse unit model

Figure 7-4: Model views of the building and Pulse unit

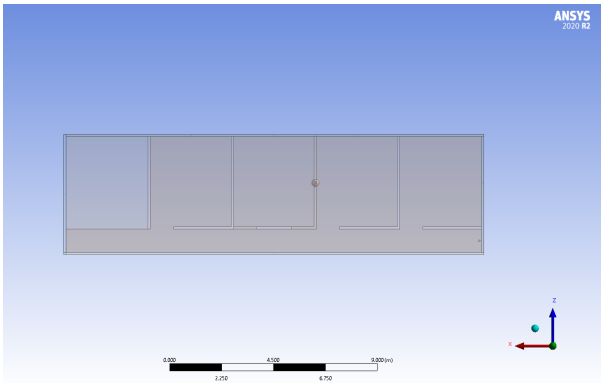
The established SolidWorks model is then imported into the ANSYS Fluent 2020R2 platform for programming and simulation. Figure 7-5 presents views of the building model in the Fluent interface. The nozzle of the Pulse unit is defined as the inlet for transient simulation, while the ten circular openings are the outlets, and others are defined as wall elements.



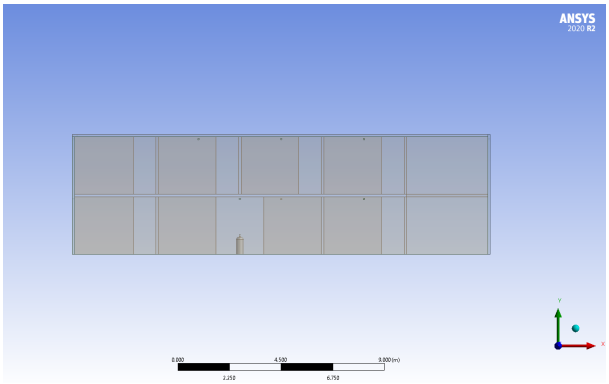
(a) 3D perspective view



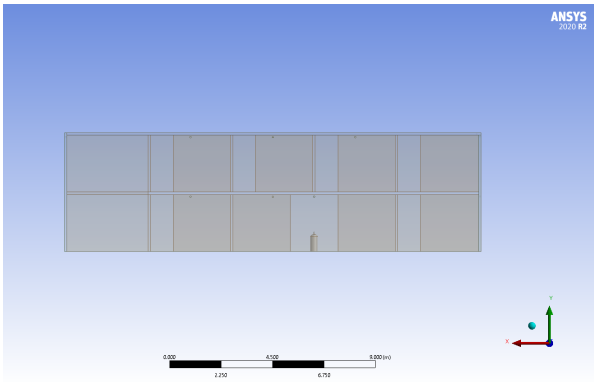
(b) 3D perspective view



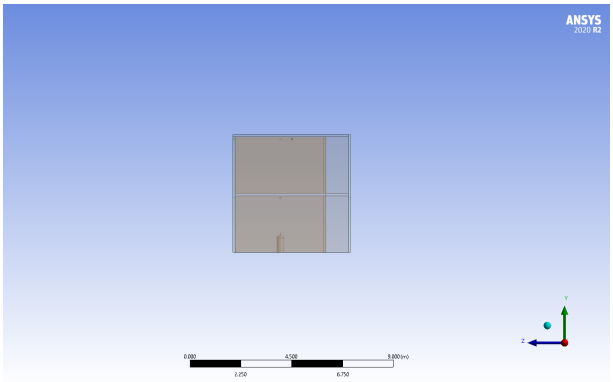
(c) Model top view



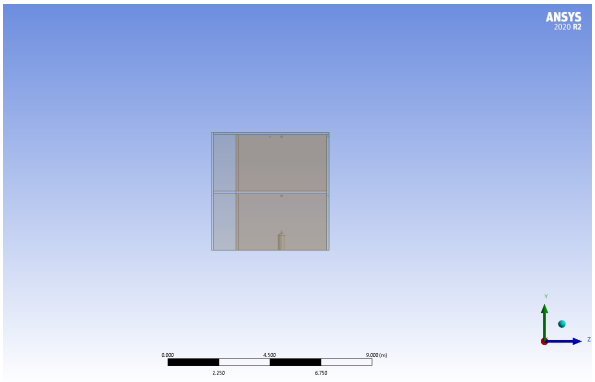
(d) Model front view



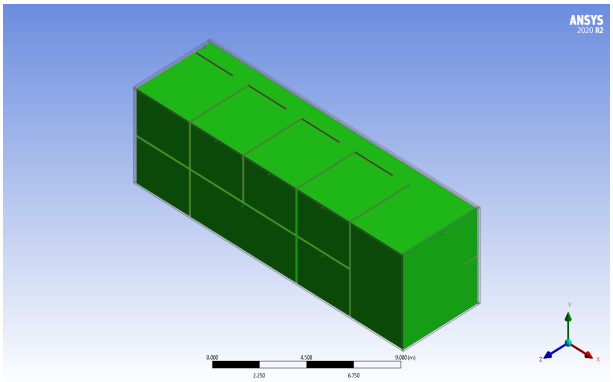
(e) Model back view



(f) Model right view



(g) Model left view



(h) Fluid domain (Building internal space)

Figure 7-5: Views of building model and Pulse unit in Fluent

Mesh and grid analysis

A mix of tetrahedral and hexahedral cells is generated for the mesh with better and accurate fitting to the created geometry. To define the grid resolution, the grid-sensitivity analysis is conducted by examining the different sets of grids with the corresponding convergence performance and the simulated value of building air leakage rate during the Pulse test. Three sets of grids are proposed for comparison, namely a coarse grid with an element size of 0.15m, a basic grid with an element size of 0.1m and a fine grid with an element size of 0.07m. The grid-convergence index (GCI) can be calculated referring to Roache [243]'s method:

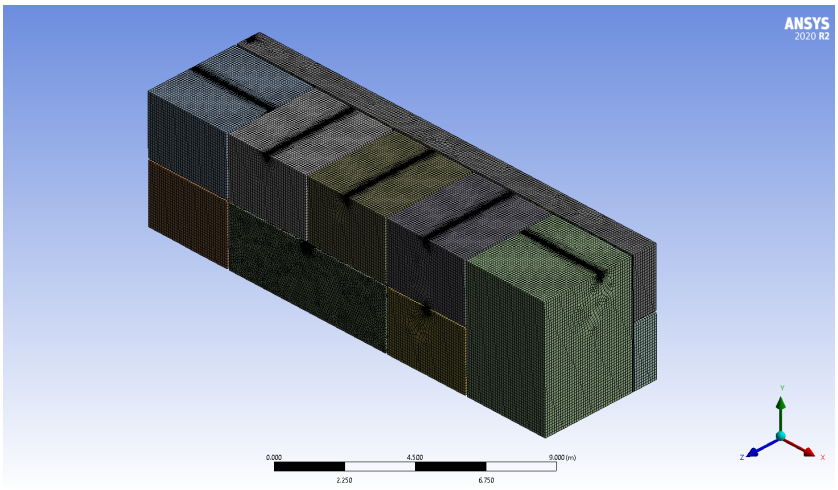
$$GCI_{coarse}=F_s\left|\frac{(Q_{coarse}-Q_{fine})\cdot r^p}{1-r^p}\right| \quad \text{for a coarse-grid solution} \quad (7\text{-}1)$$

$$GCI_{fine}=F_s\left|\frac{(Q_{coarse}-Q_{fine})}{1-r^p}\right| \quad \text{for a fine-grid solution} \quad (7\text{-}2)$$

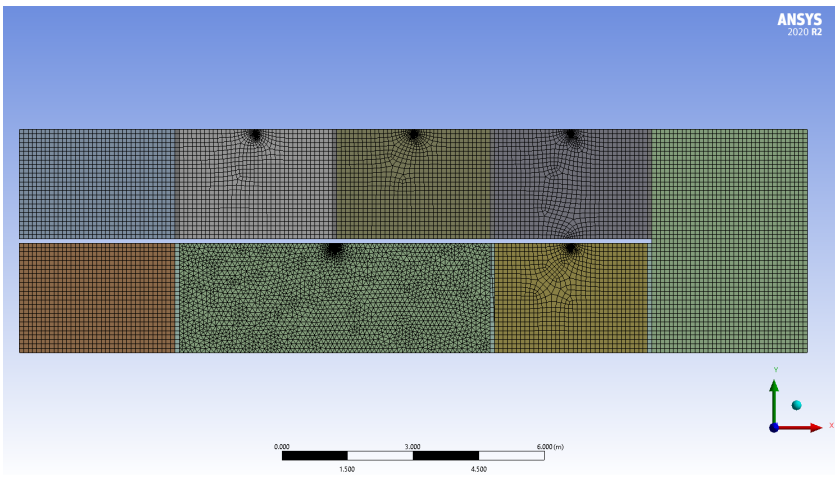
Where r is the linear grid refinement factor (i.e., 1.5 is used in this grid refinement study). p represents the formal order of accuracy. As recommended by the ANSYS Fluent Theory Guide [244] and Roy [245], the second-order discretisation scheme is preferred for cases with tetrahedral/hexahedral meshes with more accurate results and stability. Michalcová, et al. [246] also evaluated the physical accuracy of the calculation in the ANSYS Fluent for different mesh types and discretisation schemes and found that the second-order scheme achieved more accurate results than the first-order scheme for tetrahedral meshes. Therefore, p=2 for the second order of accuracy is used in the numerical analysis. F_s is the safety factor. As stated by Roache in his grid refinement studies [243, 247], F_s=1.25 is adequate for grid convergence studies using three or more grid solutions. In this grid-sensitivity study, three grid sets are proposed and assessed, including a coarse, a basic and a fine grid.

Q_{coarse} represents the simulated building air leakage rate from a relatively coarse grid, and Q_{fine} is for a relative fine grid. In the Pulse test, the measured building air leakage rate is reported at 4Pa, and the simulated air leakage rate is derived through the total volumetric flow rate of the ten openings at 4Pa. Based on the numerical results, the simulated air leakage rate is 0.09880m^3/s for the simulation with the coarse grid, 0.08916m^3/s for the basic grid, and 0.07966m^3/s for the fine grid. Therefore, GCI_{coarse} is 2.17% for comparing the coarse and basic grids, and GCI_{fine} is 0.95% for comparing the basic and fine grids. The corresponding grid convergence is also checked within the asymptotic range of convergence (i.e., $\frac{GCI_{coarse}}{r^p \cdot GCI_{fine}} = 1.015 \cong 1$); thus, the basic grid with the element size of 0.1m is used for the entire computational domain, providing

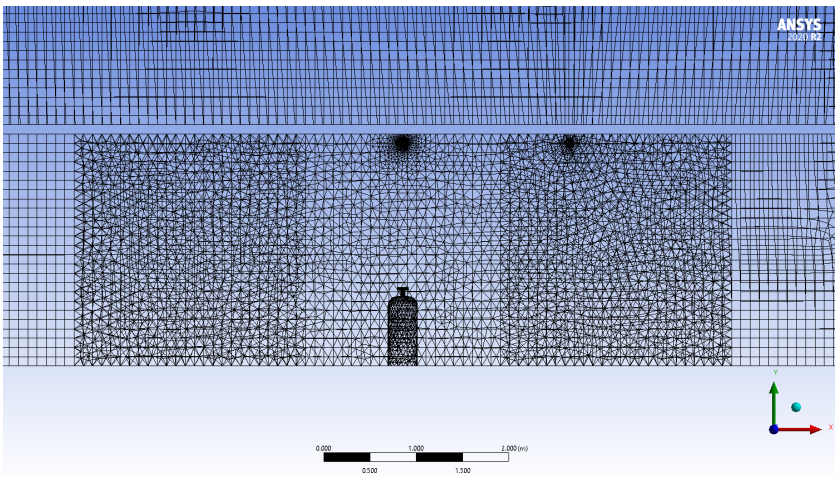
nearly grid-independent results. Moreover, a finer mesh is applied to the areas around the Pulse unit outlet (i.e., an element size of 0.002m) and at the ten openings (i.e., an element size of 0.008m) for simulations with more details. The grid has in total 909,028 cells, and Figure 7-6 provides the view of the building mesh.



(a) 3D model perspective view of building mesh



(b) Front view of building mesh



(c) Finer mesh for circular openings and Pulse unit

Figure 7-6: Building model mesh in Fluent

Solver settings

During the Pulse test, a rapid burst of air is released through the nozzle at a supersonic speed, and then the compressed air quickly diffuses within the building internal spaces; thus, the air velocity of the internal spaces reduces with distance from the nozzle. In this numerical study, the aspects of the investigation are concerned with how the pressure wave propagates within the internal spaces and the uniformity of (or lack of) the pressure rise across different zones within the building. In addition, the air is treated as a compressible fluid in this study so to present accurately how the internal building pressure physically changes when the air pulse is added into the indoor spaces. The pressure-based solver is employed for transient simulation, with additional considerations of computing time and memory requirement issues. The pressure-based solver has been dramatically improved, advanced, and extended to operate for a broad range of flows, from incompressible to compressible, in subsonic, transonic, and supersonic speed regimes and with the capability of handling complex geometries and unstructured grids, which has been examined and proved in extensive research in the literature [248-253]. For instance, Xiao, et al. [250] demonstrated the applicability and the robustness of the pressure-based method in various transient simulation cases for all flow regimes, from quasi-incompressible subsonic flows to transonic and supersonic compressible flows, on structured and unstructured meshes. Kraposhin, et al. [253] demonstrated the capability of the pressure solver in simulating compressible flows at different speeds. Basically, the pressure-based method solves the governing equations sequentially, and SIMPLE (Semi-Implicit Method for Pressure-Linked Equations) is selected as the pressure-velocity coupling algorithm. The SIMPLE algorithm is able to predict flows at all Mach numbers with good robustness and stability, using a relationship between velocity and pressure corrections to enforce mass conservation and to obtain the pressure field [254-256]. For instance, Qin, et al. [255] verified that the present SIMPLE method worked effectively for different compressible flows with stability and smooth convergence performance.

Continuity equation

$$\frac{\partial \rho}{\partial t} + \nabla \cdot \left(\rho \vec{V}\right) = 0 \tag{7-3}$$

Momentum equations

x momentum $$\frac{\partial (\rho u)}{\partial t} + \nabla \cdot \left(\rho u \vec{V}\right) = -\frac{\partial P}{\partial x} + \nabla \cdot (\mu \nabla u) + F_x \tag{7-4}$$

y momentum $$\frac{\partial (\rho v)}{\partial t} + \nabla \cdot \left(\rho v \vec{V}\right) = -\frac{\partial P}{\partial y} + \nabla \cdot (\mu \nabla v) + F_y \tag{7-5}$$

z momentum $$\frac{\partial(\rho w)}{\partial t} + \nabla \cdot \left(\rho w \vec{V}\right) = -\frac{\partial P}{\partial z} + \nabla \cdot (\mu \nabla w) + F_z \quad (7\text{-}6)$$

Energy equation

$$\frac{\partial}{\partial t}(\rho T) + \nabla \cdot \left(\rho \vec{V} T\right) = \nabla \cdot \left(\frac{k}{c_p} \nabla T\right) + S_T \quad (7\text{-}7)$$

The Energy equation is used in conjunction with Menter's shear stress transport (SST) turbulence model, which is a hybrid model combing K-omega and the K-epsilon models. By using a blending function, the SST turbulence model combines the standard K-omega model for near-wall treatment, which is robust across a wide range of flow types, and the standard K-epsilon model away from walls, which overcomes the problem of the K-omega model, of being sensitive to the inlet freestream turbulence properties [257, 258]. Zhao, et al. [259] performed a sensitivity analysis of the SST model in simulating hypersonic flows and demonstrated the SST model's capability of providing accurate predictions of flow separation under adverse pressure gradients.

In terms of the gradient solving method, Least-Squares Cell-Based method is chosen. Based on the comparative assessment of the gradient solving methods for different mesh types, Michalcová, et al. [246] recommended using the Least-Squares Cell-Based method for hexahedral and tetrahedral mesh types for good accuracy. The accuracy of the least-squares gradient method on the unstructured meshes was also examined and verified in the studies by Mavriplis [260] and Wang, et al. [261]. As discussed previously, the second-order upwind scheme is selected for the discretisation of pressure, density, momentum, and turbulent kinetic energy, with considerations of the defined mesh type, good result accuracy and computational stability. Additionally, Bailey [262] also demonstrated the second-order upwind method could reduce the false diffusion on unstructured meshes, and also balanced with concerns of complexity, computational time and stability.

Boundary conditions

For the transient simulations in this study, the calculation of air properties is performed by using the Soave-Redlich-Kong equation of state. Lin, et al. [263] presented the great flexibility and accuracy of using the Soave-Redlich-Kong equation of state for fluids in wider ranges of temperature and pressure. The nozzle of the Pulse unit is determined as the velocity inlet. In order to validate against the experimental studies, the model of the air tank with its nozzle is established based on the real size of the PULSE-60 unit. Therefore, the tank volumetric airflow rate that was measured continuously during the field test is used to derive the corresponding velocity at the nozzle by taking the surface area of the nozzle into account. A transient profile in a tabular format

containing the velocity at the nozzle and the corresponding time is created and assigned to the inlet with the transient inlet velocity. All the ten openings on the building envelope are set as the pressure outlet at standard atmosphere (i.e., 101,325Pa), and the gauge pressure is set at 0Pa. The wall boundary condition is set as default, i.e., the stationary wall with no slip. Initially, the entire computational domain is set with a gauge pressure of 0Pa, an initial temperature of 288.15K and a velocity of 0m/s.

Time step

The Courant–Friedrichs–Lewy (CFL) stability condition is considered for defining the time step. According to the definition by Laney [264], the Courant number is a non-dimensional number, which is used to evaluate the time step requirement of a transient simulation for given mesh size and flow velocity. As stated by Kavetski, et al. [265], the Courant number is a critical stability criterion for the explicit schemes, while it is not a necessary condition for the implicit transient formulation owing to its unconditional stability. Considering an excessive large time step size may influence the calculation accuracy and simulation time, the CFL stability condition is assessed for this transient simulation with the semi-implicit scheme. In this study, the Courant number (*CN*) indicates how much the air pulse ($u_x/u_y/u_z$) travels across a grid cell ($\Delta x/\Delta y/\Delta z$) in a unit of time ($\Delta t$) in the three-dimensional domain.

$$CN = \frac{u_x \Delta t}{\Delta x} + \frac{u_y \Delta t}{\Delta y} + \frac{u_z \Delta t}{\Delta z} \tag{7-8}$$

According to the simulation condition, the maximum air velocity at the nozzle during the air pulse release could achieve approximately 526.45m/s, and the grid cell size around the nozzle outlet is the minimum grid spacing in the defined computational grid, which is 0.002m. Initially, the CFL limitation is set to *CN*<1.5, as the CFL condition for the semi-implicit scheme allows *CN* higher than 1. Therefore, the corresponding maximum time step (Δt) is 0.0000015s, and the total number of time steps during the transient simulation of the 6-second Pulse test is 4,110,000. However, owing to the limitations in memory storage and available computational resources, the convergence of the transient calculation was too slow, requiring a very long computation time. In addition, the solver took only a few iterations per time step, which indicates Δt of 0.0000015s is unnecessarily small and could be increased without reducing accuracy or the likelihood of convergence issues. With considerations of the computational memory storage, supporting resources and required simulation period, the grid cell size for the entire domain of 0.1m is chosen for defining the appropriate time step. Three CFL limitations (i.e., *CN*<1.5, *CN*<2 and *CN*<3) are examined based on the convergence performance and the simulated value of building air leakage

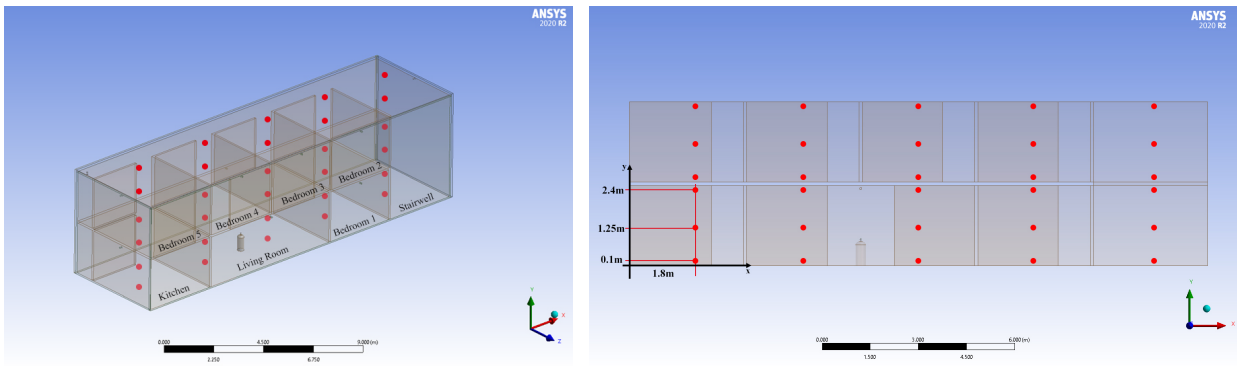
rate during the Pulse test. For the three different CFL limitations, the corresponding maximum time steps are 0.000075s, 0.0001s and 0.00015s, respectively. The difference of the building air leakage rate is approximately 3.27% between the two simulations with time steps of 0.00015s and 0.0001s, while the difference is approximately 0.86% between the two simulations with time steps of 0.0001s and 0.000075s. Therefore, the time step of 0.0001s is used for the transient simulation of the 6-second Pulse test (i.e., the total number of time steps of 60,000), with considerations of better stability and accuracy, as well as appropriate supportable computing time.

Convergence criterion

In this numerical transient simulation, the convergence criterion is set based on the residuals of the corresponding equations, including 10^{-6} for the energy equation, and 10^{-3} for all the other equations (i.e., continuity, x, y and z velocities, k, and e).

Monitoring points

In each room, three monitoring points are set to record the transient data of air pressure, air density and air velocity at different heights, except the living room has six monitoring points due to its larger size. Thus, in total, thirty indoor monitoring points are defined, as illustrated in Figure 7-7(a). As illustrated in Figure 7-7(b), in each room, all points are placed at the room centre at various heights. Specifically: the bottom point in the room is positioned at 10cm above the ground level, and the middle point is at the centre of the room, and the top point is located at 10cm below the ceiling height. The average value of all monitoring points in each room is used for data assessment. Besides, ten monitoring points at the ten openings are added to record the corresponding air volumetric flow rate and velocity. The frequency of the produced time-sequence data is set at 200Hz, allowing 200 data files to be saved every second during the transient simulation for each monitoring point.



(a) (b)

Figure 7-7: Location of indoor monitoring points: (a) 3D perspective view and (b) plan view with dimensions

7.3.2 Results and discussions: indoor pressure and velocity distributions

Due to the fact that the rapid 1.5-second pulse of air is released from the pressurised vessel, and the "quasi-steady" condition is achieved only in a very short time (i.e., approximately 0.7s in this numerical study), it would be practically challenging to gather sufficient pressure readings by the acquisition device to entirely describe the pressure variation throughout the Pulse test, which was discussed in Chapter 4. This limitation of the field testing could be addressed by the transient simulation. Based on the simulated pressure values of all monitoring points, the average indoor pressure is calculated for each room. Figure 7-8 depicts the full image of the indoor pressure variation during the entire Pulse test in each room under no wind conditions.

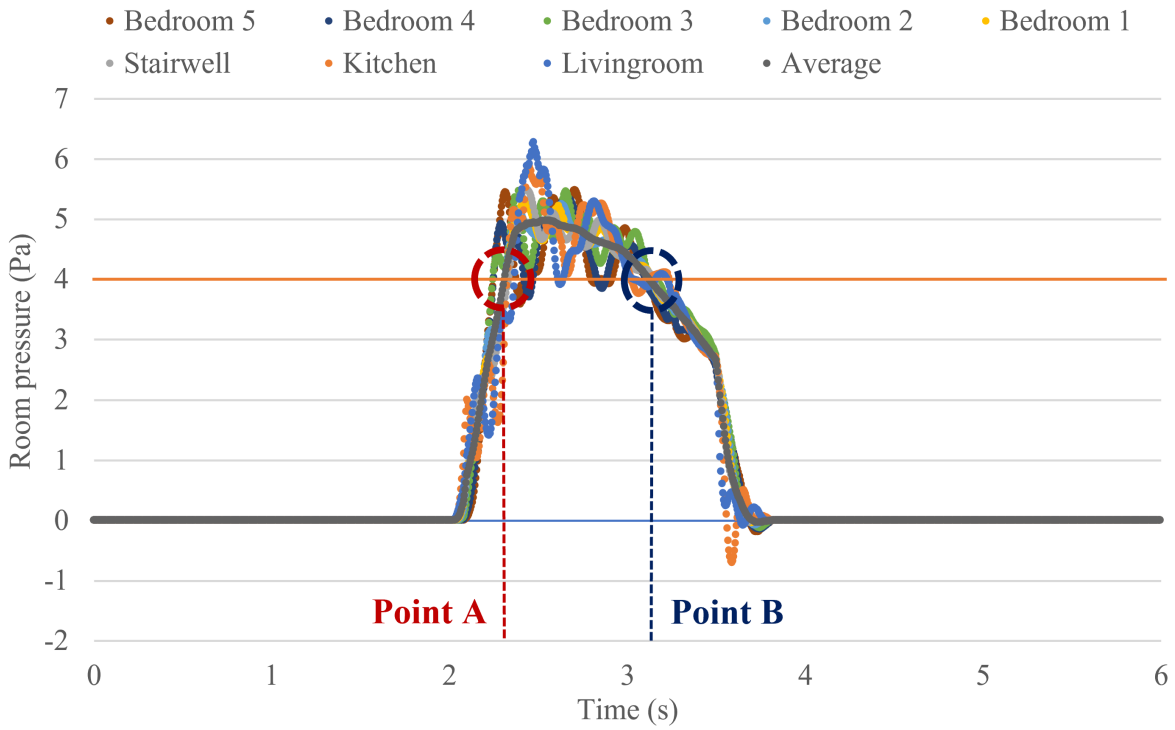


Figure 7-8: Illustration of indoor pressure variation during the entire Pulse test under no wind condition

The characteristic shape of the building pressure increase and fall can be seen in response to the air pulse. There are two time points during the entire Pulse test, at which the indoor pressure achieves 4Pa, as annotated in Points A and B. The Pulse test determines the building leakage in the range of 1-10Pa, and the measured air leakage rate of the tested building was reported at 4Pa in the field tests in Chapters 3, 4, 5 and 6. Therefore, in the numerical study, the assessment of the uniformity of the pressure distribution is conducted by evaluating Points A and B in different rooms of the building. In particular, time point B lies in the quasi-steady period, which is used for examining the building airtightness. As seen from Figure 7-8, the variation curves representing the pressure responses in all rooms show clear similarity, and minor differences of Point A and B for each room are noted as listed in Table 7-3.

Table 7-3: Time points A and B for the Pulse test under the no wind condition

	Living Room	Kitchen	Stairwell	Bedroom					Average*
				1	2	3	4	5	
Point A	2.370s	2.330s	2.335s	2.325s	2.320s	2.295s	2.285s	2.275s	2.315s
Point B	3.010s	2.990s	2.990s	2.985s	2.975s	2.975s	2.980s	2.990s	2.985s

*Average Points A and B are obtained based on the average pressure of all rooms.

Based on the average pressure of all rooms, the corresponding Point A is approximately 2.315s, indicating that the average indoor pressure reached 4Pa after 0.315s once the air pulse has been released. For clarity, note herein within this discussion, t=2s is the point of air pulse release. The Point A of each room is compared with that of the living room, as the air pulse was released in the living room. The largest difference of Point A among all rooms is approximately 0.095s, which is because that Point A falls within the unsteady period of the rapid pressure rise during the air pulse release. The average value of Point B based on the average indoor pressure is around 2.985s, within the quasi-steady period (i.e., 2.8s-3.5s). By comparing Point B of each room with that of the living room, the largest difference is only approximately 0.035s, which reveals that the pressures of different rooms match well at 4Pa. The numerical results verify the dynamic nature of the Pulse test and the capability of achieving a uniform pressure distribution within the indoor spaces in a very short time during the measurement.

Regarding the pressure distribution within the building internal spaces during the quasi-steady period, Table 7-4 lists the corresponding pressure level in each room achieved at t=3.25s. Another reason for assessing the indoor pressure distribution at t=3.25s is for considering the cross-validation of the experimental work presented in Chapter 4, as the pressure data were recorded at 4Hz. The detailed cross-validation is presented in later Section 7.3.3. The overall average pressure of the internal spaces is approximately 3.553Pa at t=3.25s. As the Pulse unit is placed in the living room, therefore, relative percentage difference (*RPD*) is calculated by comparing the pressure level in the living room with that of the other rooms. As seen from Table 7-4, the *RPD* could be as small as 1.10%, and the most significant *RPD* at t=3.25s is approximately -6.39% (i.e., by 0.233Pa), which reveals the uniformity of the pressure distribution across the internal zones during the quasi-steady period.

Table 7-4: Simulated pressure level in each room at 3.25s under the no wind condition

	Living Room	Kitchen	Stairwell	Bedroom				
				1	2	3	4	5
Maximum Pressure Level	3.648Pa	3.688Pa	3.574Pa	3.591Pa	3.548Pa	3.505Pa	3.451Pa	3.415Pa
RPD	/	1.10%	-2.03%	-1.56%	-2.74%	-3.92%	-5.40%	-6.39%

For analysis of the indoor velocity distribution during the Pulse test, the air velocity of each room is calculated by averaging the obtained velocity values of all monitoring points in the room. The variations of the air velocity in each room during the Pulse test are presented in Figure 7-9.

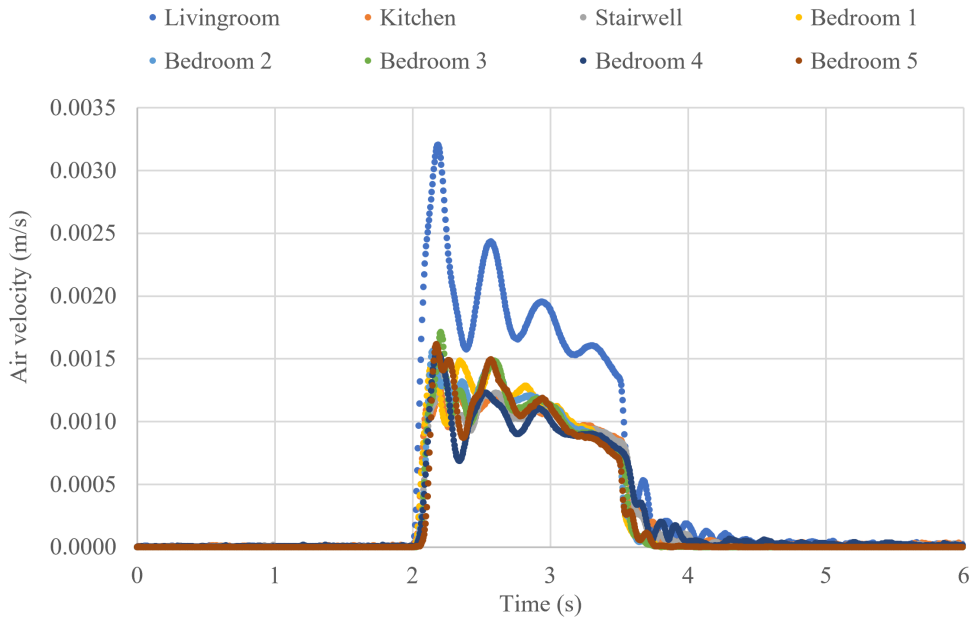


Figure 7-9: Air velocity variation in each room during the Pulse test under the no wind condition

The maximum achieved air velocity in each room during the Pulse test is listed in Table 7-5. It can be clearly seen that the average air velocity in the living room (i.e., highest achievable air velocity of 0.0032m/s) is much higher than that of the other rooms, which is due to the Pulse unit being placed in the living room for the simulation.

Table 7-5: Maximum air velocity in each room during Pulse test under the no wind condition

	Living Room	Kitchen	Stairwell	Bedroom				
				1	2	3	4	5
Maximum Air Velocity (m/s)	0.00320	0.00127	0.00142	0.00149	0.00156	0.00171	0.00155	0.00160

To analyse the air velocity distribution within the indoor spaces during the Pulse test, Figure 7-10 provides the plots of the air velocity against the distance from the nozzle of the Pulse unit at t=2.01s (i.e., a time point right after the air pulse releases), and t=3.20s (i.e., time point during the quasi-steady period). Based on the numerical simulation results, the maximum air velocity could achieve approximately 526.45m/s at the nozzle outlet over a very short distance (approximately 0.001m) when the air pulse releases, the air velocity is around the speed of sound (i.e., 340.29m/s) at the distance of 0.015m from the nozzle outlet, while at the distance of 0.341m away from the nozzle, the air velocity is only 0.08m/s. Therefore, the results demonstrate that the majority of the indoor spaces has very low air velocities when the air pulse releases; approximately 99.92% of the total building volume has an indoor air velocity below 0.08m/s. The plot of t=3.20s indicates

the fact that the compressed air diffuses quickly within the internal spaces, and the maximum obtained air velocity is 377.88m/s at the distance of 0.001m from the nozzle. At t=3.20s, more regions around the nozzle encountered light breeze; for instance, the corresponding velocity is 2.66m/s at the distance of 0.911m from the nozzle, or light airflow of 0.66m/s at the distance of 1.155m from the nozzle. The percentage of total building volume with the indoor air velocity below 0.08m/s is 93.35%; this could also be visualised in Figure 7-11(b), represented in the blue colour in the velocity contour images.

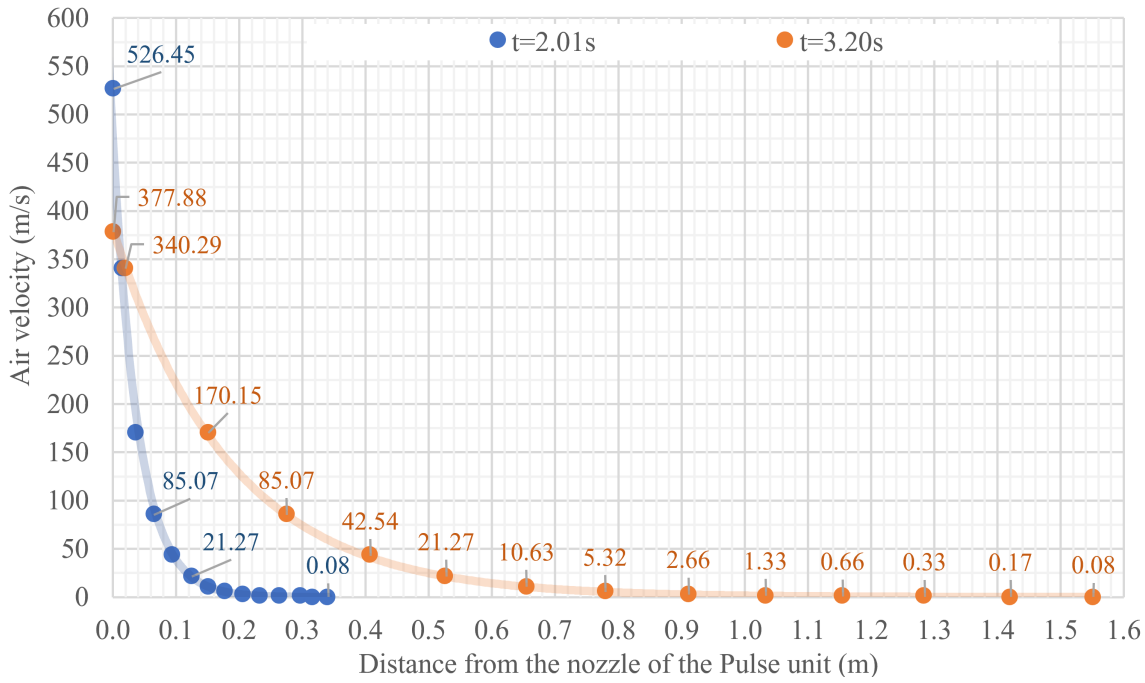
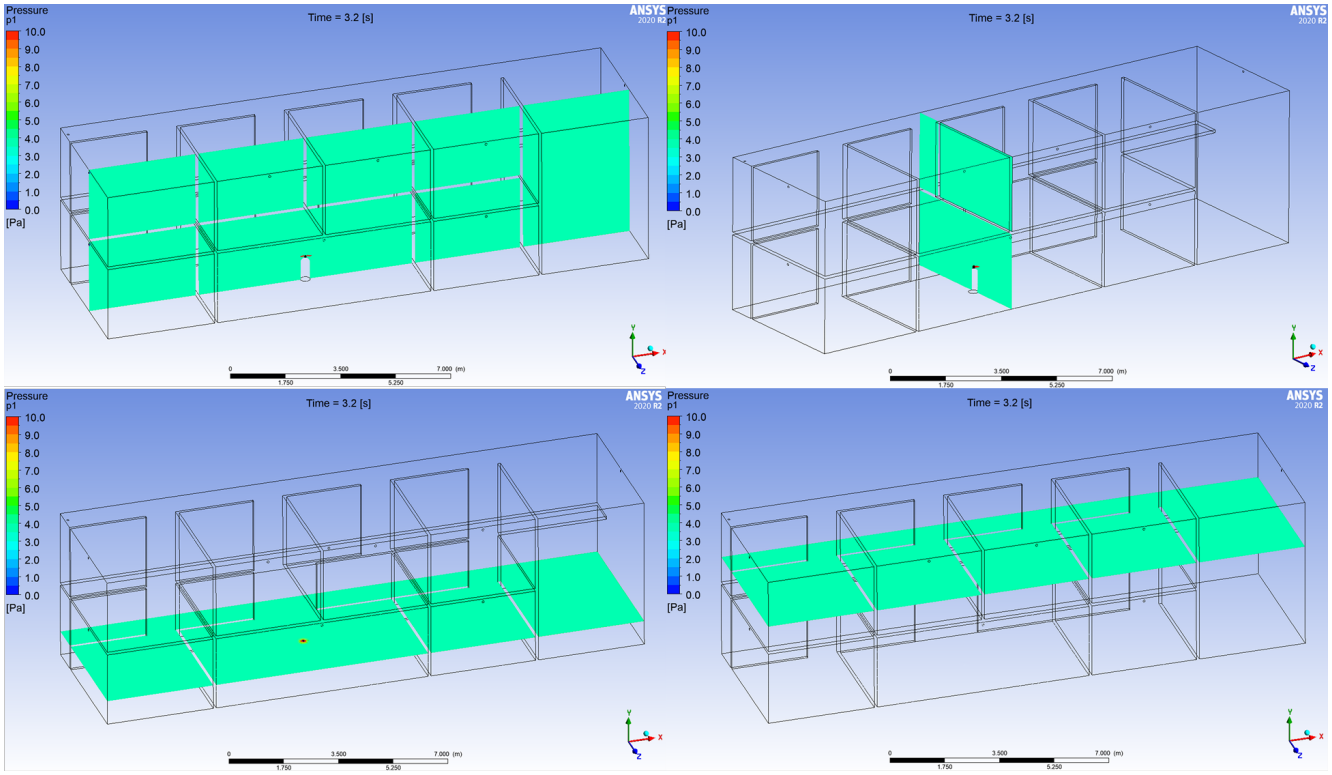


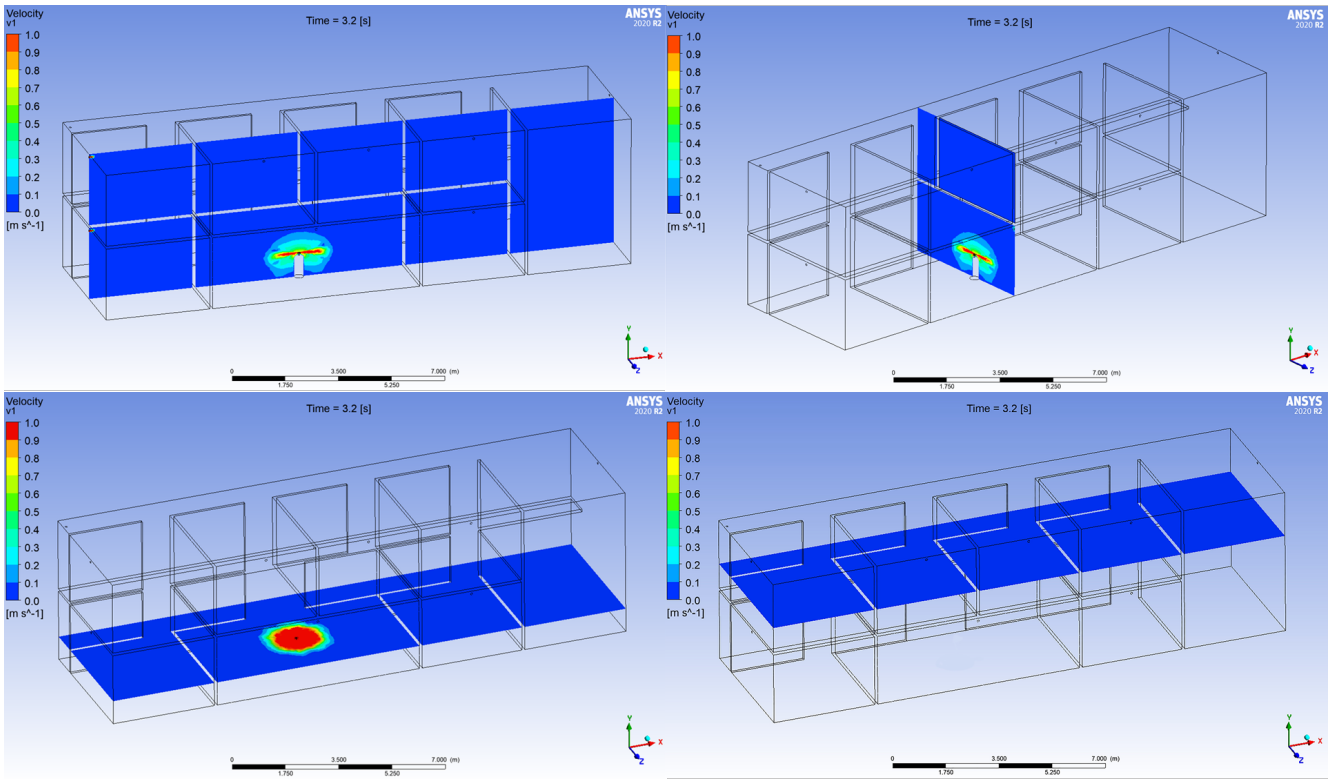
Figure 7-10: Plot of the indoor air velocity against the distance from the nozzle of the Pulse unit

This finding indicates that the high-speed airflow is only located in a very small region around the nozzle. Therefore, the simulation results provide useful information on where to place the control box of the Pulse unit in order to obtain an accurate measurement of the building pressure during the Pulse test. In addition, the results also clarify the safety concerns relating to the Pulse test, the rapid rise in the air velocity within the indoor spaces owing to the burst of air pulse release would cause low impacts on the building integrity, fabric, structure, indoor household facilities, as well as low disruption to occupants and testers during operation.

Moreover, the contour images of the indoor pressure distribution at 3.2s are shown in Figure 7-11(a) from the three-dimensional vertical and horizontal perspective views, demonstrating a uniform pressure distribution within the indoor spaces of the building during the quasi-steady period. Additionally, the vertical and horizontal contour images of the indoor air velocity distribution at 3.2s in Figure 7-11(b) show that the overall indoor spaces have very low air velocities during the quasi-steady period, except a small region near the pulse unit.



(a) Pressure distribution



(b) Velocity distribution

Figure 7-11: Contour images of indoor pressure and air velocity at 3.2s under no wind condition

7.3.3 Results and discussions: validation with experimental data

Table 7-6 lists the measured pressure level in each room at 3.25s based on the field testing in Chapter 4. The largest *RPD* of the field test results is smaller than that of simulation results, as mentioned in Section 7.3.2 (i.e., the largest *RPD* of -6.39%). The discrepancy is perhaps owing to the data recording frequency and the setup of the monitoring points. During the field testing presented in Chapter 4, only five pressure measurement points were set for five rooms, and the recording frequency of the adopted data acquisition device was limited to 4Hz. In contrast, the frequency of 200Hz was defined for the simulation data recording, which could capture more details to provide a full image of the indoor pressure variation during the Pulse test.

Table 7-6: Measured pressure level in each room at 3.25s in field testing

	Living Room	Kitchen	Bedroom 1	Bedroom 2	Bedroom 3
Pressure Level	3.343Pa	3.341Pa	3.338Pa	3.335Pa	3.333Pa
RPD	-	-0.06%	-0.15%	-0.24%	-0.30%

As monitoring points are set in each room to record the pressure variation during the Pulse test, the air leakage rate (ALR) of the building can be calculated based on the obtained pressure result of each room. The calculated ALR values are listed in Table 7-7 according to different rooms' pressure variations. Slight differences are observed among all calculated ALRs, with the largest difference of 3.69% (i.e., between the living room and Bedroom 5). Therefore, this finding suggests a good uniform indoor pressure distribution is achieved during the Pulse test. The obtained results also provide numerical evidence to confirm the minor impact of the Pulse unit location on the Pulse measurement, as similar values of the air leakage rate can be obtained based on the pressure variations in different rooms. Table 7-7 also lists the deviation of the calculated ALR with the obtained measurement from the field testing (i.e., Section 5.3.2 Case A). Only a slight deviation is noted between the air leakage rate calculated based on the living room pressure variation and the field test result (i.e., 0.08979m^3/s), while relatively more significant deviations are found for the calculated air leakage rate values based on the pressure variation of the other rooms. The average building air leakage rate is also calculated according to the average indoor pressure of all rooms, 0.08916m^3/s, which is 0.70% smaller than the obtained data from the field test in the five-bedroom dwelling. The discrepancies are mainly attributed to the facts that: (a) the air leakage rate of the field testing was obtained based on the measured pressure variation in the living room; (b) the tested dwelling has a different building shape from the building model (i.e., L shape); and (c) the tested calm condition was at a wind speed of 0.05m/s at the height of 2.2m

above ground level. Overall, the comparison demonstrates the good agreement of the air leakage rate between the simulation results and field test measurements.

Table 7-7: Simulated ALR results under the no wind condition

	Air Leakage Rate (m^3/s)								
	Living Room	Kitchen	Stairwell	Bedroom					Average
				1	2	3	4	5	
Simulation	0.08966	0.08953	0.08924	0.08897	0.08882	0.08809	0.08744	0.08647	0.08916
Deviation from the Field Test Result*	-0.14%	-0.29%	-0.61%	-0.91%	-1.08%	-1.89%	-2.62%	-3.70%	-0.70%

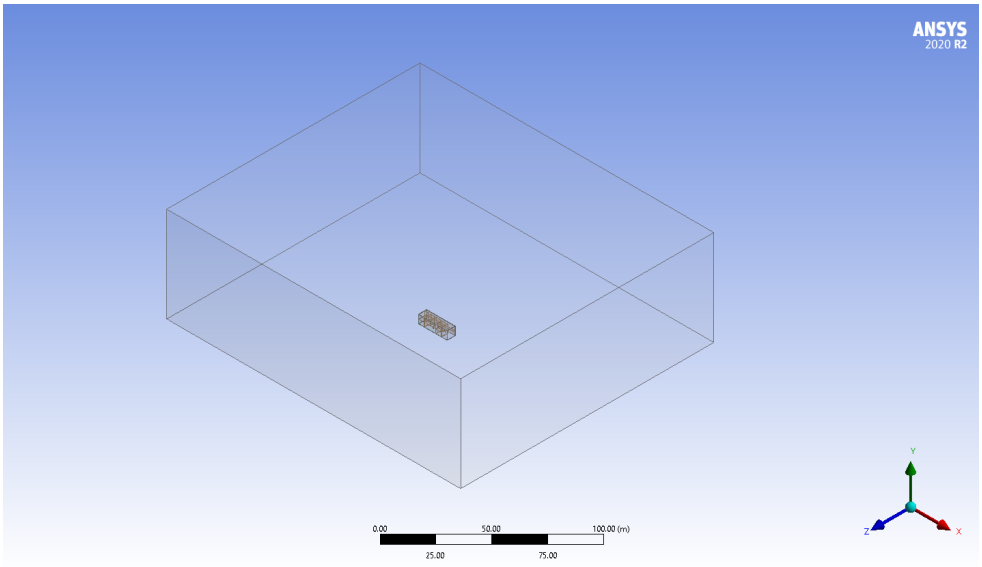
*Deviation is calculated by comparing the simulated ALR with the measured ALR from the field testing (i.e., 0.08979m^3/s).

7.4 The impact of steady wind on the Pulse test

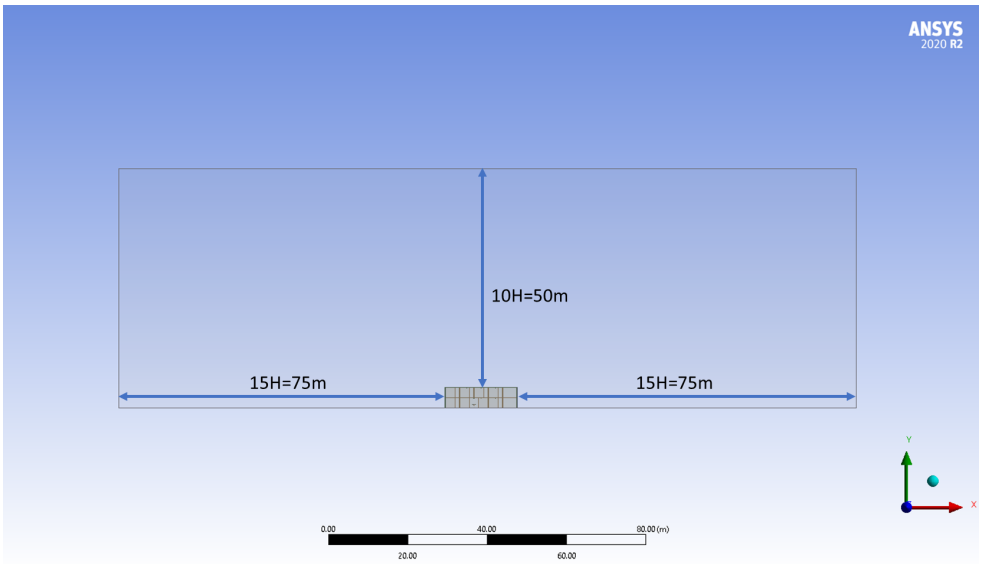
To numerically investigate the steady wind impact on the Pulse test, transient simulations are then performed to investigate the pressure wave propagation within the building internal spaces and pressure distribution across different zones during the Pulse test under different wind speed conditions.

7.4.1 Computational domain and configurations

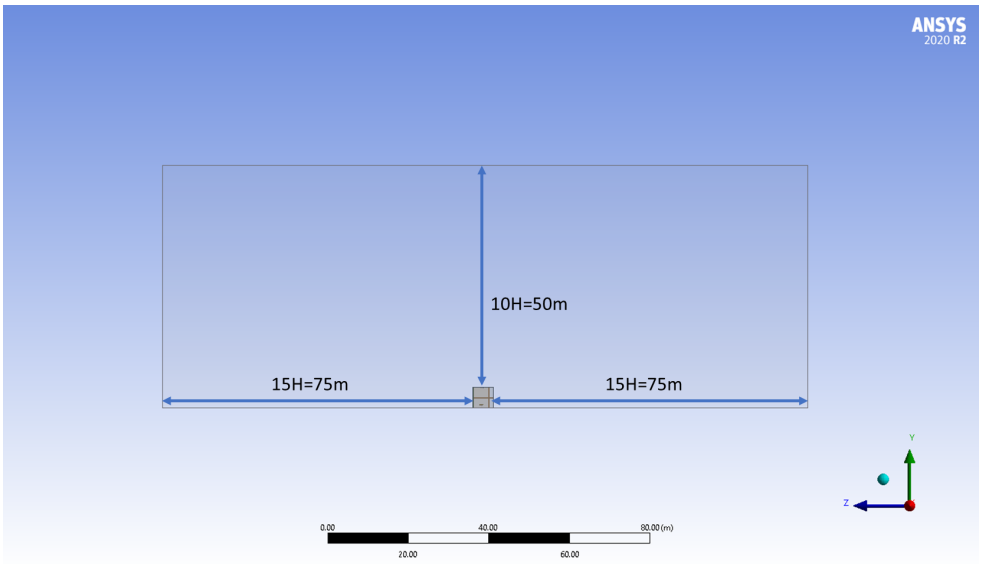
An outer computational domain is created to enclose the existing building model in the Design Modeler, to simulate the urban environment. The dimension of the outer domain is determined based on the best practice guidelines provided by Franke [266], Cowan, et al. [267], Bartzis [268]. Based on their suggestions, the established urban environment needs to be at least 5H (i.e., H=building height) above the building roof and 15H behind the building to allow the flow to fully develop. As simulations are conducted for different wind conditions, the four façades of the building can be either windward or leeward, depending on the simulated wind direction. Therefore, 15H is used as the distance between each sidewall of the building and the side plane of the outer domain, while 10H is used as the distance between the building roof and the top plane of the outer domain. As the height of the established building model is 5m; therefore, the dimension of the outer domain is set as 168m (L)*155m (W)*55m (H). The views of the outer domain with dimensions are shown in Figure 7-12.



(a) 3D view



(b) Front view



(c) Side view

Figure 7-12: Views of outer domain with building model in Fluent

The mesh of the building model is kept the same as presented in Section 7.3.1, while tetrahedral cells are generated for the mesh of the outer domain. Similarly, the grid-sensitivity analysis is performed to define the optimal grid resolution for the outer domain. Considering the simulated condition and supportable computational time, the three sets of grids for assessment are a coarse grid with an element size of 1.5m, a basic grid with an element size of 1m and a fine grid with an element size of 0.6m. Based on the simulation results, GCI_{coarse} is 2.67% for comparing the coarse and basic grids, and GCI_{fine} is 1.17% for comparing the basic and fine grids. In addition, the corresponding grid convergence is checked within the asymptotic range of convergence (i.e., $\frac{GCI_{coarse\text{-}basic}}{r^p \cdot GCI_{basic\text{-}fine}} = 1.014 \cong 1$), the basic grid with the element size of 1m is used for the outer computational domain (as seen in Figure 7-13), providing nearly grid-independent results. The total number of generated cells of the entire model is 23,091,148 cells.

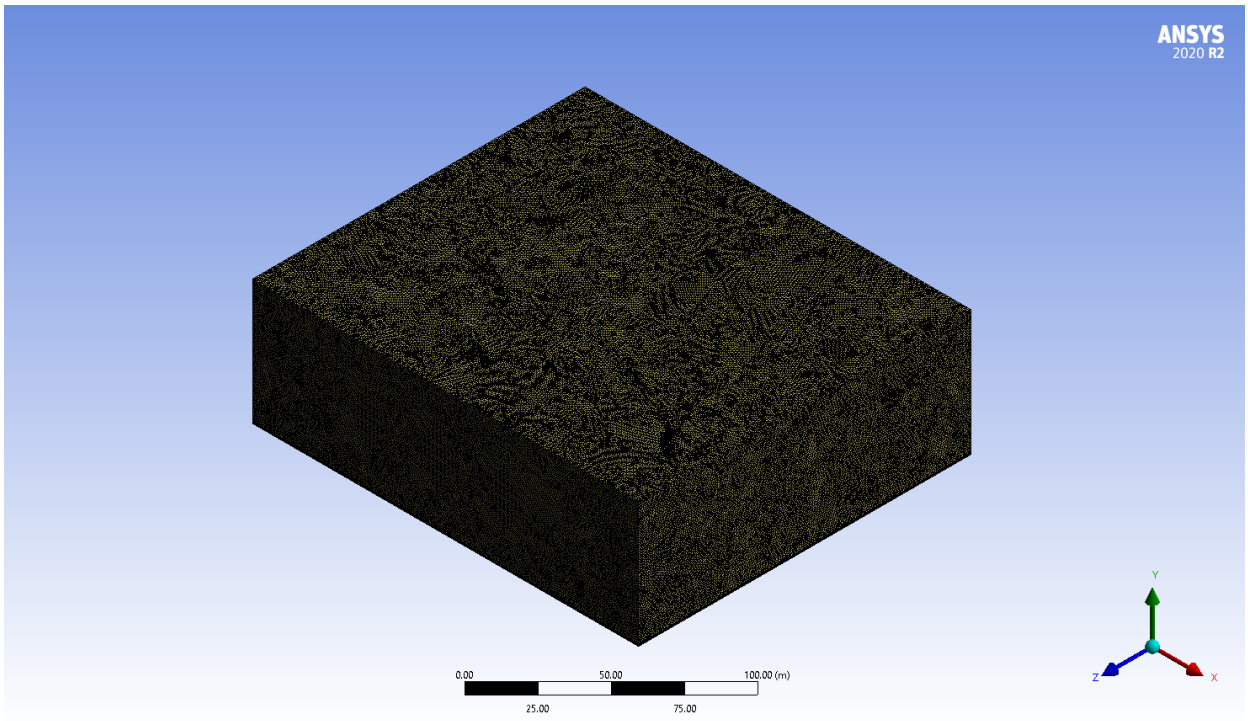


Figure 7-13: View of the outer domain mesh in Fluent

Same solver settings for the transient simulation are applied, as described in Section 7.3.1. In terms of the boundary condition, the nozzle of the Pulse unit is determined as the velocity inlet and attached with the transient profile. All the ten openings on the building envelope are set as the pressure outlet and specified as interior type to connect with the outer domain for simulation. For the outer computational domain, the simulated steady wind direction is determined as flowing along the positive x-axis, as shown in Figure 7-14.

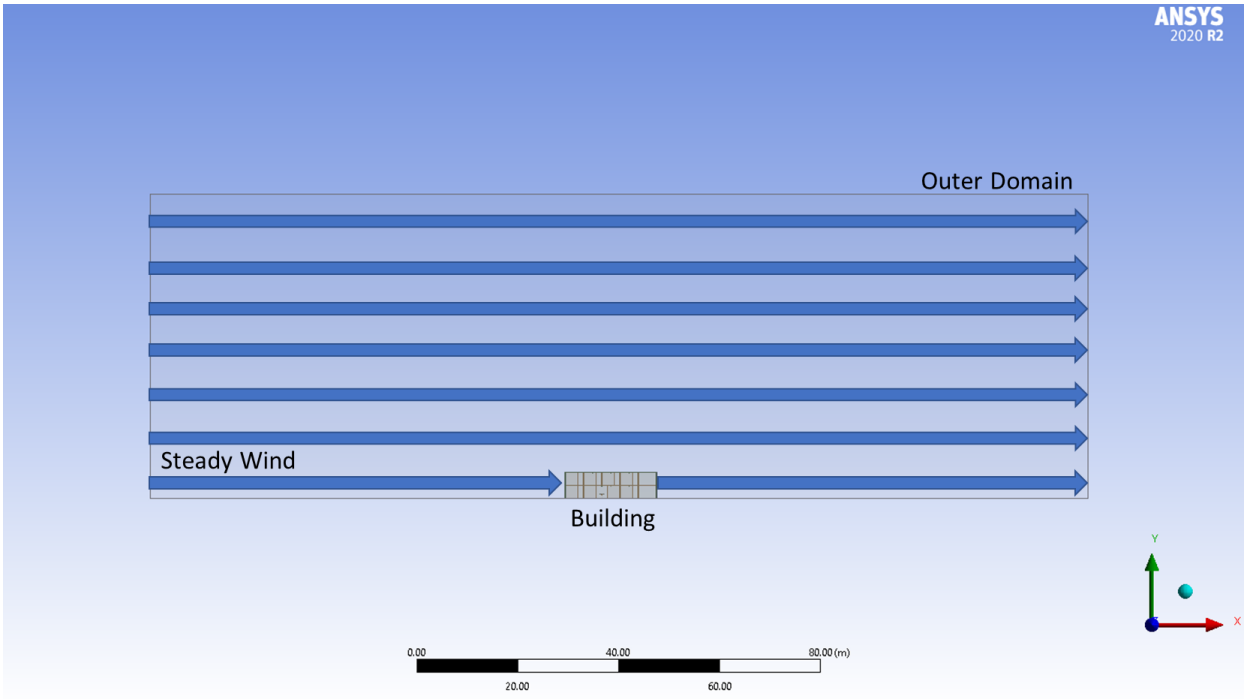


Figure 7-14: Illustration of the simulated steady wind condition in the outer domain in Fluent

According to the ISO 9972 standard, the fan pressurisation test is not recommended at the meteorological wind speed above 6m/s. Typically, the meteorological wind speed refers to the wind speed measured at the height of 10 metres above ground level. In this study, four cases with different steady wind speed levels are proposed to simulate various scenarios, including: a no wind condition (i.e., Case I), a low wind speed condition (i.e., Case II), a moderate wind speed condition (i.e., Case III) to check whether the wind speed limit mentioned in the ISO 9972 standard is also applicable to the Pulse test and a windy condition (i.e., Case IV) to investigate the limit of performing the Pulse test in wind conditions. Table 7-8 lists the detailed wind speed conditions for the four cases.

Table 7-8: Simulated wind speed level for Cases I, II, III and IV

Case	Wind Speed Level	
	At 1m above Ground	At 10m above Ground
I (No wind)	0m/s	0m/s
II (Gentle breeze-Beaufort number 3)	2m/s	4m/s
III (Moderate breeze-Beaufort number 4)	3m/s	6m/s
IV (Fresh breeze-Beaufort number 5)	5m/s	10m/s

Based on the method presented in Section 5.2.1 (i.e., eq. 5-1), the wind speed profile with height above the ground level is created for each case, as illustrated in Figure 7-15. The user-defined function is used to specify the wind speed profile along the x-axis to the outer domain.

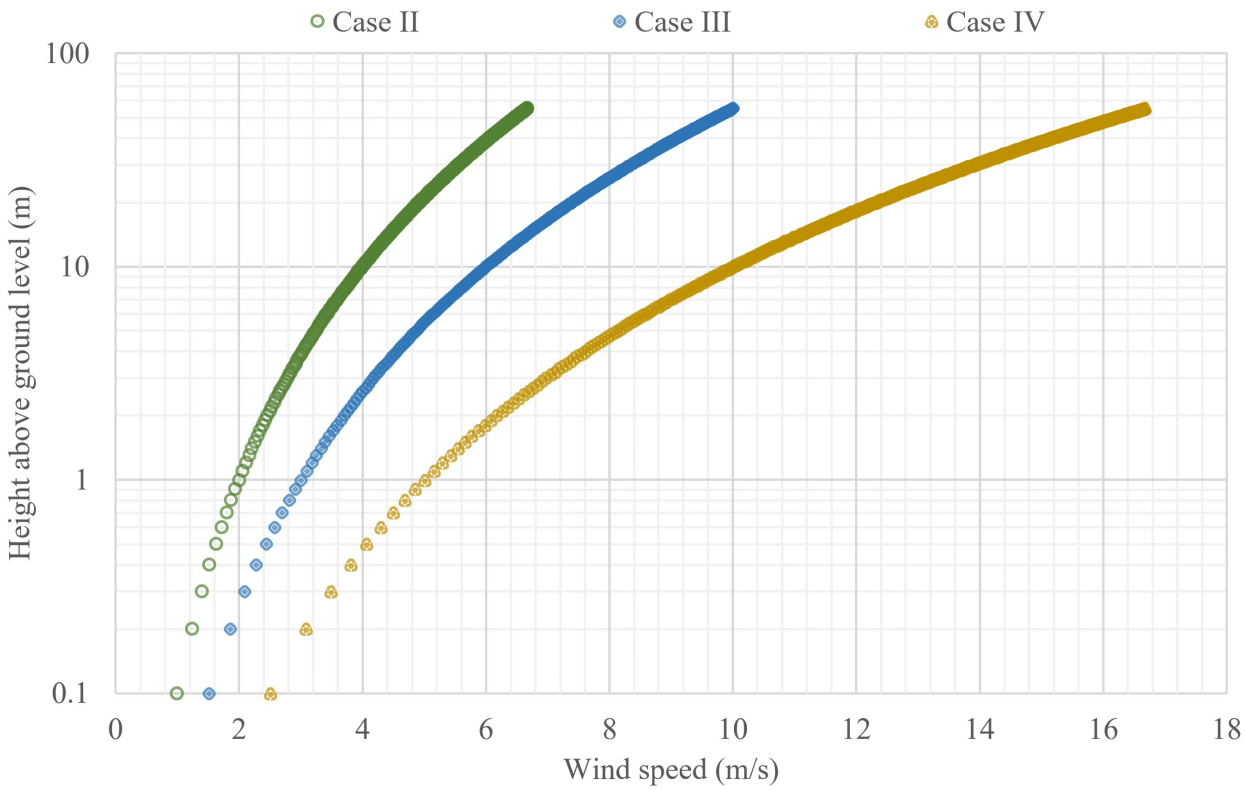
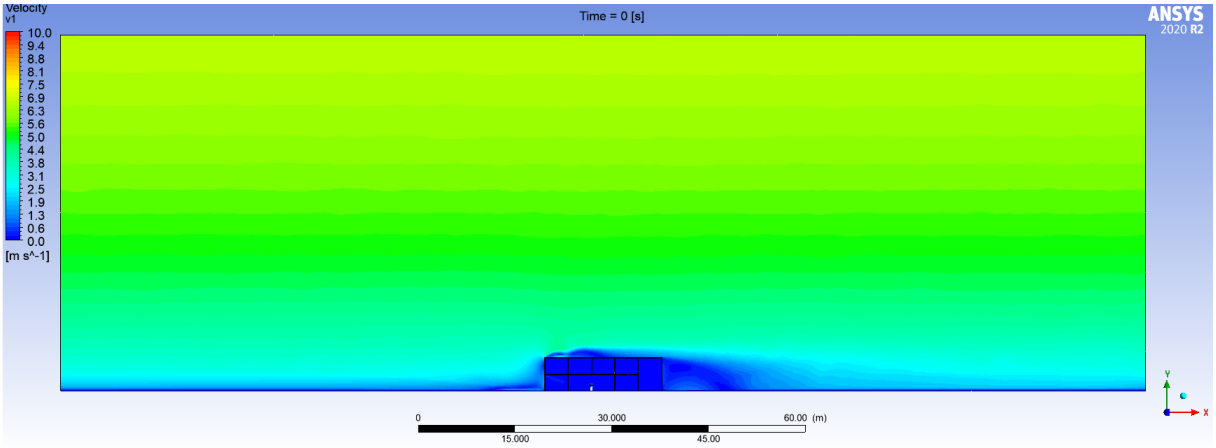
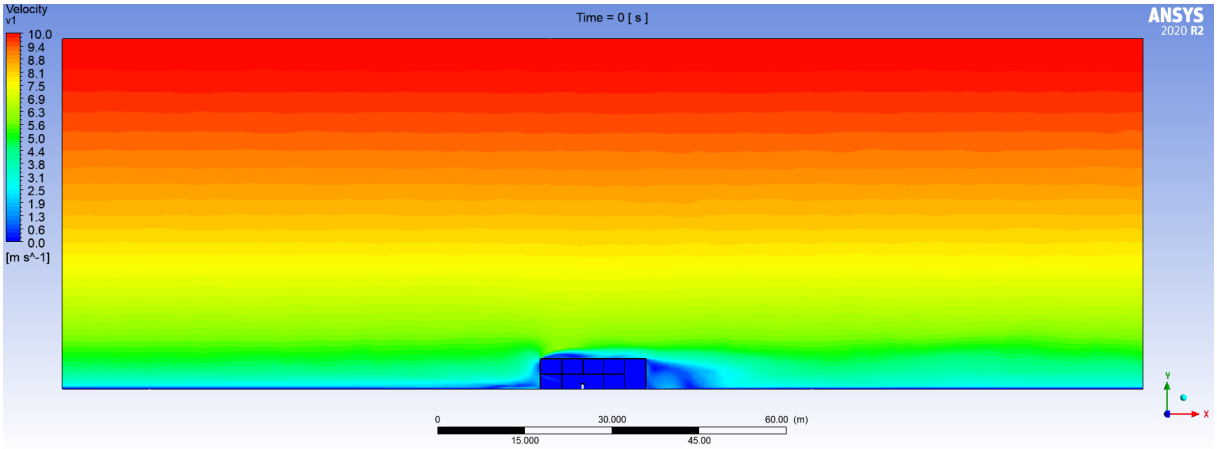


Figure 7-15: Wind speed profiles for Cases II, III and IV

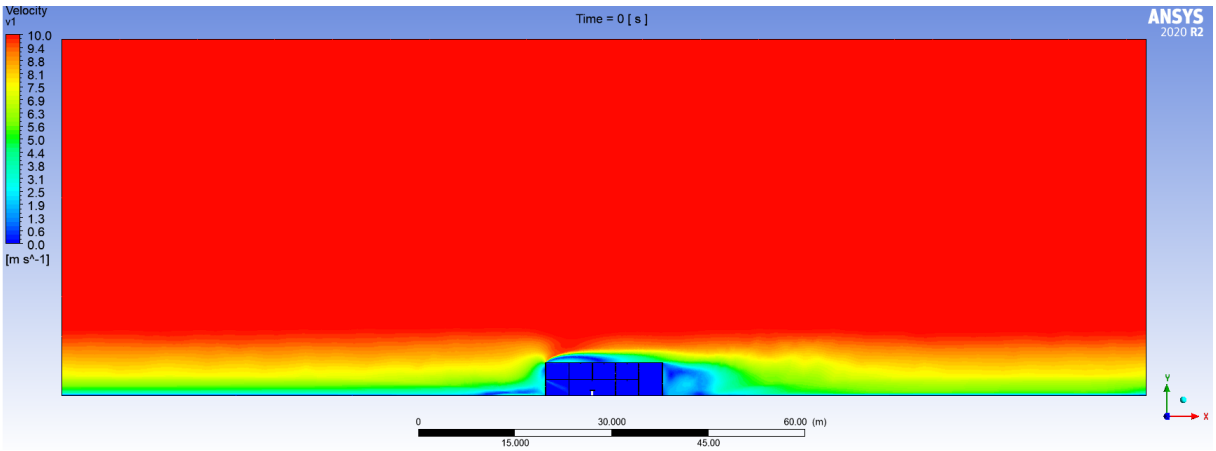
Heiselberg, et al. [269] proved that the initial condition is critical to the predictions of natural airflows in building, as it could affect the stability, convergence performance and computational time. In this numerical study, the steady-state simulation was firstly performed with only one velocity inlet using the wind speed profile and the inlet profile of the nozzle set to zero in order to derive a steady initialisation of the flow field in the entire domain. Once the residuals were stable, and a steady-state solution was achieved by examining the stability of the flow field (i.e., velocity and pressure), the data was then saved and used as the initial condition of the flow field for the transient simulation. If the steady-state simulation fails to converge, the transient simulation would proceed until a steady flow field is achieved. The evaluation of the CFL stability condition to define the time step is conducted, and the same CFL limitations (i.e., $CN<1.5$, $CN<2$ and $CN<3$) are used as discussed in Section 7.3.1. Based on the convergence performance, the simulated value of building air leakage rate during the Pulse test and overall computational period, the time step of 0.0001s is used due to its better stability and accuracy. Figure 7-16 presents the contour images of the front view for Cases II, III and IV at the beginning of the transient simulation of the Pulse test (t=0s), showing the different velocity fields in the outer domain.



(a) Case II (at the meteorological speed of 4m/s)



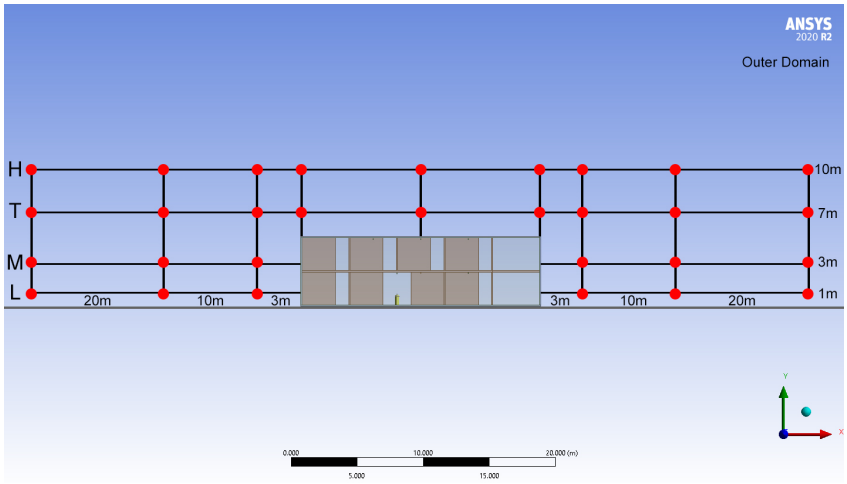
(b) Case III (at the meteorological speed of 6m/s)



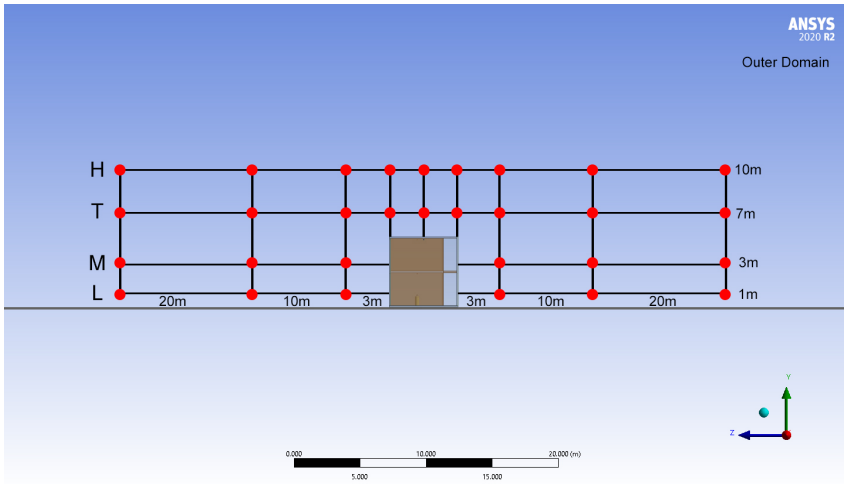
(c) Case IV (at the meteorological speed of 10m/s)

Figure 7-16: Contour images of the simulated velocity field at 0s for Cases II, III and IV

In terms of monitoring points, the same monitoring points are defined for the indoor spaces, as shown in Figure 7-7. Besides, a set of monitoring points (i.e., 9 points at H level-10m above the ground level, 9 points at T level-7m above the ground level, 6 points are M level-3m above the ground level and 6 points at L level-1m above the ground level) are defined to monitor the ambient condition at different heights and locations near the building within the outer domain as shown Figure 7-17.



(a) Front view



(b) Side view

Figure 7-17: Location of monitoring points in the outer computational domain

7.4.2 Results and discussions: indoor pressure distribution

As described in Section 5.3.1, the raw recorded data of the tank and building pressures during the Pulse field test are processed by an adjustment method to minimise the wind and buoyancy impact to the measurement of the building pressure induced by the air pulse released during the Pulse testing. In the numerical study, the pressure of the room is calculated by averaging the obtained values of all monitoring points in the room. Then the room pressures are also adjusted with the same curve-fit approach mentioned in Section 5.3.1.

Figure 7-18 presents the variation of the adjusted pressure in each room during the Pulse test for the four cases, and the overall average indoor pressure for each case is also plotted. As seen from the average indoor pressure curves for the four cases, the indoor pressure distribution during the Pulse test is greatly affected by the outdoor wind speed. Different indoor pressure curves can be noted for Cases II, III and IV with different wind speed levels, and the indoor pressure fluctuations

during the Pulse test become more noticeable when the wind speed increases. In addition, due to the wind impact, the achieved maximum pressure levels within the building during the Pulse test for the four cases are different, with different magnitudes as seen from the graphs. For instance, the maximum pressure of the average indoor pressure during the Pulse test for Case I is about 4.98Pa, while the peak average pressure level is 6.59Pa for Case IV.

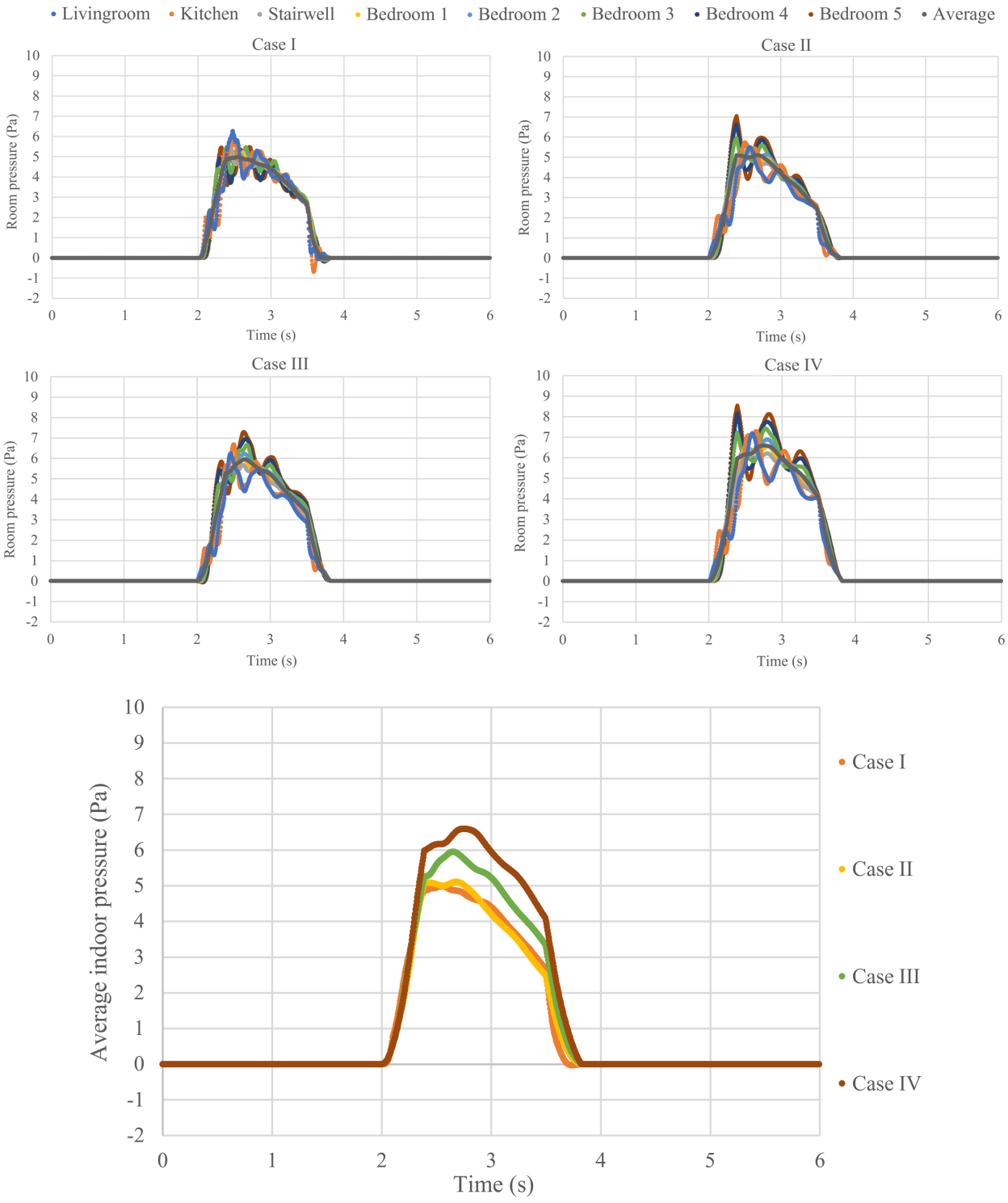


Figure 7-18: Pressure curves of each room and overall average during the Pulse test for different wind speed Cases I, II, III and IV

Similar to the analysis presented in Section 7.3.2, Table 7-9 lists the corresponding time points A and B for each room of the four cases. The comparisons of Points A and B for each room were conducted with those of the living room. Overall, for each case, the maximum difference of points A and B is small, for instance, the maximum difference of Points B among all rooms could be as small as around 0.035s, and the largest is 0.135s. This also confirms that a uniform pressure distribution within the internal building spaces was achieved during the measurement for all four cases. However, when comparing the four cases, the results imply that the wind speed affects the Pulse measurement, as different Points A and B are noted. In Case I, the maximum difference of Point A among all rooms is around 0.095s, whereas Case IV has a larger time difference of 0.145s due to the influence induced by the high wind speed condition. The impact of wind speed could also be observed by assessing Point B of all cases; for instance, the average Point B is at 3.095s in Case II at the meteorological speed of 4m/s, while it increases to 3.535s in Case IV at the meteorological speed of 10m/s.

Table 7-9: Time points A and B for Cases I, II, III and IV

	Case I		Case II		Case III		Case IV	
Time Point (s)	A	B	A	B	A	B	A	B
Living Room	2.370	3.010	2.385	3.045	2.355	3.255	2.380	3.495
Kitchen	2.330	2.990	2.380	3.085	2.355	3.265	2.370	3.505
Stairwell	2.335	2.990	2.355	3.070	2.330	3.310	2.310	3.495
Bedroom 1	2.325	2.985	2.375	3.055	2.335	3.255	2.350	3.485
Bedroom 2	2.320	2.975	2.305	3.100	2.325	3.345	2.290	3.500
Bedroom 3	2.295	2.975	2.295	3.120	2.265	3.355	2.280	3.550
Bedroom 4	2.285	2.980	2.290	3.130	2.260	3.350	2.270	3.610
Bedroom 5	2.275	2.990	2.285	3.140	2.250	3.355	2.235	3.630
Average*	2.315	2.985	2.335	3.095	2.310	3.310	2.305	3.535
Maximum Difference**	0.095	0.035	0.100	0.095	0.105	0.100	0.145	0.135

*Average Points A and B are obtained based on the average pressure of all rooms.
**Maximum difference is based on the comparison of Points A/B of each room with that of the living room.

7.4.3 Results and discussions: air leakage rate

Based on the obtained pressure results of each room (in Figure 7-18), the air leakage rate can be calculated accordingly for the four cases. The average building air leakage rate of each case is derived based on the average indoor pressure of all rooms. To quantify the wind impact on the Pulse measurement, the obtained air leakage rate that is calculated based on the pressure variation

in the living room in Case I is selected as the benchmark because: (1) the Pulse unit is placed in the living room for the simulated Pulse test, and (2) similar benchmark was defined in the analysis of the field testing results. Therefore, the relative percentage difference (*RPD*) between the air leakage rates that are calculated based on the pressure variations in other rooms and the benchmark can be calculated using eq. (7-9).

$$RPD = (\Delta ALR_{Room_benchmark})/ALR_{benchmark} \quad (7\text{-}9)$$

Where $\Delta ALR_{Room_benchmark}$ represents the air leakage rate difference between the room and benchmark.

Table 7-10 lists the detailed results of calculated air leakage rates and *RPD*s for the four cases.

Table 7-10: Calculated ALRs and *RPDs* for Cases I, II, III and IV

	Case I		Case II		Case III		Case IV	
	ALR	*RPD*	ALR	*RPD*	ALR	*RPD*	ALR	*RPD*
Living Room	0.08966	-	0.08920	-0.52%	0.08730	-2.64%	0.08631	-3.75%
Kitchen	0.08953	-0.15%	0.08732	-2.62%	0.08396	-6.38%	0.08375	-6.62%
Stairwell	0.08924	-0.47%	0.08775	-2.14%	0.08429	-6.02%	0.08078	-9.95%
Bedroom 1	0.08897	-0.77%	0.08758	-2.33%	0.08449	-5.79%	0.08057	-10.18%
Bedroom 2	0.08882	-0.94%	0.08751	-2.41%	0.08457	-5.70%	0.06967	-22.39%
Bedroom 3	0.08809	-1.76%	0.08774	-2.15%	0.08592	-4.19%	0.05537	-38.41%
Bedroom 4	0.08744	-2.49%	0.08730	-2.64%	0.08676	-3.25%	0.04843	-46.18%
Bedroom 5	0.08647	-3.57%	0.08613	-3.95%	0.08598	-4.12%	0.04665	-48.18%
Average*	0.08916	-0.56%	0.08714	-2.82%	0.08480	-5.44%	0.07248	-19.24%

*The average air leakage rate of each case is calculated based on the average indoor pressure of all rooms.

The difference of the average air leakage rate between Case I and Case II is approximately 2.27%, while large deviations are noted for comparing cases under higher wind speed levels with Case I under the no wind condition, i.e., by -4.89% (Case III) and -18.71% (Case IV), respectively. Moreover, the wind speed impact on the Pulse measurement could be apparently observed, as the *RPD* varies noticeably with the four cases. The *RPD*s of Case I, Case II and Case III fall within ±10%, while larger discrepancies are found in Case IV, which were simulated at the highest wind speed level (i.e., at the meteorological speed of 10m/s). In most cases, the *RPD* becomes more significant at a higher wind speed when comparing the *RPD* of a specific room among cases, whereas the significance of the wind speed impact varies from room to room. For example, the

RPD of the living room is -0.52% in Case II and -3.75% in Case IV; and the *RPD* of Bedroom 5 is –3.95% in Case II and became -48.18% in Case IV.

The average *RPD* of Case III is beyond ±5% (i.e., -5.44%), and Case IV has the largest *RPD*, approximately -19.24%, which indicates that the high wind speed condition could induce a large uncertainty to the Pulse measurement. Based on the numerical results, the Pulse measurement is recommended to perform under the meteorological wind speed below 6m/s, ensuring *RPD* within ±10%. This finding also agrees with the wind speed limit for the fan pressurisation method stated in the ISO 9972 standard.

As discussed in Section 5.2, the wind speed impact was also quantified by evaluating the relative percentage differences, which were calculated by comparing the air leakage rate of every single test with the baseline air leakage rate. As the anemometer was installed at 2.2m above the ground level to monitor the wind condition during the field testing, the corresponding wind speed at 2.2m above the ground level is 2.54m/s for Case II, 3.81m/s for Case III, and 6.35m/s for Case IV, with reference to the wind profile presented in Figure 7-15. Therefore, the *RPD*s of the field tests at the three wind speed levels could be found from the results presented in Section 5.2.1. Table 7-11 summarises the *RPD*s of field tests and simulations at the three wind speed levels.

Table 7-11: Comparison of *RPD*s between the simulation and experimental results

	Wind Speed at 2.2m above Ground Level		
	2.54m/s	3.81m/s	6.35m/s
RPD of Simulation Results	-2.82%	-5.44%	-19.24%
RPD of Field-Testing Results	-2.97%	-7.68%	-12.59%
Deviation from Field Testing	0.15%	2.24%	-6.65%

Both simulation and field test results show the significant effect of the wind speed on the Pulse measurement. A good agreement is found between the simulation and experimental results with deviations fall within ±7%, and both results imply that the Pulse test is recommended under wind speed below 3.81m/s at 2.2m above ground level (i.e., equivalent to the meteorological wind speed of 6m/s) for the *RPD* within ±10%. It is also noteworthy that the *RPD* deviation between the simulation and experimental results is slightly under the low wind speed (i.e., 0.15% at a wind speed of 2.54m/s), while it becomes larger at a higher wind speed (i.e., -6.65% at a wind speed of 6.35m/s). This is maybe because of the more significant errors caused by the high wind speed level.

7.4.4 Results and discussions: air flow rate of openings

Figure 7-19 presents the variation of the volumetric air flow rate at each opening during the Pulse test for the four cases. The positive values of the volumetric flow rate indicate that the air leaks out from the openings to the ambient during the Pulse test, while negative values mean that the outdoor air enters the building interior through the openings. It can be seen that the ten openings have different air leakage patterns during the Pulse measurement under different wind speed conditions. A larger deviation of the air flow rate among the ten openings can be observed under a higher wind speed condition; for instance, the air flow rate variations of the ten openings match well in Case I under no wind condition, while larger discrepancies are found for Opening 1 and 2 compared with those of other openings in Case IV under a windy condition.

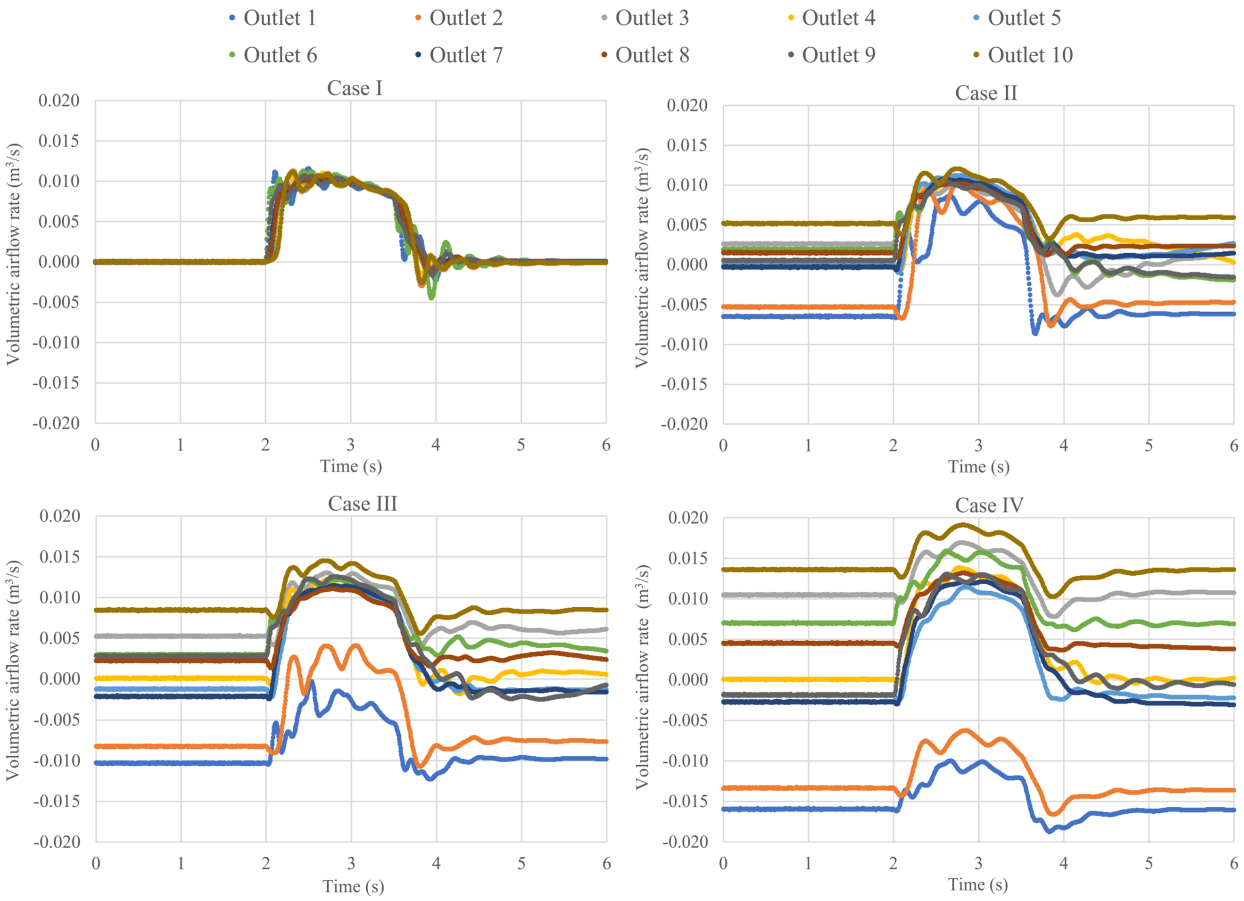


Figure 7-19: Variations of volumetric airflow rate at ten openings during the Pulse test for Cases I, II, III and IV

Although a noticeable difference of the volumetric flow rate at ten openings during the Pulse test for the four cases is found in Figure 7-19, similar curves are noted in Figure 7-20 for considering the total leakage flow rate at the ten openings. During the quasi-steady period (i.e., 2.8s-3.5s), Cases II, III, and IV have similar curve patterns, while Case I faced a relatively larger flow rate of the air leaking from the ten outlets, which is because Case I is simulated under no wind condition.

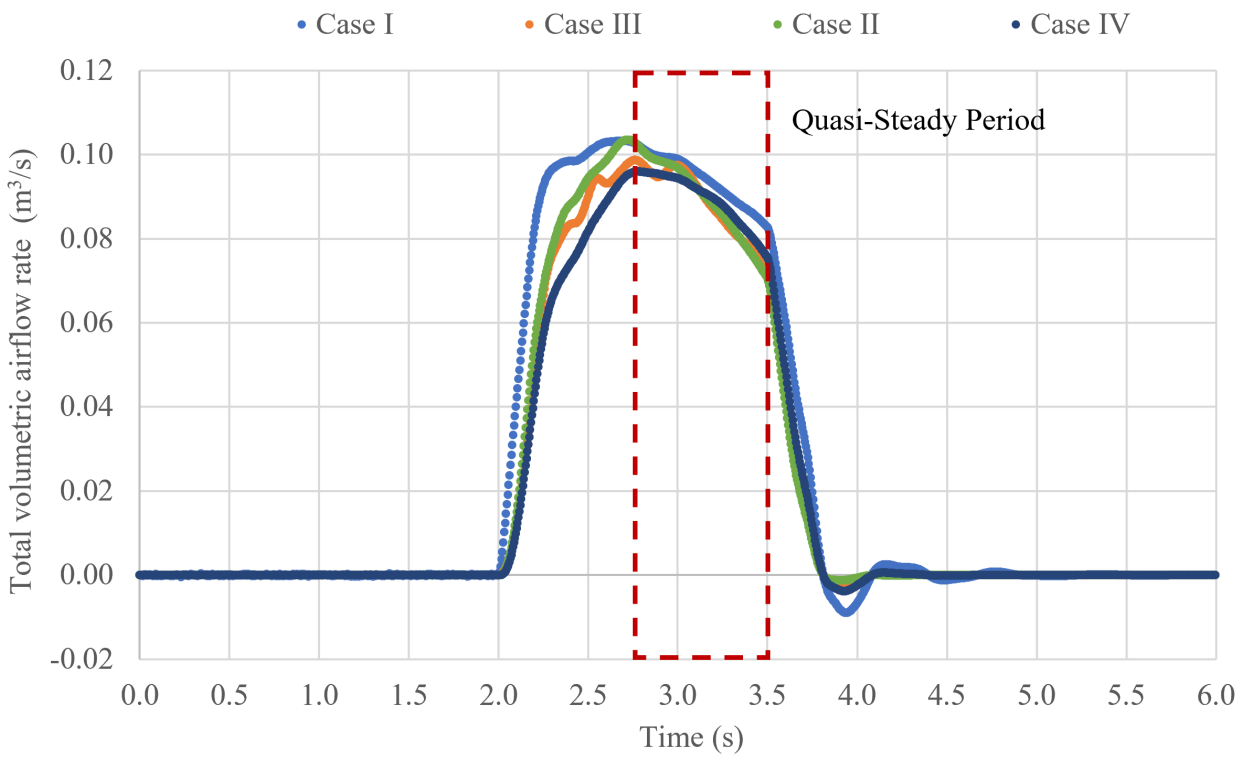


Figure 7-20: Total volumetric airflow rate of ten openings during the Pulse test for Cases I, II, III and IV

For practical Pulse applications, the quasi-steady period is selected for examining the building airtightness. Therefore, to evaluate the impact of the wind speed on the volumetric flow rate of each opening, detailed analyses of the simulation results are conducted by focusing on the quasi-steady period. Depending on the specific location on the building envelope, the opening could be windward or leeward, which also affects the flow rate of the air leaking from the opening. The average of the obtained volumetric flow rate of each opening during the quasi-steady period is calculated firstly for each case. To quantify the wind speed impact, the volumetric flow rate of each opening is plotted by deducting the average value as presented in Figure 7-21. The results clearly show that the volumetric flow rates of Openings 1 and 2 are more remarkably influenced by the outdoor wind speed. This is mainly attributed to the locations of the two openings, i.e., on the upwind side of the building envelope. In particular, Opening 1 is located on the upper level on the windward side; thus, the strong outdoor wind prevents the inside air from leaking out during the Pulse test in Case IV. Based on the results of Figure 7-21, the average deducted volumetric flow rate of each opening can be obtained, as presented in Figure 7-22.

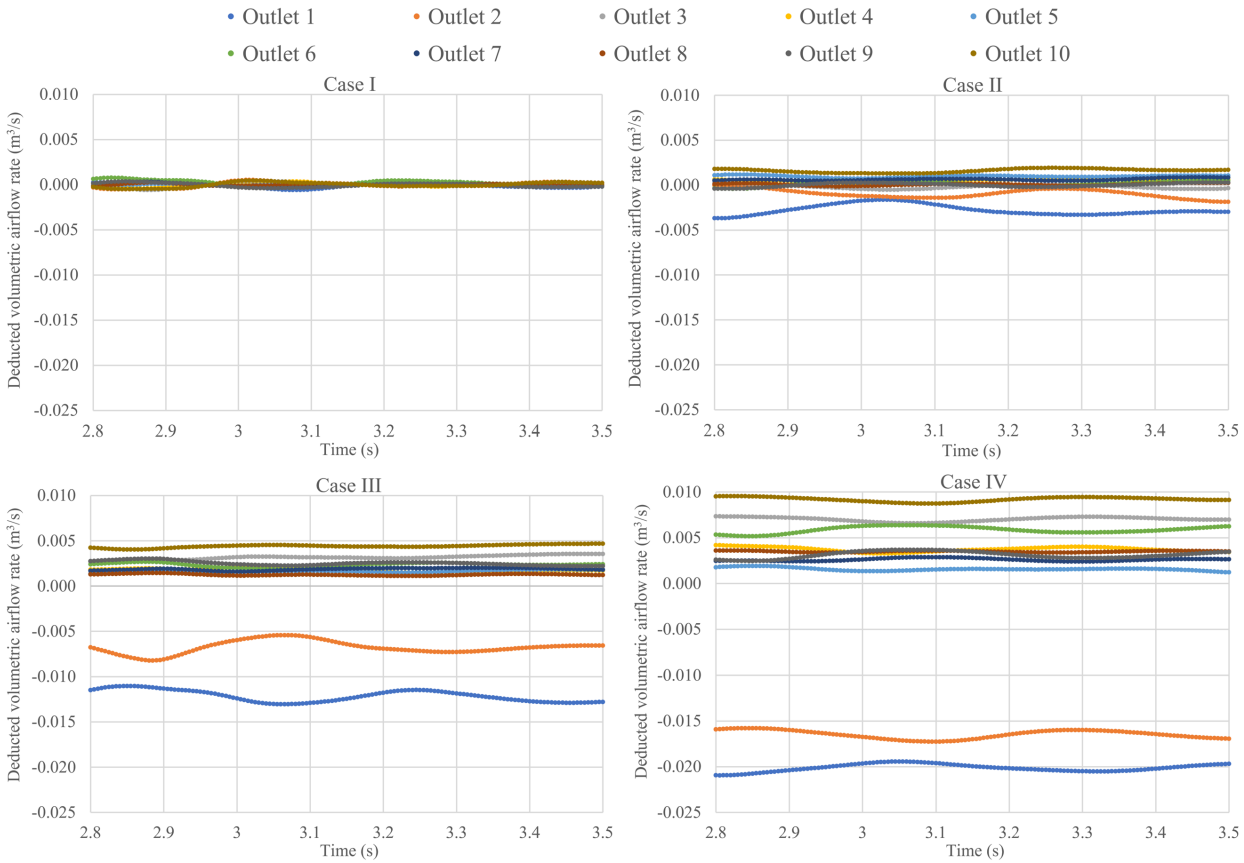


Figure 7-21: Deducted volumetric flow rate at ten openings during quasi-steady period for Cases I, II, III and IV

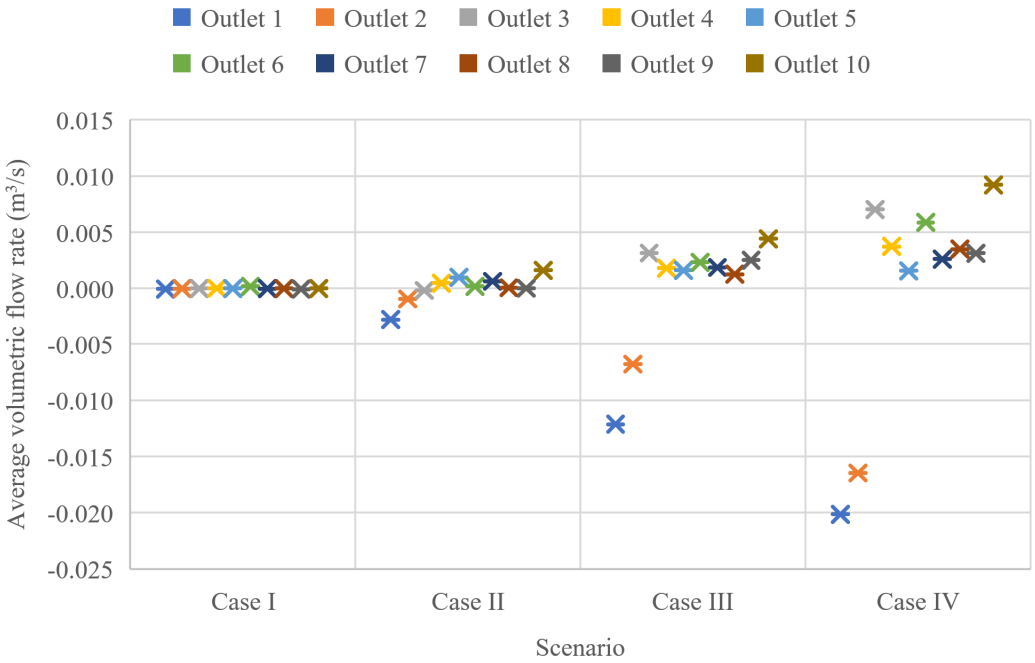


Figure 7-22: Average volumetric flow rate at ten openings during quasi-steady period for Cases I, II, III and IV

The deviation of the average deducted volumetric flow rate for the ten outlets becomes more noticeable with the increasing outdoor wind speed. For instance, the difference of the average volumetric flow rate between Opening 1 and Opening 6 is approximately 0.003m^3/s in Case II, while a larger difference can be observed in Case IV, approximately 0.026m^3/s. The results also

imply how the pressure difference across all the openings varies under various wind speed levels. For instance, when the steady wind blows to the building at a higher level, the wind pressure induces more air flow into the indoor spaces through Openings 1 and 2 in the windward façade, while the airflow rate leaking out from openings in the leeward façade is accelerated, such as Openings 3, 6 and 10.

Figure 7-23 shows the plot of the average indoor pressure against the total volumetric flow rate of ten openings during the quasi-steady period for each case. The four plots have distinct gradients, which reveals that the Pulse measurement is greatly influenced by the wind speed. At the average indoor pressure of 4Pa, the difference of the total volumetric flow rate between Case I and Case II is 1.17%, while it reaches 20.92% with the comparison between Case I and Case IV. The results reflect the importance of considering the wind condition for an accurate and valid Pulse measurement.

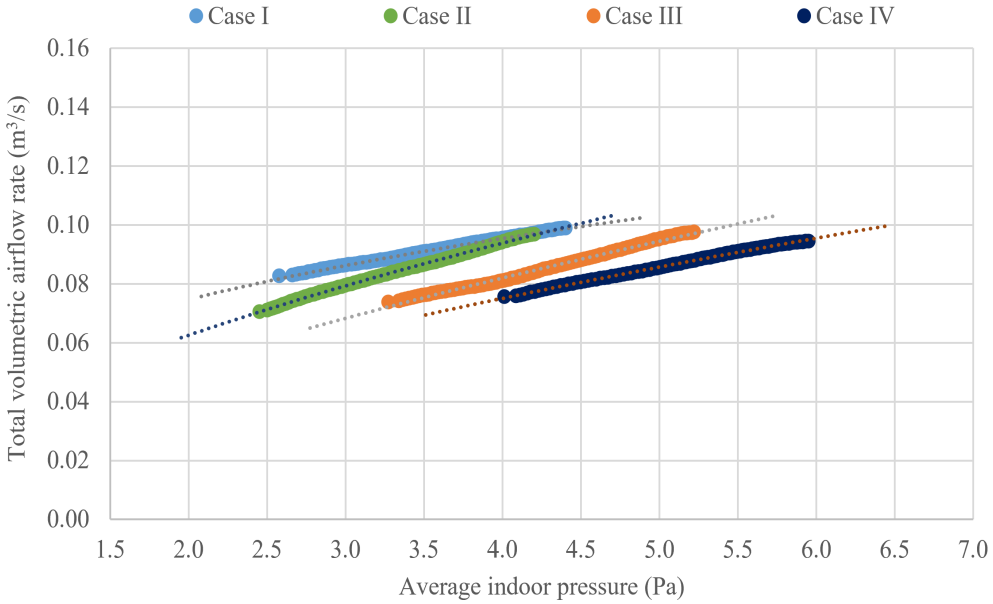
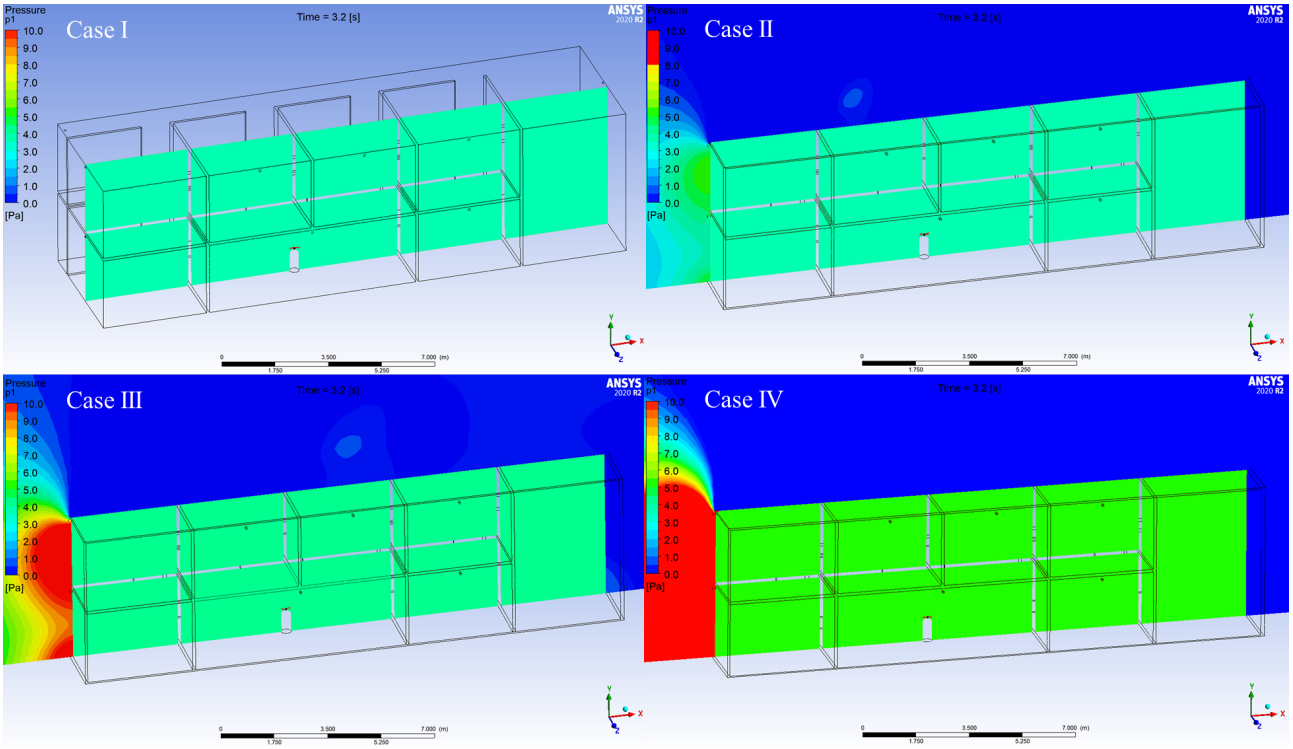
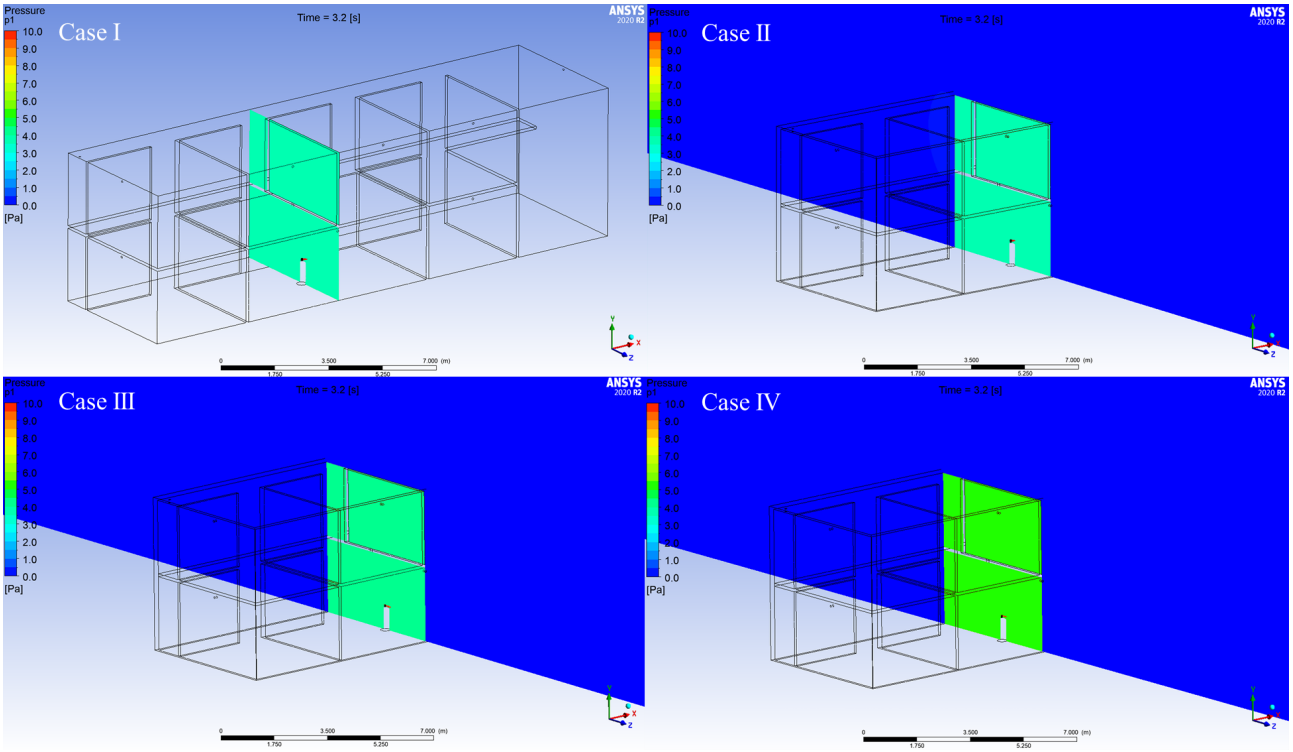


Figure 7-23: Plots of the average indoor pressure against the total volumetric flow rate of ten openings during the Pulse test for Cases I, II, III and IV

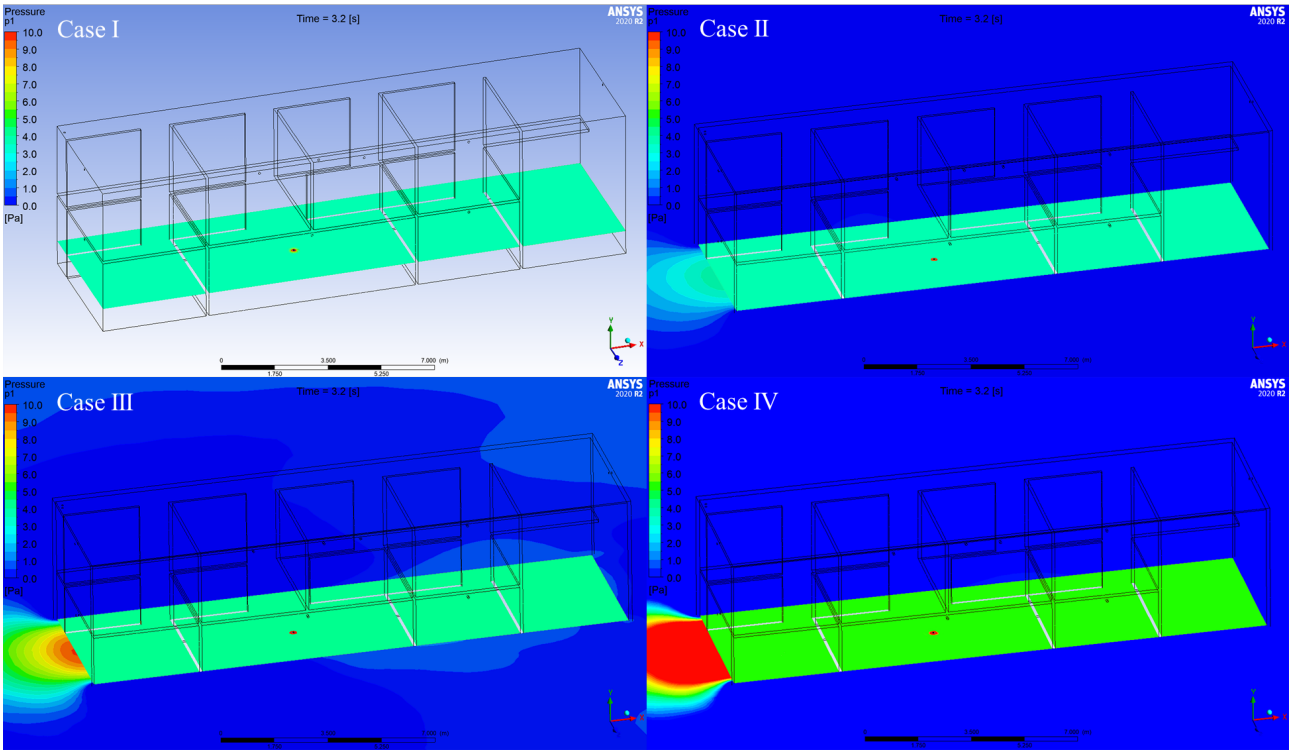
The contour images of the indoor pressure at 3.2s for the four cases are shown in Figure 7-24 from various perspective views (i.e., 7-24(a) from the vertical front view, 7-24(b) from the vertical side view, 7-24(c) and 7-24(d) from the top horizontal view). The multi-view contour images help visualise how the steady outdoor wind affects the pressure distribution within and around the building and how the pressure difference across all the openings have changed by the wind conditions. Figure 7-25 presents contour images of the indoor air velocity at 3.2s for the four cases from multiple views, depicting that the wind pressure induces air flows into the interior via the openings in the windward façade and the corresponding airflow rate increases with the increase in the wind speed level.



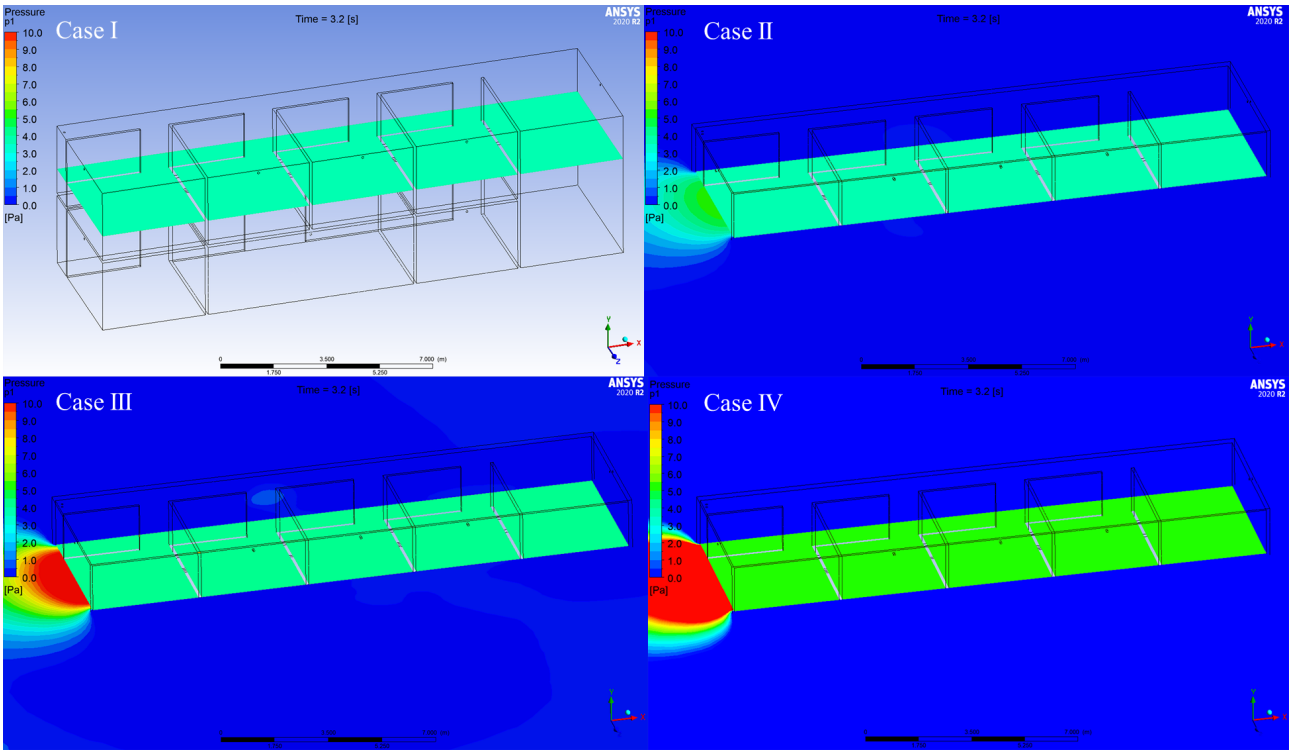
(a) Vertical front view



(b) Vertical side view

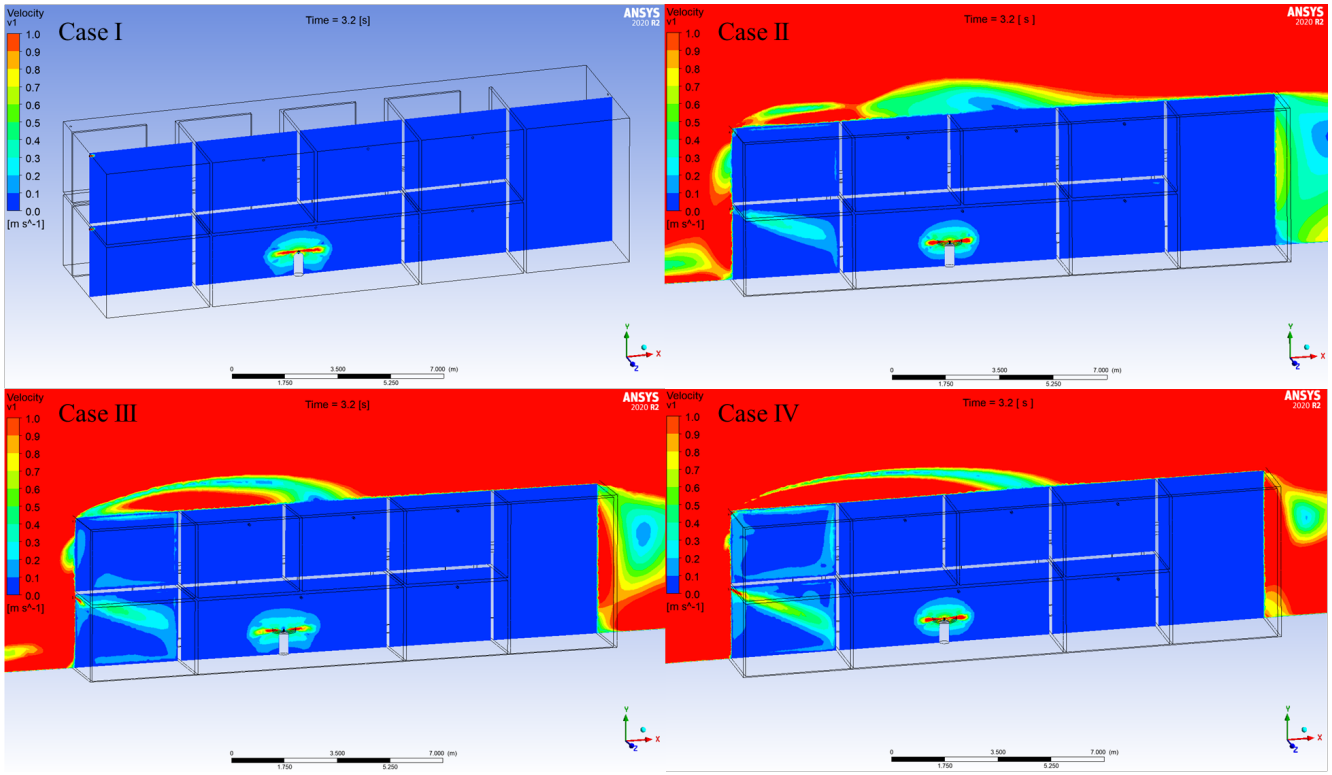


(c) Horizontal view of ground floor

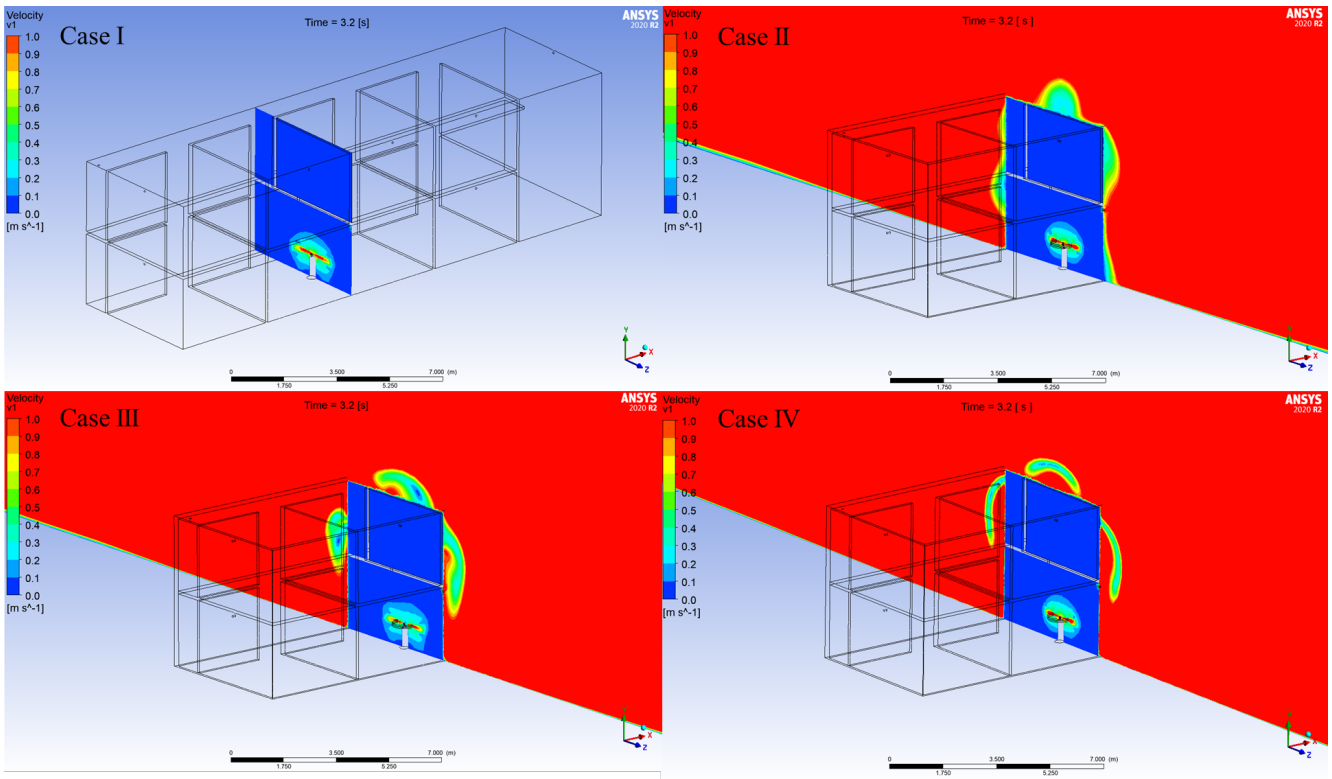


(d) Horizontal view of first floor

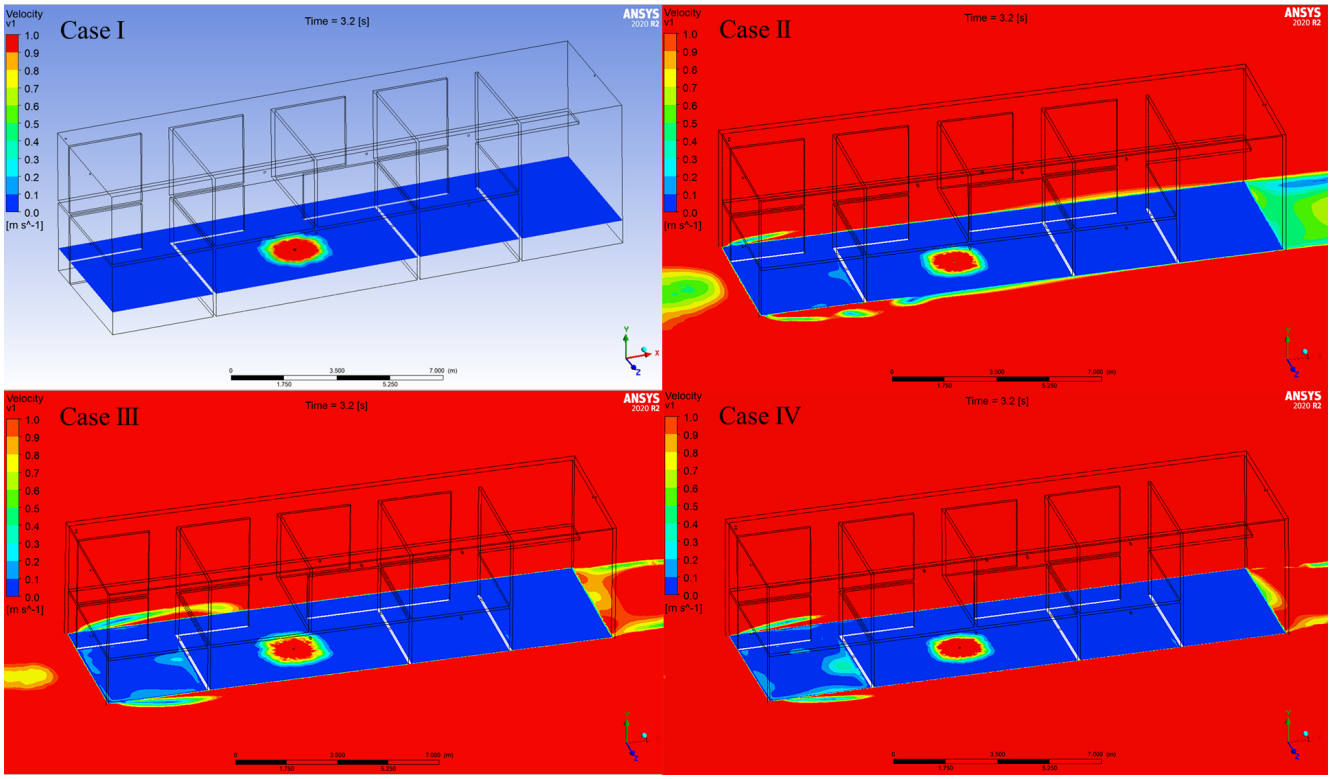
Figure 7-24: Perspective contour images of the indoor pressure at 3.2s for Cases I, II, III and IV



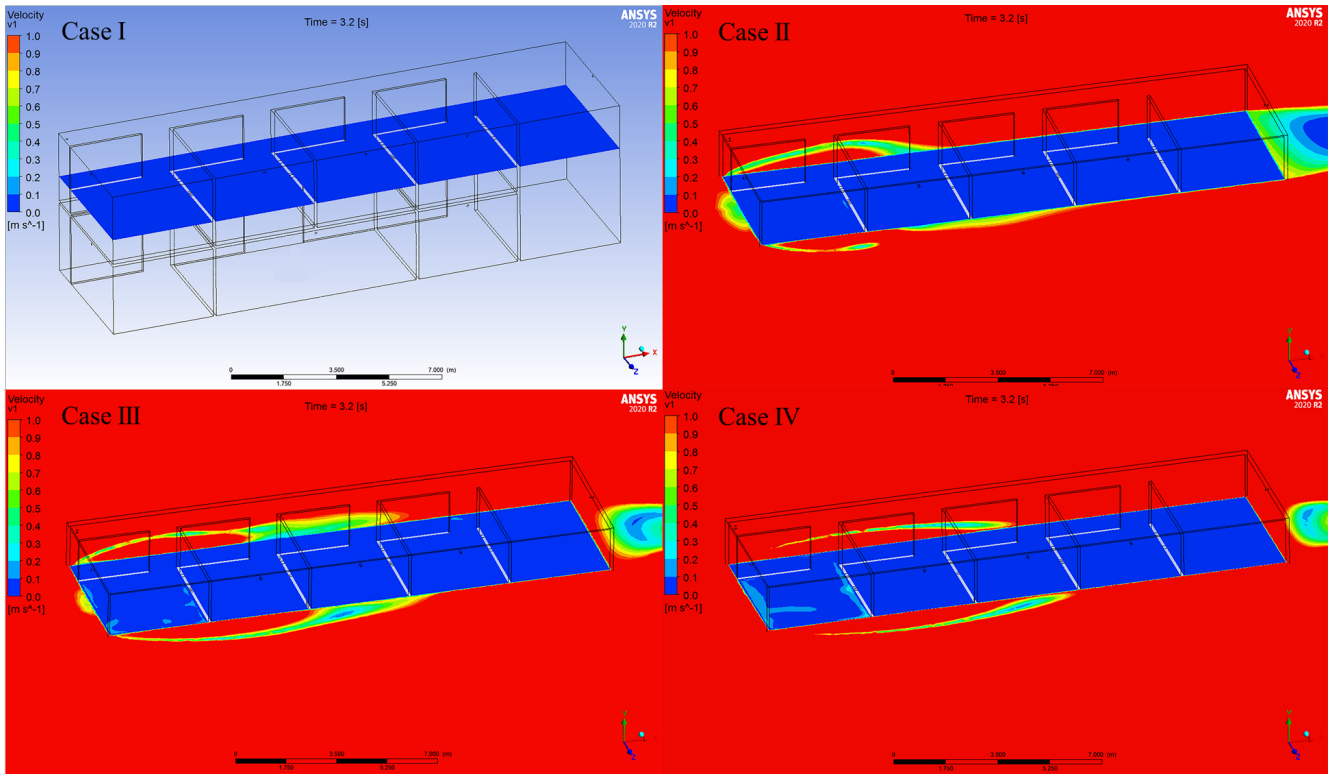
(a) Vertical front view



(b) Vertical side view



(c) Horizontal view of ground floor



(d) Horizontal view of first floor

Figure 7-25: Perspective contour images of the indoor velocity at 3.2s for Cases I, II, III and IV

7.5 The impact of wind direction on the Pulse test

Simulations were then carried out to evaluate how the pressure distributes across different zones within the building during the Pulse test under different wind directions.

7.5.1 Computational domain and configurations

Case III (at the meteorological wind speed of 6m/s) presented in Section 7.4 is used as the benchmark for examining the wind direction impact on Pulse. Therefore, another three cases with different wind directions are proposed (i.e., Cases V, VI and VII), as illustrated in Figure 7-26. As the input flow direction in the outer domain is variable for the four cases, the same settings described in Section 7.4 are used, including model configuration, grid and solver settings, wind speed profile and the setup of indoor and outdoor monitoring points. The steady-state solution was first obtained and then applied as the initial condition for each case to proceed with the further transient simulation. In terms of the determination of time steps, for each case, the assessment of CFL limitation was conducted to check the stability and accuracy of the time step of 0.0001s. Table 7-12 lists the simulated wind conditions for the four cases. The contour images of Cases III, V, VI and VII, are presented in Figure 7-27, showing the different velocity fields at the beginning of the transient simulation of the Pulse test for the four cases.

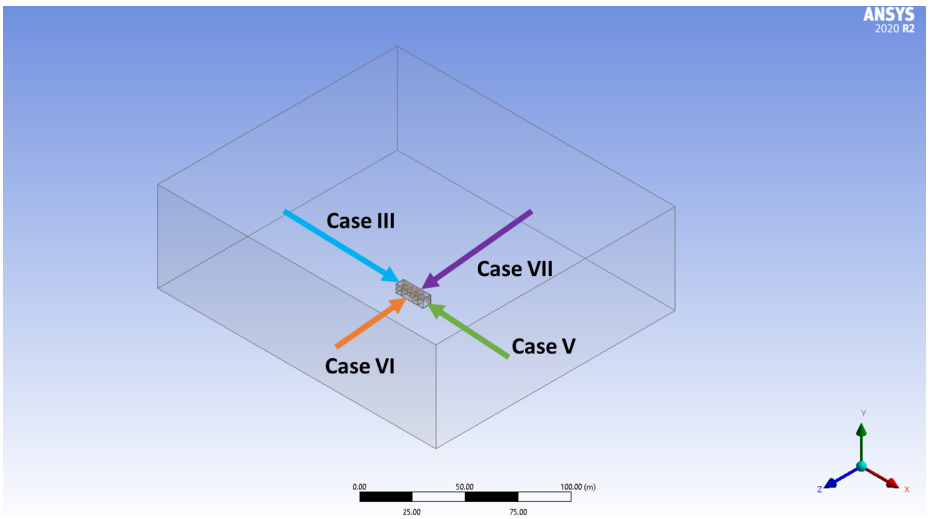
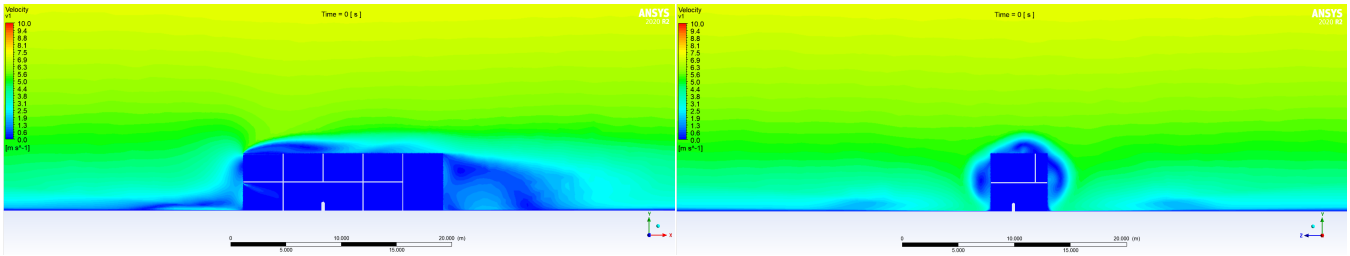


Figure 7-26: Illustration of Cases III, V, VI and VII with different wind directions

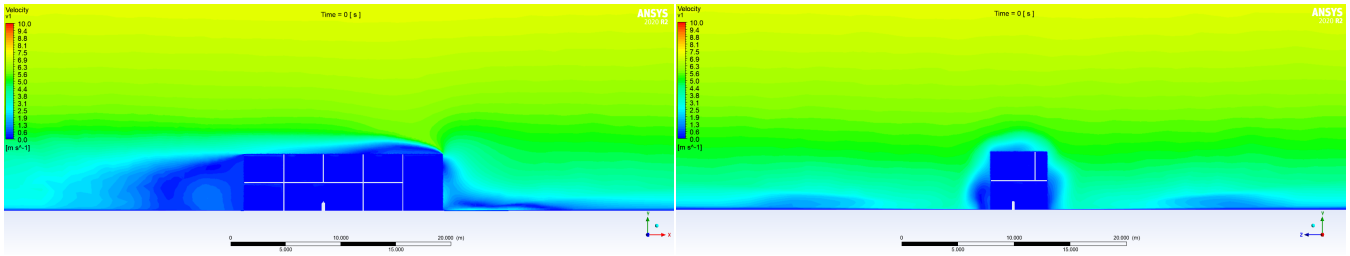
Table 7-12: Simulated wind conditions for Cases III, V, VI, VII

Case	Wind Direction (Coordinate Axis)	Wind Speed	
		At 1m above Ground	At 10m above Ground
III	along positive x-axis	3m/s	6m/s
V	along negative x-axis	3m/s	6m/s
VI	along negative z-axis	3m/s	6m/s
VII	along positive z-axis	3m/s	6m/s

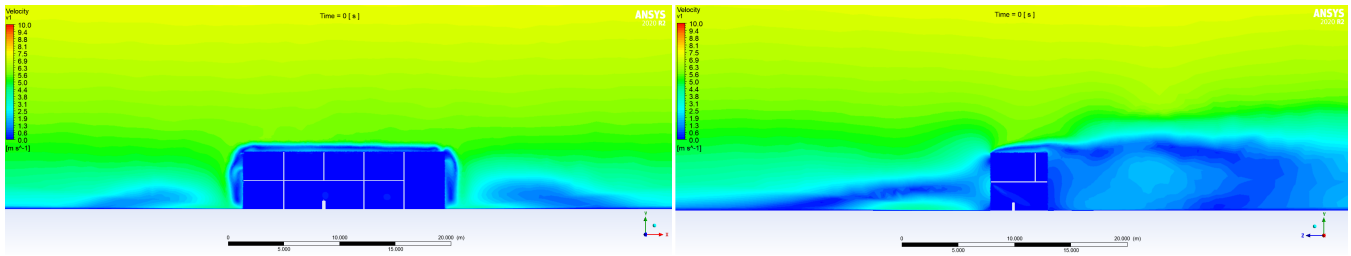
Front view Side view



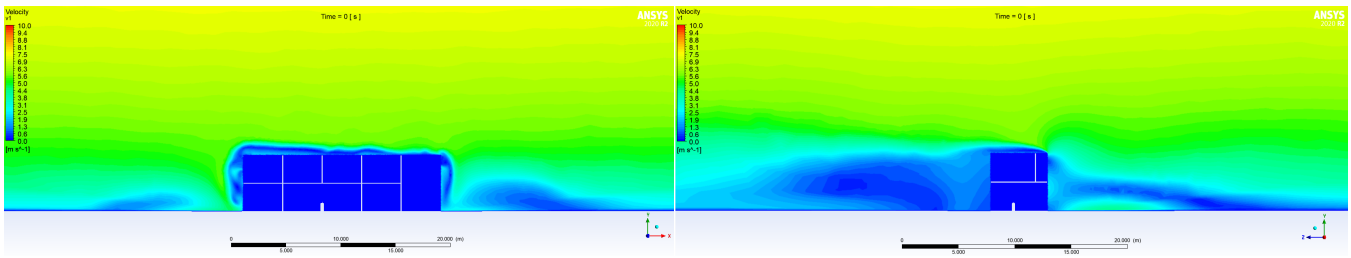
(a) Case III (wind direction: along positive x-axis)



(b) Case V (wind direction: along negative x-axis)



(c) Case VI (wind direction: along negative z-axis)



(d) Case VII (wind direction: along positive z-axis)

Figure 7-27: Contour images of the simulated wind condition at 0s for Cases III, V, VI and VII

7.5.2 Results and discussions: indoor pressure distribution

The obtained raw data of the room pressures are firstly processed with the adjustment method, as mentioned in Section 7.4.2. The variations of each room pressure and the overall average indoor pressure during the Pulse test for the four cases are presented in Figure 7-28. As seen from the graphs, the pressure curves of the four cases are different. Due to the change in the wind direction, the wind pressure distribution around the building varies, which can be observed in the pressure contour images in Figure 7-34. Moreover, as the designated openings are located in different

places across the building envelope, the ratio of the opening area in the windward to that in the leeward façade varies in accordance with the wind direction, causing different indoor pressure distributions in each room within the building. For example, the percentage of the openings in windward façade is 20% for Case III, 10% for Case V, 50% for Case VI and 10% for Case VII. Although the peak pressure of the rooms during the Pulse test varies with different wind directions, the peak values of the overall average indoor pressures are similar for the four cases, around 6Pa.

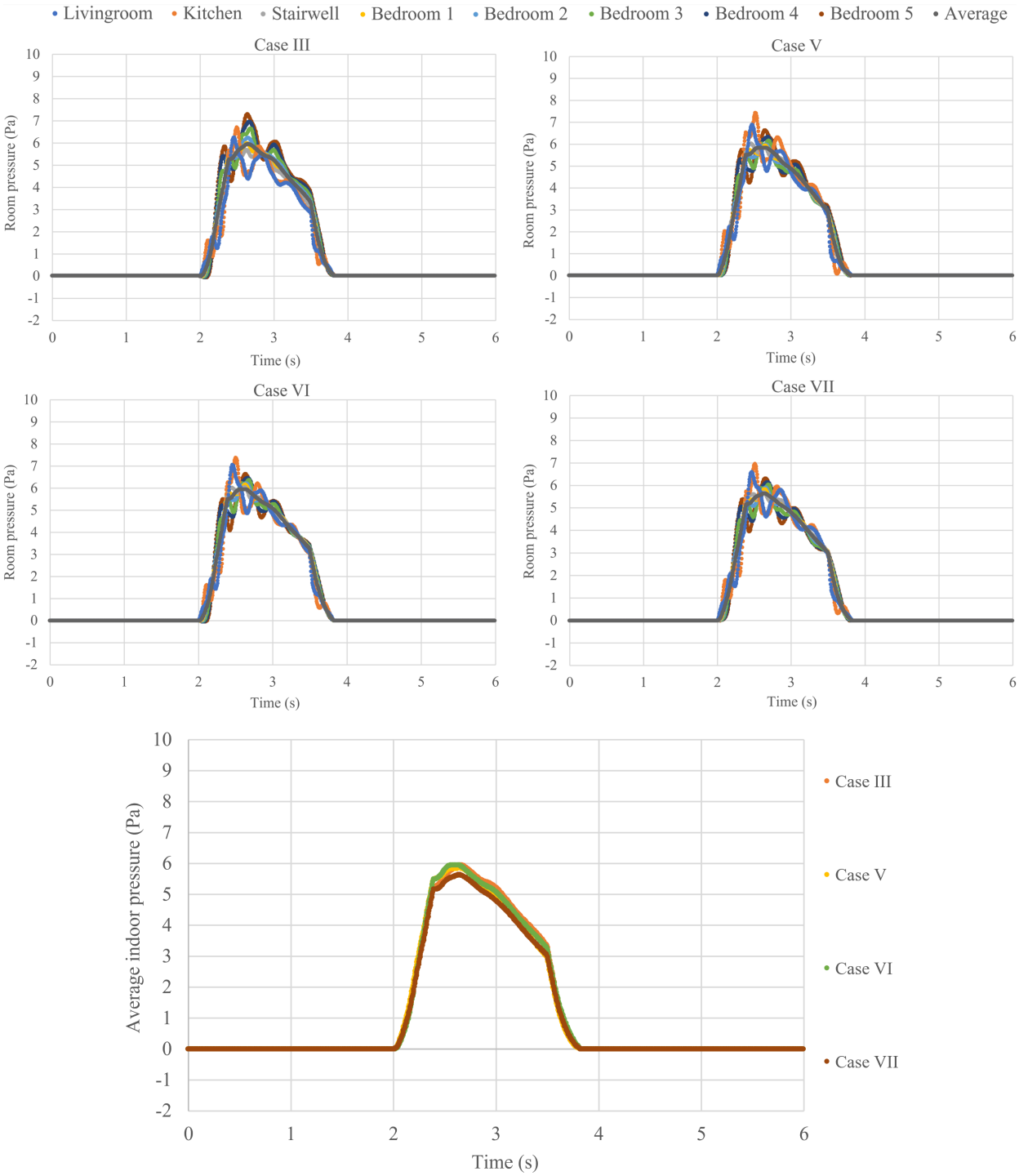


Figure 7-28: Pressure curves of each room and overall average during the Pulse test for different wind condition Cases III, V, VI and VII

The corresponding time points A and B for each room are found for each case as presented in Table 7-13. The average value of time point A is found based on the average indoor pressure of each case; it varies slightly for the four cases, ranging from 2.300s to 2.315s. Results show that the maximum difference of Point A among all rooms is 0.105s in Case III, which is similar to that of Case V with the wind direction along the x-axis. Case VII has the largest time difference of Point A, approximately 0.130s. The average value of time point B ranges from 3.245s to 3.310s for the four cases. The maximum difference of Point B among all rooms could be as small as 0.100s, and the largest difference is 0.120s. The results again provide numerical evidence to prove how quickly the pressure wave propagates within the internal building spaces during the Pulse test and achieves a uniform indoor pressure distribution under various wind direction conditions.

Table 7-13: Time points A and B for Cases III, V, VI and VII

	Case III		Case V		Case VI		Case VII	
Time Point (s)	A	B	A	B	A	B	A	B
Living Room	2.355	3.255	2.335	3.205	2.345	3.320	2.360	3.320
Kitchen	2.355	3.265	2.335	3.215	2.345	3.325	2.355	3.335
Stairwell	2.330	3.310	2.330	3.290	2.325	3.280	2.335	3.230
Bedroom 1	2.335	3.255	2.325	3.295	2.325	3.290	2.340	3.240
Bedroom 2	2.325	3.345	2.330	3.290	2.320	3.270	2.330	3.225
Bedroom 3	2.265	3.355	2.270	3.305	2.270	3.255	2.280	3.215
Bedroom 4	2.260	3.350	2.260	3.295	2.260	3.230	2.270	3.205
Bedroom 5	2.250	3.355	2.230	3.300	2.230	3.215	2.230	3.200
Average*	2.310	3.310	2.300	3.275	2.305	3.275	2.315	3.245
Maximum Difference**	0.105	0.100	0.105	0.100	0.115	0.105	0.130	0.120

*Average Points A and B are obtained based on the average pressure of all rooms.
**Maximum difference is based on the comparison of Points A/B of each room with that of the living room.

7.5.3 Results and discussions: air leakage rate

The air leakage rates of the building are calculated based on the obtained room pressures for the four cases. Similar to the analysis conducted in Section 7.4.3, the same benchmark (i.e., the air leakage rate that is calculated based on the simulated pressure variation in the living room in Case I) is selected, *RPD*s can be calculated accordingly for the four cases. The detailed data of ALRs and *RPD*s are provided in Table 7-14.

Comparatively, the lowest average ALR is given by Case III, and the largest deviation is found by comparing with that of Case V (i.e., by approximately 3.93%), which has the opposite wind direction from Case III. The difference of the average ALR between Case V and Case VII is

-2.35%, which have opposite wind directions along the z-axis. Depending on the room location within the building, the impact of wind direction on the calculated air leakage rate varies. For instance, the air leakage rates calculated based on the pressure variation in the living room are similar in Case III and Case V, which deviate from those of Cases VI and VII. It is because that the location of the living room faces negative z-axis; thus, the measurement could be more sensitive to the wind flows along the z-axis (i.e., Case VI and VII). In particular, Case VI has the lowest value of ALR calculated based on the pressure of the living room, which could be owing to the largest percentage of openings on the windward façade (i.e., 50%). The living room is located in the windward direction; thus, openings on the living room's windward facade encounter the wind flows, causing fewer airflows could be leaked out.

It can also be seen from the table that the majority of the *RPD*s fall within ±10%. In terms of the comparison of the average *RPD* among the four cases, Cases III and VI have similar results (i.e., -5.44% and -4.56%, respectively), while smaller discrepancies are observed for Case V and VII (i.e., -1.71% and -2.31% respectively). This may be attributed to the more numbers of openings on the windward façades in Cases III and VI. Only one opening is located on the right side and back of the building envelope; thus, the air leakage rate measurement is less affected by the wind coming from the right and back sides (i.e., Cases V and VII). In the experimental study presented in Section 5.2.3, similar findings were noted when south-western winds were incident upon the tested dwelling. Due to the larger envelope area and window openings of the corresponding windward façade, it is therefore likely to be proportionality leakier than other facades.

Table 7-14: Calculated ALR and *RPDs* for Cases III, V, VI and VII

	Case III		Case V		Case VI		Case VII	
	ALR	*RPD*	ALR	*RPD*	ALR	*RPD*	ALR	*RPD*
Living Room	0.08730	-2.64%	0.08516	-5.04%	0.08047	-10.29%	0.08178	-8.83%
Kitchen	0.08396	-6.38%	0.08180	-8.80%	0.07937	-11.53%	0.08080	-9.92%
Stairwell	0.08429	-6.02%	0.08814	-1.70%	0.08495	-5.28%	0.08716	-2.80%
Bedroom 1	0.08449	-5.79%	0.08716	-2.80%	0.08391	-6.44%	0.08594	-4.17%
Bedroom 2	0.08457	-5.70%	0.08907	-0.66%	0.08603	-4.07%	0.08833	-1.49%
Bedroom 3	0.08592	-4.19%	0.09065	1.11%	0.08770	-2.20%	0.08983	0.19%
Bedroom 4	0.08676	-3.25%	0.09266	3.36%	0.08854	-1.25%	0.09064	1.10%
Bedroom 5	0.08598	-4.12%	0.09522	6.23%	0.08882	-0.94%	0.09130	1.84%
Average*	0.08480	-5.44%	0.08813	-1.71%	0.08559	-4.56%	0.08760	-2.31%

*The average air leakage rate of each case is calculated based on the average indoor pressure of all rooms.

7.5.4 Results and discussions: air flow rate of openings

The variations of the volumetric airflow rate through ten openings during the Pulse test for the four cases are plotted in Figure 7-29. As the wind direction changes, the openings change between leeward and windward, which lead to different variations of the volumetric airflow rate during the Pulse test. For instance, the volumetric airflow rates at Openings 1 and 2 are lower than others in Case III, as they are located in the windward façade with less airflow being leaked out. When the wind direction changes to the opposite direction (i.e., Case V), the volumetric airflow rate at Opening 8 becomes the smallest because Opening 8 encounters the wind flows, where the pressure difference across the opening is decreased. On the other hand, Openings 3, 4, 5, 6 and 7 located on the windward walls have a lower airflow rate in Case VI, while the lowest airflow rate occurs at Opening 9 in Case VII with air blown into the indoor spaces.

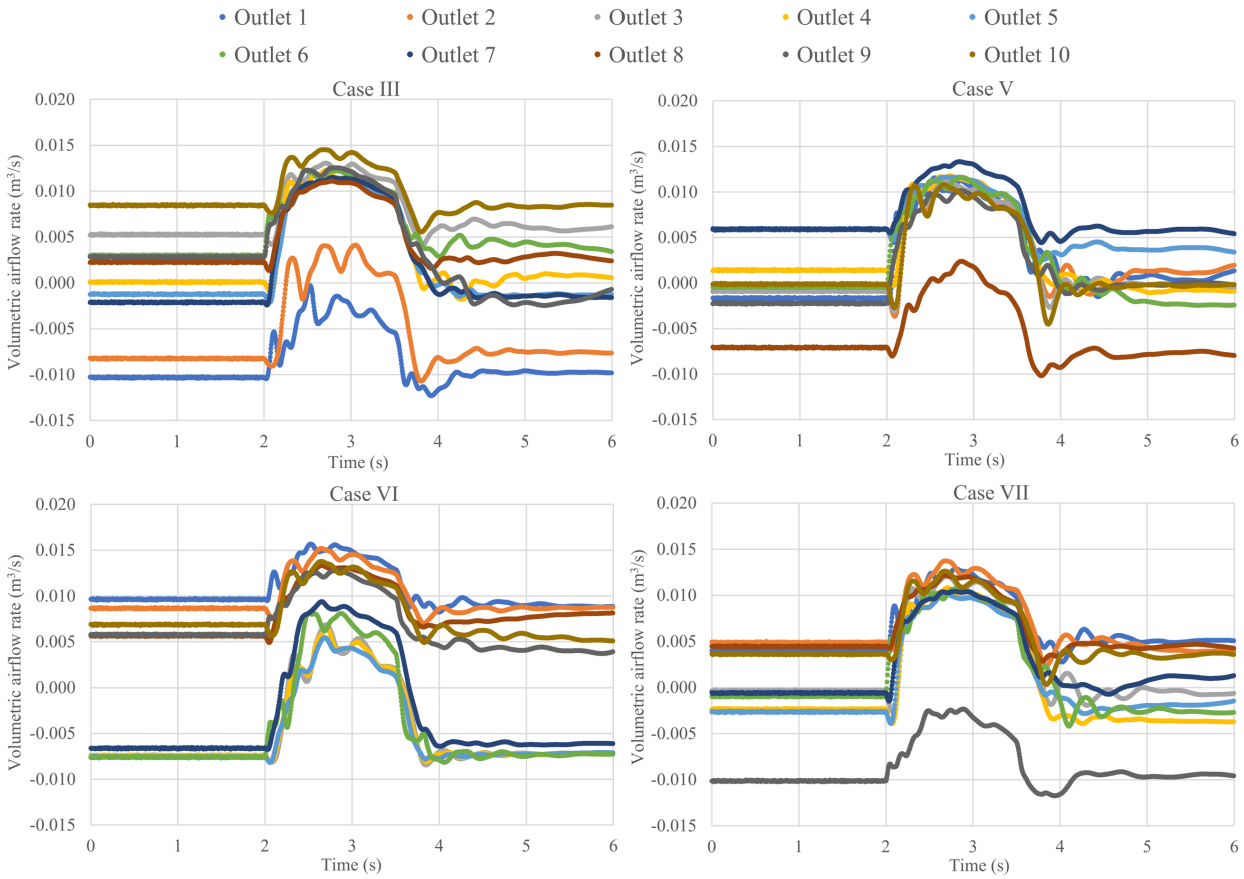


Figure 7-29: Variations of volumetric flow rate at ten openings during the Pulse test for Cases III, V, VI and VII

As seen in Figure 7-30, curves of the total volumetric flow rate at the ten openings are similar for the four cases, especially during the quasi-steady period (i.e., 2.8s to 3.5s).

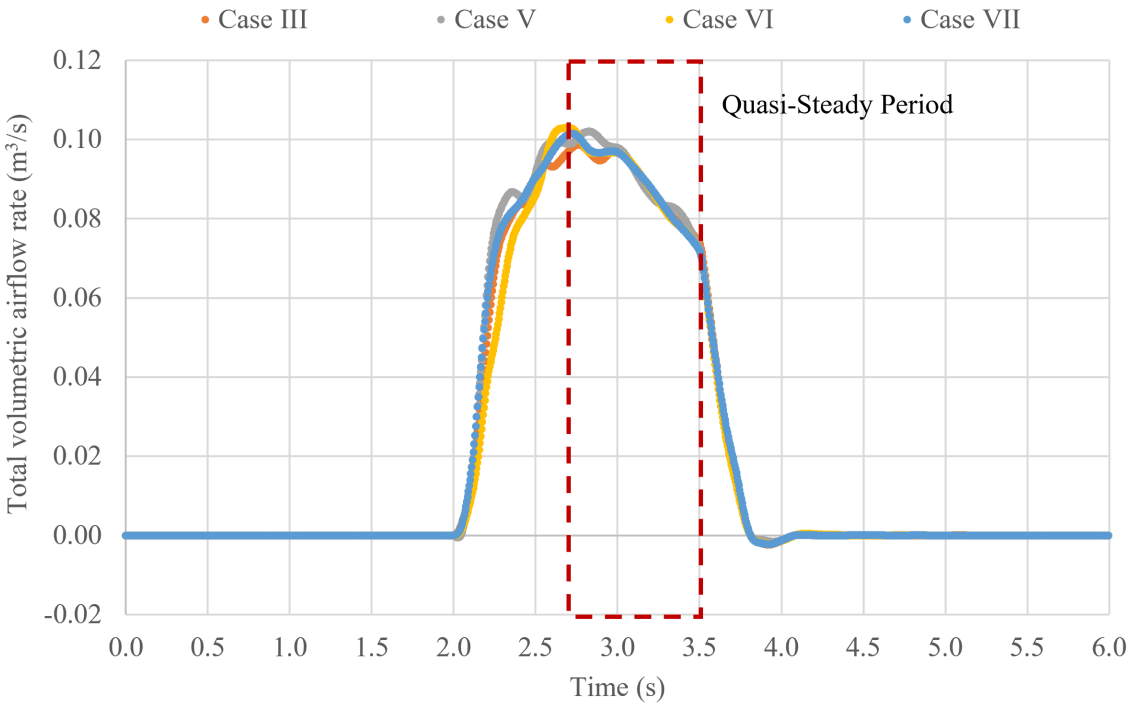


Figure 7-30: Total volumetric flow rate of ten openings during the Pulse test for Cases III, V, VI and VII

Calculations of the average volumetric airflow rate during the quasi-steady period are conducted for each opening in the four cases. The processed volumetric flow rate of each opening is then deducted by the calculated average value and plotted in Figure 7-31.

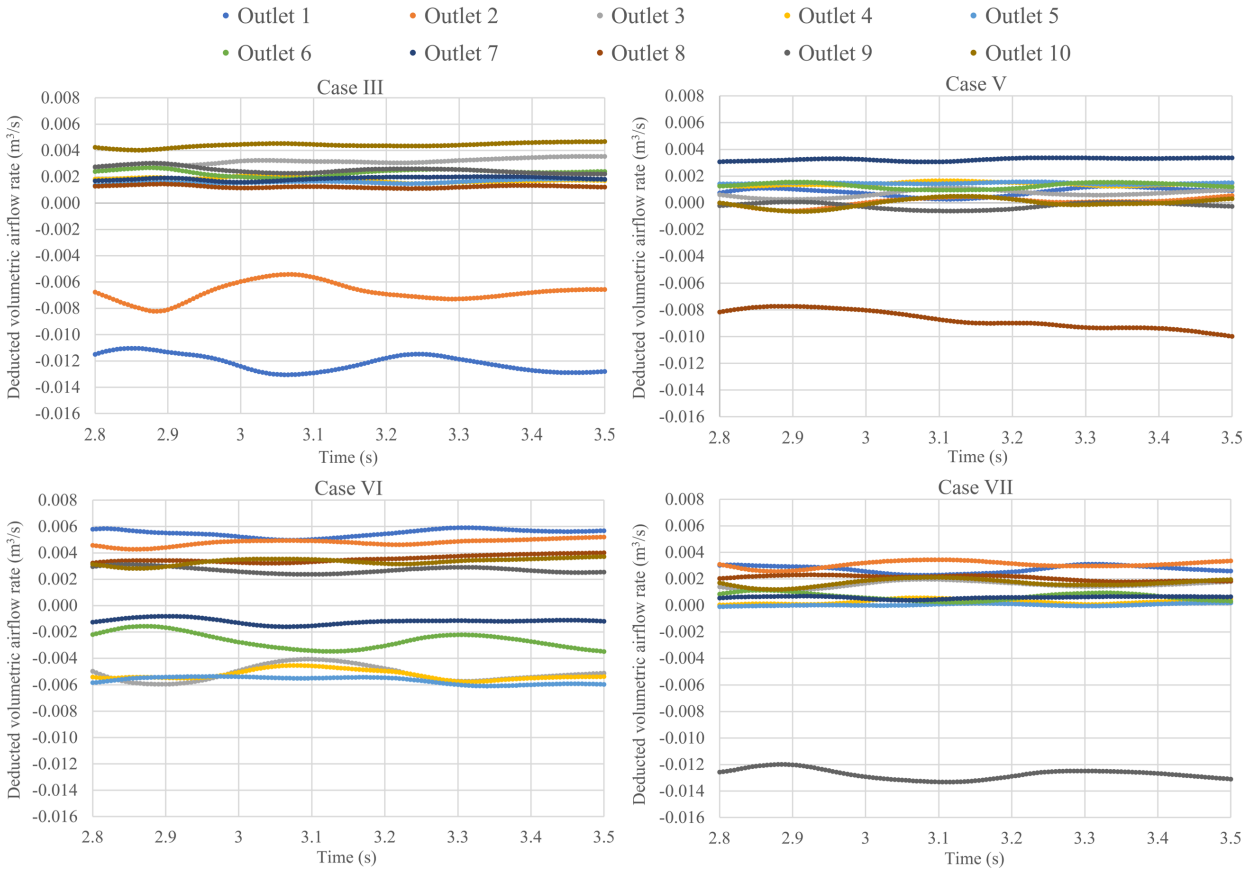


Figure 7-31: Deducted volumetric flow rate at ten openings during quasi-steady period for Cases III, V, VI and VII

It can be seen that the change of wind direction causes a different impact on the ten openings in the four cases. In Case III, airflow is induced into the indoor spaces through Openings 1 and 2 located in the windward façade, and Opening 8 observed an induced airflow into the interior spaces in Case V. In Case VI, 50% of the openings are in the windward façade, causing more airflows to leak into the indoor spaces, while in Case VII, only Opening nine encounters the incoming wind flows. These findings can be visualised in the perspective contour images of the velocity field in Figure 7-35.

The average of the processed volumetric flow rate of each opening is calculated and presented in Figure 7-32. In the graph, the openings with a negative value of volumetric airflow rate are those in the windward facades for the four cases. The velocity contour images in Figure 7-35 help to visualise that the outdoor air could be blown into the interior spaces via the windward openings, which causes indoor air cannot easily leak out during the Pulse test. In addition, the volumetric flow rate is smaller for the windward opening located on the upper level than the ground level. This is mainly due to the fact that the first-floor opening faces the wind at a higher speed than that on the ground floor.

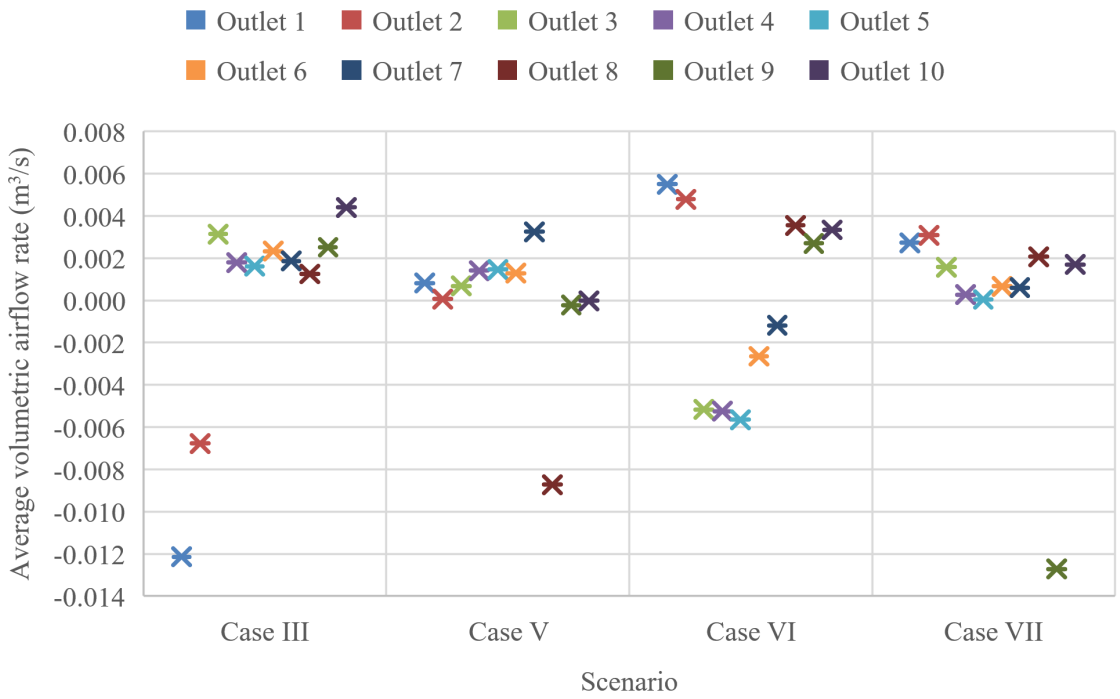


Figure 7-32: Average volumetric flow rate at ten openings during quasi-steady period for Cases III, V, VI and VII

Figure 7-33 presents the plot of the average indoor pressure against the total volumetric flow rate during the quasi-steady period for the four cases. The results demonstrate that the wind direction impact on the Pulse measurement is not as remarkable as that of the wind speed. At the average indoor pressure of 4Pa, the largest difference of the corresponding total volumetric flow rate is approximately 5.43%.

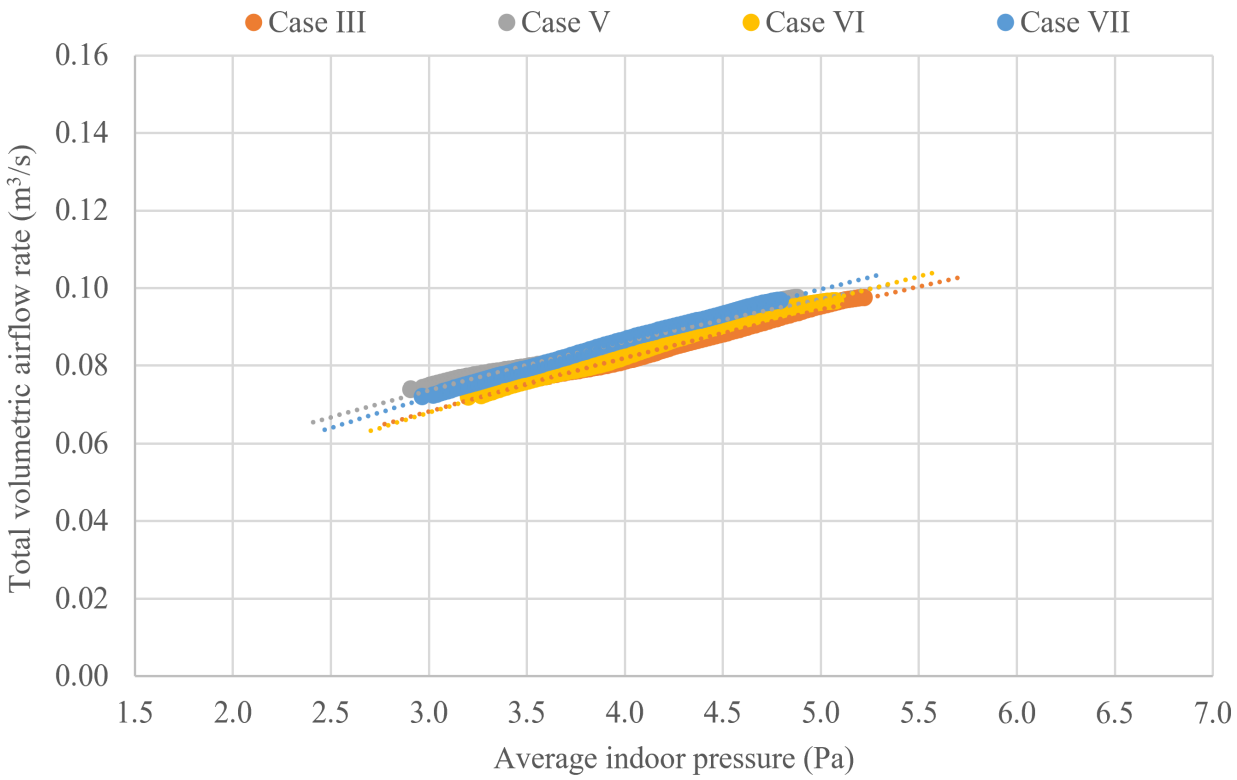
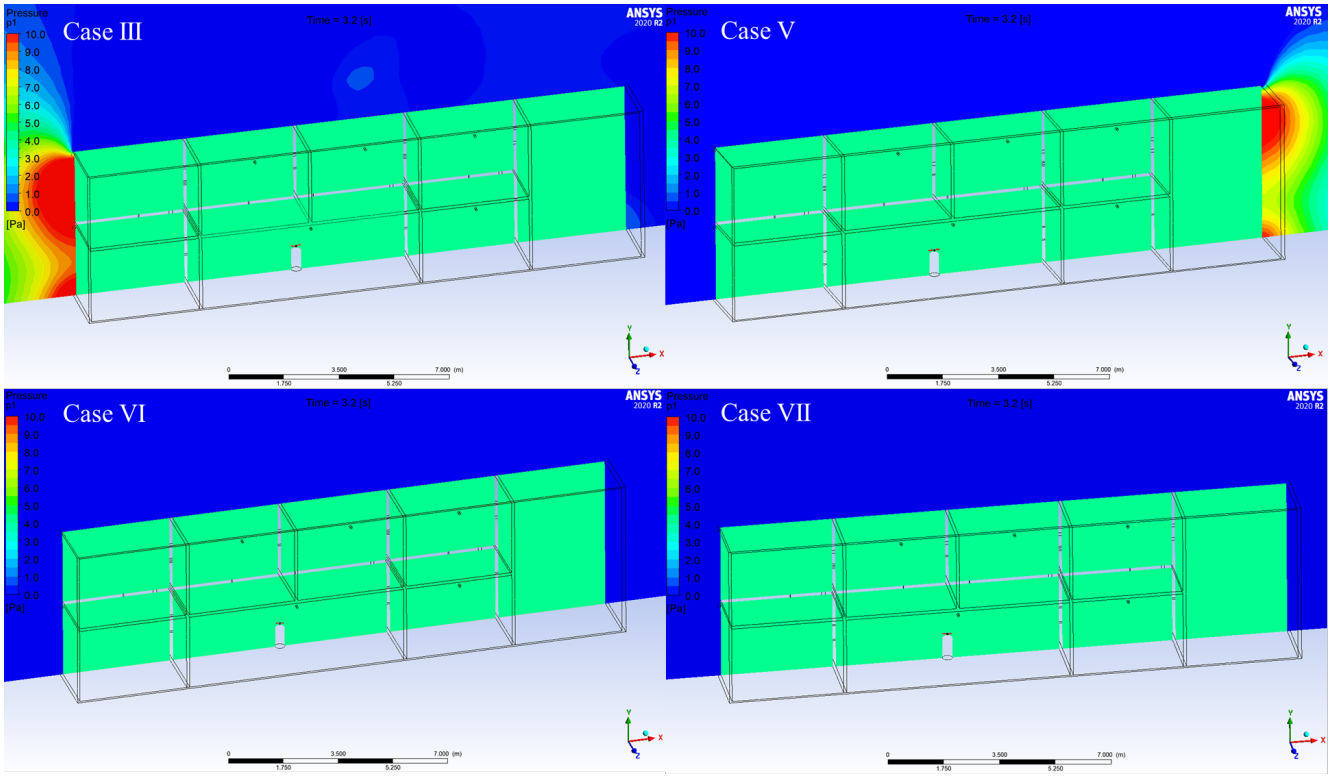
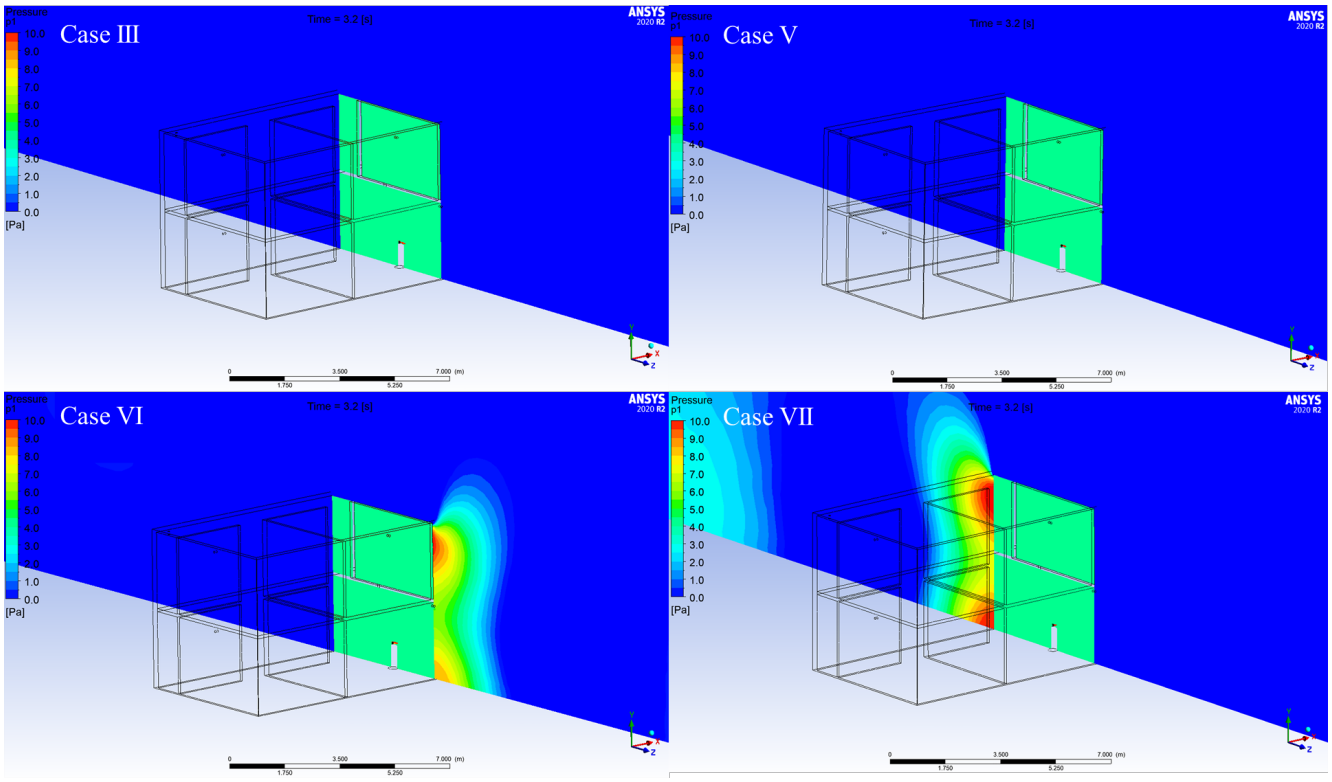


Figure 7-33: Plots of the average indoor pressure against the total volumetric flow rate of ten openings during the Pulse test for Cases III, V, VI and VII

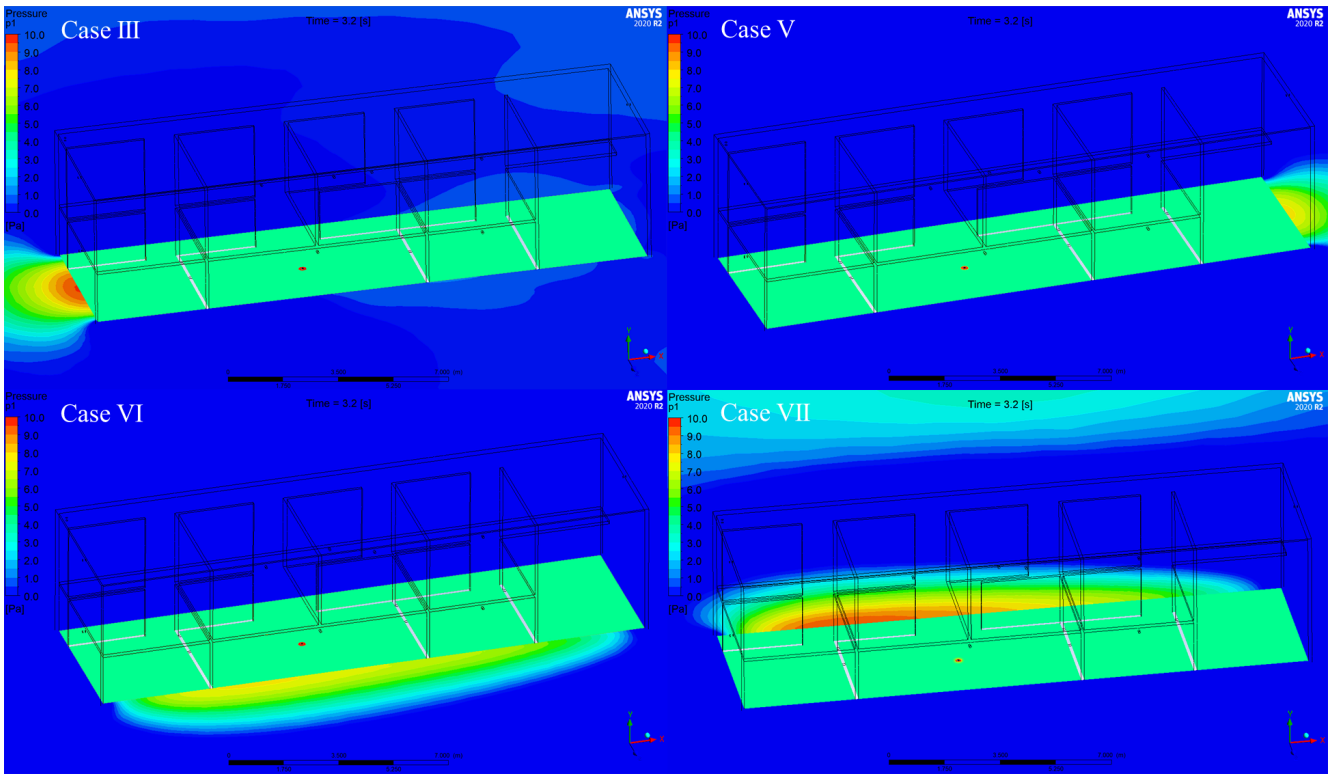
Figure 7-34 shows the perspective contour images of the indoor building pressure at 3.2s for the four cases, which depict the different wind pressure distributions around the building due to different wind directions for the four cases. As seen from both horizontal and vertical views, the indoor pressure would remain elevated in the areas with openings in the windward façade, owing to air being unable to move from the inside to the outside. However, the leakage speed could be accelerated if the leakage direction is in the same direction as that of the wind flows, which causes the indoor environment to have negative pressure. The multi-view contour images of the indoor air velocity at 3.2s for the four cases are provided in Figure 7-35. It can be clearly noticed that different velocity fields around the openings have resulted from the change of wind direction. The outdoor airflow could be induced into the indoor spaces via the windward openings during the Pulse test, while more airflow leaks out from the openings in the leeward façade, which lead to various volumetric airflow rates through different openings in the four cases.



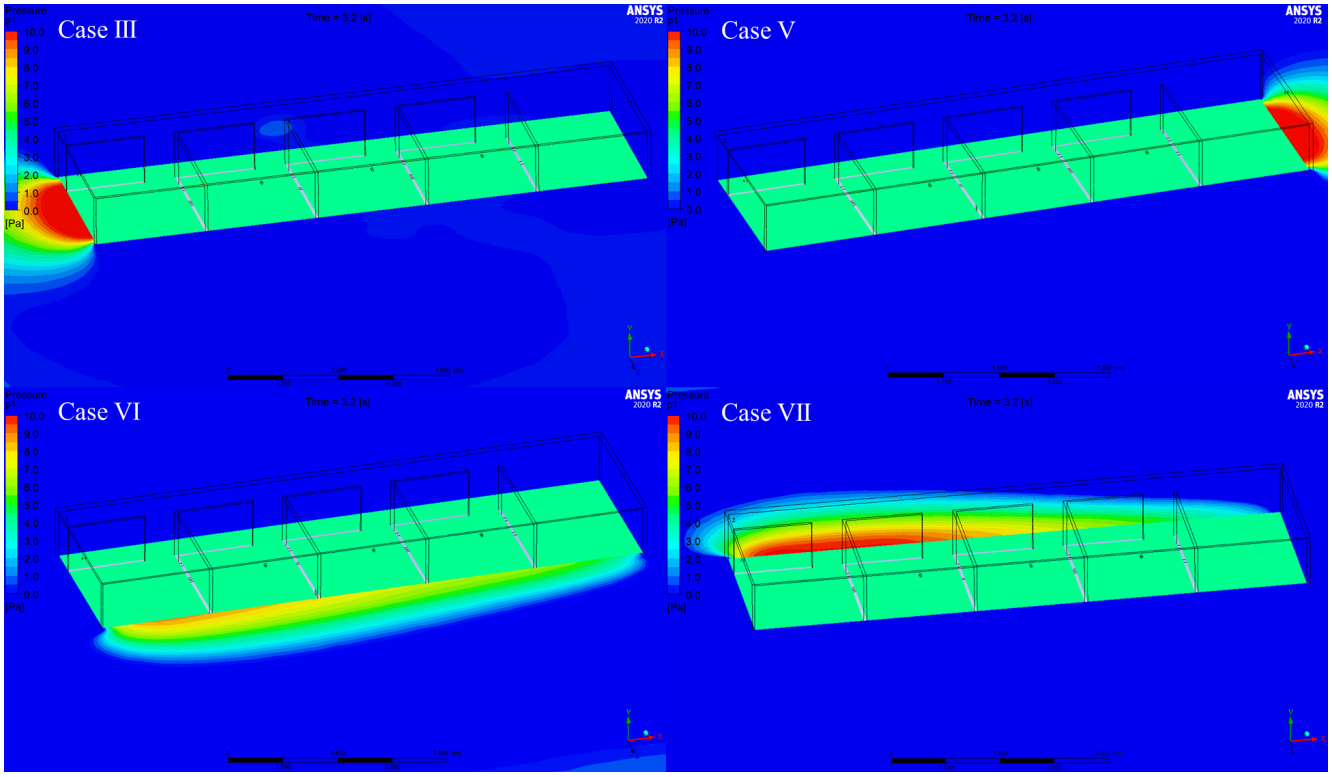
(a) Vertical front view



(b) Vertical side view

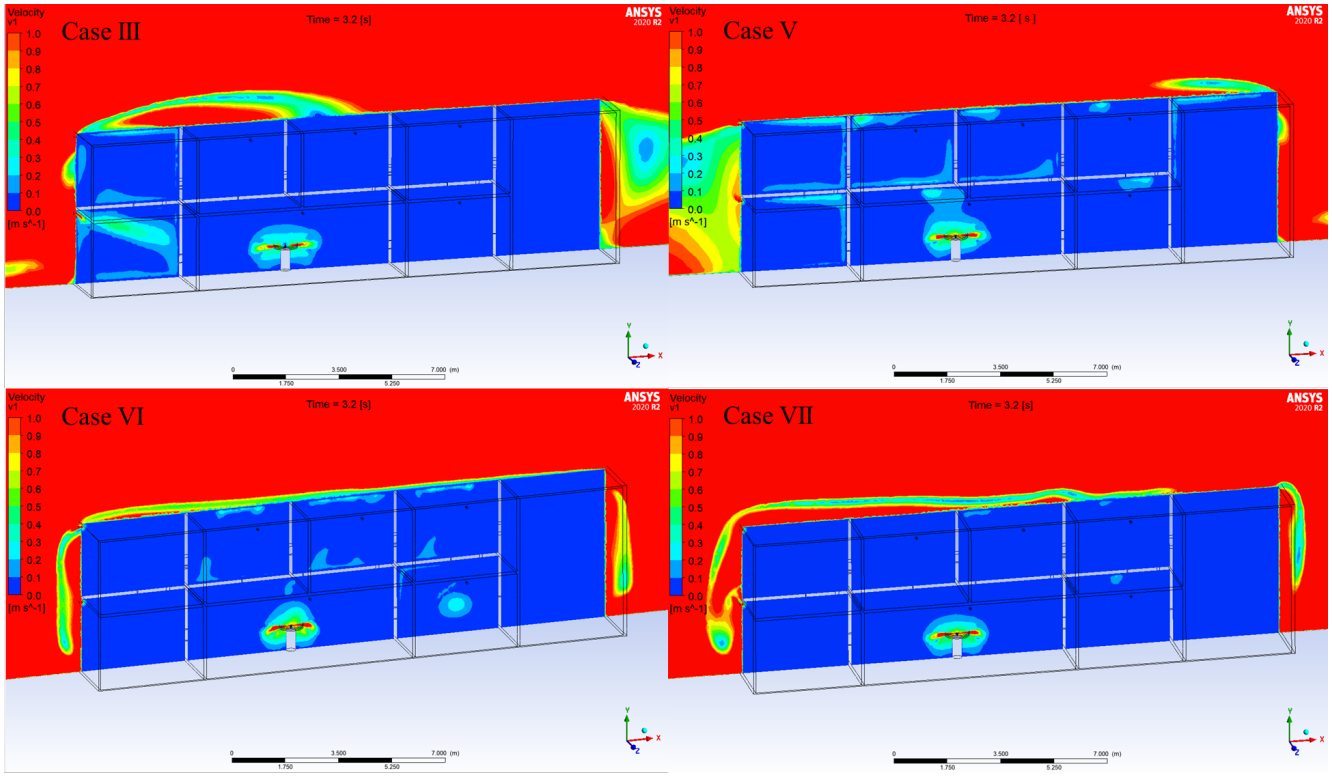


(c) Horizontal view of ground floor

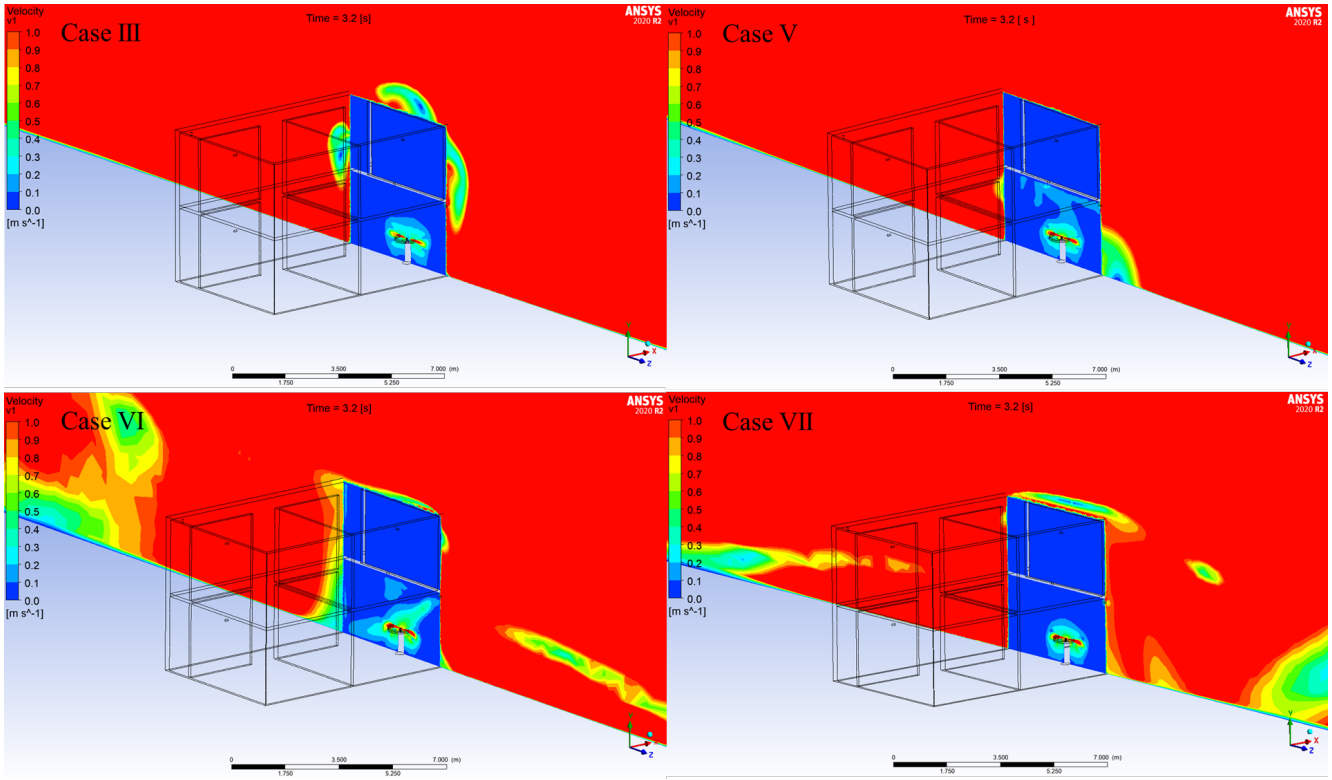


(d) Horizontal view of first floor

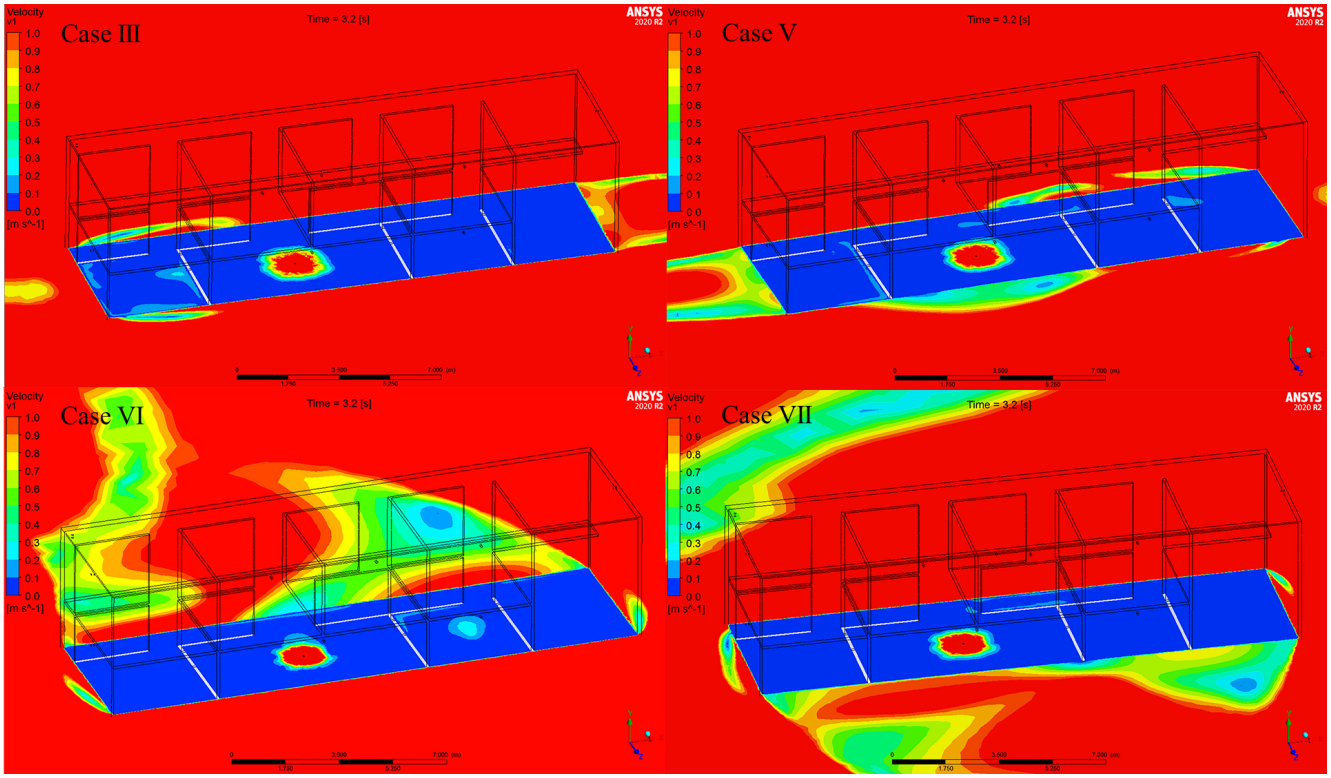
Figure 7-34: Perspective contour images of the indoor pressure at 3.2s for Cases III, V, VI and VII



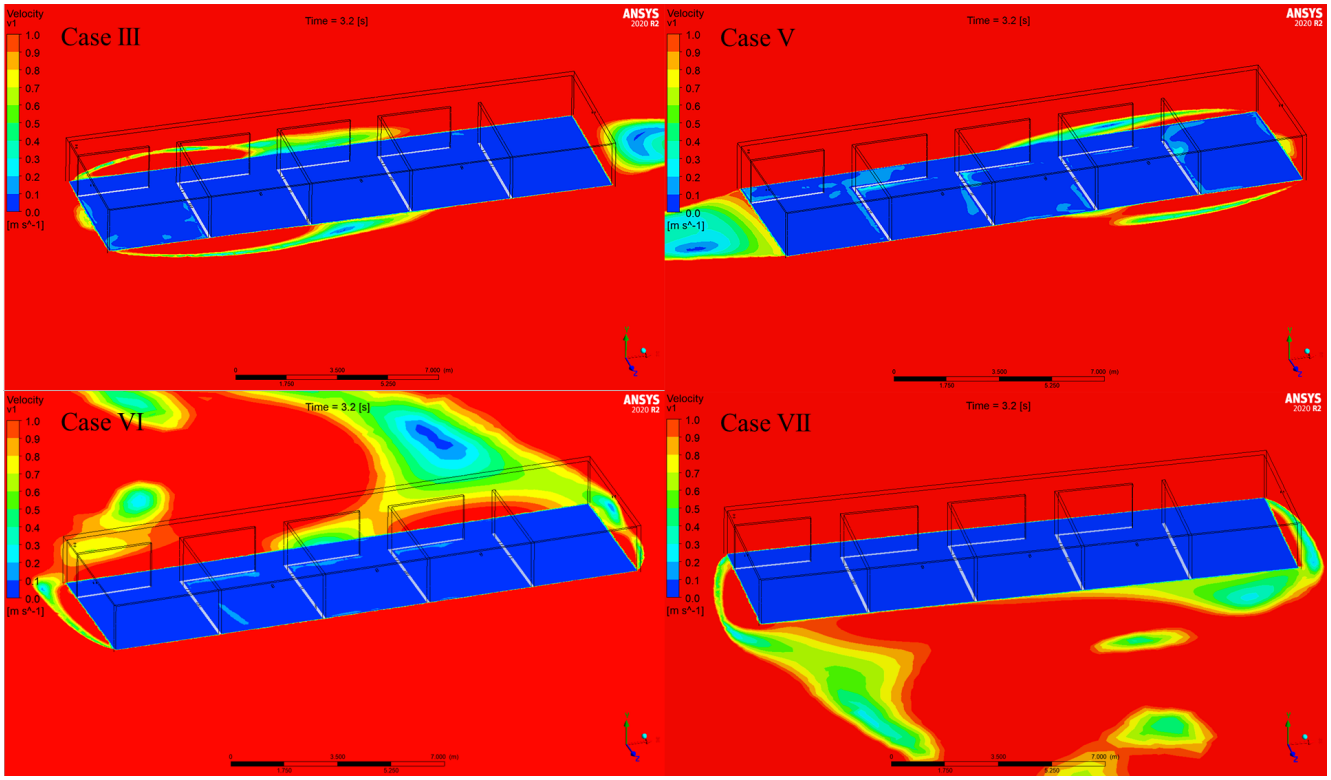
(a) Vertical front view



(b) Vertical side view



(c) Horizontal view of ground floor



(d) Horizontal view of first floor

Figure 7-35: Perspective contour images of the indoor air velocity at 3.2s for Cases III, V, VI and VII

7.6 Simulation of the Pulse test in a building with a gable roof

The most common roof types in the UK are the flat roof and the pitched type. In this section, extended simulations were implemented for a building model with a gable roof to evaluate the impact of the presence of a pitched roof on the indoor pressure distribution during the Pulse test and on the Pulse measurement by comparing with simulations of the building model with a flat roof.

7.6.1 Computational domain and configurations

The building model with a gable roof at a pitch angle of 45° is established, as shown in Figure 7-36. Two gable vents are created on opposite sides in the roof, offering ventilation of the attic space; thus, an equilibrium pressure between the attic and the outer domain would be achieved during the transient simulation.

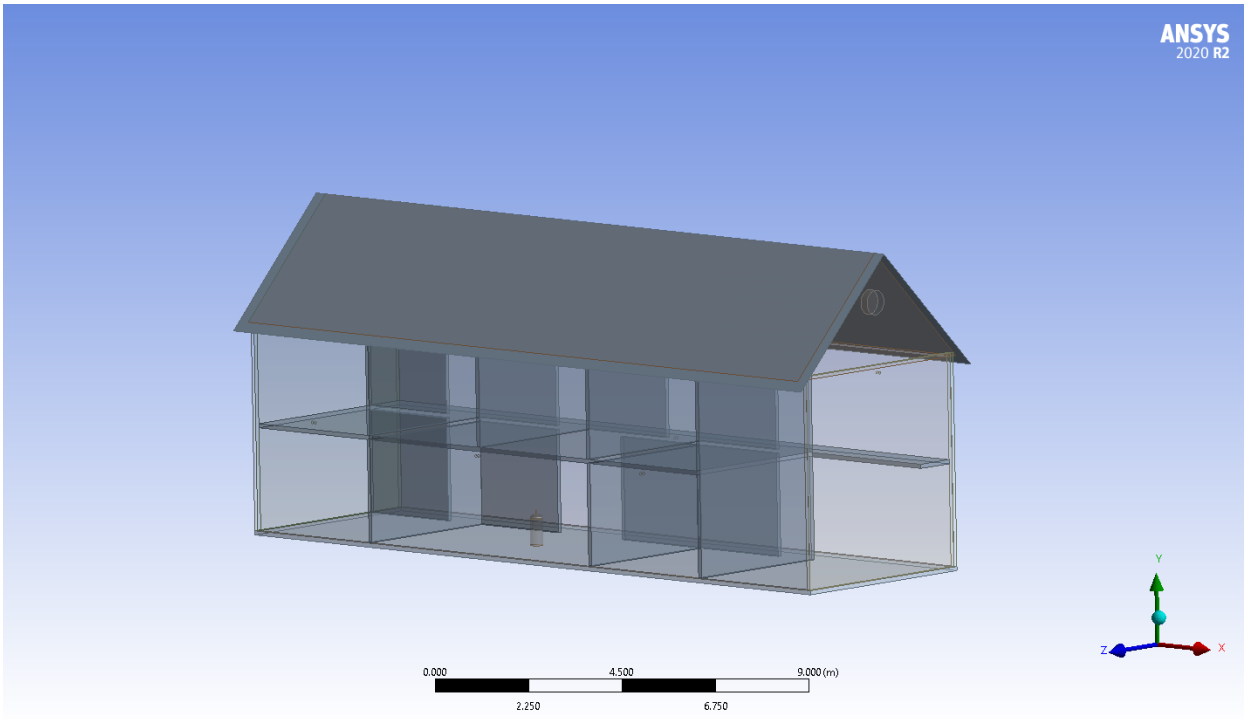


Figure 7-36: View of building model with a gable roof in Fluent

The same mesh configuration with the element size of 0.1m for the building model and 1m for the outer domain is adopted, which could provide a nearly grid-independent result. Same solver settings are applied, and the steady-state solution is firstly obtained for the initialisation of the transient simulation. In addition to the monitoring points mentioned in Section 7.3, three indoor monitoring points are added, as shown in Figure 7-37, including one in the centre of the attic area and two at the two gable vents to record the data of pressure, velocity, and air flow rate.

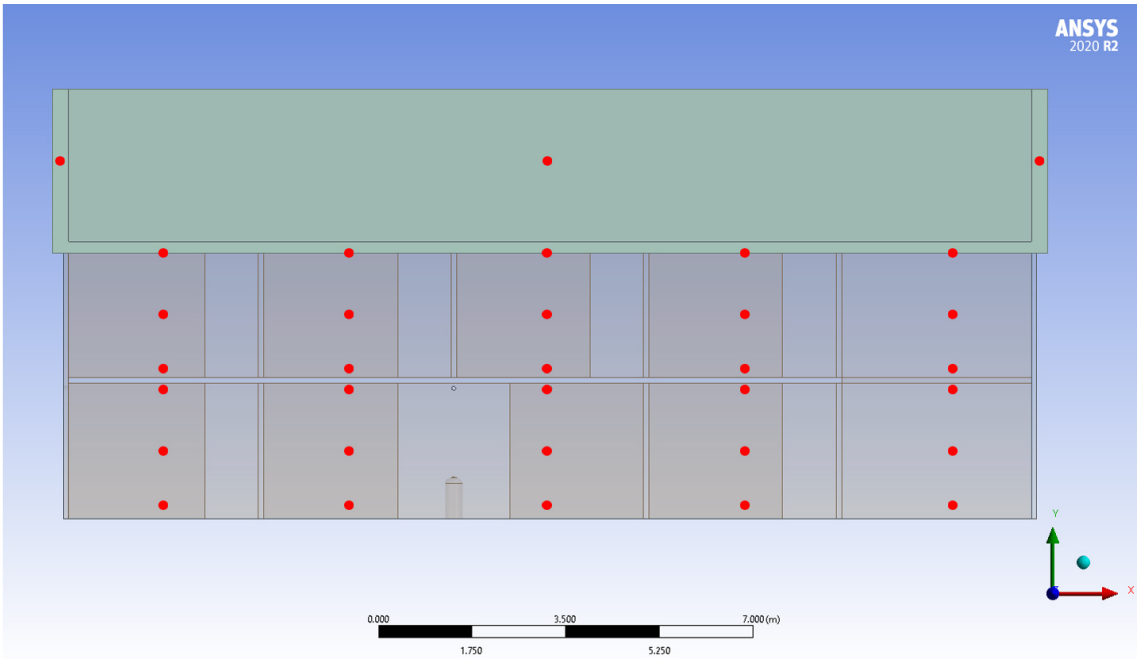


Figure 7-37: Front view of the location of indoor monitoring points

Considering the presence of the gable roof, two cases are proposed with different wind directions for comparing with the cases of a flat roof, which are: (1) Case VIII with the same wind condition of Case III, and (2) Case IX with the same wind direction of Case VI. The simulated wind condition of the two cases is illustrated in Figure 7-38.

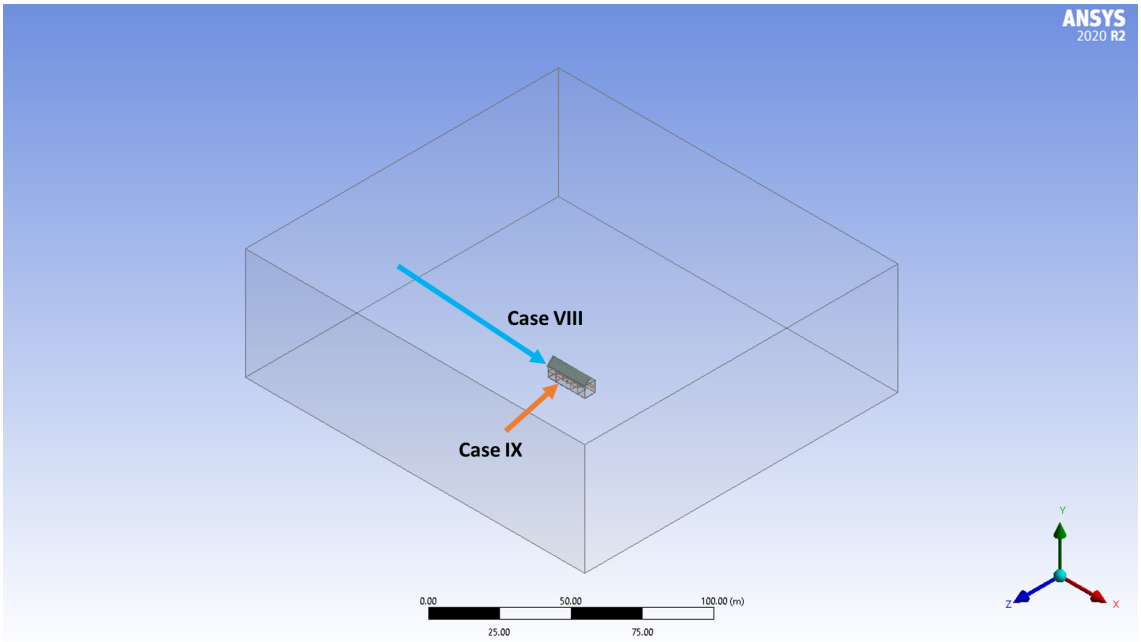


Figure 7-38: Illustration of Cases VIII and IX with different wind directions

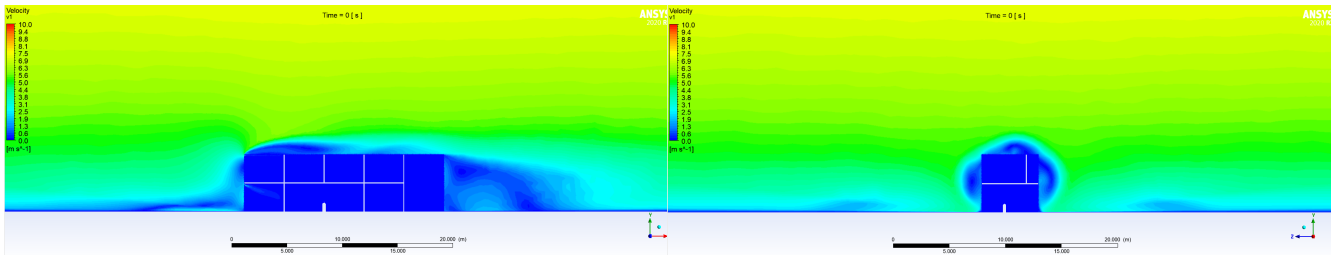
In this section, result analyses are conducted for four cases, including Cases III, VIII, VI and IX, for the comparison between the building with a flat roof and the building with a gable roof. Table 7-15 lists the detailed configuration for the four cases.

Table 7-15: Building configuration and wind condition for Cases III, VIII, VI and IX

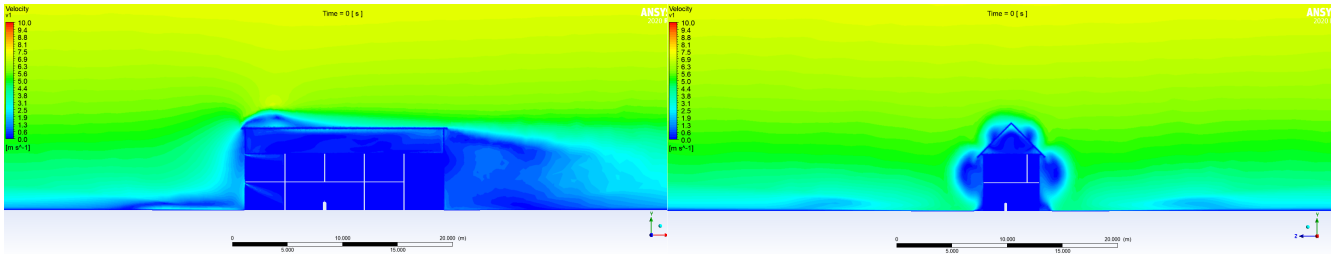
Case	Roof Type	Wind Direction (Coordinate Axis)	Wind Speed	
			At 1m above Ground	At 10m above Ground
III	Flat	along positive x-axis	3m/s	6m/s
VIII	Gable	along positive x-axis	3m/s	6m/s
VI	Flat	along negative z-axis	3m/s	6m/s
IX	Gable	along negative z-axis	3m/s	6m/s

The contour images of Cases III, VIII, VI and IX, are presented in Figure 7-39, showing the different airflow patterns around the building at the beginning of the transient simulations for cases with a flat roof and a gable roof. The contour images also depict how the wind flows over the gable roof under two different wind direction conditions.

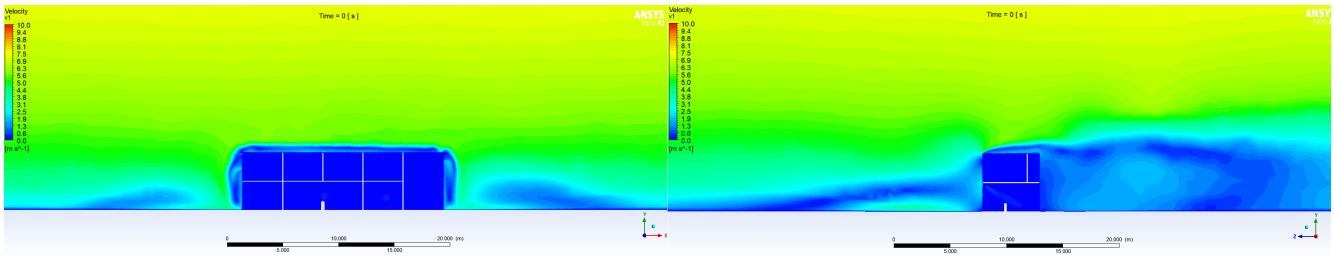
Front view Side view



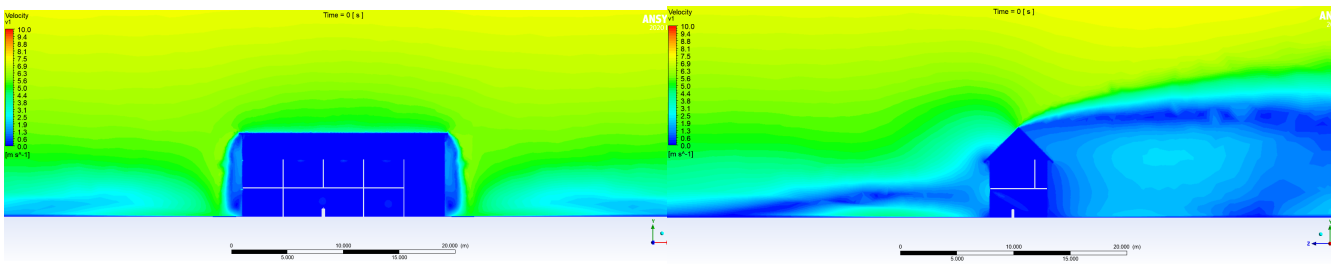
(a) Case III with a flat roof (wind direction: along positive x-axis)



(b) Case VIII with a gable roof (wind direction: along positive x-axis)



(c) Case VI with a flat roof (wind direction: along negative z-axis)



(d) Case IX with a gable roof (wind direction: along negative z-axis)

Figure 7-39: Contour images of the simulated wind condition at 0s for Cases III, VIII, VI and IX

7.6.2 Comparison of indoor pressure distribution

The same result process method was adopted as presented in Section 7.4.2 and 7.5.2, Figure 7-40 presents the variations of each room pressure and the overall average indoor pressure during the Pulse test for the four cases.

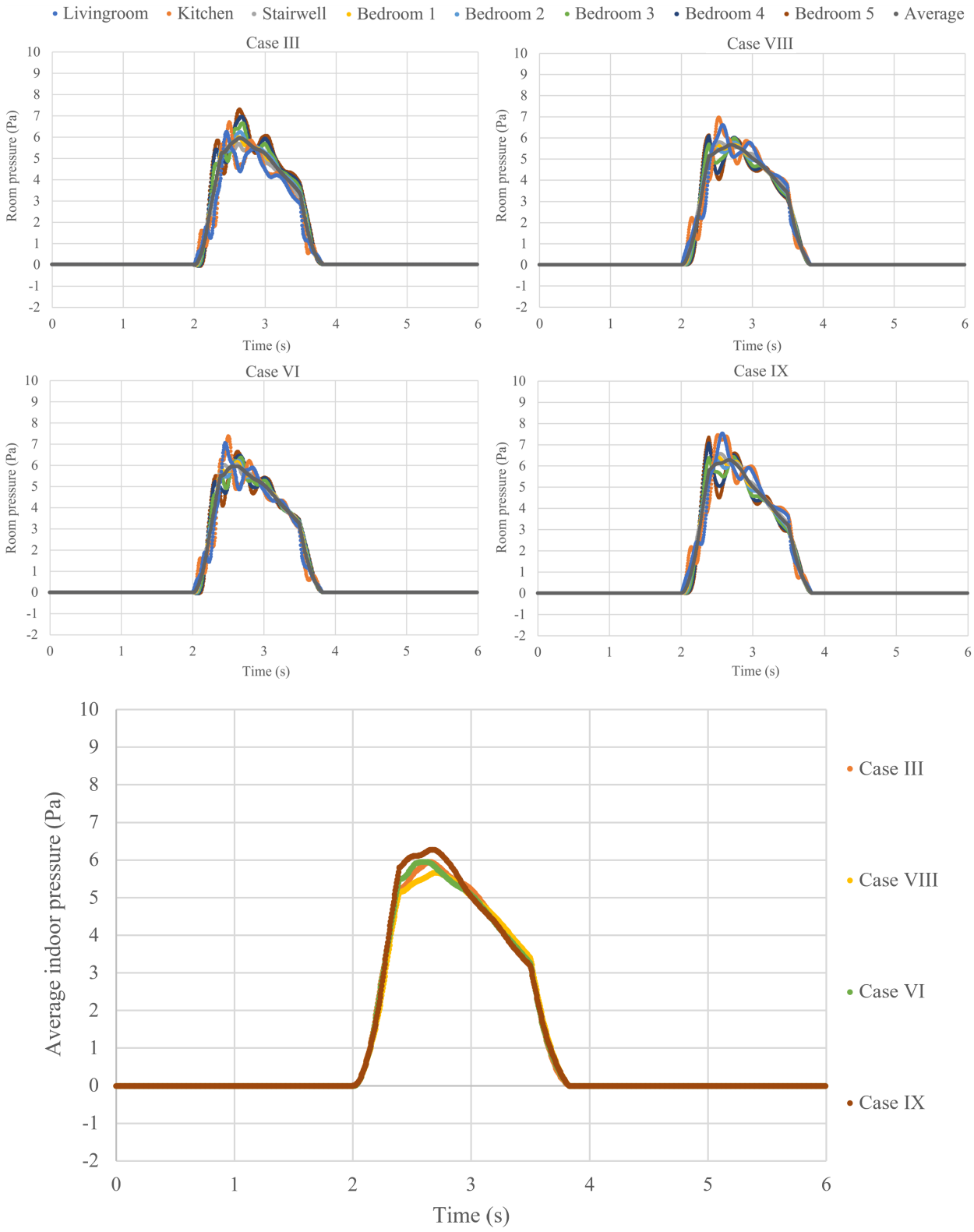


Figure 7-40: Pressure curves of each room and overall average during the Pulse test for Cases III, VIII, VI and IX

It can be seen that the presence of the gable roof results in different indoor pressure curves from those of the flat roof. For instance, for the wind direction along the positive x-axis, the peak room pressures during the Pulse test in Case VIII with a gable roof are smaller than those of Case III with a flat roof. For the wind flowing along the negative z-axis, Case IX with a gable roof has higher peak room pressures than Case VI with a flat roof.

Table 7-16 presents the corresponding time points A and B for each case. Although Case III and Case VIII have different roof geometries, the time point A varies very slightly; for instance, the average point A is approximately at 2.310s in Case III, and Case VIII is at 2.330s. In terms of the average Point B, the difference between Case III and VIII is 0.030s, between Case VI and Case IX, is only approximately 0.020s. The results indicate that the presence of the gable roof results in a minor effect on time points A and B during the Pulse test of the established building model.

Table 7-16: Time points A and B for Cases III, VIII, VI and IX

	Case III		Case VIII		Case VI		Case IX	
Time Point (s)	A	B	A	B	A	B	A	B
Living Room	2.355	3.255	2.380	3.265	2.345	3.320	2.380	3.350
Kitchen	2.355	3.265	2.385	3.280	2.345	3.325	2.390	3.370
Stairwell	2.330	3.310	2.345	3.360	2.325	3.280	2.320	3.305
Bedroom 1	2.335	3.255	2.360	3.310	2.325	3.290	2.345	3.315
Bedroom 2	2.325	3.345	2.320	3.350	2.320	3.270	2.300	3.295
Bedroom 3	2.265	3.355	2.300	3.360	2.270	3.255	2.290	3.260
Bedroom 4	2.260	3.350	2.290	3.385	2.260	3.230	2.280	3.230
Bedroom 5	2.250	3.355	2.245	3.390	2.230	3.215	2.240	3.215
Average*	2.310	3.310	2.330	3.340	2.305	3.275	2.320	3.295
Maximum Difference**	0.105	0.100	0.135	0.125	0.115	0.105	0.140	0.135

*Average Points A and B are obtained based on the average pressure of all rooms.
**Maximum difference is based on the comparison of Points A/B of each room with that of the living room.

7.6.3 Comparison of simulated air leakage rate

Table 7-17 presents the calculated ARLs based on the room pressures for the four cases. The same benchmark (i.e., the air leakage rate that is calculated based on the simulated pressure variation in the living room in Case I) was selected to calculate the *RPD*s, and the calculated *RPD*s for the four cases are shown in Table 7-17. The average air leakage rate of Case III with a flat roof is only approximately 1.25% higher than that of Case VIII with a gable roof, while the average air leakage rates of Case VI with Case IX are similar (only deviates by 0.5%). There is a slight

difference in the average *RPD* between Case III and VIII (i.e., by -1.19%), which could be attributed to the change in the wind pressure distribution around the building by different roof geometries. The difference becomes less significant by comparing Case VI and Case IX, with approximately 0.49% difference in the average *RPD*. Therefore, the comparisons of the simulated ALRs and *RPD*s between the cases of a flat roof and a gable roof demonstrate that the Pulse measurement of the established building model was insignificantly influenced by the change in the roof geometry.

Table 7-17: Calculated ALRs and *RPDs* for Cases III, VIII, VI and IX

	Case III		Case VIII		Case VI		Case IX	
	ALR	*RPD*	ALR	*RPD*	ALR	*RPD*	ALR	*RPD*
Living Room	0.08730	-2.64%	0.08504	-5.17%	0.08047	-10.29%	0.07915	-11.77%
Kitchen	0.08396	-6.38%	0.08340	-7.01%	0.07937	-11.53%	0.07855	-12.44%
Stairwell	0.08429	-6.02%	0.08236	-8.18%	0.08495	-5.28%	0.08454	-5.74%
Bedroom 1	0.08449	-5.79%	0.08263	-7.87%	0.08391	-6.44%	0.08367	-6.71%
Bedroom 2	0.08457	-5.70%	0.08211	-8.46%	0.08603	-4.07%	0.08552	-4.64%
Bedroom 3	0.08592	-4.19%	0.08281	-7.67%	0.08770	-2.20%	0.08558	-4.57%
Bedroom 4	0.08676	-3.25%	0.08336	-7.06%	0.08854	-1.25%	0.08679	-3.21%
Bedroom 5	0.08598	-4.12%	0.08294	-7.53%	0.08882	-0.94%	0.08588	-4.23%
Average*	0.08480	-5.44%	0.08374	-6.63%	0.08559	-4.56%	0.08515	-5.05%

*The average air leakage rate of each case is calculated based on the average indoor pressure of all rooms.

7.6.4 Comparison of the air flow rate of openings

Figure 7-41 shows the volumetric airflow rate variation at each opening during the Pulse test for the four cases. As Case III and Case VIII are implemented at the same wind direction (i.e., along the positive x-axis), both cases have lower volumetric airflow rates at Opening 1 and Opening 2 on the windward façade. Differently, Case VIII observers a low volumetric airflow rate at Opening 10 located at the first-floor ceiling level. For the building with a gable roof, the outdoor wind could be blown into the attic space through the gable vent; thus, a negative airflow rate is noted at Opening 10 prior to the air pulse release, indicating that air could enter through. In terms of Case VI and Case IX with the wind direction along the negative z-axis, Openings 3, 4, 5, 6 and 7 have much lower airflow rates as they are located on the windward side.

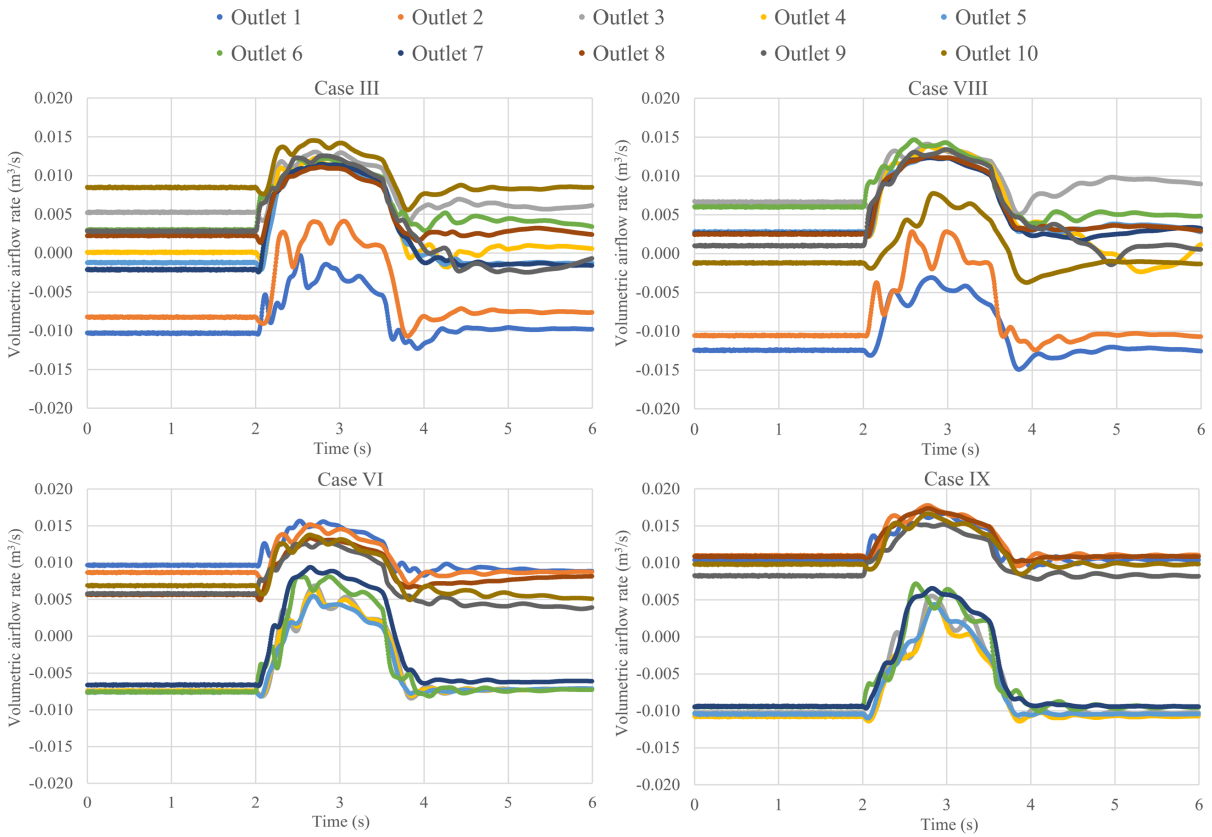


Figure 7-41: Variations of volumetric flow rate at ten openings during the Pulse test for Cases III, VIII, VI and IX

The total volumetric airflow rate of the ten openings is plotted in Figure 7-42 for each case, which shows that all four cases have similar variations of the total volumetric flow rate, especially during the quasi-steady period from 3.0s to 3.5s.

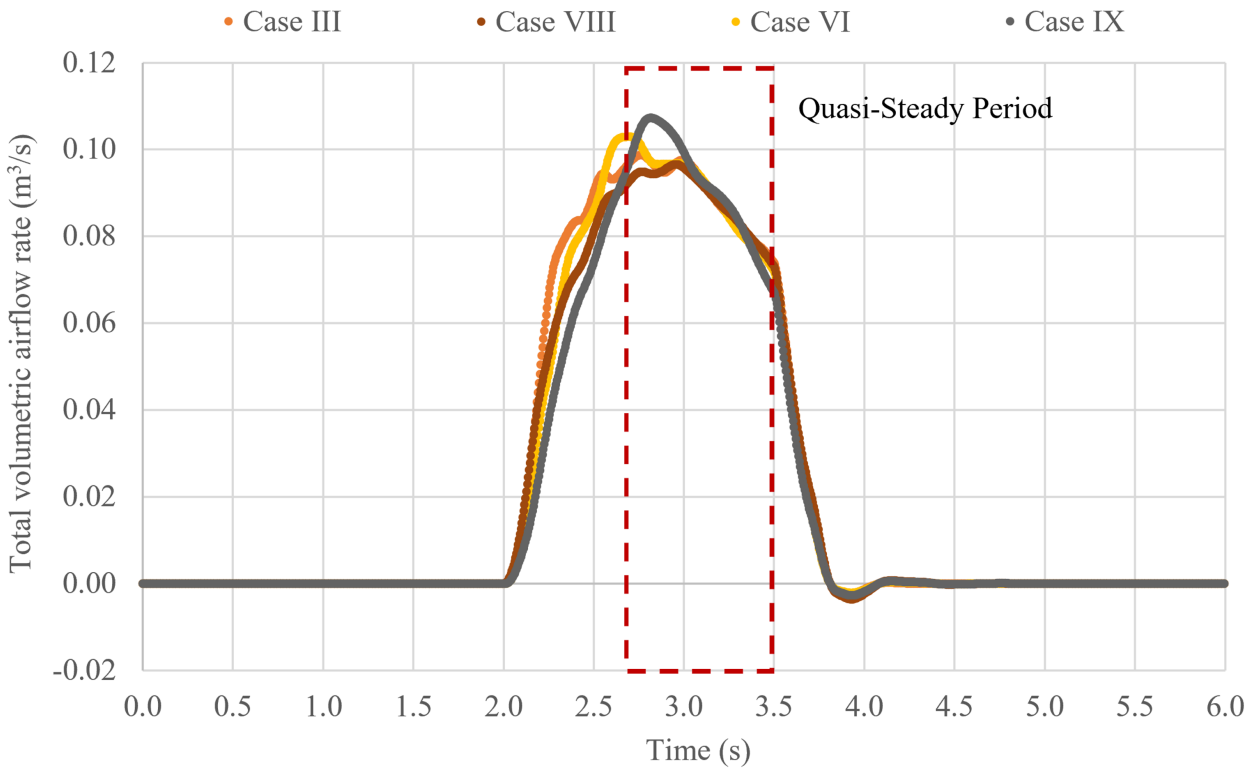
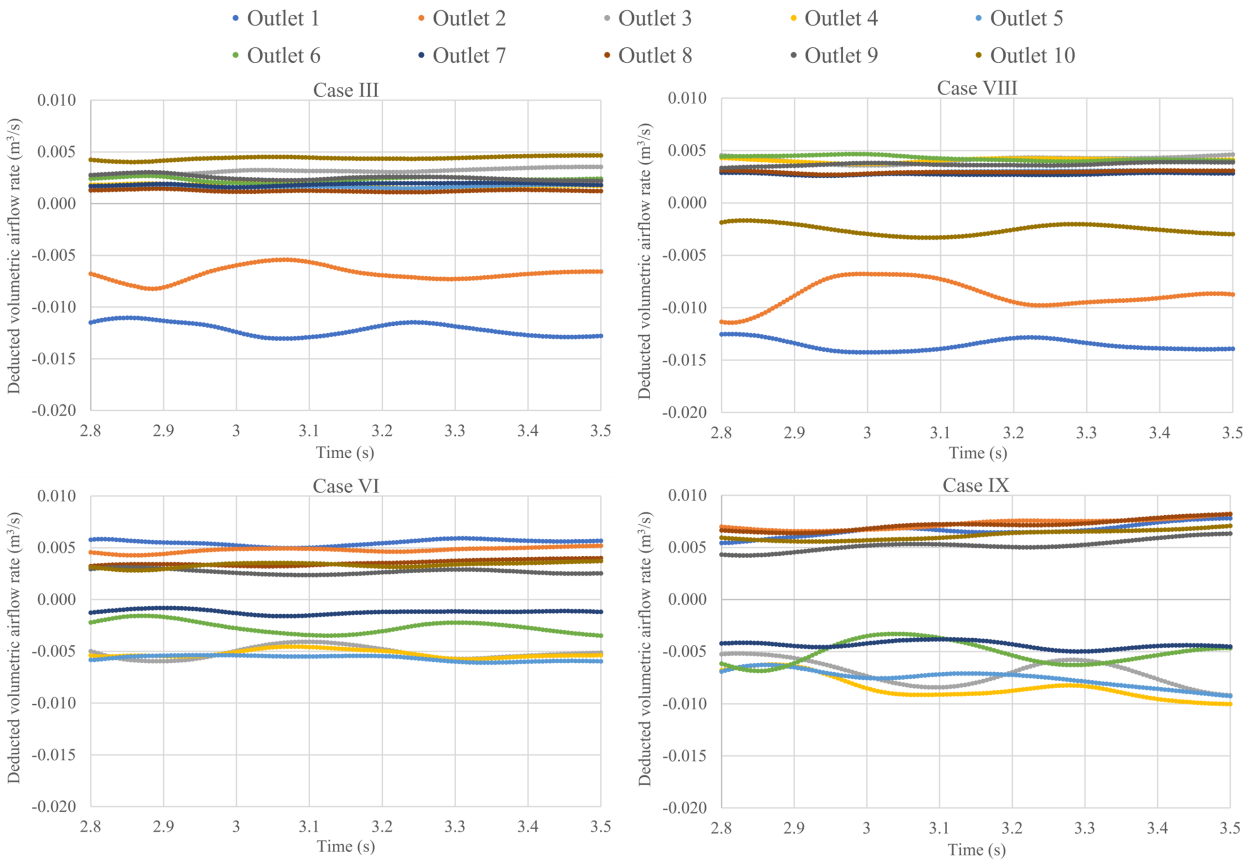
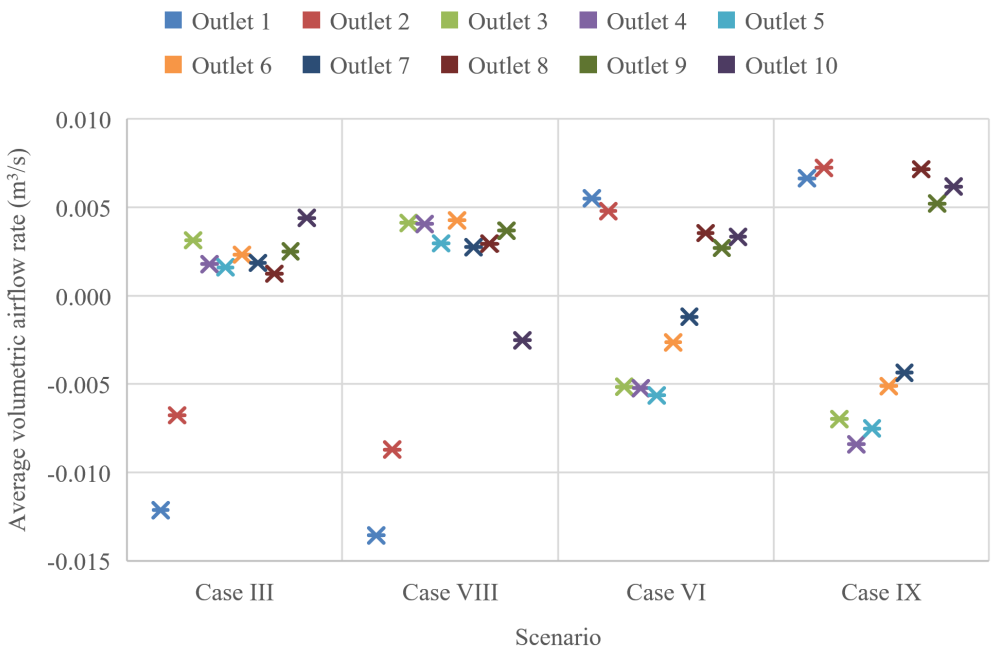


Figure 7-42: Total volumetric flow rate of ten openings during the Pulse test for Cases III, VIII, VI and IX

Figure 7-43a presents the plots of the processed volumetric flow rate of each opening for the four cases, which were calculated based on the same method as mentioned in Section 7.4.4 and 7.5.4. Based on the data presented in Figure 7-43(a), the averaged volumetric flow rate at each opening can be calculated and plotted in Figure 7-43(b). The results show a noticeable variation of the deducted volumetric airflow rate at Opening 10 between Case III with a flat roof and Case VIII with a gable roof. In Case III, with a flat roof, the airflows leak out from Opening 10 during the quasi-steady period; contrarily, the airflow is induced into the indoor spaces through Opening 10 in Case VIII with a gable roof, which is attributed to the increased pressure in the loft. The noticeable difference in the average volumetric flow rate can also be observed in Figure 7-43(b). In terms of Case VI and IX, more noticeable variations on the volumetric flow rate of the openings on the windward wall are seen in Case IX with a gable roof. For Case VI and IX, the averaged volumetric flow rate at the first-floor's Openings 3, 4, 5 deviate significantly from that of Openings 6 and 7 located on the ground floor, which may be due to the higher wind speed at a higher level above ground level.



(a)



(b)

Figure 7-43: (a) Deducted volumetric flow rates and (b) average volumetric flow rates at ten openings during quasi-steady period for Cases III, VIII, VI and IX

Figure 7-44 presents the plot of the average indoor pressure against the total volumetric flow rate during the quasi-steady period for the four cases. The results reveal that the roof type has a minor impact on the Pulse measurement of the building model. For instance, at the average indoor pressure of 4Pa, the difference of the corresponding total volumetric flow rate is approximately 0.50% between Case III and Case VIII with two different roof geometries, and the difference is 3.65% with the comparison between Case VI and Case IX.

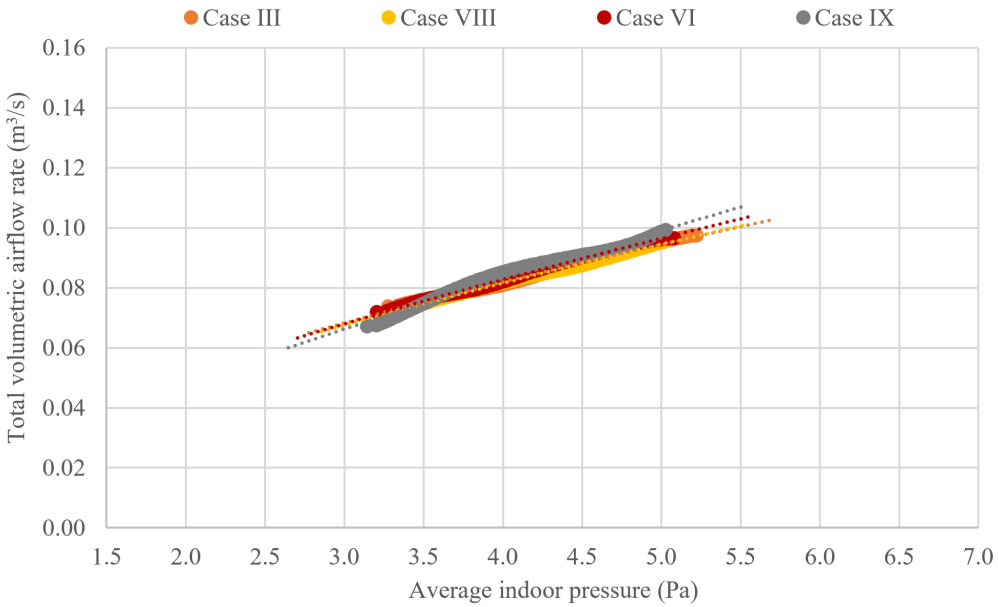
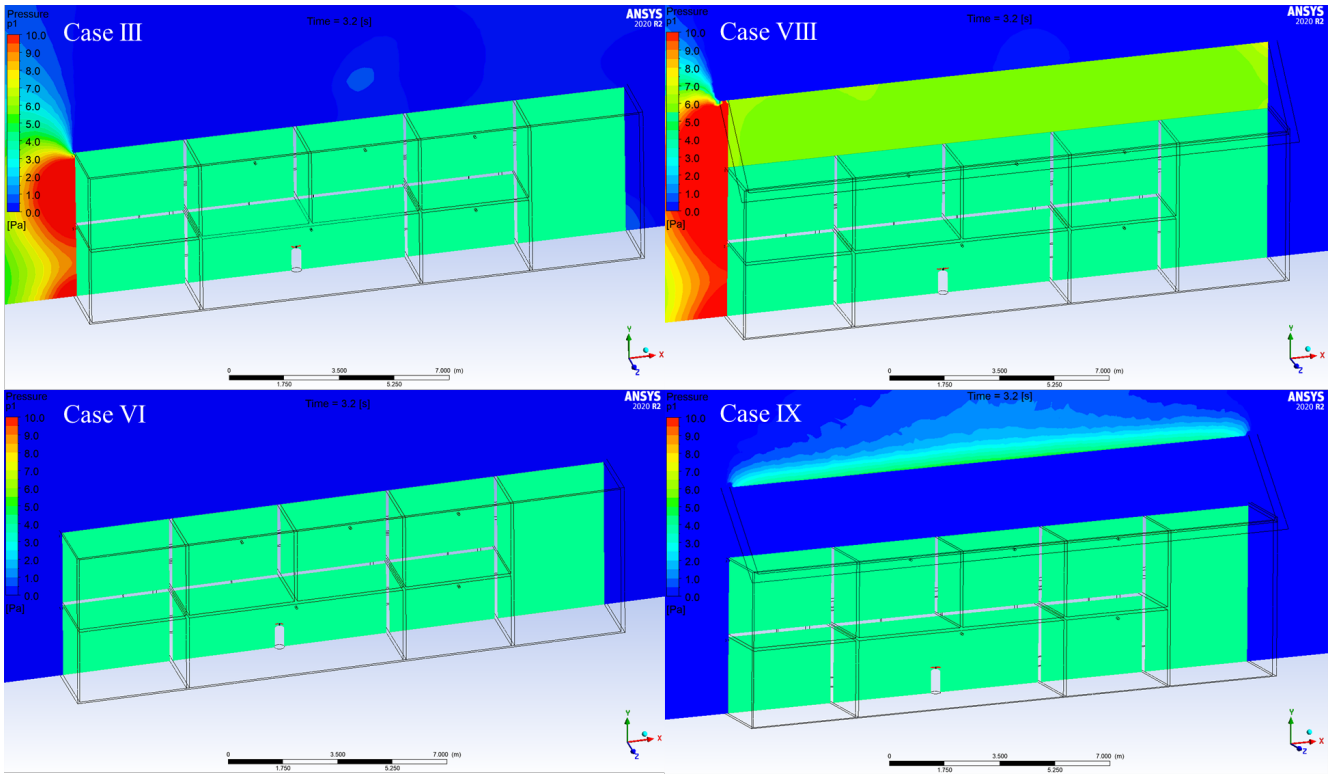
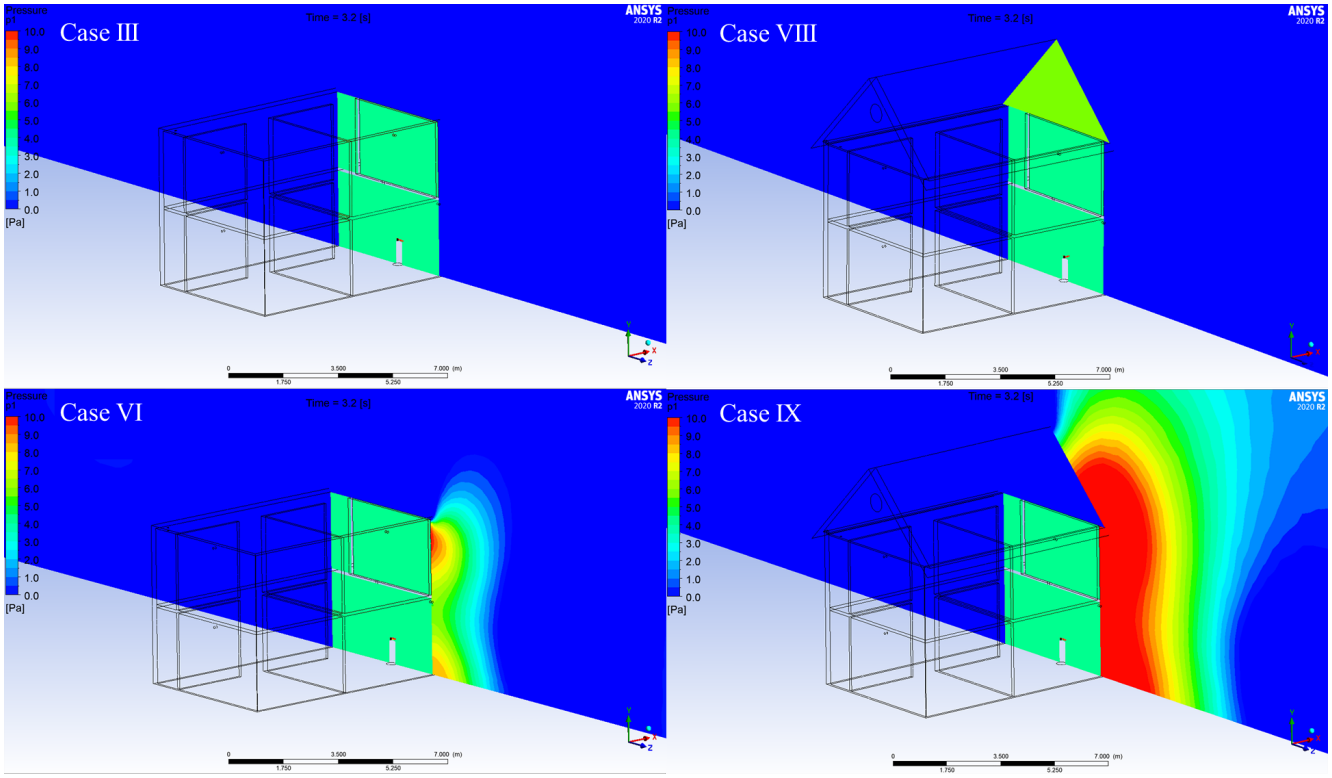


Figure 7-44: Plots of the average indoor pressure against the total volumetric flow rate of ten openings during the Pulse test for Cases III, VI, VIII and IX

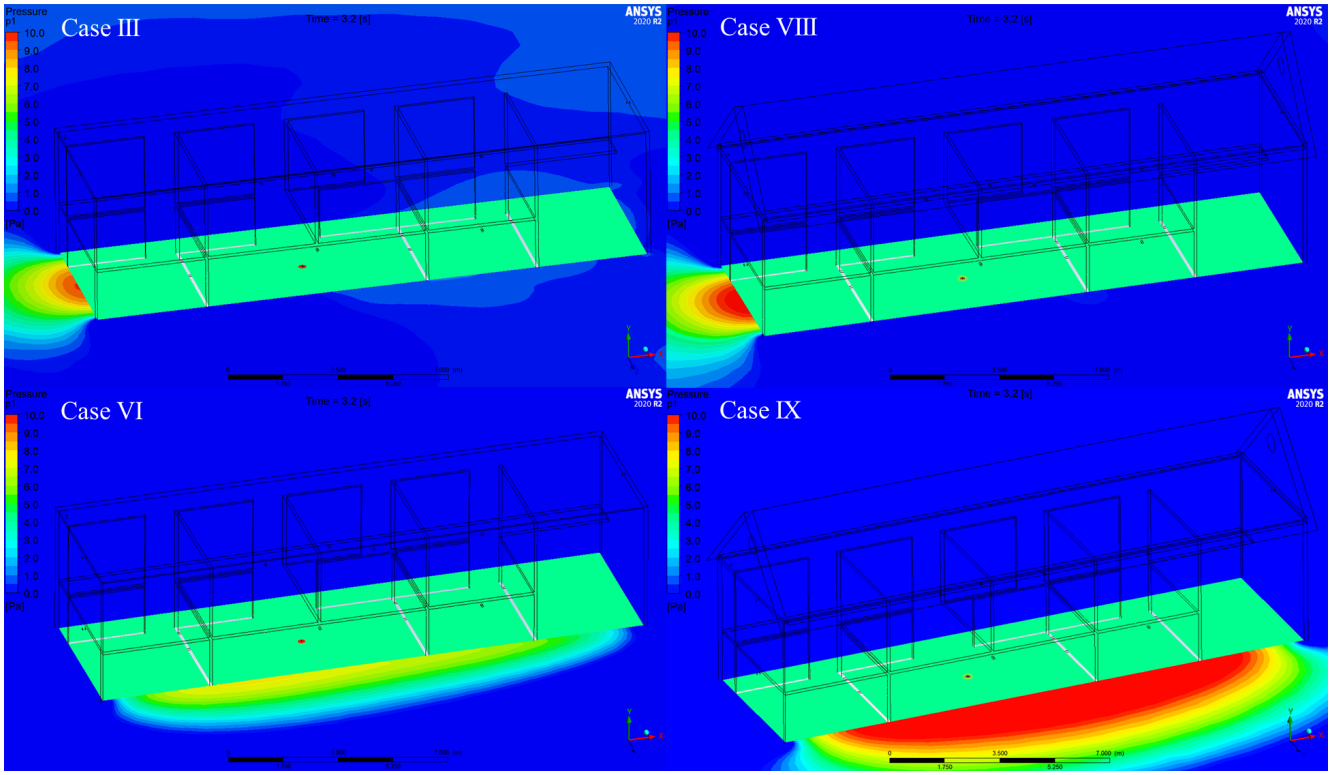
Figure 7-45 and Figure 7-46 show the perspective contour images of the indoor pressure and velocity during the quasi-steady period (i.e., at 3.2s) for the two cases with a flat roof and two cases with a gable roof. It can be observed from the horizontal and vertical views; there is an increased pressure inside the loft space when the wind flows along the positive x-axis, while the pressure inside the loft is equalised with the outdoor condition when the wind flows along the negative z-axis. On the other hand, the multi-view contour images help to visualise that the wind flows into the indoor spaces as well as the loft space through the windward openings in Case VIII, while no wind is observed in the loft space in Case IX due to the different wind conditions.



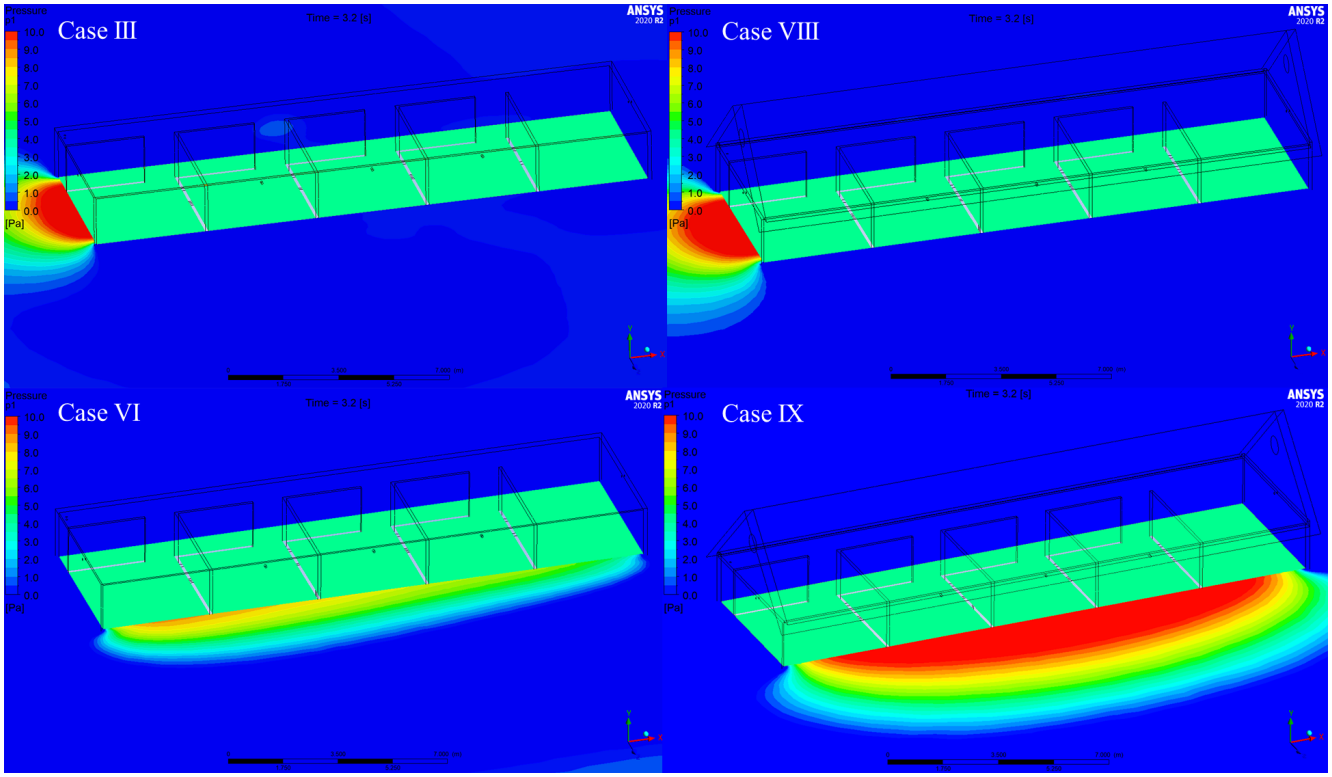
(a) Vertical front view



(b) Vertical side view

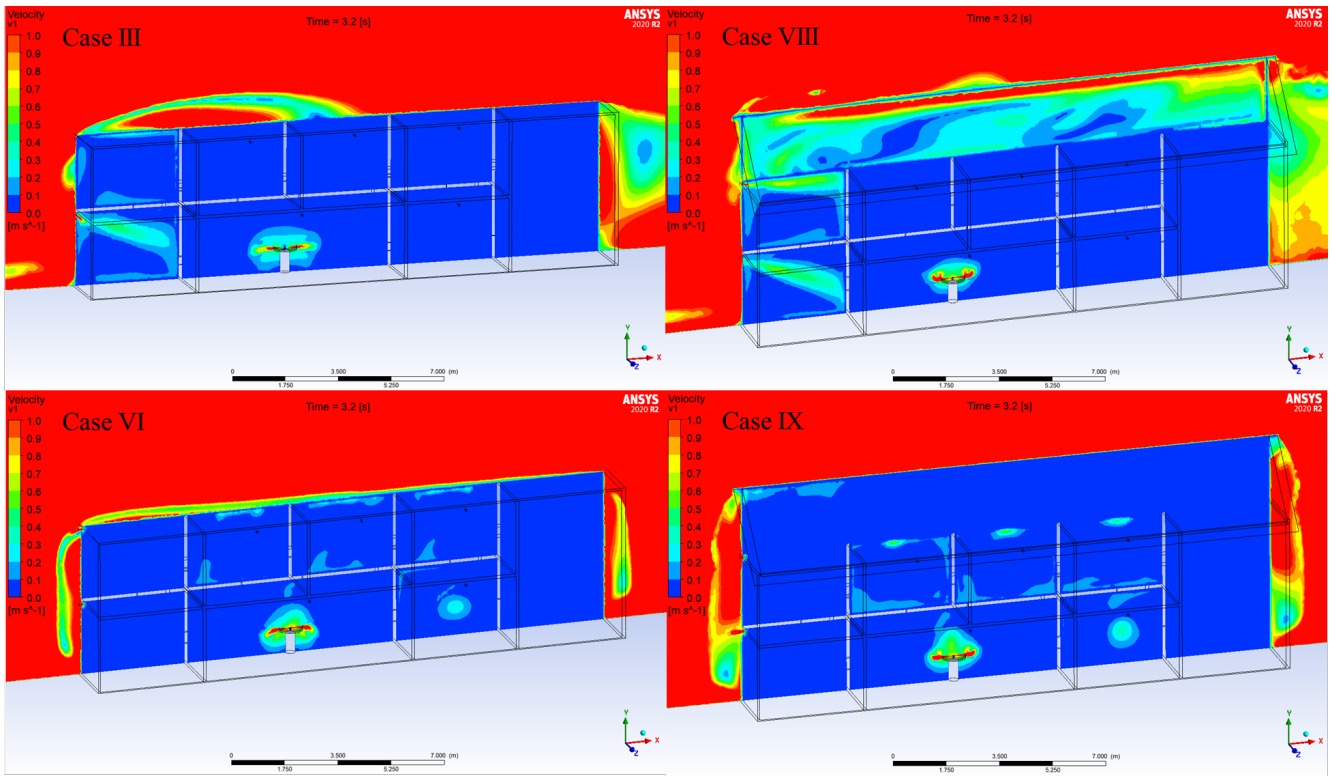


(c) Horizontal view of ground floor

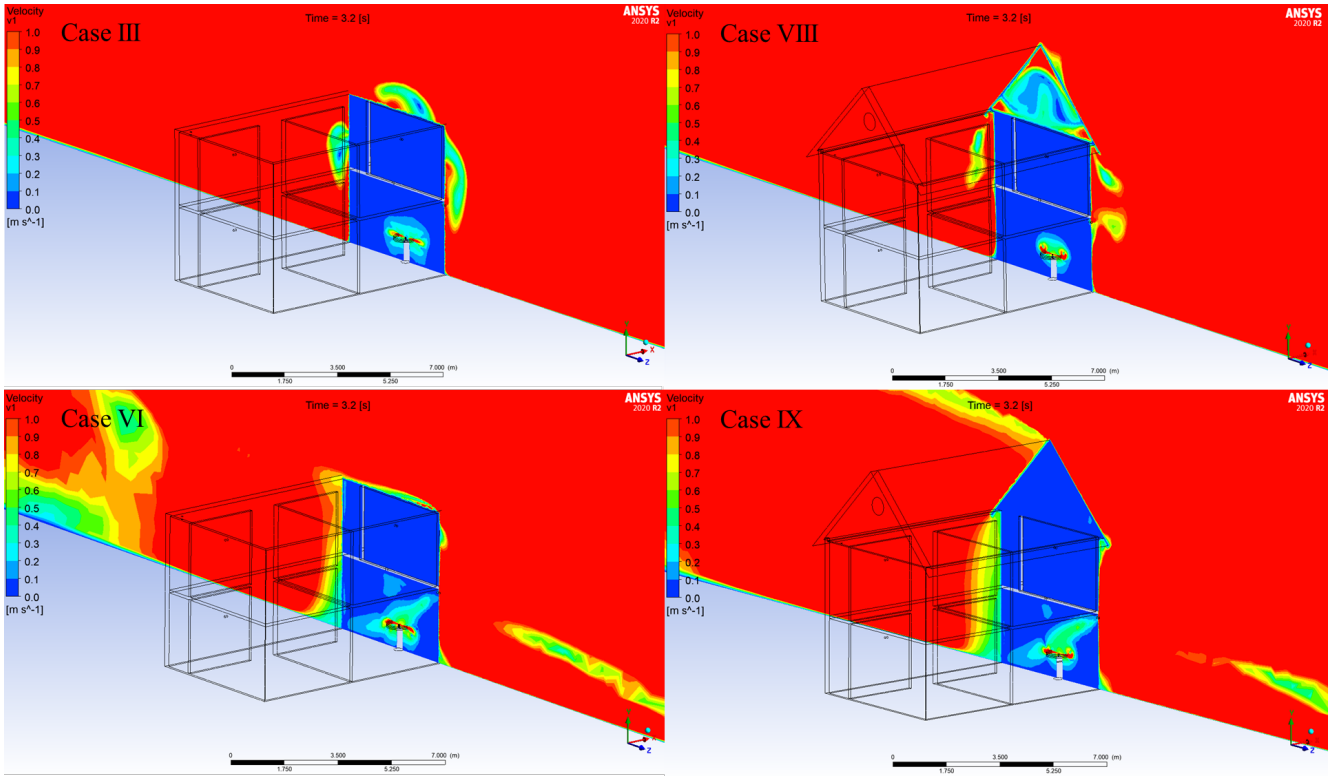


(d) Horizontal view of first floor

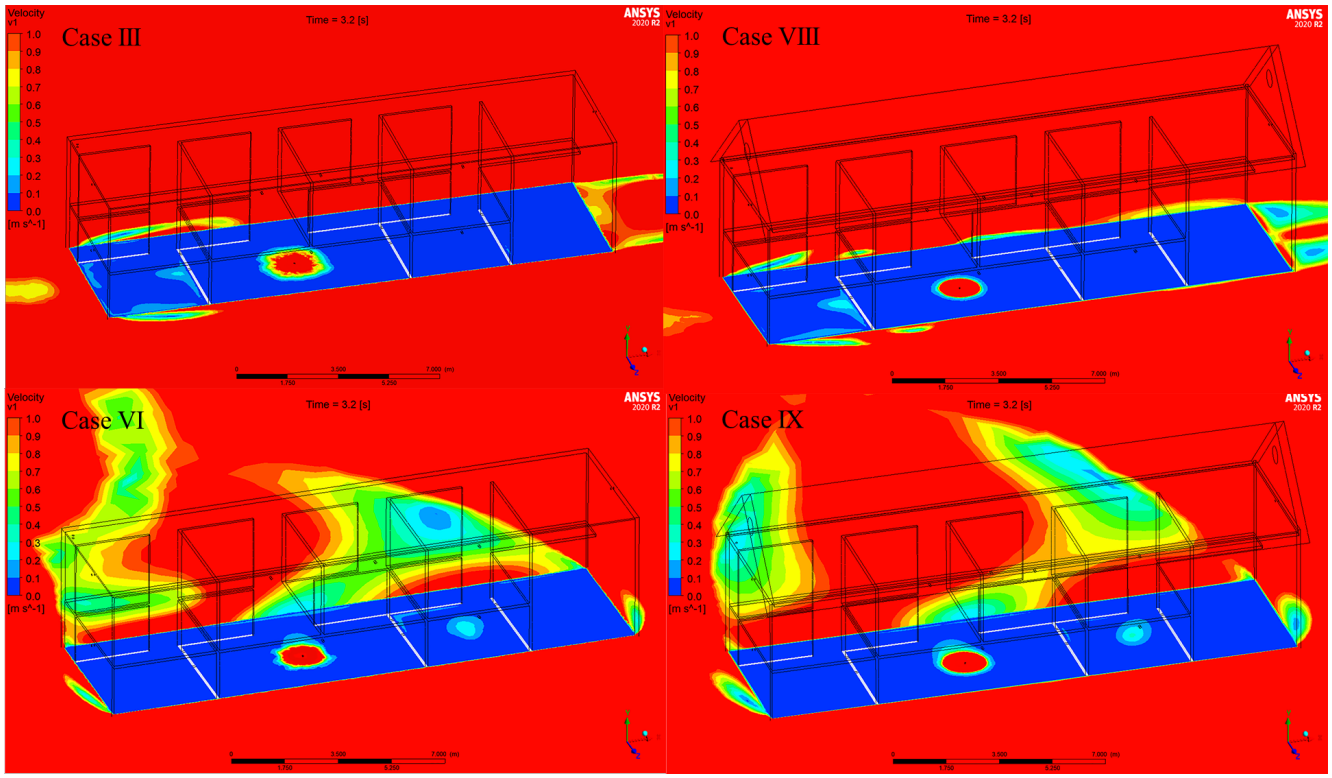
Figure 7-45: Perspective contour images of indoor pressure at 3.2s for Cases III, VIII, VI and IX



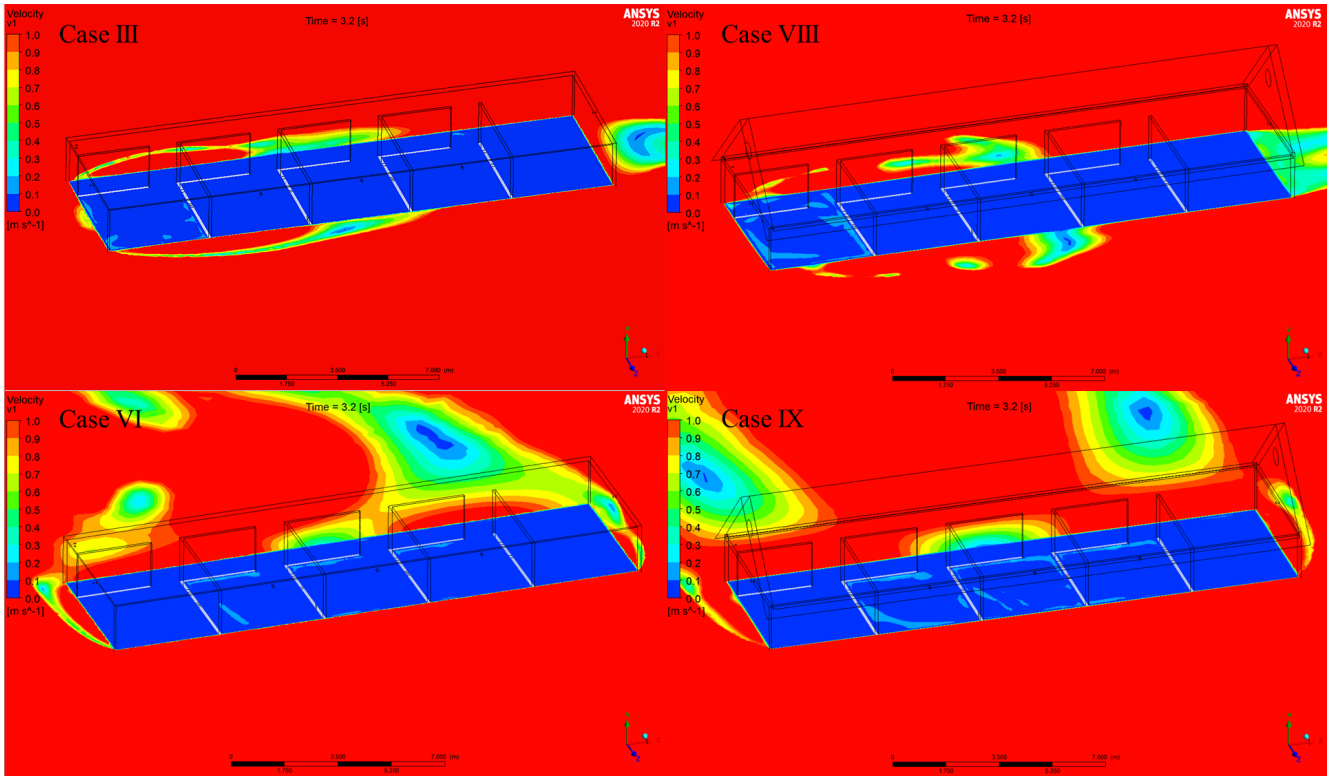
(a) Vertical front view



(b) Vertical side view



(c) Horizontal view of ground floor



(d) Horizontal view of first floor

Figure 7-46: Perspective contour images of indoor velocity at 3.2s for Cases III, VIII, VI and IX

7.7 Summary

In this chapter, a number of transient simulations were implemented using the ANSYS Fluent to visualise the dynamic process of the Pulse test and examine the steady wind impact on the Pulse measurement. Validation has been conducted by comparing the simulation results with the results obtained in field testing, and good agreements of the indoor pressure distribution and air leakage rate with experimental results were noted. The results of numerical simulation provide a detailed view of the pressure distribution across the internal spaces of the building and pressure profiles around the building envelope during the Pulse test, which in turn answer some of the frequently raised questions regarding the operation safety, reliability, and accuracy of Pulse. In addition, the numerical simulation results showed that the majority of the indoor spaces (i.e., 99.92%) has very low air velocities (i.e., below 0.08m/s) when the air pulse releases; and 93.35% of the total building volume with the indoor air velocity below 0.08m/s during the quasi-steady period. Hence, the findings confirm that the Pulse test could have low disruption and disturbance to the building fabric and occupants.

The numerical studies also allow us to assess how the steady wind might affect the Pulse measurement, which could not be practically realised in the field testing. In terms of the wind

speed impact on the Pulse test, similar findings were obtained, as mentioned in Chapters 5 and 6, that larger uncertainty could be induced to the Pulse measurement by a high wind speed level. Based on the results in this numerical study, performing the Pulse test is not recommended when the meteorological wind speed is above 6m/s to ensure the corresponding relative percentage difference within ±10%. The finding matches well with the wind limit statement for the fan pressurisation testing in the ISO 9972 standard. The simulation results of the steady wind impact also imply a difference of the identified threshold values compared with the field testing, as the meteorological wind speed limit of 7.91m/s was found in Chapter 5 (i.e., RPD <±10%.), and 14.34m/s in Chapter 6. The reasons could be: (a) the test building configurations are different, (b) numerical study considered steady wind conditions, while the experimental works were conducted under various natural wind conditions, and (c) discrepancies in numerical simulation and field test methods.

On the other hand, though the variation in the wind direction influences the indoor pressure distribution during the Pulse test, the associated impact on the Pulse measurement is less remarkable than that of the wind speed. It is also found that the building geometry and orientation affect the degree of the wind direction impact on the Pulse measurement, such as the envelope area of the windward façade and the location of the windows/openings. Moreover, the extended numerical investigation was carried out on the building model with a gable roof, and the comparison was made with the simulation of the building with a flat roof. The numerical results demonstrated that although there is a noticeable difference in the indoor pressure distribution during the Pulse test due to the two different roof types, the presence of the gable roof resulted in an insignificant impact on the Pulse measurement of the established building model. Comparing the cases with a flat roof and a gable roof, the largest deviations were 1.25% for the simulated average air leakage rate and 3.65% for the total volumetric flow rate of the openings during the quasi-steady period. Therefore, the comparisons verify that the simulations of the building models with a flat roof and a gable roof have very similar results.

To sum up, the numerical study addresses the research gap in the literature, providing valuable information to understand the dynamic nature of Pulse from the numerical perspective, the reliability and applicability of Pulse under different wind conditions and the wind limit for a valid Pulse test.

8. Conclusions

8.1 Introduction

This chapter summarises the major findings of the research based on the work presented from Chapter 2 to Chapter 7 and provides recommendations for future work. The research conducted provides in-depth insights into the wind impact on the Pulse measurement through both field tests under various natural wind conditions and numerical simulations under steady wind conditions. Based on findings of the field tests and CFD-based numerical simulations, it can be concluded that the wind condition does indeed play an influential role in the results obtained for building air leakage by means of the Pulse test. For example, higher wind speed conditions would induce an increasingly greater uncertainty to the Pulse measurement, and the change of the wind direction could also affect the Pulse measurement, especially under a high wind speed condition. This work contributes to extended explorations of Pulse from practical and numerical perspectives.

8.2 Major findings

In total, nine objectives were defined for achieving the research aim as presented in Section 1.3, and these have been accomplished. The major findings in each chapter are presented in the sections below, and the degree to which each objective has been completed is discussed, respectively.

Chapter 2: with the objective of 'A comprehensive review of the existing literature to analyse, define the importance of the research and identify the research gap'

In Chapter 2, the importance of the building airtightness was firstly discussed with reviews of the relevant available regulations in different regions and studies. The steady pressurisation method has been widely applied as a standard method for the building airtightness measurement, while Pulse offers an alternative solution, providing new metrics for both existing and new builds. The extensive literature review revealed that the wind impact on measuring building airtightness has comprehensively been investigated in relation to the steady pressurisation method, i.e., the blower door. These investigations have taken the direction of different perspectives, such as understandings of the uncertainties caused by the zero-flow pressure measurement, the steady wind and wind fluctuations through numerical and experimental approaches, and solutions to minimise the wind effect have been proposed. Therefore, the research gap has been highlighted as limited studies have been conducted to explore the impact of the wind condition on the Pulse

measurement through field testing and numerical simulation. In addition, there is a need to conduct more in-depth investigations and provide new insights into the Pulse test, as it is expected that the adoption of Pulse as an alternative airtightness test method for new buildings will be included in the forthcoming revisions to the Approved Documents providing guidance on Part L of the Building Regulations in England and Wales. No previous works have been reported on comprehensive understandings of the wind impact on the Pulse test through both numerical studies and field testing, which implies the novelty and significance of this research.

Chapter 3: with the objective of 'Comparison between Pulse and the steady pressurisation method'

Previous works regarding the comparison between the conventional steady pressurisation method and Pulse were found in the literature, and the experimental investigations presented in Chapter 3 provided complementary insights into the practical measurements when both test methods were applied to the same house in real scenarios. The results obtained from the airtightness measurements of a five-bedroom dwelling under calm weather conditions showed a good overall agreement between the two test methods, with deviations of 3.93% at 7.1Pa and 4.56% at 10.6Pa for the overlapped building pressure range. To prove the assessment validity, the error analysis was included for both test methods; the average overall error over the tested building pressure range was 1.60% for the Pulse testing, 2.94% for pressurisation testing and 7.46% for depressurisation testing. The overall measurement errors of both testing methods aligned with the uncertainty values reported in the literature. The findings also verified the applicability and reliability of Pulse.

Chapter 4: with the objective of 'Investigation of the uniformity of pressure distribution during the Pulse test through field testing'

As Pulse adopts an unsteady approach to airtightness testing, a question frequently raised by peer researchers and practitioners concerns a presumption of the potential for uneven pressure distribution, which influences the test accuracy. Experimental work of a five-bedroom detached house was presented in Chapter 4, which confirmed the achievement of a uniform indoor pressure distribution during the pulse pressurisation process. The highest deviation of 1.45% was obtained when comparing the achieved pressure in each room with the living room pressure during the three-step Pulse test. In addition, the complementary comparison test between the Pulse and the fan pressurisation method and the error analysis supported the finding of the uniformity of

pressure distribution. The overall error for the pressure distribution measurement was approximately 1.62% for the Pulse test and 2.95% for the blower door pressurisation testing at 10Pa and 15Pa.

On the other hand, the practicality of Pulse has been examined, and results demonstrated a minor impact of the Pulse test location on the building airtightness measurement. The work extended the explorations of Pulse by providing a full image of the uniform pressure distribution within the building during the Pulse test and therefore proving the applicability and reliability of the technique. The tests performed with a single Pulse unit in a five-bedroom dwelling of a relatively large volume, represented the worst-case scenario; thus, these findings are also applicable to smaller buildings.

Chapter 5: with the objectives of 'Short-term field testing to examine the wind impact on the building airtightness measurement with Pulse in a large, detached UK dwelling'; 'Identification of the threshold of wind speed that causes results with unacceptable errors and practical suggestions for the Pulse test to minimise the wind effect' and 'Improvement on the adjustment method for the Pulse measurement to reduce wind impact'

The literature review has highlighted the gap of investigations of the Pulse test performance under different natural wind conditions and addressing wind impact on the building airtightness measurement. To fill the identified research gap, in total, 423 Pulse tests have been implemented over seven days in a five-bedroom detached house to examine the wind impact under various natural wind conditions. Based on the measured air leakage rate results of the tested dwelling, the preferred test wind speed for the Pulse test was below 3.14m/s at 2.2m above ground level (i.e., approximately equivalent to the meteorological wind speed 4.95m/s based on the test location) with the *RPD* within ±5% (i.e., *RPD* against the calm wind condition of <0.5m/s). The observed threshold of wind speed that caused the Pulse measurements with unacceptable errors is 5.02m/s at 2.2m above ground level (i.e., approximately equivalent to meteorological wind speed 7.91m/s based on test the location) with the *RPD* <±10%. While above 7.37m/s at 2.2m above ground level (i.e., approximately equivalent to meteorological wind speed 11.61m/s based on test the location) would lead to the *RPD* of a single Pulse test in the tested dwelling exceeding ±20%.

On the other hand, the directional wind studies showed that at lower wind speeds, wind direction has a lesser influence on the Pulse measurement than the wind speed itself. In this study, tests were mostly conducted at the wind direction of 217°-273°, with smaller *RPD*s than those of other wind directions, which was attributed to the prevailing west to south-westerly winds in the UK.

To minimise the wind impact, the research considered performing the multiple Pulse tests, or multiple-step Pulse testing in practical testing due to the wider range of the measured pressure and improving the algorithm for adjusting the obtained Pulse measurements in the tested dwelling. The findings provide valuable information on how the Pulse measurement can be obtained practically with minimised wind and buoyancy effects using the optimal curve-fitting adjustment. Such adjustments include: (1) imposing three separate air pulses in a complete Pulse test; (2) record of the background pressure for 1.5s before the air pulse release and 1.5s after the pulse completion to ensure the recorded duration of the background pressure measurement to be long enough to capture the representative background pressure trend; and (3) determining the fitted curve based on the measured background pressure at the start point, the average pressure during recording period and at the endpoint. The work could provide practical guidance for deploying Pulse to measure building airtightness more accurately with minimised wind impact, which will be also beneficial for the wider applicability of Pulse.

Chapter 6: with the objectives of 'Long-term observations of the wind impact on the building airtightness measurement with Pulse in an outdoor chamber' and 'Identification of the threshold value of wind speed that causes results with unacceptable errors and practical suggestions for the Pulse test to minimise the wind effect'

The investigations of the wind impact were extended in this chapter through eight-month observations on the leakage variation of an outdoor chamber under various wind conditions. The measured data of the 1096 Pulse tests demonstrated the noticeable impact of the wind speed, as discussed in Chapter 5, as a higher wind speed led to a large deviation of the airtightness measurement. In terms of the threshold of wind speed that causes results with unacceptable errors, the Pulse test in the outdoor chamber with the *RPD* within ±10%, the wind speed should be less than 11.65m/s at 5m above ground level (i.e., approximately equivalent to meteorological wind speed 14.34m/s). This finding is different from the suggestion for the fan pressurisation method stated in the ISO 9972 standard (i.e., below the meteorological wind speed of 6m/s). It is also different to that of the findings in Chapter 5 (i.e., below meteorological wind speed 7.91m/s), due to the test building configuration, the position of the ultrasonic anemometer and the surrounding environment in the test location. It is also noteworthy that the threshold value of wind velocity (i.e., at a meteorological wind speed of 11.61m/s with the *RPD* within ±20%) identified in Chapter 5 was not applicable to the Pulse test in the outdoor chamber, as the corresponding *RPD* fell in the range of 6-7%. This is because the two tested buildings have different building configurations and airtightness levels, causing the wind impact on the Pulse measurement of the outdoor chamber

to be not as significant as that of the five-bedroom dwelling presented in Chapter 5. The results also indicate the importance of clarifying the specific wind speed reference point for the building airtightness measurement conducted in the field test.

Moreover, a less noticeable impact of the wind direction was also noted under the lower wind speed condition, as discussed in Chapter 5. A minor seasonal variation of the Pod's airtightness was observed over the eight months; nevertheless, the average ALR is slightly higher in winter than that of summer, which might also be caused due to the degradation of the sealing tapes around windows and doors. The work provided complementary insights into the understandings of the wind impact on the Pulse test in real scenarios and demonstrated the importance of the consideration of the dynamic wind condition in practical airtightness measurements for different buildings.

Chapter 7: with the objective of 'Numerical investigations of how different wind conditions affect the indoor and outdoor pressures of the building, and the air leakage measurement during the Pulse test'

CFD-based numerical simulations were implemented in the ANSYS Fluent based on a full-scale three-dimensional model of the building and the Pulse unit, which were established according to the configurations of the tested dwelling and experimental setup in the field testing. The simulation results were cross-validated with the obtained experimental data, and good agreements were found for the indoor pressure distribution and air leakage rate. The simulations provide answers to how different wind speed levels and directions affect the indoor pressure distribution and the air leakage measurement during the Pulse test. Based on the simulations of different steady wind speed levels, the meteorological wind speed limit for the Pulse measurement with the *RPD* within ±10% was below 6m/s, which is in line with the wind speed limit for the fan pressurisation method stated in the ISO 9972 standard. Similar to the findings discussed in Chapters 5 and 6, the Pulse measurement is less sensitive to the variation in the wind direction than the wind speed level. The largest difference of the simulated average air leakage rate among the four cases with different wind directions was about 3.93%. It was also numerically observed that the degree of the wind direction impact on the Pulse measurement also depends on the building configuration and location, such as the envelope area of the windward façade and the location of the windows/openings. Moreover, the comparison between the building model with a flat roof and gable roof demonstrated the insignificant impact caused by the presence of the gable roof, as the obtained air leakage rates were similar with a slight deviation of approximately 1.25%.

The simulation study contributes to the knowledge of computational modelling of the Pulse unit and the Pulse test, visually demonstrating how the pressure uniformly distributes across the internal spaces during the air pulse release. The study also provides complementary insights into the steady wind impact on the Pulse measurement from the numerical perspective, as well as verifying the reliability and applicability of Pulse in different building types and under various wind conditions.

And finally

Overall, the identified research gap has been filled, and the main research aim has been successfully achieved through the implementation of the nine objectives. The research has been routinely conducted as part of the ongoing Pulse development, providing progress to the knowledge of comprehensive understandings of the wind impact on the Pulse test under natural wind conditions and computationally simulated steady wind conditions. The findings of the wind impact in this research provide valuable supporting information for the improvement of protocols that are used to characterise building airtightness measurement and for the significance of building airtightness on the energy performance of buildings.

8.3 Recommendations for future work

Based on the major findings presented in Section 8.2, recommendations for future work are presented as follows:

- As discussed in Chapter 4, one technical limitation was the sampling rate of 4Hz of the employed acquisition device in the field testing. Therefore, an acquisition device coupled with multiple pressure transducers at a higher sampling rate could be used to improve the measurement frequency in the field test study and capture sufficient pressure readings to reflect the complete profile of how the indoor pressures across the internal spaces might vary during the rapid and dynamic air pulse releasing process.

- There is a research gap of experimental studies on exploring the wind impact on the building airtightness measurement using a wind tunnel. The wind tunnel experiment could allow investigations with a more configurable building model to achieve various leakage scenarios (e.g., leakage type and distribution) and under more controllable wind speed conditions. However, due to the global pandemic since March 2020, the model-scale experiment with the wind tunnel facilities was not able to be performed. The preliminary work conducted for

the proposed model-scale experiment was reported in Appendix-A, including the literature review, the test arrangement, the test methodology and the design of experimental facilities for the proposed model-scale experiment using a wind tunnel. Hence, the model scale experiment using a wind tunnel to explore the wind impact on Pulse could be conducted in the future based on the presented design of experimental facilities.

- As the presented experiment works were mainly focused on the domestic application, future works could be carried out through numerically exploring the use of various capacity Pulse units in large buildings and experimental tests in large buildings by adopting multiple Pulse units that operate simultaneously. The uniformity of pressure distribution within the internal spaces during the Pulse testing and the applicability of Pulse in a variety of building types under various weather conditions can be evaluated.

- In addition to the computational simulation of the steady wind impact presented in this research, it would be interesting to numerically explore the impact of unsteady wind conditions on the Pulse measurement, such as simulation of wind gusts at different frequencies and directions.

References

1. Department for Business, E.I.S., Energy consumption in the UK (ECUK) 1970 to 2020, E.I.S. Department for Business, Editor. 2021, National Statistics.
2. Nicol, S., et al., The cost of poor housing in the European Union. 2016, BRE Group.
3. Committee, B., Energy efficiency: building towards net zero, E.I.S. Department for Business, Editor. 2019.
4. Connolly, D., et al., Heat Roadmap Europe: Combining district heating with heat savings to decarbonise the EU energy system. Energy Policy, 2014. 65: p. 475-489.
5. Hübler, M. and A. Löschel, The EU decarbonisation roadmap 2050—What way to walk? Energy Policy, 2013. 55: p. 190-207.
6. European-Commission. Energy Efficiency in Buildings. 2014.
7. Ekins, P. and E. Lees, The impact of EU policies on energy use in and the evolution of the UK built environment. Energy Policy, 2008. 36(12): p. 4580-4583.
8. Talus, K., EU energy law and policy: a critical account. 2013: Oxford University Press.
9. Lerma, C., E. Barreira, and R.M.S.F. Almeida, A discussion concerning active infrared thermography in the evaluation of buildings air infiltration. Energy and Buildings, 2018. 168: p. 56-66.
10. Wang, Z., et al., Indoor environment quality in a low-energy residential building in winter in Harbin. Building and Environment, 2018. 135: p. 194-201.
11. Jokisalo, J., et al., Building leakage, infiltration, and energy performance analyses for Finnish detached houses. Building and Environment, 2009. 44(2): p. 377-387.
12. Han, G., J. Srebric, and E. Enache-Pommer, Different modeling strategies of infiltration rates for an office building to improve accuracy of building energy simulations. Energy and Buildings, 2015. 86: p. 288-295.
13. Brinks, P., O. Kornadt, and R. Oly, Air infiltration assessment for industrial buildings. Energy and Buildings, 2015. 86: p. 663-676.
14. Feijó-Muñoz, J., et al., Energy impact of the air infiltration in residential buildings in the Mediterranean area of Spain and the Canary islands. Energy and Buildings, 2019. 188-189: p. 226-238.
15. Guillén-Lambea, S., B. Rodríguez-Soria, and J.M. Marín, Air infiltrations and energy demand for residential low energy buildings in warm climates. Renewable and Sustainable Energy Reviews, 2019. 116: p. 109469.
16. Walker, I. and D. Wilson, Evaluating models for superposition of wind and stack effect in air infiltration. Building and Environment, 1993. 28(2): p. 201-210.
17. Chan, W.R., J. Joh, and M.H. Sherman, Analysis of air leakage measurements of US houses. Energy and Buildings, 2013. 66: p. 616-625.
18. Carrié, F.R. and B. Rosenthal, An overview of national trends in envelope and ductwork airtightness. Ventilation Information Paper, 2008. 29(1).
19. Ji, Y., et al., Air infiltration rate of typical zones of public buildings under natural conditions. Sustainable Cities and Society, 2020. 61: p. 102290.

20. Guyot, G., et al., Stimulation of good building and ductwork airtightness through EPBD. 2010.

21. Coxon, R., Research into the effect of improving air tightness in a typical uk dwelling. Building and ductwork airtightness selected papers from the rehva special journal issue on 'Airtightness', 2013: p. 19.

22. Crawley, D.B., et al., Contrasting the capabilities of building energy performance simulation programs. Building and environment, 2008. 43(4): p. 661-673.

23. Stasiulaitiene, I., et al., Infiltration of outdoor combustion-generated pollutants to indoors due to various ventilation regimes: A case of a single-family energy efficient building. Building and Environment, 2019. 157: p. 235-241.

24. Zheng, X., et al., A practical review of alternatives to the steady pressurisation method for determining building airtightness. Renewable and Sustainable Energy Reviews, 2020. 132: p. 110049.

25. British Standards Institute, BS EN ISO 9972: Thermal performance of buildings - Determination of air permeability of buildings - Fan pressurization method. 2015: British Standards Institute.

26. Sherman, M.H. and N.E. Matson, Air tightness of new US houses: A preliminary report. Lawrence Berkeley National Laboratory, LBNL-48671, 2002.

27. Okuyama, H. and Y. Onishi, Reconsideration of parameter estimation and reliability evaluation methods for building airtightness measurement using fan pressurization. Building and environment, 2012. 47: p. 373-384.

28. Carey, P. and D. Etheridge, Leakage measurements using unsteady techniques with particular reference to large buildings. Building Services Engineering Research and Technology, 2001. 22(2): p. 69-82.

29. Cooper, E. and D. Etheridge, Determining the adventitious leakage of buildings at low pressure. Part 1: uncertainties. Building Services Engineering Research and Technology, 2007. 28(1): p. 71-80.

30. Cooper, E. and D. Etheridge, Determining the adventitious leakage of buildings at low pressure. Part 2: pulse technique. Building Services Engineering Research and Technology, 2007. 28(1): p. 81-96.

31. Cooper, E., et al. A nozzle pulse pressurisation technique for measurement of building leakage at low pressure. in 35th AIVC conference, Poznan, September 2014. 2014.

32. Cooper, E., et al., Field trialling of a pulse airtightness tester in a range of UK homes. International Journal of Ventilation, 2016: p. 1-18.

33. Cooper, E., X. Zheng, and C.J. Wood, Numerical and experimental validations of the theoretical basis for a nozzle based pulse technique for determining building airtightness. Building and Environment, 2020: p. 107459.

34. Cooper, E. and D. Etheridge. Measurement of building leakage by unsteady pressurisation. in 25th AIVC Conference "Ventilation and retrofitting. 2004.

35. Zheng, X., et al. A comparison study of the blower door and novel pulse technique on measuring enclosure airtightness in a controlled environment. in 38th AIVC - 6th TightVent & 4th venticool Conference, 2017. 2017. Nottingham, UK.

36. Sherman, M. and L. Palmiter, Uncertainties in fan pressurization measurements, in Airflow performance of building envelopes, components, and systems. 1995, ASTM International.

37. Andrews, J., Error analysis for duct leakage tests in ASHRAE Standard 152P. 1997, Brookhaven National Lab., Upton, NY (United States).

38. Kraniotis, D., T.K. Thiis, and T. Aurlien, A numerical study on the impact of wind gust frequency on air exchanges in buildings with variable external and internal leakages. Buildings, 2014. 4(1): p. 27-42.

39. Leprince, V. and F.R. Carrié, Uncertainties due to steady wind in building pressurisation tests. REHVA Journal, 2018. 03: p. 53-57.

40. Haghighat, F., H. Brohus, and J. Rao, Modelling air infiltration due to wind fluctuations—a review. Building and Environment, 2000. 35(5): p. 377-385.

41. Carrié, F.R. and V. Leprince, Uncertainties in building pressurisation tests due to steady wind. Energy and Buildings, 2016. 116: p. 656-665.

42. Wu, Y., J. Niu, and X. Liu. Air infiltration induced inter-unit dispersion and infectious risk assessment in a high-rise residential building. in Building Simulation. 2018. Springer.

43. Hill, J. and T. Kusuda, Dynamic characteristics of air infiltration. ASHRAE Trans, 1975. 81(1): p. 168-185.

44. Pasos, A.V., et al., Experimental Study on the Measurement of Building Infiltration and Air Leakage Rates (at 4 and 50 Pa) by Means of Tracer Gas Methods, Blower Door and the Novel Pulse Technique in a Detached UK Home, in 39th AIVC - 7th TightVent & 5th venticool Conference Smart ventilation for buildings. 2018: Antibes Juan-Les-Pins, France.

45. Taddeo, P., et al., Comparison of Experimental Methodologies to Estimate the Air Infiltration Rate in a Residential Case Study for Calibration Purposes, in 39th AIVC - 7th TightVent & 5th venticool Conference Smart ventilation for buildings. 2018: Antibes Juan-Les-Pins, France.

46. Lanooy, T., et al., A New Method to Measure Building Airtightness, in 39th AIVC - 7th TightVent & 5th venticool Conference Smart ventilation for buildings. 2018: Antibes Juan-Les-Pins, France.

47. Remion, G., et al., Assessing the Performance of Hybrid and Natural Ventilation Systems: A Review of Existing Methods, in 39th AIVC - 7th TightVent & 5th venticool Conference Smart ventilation for buildings. 2018: Antibes Juan-Les-Pins, France.

48. Yamasawa, H., et al., Ventilation Performance of Natural Ventilation Building with Solar Chimney, in 39th AIVC - 7th TightVent & 5th venticool Conference Smart ventilation for buildings. 2018: Antibes Juan-Les-Pins, France.

49. Sajima, T., et al., Ventilation Performance of Office Building with Natural Ventilation Shaft, in 39th AIVC - 7th TightVent & 5th venticool Conference Smart ventilation for buildings. 2018: Antibes Juan-Les-Pins, France.

50. Prignon, M., A. Dawans, and G.v. Moeseke, Uncertainties in Airtightness Measurements: Regression Methods and Pressure Sequences, in 39th AIVC - 7th TightVent & 5th venticool Conference Smart ventilation for buildings. 2018: Antibes Juan-Les-Pins, France.

51. Mélois, A.B., et al., Wind Speed in Building Airtightness Test Protocols: A Review, in 39th AIVC - 7th TightVent & 5th venticool Conference Smart ventilation for buildings. 2018: Antibes Juan-Les-Pins, France.
52. Novák, J., Assessment of durability of airtightness by means of repeated testing of 4 passive houses, in 39th AIVC - 7th TightVent & 5th venticool Conference Smart ventilation for buildings. 2018: Antibes Juan-Les-Pins, France.
53. Marrero, M., J.D. Carrilho, and M.G.d. Silva, Effects of Meteorological Factors on CO2 Concentrations, in 39th AIVC - 7th TightVent & 5th venticool Conference Smart ventilation for buildings. 2018: Antibes Juan-Les-Pins, France.
54. Qabbal, L., et al., Numerical and Experimental Identification of Factors Influencing the Pressure Homogeneity during an Airtightness Test in a Large Building, in 39th AIVC - 7th TightVent & 5th venticool Conference Smart ventilation for buildings,. 2018: Antibes Juan-Les-Pins, France.
55. Breesch, H., B. Merema, and A. Versele, Ventilation cooling in a school building: evaluation of the measured performances, in 39th AIVC - 7th TightVent & 5th venticool Conference Smart ventilation for buildings. 2018: Antibes Juan-Les-Pins, France.
56. Walker, I., et al., Applying Large Datasets to Developing a Better Understanding of Air Leakage Measurement in Homes. International Journal of Ventilation, 2013. 11(4): p. 323-338.
57. Carrié, F.R. and A. Mélois, Modelling building airtightness pressurisation tests with periodic wind and sharp-edged openings. Energy and Buildings, 2020. 208: p. 109642.
58. Mees, C. and X. Loncour, Quality framework for reliable fan pressurisation tests. Qualicheck fact sheet, 2016(21).
59. Friedler, C. and C. Kumar, Reinventing retrofit: How to scale up home energy efficiency in the UK. 2019: Green Alliance.
60. Etheridge, D.W. and M. Sandberg, Building ventilation: theory and measurement. Vol. 50. 1996: John Wiley & Sons Chichester, UK.
61. Kraniotis, D., Dynamic characteristics of wind-driven air infiltration in buildings The impact of wind gusts under unsteady wind conditions. 2014, Norwegian University of Life Sciences.
62. Sherman, M.H., Air change rate and airtightness in buildings. Vol. 1067. 1990: ASTM International.
63. Younes, C., C.A. Shdid, and G. Bitsuamlak, Air infiltration through building envelopes: A review. Journal of Building Physics, 2012. 35(3): p. 267-302.
64. Pan, W., Relationships between air-tightness and its influencing factors of post-2006 new-build dwellings in the UK. Building and Environment, 2010. 45(11): p. 2387-2399.
65. Liddament, M.W., Air Infiltration Calculation Techniques: An Application Guide. 1986: Air Infiltration and Ventilation Centre.
66. Santamouris, M. and P. Wouters, Building Ventilation: The State of the Art. 2006: Taylor & Francis.
67. Tamura, G.T., Measurement of air leakage characteristics of house enclosures. ASHRAE transactions, 1975. 81(1): p. 202-211.
68. Persily, A.K., Understanding air infiltration in homes. 1982.

69. VanBronkhorst, D., A. Persily, and S. Emmerich. Energy impacts of air leakage in US office buildings. in Document-air infiltration centre aic proc. 1995. OSCAR FABER PLC.

70. Emmerich, S. and A. Persily, Energy impacts of infiltration and ventilation in US office buildings using multizone airflow simulation. IAQ and Energy'98. Atlanta: American Society of Heating, Refrigerating and Air-Conditioning Engineers. 1998, Inc.

71. Stephen, R., Airtightness in UK dwellings: BRE's test results and their significance. 1998: CRC.

72. Harrje, A.B.D., Approaches to Evaluation of Air Infiltration Energy Losses in Buildings. ASHRAE Trans~. Part I: PH-79-10, 1979.

73. Dickerhoff, D., D.T. Grimsrud, and R.D. Lipschutz, Component leakage testing in residential buildings. 1982.

74. Harrje, D. and G. Born. Cataloguing air leakage components in houses. in Proceedings of the ACEEE. 1982.

75. Anderlind, G. Energy consumption due to air infiltration. in Proceedings of the 3rd ASHRAE/DOE/BTECC Conference on Thermal Performance of the Exterior Envelopes of Buildings. 1985.

76. Claridge, D.E. and S. Bhattacharyya, The measured energy impact of infiltration in a test cell. Journal of Solar Energy Engineering, 1990. 112(2): p. 132-139.

77. Liu, M., Study of air infiltration energy consumption. 1992.

78. Energy Star, A guide to energy-efficient heating and cooling. United States Environmental Protection Agency, 2009.

79. Kalamees, T., Air tightness and air leakages of new lightweight single-family detached houses in Estonia. Building and Environment, 2007. 42(6): p. 2369-2377.

80. Binamu, A., Integrating building design properties" air tightness" and ventilation heat recovery for minimum heating energy consumption in cold climates. 2002: Tampereen Teknillinen Korkeakoulu.

81. Jokisalu, J. and J. Kurnitski, Simulation of energy consumption in typical Finnish detached house. Helsinki University of Technology, HVAC Laboratory, report B, 2002. 74: p. 2002.

82. Kraus, M. and D. Kubečkova, Airtightness of Energy Efficient Buildings. Vol. 2. 2013.

83. Lstiburek, J., K. Pressnail, and J. Timusk, Air pressure and building envelopes. Journal of Thermal Envelope and Building Science, 2002. 26(1): p. 53-91.

84. Kirkwood, R., Fuel consumption in industrial buildings. Build. Serv. Eng, 1977. 45: p. 23-31.

85. Nevrala, D. and D. Etheridge. Natural ventilation in well-insulated houses. in Proceedings of International Centre for Heat and Mass Transfer, International Seminar, UNESCO, Dubrovnik, Croatia. 1977.

86. Dorer, V., C. Tanner, and A. Weber, Airtightness of buildings. AIVC VIP, 2004. 8: p. 2003-2006.

87. Jokisalo, J., et al., A comparison of measured and simulated air pressure conditions of a detached house in a cold climate. Journal of Building Physics, 2008. 32(1): p. 67-89.

88. Airaksinen, M., et al., Microbial contamination of indoor air due to leakages from crawl space: A field study. Indoor Air, 2004. 14(1): p. 55-64.

89. Mattson, J., O. Carlson, and I. Engh. Negative influence on IAQ by air movement from mould contaminated constructions into buildings. in Proceedings of Indoor Air 2002. 2002.

90. Emmerich, S.J., J.E. Gorfain, and C. Howard-Reed, Air and pollutant transport from attached garages to residential living spaces–literature review and field tests. International Journal of Ventilation, 2003. 2(3): p. 265-276.

91. Nazaroff, W. and S. Doyle, Radon entry into houses having a crawl space. 1983.

92. Jones, A.P., Indoor air quality and health. Atmospheric environment, 1999. 33(28): p. 4535-4564.

93. Pessi, A.-M., et al., Microbial growth inside insulated external walls as an indoor air biocontamination source. Applied and Environmental Microbiology, 2002. 68(2): p. 963-967.

94. Janssens, A. and H. Hens, Interstitial condensation due to air leakage: a sensitivity analysis. Journal of Thermal Envelope and Building Science, 2003. 27(1): p. 15-29.

95. Hagentoft, C.-E. and E. Harderup, Moisture conditions in a north facing wall with cellulose loose fill insulation: Constructions with and without vapor retarder and air leakage. Journal of Thermal Insulation and Building Envelopes, 1996. 19(3): p. 228-243.

96. Krstić, H., et al. Measurements and analysis of air tightness and indoor air quality in non-residential buildings. in International Conference Management of Technology–Step to Sustainable Production (MOTSP 2018). 2018.

97. Etheridge, D., A perspective on fifty years of natural ventilation research. Building and Environment, 2015. 91: p. 51-60.

98. Siimes, S.-A., Thermal insulation in a building. 2002, C3 National Building Code Of Finland: Helsinki.

99. NBN, N., 50-001 Ventilatievoorzieningen in woongebouwen. 1991, Brussels.

100. Perera, E. and L. Parkins, Build tight–ventilate right. Building Services, CIBSE June, 1992.

101. Gałaj, J. and D. Saleta, Impact of Apartment Tightness on Temperature Variability during a Fire. International journal of environmental research and public health, 2020. 17(12): p. 4590.

102. Kukadia, V. and S. Upton, Ensuring good indoor air quality in buildings. BRE Trust, Bucknalls lane, Watford, Herts, WD25 9XX, 2019.

103. McGill, G., et al., Health effects of Modern Airtight Construction: HEMAC Multidisciplinary Network Summary Report. 2017.

104. Vinha, J., et al., Airtightness of residential buildings in Finland. Building and Environment, 2015. 93: p. 128-140.

105. Laboratory, L.B.N., U.S.D.o.E.O.o. Scientific, and T. Information, Analysis of Air Leakage Measurements from Residential Diagnostics Database. 2012: Lawrence Berkeley National Laboratory. Environmental Energy Technologies Division.

106. Colliver, D.G. Predictive method to determine the leakage area needed in residences for IAQ control by infiltration. Citeseer.

107. Hunt, C.M., J. King, and H.R. Trechsel, Building air change rate and infiltration measurements. Vol. 719. 1980: ASTM International.

108. Sherman, M.H. and W.R. Chan, Building air tightness: research and practice, in Building Ventilation. 2006, Routledge. p. 155-180.

109. ISO, BS EN ISO 9972: Thermal performance of buildings - Determination of air permeability of buildings - Fan pressurization method. 2015: British Standards Institute.

110. ASTM, A., E779–99. Standard Test Method for Determining Air Leakage Rate by Fan Pressurization, American Society for Testing and Materials, West Conshohocken, Pennsylvania, USA, 2004.

111. Bramiana, C., A.G. Entrop, and J.I. Halman, Relationships between building characteristics and airtightness of Dutch dwellings. Energy procedia, 2016. 96: p. 580-591.

112. Walker, I. and M. Sherman, An Easier Way to Measure Duct Leaks. Home Energy, 2002. 19(5): p. 34-36.

113. Love, J., et al., 'Hitting the target and missing the point': Analysis of air permeability data for new UK dwellings and what it reveals about the testing procedure. Energy and Buildings, 2017. 155: p. 88-97.

114. Henry, R., et al., Measurements of window air leakage at cold temperatures and impact on annual energy performance of a house. ASHRAE Transactions, 1998. 104: p. 1254.

115. Czech Office for Standards Metrology and Testing, ČSN 73 0540-2, in Thermal Protection of Buildings–Part 2: Requirements. 2011: Prague.

116. Danish Ministry of Housing, Danish Building and Housing Agency: Danish Building Regulations. 2015.

117. Leblond, P., L'essentiel de la RT 2012-2e éd.: Obligations et mise en oeuvre de la réglementation thermique. 2015: Dunod.

118. Federal Government of Germany, Energieeinsparverordnung (EnEV). 2009.

119. DIN4108-7, Wärmeschutz und Energie-Einsparung in Gebäuden–Teil 7: Luftdichtheit von Gebäuden, Anforderungen, Planungs-und Ausführungsemp-fehlungen sowie-beispiele. 2011.

120. Andreas Enseling, E.H., Wirtschaftlichkeit energiesparender Maßnahmen im Bestand vor dem Hintergrund der novellierten EnEV. Vol. 23. 2008: IWU Darmstadt.

121. Kommunal- og regionaldepartementet, nr 489, in Forskrift om tekniske krav til byggverk (Byggtekniskforskrift). 2010.

122. Norge, S., NS 3700: 2013 Kriterier for passivhus og lavenergibygninger–Boligbygninger. Standard Norge, 2013.

123. Energihushållning Boverket- Swedish National Board of Housing, BFS 2011:26 - BBR 19, in Building and Planning. 2012.

124. Swiss Society of Engineers and Architects, SIA 180, in Isolamento Termico, Protezione Contro L'umdità e Clima Interno Degli Edifici. 2014: Zurich, Switzerland.

125. H. Government, The Building Regulations 2010, in Approved Document L1A: Conservation of Fuel and Power in New Dwellings, with 2016 Amendments. 2016.

126. CIBSE, Testing buildings for air leakage: CIBSE Technical Memoranda TM23: 2000. 2000, The Chartered Institute of Building Services Engineers London.

127. Waters, J., Energy conservation in buildings: a guide to Part L of the Building regulations. 2008: John Wiley & Sons.

128. ASHRAE, Standard 136-1993, in A Method of Determining Air Change Rates in. 1993.

129. Limb, M., AIVC TN 55: A review of international ventilation, airtightness, thermal insulation and indoor air quality criteria. Coventry, UK, AIVC, 2001.

130. Anderson, B., Conventions for U-value calculations. 2002: CRC.

131. Lee, Y.G. and C.W. Shin, The air leakage characteristics and airtightness performance of a newly built apartment. Korean Journal of Air-Conditioning and Refrigeration Engineering, 2013. 25(11): p. 606-611.

132. The Air Tightness Testing & Measurement Association, Technical Standard L1: Measuring Air Permeability in the Envelopes of Dwellings. 2010: Amersham.

133. Blower Door Tests | Department of Energy, U.S. Department of Energy. 2015.

134. Unmasking Commercial Building Energy Loss, RSES Journa. 2014.

135. Chen, S., et al., Measured air tightness performance of residential buildings in North China and its influence on district space heating energy use. Energy and buildings, 2012. 51: p. 157-164.

136. Stabile, L., et al., Effect of natural ventilation and manual airing on indoor air quality in naturally ventilated Italian classrooms. Building and Environment, 2016. 98: p. 180-189.

137. Erhorn-Kluttig, H., et al., Airtightness requirements for high performance building envelopes. ASIEPI European Project, Report P, 2009. 157: p. 05.03.

138. Ruhnke, J. and J. Distinti, System for determining overall heating and cooling system efficienies. 2007, Google Patents.

139. Stephens, B., Energy implications of filtration in residential and light-commercial buildings. ASHRAE Transactions, 2010. 116: p. 346.

140. Testing, A.T. and M. Association., Technical Standard L1: Measuring Air Permeability of Building Envelopes (Dwellings). 2010, Northampton: Author.

141. Elzafraney, M., P. Soroushian, and M. Deru, Development of energy-efficient concrete buildings using recycled plastic aggregates. Journal of architectural engineering, 2005. 11(4): p. 122-130.

142. Zheng, X.F., et al., Experimental Studies of a Pulse Pressurisation Technique for Measuring Building Airtightness. Future Cities and Environment, 2019. 5(1): p. 10.

143. Krishnamoorthy, S., M. Modera, and C. Harrington, Efficiency optimization of a variable-capacity/variable-blower-speed residential heat-pump system with ductwork. Energy and Buildings, 2017. 150: p. 294-306.

144. ASTM, A., E779-10 Standard Test Method for Determining Air Leakage Rate by Fan Pressurization. Philadelphia: American Society of Testing and Materials, 2010.

145. Labat, M., et al., Assessment of the air change rate of airtight buildings under natural conditions using the tracer gas technique. Comparison with numerical modelling. Building and Environment, 2013. 60: p. 37-44.

146. Carey, P.S. and D.W. Etheridge, Leakage measurements using unsteady techniques with particular reference to large buildings. Building Services Engineering Research and Technology, 2001. 22(2): p. 69-82.

147. Cooper, E., D. Etheridge, and S. Smith, Determining the adventitious leakage of buildings at low pressure. Part 2: pulse technique. Building Services Engineering Research and Technology, 2007. 28(1): p. 81-96.

148. Zheng, X., et al., Experimental insights into the airtightness measurement of a house-sized chamber in a sheltered environment using blower door and pulse methods. Building and Environment, 2019: p. 106269.

149. Sharples, S., S. Closs, and N. Chilengwe, Airtightness testing of very large buildings: a case study. Building Services Engineering Research and Technology, 2005. 26(2): p. 167-172.

150. Zheng, X., et al., Airtightness measurement of an outdoor chamber using the Pulse and blower door methods under various wind and leakage scenarios. Building and Environment, 2020: p. 106950.

151. Zheng, X. and C.J. Wood, On the power law and quadratic forms for representing the leakage-pressure relationship–Case studies of sheltered chambers. Energy and Buildings, 2020. 226: p. 110380.

152. Build Test Solutions Ltd. Pulse 2.0 Brochure. 2021 [cited 2021 28.04]; Available from: https://buildtestsolutions.com/wp-content/uploads/2021/02/Pulse-Brochure-v006.pdf.

153. Sherman, M. and D. Dickerhoff. Air-tightness of US dwellings. in Document-air infiltration centre aic proc. 1994. OSCAR FABER PLC.

154. Sherman, M., Infiltration in ASHRAE's residential ventilation standards. 2008.

155. Sherman, M. and M. Modera, Low-frequency measurement of leakage in enclosures. Review of Scientific Instruments, 1986. 57(7): p. 1427-1430.

156. Watanabe, Y., H. Kobayashi, and Y. Utsumi. Development of validation of AC-pressurization measuring of leakage area of houses. in Building Simulation'99. 1999.

157. Dewsbury, J., AC pressurisation: Analysis by non-linear optimisation. Building Services Engineering Research and Technology, 1996. 17(2): p. 65-71.

158. Nishioka, T., et al. Unsteady pressurization method to measure the airtightness of the building envelope. in Research in building physics international conference; 2nd, Building physics; Research in building physics. 2003.

159. Mattsson, B. and J. Claesson, A Transient Pressurization Method for Measurements of Airtightness. Journal of Building Physics, 2007. 31(1): p. 35-53.

160. Mattsson, B., Studies on Building Air Leakage-a transient pressurisation method, measurements and modelling. 2007: Chalmers University of Technology.

161. Mattsson, B. and J. Claesson. Exploration of a transient method for measurements of airtightness. in Research in Building Physics and Building Engineering. The Third International Building Physics Conference, Concordia University, Montreal, Canada, 27-31 August 2006. 2006.

162. Møller, E.B., T.V. Rasmussen, and A. Nicolajsen. A simplified method using compressed air to determine air leakage. in Thermal Performance of the Exterior Envelopes of Whole Buildings XI International Conference. 2010. American Society of Heating, Refrigerating and Air-Conditioning Engineers, Inc.

163. Sonoda, T. and F. Peterson, A sonic method for building air-leakage measurements. Applied energy, 1986. 22(3): p. 205-224.

164. Iordache, V. and T. Catalina, Acoustic approach for building air permeability estimation. Building and Environment, 2012. 57: p. 18-27.

165. Varshney, K., et al., Air-Infiltration Measurements in Buildings Using Sound Transmission Loss Through Small Apertures. International Journal of Green Energy, 2013. 10(5): p. 482-493.

166. ACIN instrumenten. Air Tightness Tester. 2020 [cited 2021 21/07]; Available from: https://acin.nl/en/product/air-tightness-tester/.

167. Borsboom, W., et al. Commission and performance contracting of ventilation systems in practice. Determination, analyses and consequences for practitioners and contractors. in Presentatie tijdens AIVC Conferentie in Gent, 15-16 Oktober 2019, 1-9. 2019.

168. Lanooy, T., et al., Applicability of a simple and new airtightness measuring method and further comparisons with blower door measurements. International Journal of Ventilation, 2021: p. 1-8.

169. Lanooy, B. and B. Kornaat. Applicability of a simple and new airtightness measuring method and further comparisons with blower door measurements. in 40th AIVC Conference, 15-16 October, Gent 2019. 2019.

170. Leprince, V., B. Moujalled, and A. Litvak, Durability of building airtightness, review and analysis of existing studies. 2017.

171. Delmotte, C. and J. Laverge. Interlaboratory test for the determination of repeatability and reprocucibility of buildings airtightness measurements. in 32nd AIVC conference; 1st TightVent conference: Towards optimal airtightness performance. 2011. AIVC.

172. Bracke, W., et al., Durability and measurement uncertainty of airtightness in extremely airtight dwellings. International Journal of Ventilation, 2016. 14(4): p. 383-394.

173. Bailly, A., et al. Numerical evaluation of airtightness measurement protocols. in 33rd AIVC Conference" Optimising Ventilative Cooling and Airtightness for [Nearly] Zero-Energy Buildings, IAQ and Comfort", Copenhagen, Denmark. 2012.

174. Zheng, X., et al. Refined assessment and comparison of airtightness measurement of indoor chambers using the blower door and Pulse methods. in 40th AIVC - 8th TightVent & 6th venticool Conference. 2019. Ghent, Belgium.

175. Kim, A.K. and C.Y. Shaw, Seasonal variation in airtightness of two detached houses, in Measured air leakage of buildings. 1986, ASTM International.

176. Wahlgren, P. Seasonal variation in airtightness. in 35th AIVC Conference" Ventilation and airtightness in transforming the building stock to high performance", Poznań, Poland. 2014.

177. Domhagen, F. and P. Wahlgren, Consequences of Varying Airtightness in Wooden Buildings. Energy Procedia, 2017. 132: p. 873-878.

178. Bailly, A., G. Guyot, and V. Leprince. years of envelope airtightness measurements performed by French certified operators: analyses of about 65,000 tests. in 36th AIVC Conference, Madrid. 2015.

179. Modera, M.P. and D.J. Wilson, The effects of wind on residential building leakage measurements, in Air change rate and airtightness in buildings. 1990, ASTM International.

180. Delmotte, C. Airtightness of Buildings–Considerations regarding the Zero-Flow Pressure and the Weighted Line of Organic Correlation. in 38th AIVC Conference "Ventilating healthy low-energy buildings". 2017. Nottingham.

181. Vickery, B., Gust-factors for internal-pressures in low rise buildings. Journal of Wind Engineering and Industrial Aerodynamics, 1986. 23: p. 259-271.

182. Bankvall, C.G., Air movements and the thermal performance of the building envelope, in Thermal Insulation: Materials and Systems. 1987, ASTM International.

183. Shaw, C.Y., Correlation between air infiltration and air tightness for houses in a developed residential area. ASHRAE Trans.;(United States), 1981. 87(CONF-810657-).

184. Kraniotis, D., T. Aurlien, and T. Thiis, Investigating instantaneous wind-driven infiltration rates using the CO2 concentration decay method. International Journal of Ventilation, 2014. 13(2): p. 111-124.

185. Mattsson, B. The influence of wind speed, terrain and ventilation system on the air change rate of a single-family house. in ICHMT Digital Library Online. 2004. Begel House Inc.

186. Walker, I.S., D.J. Wilson, and M.H. Sherman, A comparison of the power law to quadratic formulations for air infiltration calculations. Energy and Buildings, 1998. 27(3): p. 293-299.

187. Anis, W.A., The impact of airtightness on system design. ASHRAE journal, 2001. 43(12): p. 31.

188. Sfakianaki, A., et al., Air tightness measurements of residential houses in Athens, Greece. Building and Environment, 2008. 43(4): p. 398-405.

189. Laverge, J., et al., Energy saving potential and repercussions on indoor air quality of demand controlled residential ventilation strategies. Building and Environment, 2011. 46(7): p. 1497-1503.

190. Relander, T.-O., S. Holøs, and J.V. Thue, Airtightness estimation—A state of the art review and an en route upper limit evaluation principle to increase the chances that wood-frame houses with a vapour-and wind-barrier comply with the airtightness requirements. Energy and Buildings, 2012. 54: p. 444-452.

191. CEN, E., CEN-EN 13829, Thermal Performance of Buildings – Determination of Air Permeability of Buildings – Fan Pressurization Method. 2001, European Committee for Standardization: Brussels.

192. Fernández-Agüera, J., J.J. Sendra, and S. Domínguez, Protocols for Measuring the Airtightness of Multi-Dwelling Units in Southern Europe. Procedia Engineering, 2011. 21: p. 98-105.

193. Nevander, L.E.K., J., Airtightness of buildings - Research in Sweden., in IEA Seminar on R&D projects in the area of infiltration in buildings. 1978: Paris, France.

194. Kronvall, J., Testing of houses for air leakage using a pressure method. ASHRAE transactions, 1978. 84(1): p. 72-9.

195. Jackman, P.J., Review of building airtightness and ventilation standards., in 5th AIVC Conference "The implementation and effectiveness of air infiltration standards in buildings". 1984: Nevada.

196. ASTM, ASTM Standard E779-81, in Standard practice for measuring air leakage by the fan pressurization method. 1981, ASTM American Society for Testing and Materials: Philadelphia, PA.

197. CGSB, Determination of the airtightness of building envelopes by the fan depressurization method. 1985, Canadian General Standards Board CAN2-149.10-M: Ottawa, Ontario, Canada.

198. NBR, N., Airtightness of buildings - Test method. 1981, Norwegian Council for Building Standardization (NBR): Oslo, Norway.

199. SIS, Thermal insulation - Determination of airtightness of buildings. 1980, Vaermeisolering-bestaemning av byggnaders lufttaetheet: Stockholm, Sweden.

200. Novák, J. Influence of the external pressure tap position on the airtightness test result. in 40th AIVC - 8th TightVent & 6th venticool Conference. 2019. Ghent, Belgium.

201. Delmotte, C. Airtightness of buildings – Considerations regarding place and nature of pressure taps. in 40th AIVC - 8th TightVent & 6th venticool Conference. 2019. Ghent, Belgium.

202. Rolfsmeier, S. New findings on measurements of very airtight buildings and apartments. in 40th AIVC - 8th TightVent & 6th venticool Conference. 2019. Ghent, Belgium.

203. Mélois, A.B., et al. Designing a model-scale experiment to evaluate the impact of steady wind on building air leakage measurements. in 40th AIVC - 8th TightVent & 6th venticool Conference. 2019. Ghent, Belgium.

204. Kraniotis, D. and A. Chaudhuri. CFD modelling of fan pressurization method in buildings – The impact of dynamic wind on airtightness tests. in 40th AIVC - 8th TightVent & 6th venticool Conference. 2019. Ghent, Belgium.

205. Ganguli, U., Wind and air pressures on the building envelope, N.R.C. (NRC), Editor. 1986.

206. Mao, J., W. Yang, and N. Gao, The transport of gaseous pollutants due to stack and wind effect in high-rise residential buildings. Building and Environment, 2015. 94: p. 543-557.

207. Etheridge, D. Unsteady wind effects in natural ventilation design. in Proceedings of the CIBSE National Conference, Harrogate, UK. 1999.

208. Cockroft, J. and P. Robertson, Ventilation of an enclosure through a single opening. Building and Environment, 1976. 11(1): p. 29-35.

209. Phaff, H. and W. De Gidds, Building ventilation, investigation of the consequence of opening one window on the internal climate of a room. IMG-TNO Report C, 1980. 448.

210. Ethridge, D. and D. Alexander, British Gas multi-cell model for calculating ventilation. ASHRAE Trans.;(United States), 1980. 86.

211. Sasaki, T., M. Hayashi, and N. Aratani. On the ventilating characteristics of the space under the fluctuating wind pressure. in Proceedings of ROOMVENT. 1987.

212. Crommelin, R. and E. Vrins, Ventilation through a single opening in a scale model. Air Infiltration Review, 1988. 9(3): p. 11-15.

213. Haghighat, F., J. Rao, and P. Fazio, The influence of turbulent wind on air change rates—a modelling approach. Building and environment, 1991. 26(2): p. 95-109.

214. Haghighat, F., J. Rao, and J. Riberon. Modelling fluctuating airflow through large openings. in Proceedings of the Thirteenth AIVC Conference, Nice, France. 1992.

215. Rao, J. and F. Haghighat. Wind induced fluctuating airflow in buildings. in Proc. of the 12th AIVC Conference. 1991.

216. Dascalaki, E., et al., Predicting single sided natural ventilation rates in buildings. Solar Energy, 1995. 55(5): p. 327-341.

217. Etheridge, D., Unsteady flow effects due to fluctuating wind pressures in natural ventilation design—mean flow rates. Building and Environment, 2000. 35(2): p. 111-133.

218. Etheridge, D., Unsteady flow effects due to fluctuating wind pressures in natural ventilation design—instantaneous flow rates. Building and Environment, 2000. 35(4): p. 321-337.

219. Miguel, A., et al., Wind-induced airflow through permeable materials part I: the motion equation. Journal of wind engineering and industrial aerodynamics, 2001. 89(1): p. 45-57.

220. Miguel, A., et al., Wind-induced airflow through permeable materials, Part II: air infiltration in enclosures. Journal of wind engineering and industrial aerodynamics, 2001. 89(1): p. 59-72.

221. Wang, H. and Q. Chen, A new empirical model for predicting single-sided, wind-driven natural ventilation in buildings. Energy and Buildings, 2012. 54: p. 386-394.

222. Ai, Z. and C. Mak, Analysis of fluctuating characteristics of wind-induced airflow through a single opening using LES modeling and the tracer gas technique. Building and environment, 2014. 80: p. 249-258.

223. Mahrt, L., J. Sun, and D. Stauffer, Dependence of turbulent velocities on wind speed and stratification. Boundary-Layer Meteorology, 2015. 155(1): p. 55-71.

224. Antoniou, N., et al., CFD and wind-tunnel analysis of outdoor ventilation in a real compact heterogeneous urban area: Evaluation using “air delay”. Building and Environment, 2017. 126: p. 355-372.

225. Kraniotis, D., T.K. Thiis, and T. Aurlien. Wind direction and leakage distribution in buildings. A CFD transient analysis of their impact on air exchange rates under unsteady wind conditions. in 6th European-African conference on wind engineering(EACWE 2013). 2013.

226. Holøs, S.B. and T.-O. Relander. Airtightness measurements of wood frame low energy row houses. in Proceedings: BEST conference. Portland. 2010.

227. Prignon, M., et al., A method to quantify uncertainties in airtightness measurements: Zero-flow and envelope pressure. Energy and Buildings, 2019. 188: p. 12-24.

228. Wood, C., et al., An extended pressure range comparison of the blower door and novel pulse method for measuring the airtightness of two outdoor chambers with different levels of airtightness, in 39th AIVC - 7th TightVent & 5th venticool Conference. 2018: Antibes Juan-Les-Pins, France.

229. Ministry of Housing, C.L.G., English Housing Survey 1967-2017, N. Statistics, Editor. 2019.

230. Ministry of Housing, C.L.G., English Housing Survey – Floor Space in English Homes. 2017.

231. Association, C.S., CAN/CGSB-149.10-2019, in Determination of the airtightness of building envelopes by the fan depressurization method. 2019.

232. Leprince, V., F. Carrié, and M. Kapsalaki, Building and ductwork airtightness requirements in Europe -Comparison of 10 European countries, in 38th AIVC Conference "Ventilating healthy low-energy buildings". 2017: Nottingham, UK.

233. Leprince, V. and F.-R. Carrié, Comparison of building preparation rules for airtightness testing in 11 European countries, in 35th AIVC Conference " Ventilation and airtightness in transforming the building stock to high performance". 2014: Poznań, Poland.

234. Meteoblue. 2021 [cited 2021 18/08]; Available from: https://www.meteoblue.com/en/weather/week/nottingham_united-kingdom_2641170.

235. Manwell, J.F., J.G. McGowan, and A.L. Rogers, Wind energy explained: theory, design and application. 2010: John Wiley & Sons.

236. Mikhail, A. and C. Justus, Comparison of height extrapolation models and sensitivity analysis. Wind Engineering, 1981: p. 91-107.

237. Dalila, K., et al., Evaluation of the adequacy of the wind speed extrapolation laws for two different roughness meteorological sites. American Journal of Applied Sciences, 2014. 11(4).

238. Zheng, X., et al. Experimental study of enclosure airtightness of an outdoor chamber using the pulse technique and blower door method under various leakage and wind conditions. in 39th AIVC - 7th TightVent & 5th venticool Conference. 2018. Antibes Juan-Les-Pins.

239. Windfinder.com, Wind, Wave & Weather Reports, Forecasts & Statistics Worldwide. 2021.

240. Huebsch, W., et al. Discharge Coefficients for Irregular Orifices. in APS Division of Fluid Dynamics Meeting Abstracts. 2013.

241. Kurita, C., Critical flow restricting orifices. 1988, Fermi National Accelerator Lab.(FNAL), Batavia, IL (United States).

242. Blair, G.P., et al., Coefficients of Discharge at the Aperatures of Engines. 1995, SAE International.

243. Roache, P.J., Quantification of uncertainty in computational fluid dynamics. Annual Review of Fluid Mechanics, 1997. 29(1): p. 123-160.

244. Fluent, A., ANSYS fluent theory guide 15.0. ANSYS, Canonsburg, PA, 2013. 33.

245. Roy, C.J., Grid Convergence Error Analysis for Mixed-Order Numerical Schemes. AIAA Journal, 2003. 41(4): p. 595-604.

246. Michalcová, V. and K. Kotrasová, The Numerical Diffusion Effect on the CFD Simulation Accuracy of Velocity and Temperature Field for the Application of Sustainable Architecture Methodology. Sustainability, 2020. 12(23): p. 10173.

247. Roache, P.J., Perspective: A Method for Uniform Reporting of Grid Refinement Studies. Journal of Fluids Engineering, 1994. 116(3): p. 405-413.

248. Acharya, S., et al., Pressure-Based Finite-Volume Methods in Computational Fluid Dynamics. Journal of Heat Transfer, 2007. 129(4): p. 407-424.

249. Denner, F., Fully-coupled pressure-based algorithm for compressible flows: Linearisation and iterative solution strategies. Computers & Fluids, 2018. 175: p. 53-65.

250. Xiao, C.-N., F. Denner, and B.G.M. van Wachem, Fully-coupled pressure-based finite-volume framework for the simulation of fluid flows at all speeds in complex geometries. Journal of Computational Physics, 2017. 346: p. 91-130.

251. Chen, Z.J. and A.J. Przekwas, A coupled pressure-based computational method for incompressible/compressible flows. Journal of Computational Physics, 2010. 229(24): p. 9150-9165.

252. Karimian, S.M.H. and G.E. Schneider, Pressure-based computational method for compressible and incompressible flows. Journal of Thermophysics and Heat Transfer, 1994. 8(2): p. 267-274.

253. Kraposhin, M.V., et al., A hybrid pressure-based solver for nonideal single-phase fluid flows at all speeds. International Journal for Numerical Methods in Fluids, 2018. 88(2): p. 79-99.

254. Caretto, L.S., et al. Two calculation procedures for steady, three-dimensional flows with recirculation. 1973. Berlin, Heidelberg: Springer Berlin Heidelberg.

255. Qin, J., et al., Introducing compressibility with SIMPLE algorithm. Mathematics and Computers in Simulation, 2021. 180: p. 328-353.

256. Moukalled, F. and M. Darwish, A unified formulation of the segregated class of algorithms for fluid flow at all speeds. Numerical heat transfer part B fundamentals, 2000. 37(1): p. 103-139.

257. Menter, F.R., Two-equation eddy-viscosity turbulence models for engineering applications. AIAA Journal, 1994. 32(8): p. 1598-1605.

258. Menter, F.R., M. Kuntz, and R. Langtry, Ten years of industrial experience with the SST turbulence model. Turbulence, heat and mass transfer, 2003. 4(1): p. 625-632.

259. Zhao, Y., et al., Uncertainty and sensitivity analysis of SST turbulence model on hypersonic flow heat transfer. International Journal of Heat and Mass Transfer, 2019. 136: p. 808-820.

260. Mavriplis, D. Revisiting the least-squares procedure for gradient reconstruction on unstructured meshes. in 16th AIAA computational fluid dynamics conference. 2003.

261. Wang, N., et al., Accuracy analysis of gradient reconstruction on isotropic unstructured meshes and its effects on inviscid flow simulation. Advances in Aerodynamics, 2019. 1(1): p. 18.

262. Bailey, R.T., Managing false diffusion during second-order upwind simulations of liquid micromixing. International Journal for Numerical Methods in Fluids, 2017. 83(12): p. 940-959.

263. Lin, H., et al., Volumetric Property Improvement for the Soave−Redlich−Kwong Equation of State. Industrial & Engineering Chemistry Research, 2006. 45(5): p. 1829-1839.

264. Laney, C.B., Computational gasdynamics. 1998: Cambridge university press.

265. Kavetski, D., P. Binning, and S.W. Sloan, Adaptive time stepping and error control in a mass conservative numerical solution of the mixed form of Richards equation. Advances in Water Resources, 2001. 24(6): p. 595-605.

266. Franke, J., Best practice guideline for the CFD simulation of flows in the urban environment. 2007: Meteorological Inst.

267. Cowan, I.R., I.P. Castro, and A.G. Robins, Numerical considerations for simulations of flow and dispersion around buildings. Journal of Wind Engineering and Industrial Aerodynamics, 1997. 67-68: p. 535-545.

268. Bartzis, J.G., Thematic area 5: Best practice advice for environmental flows. The QNET-CFD Network Newsletter, 2004. 2: p. 34-39.

269. Heiselberg, P., et al., Experimental and CFD evidence of multiple solutions in a naturally ventilated building. Indoor Air, 2004. 14(1): p. 43-54.

Appendix A: Design and Preparation of a Model-Scale Pulse for Wind Tunnel Test

This appendix contains the literature review of the wind tunnel experiment, experimental design and setup of the model-scale experiment in a wind tunnel to investigate how the steady wind affects the Pulse test.

A.1 Literature review

An Atmospheric Boundary Layer (ABL) wind tunnel can be used to investigate the wind impact on the building airtightness measurement, as the environmental and morphological parameters of the scaled buildings inside a wind tunnel can be controlled. ABL is capable of simulating the airflow as it flows over the earth's surface, which has been widely adopted for urban and environmental experiments. In general, ABL wind tunnels can be designed in open- or closed-circuit. In an open wind tunnel, the inlet and outlet are not directly coupled, while the air circulates in the closed-circuit through connected parts. Comparatively, a closed-circuit wind tunnel has more elements than an open-circuit one, as the parts that allowing returning air result in a larger dimension of the wind tunnel [1]. The main advantages of closed-circuit wind tunnels include: the recirculated air can be less disturbed with lower turbulence intensities, less power consumption and lower operation cost, but the initial cost for construction is higher [2]. In terms of the design, a number of parameters are considered, such as the fan, the test section, setting chamber etc. For open-circuit wind tunnels, the space where the air returns should not affect the inlet airflow. Axial fans can accelerate the flow parallel to the duct, which is popular for closed-circuit wind tunnels and open wind tunnels adopt either axial or centrifugal fans. A suitable fan is important to a wind tunnel for better efficiency, which needs to match the system curve [3], as seen in Figure A-1.

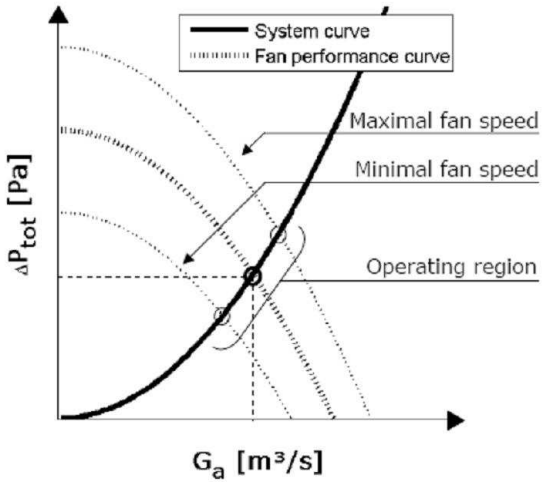


Figure A-1: Fan performance curve (dotted) and wind tunnel system curve (solid) by Moonen, et al. [4]

A diffuser decreases the velocity and converts dynamic pressure into static pressure when a diffuser reaches a certain angle where the flow near the wall separates. Separation (i.e. diffuser, exit, corner, cross-sections) should be avoided in the wind tunnel design [5], as non-continuous flow could be generated, and the velocity would fluctuate with time [6]. The settling chamber is designed to produce parallel, spatially uniform and steady airflows because a mimic of the atmospheric boundary layer is required in the test section [7]. A contraction is added to improve flow uniformity, thus enhance the circuit efficiency by reducing losses in the settling chamber [5]. For example, Vladut, et al. [8] modified an old open-circuit infrastructure for a new boundary layer wind tunnel (see Figure A-2), which is able to generate a velocity field (0.1-30m/s). They used a honeycomb together with an interchangeable grid pack to minimise the turbulence intensity. Mayer, et al. [9] designed an open-jet wind tunnel with two interchangeable rectangular nozzles and a partially shared contraction, which ensured low turbulence intensity and low flow angularity for spatially uniform steady airstreams (Figure A-3).

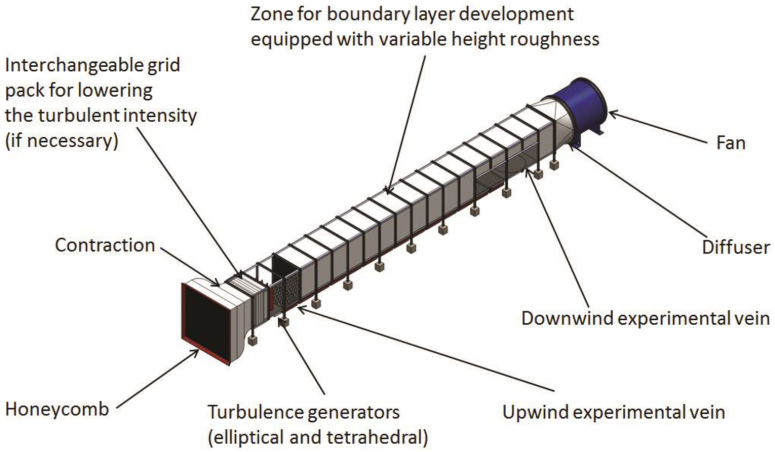


Figure A-2: Open-circuit wind tunnel by Vladut, et al. [8]

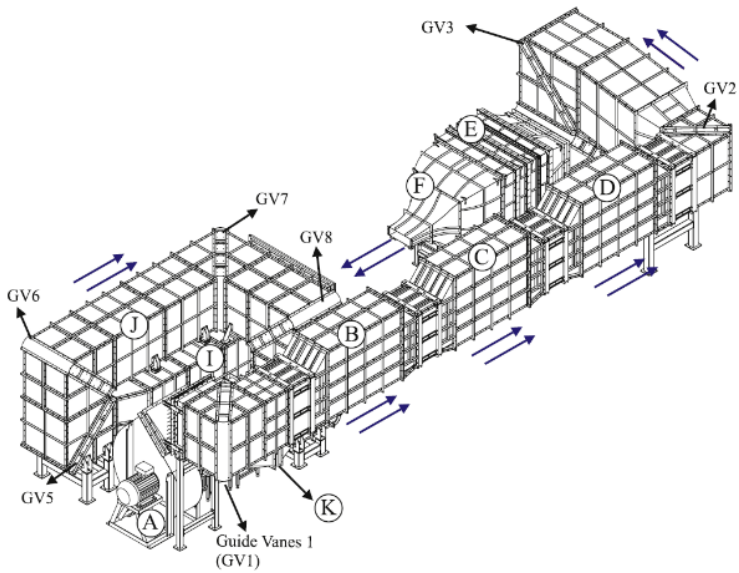


Figure A-3: Open-jet wind tunnel by Mayer, et al. [9]

Flow characteristics can be influenced by a boundary layer, where friction is caused by the solid surface over which the airflow passes. The simulation of the atmospheric boundary layer can be realised in the working section by having adjustable roughness elements along the floor to simulate a variety of urban circumstances [1].



Figure A-4: The variable roughness system by Vladut, et al. [8]

Theoretically, the total pressure decreases in flow direction along the duct of a wind tunnel, while the fan could compensate the total pressure (i.e. static and dynamic) with the amount lost through the wind tunnel [10], which can be expressed as:

$$\Delta p_{\text{fan}} = \Delta p_{wt} \tag{A-1}$$

Where $\Delta p_{wt}$is the pressure loss throughout the wind tunnel and Δp_{fan} is the pressure rise caused by the fan.

The pressure loss of a part in the wind tunnel can be obtained by multiplying the pressure loss coefficient (K) with the dynamic pressure (p_d) [11]:

$$\Delta p = K p_d \tag{A-2}$$

Where p_d is the dynamic inlet pressure of the part = $\frac{1}{2}\rho v^2$.

Figure A-5 shows an example of the pressure loss calculation containing some pressure coefficients referred to in the literature review [11, 12].

	K	q	Δp	$K_{(}ts)$
part 1	K_1	q_1	$K_1 q_1$	$K_1 \frac{q_1}{q_{ts}}$
part 2	K_2	q_2	$K_2 q_1$	$K_2 \frac{q_2}{q_{ts}}$
part 3	K_3	q_3	$K_3 q_3$	$K_3 \frac{q_3}{q_{ts}}$
part i	K_i	q_i	$K_i q_i$	$K_i \frac{q_i}{q_{ts}}$
				$\sum (K_{ts}) = \frac{\sum (K_i q_i)}{q_{ts}}$
			$\Delta p = \sum (K_i q_i)$	$\Delta p = \sum (K_{ts})\, q_{ts}$

Figure A-5: Overview of total pressure loss calculation [3]

The pressure loss in diffusers accounts for about 30% of the total pressure loss in wind tunnels, which is due to the wall friction and expansion loss [12]:

$$K_d = K_f + K_{ex} \tag{A-3}$$

Where K_d is the pressure loss coefficient of a diffuser, K_f is the wall friction coefficient, $K_f = (1 - \frac{1}{Ar^2}) \frac{f}{8 sin\partial}$ and K_{ex} is the expansion loss coefficient $K_{ex} = K_e(\frac{Ar-1}{Ar})^2$ and the area ratio $A_r = \frac{Aot}{Ain}$ is the ratio outlet cross-section to the inlet cross-section. The equivalent conical angle is obtained by $\partial = \tan^{-1}(\frac{\sqrt{Aot}-\sqrt{Ain}}{l/\pi})$ and $f = [2\log_{10}(Re\sqrt{f}) - 0.8]^{-2}$.

Figure A-6 presents the example of the pressure loss coefficient of a square diffuser (K_e) referred to van Dommelen [3].

Ke for a square cross section:

K_e = 0.09623 - 0.004152 α for $\alpha < 1.5$

K_e = 0.122156 - 0.0458960 α + 0.02202816 α^2 - 0.003269152 α^3 - 0.0006144896 α^4 + 0.00027999008 α^5 - 0.000023373888 α^6 for $1.5 \leq \alpha \leq 5$

K_e = -0.1322 + 0.05866 α for $\alpha > 5$

Ke for a circular cross section:

K_e = 0.1033 - 0.02389 α for $\alpha < 1.5$

K_e = 0.1709 - 0.1170 (α) + 0.03260 α^2 + 0.001078 α^3 - 0.0009076 α^4 - 0.00001331 α^5 + 0.00001345 α^6 for $1.5 \leq \alpha \leq 5$

K_e = -0.09661 + 0.04672 α for $\alpha > 5$

Figure A-6: Examples of K_e [3]

The pressure loss in settling chambers is the sum of the pressure losses of a honeycomb and/or screen. The pressure loss coefficient increases with the length of the honeycomb cells, which can be calculated based on eq. (A-4):

$$K = \lambda(\frac{lcell}{D_{cell}} + 3)(\frac{1}{\beta})^2 + (\frac{1}{\beta} - 1)^2 \quad \text{(A-4)}$$

where $\lambda = 0.375(\frac{\Delta_r}{Dcell})^{0.4}\mathrm{Re}\,\Delta_r^{-0.1}$ for $\mathrm{Re}\,\Delta_r \leq 275$ and $\lambda = 0.214(\frac{\Delta_r}{Dcell})^{0.4}$ for $\mathrm{Re}\,\Delta_r > 275$. D_{cell} is the hydraulic cell diameter, β is the honeycomb porosity and Δ_r is the roughness.

The pressure loss in contractions is related to the area ratio and length, which together determine the contraction angle. For curved contraction, the coefficient of pressure loss is expressed as:

$$K = 0.32 f_{av} \frac{l}{D_o} \quad \text{(A-5)}$$

Where f_{av} is the friction factor at the average diameter, l is the length of the centre line, and D_o is the outlet diameter of contraction.

The total power required for operating a wind tunnel (E_{wt}) can be calculated by multiplying the total pressure loss with the flow area [5, 12]:

$$E_{wt} = A_{\mathrm{ts}} v_{\mathrm{ts}} \sum \Delta p_{wt} \quad \text{(A-6)}$$

Where A_{ts} is the cross-section area of the test section and v_{ts} is the velocity in the test section.

Extensive studies have been found in the literature for urban and environment experiments, for instance, experiments on cross-ventilation flow for building in urban areas under various wind angle conditions [13], observations of the gusty wind effect on the structural design of high-rise buildings [14] and measurements of surface pressure and total drag on building via the wind tunnel experiment [15]. However, few experimental studies have been conducted for exploring the wind impact on the building airtightness measurement using a wind tunnel. Mélois, et al. [16] considered a model experiment in a wind tunnel to evaluate the steady wind impact on the fan pressurisation method. They designed a solid and well-sealed cube model to represent a building for model investigation and a small-scale fan pressurisation unit that could be fitted into the wind tunnel. Experimental works have been conducted for the designed wind tunnel rig by performing fan pressurisation tests in different windy conditions inside the wind tunnels [17].

A.2 Experimental set-up

Model-scale building design

The test building was assumed to be represented by a single zone model for conducting a controlled experiment in laboratory conditions [18]. Referred to previous work, to ensure similar conditions in the model-scale experiment, the building model scales were determined based on the following relationships:

$$\bar{U}=\bar{P} \qquad \bar{P}.\bar{A}^2=\bar{q}^2 \qquad \bar{A}^{0,5}=\bar{L} \qquad \bar{V}.\bar{U}=\bar{L}.\bar{q}$$

Considering a typical two-story dwelling (i.e., with a total floor area of 120m^2 and an internal volume of 320m^3) as an actual test building, and a scale ratio for the length of $\bar{L}$=1/12, the scale ratios are obtained respectively as given in Table A-1. Figure A-7 shows a sketch of the scaled model with dimensions. The building leakage is represented by four openings on the four sides of the building model.

Table A-1: Scale ratios for the model-scale building

Length	$\bar{L}$	1/12
Area of Opening	$\bar{A}$	1/144
Internal Building Volume	$\bar{V}$	1/1728
Wind Speed at the Building Level	$\bar{U}$	1
Pressure Relative to External Pressure	$\bar{P}$	1
Volumetric Airflow Rate	$\bar{q}$	1/144

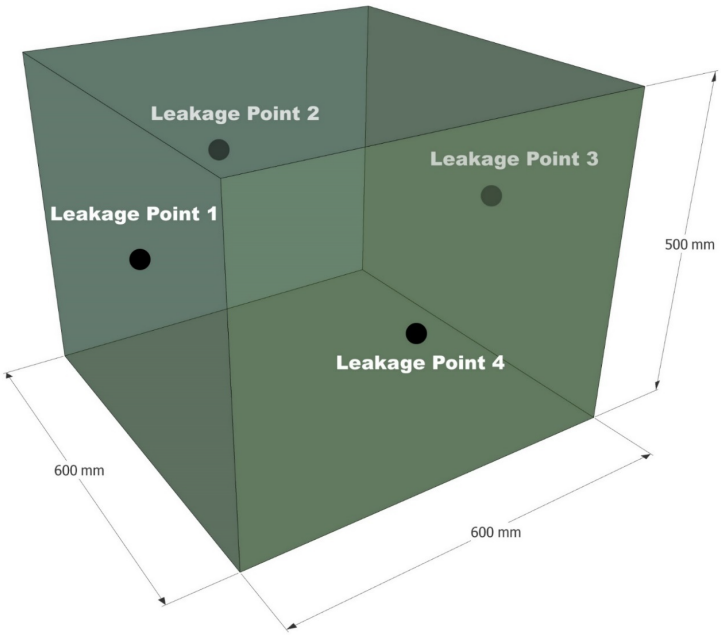


Figure A-7: Scaled building model

Model-scale Pulse unit design

A model-scale Pulse unit, which consists of a 0.5-litre air tank and oil-free compact air compressor, was designed and constructed for the wind tunnel experiment. A ¼ inch (BSP) solenoid valve was installed at the outlet for releasing compressed air from the air tank into the building model.

In addition, the Pulse test data, such as model-scale building airtightness, were recorded and analysed by the on-board Pulse control box, with results displayed on the LCD screen, as seen in Figure A-8.

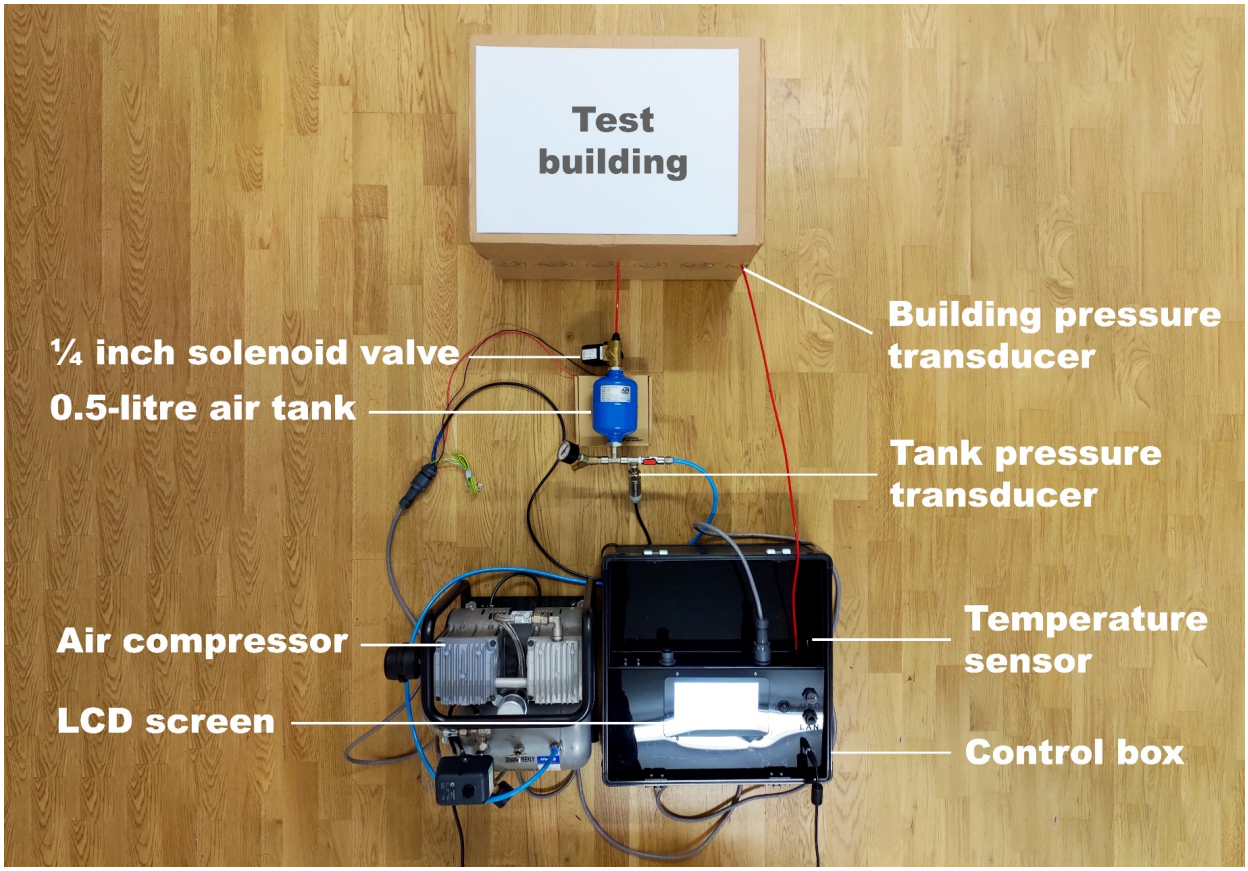


Figure A-8: Model-scale Pulse unit

A.3 Experiment design

The University of Nottingham is equipped with an open circuit low-speed wind tunnel, and the holistic illustration is given in Figure A-9, referred to work by Sofotasiou [19]. The wind tunnel is equipped with an axial fan that enables the generation of velocity speeds up to 11m/s when empty. Figure A-10 presents the photo of the inlet of the wind tunnel.

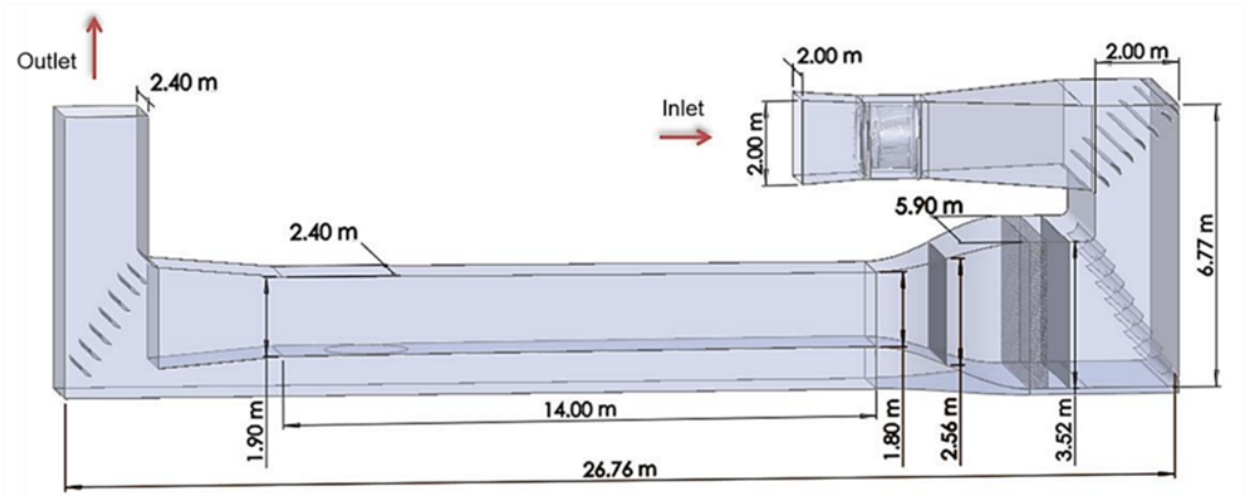


Figure A-9: Schematic diagram of the wind tunnel [19]

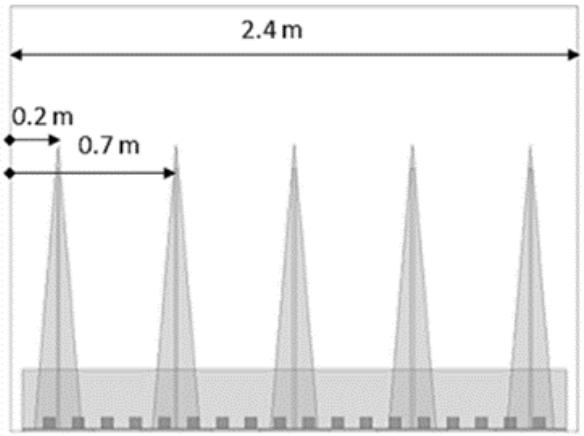


Figure A-10: Photo of the inlet of the wind tunnel in Faculty of Engineering, University of Nottingham

The wind tunnel provides the generation of a suburban terrain at a scale of 1:400, as presented in Figure A-11. The terrain is with a power-law exponent equal to 0.28 and a target boundary layer depth equal to 400m in full scale or 1m in wind tunnel scale [20]. As the building model for the experiment is designed with a scale ratio of 1:12, the scale of the suburban terrain is required at 1:12.



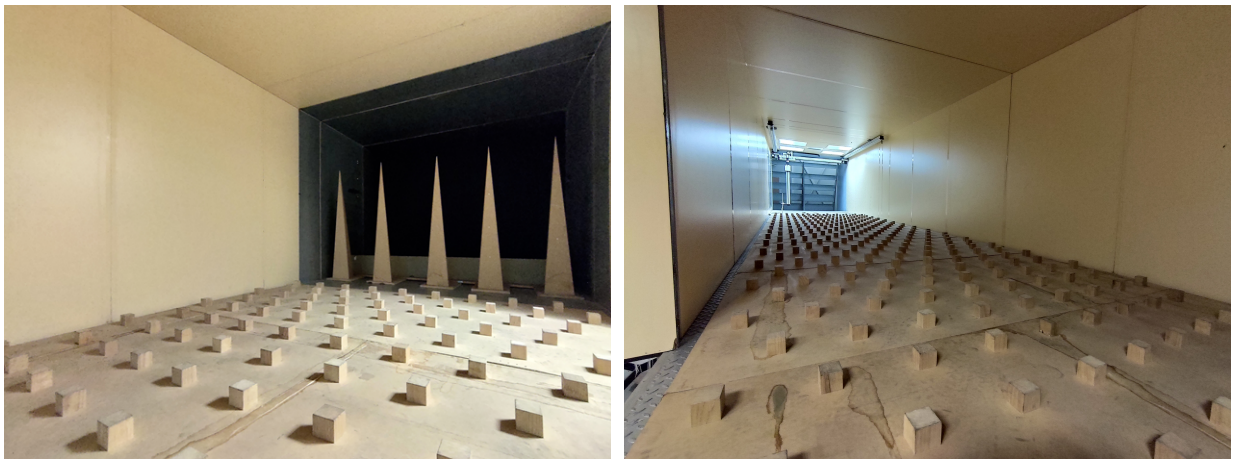
(a)



(b)

Figure A-11: Diagrams of (a) sectional view of the wind tunnel and (b) suburban terrain in the wind tunnel [19]

Figure A-12 presents the photo of the suburban terrain inside the wind tunnel.



(a) (b)

Figure A-12: Photos of the suburban terrain inside the wind tunnel in the University of Nottingham

For this study, the scaled building model will be placed on the round platform inside the wind tunnel for testing, as indicated in Figure A-13. As seen from the photo in Figure A-14, the orientation of the model will be adjusted in order to simulate different wind directions in order to investigate the impact of the steady wind direction on the building airtightness measurement using the model-scale Pulse unit. There is a space underneath the platform, as shown in Figure A-15, so that the Pulse unit could be placed for experiment with easy access and operation. Therefore, during the experiment, the air pulse would be released from the air tank located underneath the platform to the interior of the building model on the round platform. Furthermore, there are a number of designated locations inside the wind tunnel for placing various sensors, such as anemometer, pressure transducers and thermocouples.

For the wind tunnel testing, various parameters are considered; some of them are fixed, while other parameters will be adjusted in order to evaluate the steady wind impact, as listed in Table A-2.

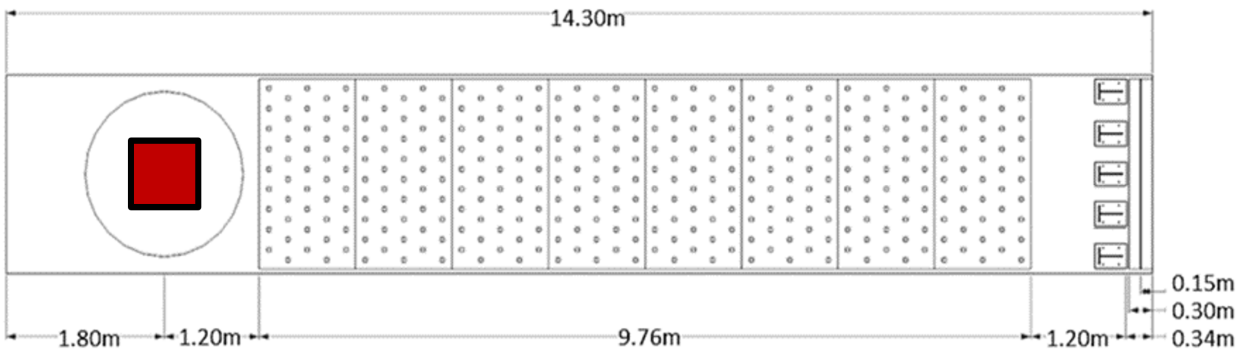


Figure A-13: Location of test building model in the wind tunnel [19]



Figure A-14: Photos of the round platform inside the wind tunnel



Figure A-15: Photos of the round platform underneath space inside the wind tunnel

Table A-2: Operating parameters of the experiment

Operating Parameters		Notes
Fixed Parameters	Initial inside and outside temperatures	The stack effect is not taken into account in the model-scale experiment to be able to estimate the wind error only.
Varying Parameters	Steady wind speed	Ranging from wind speed 0 to 11m/s
	Distribution of building leakage areas	Four respective leakage points are designed on the four walls of the building model to simulate the building leakage areas. Under different scenarios, the four leakage points will be adjusted accordingly (e.g., various leakage areas and locations), but the total building air leakage area is maintained at the same level.
	Opening areas	The openings on the four walls are adjustable in order to provide a range of leakage levels for testing.
	External pressure tap location	A reference point where the building pressure tapping is installed is determined (i.e., the centre of the building model). Tests will be repeated by placing the pressure tap at different locations around the building model and assess the measurement results.

A.4 Proposed results analysis

The obtained results from the model-scale experiments will be used to accomplish the following assessments.

1) Evaluation of the impact of steady wind at various speed levels on the Pulse test;
2) Evaluation of the impact of steady wind direction on the Pulse test;
3) Evaluation of the impact of building leakage distribution on the Pulse test;
4) Evaluation of the impact on the Pulse test for buildings with various leakage levels;
5) Improvement of the Pulse reliability with reduced uncertainty under high wind conditions.

A.5 References

1. Rae, W.H. and A. Pope, Low-speed wind tunnel testing. 1984: John Wiley.
2. Basak, R., D. Mitra, and A. Mazumdar, Design of various components of an open circuit blower tunnel without exit diffuser. International Journal of Advances in Science and Technology, page, 2011. 89.
3. van Dommelen, R., Design of an atmospheric boundary layer wind tunnel. 2013.
4. Moonen, P., et al., Numerical modeling of the flow conditions in a closed-circuit low-speed wind tunnel. Journal of Wind Engineering and Industrial Aerodynamics, 2006. 94(10): p. 699-723.

5. Johl, G., M. Passmore, and P. Render, Design methodology and performance of an indraft wind tunnel. The aeronautical journal, 2004. 108(1087): p. 465-473.

6. Chong, T., P. Joseph, and P. Davies, Design and performance of an open jet wind tunnel for aero-acoustic measurement. Applied acoustics, 2009. 70(4): p. 605-614.

7. Vignon, E., et al., Modeling the dynamics of the atmospheric boundary layer over the antarctic plateau with a general circulation model. Journal of Advances in Modeling Earth Systems, 2018. 10(1): p. 98-125.

8. Vladut, A.C., et al., A new boundary layerwind tunnel. U.P.B. Sci. Bull., Series D, 2017. 79(2): p. 159-168.

9. Mayer, Y.D., et al., Design and performance of an aeroacoustic wind tunnel facility at the University of Bristol. Applied Acoustics, 2019. 155: p. 358-370.

10. Hemphill, G.B., Practical tunnel construction. 2012: John Wiley & Sons.

11. Barlow, J.B., et al., Low-speed wind tunnel testing. 1999, New York: Wiley.

12. Eckert, W.T., K.W. Mort, and J. Jope, Aerodynamic design guidelines and computer program for estimation of subsonic wind tunnel performance. 1976.

13. Shirzadi, M., Y. Tominaga, and P.A. Mirzaei, Wind tunnel experiments on cross-ventilation flow of a generic sheltered building in urban areas. Building and Environment, 2019. 158: p. 60-72.

14. Li, X. and Q. Li, Observations of typhoon effects on a high-rise building and verification of wind tunnel predictions. Journal of Wind Engineering and Industrial Aerodynamics, 2019. 184: p. 174-184.

15. Li, B., et al., Drag distributions of non-uniform buildings from surface pressure measurements in wind tunnel. Building and Environment, 2018. 143: p. 618-631.

16. Mélois, A.B., et al. Designing a model-scale experiment to evaluate the impact of steady wind on building air leakage measurements. in 40th AIVC - 8th TightVent & 6th venticool Conference. 2019. Ghent, Belgium.

17. Mélois, A.B., et al. Assessment of wind impact on building air leakage measurements using a model scale experiment. in E3S Web of Conferences. 2020. EDP Sciences.

18. Carrié, F.R. and V. Leprince, Uncertainties in building pressurisation tests due to steady wind. Energy and Buildings, 2016. 116: p. 656-665.

19. Sofotasiou, P., Aerodynamic optimisation of sports stadiums towards wind comfort. 2017, University of Sheffield.

20. Simiu, E. and R.H. Scanlan, Wind effects on structures : fundamentals and applications to design. 3rd ed. ed. 1996: New York : John Wiley.